FRAME AND FOURIER METHODS FOR EXOTIC OPTION PRICING AND HEDGING

A Thesis
Presented to
The Academic Faculty

by

Justin Lars Kirkby

In Partial Fulfillment
of the Requirements for the Degree
Doctor of Philosophy in Operations Research in the
School of Industrial and Systems Engineering

Georgia Institute of Technology
December 2016

FRAME AND FOURIER METHODS FOR EXOTIC OPTION PRICING AND HEDGING

Approved by:

Shi-Jie Deng, Committee Chair, Advisor
School of Industrial and Systems Engineering
Georgia Institute of Technology

David Goldberg
School of Industrial and Systems Engineering
Georgia Institute of Technology

David Goldsman
School of Industrial and Systems Engineering
Georgia Institute of Technology

Ionel Popescu
School of Mathematics
Georgia Institute of Technology

Enlu Zhou
School of Industrial and Systems Engineering
Georgia Institute of Technology

Date Approved: October 19, 2016

Dedicated to my wife for her support and patience.

ACKNOWLEDGEMENTS

I would like to thank my advisor, Shi-Jie Deng, for his mentoring over the years, as well as all of my professors at Georgia Tech. I thank my committee members David Goldberg, David Goldsman, Ionel Popescu, and Enlu Zhou for their support. I thank Mike Staunton for his helpful critiques of some of the early papers, and Jeffrey Pavelka for discussions and reading of the initial drafts. I thank my wife for her support and understanding through many years in a rigorous program. I also thank the anonymous reviewers for their time and excellent suggestions that have improved the quality of this work.

TABLE OF CONTENTS

LIST OF TABLES

LIST OF FIGURES

SUMMARY

In Mathematical Finance, the field of option pricing is a wonderful intersection of many fascinating branches of mathematics. This work investigates an exciting strain of research within this field which utilizes the tools of Fourier analysis. In particular, Frame theory is introduced to the field as a means of tackling many problems in option pricing and hedging. From this theory we derive a new approach for solving pricing problems in the Fourier domain, using the characteristic function of the underlying process. The resulting method is robust, accurate and efficient. Each type of exotic contract presents unique challenges from a mathematical and numerical perspective, and much of this work is concerned with designing efficient algorithms that exploit problem structure in interesting ways. Also important is an understanding of the errors resulting from various approximations made. We present detailed error analyses to investigate the convergence properties of the method, which are verified by a series of computational experiments to test its limits. To aid in future research, large sets of benchmark prices are prepared for various models so that comparisons can be made.

CHAPTER I

INTRODUCTION

Numerical option pricing has been revolutionized with the advent of fast transform methods. While lattice and Monte Carlo based approaches remain the most generally applicable, transform based approaches, when available, provide astonishing gains in accuracy and efficiency. Problems that may take a Monte Carlo routine hours or even days can be reduced to mere seconds (or fractions thereof) by a well designed transform method. Since the seminal work of [35], which introduced the fast Fourier transform (FFT) as a means of efficiently computing a spectrum of European option prices under exponential Levy dynamics [16, 32, 117, 120], the applicability and sophistication of transform methods has rapidly evolved (see [91] for more details and [96] for a related approach).

While restricted to mixture of Gaussian models, the fast Gauss transform, applied first to European options [26], and later extended to discretely monitored exotics [27, 133], is a prominent example. Early exercise features under general Levy dynamics were effectively incorporated by the CONV method [100], based on the FFT. Around the same time, the Hilbert transform (HT) was introduced as a tool for pricing barrier options and credit default swaps (CDSs) [67]. European, lookback, and Bermudan options were soon part of its domain [64–66]. Recently, time-changed Levy processes have extended the applicable model class of HT methods [135].

Other methods have continued to refine and extend the original approach of Carr and Madan. For example, the work of [102] improves its application by optimal selection of (flat) integration contours, while [19] introduces nonlinear contours to hasten convergence. The latter approach is applied as well to discrete barrier options and CDSs [51]. Also within the numerical pricing realm, but restricted to Gaussian return distributions, is the quadrature method [7, 8], mentioned here because of its applicability to many types of options.

Perhaps the most applicable transform method for pricing options under Levy dynamics and affine jump diffusions [57] is the COS method [61], which utilizes a cosine series expansion of the risk-neutral return density. Extensions to barrier and Bermudan options [62, 63, 136], swing options [137], Asian options [138, 139], CDSs [60], and higher dimensions [118] have been developed with impressive performance.

1.1 Research Overview

This work is concerned primarily with a new option pricing framework, called the PROJ method (option pricing by frame projection) [83], which was introduced as an efficient means of pricing large European option portfolios, as arises in the context of calibration. Static hedging is also considered in [88]. The method is now applicable to forward starting options [87], barrier, Parisian (cumulative and resetting) and step options [85], Bermudan/American options [86], swing options [89], arithmetic Asian [84] and lookback options [86], as well as as credit default swaps [86]. Geometric Asian options are priced in [83].

The contribution of PROJ, in addition to providing a robust and universal pricing method, is that it performs exceptionally well in the cases for which global basis methods experiences difficulty. In particular, as monitoring frequency increases, the local basis structure of PROJ provides a critical advantage in terms of accuracy and robustness. Moreover, local bases are much simpler to work with when developing extensions to more exotic contracts. Additional flexibility is another benefit, since different basis types of varying degrees of smoothness can be used to target salient features of a problem. We also find significant speed advantages over existing state-of-the-art algorithms, especially for contracts of weekly-monitored frequency or greater and with heavy-tailed transitional densities.

On one hand, PROJ can be combined with careful numerical techniques to derive extremely robust/efficient specialized algorithms. On the other, due to the accelerated convergence of convolution, it can by applied very directly to problems for which convolution alone is too computationally burdensome. Hence, PROJ can be used as a first approach to tackling problems directly, before specialized algorithms are considered, and it is universally applicable whenever a transition density could be used. Even if a density is known in closed

form, directly convolution is much slower to converge than if a projection of the density is first performed. This work details the development of this framework for pricing and hedging vanilla and exotic options.

1.2 Outline of Dissertation

This work comprises a series of self-contained chapters, beginning with an accessible introduction to the transform-based literature in Chapter 2. The third chapter introduces the PROJ method, which applies frame theory to price large baskets of European options and geometric Asian options, most commonly used as control variates in Monte Carlo schemes. This framework is refined and extended in Chapter 4, where the convergence order of various B-splines are studied, along with alternative methods for truncation interval selection, and a method for forward-starting option pricing. Chapter 5 considers the problem of static hedging, and presents a general framework. New approximation results are obtained for the calculation of dual coefficients and have the potential for various applications.

Generalized arithmetic Asian (averaging) options are considered in Chapter 6. These contracts are highly path dependent, and the resulting method provides a substantial cost reduction over existing alternatives, often providing a several hundred fold time reduction. Chapter 7 considers the pricing of generalized barrier options using a fast Toepiltz based convolution scheme. This includes standard single and double barrier options (which are weakly path dependent) as well as their more complex counterparts, namely Parisian options, Par-asian options, and step options. While several methods exist for the Black-Scholes model and recent work has extended to Kou's jump diffusion, the PROJ method is the first to consider Parisian options for general exponential Levy processes of an arbitrary form. Finally, Chapter 8 concludes the work with a discussion of future research objectives.

CHAPTER II

FOURIER METHODS FOR OPTION PRICING

The modern landscape of financial modeling has been inexorably shaped by the seminal works of Black and Scholes [15] and Merton [106]. The original model, which has become known as the Black-Scholes-Merton (BSM) model, specifies a stochastic equation for the evolution of an underling asset price $(S_t)_{t\geq 0}$, namely the geometric Brownian motion process

$$dS_t = S_t(\mu dt + \sigma dW_t), \qquad S_0 > 0, \tag{1}$$

where $(W_t)_{t\geq 0}$ is a standard Brownian motion. For now, the constant μ is essentially arbitrary, assumed to exist for a given *real-world* measure $\mathbb{P}$, a measure which for general models will capture the observed market randomness by the triplet $(\Omega, \mathcal{F}, \{\mathcal{F}_t\}_{t\geq 0}, \mathbb{P})$ with the standard interpretation.

The traditional and perhaps most natural approach to asset modeling, in the spirit of BSM, is the specification of a dynamic process for the underlying, as in equation (1). In this case, Ito's lemma can easily verify that the following process

$$S_t = S_0 \exp\left((\mu - \tfrac{1}{2}\sigma^2)t + \sigma W_t\right), \tag{2}$$

uniquely solves equation (1). It is therefore equivalent to model $(S_t)_{t\geq 0}$ by directly assuming the form of equation (2), and the dynamics are readily available if needed. With the exception of stochastic volatility models, this is the approach we will take.

In addition to an underlying traded asset, we assume the ability to borrow and trade funds at a continuously compounding rate of interest $r \geq 0$. To formalize this notion, we consider an account bearing no risk of default, in which funds are deposited or withdrawn at our discretion. The existence of such an account, which is mostly a mathematical formalization, is essential to the theory of arbitrage-free or risk-neutral pricing.

2.1 Risk-Neutral Pricing

Our interest in this work is exclusively the pricing and hedging of financial instruments with payoffs that depend on the path of $(S_t)_{t\geq 0}$ (and possibly other random variables as well), where S_t is typically the price on an equity or index. While there are several equivalent approaches to this problem, each with a rich and vibrant theory, we take for granted their derivation and proceed immediately to the so-called *risk-neutral* world. The approach of direct risk-neutral modeling is the most convenient from a pricing perspective. We assume the existence of a measure $\mathbb{Q}$, called the *risk-neutral* or *martingale measure*, under which all underlying price processes (of traded assets) behave as martingales after discounting and (if applicable) the reinvestment of dividends[1]. This is to say that

$$\mathbb{E}[S_{t+\Delta_t}|S_t] = S_t e^{(r-q)\Delta_t}, \qquad \Delta_t > 0, \tag{3}$$

where $r, q \geq 0$ are the continuous risk-free interest rate and dividend yield, and $\mathbb{E}[\cdot] \equiv \mathbb{E}_{\mathbb{Q}}[\cdot]$. If we took equation (2) as the *risk-neutral* price process, with continuous volatility $\sigma > 0$ fixed, there is a unique value of μ for which equation (3) is satisfied, and the measure $\mathbb{Q}$ is determined by this choice of μ. In particular, $\mathbb{E}[\exp(\sigma W_t)] = \exp(\frac{1}{2}\sigma^2 t)$, so $\mu \equiv r - q$ by necessity. Hence, if we decide on a geometric Brownian motion as our underlying model, the risk-neutral model used to price contracts that depend on $(S_t)_{t\geq 0}$ is fixed by the drift $\mu = r - q$, where $\sigma > 0$ is a free parameter (determined econometrically or otherwise).

2.1.1 Derivative Contracts

Ultimately, our goal is to price contracts contingent on the path of an underlying, which requires a terminal or expiry date T, and a initial date $t_0 < T$. We assume that T and t_0 are deterministic (fixed in the contract), although in general they can be random stopping times. A *European option* is a contract of the form $g(S_T)$, depending only on S_T at expiry. For example, a European call option is mathematically equivalent to the payoff $g(S_T) = (S_T - W)^+ = (S_T - W)\mathbb{1}_{[W,\infty)}(S_T)$, for a *strike* $W > 0$.

[1]Starting from $\mathbb{P}$, we assume that $\mathbb{Q} \overset{loc}{\sim} \mathbb{P}$, ie they are locally equivalent in the sense of $\mathbb{Q}|\mathcal{F}_t$ and $\mathbb{P}|\mathcal{F}_t$ ascribing positive probability to the same sets in $\mathcal{F}_t$, $\forall t > 0$. The direct approach to risk-neutral modeling is to circumvent the specification of $\mathbb{P}$, and proceed directly to modeling $(S_t)_{t\geq 0}$ under the risk-neutral measure $\mathbb{Q}$.

An *American option* is of the form $g(S_\tau)$, where $\tau \in [t_0, T]$ is a single stopping time determined by the holder (purchaser) of the option. That is, the underlying asset is observed for $s \in [t_0, \tau]$, and at time τ the holder *exercises* the contract for a payoff $g(S_\tau)$, received immediately[2]. American options belong to the class of *early-exercise* contracts, which contain features that allow decisions of the holder, prior to expiry, to affect the ultimate payoff received. A simple example is the *Bermudan option*, which fixes a discrete set of times $\tau \in \mathcal{T}$ prior to expiry at which the holder can exercise the contract and receive the payoff $g(S_\tau)$. A more complicated example is the *swing option*, commonly featured in gas and electricity markets, which in addition to a set of guaranteed commodity deliveries, allows the holder the order additional units or even deliver units back to the option seller at a fixed set of exercise (swing) dates.

While the American option is a common *path-dependent* contract, many other examples pervade financial exchanges and over-the-counter markets. For path-dependent contract without early-exercise features, the terminal payoff is of the form $g(S) = g\left(\{S_t\}_{t\in[t_0,T]}\right)$. For example, barrier options monitor the value of an underlying at a set of times $\tau \in \mathcal{T}$, and provide a payoff which depends on whether or not the underlying crosses into (or leaves) a specified region prior to expiry. Lookback options monitor the extreme values of an asset to determine the payoff, while Asian options take some type of average of the underlying across the set of observation dates. Pricing these exotic contracts, especially in the presence of complex underlying dynamics and discrete monitoring, requires specialized numerical techniques. Even in the case of the relatively simple BSM model, no analytical formulas exist for many varieties of these contracts, especially when monitoring is discrete. This work investigates a variety of approaches that excel when an underlying process can be described by its equivalent formulation in the Fourier domain. The first step towards extracting this alternative representation of a process is to establish the price of a contract as that of an expectation in the risk-neutral measure.

[2]This, and many other assumptions to come, are made for mathematical tractability. Obviously, even the existence of a purely American contract is impossible, but in a well-functioning market it can be a suitable approximation to reality.

2.1.2 The Valuation Formula

We now discuss briefly the valuation formulas for financial options, based on the theory of risk-neutral pricing. While the eccentricities of exotic contracts present unique challenges both in theory and computation, the unifying construct which engenders pricing by Fourier methods is that the price can be represented as an expectation of the terminal payoff.

Suppose first we have a European type contract with payoff $g(S_T)$, and a model for S_t under the risk-neutral measure $\mathbb{Q}$. We assume that S_t is a Markov process, so $\mathbb{Q}(S_t \in B|\mathcal{F}_u) = \mathbb{Q}(S_t \in B|S_u)$ for $t_0 \leq u < t \leq T$, and $B \in \mathcal{F}$. At any time $t \in [t_0, T]$, we denote the price of $g(S_T)$, as a function of the currently observed price S_t, by $\mathcal{V} \circ g(S_t)$, which follows from the Markov assumption. If $g(S_T)$ is to be a traded asset, then to avoid arbitrage in the market containing the underlying and a risk-free account, not only must $e^{-(r-q)t}S_t$ behave as martingale under $\mathbb{Q}$, but so must $e^{-rt}\mathcal{V} \circ g(S_t)$. In particular,

$$e^{-rt}\mathcal{V} \circ g(S_t) = \mathbb{E}[e^{-rT}\mathcal{V} \circ g(S_T)|S_t], \qquad t \leq T. \tag{4}$$

Since $\mathcal{V} \circ g(S_T) = g(S_T)$, this yields the risk-neutral valuation formula for European options

$$\mathcal{V} \circ g(S_t) = e^{-r(T-t)}\mathbb{E}[g(S_T)|S_t], \qquad t \leq T. \tag{5}$$

If a density for S_T was known, say $f_{S_T|S_t}$, we could evaluate equation (5) by directly integrating $g(S_T)$ against $f_{S_T|S_t}$, as in BSM case. Fortunately for mathematicians (not so much for practitioners), the density of S_T is generally unknown, and valuation is much more involved than a simple integral. Even more sophistication is required to price path-dependent options.

For a path-dependent contract, with payoff $g(S) = g\left(\{S_t\}_{t\in[t_0,T]}\right)$, we denote the current price by V_t, which is a function of the entire history $\{\mathcal{F}_s\}_{s\in[t_0,t]}$. Obviously, this path dependence is much stronger than for European options, although in many cases a dimensionality reduction (akin to a sufficient statistic) allows us to write $V_t = \mathcal{V} \circ g(S_t, H_t)$, where H_t is a vector-valued process of finite dimension. For example, for stochastic volatility models, H_t is just the current volatility. For an Asian option under a time-homogeneous Markov

process, H_t is the currently observed average price. In general, all we can say is that

$$V_t = e^{-r(T-t)}\mathbb{E}[g\left(\{S_u\}_{u\in[t_0,T]}\right)|\mathcal{F}_t], \qquad t \leq T. \tag{6}$$

In some cases, as will be seen, we can reduce the problem to a sequence of intermediate valuations, each equivalent to pricing a standard European option.

Finally, we will consider the valuation problem for early-exercise contracts. For a general path-dependent option with a *single* early exercise opportunity within the set of permissible dates $\tau \in \mathcal{T}$, possibly continuous, equation (6) becomes

$$V_t = \sup_{\tau\in\mathcal{T}_t} e^{-r(\tau-t)}\mathbb{E}[g\left(\{S_u\}_{u\in[t_0,\tau]}\right)|\mathcal{F}_t], \qquad t \leq T, \tag{7}$$

where $\mathcal{T}_t = \{\tau \in \mathcal{T} : \tau \geq t\}$, so the determination of $\tau \in \mathcal{T}$ is a problem of optimal stopping. For Bermudan and vanilla American options, the formula simplifies to $\mathcal{V} \circ g(S_t) = \sup_{\tau\in\mathcal{T}_t} e^{-r(\tau-t)}\mathbb{E}[g(S_\tau)|S_t]$, which resembles the European pricing formula. Naturally, valuation is only feasible if the contract has not already been exercised. Again, these problems will be united by the ubiquitous presence of an expectation.

2.2 Fourier Transforms and Levy Processes

We next recall the crucial ingredient of the Fourier approach to option pricing, which is the characteristic function of a process. For a random variable X on $(\Omega, \mathcal{F}, \{\mathcal{F}_t\}_{t\geq 0}, \mathbb{Q})$, the *characteristic function* is defined as

$$\phi_X(\xi) := \mathbb{E}[e^{iX\xi}] = \int_\Omega e^{iX(\omega)\xi}\mathbb{Q}(d\omega) = \int_{\mathbb{R}} e^{ix\xi}\mu_X(dx), \qquad \xi \in \mathbb{R}, \tag{8}$$

where μ_X is the measure induced by X. For the majority of models considered in this work, μ_X is absolutely continuous with respect to Lebesgue measure, so X will posses a continuous density[3] $f_X(x)$. Equation (8) simplifies in this case to

$$\phi_X(\xi) = \int_{\mathbb{R}} e^{ix\xi} f_X(x)dx = \widehat{f}_X(\xi), \qquad \xi \in \mathbb{R}, \tag{9}$$

where $\widehat{f}_X(\xi)$ is the *Fourier transform* of the density f_X, which is defined for general $f \in L^1(\mathbb{R})$ as[4]

$$\mathcal{F}f(\xi) = \widehat{f}(\xi) = \int_{\mathbb{R}} e^{i\xi x} f(x)dx, \qquad \xi \in \mathbb{R}.$$

[3] All Levy processes, with the exception of compound Poisson processes, admit a continuous density.
[4] Recall that $L^1(\mathbb{R})$ is the set of Borel-measurable functions such that $\|f\|_1 := \int_{\mathbb{R}} |f(x)|dx < \infty$.

When referring to a stochastic process, we will denote the density of X_t by $f_t(x)$, and its characteristic function by $\widehat{f_t}(\xi) = \mathbb{E}[\exp(iX_t\xi)]$. At any point in time, the marginal density f_t is characterized uniquely by its characteristic function.

An immense diversity of driving stochastic processes have well-known analytical representations in terms of their characteristic functions. They include the classical geometric Brownian motion, affine-jump diffusions, stochatic volatility models, general Levy processes, and time-changed Levy processes. To establish notation and basic methodology, we focus initially on the case of exponential Levy models, which is a rich and often analytically tractable class which generalizes the tranditional BSM framework.

2.2.1 Exponential Levy Models

Recall the geometric Brownian motion in equation (2), which models the underlying as $S_t = S_0 \exp(X_t)$, where $X_t := \mu_{RN} \cdot t + \sigma W_t$, with $\mu_{RN} := (r - q - \frac{1}{2}\sigma^2)$ under the risk-neutral measure. Suppose we start with a model of the form

$$S_t = S_0 \exp(X_t) = S_0 \exp(\mu \cdot t + L_t), \tag{10}$$

where $(L_t)_{t\geq 0}$ is a stochastic process which drives the risk-neutral randomness of S_t under $\mathbb{Q}$, and X_t is the *log-return process.* A natural point of departure from the BSM framework is to consider which assumptions on L_t might be relaxed to yield a more general class of models. By requiring only that L_t posses independent, stationary increments (relaxing the assumption of normally distributed increments), and $L_0 = 0$, we have a *Levy process* model[5] for $(L_t)_{t\geq 0}$. In particular, we assume that for any $t_0 < t_1 < ... < t_n$, the random variables $L_{t_0}, L_{t_1} - L_{t_0}, ..., L_{t_n} - L_{t_{n-1}}$ are independent, and the distribution of $L_{t+\Delta_t} - L_t$ is independent of t, depending only on the time increment Δ_t.

A major appeal of Levy processes is their ability to capture jump behavior, in addition to the irratic, but continuously varying diffusive nature of a Brownian motion. In terms of the density (and characteristic function), jumps are accomodated by the *Levy measure*

[5]We also require the following stochastic continuity condition: $\forall \epsilon > 0$, $\lim_{\Delta_t \to 0} \mathbb{Q}(|L_{t+\Delta_t} - L_t| \geq \epsilon) = 0$, for any fixed time. This implies that while jumps may occur with positive probability, there is no such mass associated with any particular time.

$\Pi : \mathbb{R} \to \mathbb{R}$, which assigns to each set $A \in \mathcal{B}(\mathbb{R})$ (Borel sets) the expected number of jumps $\Pi(A)$ per *unit time* with size belonging to A. The simplest example is the compound poisson process, $L_t = \sum_{k=1}^{N_t} J_k$, where $(N_t)_{t\geq 0}$ is a rate λ Poisson process, and $J_k \overset{iid}{\sim} f_J$, independently of N_t. In this case, we have formally $\Pi(dx) = \lambda f_J(dx)$, which is the rate at which jumps occur (per unit interval) times the probability of a jump size in $[x, x+dx)$. In general, the Levy measure Π must satisfy

$$\Pi(\{0\}) = 0, \quad \int_{|x|\leq 1} x^2 \Pi(dx) < \infty, \quad \text{and} \int_{|x|>1} \Pi(dx) < \infty. \tag{11}$$

The separation of $|x| \leq 1$ and $|x| > 1$ is to accomodate processes with infinite activity of small jumps (recall that the Poisson process can have only finitely many jumps in any time interval), for which $\int_{|x|\leq 1} |x|\Pi(dx) = \infty$, and those without a finite moment for large jumps $\int_{|x|>1} |x|\Pi(dx) = \infty$.

From the perspective of Fourier based pricing, Levy processes are ideal for several reasons. The first, which follows from independence and stationarity of increments is that

$$\phi_t(\xi) = \mathbb{E}[e^{iL_t\xi}] = \Big(\mathbb{E}[e^{iL_1\xi}]\Big)^t = e^{\psi_L(\xi)t}, \qquad t \geq 0, \tag{12}$$

where $\psi_L(\xi)$ is a function called the *Levy symbol* or *Levy exponent*. Hence, the characteristic function of L_t is of the same form for all $t \geq 0$, engendering a pleasant tractability. Moreover, this symbol is given analytically by the Levy-Khintchine formula [9, 46, 120]

$$\psi_L(\xi) = i\xi b - \frac{\sigma^2}{2}\xi^2 + \int_{\mathbb{R}} \Big(e^{i\xi x} - 1 - i\xi x \mathbb{1}_{\{|x|\leq 1\}}\Big)\Pi(dx), \tag{13}$$

where $\Pi(dx)$ is the Levy measure which governs the jump behavior of L_t, b is a drift parameter, and σ corresponds to the volatility rate of a continuous diffusion component. We call (b, σ, Π) the *Levy triplet*. Because of our choice to model the log return as $X_t = \mu \cdot t + L_t$, the drift parameter b corresponding to the process L_t is irrelevant for pricing, as we will later see[6]. The geometric Brownian motion model is obtained when $\Pi \equiv 0$ (no jumps can occur), $b = 0$, and $\sigma > 0$ is the desired volatility, from which $L_t = \sigma W_t$. The characteristic exponent is simply $\psi_L(\xi) = -\frac{\sigma^2}{2}\xi^2$. When $\sigma = 0$, we obtain pure jump processes.

[6]This is analagous to the BSM framework, in which the real-world drift μ is irrelavant.

Not only does the class of exponential Levy models contain the traditional geometric Brownian motion model of BSM, but it also includes the more versatile jump diffusions that began with Merton's Jump Diffusion (MJD) developed in [106]. For example, suppose that $(N_t)_{t\geq 0}$ is a rate $\lambda > 0$ Poisson process and $(W_t)_{t\geq 0}$ a standard Brownian motion. We can form the log-return process X_t by

$$X_t = \mu \cdot t + L_t, \qquad L_t = \sigma W_t + \sum_{k=1}^{N_t} J_k,$$

where J_k are *jump sizes* with distribution f_J, independent of the number of jumps N_t. In section 2.2.3 we give a simple procedure to obtain the risk-neutral model under $\mathbb{Q}$, given arbitrary model parameters. We consider any other specification, in which risk-neutrality is not enforced, to be a model under the real-world measure $\mathbb{P}$. For this example, the characteristic function of X_t under the real-world measure is

$$\mathbb{E}_{\mathbb{P}}[\exp(iX_t\xi)] = \exp(i\xi\gamma \cdot t) \cdot \exp(-\tfrac{\sigma^2}{2}\xi^2 t) \cdot \exp\left(t \int_{\mathbb{R}} (e^{i\xi x} - 1)\lambda f_J(x)dx\right) \qquad (14)$$

which follows from indepdenence of each process, and after conditioning on the number of jumps, where $\gamma := \mu - \lambda \int_{|x|\leq 1} x f_J(x)dx$ is assumed to be finite[7]. The final term in equation (14) is simplified by

$$\lambda t \cdot \int_{\mathbb{R}} (e^{i\xi x} - 1) f_J(x)dx = \lambda t \cdot (\widehat{f}_J(\xi) - 1),$$

so $\psi_L(\xi)$ is given explicitly once a jump size distribution f_J is chosen. Merton [106] chose $J_k \sim \mathcal{N}(\mu_J, \sigma_J)$, in which case $\widehat{f}_J(\xi) - 1 = e^{i\xi\mu_J - \frac{1}{2}\sigma_J^2\xi^2} - 1$.

We will have more to say about Levy processes and the corresponding measure. For now, we acknowledge that Levy processes of financial interest can be specified by a very simple Levy symbol, where the integral in equation (13) has been derived in closed form. Since a characteristic function uniquely determines the density, all that we need to price financial contracts is the symbol ψ_L, where any parameters are chosen according to observed features of a market (e.g. by calibration to the prices of current observed contracts, or by econometric estimation using historical time series.)

[7] We will not need to explicitly evaluate this term in order to price under this model.

2.2.2 Strip of Regularity

When working in the Fourier domain, convergence rates of pricing algorithms will often depend on the regularity of characteristic functions for the underlying process. In some cases, explicit bounds on the characteristic function decay will be used as inputs to the algorithm itself. By the Riemann-Lebesgue Theorem, the Fourier transform of any $f \in \mathbb{L}^1(\mathbb{R})$ satisfies

$$\lim_{|\xi|\to\infty} \widehat{f}(\xi) = 0, \tag{15}$$

which is the minimal decay we can expect of any $\widehat{f}$. In general, the rate of decay of $\widehat{f}$ is intrinsically linked with the smoothness of f: the smoother is f, the more rapidly $\widehat{f}$ will decay, and conversely. Transform methods which incur a truncation error in the Fourier domain will benefit from a rapidly decaying $\widehat{f}$. In particular, we have the following standard results, where $C^n(\mathbb{R})$ is the space of n-th order continuously differentiable functions[8].

Theorem 2.2.1. *Suppose that $f, \widehat{f} \in \mathbb{L}^1(\mathbb{R})$. The following hold:*

(i) If $x^k f(x) \in \mathbb{L}^1(\mathbb{R})$ for $k \geq 0$, then $\widehat{f} \in C^k(\mathbb{R})$, and

$$\widehat{f}^{(k)}(\xi) = \mathcal{F}[(ix)^k f(x)](\xi).$$

(ii) If $\xi^n \widehat{f}(\xi) \in \mathbb{L}^1(\mathbb{R})$ for some $n \geq 0$, then $f \in C^n(\mathbb{R})$.

(iii) If $f \in C^n(\mathbb{R})$, and if $f^{(k)} \in L^1$ for $k = 1, ..., n$, then

$$\widehat{f^{(k)}}(\xi) = (-i\xi)^k \widehat{f}(\xi).$$

In terms of a density f_X, part (i) states that the characteristic function $\widehat{f_X}$ is continuously differentiable as many times as the random variable X has finite moments. From part (iii), and the Riemann-Lebesgue Theorem, the Fourier transform of a C^n function with integrable derivatives satisfies

$$\lim_{|\xi|\to\infty} |\widehat{f^{(k)}}(\xi)| = \lim_{|\xi|\to\infty} |\xi|^k |\widehat{f}(\xi)| = 0,$$

[8]The following theorem is related to invertability of $\mathcal{F}$, which is discussed in section 2.2.5. These are standard results in Fourier analysis. See for example [70].

from which we have the asymptotic bound

$$|\widehat{f}(\xi)| \leq \frac{M}{|\xi|^k}, \quad \text{as } |\xi| \to \infty. \tag{16}$$

In particular, the Fourier transform of a C^∞ function with integrable derivatives of all orders decays faster than any polynomial at infinity.

For most processes we study, the characteristic function can be extended to an analytic function in the complex plane, $\mathbb{C}$. This will be essential to the numerical pricing methods that follow. As a converse to part (i) of Theorem 2.2.1, if all derivatives of $\phi_X(\xi) = \mathbb{E}[e^{iX\xi}]$,

$$\phi_X^{(k)}(\xi) = \int_{\mathbb{R}} (ix)^k e^{i\xi x} f_X(x) dx, \qquad \xi \in \mathbb{R},$$

exist at the origin, then the k-th moments of X, $\mathbb{E}[X^k] = \phi^{(k)}(0)/i^k$, exist for all $k \geq 0$ (ie $x^k f_X(x) \in \mathbb{L}^1(\mathbb{R})$). Moreover, for some $\rho > 0$, the characteristic function can be expanded as

$$\phi_X(z) = \sum_{k=0}^{\infty} \frac{i^k \mathbb{E}[X^k]}{k!} z^k, \qquad |z| < \rho. \tag{17}$$

As a special case, suppose that $\int_{\mathbb{R}} e^{-\eta x} f_X(x) dx < \infty$ for $\eta \in (-\lambda, \lambda)$ containing the origin. Then clearly for any $k \geq 0$, $\int_{\mathbb{R}} x^k e^{izx} f_X(x) dx < \infty$ for $z \in \mathbb{C}$ in a neighborhood of the origin where $|x^k e^{izx}| < e^{-\eta x}$. To characterize the *strip of regularity* (or *domain of analyticity*) of ϕ_X in $\mathbb{C}$, which is the largest open set in which ϕ_X is analytic and single-valued, we have the following theorem due to [103]:

Theorem 2.2.2. *If a characteristic function $\phi_X(z)$ is analytic in a neighborhood of the origin, then it is also analytic in a horizontal strip and can be represented in this strip by a Fourier integral. Either this strip is the whole plane, or it has two horizontal boundary lines. The purely imaginary points on the boundary of the strip of convergence (if it is not the whole plane) are singular points of $\phi_X(z)$.*

For a Levy process, where $\phi_t(z) = e^{\psi_L(z)t}$, this strip coincides with the strip of regularity for ψ_L. In terms of the Levy measure Π defined in equation (13), Theorem 25.17 of [120] provides an equivalent definition of the strip[9], which depends on the following set:

$$\mathcal{I}_L = \left\{ \alpha \in \mathbb{R} : \int_{|x|>1} e^{-\alpha x} \Pi(dx) < \infty \right\}, \tag{18}$$

[9]Here we have used the notation from [67].

where $\alpha \in \mathcal{I}_L$ is equivalent to $\mathbb{E}[e^{-\alpha L_t} < \infty]$ for all $t > 0$. From equation (11), $\mathcal{I}_L$ contains the origin (ie $\int_{|x|>1} \Pi(dx) < \infty$) and it can be shown to be a convex set. Moreover, in order for the price process itself to be well defined, we must have $\mathbb{E}[S_t] = S_0 e^{\mu t}\mathbb{E}[e^{L_t}] < \infty$, so $\alpha = -1 \in \mathcal{I}_L$. We will therefore assume the necessary restriction $\psi_L(-i) < \infty$. By convexity, it follows that for any realistic exponential Levy model, $[-1, 0] \subset \mathcal{I}_L$. Now note that if $\eta \in \mathcal{I}_L$, and $z = \xi + i\eta$, the characteristic function at z is well defined:

$$|\phi_t(z)| = |\phi_t(\xi + i\eta)| \leq \int_{\mathbb{R}} |e^{ix(\xi+i\eta)}| p_t(x)dx = \int_{\mathbb{R}} e^{-\eta x} p_t(x)dx < \infty, \tag{19}$$

where the notation p_t refers to the density of log-return, X_t. However, $\mathbb{E}[e^{L_t}] < \infty \Leftrightarrow \mathbb{E}[e^{X_t}] < \infty$, so $\mathcal{I}_X = \mathcal{I}_L$. We thus characterize the strip of regularity

$$\mathcal{D}_{(\lambda_-,\lambda_+)} = \{z \in \mathbb{C} : \Im(z) \in (\lambda_-, \lambda_+)\}, \tag{20}$$

where $-\infty \leq \lambda_- \leq -1$ and $0 \leq \lambda_+ \leq \infty$ are the endpoints of $\mathcal{I}_L$. For any $z \in \mathcal{D}_{(\lambda_-,\lambda_+)}$, $\phi_t(z)$ is well defined and can be extended analytically as a function in the complex plane. Most transform methods require an open strip containing the real line (equivalently $\mathcal{I}_L \supset (-\lambda, \lambda)$ for some $\lambda > 0$), and explicit knowledge of λ_+, λ_- can be used in some cases to improve the performance of numerical procedures, and to obtain bounds on convergence.

Remark 1. For the most part, we consider models for the log-return process $X_t = \ln(S_t/S_0)$, with the corresponding density $p_t(x)$ and characteristic function $\phi_t(\xi)$. In some cases, it is more convenient (or perhaps conventional) to model the log asset process, say $Y_t = \ln(S_t)$, with density $q_t(y|\ln(S_0))$. Given an exponential Levy model, it follows that $q_t(y|\ln(S_0)) = p_t(y - \ln(S_0))$, from which $\widehat{q}_t(\xi|\ln(S_0)) = e^{i\xi \ln(S_0)}\phi_t(\xi)$. Indeed,

$$\begin{aligned}\widehat{q}_t(\xi|\ln(S_0)) = \int_{\mathbb{R}} e^{iy\xi} p_t(y - \ln(S_0))dy &= \int_{\mathbb{R}} e^{i(y+\ln(S_0))\xi} p_t(y)dy \\ &= e^{i\xi \ln(S_0)} \int_{\mathbb{R}} e^{iy\xi} p_t(y)dy.\end{aligned}$$

As we will later see, the (desirable) property that $\widehat{q}_t(\xi|s) = e^{i\xi s}\varphi_t(\xi)$, where s is a known state vector and $\varphi_t(\xi)$ is of the form $\exp(h(t, \xi, \theta))$, holds for an additional class of processes, namely the Affine Jump Diffusion (AJD) models [57], which includes Heston's stochastic volatility model [79] as a special case. In [39], the AJD models are obtained as a subclass

of time-changed Levy processes, where a given Levy model is subordinated (ie defined on a stochastic clock) by another, possibly correlated, Levy process. While exponential Levy models are capable of capturing jumps and volatility smiles, the time-changed Levy models can also capture *leverage effects*, which describe the correlation between volatility and returns.

2.2.3 Martingale Adjustment

In order to apply the risk-neutral approach to modeling the underlying, the measure $\mathbb{Q}$ must be such that discounted asset prices behave as martingales (after reinvesting dividends). For exponential models of the form of equation (10), we can start with an arbitrary[10] Levy symbol $\psi_L(\xi)$, and fix the measure $\mathbb{Q}$ by assigning a certain value to the term μ. Namely,

$$\begin{aligned}\mathbb{E}\left[e^{-(r-q)t}S_t|S_0\right] = e^{-(r-q)t}S_0\mathbb{E}\left[e^{X_t}\right] &= e^{(\mu-(r-q))t}S_0\mathbb{E}\left[e^{L_t}\right] \\ &= S_0 e^{(\mu-(r-q)+\psi_L(-i))t},\end{aligned}$$

where $\mathbb{E}[\exp(L_t)] = \exp(\psi_L(-i)t) < \infty$ by assumption (see section 2.2.2) . So in order for equation (3) to hold for an arbitrary choice of model parameters, ie in order for $\mathbb{E}\left[e^{-(r-q)t}S_t|S_0\right] = S_0$, the exponential drift must satisfy

$$\mu \equiv \mu_{RN} := r - q - \psi_L(-i), \tag{21}$$

where in general

$$\psi_L(-i) = b + \frac{\sigma^2}{2} + \int_{\mathbb{R}} \left(e^x - 1 - x\mathbb{1}_{\{|x|\leq 1\}}\right)\Pi(dx). \tag{22}$$

This is the so-called additive martingale adjustment, and it turns any Levy model of the form

$$S_t = S_0 \exp(\mu_{RN} \cdot t + L_t) \tag{23}$$

into a valid (arbitrage-free) pricing mechanism. This is why, as mentioned in section 2.2.1, the drift parameter b of L_t is irrelevant, since it always neutralized by the martingale adjustment, assuming we have modeled the process by equation (23).

[10]The only requirement is $\mathbb{E}[e^{L_1}] < \infty$, ie $\psi_L(-i) < \infty$.

2.2.4 Exponential Damping

The first transform approaches (and more recent advances) involved the Fourier transforms of non-integrable payoffs, such as call options, in addition to the characteristic function of a process. Given that the exponential moments of many model processes exist, the idea is to transfer some of this integrability to the payoff, which is typically not integrable. For example, in order for

$$\mathbb{E}_{\mathbb{Q}}[G(X_T)] = \int_{\mathbb{R}} G(x) f_T(x) dx < \infty,$$

clearly the product $G \cdot f_T \in L^1(\mathbb{R})$. Integrability becomes a more delicate issue when switching to the Fourier domain. This issue is partially resolved by extending the Fourier transform's domain into the complex plane, which has the same effect on integrability as transforming an "exponentially damped" version of the function.

The so-called *generalized Fourier transform* or *Fourier-Laplace transform* is defined as

$$\mathcal{F}f(z) = \widehat{f}(z) = \int_{\mathbb{R}} e^{ixz} f(x) dx, \qquad z = \xi + i\eta \in \mathbb{C}.$$

From equation (19), the generalized Fourier transform will exist as long as $e^{-\eta x} f(x) \in L^1(\mathbb{R})$. Clearly, the generalized Fourier transform of a function can exist for a set of $z \in \mathbb{C}$, while its traditional Fourier transform does not. As long as f is locally bounded, and grows no more than exponentially, we can define its generalized Fourier transform. To define the characteristic function $\phi_X(z)$, integrability of $f_X(x) \cdot e^{ixz}$ holds for any $z \in \mathcal{D}_{(\lambda_+, \lambda_-)}$, in which case the generalized transform exists. In particular, the Fourier transform of the exponentially damped function $e^{-\eta x} f(x)$ is given by

$$\mathcal{F}[e^{-\eta x} f(x)] = \int_{\mathbb{R}} e^{-\eta x} e^{ix\xi} f(x) dx = \int_{\mathbb{R}} e^{ix(\xi + i\eta)} f(x) dx = \widehat{f}(i\eta + \xi).$$

For a call option payoff, $G_{S_0}(x) = (S_0 e^x - W)^+$, we find the generalized Fourier transform, taken with respect to the log-return[11]

$$\widehat{G}_{S_0}(z) = \int_{\ln(W/S_0)}^{\infty} e^{ixz}(S_0 e^x - W) dx = \left(\frac{S_0}{iz+1} e^{x(iz+1)} - \frac{W}{iz} e^{x(iz)} \right|_{\ln(W/S_0)}^{\infty}.$$

[11] The approach is most often applied with respect to the log-price, though to maintain consistency with later pursuits, we will work with the log-return whenever feasible.

In order for $\widehat{G}_{S_0}(z)$ to exist for $z = \xi + i\eta$, we require $\eta > 1$, in which case

$$\widehat{G}_{S_0}(z) = \frac{W}{iz}\left(\frac{W}{S_0}\right)^{iz} - \frac{S_0}{iz+1}\left(\frac{W}{S_0}\right)^{iz+1} = \frac{W}{iz-z^2}\left(\frac{W}{S_0}\right)^{iz},$$

which is complex-analytic for $\Im(z) = \eta > 1$. For a given payoff $G_{S_0}(x) = g(S_0 e^x)$, we will denote its strip of regularity by $\mathcal{S}_G$, which is the set of $z \in \mathbb{C}$ for which $\widehat{G}_{S_0}(z)$ is well defined. The notation $\mathcal{D}_{(\lambda_-,\lambda_+)}$ is reserved for analytic characteristic functions.

2.2.5 Fourier Inversion

A duality exists between the state and Fourier spaces that facilitates pricing when the characteristic function of a process is known. We define the *conjugate* or *inverse Fourier transform* of f by

$$\mathcal{F}^{-1}f(\xi) = \widehat{f}(\xi) = \frac{1}{2\pi}\int_{\mathbb{R}} e^{-i\xi x} f(x)dx.$$

Note that $\mathcal{F}^{-1}(\bar{f}) = \frac{1}{2\pi}\overline{\mathcal{F}(f)}$, though the conjugate transform is not strictly a conjugate as defined. The following classic result provides a link between the two domains.

Theorem 2.2.3. *If $f \in L^1$ and $\widehat{f} \in L^1$, then $\mathcal{F}^{-1}\mathcal{F}f(x) = \mathcal{F}^{-1}\widehat{f}(x) = f(x)$ at all continuity points of f. That is, $f(x)$ can be recovered by*

$$f(x) = \frac{1}{2\pi}\int_{-\infty}^{\infty} e^{-i\xi x}\widehat{f}(\xi)d\xi.$$

More generally, if the generalized fourier transform exists in a strip containing $\Im(z) = \eta$, by Cauchy's theorem [47, 116] we can invert $\widehat{f}(z)$ by integrating along the contour $\Gamma_\eta := \{z \in \mathbb{C} : \Im(z) = \eta\}$ contained within the strip, from which

$$f(x) = \frac{1}{2\pi}\int_{i\eta-\infty}^{i\eta+\infty} e^{-izx}\widehat{f}(z)dz = \frac{1}{2\pi}\int_{-\infty}^{\infty} e^{-i(\xi+i\eta)x}\widehat{f}(\xi+i\eta)d\xi. \tag{24}$$

In particular, suppose that $\phi_T(z)$ is complex analytic in $\mathcal{D}_{(\lambda_-,\lambda_+)}$ with $-\eta \in (\lambda_-, \lambda_+)$, and $G_{S_0}(x) := g(S_0 e^x)$ is a European payoff for which $\eta \in \mathcal{S}_G$, as defined in section 2.2.4. The valuation formula in equation (5) provides the following:

$$\begin{aligned}
\mathcal{V} \circ g(S_0) &= e^{-rT}\mathbb{E}[G_{S_0}(X_T)] \\
&= e^{-rT}\mathbb{E}\left[\frac{1}{2\pi}\int_{\mathbb{R}} e^{-i(\xi+i\eta)X_T} \cdot \widehat{G}_{S_0}(\xi+i\eta)d\xi\right] \\
&= \frac{e^{-rT}}{2\pi}\int_{\mathbb{R}} \mathbb{E}\left[e^{i(-\xi-i\eta)X_T}\right] \cdot \widehat{G}_{S_0}(\xi+i\eta)d\xi \\
&= \frac{e^{-rT}}{2\pi}\int_{\mathbb{R}} \phi_T(-\xi-i\eta) \cdot \widehat{G}_{S_0}(\xi+i\eta)d\xi,
\end{aligned}$$

where the exchange of integrals is made only formally at this point. Aside from a change of variables, this is essentially the formula obtained by Raible [117] and later reinterpreted by Lewis [97], and it represents one of the first directions in Fourier based pricing. Utilizing the inner product structure of $L^2(\mathbb{R})$, the formula is derived as a simple corollary of Parseval's theorem, discussed next.

Not only are integral formulas of a similiar nature the subject of ongoing reseach, but these tools will be applied in different ways to derive valuation methods that are of primary interest in this work, namely the density expansion approaches of Kirkby [83] and Fang and Oosterlee [61]. The related Hilbert transform approach of Feng and Linetsky [66] is studied as well. All of these approaches and their later extensions are derived from the basic Fourier theory.

Finally, we note that equation (24) can be evaluated to numerically to obtain estimates of $f(x)$. By fixing a discrete grid of size $2N+1$, with step size $\Delta_\xi > 0$, we have a trapezoidal approximation

$$f(x) \approx \frac{1}{2\pi}\sum_{k=-N}^{N} e^{-ix(k\Delta_\xi+i\eta)}\widehat{f}(k\Delta_\xi+i\eta)\Delta_\xi.$$

In order to *efficiently* compute multiple values of $f(x)$ simultaneously, we will use the Fast Fourier transform, introduced later, which imposes certain restrictions on our grid choice.

2.2.6 Fourier Tranforms in $\mathbb{L}^2$

So far we have assumed integrability of functions (exponentially damped or otherwise). Of critical importance is the extension of the Fourier transform to the space $\mathbb{L}^2(\mathbb{R})$ of square

integrable functions, where[12] $f \in \mathbb{L}^2(\mathbb{R})$ iff $\int_{\mathbb{R}} f^2(x)dx < \infty$. Recall that $\mathbb{L}^2$ is a Hilbert space equipped with the inner product[13]

$$\langle f, g \rangle = \int_{\mathbb{R}} f(x)\overline{g(x)}dx = \int_{\mathbb{R}} g(x)\overline{f(x)}dx, \qquad f, g \in \mathbb{L}^2(\mathbb{R}). \tag{25}$$

This inner product structure, and the $\mathbb{L}^2$ norm it induces, are ideal for studying optimal approximations from sets of functions. Moreover, it simplifies the derivation of various integral formulas which arise naturally as the inner product of a payoff with the underlying density.

While the Fourier transform is originally defined for functions $f \in \mathbb{L}^1(\mathbb{R})$, it can be extended isometrically to the space $\mathbb{L}^2(\mathbb{R})$. If $f \in \mathbb{L}^2$, then $\widehat{f}$ is the $\mathbb{L}^2$-limit:

$$\int_{-n}^{n} e^{i\xi x} f(x)dx \overset{L^2}{\to} \widehat{f}(\xi) \text{ as } n \to \infty,$$

that is $\mathcal{F}[f \cdot \mathbb{1}_{[-n,n]}] \to \mathcal{F}[f]$, in mean square. The following properties hold (see for example [70]).

Theorem 2.2.4. ***(Plancherel's Extension to*** $\mathbb{L}^2$***)*** *The Fourier transform* $\mathcal{F}$ *and its inverse* $\mathcal{F}^{-1}$ *extend uniquely to isometries (modulo* $(2\pi)^{-1}$*) on* $\mathbb{L}^2(\mathbb{R})$*. The following hold for* $\mathcal{F} : \mathbb{L}^2(\mathbb{R}) \to \mathbb{L}^2(\mathbb{R})$*, and* $f, g \in \mathbb{L}^2(\mathbb{R})$*:*

(i) $\mathcal{F}\mathcal{F}^{-1}f = \mathcal{F}^{-1}\mathcal{F}f = f$ *a.e.*

(ii) $\int_{\mathbb{R}} f(x)\overline{g(x)}dx = \frac{1}{2\pi}\int_{\mathbb{R}} \widehat{f}(\xi)\overline{\widehat{g}(\xi)}d\xi = \frac{1}{2\pi}\langle \widehat{f}, \widehat{g} \rangle$.

(iii) The Fourier transform defined on $\mathbb{L}^1$ *and the extension to* $\mathbb{L}^2$ *coincide on* $\mathbb{L}^1 \cap \mathbb{L}^2$*.*

Hence from the last claim, we will continue to refer to *the* Fourier transform of a function. The first claim ensures that we can reverse the order of transform and inverse, for $f \in \mathbb{L}^2(\mathbb{R})$. Given $\mathbb{L}^1$ integrability, we would have to check that the Fourier transform was integrable as well before the exchanging operations. The second claim, known as *Parseval's Theorem*, leads to another interpretation of the valuation formula[14], summarized in the following theorem.

[12] Measurability is always assumed.
[13] The complex conjugate of $z \in \mathbb{C}$, $z = \xi + i\eta$, is $\bar{z} = \xi - i\eta$.
[14] A similar approach is even called Parsevaluation by Peter Carr.

Theorem 2.2.5. *Suppose $e^{\eta x} f_T(x), e^{-\eta x} G_{S_0}(x) \in \mathbb{L}^2(\mathbb{R})$, for some $\eta \in \mathbb{R}$, where $G_{S_0}(x) = g(S_0 e^x)$ is a European payoff, and f_T the density of $X_T = \ln(S_T/S_0)$ with characteristic function ϕ_T. Then the time zero value of G_{S_0} is given by*

$$\mathcal{V} \circ g(S_0) = \frac{e^{-rT}}{2\pi} \int_{\mathbb{R}} \phi_T(-\xi - i\eta) \cdot \widehat{G}_{S_0}(\xi + i\eta) d\xi. \tag{26}$$

Proof. First note that $f_T(x) G_{S_0}(x) = e^{\eta x} f_T(x) \cdot e^{-\eta x} G_{S_0}(x) \in \mathbb{L}^1(\mathbb{R})$ by Cauchy-Schwartz, so the price of G_{S_0} is finite. Hence

$$\begin{aligned} \mathcal{V} \circ g(S_0) &= e^{-rT} \int_{\mathbb{R}} f_T(x) G_{S_0}(x) dx \\ &= e^{-rT} \int_{\mathbb{R}} e^{\eta x} f_T(x) \cdot e^{-\eta x} G_{S_0}(x) dx \\ &= \frac{e^{-rT}}{2\pi} \int_{\mathbb{R}} \overline{\mathcal{F}[e^{\eta x} f_T(x)](\xi)} \cdot \mathcal{F}[e^{-\eta x} G_{S_0}(x)](\xi) d\xi, \end{aligned}$$

and the result follows from $\overline{\mathcal{F}[e^{\eta x} f_T(x)](\xi)} = \widehat{f}_T(-\xi - i\eta)$. □

2.3 Valuation Methods

2.3.1 Fourier Transform in Log Strike

The fast Fourier transform made its debut as European option pricing tool in the seminal work [35] of Carr and Madan (1998). They devised a way to calculate the prices of a spectrum of vanilla options simultaneously as needed for efficient calibration. The idea is to represent call prices as a function of strike, say

$$C_T(k) = \int_k^\infty e^{-rT} (e^y - e^k) q_T(y|s) dy, \tag{27}$$

where $k = \ln(K), s = \ln(S_0)$, and $q_T(y|s)$ is the conditional density of $Y_T = \ln(S_T)$ given $\ln(S_0)$. Note that for Levy models, $\widehat{q}_T(\xi|s) = e^{i\xi \ln(S_0)} \phi_T(\xi)$ where the log-return is distributed $\ln(S_T/S_0) \sim p_T$ with characteristic function $\phi_T(\xi)$ (see the remark in section 2.2.2).

Rather than apply the Fourier transform to $C_T(k)$ directly, where $C_T(k) \to S_0$ as $k \to -\infty$ (so it is not (square) integrable in k), a damping factor is introduced to obtain an integrable function $c(k)$, along with its Fourier transform $\widehat{c}_T(\xi)$,

$$c_T(k) := e^{\alpha k} C_T(k), \qquad \widehat{c}_T(\xi) = \int_{-\infty}^\infty e^{i\xi k} c_T(k) dk, \tag{28}$$

where the *damping parameter* $\alpha \in \mathbb{R}$ is chosen appropriately. In particular, they derive a closed-form expression for $\widehat{c}_T(\xi)$ given in terms of the chf $\widehat{q}_T(\xi)$ by

$$\begin{aligned}\widehat{c}_T(\xi) &= \int_{-\infty}^{\infty} e^{i\xi k} \int_k^{\infty} e^{-rT} e^{\alpha k}(e^y - e^k) q_T(y|s) dy dk \\ &= \frac{e^{-rT}\widehat{q}_T(\xi - (\alpha+1)i|s)}{\alpha^2 + \alpha - \xi^2 + i(2\alpha+1)\xi},\end{aligned}$$

which exists if and only if $\widehat{q}_T(-(\alpha+1)i|s) = \mathbb{E}[S_T^{\alpha+1}] < \infty$ (that is, $-(\alpha+1) \in \mathcal{I}_Y$, the strip of regularity of the log price). Hence, the value in log-strike space is obtainable by inversion,

$$C_T(k) = \frac{e^{-\alpha k}}{2\pi} \int_{-\infty}^{\infty} e^{-i\xi k} \cdot \widehat{c}_T(\xi) d\xi = \frac{e^{-\alpha k}}{\pi} \int_0^{\infty} e^{-i\xi k} \cdot \widehat{c}_T(\xi) d\xi, \tag{29}$$

using the fact that C_T is real. The integral in equation (29) is easily discretized and representable as a discrete Fourier transform, to which the FFT is applied to obtain $C_T(k)$ along a set of $k \in \mathbb{R}$. Recent methods offer improvements (in accuracy and speed) over this approach for pricing multiple strikes [61, 83].

2.3.2 Convolution

The convolution of two complex valued functions on $\mathbb{R}$ is defined as

$$f * g(x) = \int_{\mathbb{R}} f(x-y)g(y)dy = \int_{\mathbb{R}} f(y)g(x-y)dy, \tag{30}$$

whenever it exists. The integral exists, for example, when $f, g \in \mathbb{L}^1(\mathbb{R})$, in which case $f * g \in \mathbb{L}^1(\mathbb{R})$ and $\|f * g\|_1 \leq \|f\|_1 \|g\|_1$.[15] For $f, g \in \mathbb{L}^1(\mathbb{R})$, the Fourier transform maps convolutions into products:

$$\widehat{f * g}(\xi) = \widehat{f}(\xi) \cdot \widehat{g}(\xi), \quad \xi \in \mathbb{R}. \tag{31}$$

Similarly, the *cross-correlation* is defied by

$$f \star g(x) = \int_{\mathbb{R}} \overline{f(y)} g(y+x) dy. \tag{32}$$

Noting that $(f \star g)(x) = (\overline{f(-y)} * g(y))(x)$, equation (31) yields

$$\widehat{f \star g}(\xi) = \overline{\widehat{f}(\xi)} \cdot \widehat{g}(\xi) = \widehat{f}(-\xi)\widehat{g}(\xi). \tag{33}$$

[15] Similarly, if $f \in \mathbb{L}^1(\mathbb{R})$ while $g \in \mathbb{L}^2(\mathbb{R})$, then $f * g \in \mathbb{L}^2(\mathbb{R})$ (with existence a.e) and $\|f * g\|_2 \leq \|f\|_1 \|g\|_2$.

For example, suppose that $H(y) = g(e^y)$ is an integrable European payoff with $Y_T = \ln(S_T)$, and $q_T(y|s)$ is the density of Y_T conditioned on $s = \ln(S_0)$. Note that the dependence on S_0 is now incorporated in the variable y.

The valuation formula yields

$$\begin{aligned} e^{rT}\mathcal{V} \circ H(s) = \int_{\mathbb{R}} H(y) q_T(y|s) dy &= \int_{\mathbb{R}} H(y) p_T(y-s) dy \\ &= \int_{\mathbb{R}} H(x+s) p_T(x) dx = p_T \star H(s), \end{aligned}$$

after the change of variable $x = y - s$, since $p_T(x) = \overline{p_T(x)}$, where p_T is the density of log-return ($X_T = \ln(S_T/S_0)$ is represented by the variable x). Since $H \in \mathbb{L}^1(\mathbb{R})$, $(\mathcal{V} \circ H)(s) \in \mathbb{L}^1(\mathbb{R})$ as a function of the initial log price, where $e^{rT}\|\mathcal{V} \circ H\|_1 \leq \|p_T\|_1 \|H\|_1 = \|H\|_1 < \infty$, so we are permitted to take the Fourier transform. Hence

$$\mathcal{F}\{\mathcal{V} \circ H(s)\}(\xi) = e^{-rT}\mathcal{F}\{p_T \star H(s)\}(\xi) = e^{-rT}\phi_T(-\xi) \cdot \widehat{H}(\xi).$$

Assuming further that $\phi_T(-\xi)\widehat{H}(\xi) \in \mathbb{L}^1(\mathbb{R})$, we obtain the pricing formula by applying the inverse Fourier transform:

$$\begin{aligned} \mathcal{V} \circ H(s) = \mathcal{F}^{-1}\{\mathcal{F}\{\mathcal{V} \circ H\}(\xi)\}(s) &= e^{-rT}\mathcal{F}^{-1}\{\phi_T(-\xi) \cdot \widehat{H}(\xi)\}(s) \\ &= \frac{e^{-rT}}{2\pi} \int_{\mathbb{R}} e^{-i\xi s} \phi_T(-\xi) \cdot \widehat{H}(\xi) d\xi. \end{aligned} \tag{34}$$

In terms of our typical parameterization of the payoff function as $G_{S_0}(x) = g(S_0 e^x)$, we note that $H(y) = g(e^y) = g\left(S_0 e^{y - \ln(S_0)}\right) = G_{S_0}(y - \ln(S_0))$. Hence, $\widehat{H}(\xi) = e^{i\ln(S_0)\xi}\widehat{G}_{S_0}(\xi)$, and equation (34) becomes

$$\mathcal{V} \circ H(s) = \mathcal{V} \circ G_{S_0} = \frac{e^{-rT}}{2\pi} \int_{\mathbb{R}} \phi_T(-\xi)\widehat{G}_{S_0}(\xi) d\xi, \tag{35}$$

which is equivalent to formula (26) when $\eta = 0$, reflecting the assumed integrability of $H(y)$.

The CONV method [100] for pricing Bermudan options in exponential Levy models (extended to multi-asset options under Gaussian dynamics [92]), relies on a recursive convolution scheme for the *exponentially damped* value, as a function of current log-price, $s = \ln(S_0)$.[16] When $H(y)$ is unbounded, the value function will also be unbounded as a

[16] Their approach, which is discussed in a later chapter, computes the continuation value of the contract along the log spot grid at each observation date.

function of $\ln(S_0)$, so integrability fails. Assuming that one tail of the value function is bounded, while the other grows at most exponentially (e.g. for plain vanilla contracts), we may choose $\eta \in \mathbb{R}$ so that $e^{\eta s}(\mathcal{V} \circ H)(s) := v(s) \in \mathbb{L}^1(\mathbb{R})$.

While the Fourier transform maps the convolution of two functions to the product of their transforms, it also maps the product of two functions to the convolution of their transforms:

$$\mathcal{F}\{f \cdot g\}(\xi) = \frac{1}{2\pi}\widehat{f} * \widehat{g}(\xi) = \frac{1}{2\pi}\int \widehat{f}(\xi - \eta)\widehat{g}(\eta)d\eta, \quad \forall f, g \in \mathbb{L}^2(\mathbb{R}).$$

For example, given a density (or payoff) which is restricted to the corridor $\mathbb{1}_{(l,u)}$, we find that

$$\mathcal{F}\{\mathbb{1}_{(l,u)} \cdot f\}(\xi) = \int_{-\infty}^{\infty} e^{i(\xi-\eta)\frac{u+l}{2}} \frac{\sin\left((\xi-\eta)\frac{u-l}{2}\right)}{\pi(\xi-\eta)}\widehat{f}(\eta)d\eta.$$

2.3.3 Hilbert Transform

Another transform, which has been popularized in finance by the work of [67], is the Hilbert transform, defined as the Cauchy principal value

$$\mathcal{H}f(x) = \frac{1}{\pi}p.v.\int_{\mathbb{R}} \frac{f(y)}{x-y}dy.$$

The Hilbert transform arises natrually in the context of Fourier transform calculations. In particular,

$$\mathcal{F}\{\mathbb{1}_{(l,\infty)} \cdot f\}(\xi) = \frac{1}{2}\widehat{f}(\xi) + \frac{i}{2}e^{il\xi}\mathcal{H}\big(e^{-il\eta}\widehat{f}(\eta)\big)(\xi) \tag{36}$$

$$\mathcal{F}\{\mathbb{1}_{(-\infty,u)} \cdot f\}(\xi) = \frac{1}{2}\widehat{f}(\xi) - \frac{i}{2}e^{iu\xi}\mathcal{H}\big(e^{-iu\eta}\widehat{f}(\eta)\big)(\xi). \tag{37}$$

For example, [64] apply equation (37) to botain an alternative to the tradtional inversion formula in equation (44) for calculating a cdf. They note that

$$\begin{aligned} F(x) = \int_{-\infty}^{x} f(y)dy &= \int_{\mathbb{R}} f(y)\mathbb{1}_{(-\infty,x)}(y)dy \\ &= \mathcal{F}\{\mathbb{1}_{(-\infty,x)} \cdot f\}(0) = \frac{1}{2} - \frac{i}{2}\mathcal{H}\big(e^{-i\xi x}\widehat{f}(\xi)\big)(0). \end{aligned} \tag{38}$$

The value of a European call option $g(S_0e^{X_T}) = (S_0e^{X_T} - W)^+$ is also derived in [64] in terms of the Hilbert transform as

$$\begin{aligned}\mathcal{V} \circ g(S_0) &= S_0e^{-rT}\mathbb{E}[e^{X_T}\mathbb{1}_{[X_T>\ln(W/S_0)]}] - Ke^{-rT}\mathbb{Q}[X_T > \ln(W/S_0)] \\ &= \frac{1}{2}S_0e^{-qT} - \frac{1}{2}We^{-rT} \\ &\quad + \frac{i}{2}e^{-rT}\mathcal{H}\left(e^{-i\xi\ln(W/S_0)}(S_0\widehat{f}_T(\xi - i) - W\widehat{f}_T(\xi))\right)(0),\end{aligned}$$

where f_T is the density of $X_T = \ln(S_T/S_0)$. The final term is approximated by the real part of a trapezoidal approximation

$$\frac{i}{2}e^{-rT}\sum_{n=-N/2}^{N/2}\left(e^{-inh\ln(W/S_0)}(S_0\widehat{f}_T(nh - i) - W\widehat{f}_T(nh))\right)\frac{\cos(\pi n) - 1}{\pi n},$$

where the value corresponding to $n = 0$ in the sum is zero. For pricing a single option, this approach is often very effective. More efficient procedures are developed later for pricing large sets of options, as required for calibration.

2.3.4 Measure Changes and Transforms

In some cases, it is convenient to change to an alternative measure to reduce the problem complexity. Given a measurable space $(\Omega, \mathcal{F})$, and two equivalent measures $\mathbb{Q}, \widetilde{\mathbb{Q}}$, Bayes' theorem states that for any $X(\omega)$ which is $\mathbb{Q}$ integrable, and $\mathcal{G} \subset \mathcal{F}$, the conditional expectation of X can be found under either measure:

$$\mathbb{E}_{\mathbb{Q}}[X|\mathcal{G}] = \frac{\mathbb{E}_{\widetilde{\mathbb{Q}}}[X\zeta|\mathcal{G}]}{\mathbb{E}_{\widetilde{\mathbb{Q}}}[\zeta|\mathcal{G}]}, \quad \zeta = \frac{d\mathbb{Q}}{d\widetilde{\mathbb{Q}}}, \tag{39}$$

where ζ is the *Radon-Nikodym* derivative of $\mathbb{Q}$ with respect to $\widetilde{\mathbb{Q}}$, which satisfies $\zeta > 0$ ($\widetilde{\mathbb{Q}}$-a.s.), $E_{\widetilde{\mathbb{Q}}}[\zeta] = 1$, and $\mathbb{E}_{\mathbb{Q}}[X] = E_{\widetilde{\mathbb{Q}}}[X\zeta]$ for any $\mathbb{Q}$-integrable X.

While an inherent measure change is at the heart of risk-netural pricing, our main use of this result is to change from the pricing measure $\mathbb{Q}$ to an equivalent measure for which expecations are easier to compute. For example, suppose we wish to calculate[17] $\mathbb{E}[e^{-bX}\mathbb{1}_{\{X\leq c\}}]$, which is expectation of a product of two functions of the random variable X. Assuming that $\mathbb{E}[e^{-bX}] = \phi_X(ib)$ is finite, then the variable

$$Z := \frac{e^{-bX}}{\mathbb{E}[e^{-bX}]} = \frac{e^{-bX}}{\phi_X(ib)}$$

[17] As usual, the convention is $\mathbb{E}[\cdot] = \mathbb{E}_{\mathbb{Q}}[\cdot]$. The following result can be found in [64].

provides a change from $\mathbb{Q}$ to a new measure $\widetilde{\mathbb{Q}}$. Indeed, $Z > 0$ (a.s.) and $\mathbb{E}[Z] = 1$, so $Z = \frac{d\widetilde{\mathbb{Q}}}{d\mathbb{Q}}$ is the Radon-Nikodym derivative for the measure

$$\widetilde{\mathbb{Q}}(A) = \int_A Z(\omega) d\mathbb{Q}(\omega) = \int_A \frac{d\widetilde{\mathbb{Q}}}{d\mathbb{Q}} d\mathbb{Q}(\omega) = \mathbb{E}_{\mathbb{Q}}(Z\mathbb{1}_A).$$

Hence, we can write

$$\mathbb{E}[e^{-bX}\mathbb{1}_{\{X\leq c\}}] = \phi_X(ib)\cdot\mathbb{E}[Z\mathbb{1}_{\{X\leq c\}}] = \phi_X(ib)\cdot\mathbb{E}_{\widetilde{\mathbb{Q}}}[\mathbb{1}_{\{X\leq c\}}] = \phi_X(ib)\cdot\widetilde{\mathbb{Q}}[X\leq c].$$

As long as $\widetilde{\phi}_X$, the characteristic function of X under $\widetilde{\mathbb{Q}}$ is known, then Fourier transform methods can be used to determine $\widetilde{\mathbb{Q}}[X \leq c]$. Fortunately, it satisfies

$$\widetilde{\phi}_X(\xi) = \mathbb{E}_{\widetilde{\mathbb{Q}}}[e^{i\xi X}] = \mathbb{E}[Ze^{i\xi X}] = \frac{\mathbb{E}[e^{-bX}e^{i\xi X}]}{\mathbb{E}[e^{-bX}]} = \frac{\phi_X(\xi+ib)}{\phi_X(ib)}.$$

Thus, combining this result with the Hilbert transform formula in equation (38), we obtain

$$\begin{aligned}\mathbb{E}[e^{-bX}\mathbb{1}_{\{X\leq c\}}] &= \phi_X(ib)\widetilde{F}_X(c)\\ &= \phi_X(ib)\left(\frac{1}{2} - \frac{i}{2}\mathcal{H}\big(e^{-i\xi c}\widetilde{\phi}_X(\xi)\big)(0)\right)\\ &= \frac{\phi_X(ib)}{2} - \frac{i}{2}\mathcal{H}\big(e^{-i\xi c}\phi_X(\xi+ib)\big)(0).\end{aligned}$$

2.3.4.1 Measure Change Processes

For most interesting problems, the financial contract depends on several values assumed by the underlying prior to expiration, which is fixed as T. In this case, if $(Z_t)_{0\leq t\leq T}$ is a strictly positive (local) martingale with $\mathbb{E}[Z_t] = 1$, then $Z_t = \mathbb{E}[Z_T|\mathcal{F}_t]$ provides a Radon-Nikodym derivative *process*

$$Z_t = \frac{d\widetilde{\mathbb{Q}}}{d\mathbb{Q}}\Big|_{\mathcal{F}_t}, \quad t \leq T.$$

For example, consider the discretely monitored maximum of $X_t = \ln(S_t/S_0)$ over a set of dates $\{0, \Delta_t, 2\Delta_t, ..., M\Delta_t = T\}$, defined by

$$\mathfrak{M}_M = \max_{0\leq m\leq M} X_{t_m}.$$

To calculate the exponential moments of $\mathfrak{M}_M$, $\mathbb{E}[e^{u\mathfrak{M}_M}]$, the approach of [66] is to consider the positve martingale

$$Z_t = \frac{e^{uX_t}}{\mathbb{E}[e^{uX_t}]} = e^{uX_t - t\psi_X(-iu)}, \quad t \leq T,$$

where $u \in \mathcal{I}_L$, as defined in section 2.2.2. The characteristic functions under the resulting measure $\widetilde{\mathbb{Q}}$ satisfy

$$\widetilde{\phi}_t(\xi) = \mathbb{E}_{\widetilde{\mathbb{Q}}}[e^{iX_t\xi}] = \frac{\phi_t(\xi - iu)}{\phi_t(-iu)}, \quad \xi \in \mathbb{R}.$$

Hence,

$$\begin{aligned}
\mathbb{E}[e^{u\mathfrak{M}_M}] &= \mathbb{E}[e^{u(\mathfrak{M}_M - X_T) + uX_T}] \\
&= e^{T\psi_X(-iu)} \cdot \mathbb{E}[Z_T e^{u(\mathfrak{M}_M - X_T)}] \\
&= \phi_T(-iu) \cdot \mathbb{E}_{\widetilde{\mathbb{Q}}}[e^{u(\mathfrak{M}_M - X_T)}],
\end{aligned}$$

which expresses the expectation as one of a new variable $\mathfrak{M}_M - X_T$ under the measure $\widetilde{\mathbb{Q}}$. Later, we show how to obtain this variable recursively.

2.3.4.2 Change of Numeraire

So far we have assumed the existence of a risk-neutral pricing measure $\mathbb{Q}$ under which prices are obtained by expectation. In this case, if $M_t := e^{rt}$ denotes the price of a unit holding in the money market account, the definition of $\mathbb{Q}$ is that for any traded asset price S_t (assuming no dividend payments),

$$\frac{S_t}{M_t} = \mathbb{E}_{\mathbb{Q}}\left[\frac{S_T}{M_T}|\mathcal{F}_t\right], \qquad t \leq T. \tag{40}$$

In general, suppose there exists a *numeraire* $(N_t)_{t\geq 0}$, which is the (positive) price process of a non-dividend paying asset. Then from [72], there must exist a locally equivalent measure $\mathbb{N}$, defined by the Radon-Nikodym derivative process

$$Z_t = \left.\frac{d\mathbb{N}}{d\mathbb{Q}}\right|_{\mathcal{F}_t} = \frac{N_t/N_0}{M_t/M_0}, \qquad t \leq T, \tag{41}$$

such that the price S_t of any tradeable asset satisfies

$$\frac{S_t}{N_t} = \mathbb{E}_{\mathbb{N}}\left[\frac{S_T}{N_T}|\mathcal{F}_t\right]. \tag{42}$$

In general, if Y is $\mathcal{F}_t$ measurable and $s \leq t \leq T$,

$$\mathbb{E}_{\mathbb{N}}[Y|\mathcal{F}_s] = \frac{1}{Z_s}\mathbb{E}_{\mathbb{Q}}[Z_t Y|\mathcal{F}_s]. \tag{43}$$

2.3.5 Pricing by Probability Decomposition

One of the first approaches to option pricing by Fourier transform uses the so-called Gil-Pelaez inversion formula [74], as applied for example by Heston [79] in his seminal work. Bakshi and Madan [10] provide a generalized European option pricing formula based on this formula. If $F_X(x) := \int_{-\infty}^{x} f_X(x)dx$ is the cumulative distribution function (cdf), then we have the following standard formula:

$$\begin{aligned} F_X(x) &= \frac{1}{2} + \frac{1}{2\pi}\int_0^\infty \frac{e^{i\xi x}\phi_X(-\xi) - e^{-i\xi x}\phi_X(\xi)}{i\xi} d\xi \\ &= \frac{1}{2} - \frac{1}{\pi}\int_0^\infty \Re\left(\frac{e^{-ix\xi}\phi_X(\xi)}{i\xi}\right) d\xi. \end{aligned} \tag{44}$$

For a European call option $g(S_T) = (S_T - W)^+$, equation (5) yields

$$\begin{aligned} \mathcal{V} \circ g(S_0) &= e^{-rT}\mathbb{E}[(S_0 e^{X_T} - W)^+] \\ &= S_0 e^{-rT}\mathbb{E}[e^{X_T}\mathbb{1}_{[X_T > \ln(W/S_0)]}] - We^{-rT}\mathbb{Q}[X_T > \ln(W/S_0)], \end{aligned}$$

where the second term is just $-We^{-rT}(1 - F_X(\ln(W/S_0)))$. The first term is simplified considerably by a change of measure. In particular, if we assume a zero dividend yield so that $E_{\mathbb{Q}}[e^{X_t}] = e^{rt}$, then

$$Z_t := \frac{e^{X_t}}{e^{rt}} = \frac{e^{X_t}}{E_{\mathbb{Q}}[e^{X_t}]}, \qquad t \le T,$$

provides an appropriate measure change (Radon-Nikodym) process with $Z_0 = 1$. The first term is then simplified using

$$\begin{aligned} e^{-rT}\mathbb{E}_{\mathbb{Q}}\left[e^{X_T}\mathbb{1}_{[X_T > \ln(W/S_0)]}\right] &= \mathbb{E}_{\mathbb{Q}}\left[Z_T\mathbb{1}_{[X_T > \ln(W/S_0)]}\right] \\ &= \mathbb{E}_*\left[\mathbb{1}_{[X_T > \ln(W/S_0)]}\right] = \mathbb{Q}^*(X_T > \ln(W/S_0)), \end{aligned}$$

where $\mathbb{E}_*[\cdot]$ is the expectation under the new measure $\mathbb{Q}^*$. Hence, if we can acquire $\phi_T^*(\xi)$, the characteristic function of X_T under the measure $\mathbb{Q}^*$, equation (44) can be applied to evaluate $\mathbb{Q}^*(X_T > \ln(W/S_0))$. Well,

$$\phi_T^*(\xi) = \mathbb{E}_*\left[e^{iX_T\xi}\right] = \mathbb{E}_{\mathbb{Q}}\left[e^{iX_T\xi}Z_T\right] = \mathbb{E}_{\mathbb{Q}}\left[e^{X_T(1+i\xi)}\right]e^{-rT} = e^{-rT}\phi_T(\xi - i).$$

Hence, both terms can be evaluated using equation (44), so after two numerical integrations an approximate value is obtained. The main observation is that, as long as the characteristic

function after an appropriate measure change is known in closed form, Fourier techniques still apply. A similar approach is used to price discretely monitored lookback options, in which case the change of measure is essential.

2.3.6 Spread Options

While this work focuses primarily on one dimensional problems, transform methods have been applied successfully for low-dimensional multi-asset contracts. For high-dimensional problems, Monte Carlo simulation remains the most generally applicable. In some cases, the formula of Lewis [97] and Raible [117] can be extended by a successful damping of the terminal payoff. In [92], the CONV method is used to value higher dimensional basket options, for which damping cannot be applied. We also mention the work of [53], which directly extends the Carr and Madan framework [35] to spread option pricing. For more details on spread options, see [28]. Also see [98] for closed-form approximation strategies.

A two-dimensional *spread option* on (S_T^1, S_T^2) specifies the payoff

$$(S_T^1 - S_T^2 - W)^+ = W \cdot \left(e^{Y_T^1} - e^{Y_T^2} - 1\right)^+,$$

where $(Y_T^1, Y_T^2) = \big(\ln(S_T^1/W), \ln(S_T^2/W)\big)$. According to [80], the payoff function $H(y_1, y_2) := (e^{y_1} - e^{y_2} - 1)^+$ can be represented as follows.

Theorem 2.3.1. *For $\eta = (\eta_1, \eta_2) \in \mathbb{R}^2$, with $\eta_2 > 0$ and $\eta_1 + \eta_2 < -1$,*

$$H(y_1, y_2) = \int\int_{\mathbb{R}^2 + i\eta} e^{i\langle z, y\rangle} \check{H}(z) dz, \quad \check{H}(\xi_1, \xi_2) = \frac{\Gamma(i(\xi_1 + \xi_2) - 1) \cdot \Gamma(-i\xi_2)}{(2\pi)^2 \cdot \Gamma(i\xi_1 + 1)}, \tag{45}$$

where $\Gamma(v)$ is the complex gamma function defined by $\Gamma(v) = \int_0^\infty e^{-t} t^{v-1} dt$, for $\Re(v) > 0$.

This theorem provides an analytic expression, in the case of a two dimensional spread option, for the general statement $H = \mathcal{F}\{\mathcal{F}^{-1}\{H\}\}$. The integral is taken over the contour $\{z \in \mathbb{C}^2 : (z_1, z_2) = (\xi_1 + i\eta_1, \xi_2 + i\eta_2), \quad \eta, \xi \in \mathbb{R}^2\}$.

If $Y_0 := (Y_0^1, Y_0^2) = \big(\ln(S_0^1/W), \ln(S_0^2/W)\big)$, the spread option value is found by replacing H with its inverse transform representation, as was done in section 2.2.5 for one dimensional

case[18]:

$$
\begin{aligned}
e^{rT}\mathcal{V} \circ H(Y_0) &= W \cdot \mathbb{E}\left[\left(e^{Y_T^1} - e^{Y_T^2} - 1\right)^+\right] \\
&= W \cdot \mathbb{E}\left[\int\int_{\mathbb{R}^2+i\eta} e^{i\langle z, Y_T\rangle} \check{H}(z)dz\right] \\
&= W \int\int_{\mathbb{R}^2+i\eta} \mathbb{E}\left[e^{i\langle z, Y_T\rangle}\right] \check{H}(z)dz = W \int\int_{\mathbb{R}^2+i\eta} \phi_{Y_T}(z)\check{H}(z)dz.
\end{aligned}
$$

Proof of Theorem 2.3.1. With the parameters (η_1, η_2) chosen as directed, $e^{\langle \eta, y\rangle}H(y) \in \mathbb{L}^2(\mathbb{R}^2)$, so the Fourier transform exists. By restricting the domain to $\{y : y_1 > 0, e^{y_2} < e^{y_1} - 1\}$, it follows

$$
\begin{aligned}
g(\xi) &:= \int\int_{\mathbb{R}^2} e^{-i\langle \xi, y\rangle} H(y)dy \\
&= \int_0^\infty e^{-i\xi_1 y_1} \left[\int_{-\infty}^{\log(e^{y_1}-1)} e^{-i\xi_2 y_2}[(e^{y_1} - 1) - e^{y_2}]dy_2\right] dy_1 \\
&= \int_0^\infty e^{-i\xi_1 y_1}(e^{y_1} - 1)^{1-i\xi_2} \left[\frac{1}{-i\xi_2} - \frac{1}{1 - i\xi_2}\right] dy_1.
\end{aligned}
$$

After the change of variables $u = e^{-y_1}$,

$$
g(\xi) = \frac{1}{(1 - i\xi_2)(-i\xi_2)} \int_0^1 u^{i\xi_1 - 1} \left(\frac{1-u}{u}\right)^{1-i\xi_2} du.
$$

□

2.4 Option Pricing By Basis Expansion

The classical transform techniques provide a solid foundation for option pricing in the Fourier domain. Recently, significant improvements in terms of accuracy, computational efficiency, and generality have resulted from a new perspective in this domain. Rather than approach the valuation formula directly, the characteristic function of a process leads to a representation of the density in terms of a countable set of basis elements, $\{\Psi_k\}_{k\in\mathcal{K}}$, spanning the function space $\mathcal{M} := \overline{\text{span}}\{\Psi_k\}_{k\in\mathcal{K}}$. The idea is to determine the "best" approximation of the density by a member in $\mathcal{M}$, and to integrate the payoff directly against this approximate density. This chapter considers basis projection methods in the

[18]Note, however, that the order of Fourier transform and inversion has been reversed, at least in terms of our definition of the two.

generalized framework initiated in [83, 88]. The unifying theory is that of frames and Reisz bases, which is the subject of the next section.

For now, suppose that $G_{S_0}(y) = g(S_0 e^y)$ is a European type payoff function which is supported (and bounded) on the compact set $y \in [l, u]$, and let $p_{[l,u]}(y) := p_T(y)\mathbb{1}_{[l,u]}(y)$ denote the terminal density restricted to the payoff support.[19] Suppose further that the following representation of $p_{[l,u]}$ in terms of $\{\Psi_k\}_{k\in\mathcal{K}}$ holds:

$$p_{[l,u]}(x) = \sum_{k\in\mathcal{K}} \alpha_k \Psi_k(x), \qquad \alpha_k \in \mathbb{R}.$$

The value of g is then given simply by

$$\mathcal{V} \circ g(S_0) = e^{-rT} \int_{[l,u]} G_{S_0}(y) p_{[l,u]}(y) dy = e^{-rT} \sum_{k\in\mathcal{K}} \alpha_k \int_{[l,u]} G_{S_0}(y) \Psi_k(y) dy \tag{46}$$

where for the moment we assume that passing the integral is justified. If G_{S_0} is actually unbounded but finitely priced, the formula in equation (46) will contain a truncation error as well, which can be made arbitrarily small by a judicious choice of $[l, u]$. We will discuss this and other approximation issues in detail. As an important example, and to our knowledge the first of its kind, Fang and Oosterlee [61] consider the set $\Psi_k(x) := \cos\left(k\pi \frac{x-l}{u-l}\right)$, which leads to the cosine series expansion method (COS), introduced in section 2.4.2.

For a general basis, assuming that α_k are readily available as well as the inner products $\langle G_{S_0}, \Psi_k \rangle$, the option value can be determined. Compared to previous transform approaches, which require the computation of just one or two integrals, it seems that we have succeeded only in complicating the problem further, and for pricing a *single European* option, this observation is not entirely incorrect.[20] However, the pricing of a single European option is something of fait accompli in the field of option pricing,[21] and plenty of infrastructure exists for pricing these contracts in practice with reasonable efficiency.

[19] Restricting an expansion of $p_T(y)$ to $[l, u]$ is not the same as expanding $p_T(y)\mathbb{1}_{[l,u]}(y)$, as the later is subject to Gibbs oscillations. For now we ignore this distinction. The PROJ method presented below uses the former, while the COS method applies the latter. When $[l, u]$ is chosen sufficiently wide, the distinction is immaterial.

[20] For many underlying processes, especially those with heavy tails and sharp peaks, the new approach will still substantially outperform traditional methods, even for a single European option.

[21] New approaches are still being developed which can shed additional light on the nature of this problem, aside from providing an alternative solution. For example see [131] for an interesting approach based on Hermite polynomial expansions.

An obvious advantage of basis expansion methods lies in the fact that, assuming the coefficients α_k are obtainable, they can be reused in successive calculations. For pricing discretely monitored exotic contracts, this feature is essential.

While the theory of bases and frames is rich in the context of general Banach spaces, we restrict our attention to separable Hilbert spaces which provide a wealth of established results without unduly constraining the analysis. More details on basis theory can be found in [44, 50, 78, 134]. We also refer the reader to [1, 52, 109], which are excellent texts on the theory of Hilbert spaces and linear operators.

Recall that a Hilbert space, $\mathbb{H}$, is an inner product space which is complete[22] with respect to the inner product induced norm in that any Cauchy sequence of elements in $\mathbb{H}$ converges to a function in $\mathbb{H}$. In most applications, $\mathbb{H} = \mathbb{L}^2(\mathbb{R}^d)$ or $\mathbb{H} = \mathbb{L}^2(E)$ for some $E \subset \mathbb{R}^d$, where

$$\mathbb{L}^2(E) = \{f : \int_E f^2(x)dx < \infty,\ f \text{ measurable on } E\},$$

from which we define the norm $\|f\|_2 := \langle f, f\rangle = \int_E f^2$. The underlying set E should be clear from the context. Given the norm structure on $\mathbb{H}$, any two functions f, g are considered "equivalent", that is $f \equiv g$ in $\mathbb{H}$, whenever $\|f - g\|_2 = 0$. They are *orthogonal* if $\langle f, g\rangle = 0$, in which case $\|f + g\|_2^2 = \|f\|_2^2 + \|g\|_2^2$ by the Pythagorean Theorem.

2.4.1 Basis Representation and Duality

Separability of $\mathbb{L}^2$ spaces guarantees the existence of a countable set of functions that is capable of reproducing (representing)[23] any other element in the space. As a minimal requirement, a sequence of elements $\{\Psi_k\}_{k\in\mathcal{K}} \subset \mathbb{H}$ is said to be *maximal*(*complete*) if $\overline{\text{span}}\{\Psi_k\}_{k\in\mathcal{K}} = \mathbb{H}$, which says that $\{\Psi_k\}_{k\in\mathcal{K}}$ is capable of *representing* any function in $\mathbb{H}$. A maximal sequence $\{\Psi_k\}_{k\in\mathcal{K}} \subset \mathbb{H}$ is called a *basis* for $\mathbb{H}$ if to every element $f \in \mathbb{H}$ there

[22] This should not be confused with a separate notion of completeness, defined next.

[23] In the sense that the original function and the representation are indistinguishable under the norm.

corresponds a *unique* sequence of coefficient functionals[24] $\{A_k(f)\}_{k\in\mathcal{K}} \subset \mathbb{C}$ satisfying

$$f = \sum_{k\in\mathcal{K}} A_k(f)\Psi_k, \tag{47}$$

where convergence is with respect to the norm on $\mathbb{H}$. For example, when $\mathcal{K} = \mathbb{N}_+$, equation (47) is interpreted as $\mathbb{L}^2$ convergence:

$$\left\| f - \sum_{k=1}^{N} A_k(f)\Psi_k \right\|_2 \to 0 \quad \text{as} \quad N \to \infty.$$

We say that two sequences $\{\Psi_k\}$ and $\{\widetilde{\Psi}_k\}$ are *biorthogonal* if for all k, j

$$\langle \widetilde{\Psi}_k, \Psi_j \rangle = \int_E \widetilde{\Psi}_k(x)\overline{\Psi_j(x)}dx = \delta_{j-k},$$

where $\delta_{j-k} = \mathbb{1}\{j = k\}$. The next theorem, which holds in a similar form for more general frames, is a key result concerning basis representations.

Theorem 2.4.1. ***(Representation Theorem)*** *If $\{\Psi_k\}_{k\in\mathcal{K}}$ is a basis for $\mathbb{H}$, there exists a unique family $\{\widetilde{\Psi}_k\}_{k\in\mathcal{K}} \subset \mathbb{H}$ such that for any $f \in \mathbb{H}$,*

$$f = \sum_{k\in\mathcal{K}} \langle f, \widetilde{\Psi}_k \rangle \Psi_k,$$

where $\{\widetilde{\Psi}_k\}$ is also a basis for $\mathbb{H}$, and $\{\widetilde{\Psi}_k\}$ and $\{\Psi_k\}$ are biorthogonal. We call $\{\widetilde{\Psi}_k\}$ the dual basis *corresponding to $\{\Psi_k\}$.*

As a first example, it can be shown[25] that $\Psi_k(x) = \mathcal{E}_k(x)$ defined by

$$\mathcal{E}_k(x) := \frac{1}{\sqrt{u-l}} \exp\left(2\pi i k \frac{x-l}{u-l}\right), \qquad k = 0, 1, ...,$$

is a maximal *orthonormal* set in $\mathbb{L}^2([l, u])$ with the complex scalar field[26], $\mathbb{C}$, where orthonormality implies that $\langle \Psi_k, \Psi_j \rangle = \delta_{j-k}$. In the special case of orthormality, $\{\Psi_k\}$ is self-dual in that $\widetilde{\Psi}_k = \Psi_k$ for all k. This leads to the familiar formula $f = \sum_{k=1}^{\infty} \langle f, \Psi_k \rangle \Psi_k$. More generally, the basis and its dual yield unconditionally convergent representations for their closed span, providing alternative descriptions of the same space.

[24] Each $A_k : \mathbb{H} \to \mathbb{C}$ is a *continuous linear functional*. That is, in addition to linearity, boundedness holds: $|A_k(f)| \leq C_k \|f\|_2$, $\forall f \in \mathbb{H}$, where $C_k \in \mathbb{R}_+$. In particular, small perturbations in a function lead to small changes in the values prescribed by the coefficient functionals.

[25] See for example [52, 109].

[26] That is, it is maximal for the space of complex valued functions. The COS method, in contrast, uses a cosine basis which is maximal over the real scalar field.

Theorem 2.4.2. ***(Duality)*** *If $\{\Psi_k\}_{k\in\mathcal{K}}$ and $\{\widetilde{\Psi}_k\}_{k\in\mathcal{K}}$ are dual bases for a Hilbert space $\mathbb{H}$ with countable index set $\mathcal{K}$, the following hold:*

(i) $f = \sum_{k\in\mathcal{K}}^{\infty}\langle f, \widetilde{\Psi}_k\rangle\Psi_k, \quad \forall f \in \mathbb{H}.$

(ii) $f = \sum_{k\in\mathcal{K}}^{\infty}\langle f, \Psi_k\rangle\widetilde{\Psi}_k, \quad \forall f \in \mathbb{H}.$

(iii) $\langle f, g\rangle = \sum_{k\in\mathcal{K}}^{\infty}\langle f, \Psi_k\rangle\langle\widetilde{\Psi}_k, g\rangle, \quad \forall f, g \in \mathbb{H}.$

In fact, any one of these characterizations is equivalent for the pair $\{\Psi_k\}_{k\in\mathcal{K}}$ and $\{\widetilde{\Psi}_k\}_{k\in\mathcal{K}}$ to be dual bases (as long as representations are unique).

Again consider the (self-dual) exponential basis $\{\mathcal{E}_k\}_{k=0}^{\infty}$, and the payoff $G_{S_0}(y)$ supported on $[l, u]$ with p_T the risk-neutral log-return density[27]. Theorem 2.4.2 immediately provides the formula:

$$\mathcal{V}\circ g(S_0) = e^{-rT}\sum_{k=0}^{\infty}\langle p_{[l,u]}, \mathcal{E}_k\rangle\overline{\langle G, \mathcal{E}_k\rangle} = \frac{e^{-rT}}{u-l}\sum_{k=0}^{\infty}\mathcal{D}_k^{p_T}\cdot\overline{\mathcal{D}_k^{G}} \tag{48}$$

which is an inner product of the Fourier series coefficients of $p_{[l,u]}$ and G where, for example, $\mathcal{D}_k^{p_T} = \int_{[l,u]} p_T(x)\cdot\exp\left(2\pi ik\frac{x-l}{u-l}\right)dx$. Since $\{\mathcal{E}_k\}$ forms a basis, this provides a (semi)-analytical expression for the option price, which can be calculated numerically.

However, it is not always true that analytical results are preferred to approximations, as will be seen several times in the course of this work. An alternative approach, which more directly incorporates the known characteristic function of f_T, is as follows. With convergence in the mean square sense[28], and $\gamma := \frac{2\pi}{u-l}$

$$\begin{aligned}
p_{[l,u]}(x) &= \sum_{k=0}^{\infty}\langle p_{[l,u]}, \mathcal{E}_k\rangle\mathcal{E}_k(x) \\
&\approx \sum_{k=0}^{N-1}\left(\int_{[l,u]} p_T(x)\mathcal{E}_k(x)dx\right)\cdot\mathcal{E}_k(x) \\
&= \sum_{k=0}^{N-1}\frac{1}{\sqrt{u-l}}\left(\int_{[l,u]} p_T(x)\exp\left(2\pi ik\frac{x-l}{u-l}\right)dx\right)\cdot\mathcal{E}_k(x) \\
&\approx \sum_{k=0}^{N-1}\frac{e^{-i\gamma kl}}{\sqrt{u-l}}\left(\int_{-\infty}^{\infty} p_T(x)e^{i\gamma kx}dx\right)\cdot\mathcal{E}_k(x) = \sum_{k=0}^{N-1}\frac{e^{-i\gamma kl}}{\sqrt{u-l}}\phi_T(\gamma k)\cdot\mathcal{E}_k(x)
\end{aligned}$$

[27] Assuming that G is locally bounded, $G \in \mathbb{L}^2([l, u])$. Similarly, $p_T \in \mathbb{L}^2([l, u])$.

[28] For this particular basis, which has been extensively studied over the years, we can speak of pointwise and uniform convergence as well, though it will not be necessary for our purposes.

where $N \in \mathbb{N}_+$ is a sufficiently large truncation parameter. Valuation proceeds by equation (46) with $A_k = (u-l)^{-1/2} e^{-i\gamma kl} \phi_T(\gamma k)$, $k = 0, ..., N-1$. While the new formula is a considerable simplification as compared with (48), this approach is only valid if $[l, u]$ is sufficiently large so that

$$\int_l^u p_T(x) e^{i\xi x} dx \approx \int_{-\infty}^{\infty} p_T(x) e^{i\xi x} dx = \phi_T(\xi),$$

which we assume for now to be the case, returning later to this and other issues concerning convergence rates of expansion methods. Approximating the above integral by $\phi_T(\xi)$ was applied by [61] in deriving the COS method.

2.4.2 COS Density Expansion

The method of Fang and Oosterlee (2008) considers a cosine series expansion of the truncated density, rather than the full Fourier series illustrated above. In the context of duality, we can fix the following basis for $\mathbb{L}^2([l, u])$ of real-valued functions and its dual:

$$\{\Psi_k\}_{k\geq 0} = \left\{ \frac{1}{u-l} \mathbb{1}_{[l,u]}(x) \right\} \bigcup \left\{ \frac{2}{u-l} \cos\left(k\pi \frac{x-l}{u-l} \right) \right\}_{k\geq 1},$$

$$\{\widetilde{\Psi}_k\}_{k\geq 0} = \left\{ \mathbb{1}_{[l,u]}(x) \right\} \bigcup \left\{ \cos\left(k\pi \frac{x-l}{u-l} \right) \right\}_{k\geq 1},$$

where biorthogonality is easily verified. In particular, any $f \in \mathbb{L}^2([l, u])$, *f real-valued*, is representable by

$$f(x) = \sum_{k=0}^{\infty} \langle f, \widetilde{\Psi}_k \rangle \cdot \Psi_k(x) = \frac{2}{u-l} {\sum}'_{k=0}^{\infty} A_k \cdot \cos\left(k\pi \frac{x-l}{u-l} \right), \tag{49}$$

where

$$A_k = \int_l^u f(x) \cos\left(k\pi \frac{x-l}{u-l} \right) dx, \qquad k \geq 0,$$

and the summation prime designates that the first coefficient is weighted by 1/2.

Noting that $f(x) \in \mathbb{R}$ implies $f(x) = \Re\{f(x)\}$, for $[l, u]$ sufficiently large it then follows

$$\begin{aligned} A_k &\approx \int_{-\infty}^{\infty} \Re\left\{ f(x) \cos\left(k\pi \frac{x-l}{u-l} \right) \right\} dx \\ &= \int_{-\infty}^{\infty} \Re\left\{ f(x) \exp\left(i \cdot k\pi \frac{x-l}{u-l} \right) dx \right\} \\ &= \Re\left\{ \exp\left(-i \frac{kl\pi}{u-l} \right) \int_{-\infty}^{\infty} f(x) \exp\left(i \frac{k\pi}{u-l} x \right) dx \right\} = \bar{A}_k, \end{aligned}$$

where

$$\bar{A}_k := \Re\left\{\exp\left(-i\frac{kl\pi}{u-l}\right)\widehat{f}\left(\frac{k\pi}{u-l}\right)\right\}. \tag{50}$$

When working with the log return variable, $\ln(S_T/S_0)$, which has density p_T and characteristic function ϕ_T, the coefficients in equation (50) are found by replacing $\widehat{f}$ with ϕ_T. In this case, dependence of the option price on S_0 is incorporated in the payoff $g(S_0e^y)$.

Remark 2. Depending on the context, it may be more convenient to work with the density of $\ln(S_T)$, or even that of $\ln(S_T/W)$ for a parameter $W > 0$ (usually an option strike), rather than the log return. First consider $q_T(y|S_0)$, the conditional density of $Y_T = \ln(S_T)$ given S_0. For Levy models, equation (50) is applied with $\widehat{q}_T(\xi) = e^{i\xi\ln(S_0)}\phi_T(\xi)$, since $q_T(y|S_0) = p_T(y - \ln(S_0))$. The parameterization of [61] is to define $y = \ln(S_T/W)$ and $x = \ln(S_0/W)$, and $f_T(y|x)$ corresponds to the characteristic function $\widehat{f}_T(\xi|x) = e^{i\ln(S_0/W)\xi}\phi_T(\xi)$. In the latter two cases, the density expansion incorporates S_0, while the payoff is independent of S_0.

2.4.3 COS Valuation Formula: European Options

In the original work by Fang and Oosterlee (2008), European options are priced by as follows. For a given strike $W > 0$, define $x = \ln(S_0/W)$ and $y = \ln(S_T/W)$. The truncated density support, $[l, u]$, is now in the space of $\ln(S_T/W)$. After fixing a series trunction parameter, $N \in \mathbb{N}$, the density of $f_T(y|x)$ is approximated by the truncated cosine series expansion with coefficients prescribed by equation (50):

$$\bar{f}_T(y|x) := \frac{2}{u-l}{\sum}'_{k=0}^{N-1}\bar{A}_k(x)\cdot\cos\left(k\pi\frac{x-l}{u-l}\right), \tag{51}$$

where, given the characteristic function $\widehat{f}_T(\xi|x) = e^{ix\xi}\phi_T(\xi)$, we have

$$\begin{aligned}\bar{A}_k(x) &:= \Re\left\{\exp\left(-i\frac{kl\pi}{u-l}\right)\widehat{f}_T\left(\frac{k\pi}{u-l}\Big|x\right)\right\}\\ &= \Re\left\{\exp\left(ik\pi\frac{x-l}{u-l}\right)\phi_T\left(\frac{k\pi}{u-l}\right)\right\}.\end{aligned}$$

Now let $G(y) = g(e^y)$ denote a European payoff. We have the value approximation

$$\mathcal{V}\circ g(S_0) \approx e^{-rT}{\sum}'_{k=0}^{N-1}\bar{A}_k(x)\cdot G_k,$$

where[29]

$$G_k := \langle G \cdot \mathbb{1}_{[l,u]}, \Psi_k \rangle = \frac{2}{u-l} \int_l^u G(y) \cos\left(k\pi \frac{y-l}{u-l}\right) dy$$

are the payoff coefficients. For example,

$$G(y) = [\alpha \cdot W\,(e^y - 1)]^+ \quad \text{with} \quad \alpha = \begin{cases} 1 & \text{for a call,} \\ -1 & \text{for a put.} \end{cases}$$

Simple calculus derives the necessary integrals required to evaluate call and put payoff coefficients, where $[c,d] \subset [l,u]$:

$$\begin{aligned} \chi_k(c,d) &:= \int_c^d e^y \cos\left(k\pi \frac{y-l}{u-l}\right) dy \\ &= \frac{1}{1+\left(\frac{k\pi}{u-l}\right)^2} \left[\cos\left(k\pi \frac{d-l}{u-l}\right) e^d - \cos\left(k\pi \frac{c-l}{u-l}\right) e^c \right. \\ &\qquad \left. + \frac{k\pi}{u-l} \sin\left(k\pi \frac{d-l}{u-l}\right) e^d - \frac{k\pi}{u-l} \sin\left(k\pi \frac{c-l}{u-l}\right) e^c \right] \end{aligned} \tag{52}$$

and

$$\psi_k(c,d) := \begin{cases} \frac{u-l}{k\pi} \left[\sin\left(k\pi \frac{d-l}{u-l}\right) - \sin\left(k\pi \frac{c-l}{u-l}\right)\right] & k \neq 0, \\ (u-l) & k = 0. \end{cases} \tag{53}$$

For example, the call option payoff coefficients satisfy

$$\begin{aligned} G_k^{call} &= \frac{2}{u-l} \int_0^u W(e^y - 1) \cos\left(k\pi \frac{y-l}{u-l}\right) dy \\ &= \frac{2W}{u-l} (\chi_k(0,u) - \psi_k(0,u)), \end{aligned} \tag{54}$$

while for the vanilla put,

$$\begin{aligned} G_k^{put} &= \frac{2}{u-l} \int_l^0 W(1 - e^y) \cos\left(k\pi \frac{y-l}{u-l}\right) dy \\ &= \frac{2W}{u-l} (\psi_k(l,0) - \chi_k(l,0)). \end{aligned} \tag{55}$$

Formulas for digital and "cash-or-nothing" European options are derived similarly. These formulas will also be used in the derivation of exotic pricing algorithms.

[29] Multiplying G by $\mathbb{1}_{[l,u]}$ is redundant because of the basis support, but it is important to keep in mind that the choice of basis support is a choice of truncation, in is an important factor in the error analysis.

2.4.4 Frames

Before moving on to additional applications, we consider a construct that generalizes the notion of a basis by relaxing the uniqueness requirement of representations. While this notion is directly applicable to the practice (and theory) of static hedging [88], our goal for now is to establish enough background to motivate what are called bases of translates, which will allow us to specify approximation spaces by modifying a single "shape" function. Readers with a more practice-oriented interest are encouraged to proceed directly to section 2.5, which is self-contained.

Consider a sequence $\{\Psi_k\}_{k\in\mathcal{K}} \subset \mathbb{H}$, indexed by a countable set $\mathcal{K}$. Recall *Bessel's equality*, which states that if $\{\Psi_k\}_{k\in\mathcal{K}}$ is a maximal orthonormal sequence in $\mathbb{H}$, then

$$\sum_{k\in\mathcal{K}} |\langle f, \Psi_k\rangle|^2 = \|f\|_2^2, \quad \forall f \in \mathbb{H}, \tag{56}$$

and this is an equivalent condition for orthonormality.[30] If, instead of satisfying Bessel's equality strictly, there exists some $B > 0$ for which

$$\sum_{k\in\mathcal{K}} |\langle f, \Psi_k\rangle|^2 \leq B\|f\|_2^2, \qquad \forall f \in \mathbb{H},$$

we call $\{\Psi_k\}_{k\in\mathcal{K}}$ a *Bessel sequence* in $\mathbb{H}$, and the defining inequality is called *Bessel's inequality*. This inequality is necessary to obtain *unconditionally convergent* representations (convergence regardless of how the elements are ordered).

Theorem 2.4.3. *If $\{\Psi_k\}_{k\in\mathcal{K}}$ is a Bessel sequence in $\mathbb{H}$ with bound B, then $\sum_{k\in\mathcal{K}} A_k\Psi_k$ converges unconditionally for every $\{A_k\}_{k\in\mathcal{K}} \in l^2(\mathcal{K})$. In particular, the operator $T : l^2(\mathcal{K}) \to \mathbb{H}$ defined by*

$$T\{c_k\} = \sum_{k\in\mathcal{K}} A_k\Psi_k$$

is a well defined, bounded linear operator with $\|T\| \leq \sqrt{B}$. Further, the adjoint of T, $T^* : \mathbb{H} \to l^2(\mathcal{K})$, is given by

$$T^*f = \{\langle f, \Psi_k\rangle\}_{k\in\mathcal{K}}.$$

[30] Not only is an orthonormal basis, say $\{e_k\}_{k\in\mathcal{K}}$, guaranteed to exist for any Hilbert space, but knowing just one such basis allows us to determine the entire realm of orthonormal bases by unitary mappings of $\{e_k\}$. Namely, any other orthonormal basis is of the form $\{Ue_k\}_{k\in\mathcal{K}}$, where $U : \mathbb{H} \to \mathbb{H}$ is a unitary operator: $UU^* = U^*U = I$, where U^* is the adjoint of U, and I the identity operator on $\mathbb{H}$ (see [44], Theorem 3.4.7).

For a given Bessel sequence $\{\Psi_k\}_{k\in\mathcal{K}}$ we call T the *synthesis operator*, and T^* the *analysis operator*. By mandating in addition a lower bound,

$$A\|f\|_2^2 \leq \sum_{k\in\mathcal{K}} |\langle f, \Psi_k\rangle|^2 \leq B\|f\|_2^2, \quad \forall f \in \mathbb{H}, \tag{57}$$

we call $\{\Psi_k\}_{k\in\mathcal{K}}$ a *frame* for $\mathbb{H}$, and A, B the lower and upper *frame bounds*. By the lower bound, $\mathcal{M} := \overline{\text{span}}\{\Psi_k\}$ is a complete sequence for $\mathbb{H}$. Indeed, $\mathcal{M}$ is a closed linear space satisfying $\mathcal{M}^\perp = \{0\}$, so $\mathcal{M} = \mathbb{H}$. In general, frames are *not* bases for $\mathbb{H}$. Thus, we see that frames offer a natural generalization to the traditional basis concept since they provide completeness without requiring Bessel's *equality* (or normalization).

A special type of frame is a *Riesz basis*, which in addition to equation (62) must also provide unique representations. If fact, every Riesz basis is a sequence of the form $\{Ue_k\}_{k=1}^\infty$, where $\{e_k\}_{k=1}^\infty$ is an orthonormal basis for $\mathbb{H}$, and $U : \mathbb{H} \to \mathbb{H}$ is a bounded, bijective operator. We are not required to produce U or $\{e_k\}$ for which the definition holds, as simpler criteria (to be presented) exists. Yet another equivalent characterization of a Riesz basis is as an ω-independent frame, where a sequence $\{\Psi_k\}_{k\in\mathcal{K}}$ is *ω-independent* if whenever the series $\sum_{k\in\mathcal{K}} c_k\Psi_k$ converges to zero for some scalars $\{c_k\}_{k\in\mathcal{K}}$, then $c_k = 0\ \forall k$.[31] Similarly, if by removing any arbitrary element from a frame we destroy the frame property, that frame is necessarily a Riesz basis and conversely.[32]

2.4.5 Function Representation Via Frames

We turn now to the general representation theorem for frames. Since the Bessel upper bound holds for any frame $\{\Psi_k\}_{k=1}^\infty$, the corresponding operator $T^* : \mathbb{H} \to l^2(\mathbb{N})$ returns a sequence in $l^2(\mathbb{N})$ for any function in $\mathbb{H}$, and composition by T yields the well defined operator $S : \mathbb{H} \to \mathbb{H}$ given by

$$Sf = TT^*f = \sum_{k\in\mathcal{K}} \langle f, \Psi_k\rangle \Psi_k,$$

[31] Compare this to the weaker definition of linear independence, which only requires that every finite subset of $\{c_k\}_{k\in\mathcal{K}}$ is linearly independent.

[32] In frame parlance, one often encounters the term *exact frame* to describe a frame with this property. Any frame which does not have this property, i.e a frame which is not also a Riesz basis, is called *redundant* or *overcomplete*.

which is called the *frame operator*. For an orthonormal basis, S is simply the identity on $\mathbb{H}$.

Theorem 2.4.4. ***(Frame Representation Theorem)*** *For any frame $\{\Psi_k\}_{k\in\mathcal{K}} \subset \mathbb{H}$ with frame bounds A, B, the following hold on $\mathbb{H}$:*

(i) S is bounded, invertible, and self-adjoint.

(ii) The sequence $\{S^{-1}\Psi_k\}_{k\in\mathcal{K}}$ is a frame with bounds B^{-1}, A^{-1}:

$$B^{-1}\|f\|^2 \leq \sum_{k\in\mathcal{K}} |\langle f, S^{-1}\Psi_k\rangle|^2 \leq A^{-1}\|f\|^2, \ \forall f \in \mathcal{H},$$

and S^{-1} is the frame operator for $\{S^{-1}\Psi_k\}_{k\in\mathcal{K}}$.

(iii) The representation

$$f = \sum_{k\in\mathcal{K}} \langle f, S^{-1}\Psi_k\rangle \Psi_k$$

holds for every $f \in \mathbb{H}$.

The frame $\{S^{-1}\Psi_k\}_{k\in\mathcal{K}}$ is called the *canonical dual* of $\{\Psi_k\}_{k=1}^{\infty}$, and the scalars $\langle f, S^{-1}\Psi_k\rangle$ are the *frame coefficients*. Since a frame is not generally a basis, the frame coefficients are not generally biorthogonal. On the other hand, since a Riesz basis is a frame for which the dual basis $\{\widetilde{\Psi}_k\} \subset \mathbb{H}$ is unique and biorthogonal (as is the case with any true basis), we see that $\{S^{-1}\Psi_k\} \equiv \{\widetilde{\Psi}_k\}$ is the unique biorthogonal basis corresponding to $\{\Psi_k\}$, and this dual basis is also a Riesz basis for the same space.[33] For a general frame however, there may be other dual frames for which the representation holds and we always reserve the notation $\widetilde{\Psi}$ for the canonical dual.

2.5 Bases From a Generator

To motivate the framework of density expansion in a basis, we considered the cosine series basis for $\mathbb{L}^2([l,u])$, in order to reconstruct the truncated density $f_T \mathbb{1}_{[l,u]}$. Coefficients of the expansion of $f_T \mathbb{1}_{[l,u]}$ (a localization of the density) were obtained by global information of f_T on $\mathbb{R}$, in terms of $\widehat{f_T}(\xi)$. With the Hilbert space interpretation, the truncated series

[33] A subtlety worth mentioning is that uniqueness applies to a biorthogonal Riesz basis living in the same space as $\{\Psi_k\}$. It is possible, however, that additional biorthogonal bases exist within a larger space.

expansion in equation (51) is an approximation of the *orthogonal projection* of $f_T \mathbb{1}_{[l,u]}$ onto $\mathcal{M}_N := \text{span}\{\Psi_k\}_{k=0}^{N-1}$, given by $P_{\mathcal{M}_N} f_{[l,u]}(x) = \sum_{k=0}^{N-1} \langle f_T \mathbb{1}_{[l,u]}, \widetilde{\Psi}_k \rangle \cdot \Psi_k(x)$.

An alternative approach is to consider $\mathbb{H} = \mathbb{L}^2(\mathbb{R})$, and find an expansion of the density p_T (or f_T) on all of $\mathbb{R}$. Values will then be obtained upon integrating a truncated expansion, rather than expanding a truncated density. A flexible and powerful approach to this problem is to consider approximation spaces[34] spawned by a single function φ, called a *generator*.

2.5.1 Riesz Sequence of Translates

Suppose that $\varphi \in \mathbb{L}^2(\mathbb{R})$, and define the translation operator $T_k : \varphi \to T_k\varphi$ by $T_k\varphi(x) = \varphi(x-k)$. Considering the translations of φ for $k \in \mathcal{K}$, where for concreteness we take $\mathcal{K} \equiv \mathbb{Z}$, the closed subspace $\mathcal{M} := \overline{\text{span}}\{T_k\varphi\}_{k\in\mathbb{Z}}$ is also a Hilbert space, and the frame operator is a map $S : \mathcal{M} \to \mathcal{M}$ by $Sf = \sum_{k\in\mathbb{Z}} \langle f, T_k\varphi \rangle T_k\varphi$. Assuming that $\{T_k\varphi\}$ is a frame for $\mathcal{M}$, we have

$$P_{\mathcal{M}} f = \sum_{k\in\mathbb{Z}} \langle f, S^{-1}T_k\varphi \rangle \cdot T_k\varphi, \quad f \in \mathbb{L}^2(\mathbb{R}),$$

where $P_{\mathcal{M}} : \mathbb{L}^2(\mathbb{R}) \to \mathcal{M}$ is the orthogonal projection operator. For a general frame, it can be shown that

$$ST_k = T_kS \qquad \text{and} \qquad S^{-1}T_k = T_kS^{-1}, \quad \forall k \in \mathbb{Z}.$$

The fact that S and S^{-1} commute with integer translation enables a very simple characterization of the (canonical) dual frame:

$$\{\widetilde{\varphi}_k\}_{k\in\mathbb{Z}} := \{S^{-1}T_k\varphi\}_{k\in\mathbb{Z}} = \{T_kS^{-1}\varphi\}_{k\in\mathbb{Z}} = \{T_k\widetilde{\varphi}\}_{k\in\mathbb{Z}},$$

where $\widetilde{\varphi} := S^{-1}\varphi$ is the canonical dual to φ (i.e $\{T_k\widetilde{\varphi}\}$ and $\{T_k\varphi\}$ are dual frames). As a consequence, the dual sequence is attainable without analyzing each individual $\widetilde{\varphi}_k$, as long as $\widetilde{\varphi}$ is computable.

It turns out that the frame properties of a sequence of the form $\{T_k\varphi\}$ can be completely characterized by the 2π-periodic function $\mathbf{\Phi} : \mathbb{R} \to \mathbb{R}$ defined as

$$\mathbf{\Phi}(\gamma) = \sum_{k\in\mathbb{Z}} |\widehat{\varphi}(\gamma + 2\pi k)|^2 .$$

[34] In contrast to the truncated cosine expansion, the approximations spaces are each infinitely dimensional, and generally nested.

One way to obtain an expression for $\mathbf{\Phi}$ is via Fourier series (FS) expansion:

Theorem 2.5.1. *Let $\varphi \in \mathbb{L}^2(\mathbb{R})$. Then $\mathbf{\Phi} \in L^1(0, 2\pi)$, and the Fourier coeffients of $\mathbf{\Phi}$ with respect to the orthonomal basis $\{e^{-ikx}\}_{k\in\mathbb{Z}}$ are given by*

$$c_k = 2\pi \int_{-\infty}^{\infty} \varphi(x)\overline{\varphi(x-k)}dx, \qquad k \in \mathbb{Z}.$$

Moreover, when φ is a compactly supported real-valued function, the FS expansion has only finitely many terms:

$$\mathbf{\Phi}(\gamma) = c_0 + 2\sum_{k=1}^{N} c_k \cos(k\gamma), \quad \textit{for some } N \in \mathbb{N}.$$

Proof. We have

$$\int_0^{2\pi} \mathbf{\Phi}(\gamma)d\gamma = \sum_n \int_0^{2\pi} |\widehat{\varphi}(\gamma + 2\pi n)|^2 = \int_{\mathbb{R}} |\widehat{\varphi}(\gamma)|^2 d\gamma < \infty,$$

so $\mathbf{\Phi} \in L^1(0, 2\pi)$. Thus, since $\mathbf{\Phi}$ is 2π-periodic, the FS coefficients are given by

$$\begin{aligned} c_k := \int_0^{2\pi} \mathbf{\Phi}(\gamma)e^{ik\gamma}d\gamma &= \int_0^{2\pi} \sum_n |\widehat{\varphi}(\gamma + 2\pi n)|^2 \, e^{ik\gamma}d\gamma \\ &= \int_0^{2\pi} \sum_n |\widehat{\varphi}(\gamma + 2\pi n)|^2 \, e^{ik(\gamma+2\pi n)}d\gamma \\ &= \int_{\mathbb{R}} |\widehat{\varphi}(\gamma)|^2 e^{ik\gamma}d\gamma \\ &= 2\pi \int_{\mathbb{R}} \varphi(x)\overline{\varphi(x-k)}dx. \end{aligned}$$

Finally, if φ is real-valued, the conjugation may be dropped and $c_k = c_{-k}$. Compactness yields an N for which $c_k = 0$ for $|k| > N$, and so

$$\begin{aligned} \mathbf{\Phi}(\gamma) = \sum_{|k|\le N} c_k e^{-ik\gamma} &= c_0 + \sum_{k=1}^{N} c_k \left(e^{-ik\gamma} + e^{ik\gamma}\right) \\ &= c_0 + \sum_{k=1}^{N} c_k \cdot 2\cos(k\gamma). \end{aligned}$$

□

Not only does $\mathbf{\Phi}$ characterize the frame properties of a generator, but the Fourier transform of the corresponding dual generator is given explicitly in terms of $\mathbf{\Phi}$, as demonstrated in the following theorem (see [44] for a proof).

Theorem 2.5.2. *Let $\varphi \in \mathbb{L}^2(\mathbb{R})$, and fix $A, B > 0$. Let S denote the frame operator for $\{T_k\varphi\}$. Then:*

(i) $\{T_k\varphi\}_{k\in\mathbb{Z}}$ is a Riesz sequence with bounds A, B iff

$$A \leq \mathbf{\Phi}(\gamma) \leq B, \qquad a.e.\ \gamma \in [0, 2\pi].$$

In this case, $S^{-1}\varphi = \widetilde{\varphi}$, which is given in terms of its Fourier transform:

$$\widehat{\widetilde{\varphi}}(\gamma) = \frac{\widehat{\varphi}(\gamma)}{\mathbf{\Phi}(\gamma)}.$$

(ii) $\{T_k\varphi\}_{k\in\mathbb{Z}}$ is a frame sequence with bounds A, B iff

$$A \leq \mathbf{\Phi}(\gamma) \leq B, \qquad a.e.\ \gamma \in [0, 2\pi] \setminus N_0,$$

where $N_0 := \{\gamma \in [0, 2\pi] : \mathbf{\Phi}(\gamma) = 0\}$. In this case, $S^{-1}\varphi = \widetilde{\varphi}$, which is given in terms of its Fourier transform:

$$\widehat{\widetilde{\varphi}}(\gamma) = \frac{\widehat{\varphi}(\gamma)}{\mathbf{\Phi}(\gamma)}.\mathbb{I}_D(\gamma),$$

where $D := \{\gamma \in \mathbb{R} : \mathbf{\Phi}(\gamma) \neq 0\}$.

Thus, if $\widehat{\varphi}$ is known along with $\mathbf{\Phi}$ (e.g by Theorem 2.5.1), then the Fourier transform of the dual can be found. Our goal is to combine knowledge of the primal dual pair $(\varphi, \widetilde{\varphi})$, or equivalently the pair of Fourier transforms, to obtain closed-form expressions of orthogonally projected risk-neutral densities.

Another simple operation is required to broaden the scope of this procedure, which results in a parameterization of the approximation space in terms of a *resolution*, which is a measure of its granularity. We denote the dilation operator by D_a for $a \neq 0$, which acts on a function according to $D_a\varphi(x) = |a|^{1/2}\varphi(ax) := \varphi^a(x)$.

Lemma 2.5.3. *If $\varphi \in \mathbb{L}^2$, and $\{T_k\varphi\}_{k\in\mathbb{Z}}$ is a frame sequence, then $\{T_{\frac{k}{a}}\varphi^a\}_{k\in\mathbb{Z}} = \{D_aT_k\varphi\}_{k\in\mathbb{Z}}$ is also a frame sequence with the same frame bounds. The canonical dual is given by $\{T_{\frac{k}{a}}S^{-1}\varphi^a\}_{k\in\mathbb{Z}}$. In particular, if $\{T_k\varphi\}_{k\in\mathbb{Z}}$ is a Riesz sequence in $\mathbb{H}$, and $\mathcal{M}_a := \overline{span}\{D_aT_k\varphi\}_{k\in\mathbb{Z}}$, then $\{D_aT_k\widetilde{\varphi}\}_{k\in\mathbb{Z}}$ is the biorthogonal dual of $\{D_aT_k\varphi\}_{k\in\mathbb{Z}}$ on $\mathcal{M}_a$.*

This result, which is proved in [44], justifies our special interest in Riesz sequences as opposed frames in general, at least when the objective is to efficiently project a density[35]. Specifically, the dual to a general frame is described in terms of $S^{-1}\varphi^a$, and it can depend in a nontrivial way on the scaling parameter a. In contrast, a Riesz sequence and its corresponding dual are described entirely by the pair scaling functions $(\varphi, \widetilde{\varphi})$. This is essential when the resolution required to obtain a desired accuracy is unknown, and several approximations may be made prior to terminating with a reasonable estimate.

[35]For static hedging, the generality of frames allows us to study spaces of redundant functions, and efficiency is not always the primary consideration when constructing a static hedge.

CHAPTER III

OPTION PRICING BY FRAME DUALITY

This chapter is based on the paper [83], published in SIAM Journal on Financial Mathematics.

3.1 Introduction

The emergence of increasingly sophisticated models for asset price dynamics has stimulated the development of efficient pricing and calibration procedures to value derivatives. An especially fruitful direction in asset modeling has been the application of Levy processes [12, 32, 73, 104] as drivers of asset dynamics. As Levy driven models (and affine models [57] such as those of Heston [79] or Bates [101]) are often specified by the characteristic function of the log asset price, Fourier transform techniques have emerged as indispensable tools for the valuation of financial products. This is especially true for numerical integration-based option pricing, which is the focus of this paper. In particular, we develop a density projection method using Riesz bases of translates, which includes the class of B-splines, as well as other compactly supported kernels, bell functions, and window functions used in signal processing.

Efficient procedures utilizing the fast Fourier transform (FFT) were pioneered by Carr and Madan [35] where prices across a range of (log) strikes were computed simultaneously, enabling the calibration of exponential Levy models to market prices. Additional details and error bounds can be found in [91]. Recent advances in numerical option pricing include the COS method [61, 62], in which the log return relative is expanded in a Fourier cosine series, and the CONV method [100], in which the valuation operator is expressed as a cross-correlation and the FFT is applied. In [112, 113], B-splines are introduced as an effective means of locally approximating a density function, providing an alternative to the global basis representation of [61].

Density approximation methods are distinguished by the determination of coefficients in

the basis expansion, much like quadrature rules are distinguished by the choice of nodes and weights. In [113], the coefficients of a B-spline basis are approximated numerically by first determining the Fourier transform of a truncated density expansion[1], and then by applying a numerical approximation of Cauchy's integral formula to the resulting polynomial.

The main contribution of our work is in the novel application of frame duality theory to derive the exact integral representation of the true orthogonal projection coefficients, which applies to compactly supported basis elements in general, and to B-splines in particular. Orthogonal projections, as opposed to alternative representations with the same basis, lead to accelerated convergence of integrals (see [127] for a detailed study and [85] for an example with barrier options). While the integral representation of projection coefficients must be truncated to obtain numerical coefficients, the quadrature and truncation errors are exponentially decaying. Hence the convergence acceleration afforded by the true orthogonal projection is maintained. The error analysis demonstrates that the departure of numerical coefficients from the analytical representation is negligible in comparison to the projection error itself. Since our approach applies to a larger class of generators, it motivates the search for specialized bases that can, for example, robustly price highly peaked densities. The possibility exists as well that generators can be adapted to the eccentricities of a particular model class, such as the variance gamma processes.

By appealing to the duality of frame sequences, we utilize the frame representation theorem to obtain an analytical expression for the optimal coefficients, which are then obtained efficiently using the fast Fourier transform with exponential convergence. The analytical expressions are derived from the fact that the dual scaling functions of B-splines (and other compactly supported generators) can be obtained explicitly, allowing for a direct expansion of the density. The method, which we call PROJ (for projection), outperforms that of its nearest rival, COS [61], in the context of pricing large sets of European options. From a practitioner's standpoint where pricing occurs in real time, PROJ does not require the delicate selection of control parameters to hasten let alone obtain convergence, as do

[1]Either by first truncating the support, or by truncating a series expansion in the case of unbounded support.

other transform methods [35, 96, 102, 112, 113].

The compact support of the basis elements, and the use of the FFT to calculate projection coefficients, facilitate the extension of PROJ to the pricing of complex path-dependent options where repeated expansions are required. Most importantly, the convergence acceleration that derives from the use of orthogonal projection coefficients applies to the calculation of intermediate value functions for exotic options. This acceleration greatly reduces the resolution required to obtain a desired accuracy. Because of the nature of discretely monitored exotic option pricing, the error analysis presented in this work is valuable for analyzing extensions to more complicated settings. Aside from an interesting application of duality, the generality of the PROJ method in terms of vanilla and exotic option pricing makes it an effective local basis complement to the COS method.

3.2 Motivation

Research on the use of basis functions to represent probability densities has led to more efficient schemes for option pricing when the underlying characteristic function is known. For example, in the COS method of [61], the risk-neutral density is expanded in a cosine basis on $[l, u]$ as

$$f_T(y) \approx \sum\nolimits'_{k=0}^{N-1} \Re\left\{\widehat{f}_T\left(\frac{k\pi}{u-l}\right) e^{ik\pi\frac{y-l}{u-l}}\right\} \cos\left(k\pi\frac{y-l}{u-l}\right)$$

where[2] $y = \ln(S_T)$. Here, $[l, u]$ is a truncated support chosen to capture the mass of f_T to within a given tolerance. This approach has been used to priced vanilla as well as exotic options, although the global support of the cosine basis functions can lead to difficulties in the path-dependent case.

Alternatively, one can consider compactly supported basis functions, such as the class of B-splines. The approach of [113] is to utilize cardinal B-splines of order zero and one (Haar and linear) to approximate the Fourier transform of $f_T(y)\mathbb{1}_{[l,u]}(y)$, which is used to approximate the coefficients of an expansion in the basis at a resolution $a = 2^P$, $P \in \mathbb{N}$.

[2] In the context of pricing an option with strike K, $y = \ln(S_T/K)$.

For example, with $\varphi^c(x)$ the linear spline on $[0,2]$, an approximation over $[l,u]$ is given by[3]

$$f_T(y) \approx \sum_{k=0}^{2(a-1)} c_{a,k} \cdot \varphi^c_{a,k}\left(2\frac{y-l}{u-l}\right),$$

where for $k \geq 1$

$$c_{a,k} \approx \frac{4a^{1/2}}{\pi r^k (u-l)} \int_0^\pi \Re\left\{\widehat{f}_T\left(\frac{2ai}{u-l}\ln(re^{i\xi})\right)\frac{\ln^2(re^{i\xi})\cdot(re^{i\xi})^{-\frac{2al}{u-l}}}{(re^{i\xi}-1)^2}\cdot\cos(k\xi)\right\}du, \quad (58)$$

and the formula for $k=0$ is multiplied by $1/2$. Here, $r>0$, $r\neq 1$ is a user specified parameter which is chosen to control truncation and discretization errors. To calculate each integral, $k=0,...,2^{P+1}-2$, the authors use a trapezoidal approximation with step size $h=\pi/a$.

We approach the problem from a different perspective, which applies not only to B-splines, but to any compactly supported scaling functions that generate a Riesz basis. It further dispenses with the control parameter r, which contributes to our method's robustness and implementation ease. By utilizing duality, we are able to compute the exact projection coefficients of the infinite basis expansion of f_T, which for the linear basis[4] are given by

$$\beta^{L^2}_{a,k} = \frac{12a^{1/2}}{\pi}\Re\left\{\int_0^\infty \widehat{f}_T(a\xi)\frac{\sin^2(\xi/2)}{\xi^2(2+\cos(\xi))}e^{-iax_k\xi}d\xi\right\}. \quad (59)$$

These coefficients are then calculated simultaneously with complexity $\mathcal{O}(N\log_2(N))$ using the FFT, where N is the number of basis elements, rather than individually as is required by equation (58). For Levy models used in practice (see Figure 43), the trapezoidal rule used in conjunction with the FFT results in exponentially convergent discretization as well as truncation errors[5].

In addition to computational efficiency, our method enjoys the advantages of a compact basis, which is crucial for extensions to path dependent contracts which require repeated density expansions. The extensions derived in [84, 85] build on the theory and underlying algorithms developed in this work.

[3] They also use an infinite basis, for which a series is then truncated. In either case, the resulting approximation corresponds to a representation of f_T with compact support

[4] We will utilize scaling functions centered about the origin, rather than the cardinal splines used in [113].

[5] The exception to exponentially convergent truncation errors is the variance gamma (VG) model when $T \ll 1$.

3.3 Valuation by Basis Duality

In this section we study the valuation problem for models that can be described by the characteristic function of a driving source of randomness. Of particular interest are Heston's stochastic volatility model [79] and models driven by an underlying Levy process (see [46, 121] for a financial background on Levy processes).

3.3.1 Characteristic Function of Risk Neutral Log Return

Consider a Levy process $L(t), t \geq 0$, with *characteristic exponent(symbol)* $\psi_L(\xi) := \ln \mathbb{E}[\exp(i\xi L(1))]$, which is the log characteristic function of the process at $t = 1$. The process increments, $L(t + \Delta_t) - L(t)$, are stationary and independent, and by the Levy-Khintchine theorem the characteristic function satisfies

$$\phi_{L(t)}(\xi) := \mathbb{E}[e^{iL(t)\xi}] = e^{t\psi_L(\xi)}, \quad t \geq 0.$$

Processes of interest in finance satisfy the exponential moment condition $\mathbb{E}[e^{-\alpha L(t)}] < \infty$, $\forall t \geq 0$, where the set of all such α is an interval $\mathcal{I}_L = (\lambda_-, \lambda_+)$, where $-\infty \leq \lambda_- \leq 0 \leq \lambda_+ \leq \infty$, and the endpoints may be included. In particular, as a function of $z = \xi + iw$, $\psi_L(z)$ is complex analytic in the strip[6] $\mathcal{D}_{(\lambda_-,\lambda_+)} := \{z \in \mathbb{C} : \Im(z) \in (\lambda_-, \lambda_+)\}$. This fact will be used to quantify certain approximation errors in the algorithms to follow. Note that for the processes given in Figure 43, $\mathcal{I}_L \supset (-d, d)$ for some $0 < d \leq \infty$.

To model the underlying randomness, we consider exponential Levy processes of the form

$$S(t) = S(0)e^{Y(t)} = S(0)e^{(r-q+\omega)t+L(t)}, \quad \omega = -\psi_L(-i),$$

where $r \geq 0$ and $q \geq 0$ are the interest rate and dividend yeild. One can easily deduce that $\mathbb{E}[S^{-\alpha}(t)] < \infty$ for $\alpha \in \mathcal{I}_L$ and $t > 0$. Here ω is a "convexity correction" that is used to fix a risk-neutral measure, as incomplete markets lead to a spectrum of arbitrage-free pricing measures.

[6]The size of this strip is determined by the Levy measure, ν_L, since $\mathbb{E}[e^{-\alpha L(t)}] < \infty$ for all $t > 0$ if and only if $\int_{|x|\geq 1} e^{-\alpha x}\nu_L(dx) < \infty$, independently of t (see [120], Theorem 25.17).

Table 1: Symbols, parameter restrictions and strip of analyticity $\mathcal{I}_L$ for tractable Levy processes.

Model	$\psi_L(\xi)$	Param. Restrict.	$\mathcal{I}_L$
BSM	$-\frac{\sigma^2}{2}\xi^2$	$\sigma > 0$	$\mathbb{R}$
MJD	$-\frac{\sigma^2}{2}\xi^2 + \lambda\Big(e^{i\xi\mu_J - \frac{\sigma_J^2}{2}\xi^2} - 1\Big)$	$\lambda, \sigma_J, \sigma > 0$	$\mathbb{R}$
CGMY	$C\Gamma(-Y)\left((M-i\xi)^Y - M^Y + (G+i\xi)^Y - G^Y\right)$	$C, G > 0, M > 1$ $Y \in (0,1)\cup(1,2)$	$[-M, G]$
NIG	$-\delta\left(\sqrt{\alpha^2 - (\beta+i\xi)^2} - \sqrt{\alpha^2-\beta^2}\right)$	$\alpha, \delta > 0$ $\beta \in (-\alpha, \alpha-1)$	$[\beta \pm \alpha]$
KOU	$-\frac{\sigma^2}{2}\xi^2 + \lambda\Big(\frac{(1-p)\eta_2}{\eta_2+i\xi} + \frac{p\eta_1}{\eta_1-i\xi} - 1\Big)$	$\lambda, \sigma > 0$, $p \in [0,1]$ $\eta_1 > 1, \eta_2 > 0$	$(-\eta_1, \eta_2)$
VG	$-\frac{\sigma^2}{2}\xi^2 - \frac{1}{\nu}\ln\Big(1 - i\nu\theta\xi + \nu\frac{\sigma_V^2}{2}\xi^2\Big)$	$\nu, \sigma_V > 0$, $\sigma \geq 0$ $\zeta := \sqrt{\frac{\theta^2}{\sigma_V^4} + \frac{2}{\nu\sigma_V^2}}$	$\big[\frac{\theta}{\sigma^2} \pm \zeta\big]$

The characteristic function of $Y(T)$, for which we assume the density $f_T(y)$, is given by

$$\widehat{f}_T(\xi) = e^{i\xi(r-q-\psi_L(-i))T} e^{\psi_L(\xi)T}, \quad T > 0. \tag{60}$$

With the exception of the pure jump VG (ie when $\sigma = 0$), the processes of interest satisfy

$$|\widehat{f}_T(\xi)| = |e^{\psi_L(\xi)T}| \leq \kappa e^{-Tc|\xi|^\nu}, \tag{61}$$

where $c, \kappa > 0$ and $\nu \in (0, 2]$. For any process with a diffusive (Brownian motion) component, $-\frac{\sigma^2}{2}\xi^2$, (193) is satisfied with $\nu = 2$, which is the ideal case from a computational perspective ($\nu = 1$ for NIG while $\nu = Y$ for CGMY, both of the pure jump type). For the pure jump VG, $|\widehat{f}_T(\xi)| = \mathcal{O}(\kappa|\xi|^{-2T/\nu})$, so that $\widehat{f}_T(\xi)$ fails to be integrable for $T \leq \nu/2$.

3.3.2 Density Projection by Duality

To obtain density projections, we restrict our attention to Riesz basis of translates[7], generated by a real-valued function of compact support. In particular, given a compactly supported *generator* φ, and a fixed *resolution* a, we form the *sequence (of translates)* generated by φ, $\{\varphi_{a,k}(x)\}_{k\in\mathbb{Z}} := \{a^{1/2}\varphi(a(x-x_k))\}_{k\in\mathbb{Z}}$, where $x_k := x_1 + (k-1)/a$, $k \in \mathbb{N}$. The point

[7] A Riesz basis is a special type of frame for which representations are unique.

x_1 will be chosen according to the application. The defining property which makes $\{\varphi_{a,k}\}_{k\in\mathbb{Z}}$ a Riesz sequence, or equivalently a Riesz basis for its closed span $\mathcal{M}_a := \overline{\text{span}}\{\varphi_{a,k}\}_{k\in\mathbb{Z}}$, is that

$$A\|f\|^2 \leq \sum_{k\in\mathbb{Z}} |\langle f, \varphi_{a,k}\rangle|^2 \leq B\|f\|^2, \quad \forall f \in L^2(\mathbb{R}), \tag{62}$$

for some $0 < A \leq B$ called the *frame bounds*. We now show how analytical formulas for the orthogonal projections of probability densities are obtained.

For simplicity, we assume that φ is real-valued and symmetric. From the duality theory of Reisz bases [44, 78, 134], to each φ which satisfies (62), there must exist a *dual generator* $\widetilde{\varphi}$ such that for any $f_T \in L^2(\mathbb{R})$, the orthogonal projection of f_T onto $\mathcal{M}_a := \overline{\text{span}}\{\varphi_{a,k}\}_{k\in\mathbb{Z}}$ is given by

$$P_{\mathcal{M}_a} f_T(y) = \sum_{k\in\mathbb{Z}} \left(\int_{-\infty}^{\infty} f_T(x)\overline{\widetilde{\varphi}_{a,k}(x)}dx \right) \varphi_{a,k}(y) = \sum_{k\in\mathbb{Z}} \beta_{a,k}^{L^2} \cdot \varphi_{a,k}(y),$$

where[8] $\beta_{a,k}^{L^2} := \mathbb{E}[\widetilde{\varphi}_{a,k}(Y_T)]$. In fact, $\{\widetilde{\varphi}_{a,k}(x)\}_{k\in\mathbb{Z}} := \{a^{1/2}\widetilde{\varphi}(a(x - x_k))\}_{k\in\mathbb{Z}}$ is itself a Riesz basis for $\mathcal{M}_a$. Obviously, in the special case of orthonormal φ, it holds $\varphi \equiv \widetilde{\varphi}$. In order to derive $\widetilde{\varphi}$, it can be shown that the bounds in (62) are equivalent to

$$A \leq \sum_{k\in\mathbb{Z}} |\widehat{\varphi}(\xi + 2\pi k)|^2 \leq B, \quad \xi \in [0, 2\pi].$$

It then follows that the Fourier transform of $\widetilde{\varphi}$ satisfies

$$\widehat{\widetilde{\varphi}}(\xi) = \frac{\widehat{\varphi}(\xi)}{\mathbf{\Phi}(\xi)}, \qquad \mathbf{\Phi}(\xi) := \sum_{k\in\mathbb{Z}} |\widehat{\varphi}(\xi + 2\pi k)|^2, \quad \xi \in \mathbb{R}. \tag{63}$$

In fact, by the compact support of φ, $\text{supp}(\varphi) \subset [-\alpha, \alpha]$, $\mathbf{\Phi}(\xi)$ is actually a trigonometric polynomial, which by symmetry admits a finite cosine series expansion

$$\mathbf{\Phi}(\xi) = c_0 + 2\sum_{k=1}^{M} c_k \cos(k\xi), \quad c_k = \int_{-\alpha}^{\alpha} \varphi(x)\varphi(x - k)dx, \qquad k = 1, .., M. \tag{64}$$

We are then able to derive exact expressions for $\mathbf{\Phi}(\xi)$ and in turn for the dual transform. In section 3.3.3, explicit formulas for $\mathbf{\Phi}(\xi)$ are given for the B-splines of orders up to three.

[8] The conjugate has been dropped by assuming that φ is real-valued and symmetric.

Hence, denoting by $\bar{\mathcal{F}}(g)(\xi) := \overline{\mathcal{F}(g)(\xi)}$ we have

$$\begin{aligned}\beta_{a,k}^{L^2} &= \int_{-\infty}^{\infty} f_T(x)\overline{\widetilde{\varphi}_{a,k}(x)}dx = a^{1/2}\int_{-\infty}^{\infty} f_T(x)\overline{\widetilde{\varphi}(a(x-x_k))}dx \\ &= \frac{a^{1/2}}{2\pi}\int_{-\infty}^{\infty}\widehat{f}_T(\xi)\bar{\mathcal{F}}[\widetilde{\varphi}(a(\cdot - x_k))](\xi)d\xi \\ &= \frac{a^{-1/2}}{2\pi}\int_{-\infty}^{\infty}\widehat{f}_T(\xi)\exp(-ix_k\xi)\widehat{\widetilde{\varphi}}\Big(\frac{-\xi}{a}\Big)d\xi.\end{aligned}$$

Note that the symmetry and reality of φ imply the same of $\widehat{\widetilde{\varphi}}(\xi/a)$. Moreover, since $\beta_{a,k}^{L^2} = \Re[\beta_{a,k}^{L^2}]$, we have

$$\begin{aligned}\beta_{a,k}^{L^2} &= \frac{a^{-1/2}}{2\pi}\Re\left\{\int_{-\infty}^{\infty}\widehat{f}_T(\xi)\exp(-ix_k\xi)\widehat{\widetilde{\varphi}}\Big(\frac{-\xi}{a}\Big)d\xi\right\} \\ &= \frac{a^{-1/2}}{2\pi}\left(\Re\left\{\int_{-\infty}^{0}\overline{e^{-ix_k\xi}\widehat{f}_T(\xi)\widehat{\widetilde{\varphi}}\Big(\frac{-\xi}{a}\Big)}d\xi\right\} + \Re\left\{\int_0^{\infty}e^{-ix_k\xi}\widehat{f}_T(\xi)\widehat{\widetilde{\varphi}}\Big(\frac{-\xi}{a}\Big)d\xi\right\}\right) \\ &= \frac{a^{-1/2}}{\pi}\Re\left\{\int_0^{\infty}\exp(-ix_k\xi)\cdot\widehat{f}_T(\xi)\widehat{\widetilde{\varphi}}\Big(\frac{\xi}{a}\Big)d\xi\right\}. \qquad (65)\end{aligned}$$

Given the coefficients $\{\beta_{a,k}^{L^2}\}_{k\in\mathbb{Z}}$, the value of a $T-$expiry European contract $g(S_T)$, as a function of the currently observed price S_0, is given by

$$\begin{aligned}\mathcal{V}\circ g(S_0) &= e^{-rT}\int_{-\infty}^{\infty} g(S_0e^y)f_T(y)dy \\ &\approx e^{-rT}\sum_{k\in\mathbb{Z}}\beta_{a,k}^{L^2}\int_{-\infty}^{\infty}\varphi_{a,k}(y)g(S_0e^y)dy, \qquad (66)\end{aligned}$$

where $r, q \geq 0$ are the continuous interest rate and dividend yield, fixed over $[0, T]$.

Before stating the main proposition, we define $\mathcal{H}(\mathcal{D}_d)$ to be the set of analytic functions in the strip $\mathcal{D}_d = \{z \in \mathbb{C} : \Im(z) \in (-d, d)\}$ which satisfy

$$\int_{-d}^{d}|h(x+iy)|dy \to 0, \quad \text{as } |x| \to \infty.$$

For $h \in \mathcal{H}(\mathcal{D}_d)$, we define the Hardy norm

$$\|h\|^{\mathcal{H}_d} := \lim_{\epsilon\to 0^+}\left[\int_{\mathbb{R}}|h(x+i(d-\epsilon))|dx + \int_{\mathbb{R}}|h(x-i(d-\epsilon))|dx\right].$$

By considering Fourier integrals on the real line, we obtain the following result, which is a simple corollary of Theorem 3.2.1 in [123] (see also [67] for applications to the Hilbert transform).

Lemma 3.3.1. *Suppose that $h \in \mathcal{H}(\mathcal{D}_d)$ for some $d > 0$. Fix $a = 2^P$ and $\bar{a} = 2^{\bar{P}}$, $P, \bar{P} \in \mathbb{N}$. Then for $\Delta_\xi := 2\pi/\bar{a}$ and $x \in \mathbb{R}$, we have*

$$\left| \Delta_\xi \sum_{j=-\infty}^{\infty} e^{ix\xi_j} h(\xi_j) - \int_{\mathbb{R}} e^{ix\xi} h(\xi) d\xi \right| \leq \frac{e^{-(\bar{a}-|x|)d}}{1 - e^{-\bar{a}d}} \|h\|^{\mathcal{H}_d}. \tag{67}$$

By combining this with the expression derived for $\beta_{a,k}^{L^2}$, we have the following result.

Proposition 3.3.1. *Suppose that φ is a compactly supported Riesz generator, real-valued and symmetric about the origin. Given the characteristic function $\widehat{f}_T(\xi)$ of a density $f_T \in L^2(\mathbb{R})$, we have the following.*

(i) For any resolution $a > 0$, the orthogonal projection coefficients satisfy

$$\beta_{a,k}^{L^2} = \frac{a^{-1/2}}{\pi} \Re \left\{ \int_0^\infty \exp(-ix_k\xi) \cdot \widehat{f}_T(\xi) \frac{\widehat{\varphi}(\xi/a)}{\mathbf{\Phi}(\xi/a)} d\xi \right\}, \qquad k \in \mathbb{Z}.$$

(ii) For some $\eta > 0$, $\widehat{\widetilde{\varphi}}(z)$ is analytic in the strip $\mathcal{D}_\eta$, and satisfies $|\widehat{\widetilde{\varphi}}(z)| \leq C_\eta(\varphi)$ uniformly on $\mathcal{D}_\eta$, where $0 < C_\eta(\varphi) < \infty$.

(iii) If in addition, $\widehat{f}_T(z) \in \mathcal{H}(\mathcal{D}_d)$, then for some $0 < C(f_T) \leq C_{\eta \wedge d}(\varphi) \|\widehat{f}_T\|^{\mathcal{H}_d}$ and $0 < \gamma(a) \leq d$,

$$\left| \beta_{a,k}^{L^2} - \Delta_\xi {\sum}'_{j \geq 0} e^{-ix_k\xi_j} \widehat{f}_T(\xi_j) \widehat{\widetilde{\varphi}}(\xi_j/a) \right| \leq \frac{e^{-(\bar{a}-|x_k|)\gamma(a)}}{1 - e^{-\bar{a}\gamma(a)}} \frac{C(f_T)}{\pi a^{1/2}},$$

where $\bar{a} > 0$, $\Delta_\xi := 2\pi/\bar{a}$, and $\xi_j = (j-1)\Delta_\xi$, and the summation prime indicates the first term should be halved. Hence the trapezoidal rule results in exponentially convergent discretization errors. Moreover, $\gamma(a)$ can be made arbitrarily close to d for a sufficiently large.

Proof. The first claim follows immediately from equation (65). To prove the second, note first that by compactness of φ,

$$\begin{aligned} \mathbf{\Phi}(\xi + i\eta) &= c_0 + 2 \sum_{k=1}^{M} c_k \cos(k(\xi + i\eta)) \\ &= c_0 + \sum_{k=1}^{M} c_k \cos(k\xi) \left(e^{k\eta} + e^{-k\eta} \right) + i \sum_{k=1}^{M} c_k \sin(k\xi) \left(e^{-k\eta} - e^{k\eta} \right), \end{aligned} \tag{68}$$

and let $A > 0$ be the corresponding lower frame bound. For $\nu > 0$, define $\Gamma_\nu := \{z \in \mathbb{C} : \Re[z] \in [0, 2\pi], \Im[z] \in [-\nu, \nu]\}$. It follows that $\Phi(\xi + i\eta)$ has finitely many zeros on any compact set of the form Γ_ν (else its null set has an accumulation point, from which $\Phi \equiv 0$ on Γ_ν, contradicting $\Phi(\xi + i\eta) \geq A$ for $\eta = 0$), and in particular no point on Γ_0 is an accumulation point of its null set. Since $\Phi(z)$ is complex analytic as trigonometric polynomial with $\Phi(\Gamma_0) \geq A > 0$, by uniform continuity in η, ξ there exists $\gamma > 0$ such that $\Phi(z) > 0$ on Γ_γ. With $\eta \leq \gamma$ fixed, we see from equation (68) that $\Re[\mathbf{\Phi}(\xi + i\eta)]$ is 2π periodic in ξ, from which the set Γ_γ can be extended horizontally to the strip $\mathcal{D}_\gamma$, on which $\Phi(z)$ is bounded below. Now consider

$$\widehat{\varphi}(\xi + i\eta) = \int_{[-\alpha,\alpha]} \varphi(x) e^{ix\xi} e^{-x\eta} dx \leq e^{\alpha|\eta|} \int_{[-\alpha,\alpha]} |\varphi(x)| dx, \tag{69}$$

again by the compactness of φ. Hence, $\widehat{\widetilde{\varphi}}(\xi + i\eta) = \widehat{\varphi}(\xi + i\eta)/\mathbf{\Phi}(\xi + i\eta)$ can be bounded above on $\mathcal{D}_\gamma$. Thus, the Hardy norm of $\widehat{\widetilde{\varphi}}(\xi/a)\widehat{f}_T(\xi)$ can be bounded above by a constant multiple of $\|\widehat{f}_T\|^{\mathcal{H}_d}$. Analyticity of the product in a common strip allows us to apply Lemma 3.3.1, and the final claim follows. □

In order apply the FFT to compute $\beta^{L^2}_{a,k}$, we fix a resolution $a = 2^P$ ($\Delta = \Delta_x = 1/a$), and a truncation parameter $\bar{a} = 2^{\bar{P}}$, $P, \bar{P} \in \mathbb{N}$, which will be discussed in section 3.4. In what follows, $\mathcal{D}$ denotes the discrete Fourier transform (DFT) of a vector:

$$\mathcal{D}_n\{y_j\} = \sum_{j=1}^{N} e^{-i\frac{2\pi}{N}(j-1)(n-1)} y_j, \quad n = 1, ..., N.$$

The trapezoidal approximation of the coefficients over $x_k = x_1 + (k-1)\Delta_x$, $k = 1, ..., N$, is given by

$$\begin{aligned}
\beta^{L^2}_{a,k} &\approx \frac{a^{-1/2}}{\pi} \Re \left\{ \sum_{j=1}^{N} \exp(-ix_k\xi_j) \cdot \widehat{f}_T(\xi_j) \widehat{\widetilde{\varphi}}\Big(\frac{\xi_j}{a}\Big) v_j \Delta_\xi \right\} \\
&= \frac{a^{-1/2}}{\pi} \Re \sum_{j=1}^{N} e^{-i(j-1)(k-1)\Delta_x\Delta_\xi} \cdot e^{-ix_1(j-1)\Delta_\xi} \widehat{f}_T(\xi_j) \widehat{\widetilde{\varphi}}\Big(\frac{\xi_j}{a}\Big) v_j \Delta_\xi \\
&= \frac{2a^{1/2}}{N} \Re \sum_{j=1}^{N} e^{-i\frac{2\pi}{N}(j-1)(k-1)} F_j,
\end{aligned} \tag{70}$$

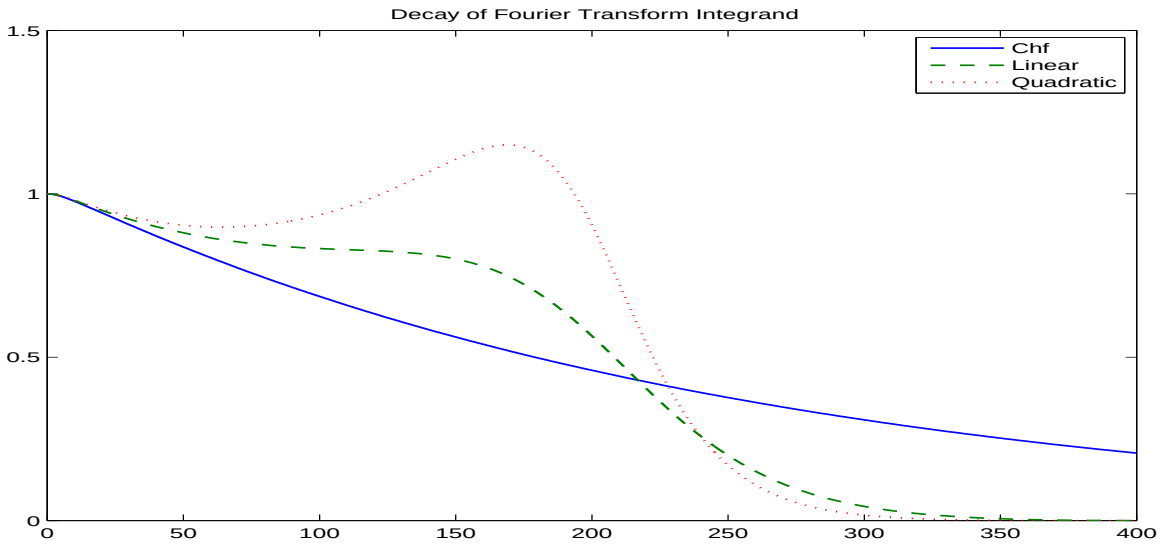

Figure 1: Integrand decay under Normal Inverse Gaussian model, $T = .01$. Modulus of characteristic function (Chf), $\widehat{f}(\xi_j)$, versus the Fourier transform integrands used in linear and quadratic projection, $\widehat{f}(\xi_j)\widehat{\widetilde{\varphi}}(\xi_j/a)$, where $\xi_j \in [0, 2\pi a)$, at a spacing $\Delta_\xi = 2\pi/\bar{a}$, with $\bar{a} = 2^2$, $a = 2^6$.

so that $\beta^{L^2}_{a,k} \approx \widetilde{\beta}_{a,k}$ where

$$\widetilde{\beta}_{a,k} := \frac{2a^{1/2}}{N}\Re[\mathcal{D}_n\{F_j\}_{j=1}^N], \qquad F_j := \exp\left(-ix_1\xi_j\right)\widehat{f}_T(\xi_j)\cdot\widehat{\widetilde{\varphi}}(\xi_j/a)v_j, \tag{71}$$

and $\nu_j := 1 - (\delta_{j,1} + \delta_{j,N})/2$ (although in practice we can safely neglect $\delta_{j,N}$). The discrete transform approximation to $\beta^{L^2}_{a,k}$ is analyzed in detail in the error analysis. We next develop the application of duality to density projection onto members of the B-spline class.

3.3.3 Orthogonal Projection Onto B-Splines

Starting with the Haar scaling function $\varphi^{[0]}(y) := \mathbb{1}_{[-\frac{1}{2},\frac{1}{2}]}(y)$, we can define the p-th order B-splines successively by the convolution

$$\varphi^{[p]}(x) = \varphi^{[0]} \star \varphi^{[p-1]}(x) = \int_{-\infty}^{\infty} \varphi^{[p-1]}(y-x)\mathbb{1}_{[-\frac{1}{2},\frac{1}{2}]}(y)dy,$$

from which it is derived that

$$\widehat{\varphi}^{[p]}(\xi) = \left(\frac{\sin(\xi/2)}{(\xi/2)}\right)^{p+1}, \quad \widehat{\varphi}^{[p]}(0) = \int_{-\infty}^{\infty}\varphi^{[p]}(x)dx = 1. \tag{72}$$

Since $\text{supp}(\varphi^{[p]}) = \left[-\frac{p+1}{2}, \frac{p+1}{2}\right]$, it follows that

$$\mathbf{\Phi}^p(\xi) = c_0^p + 2\sum_{k=1}^{p+1} c_k^p \cos(k\xi), \quad c_k^p = \int_{-\frac{p+1}{2}}^{\frac{p+1}{2}} \varphi^{[p]}(x)\varphi^{[p]}(x-k)dx, \tag{73}$$

for $k = 1, .., p+1$. For example, we derive

$$\begin{aligned}
\mathbf{\Phi}^0(\xi) &= 1 \\
\mathbf{\Phi}^1(\xi) &= \frac{1}{3}(2 + \cos(\xi)) \\
\mathbf{\Phi}^2(\xi) &= \frac{1}{60}\left(33 + 26\cos(\xi) + \cos(2\xi)\right) \\
\mathbf{\Phi}^3(\xi) &= \frac{1}{2520}\left(1208 + 1191\cos(\xi) + 120\cos(2\xi) + \cos(3\xi)\right),
\end{aligned}$$

and similarly for higher orders. An immediate benefit of the use of frame duality is illustrated in figure 1. Direct integration requires a much larger truncation integral in the Fourier domain, whereas the integrands prescribed by linear and quadratic projection exhibit rapid decay and a truncation error reduction. Note too that $\widehat{\widetilde{\varphi}}(\xi_j/a) = \widehat{\widetilde{\varphi}}(2\pi(j-1)/\bar{a})$, so its shape is unaffected by the choice of a. Hence, to control the source of error caused by truncating in the Fourier domain, a model independent choice is to fix $a \geq \tilde{a}$, where $\widehat{\widetilde{\varphi}}(2\pi\tilde{a}) < TOL$.

The following proposition, proved in [127] (see also [128]), justifies the observation that at coarse resolutions, orthogonal projection onto a B-spline basis behaves as that of an interpolation with twice the order of accuracy. For this reason, using just piecewise linear and quadratic bases, we typically observe rapid initial convergence, followed by an eventual approach to the asymptotic regime. For lower order B-splines, this property facilitates their ability to provide accurate approximations at a low cost. We denote by W_2^L the space of functions whose first L derivatives exist in the $L^2(\mathbb{R})$ sense.

Proposition 3.3.2. *[127] If for $m = 0, ..., L-1$, $\widehat{\varphi}^{(m)}(2\pi k) = 0$, $k \in \mathbb{Z}$, $k \neq 0$, then for a constant $K_{\varphi,2L}$, it holds $\forall f \in W_2^L$*

$$\|f - P_{\mathcal{M}_a} f\|_2 \leq K_{\varphi,2L} \cdot \Delta^{2L} \cdot \|f^{(2L)}\|_2 + K_{\varphi,2L}^{1/2} \cdot \Delta^L \cdot \|f^{(L)}\|_2, \tag{74}$$

where $\mathcal{M}_a = \mathcal{M}_a(\varphi) := \overline{span}\{\varphi_{a,k}\}_{k\in\mathbb{Z}}$.

Clearly, for small enough Δ, the error is dominated by the order $\mathcal{O}(\Delta^L)$ term, but only after enjoying an initially rapid decay. In particular, this result applies to the p-th order B-splines with generator $\varphi^{[p]}$ where $L = p$.

Remark 3. We also note that, for characteristic functions satisfying equation (193), ie those in Figure 43 with the exception of the pure jump VG model, the coefficient errors can be bounded by

$$|\beta_{a,k}^{L^2} - \widetilde{\beta}_{a,k}| \leq \frac{a^{-1/2}}{\pi}\left(\frac{\kappa \cdot C_p(a)}{p \cdot (2\pi)^p} \cdot \exp(-Tc \cdot (2\pi a)^\nu) + \frac{e^{-(\bar{a}-|x_k|)\gamma(a)}}{1-e^{-\bar{a}\gamma(a)}} C(f_T)\right),$$

where $C_p(a) = \mathcal{O}(a)$, as discussed in the error analysis, and the other constants are as in Proposition 3.3.1. Hence, with $\bar{a}$ fixed sufficiently large, the convergence is exponential in a. It then follows from Proposition 3.3.2 that for a modest choice of a, the projection errors will dominate (this will be made more precise in the error analysis). Consequently, our ability to control the sources of error is not significantly restricted by the Nyquist relation, which entangles the grids in the Fourier and state space. In fact, this relationship simplifies the implementation by reducing the number of user supplied inputs.

3.4 Valuation with the Piecewise Linear Basis

At a fixed resolution a, the piecewise linear approximation space is spanned by the functions $\{\varphi_{a,n}\}_{n\in\mathbb{Z}}$ given by

$$\varphi_{a,n}(y) = \begin{cases} a^{3/2}\left[y - \left(x_1 + \frac{n-2}{a}\right)\right] & \text{if } y \in \left[x_1 + \frac{n-2}{a}, x_1 + \frac{n-1}{a}\right] \\ a^{3/2}\left[\left(x_1 + \frac{n}{a}\right) - y\right] & \text{if } y \in \left[x_1 + \frac{n-1}{a}, x_1 + \frac{n}{a}\right], \end{cases} \tag{75}$$

so that $\varphi_{a,n}(y)$ is centered over $x_n = x_1 + (n-1)/a$. As discussed below, $x_1 \in \mathbb{R}$ and $N \in \mathbb{N}$ are chosen so that $\{\varphi_{a,n}\}_{n=1}^N$ corresponds to a finite dimensional approximation. Note too that $\sum_{k=1}^N \beta_{a,k}^{L^2}\varphi_{a,k}$ is the orthogonal projection of $P_{\mathcal{M}_a} f_T$ onto $\{\varphi_{a,n}\}_{n=1}^N$. Rather than approximate $f_T(y)\mathbb{1}_{[l,u]}$, the approach of restricting the infinite dimensional projection avoids Gibbs oscillations in this respect.

3.4.1 The Valuation Formula

The Fourier transform of the dual generator is found from equations (110) and (73) to satisfy

$$\widehat{\widetilde{\varphi}}^{[1]}(\xi) = \frac{12\sin^2(\xi/2)}{\xi^2(2+\cos(\xi))},$$

from which the frame projection coefficients (beta) can be determined.

In order to simplify constants in the final valuation formula, we define

$$\bar{\beta} := \Re[\mathcal{D}\{H_j\}_{j=1}^{N}], \tag{76}$$

where

$$H_1 = 1/24a^2, \quad H_j = \exp(-ix_1\xi_j) \cdot \widehat{f_T}(\xi_j) \cdot \frac{\sin^2(\xi_j/2a)}{\xi_j^2(2+\cos(\xi_j/a))} \quad j \geq 2. \tag{77}$$

We now define $\bar{N} \leq N$ according to two approaches. In the first, assuming that the density is centered near its mean, $\bar{N} = N$ can be safely chosen. This approach is used for barrier and Asian option pricing in [84,85]. However, we often find it convenient to fix x_1 according to the extreme strike in a set of options, in which case $\bar{N} := N/2$, in order to avoid wrap-around effects (caused by setting one of the support boundaries at a point of relatively high mass). After simplifying constants, the valuation formula in equation (66) becomes

$$\mathcal{V}_{\bar{N}} \circ g := \frac{24a^2e^{-rT}}{N} \sum_{n=1}^{\bar{N}} \bar{\beta}_{a,n} \cdot g_{a,n}, \tag{78}$$

where

$$g_{a,n} := a^{1/2} \int_{x_{n-1}}^{x_{n+1}} \varphi_{a,n}(y) g(S_0 e^y) dy, \quad n = 1, ...\bar{N}. \tag{79}$$

As an empirically conservative rule of thumb, if the resolution is chosen as $a = 2^P$ for some $P \in \mathbb{N}$, for *European* options we select $N, \bar{N}$ according to

$$T \in [.1, 1] : \bar{N} = 2^{P+3}, \qquad T < .1 : \bar{N} = 2^{P+2}, \tag{80}$$

and $N = 2\bar{N}$. Again, this is chosen to simplify the implementation as much as possible. More explicit bounds can be derived (see [61] for a cumulant based prescription), which are especially recommended for large $T \gg 1$. Depending on the application, one may wish to choose a more or less conservative interval, or apply an adaptive procedure by which the magnitudes of $\bar{\beta}_{a,1}$ and $\bar{\beta}_{a,N}$ are used a stopping criteria.

To derive payoff coefficients with respect to the linear basis, we introduce the following functions:

$$\varphi^L(y) := y + 1, \quad \text{and} \quad \varphi^R(y) := 1 - y,$$

which represent the left and right portions of φ on $[-1,1]$. Moreover, the following integrals will be needed:

$$\vartheta_L(\gamma_1,\gamma_2) := \int_{\gamma_1}^{\gamma_2} e^{\frac{y}{a}}\varphi^L(y)dy, \qquad \bar{\vartheta}_L(\gamma_1,\gamma_2) := \int_{\gamma_1}^{\gamma_2} \varphi^L(y)dy. \tag{81}$$

The integrals ϑ_R and $\bar{\vartheta}_R$ are defined analogously.

3.4.2 Geometric Asian Options

We now consider a path-dependent option, the geometric Asian option,[9] which is priced efficiently by a linear basis implementation of PROJ. Given a uniform set of monitoring dates, $t_m = (m-1)\frac{T}{M}$, $m = 1,...,M+1$, at which the prices $S_m := S(t_m)$ are to be observed, Asian contracts with geometric averaging are payoffs contingent on

$$G_M := \left(\prod_{m=0}^{M} S_m\right)^{\frac{1}{M+1}}.$$

These products are priced analogously to European options, since the characteristic function of $\ln(G_M)$ is explicitly available. Namely, with

$$L_M := \ln(G_M) = \frac{1}{M+1}\sum_{m=0}^{M}\ln(S_m),$$

independence of increments can be used to derive (see [69]) the chf $\widehat{f}_{L_M}(\xi;\ln(S_0)) := \mathbb{E}\left[e^{i\xi L_M}|\ln(S_0)\right]$, which satisfies

$$\begin{aligned}\widehat{f}_{L_M}(\xi) &= e^{i\xi\ln(S_0)}\prod_{m=1}^{M}\widehat{f}_{\Delta_t}\left(\xi\frac{M+1-m}{M+1}\right)\\ &= \exp\left(i\xi\left(\ln(S_0)+\frac{T}{2}(r-q-\psi_L(-i))\right)+\frac{T}{M}\sum_{m=1}^{M}\psi_L\left(\xi\frac{M+1-m}{M+1}\right)\right),\end{aligned}$$

where $\widehat{f}_{\Delta_t}$ is defined as in equation (108). Fixed strike Asian option payoffs are then expressed as

$$g(L_M) := \begin{cases}\left(e^{L_M}-W\right)\mathbb{1}_{[L_M\geq\ln(W)]}, & \text{for a call,}\\ \left(W-e^{L_M}\right)\mathbb{1}_{[L_M\leq\ln(W)]}, & \text{for a put.}\end{cases} \tag{82}$$

[9] Geometric Asian options are often used as control variates in Monte Carlo methods for their arithmetic counterparts. Using them as such requires that we can price geometric Asian options efficiently.

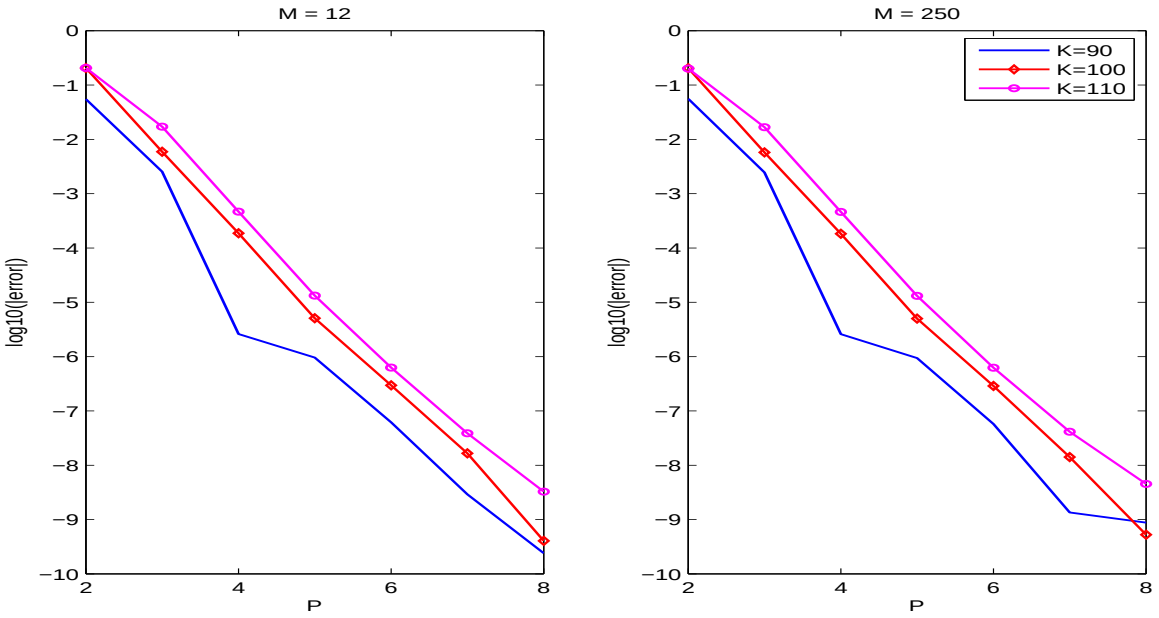

Figure 2: Geometric Asian options priced by PROJ under the Normal Inverse Gaussian model. Parameters and reference values as in [69]: $S_0 = 100, T = 1, r = 0.0367$, and NIG parameters: $\alpha = 6.1882, \beta = -3.8941, \delta = .1622$.

Hence, given an approximation to $f_{L_M}(u; S_0)$, it follows e.g for a call

$$\mathcal{V} \circ g(S_0) = e^{-rT} \int_{\ln(W)}^{\infty} \left(e^{L_M} - W\right) f_{L_M}(u; S_0) du. \tag{83}$$

Remark 4. There are two approaches to determine the point about which we expand f_{L_M} by frame projection. The first is to center the density about $\mathbb{E}[L_M]$, which can be found by

$$\mathbb{E}[L_M] = \frac{1}{M+1}\mathbb{E}\left[(M+1)\ln(S_0) + \sum_{m=1}^{M} \ln\left(\frac{S_m}{S_0}\right)\right] = \ln(S_0) + \frac{T}{2}\mu,$$

where $\mu = \mathbb{E}[S_{t+1}/S_t]$. We then perturb $\mathbb{E}[L_M]$ slightly so that $\ln(W)$ belongs to the grid. The second approach is to fix the initial grid point by $x_1 := \ln(W)$. To account for the periodicity of the discrete Fourier transform, only the first $N/2$ coefficients should be used to determine the price with the second approach. In either case, the payoff coefficients are simple to calculate.

3.4.2.1 A Numerical Example

For example, fixing $x_1 := \ln(W)$, we approximate the geometric Asian call value by equation (78) where

$$g_{a,1} := \exp(x_1) \cdot a\left(a(e^{\Delta} - 1) - 1\right) - W,$$

and

$$g_{a,n} := \frac{\exp(x_n)}{3}\left(1 + e^{\frac{\Delta}{2}} + e^{-\frac{\Delta}{2}}\right), \quad n = 2, ..., \bar{N} = N/2.$$

Specifying the Normal Inverse Gaussian model (NIG), discussed in section 3.7.5, we validate the reference prices given in [69] to the precision provided (up to six decimals), after which PROJ with $a = 2^{11}, \bar{a} = 2^{\bar{P}} = 2^4$ is used to obtain further precision. The convergence for three strikes and maturities $M \in \{12, 250\}$ are given in figure 2. Not only is a practical level of precision reached rapidly, we see that doubling the resolution reduces the error ten-fold. A similar convergence rate is observed for the extension of PROJ to arithmetic Asian options [84]. Since the chf of L_M is relatively expensive to compute, zero padding can be used to obtain coefficients at higher resolutions, without further samples from the chf.

Remark 5. We also note that by [69], floating strike geometric options (with $\alpha = \pm 1$) are priced according to

$$\begin{aligned} e^{-rT}\mathbb{E}(\alpha(G_M - WS_M))^+ =& e^{-rT}S_0 \cdot \mathbb{E}\left(\alpha\frac{S_M}{S_0}\left(\frac{G_M}{S_M} - W\right)\right)^+ \\ &= e^{-rT}S_0 \cdot \widetilde{\mathbb{E}}\left(\alpha\left(e^{\widetilde{L}_M} - W\right)\right)^+, \end{aligned}$$

where under the change of numeraire the variable $\widetilde{L}_M := \ln(G_M/S_M)$ has characteristic function

$$\phi_{\widetilde{L}_M}(\xi) = \exp\left(-i\xi(r - q + \psi(i))\frac{T}{2} + \Delta_t \sum_{m=1}^{M} \psi\left(-\xi\frac{m}{M+1}\right)\right).$$

The same pricing technique then applies.

3.4.3 Pricing Multiple Vanilla Options Simultaneously

Since much of the computational overhead is due to the determination of $\bar{\beta}$, this cost can be spread across multiple payoffs by pricing them together, where $\bar{\beta}$ is computed once after initialization. The result is an efficient means of vanilla pricing to accompany calibration procedures and to expedite the valuation of large portfolios.

Let $W := \{W_1, ...W_K\}$ denote the strike set of a basket of call options on S_T, so that

$$g_{W_k}(S_0e^{Y_T}) := (S_0e^{Y_T} - W_k)^+ = (S_0e^{Y_T} - W_k)\mathbb{1}_{Y_T \geq \ln(W_k/S_0)}, \quad k = 1, ..., K.$$

With $x_n = x_1 + (n-1)/a$, $n = 1, ..., \bar{N}$, we determine for each W_k the smallest index n for which the supports of $\varphi_{a,n}$ and g_{W_k} overlap, and denote this index by $n(k)$. Hence $n(k)$ satisfies

$$x_1 + (n(k)-1)/a \leq \ln(W_k/S_0) < x_1 + n(k)/a,$$

so that

$$n(k) := \lfloor a(\ln(W_k/S_0) - x_1) + 1 \rfloor, \quad k = 1, ..., K.$$

We thus define the matrix G as follows:

$$G_{k,n} := a^{1/2} \int_{x_{n-1}}^{x_{n+1}} \varphi_{a,n}(y) g_{W_k}(S_0 e^y) dy = \begin{cases} 0, & n \leq n(k) - 1 \\ I_1(k,n), & n = n(k) \\ I_2(k,n), & n = n(k)+1 \\ I_3(k,n), & n \geq n(k)+2 \end{cases}$$

By our choice of x_1, this results in an upper triangle structure for G, with $G_{1,1}$ nonzero. With

$$d_k := x_{n(k)+1} - \ln(W_k/S_0) + 1, \quad \Delta := 1/a,$$

we have the following:

Result 3.4.1. *The values* $\boldsymbol{\mathcal{V}}_{\bar{N}} \circ g_W := [\mathcal{V}_{\bar{N}} \circ g_{W_1}, ..., \mathcal{V}_{\bar{N}} \circ g_{W_K}]^\top$ *are computed with complexity* $\mathcal{O}(K\bar{N} + N \log_2 N)$ *using*

$$\boldsymbol{\mathcal{V}}_{\bar{N}} \circ g_W = \frac{24a^2 e^{-rT}}{N} G\{\bar{\beta}\}_{n=1}^{\bar{N}}, \tag{84}$$

where $G_{k,n}$ *satisfy*

$$I_1(k,n) = a^2 \left(S_0 \exp(x_{n+1}) - \frac{W_k}{2} \left(d_k^2 + 1 \right) \right), \quad n = n(k) \tag{85}$$

$$I_2(k,n) = a^2 \left(S_0 \exp(x_n) \left(e^{\Delta} - 2 \right) + \frac{W_k}{2} \left((d_k - \Delta)^2 - 2\Delta^2 + 1 \right) \right), n = n(k)+1 \tag{86}$$

$$I_3(k,n) = a^2 S_0 \exp(x_{n-1}) \left(1 - 2e^{\Delta} + e^{2\Delta} \right) - W_k, \quad n = n(k)+2, ..., \bar{N}. \tag{87}$$

As shown in the error analysis, $|\boldsymbol{\mathcal{V}}_{\bar{N}} \circ g_W - \boldsymbol{\mathcal{V}} \circ g_W| \sim \mathcal{O}(\Delta^2)$*, while for coarser scales,* $O(\Delta^4)$ *governs the decay. When* K *is large, the complexity is* $\mathcal{O}(K\bar{N})$ *for a fixed choice of* N*.*

Proof. We outline here the strategy used to evaluate G, which can be followed to derive coefficients for various other payoffs (e.g. digitals) as well as "Greeks." With $l_k := \ln(W_k/S_0)$ and $c_k := a(l_k - x_{n(k)})$ we can compute $I_1 = I_1(k, n(k))$ for each k and $n(k)$:

$$\begin{aligned} I_1 &= a^{1/2} \int_{l_k}^{x_{n(k)+1}} a^{1/2} \varphi(a(y - x_{n(k)}))(S_0 e^y - W_k) dy \\ &= \int_{c_k}^{1} \varphi^R(y)(S_0 e^{x_{n(k)}} e^{\frac{y}{a}} - W_k) dy = S_0 e^{x_{n(k)}} \vartheta_R(c_k, 1) - W_k \bar{\vartheta}_R(c_k, 1), \end{aligned}$$

which follows from a change of variables. Similarly, defining $\bar{c}_k := a(l_k - x_{n(k)+1})$, $I_2 = I_2(k, n(k)+1)$ is given by

$$\begin{aligned} I_2 &= a^{1/2} \int_{l_k}^{x_{n(k)+2}} a^{1/2} \varphi(a(y - x_{n(k)+1}))(S_0 e^y - W_k) dy \\ &= \int_{\bar{c}_k}^{0} \varphi^L(y)(S_0 e^{x_{n(k)+1}} e^{\frac{y}{a}} - W_k) dy + \int_{0}^{1} \varphi^R(y)(S_0 e^{x_{n(k)+1}} e^{\frac{y}{a}} - W_k) dy \\ &= S_0 e^{x_{n(k)+1}} (\vartheta_L(\bar{c}_k, 0) + \vartheta_R(0, 1)) - W_k (\bar{\vartheta}_L(\bar{c}_k, 0) + \bar{\vartheta}_R(0, 1)). \end{aligned}$$

For the final integral,

$$\begin{aligned} I_3(k, n) &= a^{1/2} \int_{x_{n-1}}^{x_{n+1}} a^{1/2} \varphi(a(y - x_n))(S_0 e^y - W_k) dy \\ &= S_0 e^{x_n} (\vartheta_L(-1, 0) + \vartheta_R(0, 1)) - W_k (\bar{\vartheta}_L(-1, 0) + \bar{\vartheta}_R(0, 1)), \end{aligned}$$

for each k and for $n = n(k) + 2, ..., \bar{N}$.

Simple calculus then yields the integrals in (81)

$$\vartheta_L(\gamma_1, \gamma_2) = a(a - (1 + \gamma_1)) e^{\frac{\gamma_1}{a}} + a(-a + (1 + \gamma_2)) e^{\frac{\gamma_2}{a}},$$

$$\vartheta_R(\gamma_1, \gamma_2) = a(-a + (\gamma_1 - 1)) e^{\frac{\gamma_1}{a}} + a(a - (\gamma_2 - 1)) e^{\frac{\gamma_2}{a}},$$

$$\bar{\vartheta}_L(\gamma_1, \gamma_2) = \frac{1}{2}(\gamma_2^2 - \gamma_1^2) + \gamma_2 - \gamma_1, \quad \text{and} \quad \bar{\vartheta}_R(\gamma_1, \gamma_2) = \frac{1}{2}(\gamma_1^2 - \gamma_2^2) + \gamma_2 - \gamma_1.$$

After evaluating these expressions at the required points and rearranging, one obtains the formulas given above. □

Remark 6. In addition to the upper triangular structure of G, inspection of equation (87) reveals an important feature of the method. The values $\{S_0 \exp(x_n)\}_{n=1}^{\bar{N}}$ can be calculated

at initialization, independent of the number K of strikes, so the cost of populating G grows very slowly with K.

In practice, we utilize an equally simple approximate formula for equation (87), which is discussed next. Generally, European call options are priced most effectively by put-call parity, a technique reviewed shortly in this context. However, we have found the direct approach to be successful at pricing knock-out barrier options.

3.4.3.1 Approximation of Payoff Coefficients

As the resolution increases, numerical errors can become non-negligible when computing the $I_j(k,n)$. For example, in equation (87), $1 - 2e^{\Delta} + e^{2\Delta} \approx 1 - 1$ for small Δ. At high resolutions one can safely apply the following Simpson's approximation to the integrals in (79):

$$\begin{aligned} g_n &= a^{1/2}\left[\int_{x_{n-1}}^{x_n} a^{3/2}(y - x_{n-1})g(S_0e^y)dy + \int_{x_n}^{x_{n+1}} a^{3/2}(x_{n+1} - y)g(S_0e^y)dy\right] \\ &\approx \frac{1}{3}\left[g\left(S_0e^{x_n - 1/2a}\right) + g\left(S_0e^{x_n}\right) + g\left(S_0e^{x_n + 1/2a}\right)\right]. \end{aligned}$$

Though it is not always the case, the application of Simpson's rule can result in accurate approximations which are less prone to numerical error at high resolutions. For a call option with strike W_k, the approximation becomes:

$$I_3(k,n) \approx \frac{1}{3}\left(S_0\exp(x_n)\left(1 + e^{\Delta/2} + e^{-\Delta/2}\right) - 3W_k\right), \tag{88}$$

which is numerically superior to the exact solution given by equation (87), since the subtraction of terms with similar magnitudes has been replaced by addition. We find that (88) provides comparable results at lower resolutions, so we use this approximation in general.

3.4.4 Efficient Computation of Greeks

The allure of closed form expressions for option values is due partially to the ability to compute portfolio sensitives quickly and easily, so that traders may engage in various hedging practices as market information updates. Using the PROJ method, one can obtain "Greeks" efficiently and simultaneously for many strikes.

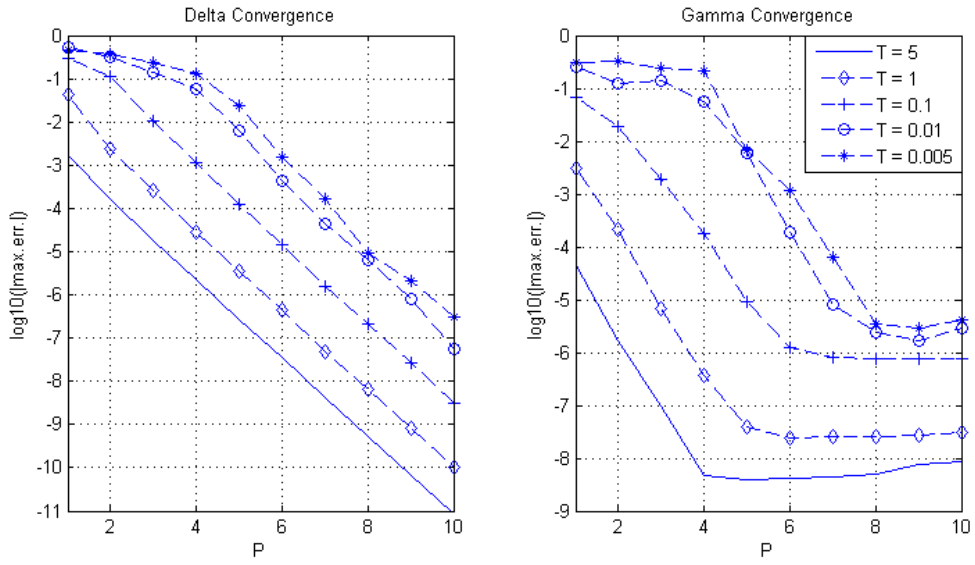

Figure 3: Greeks: convergence of Deltas (left) and Gammas (right) in BSM model for various maturities T. Log of maximum absolute error taken over 50 strikes centered about $S_0 = 50$, with $r = 0.05$ and volatility $\sigma = 0.3$.

To obtain the portfolio "Delta", denoted $\mathbf{\Delta}$ (to distinguish from $\Delta := 1/a$), we formally differentiate the value approximation with respect to S_0, which for the linear basis yields

$$\mathbf{\Delta} \approx \frac{24a^2 e^{-rT}}{N} \sum_{n=1}^{\bar{N}} \bar{\beta}_n \cdot a^{1/2} \int_{x_{n-1}}^{x_{n+1}} \varphi_{a,n}(y) \cdot e^y \mathbb{1}_{[y>\ln(W/S_0)]} dy.$$

One then proceeds exactly as for pricing, by computing the matrix G with entries given by $I_j^{\Delta}, j = 1, 2, 3$. With $b_{1,k} := l_k - x_{n(k)}$ and $b_{2,k} := l_k - x_{n(k)+1}$, these are easily obtained:

$$I_1^{\Delta} = e^{x_{n(k)}} \vartheta_R(a \cdot b_{1,k}, 1) = a^2 \left(\frac{W_k}{S_0} (b_{1,k} - 1 - \Delta) + e^{x_{n(k)}} e^{\Delta} \right)$$

$$I_2^{\Delta} = e^{x_{n(k)+1}} [\vartheta_L(a \cdot b_{2,k}, 0) + \vartheta_R(0, 1)] = a^2 \left(\frac{W_k}{S_0} (1 - b_{1,k}) + e^{x_{n(k)+1}} \left(e^{\Delta} - 2 \right) \right)$$

$$I_3^{\Delta} \approx \frac{1}{3} e^{x_n} \left(1 + e^{\Delta/2} + e^{-\Delta/2} \right), \quad n \geq n(k) + 2,$$

where $I_3^{\Delta}(k, n)$ is approximated by Simpson's rule for better accuracy.

More care is needed to calculate $\mathbf{\Gamma}$, which represents the second derivative of $\mathcal{V} \circ g_W$ with respect to S_0. In this case, one can rely on numerical differentiation which approximates Gamma, for example, by the second order scheme

$$\mathbf{\Gamma} \approx \frac{\mathcal{V} \circ g_W(S_0 - h) - 2\mathcal{V} \circ g_W(S_0) + \mathcal{V} \circ g_W(S_0 + h)}{h^2}$$

which achieves an accuracy of at least 5 digits for each maturity tested in just milliseconds of cpu time. Figure 3 displays Delta and Gamma convergence for the BSM model, where reference values can be obtained by exact formulas. To compute Gammas, we find $h = 0.05$ works well for $T \geq 0.1$, and $h = 0.01$ for $T < 0.1$, while results deteriorate as h is taken much smaller. Higher order difference schemes are easily implemented as well.

Remark 7. An alternative approach to calculating Gammas is obtained by Leibniz's rule, where

$$\mathbf{\Gamma} = e^{-rT}\frac{\partial}{\partial S_0}\int_{\ln\left(\frac{W}{S_0}\right)}^{\infty} e^y f_T(y)dy = e^{-rT}\frac{W}{S_0^2}f_T\left(\ln\left(\frac{W}{S_0}\right)\right).$$

For the single strike case $f_T(\ln(W/S_0)) \approx \frac{24a^3}{N}\bar{\beta}_{a,1}$, which is highly accurate for $T \geq .01$ at modest resolutions.[10] However, given the speed by which PROJ obtains prices across multiple strikes, a finite difference approach is sufficient in the European case. For exotic instruments, where pricing is more expensive, this alternative is preferred since all the required inputs are obtained as byproducts of the pricing algorithm [84].

3.4.5 Put Options and Pricing by Put-Call Parity

Now let $W := \{W_1, ...W_K\}$ denote the strike set of a basket of European put options on S_T, so that

$$g_{W_k}(S_0e^{Y_T}) := (W_k - S_0e^{Y_T})^+ = (W_k - S_0e^{Y_T})\mathbb{1}_{Y_T \leq \ln(W_k/S_0)}, \quad k = 1, ..., K.$$

To determine the initial grid point, we fix x_1 so that $x_{\bar{N}} := x_1 + (\bar{N} - 1)\Delta = \ln(W_K/S_0)$. That is, $x_1 := \ln(W_K/S_0) - (\bar{N} - 1)\Delta$, and $x_n = x_1 + (n-1)/a$, $n = 1, ..., \bar{N}$. We then determine for each W_k the *largest* index n for which the supports of $\varphi_{a,n}$ and g_{W_k} overlap, and denote this index by $n(k)$. Hence $n(k)$ satisfies

$$x_1 + (n(k) - 2)/a \leq \ln(W_k/S_0) < x_1 + (n(k) - 1)/a,$$

so that

$$n(k) := \lceil a(\ln(W_k/S_0) - x_1) + 1\rceil, \quad k = 1, ..., K.$$

[10] To price multiple strikes, an interpolation procedure can be applied.

Analogous to the case of call options, we define the matrix G as follows:

$$G_{k,n} := a^{1/2} \int_{x_{n-1}}^{x_{n+1}} \varphi_{a,n}(y) g_{W_k}(S_0 e^y) dy = \begin{cases} 0, & n \geq n(k)+1 \\ I_1(k,n), & n = n(k) \\ I_2(k,n), & n = n(k)-1 \\ I_3(k,n), & n \leq n(k)-2 \end{cases}$$

With

$$d_k := \ln(W_k/S_0) - x_{n(k)-1} - 1,$$

we have:

Result 3.4.2. *The payoff coefficients $G_{n,k}$ for vanilla put options are given by*

$$I_1(k, n(k)) = a^2 \left(\frac{W_k}{2}(d_k^2 + 1) - S_0 \exp(x_{n(k)-1}) \right) \tag{89}$$

$$I_2(k, n(k)-1) = a^2 \left(-\frac{W_k}{2} \left((d_k - \Delta)^2 - 2\Delta^2 + 1 \right) - S_0 \exp(x_{n(k)-1}) \left(e^{-\Delta} - 2 \right) \right) \tag{90}$$

$$I_3(k,n) \approx W_k - \frac{S_0}{3} \exp(x_n) \left(1 + e^{\Delta/2} + e^{-\Delta/2} \right), \quad n \leq n(k) - 2. \tag{91}$$

As with call options, equation (91) is obtained by Simpson's approximation, which is more robust than the exact integral.

An equivalent call option formula can be obtained using put-call parity. Given a strike set $W := \{W_1, ..., W_K\}$, with respective sets of call and put option payoffs $\{C_{W_k}\}_{k=1}^K$ and $\{P_{W_k}\}_{k=1}^K$ of maturity T, once can express the call values as

$$\boldsymbol{\mathcal{V}} \circ C_W = \boldsymbol{\mathcal{V}} \circ P_W + S_0 e^{-qT} - W \cdot e^{-rT}, \tag{92}$$

where zero dividends are assumed for simplicity. While payoff coefficients for call options grow exponentially (in the money), the payoff coefficients for put options are bounded above. Vanilla option valuation in the linear basis is summarized by Algorithm 4.

3.5 Valuation with the Piecewise Quadratic Basis

At low to moderate resolutions (specified below), we can improve the valuation accuracy by projecting f_T onto a smoother frame sequence, given by the quadratic B-Splines. The

Algorithm 1 Vanilla Option Valuation: Linear Basis

$x_1 \leftarrow \ln(W_K/S_0) - (\bar{N}-1)\Delta$
$H_1 \leftarrow 1/(24a^2)$, H_j for $j = 2, ..., N$ is given by (266)
$\bar{\beta} \leftarrow \Re\left[\text{FFT}\{H_j\}\right]$
$G(k,n) \leftarrow 0$, $k = 1, ..., K$, $n = 1, ..., \bar{N}$
$e_n \leftarrow \exp(x_1 + (n-1)\Delta), n = 1, ..., \bar{N}$
for $k \leftarrow 1, K$ **do**
  $l_k \leftarrow \ln(W_k/S_0)$; $n_k \leftarrow \lceil a(l_k - x_1) + 1 \rceil$; $d_k \leftarrow l_k - (x_1 + (n_k - 2)\Delta) - 1$
  $G(k,1), ..., G(k,n_k)$ determined by equations (89)-(91)
end for
if put == 1 **then**
  return $\mathcal{V} = 24a^2 e^{-rT}/NG\{\bar{\beta}\}_{n=1}^{\bar{N}}$
else
  return $\mathcal{V} = 24a^2 e^{-rT}/NG\{\bar{\beta}\}_{n=1}^{\bar{N}} + S_0 e^{-qT} - W^\top e^{-rT}$
end if

generator $\phi(y) \equiv \varphi^{[2]}(y)$ is defined as

$$\phi(y) := \begin{cases} \frac{1}{2}y^2 + \frac{3}{2}y + \frac{9}{8}, & y \in [-3/2, -1/2) \\ -y^2 + \frac{3}{4} & y \in [-1/2, 1/2) \\ \frac{1}{2}y^2 - \frac{3}{2}y + \frac{9}{8}, & y \in [1/2, 3/2). \end{cases}$$

To simplify derivations, we will use the notation ϕ^L, ϕ^M, and ϕ^R to specify ϕ on each of the intervals $[-3/2, -1/2), [-1/2, 1/2)$ and $[1/2, 3/2)$ respectively. As noted in equation (110), $\widehat{\phi}(\xi) = \widehat{\varphi}^{[2]}(\xi) = (\sin(\xi/2)/(\xi/2))^3$, and $\mathbf{\Phi}(\xi)$ is easily determined using equation (64). Hence we derive

$$\widehat{\widetilde{\phi}}(\xi) = \frac{480\sin^3(\xi/2)}{\xi^3(26\cos(\xi) + \cos(2\xi) + 33)}.$$

We then define[11]

$$H_j = \left(\frac{\sin(\xi_j/2a)}{\xi_j}\right)^3 \frac{\exp(-ix_1\xi_j)\cdot \widehat{f}_T(\xi_j)}{26\cos(\xi_j/a) + \cos(2\xi_j/a) + 33} \quad j \geq 2, \tag{93}$$

and $H_1 = 1/(960a^3)$. The beta coefficients $\bar{\beta} = \{\bar{\beta}_n\}_{n=1}^N$ are obtained using:

$$\bar{\beta} = \Re[\mathcal{D}\{H_j\}_{j=1}^N],$$

where constants will again be consolidated in the pricing formula.

[11]The adjustment by 1/2 of H_N is neglected due to insignificance.

3.5.1 Pricing Call Option Portfolios

The payoff coefficients in the case of quadratic splines are slightly more involved than in the linear case. Given a strike set $W := \{W_1, ..., W_K\}$, we define $x_1 := \ln(W(1)/S_0) - \Delta$, and $x_n := x_1 + (n-1)\Delta$, $n = 1, ..., \bar{N}$. The initial grid point x_1 accounts for the extended support of ϕ. For each k, we determine the *smallest* index $n(k)$ for which the support of $\phi_{a,n(k)}$ overlaps that of g_{W_k}. Specifically,

$$x_1 + (n(k)-1)\Delta + \Delta/2 \leq \ln(W(k)/S_0) < x_1 + (n(k)-1)\Delta + 3\Delta/2,$$

which yields

$$n(k) := \lfloor a(\ln(W(k)/S_0) - x_1) + 1/2 \rfloor.$$

The payoff coefficients are organized in the matrix

$$G_{k,n} := a^{1/2} \int_{x_n - \frac{3}{2}\Delta}^{x_n + \frac{3}{2}\Delta} \phi_{a,n}(y) g_{W_k}(S_0 e^y) dy = \begin{cases} 0, & n \leq n(k) - 1 \\ I_1(k,n), & n = n(k) \\ I_2(k,n), & n = n(k)+1 \\ I_3(k,n), & n = n(k)+2 \\ I_4(k,n), & n \geq n(k)+3 \end{cases}$$

for which we will need the integrals $\varrho^L, \bar{\varrho}^L, \varrho^M, \bar{\varrho}^M$, and $\varrho^R, \bar{\varrho}^R$, where

$$\varrho^L(\gamma_1, \gamma_2) := \int_{\gamma_1}^{\gamma_2} \phi^L(y) e^{\frac{y}{a}} dy, \quad \bar{\varrho}^L(\gamma_1, \gamma_2) := \int_{\gamma_1}^{\gamma_2} \phi^L(y) dy.$$

The other integrals are defined analogously. To further simplify notation, let

$$b_{1,k} := \ln(W(k)/S_0) - x_{n(k)}, \quad b_{2,k} := b_{1,k} - \Delta, \quad b_{3,k} := b_{2,k} - \Delta. \tag{94}$$

Finally, define

$$\begin{aligned} c_1 &:= a^3 S_0 \cdot e^{3\Delta/2}, \\ c_2 &:= a^3 S_0 \cdot \left(e^{3\Delta/2} - 3e^{\Delta/2} \right), \\ c_3 &:= a^3 S_0 \cdot \left(e^{3\Delta/2} - 6\sinh(\Delta/2) \right), \\ c_4 &:= a^3 S_0 \cdot \left(2\sinh(3\Delta/2) - 6\sinh(\Delta/2) \right). \end{aligned} \tag{95}$$

With this notation, we have the following:

Result 3.5.1. *European call options are priced in the quadratic spline basis according to*

$$\boldsymbol{\mathcal{V}}_{\bar{N}} \circ g_W \approx \frac{960 \cdot a^3 e^{-rT}}{N} G\{\bar{\beta}\}_{n=1}^{\bar{N}}, \tag{96}$$

where the payoff coefficients $G_{n,k}$ are given by

$$I_1(k, n(k)) = \left(\frac{1}{48}(2a \cdot b_{1,k} - 3)^3 - \frac{b_{1,k}^2}{2} a^3 + a^2 \Big(\frac{3}{2} + a \Big)(b_{1,k} - 1) - \frac{9}{8} a \right) W_k \tag{97}$$

$$+ c_1 \exp(x_{n(k)})$$

$$I_2(k, n(k)+1) = \left(\frac{3a - 8a^3}{4}(b_{2,k} - 1) - \frac{1}{2} + a^3 b_{2,k}^2 \Big(1 - \frac{b_{2,k}}{3} \Big) \right) W_k \tag{98}$$

$$+ c_2 \exp(x_{n(k)+1})$$

$$I_3(k, n(k)+2) = a^2 \left(b_{3,k}^2 \Big(\frac{b_{3,k}}{6} a + \frac{3}{4} - \frac{a}{2} \Big) + (b_{3,k} - 1) \Big(\frac{9\Delta - 12}{8} + a \Big) \right) W_k \tag{99}$$

$$+ c_3 \exp(x_{n(k)+2})$$

$$I_4(k, n) = -W_k + c_4 \exp(x_n), \quad n = n(k) + 3, ..., \bar{N}. \tag{100}$$

The convergence rate for a piecewise quadratic basis obeys $|\boldsymbol{\mathcal{V}}_{\bar{N}} \circ g_W - \boldsymbol{\mathcal{V}} \circ g_W| \sim \mathcal{O}(\Delta^3)$, and $O(\Delta^6)$ for coarse scales, as described in the error analysis.

Proof. We outline the basic steps used to determine the payoff matrix G as follows. With $l_k := \ln(W(k)/S_0)$,

$$\begin{aligned} I_1(k, n(k)) &= a^{1/2} \int_{l_k}^{x_{n(k)} + \frac{3}{2}\Delta} (S_0 e^y - W_k) a^{1/2} \phi(a(y - x_{n(k)})) dy \\ &= \int_{b_{1,k}}^{3/2} (S_0 e^{x_{n(k)}} e^{\frac{y}{a}} - W_k) \phi^R(y) dy \\ &= S_0 e^{x_{n(k)}} \varrho^R \Big(b_{1,k}, \frac{3}{2} \Big) - W_k \bar{\varrho}^R \Big(b_{1,k}, \frac{3}{2} \Big). \end{aligned}$$

Next, with $S_1(k) := S_0 e^{x_{n(k)+1}}$, $I_2 = I_2(k, n(k)+1)$ satisfies

$$\begin{aligned} I_2 &= \int_{b_{2,k}}^{1/2} (S_1(k) e^{\frac{y}{a}} - W_k) \phi^M(y) dy + \int_{1/2}^{3/2} (S_1(k) e^{\frac{y}{a}} - W_k) \phi^R(y) dy \\ &= S_1(k) \Big(\varrho^M \Big(b_{2,k}, \frac{1}{2} \Big) + \varrho^R \Big(\frac{1}{2}, \frac{3}{2} \Big) \Big) - W_k \Big(\bar{\varrho}^M \Big(b_{2,k}, \frac{1}{2} \Big) + \bar{\varrho}^R \Big(b_{2,k}, \frac{1}{2} \Big) \Big). \end{aligned}$$

The other two integrals are determined analogously, after which these expressions are evaluated using exact formulas for $\varrho, \bar{\varrho}$, which are found by simple calculus. □

The implementation using a quadratic basis is given in Algorithm 2, which provides accelerated convergence of value approximations at low resolutions, usually $P \leq 8$ (though depending on contract maturity T), after which linear projection is more effective. Put-call parity can be used to price options with the quadratic basis.

Algorithm 2 Vanilla Option Valuation: Quadratic Basis

$x_1 \leftarrow \ln(W_1/S_0) - \Delta$; $\quad c_1, .., c_4$ defined by (95)
$H_1 \leftarrow 1/(960a^3)$, H_j for $j = 2, ..., N$ is given by (93)
$\bar{\beta} \leftarrow \Re[\text{FFT}\{H_j\}]$
$G(k, n) \leftarrow 0$, $k = 1, ..., K$, $n = 1, ..., \bar{N}$
$e_n \leftarrow \exp(x_1 + (n-1)\Delta), n = 1, ..., \bar{N}$
for $k \leftarrow 1, K$ **do**
  $l_k \leftarrow \ln(W_k/S_0)$; $\quad n_k \leftarrow \lfloor a(l_k - x_1) + .5 \rfloor$
  b_k defined by (94)
  $G(k, n_k), ..., G(k, \bar{N})$ determined by equations (97)-(100)
end for
if put $== 1$ **then**
  return $\mathcal{V} = 960a^3 e^{-rT}/NG\{\bar{\beta}\}_{n=1}^{\bar{N}} - S_0 e^{-qT} + W^\top e^{-rT}$
else
  return $\mathcal{V} = 960a^3 e^{-rT}/NG\{\bar{\beta}\}_{n=1}^{\bar{N}}$
end if

The PROJ method, provided in Algorithm 3, is a hybrid of linear and quadratic projection, employed according to their relative strengths[12] (as a function of P and T). This algorithm is analyzed in the numerical results section. As mentioned for geometric Asian

Algorithm 3 Hybrid PROJ Method for Vanilla Options

Choose $\bar{N}$ by equation (80)
$N \leftarrow 2\bar{N}$
$K :=$ length(W); $\quad a := 2^P$; $\quad \Delta := 1/a$; $\quad \Delta_\xi := 2\pi a/N$
$\xi_j \leftarrow (j-1)\Delta_\xi, j = 1, ..., N$
$Quadratic \leftarrow (P \leq 6) | (P \leq 7 \ \& \ 0.1 \leq T \leq 2) | (P \leq 8 \ \& \ T \leq 0.1)$
if $Quadratic == 1$ **then**
  Call Algorithm 4
else
  Call Algorithm 2
end if

options, when pricing contracts of longer maturities, faster decay of the chf tails (combined with the windowing effect demonstrated in figure 1), implies that zero padding (extending

[12] We determined a simple set of rules by empirical testing on a large number of different models. Numerical results are later provided using different parameter settings.

the dual integrand sample in Fourier space by zeros) can be used to obtain coefficients at higher resolutions at a reduced cost.

3.6 Error Analysis

3.6.1 Discrete Transform Error

To study the error implicit in $\widetilde{\beta}_{a,k}$, we decompose $\mathcal{E}_k := \beta^{L^2}_{a,k} - \widetilde{\beta}_{a,k}$ as

$$\begin{aligned}\mathcal{E}_k &= \frac{a^{-1/2}}{\pi}\Re\left\{\int_0^\infty h_{a,k}(\xi)\cdot\widehat{f}_T(\xi)d\xi - \Delta_\xi\sum_{j=1}^{N} v_j h_{a,k}(\xi_j)\cdot\widehat{f}_T(\xi_j)\right\}\\ &= \frac{a^{-1/2}}{\pi}\Re\left\{\int_0^\infty h_{a,k}(\xi)\cdot\widehat{f}_T(\xi)d\xi - \Delta_\xi{\sum_{j=1}^{\infty}}' h_{a,k}(\xi_j)\cdot\widehat{f}_T(\xi_j)\right\}\\ &\quad + \frac{a^{-1/2}}{\pi}\Re\left\{\Delta_\xi{\sum_{j=N}^{\infty}}' h_{a,k}(\xi_j)\cdot\widehat{f}_T(\xi_j)\right\} := \mathcal{E}_k^1 + \mathcal{E}_k^2, \end{aligned} \tag{101}$$

where the prime indicates the first term in the sum is halved, and

$$h_{a,k}(\xi) := \exp(-ix_k\xi)\cdot\widehat{\widetilde{\varphi}}\Big(\frac{\xi}{a}\Big).$$

The infinite trapezoidal error, $\mathcal{E}_k^1$, is quantified in Proposition 3.3.1. Assuming for now that[13] $|h_{a,k}(\xi)| \le 1$ for $\xi \ge 2\pi a$ (in general the decay of $|h_{a,k}(\xi)|$ hastens that of $\mathcal{E}_k^2$, as illustrated in figure 1),

$$|\mathcal{E}_k^2| \le \frac{a^{-1/2}}{\pi}\cdot\Delta_\xi{\sum_{j=N}^{\infty}}'|\widehat{f}_T(\xi)|d\xi \le \frac{a^{-1/2}}{\pi}\int_{2\pi a}^{\infty}\Theta(\xi)d\xi,$$

where $\Theta(\xi)$ is any monotone decreasing function that majorizes $|\widehat{f}_T(\xi)|$ over $[2\pi a,\infty)$. In particular, if for some $c,\kappa>0$ and $\nu\in(0,2]$, $\widehat{f}_T(\xi)$ satisfies

$$|\widehat{f}_T(\xi)| \le \kappa\exp(-Tc|\xi|^\nu), \quad \xi\in\mathbb{R}, \tag{102}$$

then

$$\begin{aligned}|\mathcal{E}_k^2| \le \frac{a^{-1/2}}{\pi}\kappa\int_{2\pi a}^{\infty}\exp(-Tc\cdot\xi^\nu)d\xi &= \frac{a^{-1/2}}{\pi}\frac{\kappa}{\nu(Tc)^{1/\nu}}\Gamma\left(\frac{1}{\nu},Tc(2\pi a)^\nu\right)\\ &\sim \frac{a^{-1/2}}{\pi}\frac{\kappa(2\pi a)^{1-\nu}}{Tc\nu}\exp(-Tc\cdot(2\pi a)^\nu),\end{aligned} \tag{103}$$

[13] This holds for the B-spline generators and simplifies notation. Otherwise, a constant multiple is introduced.

which holds independently of k. The last term governs the behavior of $|\mathcal{E}_k^2|$ for large a. More explicit bounds are given for the B-spline basis below.

On the other hand, given a chf with polynomial decay, such as that of the pure jump VG, where $|\widehat{f}_T(\xi)| \leq \kappa|\xi|^{-2T/\nu}$ for large $|\xi|$, it follows that

$$|\mathcal{E}_k^2| \leq \frac{a^{-1/2}}{\pi}\kappa \int_{2\pi a}^{\infty} \xi^{-2T/\nu} d\xi = \frac{a^{-1/2}}{\pi}\frac{\nu}{2T-\nu}(2\pi a)^{(\nu-2T)/\nu},$$

so at the very least we require $\nu < 2T$ for the tail integral to exist. However, if for some $p \geq 1$, and for $|\xi|$ large, we have $|h_{a,k}(\xi)| = \mathcal{O}((\xi/a)^{-p})$, as is the case of p-th order B-splines, integrability is always satisfied, since $p + 2T/\nu > 1$, independently of T. Hence, for very short maturities, the PROJ method is capable of pricing with densities for which the characteristic function is not integrable, which is a major drawback of other transform methods. This suggests that techniques such as spectral filtering, may not be required.

We now have the following truncation error bound for B-splines, which is derived similarly to the discussion above.

Proposition 3.6.1. *Given $p \geq 1$, and $\varphi^{[p]}$ the p-th order B-spline generator, then for any $\widehat{f}_T(\xi)$ satisfying equation (199) above, $\mathcal{E}^2 := \sup_{1\leq k\leq N} |\mathcal{E}_k^2|$ satisfies*

$$\mathcal{E}^2 \leq \frac{a^{-1/2}}{\pi}\frac{\kappa \cdot C_p(a)}{p \cdot (2\pi)^p} \cdot \exp(-Tc \cdot (2\pi a)^\nu),$$

where $C_p(a) = \mathcal{O}(a)$.

Note that for the Haar ($p = 0$) basis, (103) provides a conservative bound.

3.6.2 Valuation Error

For simplicity assume $r = 0$. Further, we consider the case where $N := 2\bar{N}$, so that $G := [x_1, x_1 + \bar{a}/2]$ is the approximate integration range.[14] For a European payoff $g(S_0e^y)$,

[14] In the case that $N := \bar{N}$, the density is centered roughly over $[-\bar{a}/2, \bar{a}/2]$, and the analysis is similar.

with $\widetilde{f}_T^{\bar{N}} := \sum_{k=1}^{\bar{N}} \widetilde{\beta}_{a,k}\varphi_{a,k}(y)$,

$$\begin{aligned}
\mathcal{V} \circ g(S_0) &= \int_{-\infty}^{\infty} g(S_0e^y) f_T(y)dy \\
&= \int_G g(S_0e^y)\widetilde{f}_T^{\bar{N}}(y)dy + \int_G g(S_0e^y)\left(P_{\mathcal{M}_a} f_T(y) - \widetilde{f}_T^{\bar{N}}(y)\right)dy \\
&\quad + \int_G g(S_0e^y)\left(P_{\mathcal{M}_a} f_T(y) - f_T(y)\right)dy + \int_{\mathbb{R}/G} g(S_0e^y) f_T(y)dy \\
&:= \int_G g(S_0e^y)\widetilde{f}_T^{\bar{N}}(y)dy + \mathcal{E}^3 + \mathcal{E}^4 + \tau(G). \qquad (104)
\end{aligned}$$

When $g_{a,n}$ are computed numerically, we introduce the additional error

$$\mathcal{E}^g = \sum_{k=1}^{\bar{N}} \widetilde{\beta}_{a,k}\left(\int_G g(S_0e^y)\varphi_{a,k}(y) - a^{-1/2}g_{a,k}\right),$$

which converges in accordance to the integration scheme used to compute $g_{a,k}$. Otherwise, when $g_{a,k}$ are given explicitly (such as for vanilla options, digitals, etc.)

$$\mathcal{V}_{\bar{N}} \circ g(S_0) = \int_G g(S_0e^y)\widetilde{f}_T^{\bar{N}}(y)dy,$$

from which equation (104) implies

$$\left|\mathcal{V} \circ g - \mathcal{V}_{\bar{N}} \circ g\right|(S_0) \le |\mathcal{E}^3| + |\mathcal{E}^4| + |\tau(G)|. \qquad (105)$$

Specifically,

$$\begin{aligned}
\mathcal{E}^3 &= \int_G g(S_0e^y) \sum_{k=1}^{\bar{N}} \left(\beta_{a,k}^{L^2} - \widetilde{\beta}_{a,k}\right)\varphi_{a,k}(y) \\
&\le \|g(S_0e^y)\|_\infty^G \cdot \sup_{1\le k\le \bar{N}} |\beta_{a,k}^{L^2} - \widetilde{\beta}_{a,k}| \cdot \bar{N}a^{-1/2}.
\end{aligned}$$

When $x_1 > 0$, $|x_k| = x_1 + (k-1)/a \le x_1 + \frac{\bar{a}}{2}$, so $\bar{a} - |x_k| \ge \frac{\bar{a}}{2} - x_1$. Similarly, if $x_1 < 0$, $|x_k| \le \max\{|x_1|, \frac{\bar{a}}{2}\}$, from which $\bar{a} - |x_k| \ge \min\{\bar{a} - |x_1|, \frac{\bar{a}}{2}\}$. In either case, assuming $\bar{a} - |x_k| > 0$, $1 \le k \le \bar{N}$, $\mathcal{E}^3$ converges exponentially in $a, \bar{a}$. Practically speaking, with $\bar{a}$ fixed to limit the density truncation error $\tau(G)$, the convergence is exponential in a. For densities that correspond to $\widehat{f}_T(\xi) \in \mathcal{H}(\mathcal{D}_d)$, with $d > 0$ (all models in Figure 43; for pure jump VG, one must have $\nu < 2T$), it can be shown (cf [120]) that $f_T(y)$ has exponentially decaying (semi-heavy) tails, from which $\tau(G)$ can be controlled. See equation (136) for a clever method developed by [61] that utilizes the cumulants of f_T to control $\tau(G)$ (in most

cases observed in practice, especially for $T \ll 1$, our empirical rule of thumb is conservative compared to the rule suggested in [61]).

Finally, we have the bound

$$|\mathcal{E}^4| \leq \|g(S_0 e^y)\|_2^G \|P_{\mathcal{M}_a} f_T - f_T\|_2.$$

Hence, for an L-th order generator, such as $\varphi^{[L]}$,

$$|\mathcal{E}^4| \leq C(\mathcal{E}^4)\Delta^{2L} + \mathcal{O}(\Delta^L)$$

where $C(\mathcal{E}^4) := K_{\varphi,2L} \cdot \|g(S_0 e^y)\|_2^G \cdot \|f_T^{(2L)}\|_2$. The $\mathcal{O}(\Delta^L)$ term governs the fine scale behavior, while the initial decay behaves as $\mathcal{O}(\Delta^{2L})$. With $\bar{a}$ sufficiently large, chosen in particular to control the truncation error $\tau(G)$, it follows that

$$|\mathcal{V} \circ g - \mathcal{V}_{\bar{N}} \circ g|\,(S_0) = \mathcal{O}(\mathcal{E}^4).$$

Thus, the value error decays on the order of the projection error.

3.7 Numerical Experiments

In this section, we perform a series of numerical experiments to analyze the efficiency and accuracy of PROJ as a pricing method, as given by Algorithm 3. Specifically, we assess the utility of PROJ as a the pricing component of a numerical calibration routine in which multiple strikes of European call options are priced simultaneously. Tests are conducted with Heston, CGMY, and NIG specifications of the log return distribution, with several parameter settings in each case.

Aside from this particular application to calibration, this section is intended to demonstrate in a familiar setting the convergence behavior of this novel method for a variety of models. While the relative power of PROJ is most pronounced for path dependent applications, where its compactly supported basis elements along with the FFT implementation are fully harnessed, robust and efficient pricing of vanilla options is a prerequisite for any density approximation method.

For experiments involving Levy models, reference parameters are calculated by the COS method of Fang and Oosterlee [61], which is reviewed briefly in the next section. For

Heston's model, the industry standard of Carr and Madan [35] is employed. Since COS is the fastest available method (at each desired accuracy level) for pricing European options across *multiple strikes*, we compare our results to COS with the recommended parameter settings.

While not reported here due to length constraints, we confirmed the findings of [61] with respect to other popular pricing methods. Namely, the method of Carr and Madan (CM), while accurate for large N, is very slow to converge compared to PROJ and COS. Similarly we found that CONV was slower to reach the same accuracy (and increasingly so for higher accuracies), though it showed an improvement over CM. We also consider methods of direct integration, with the same findings.

3.7.1 Comparison

The COS method is parameterized by N_{COS}, which is the number of terms included in the Fourier cosine series expansion. For PROJ the results are reported at the level of P, where $a = 2^P$ gives the basis support length. When $T < 1$, $\bar{N} = 4a$, otherwise $\bar{N} = 8a$. Results are presented in a way that highlights the required parameter setting in each method to achieve a comparable level of accuracy. Maximum and average absolute errors are presented, as well as cpu time in milliseconds for each method.

The COS method has been implemented to the best of the author's ability. For a conservative comparison, times reported for PROJ do not reflect certain additional time saving techniques that could be employed. For example, symmetry of $\mathbf{\Phi}(\xi)$ can be used to cut its initialization cost in half. Moreover, as illustrated in figure 1, dual integrands decay much faster than the chf itself, so zero padding can be used to obtain coefficients at higher resolutions without additional samples from the dual integrand. This is especially useful for longer maturities ($T \geq 1$) for which the chf becomes peaked, rapidly decaying chf tails (e.g. Heston, Merton, BSM, etc.) as well as when the chf itself is expensive to evaluate, as for geometric Asian options.

Reported cpu times are given in milliseconds (msec) and are derived from the average over 200 replications of each experiment. The code is written in MATLAB 8.1, and the

computer has an Intel(R) Core(TM) i5-3470T CPU, 2.90GHz with 3MB cache size.

3.7.2 COS Implementation Details

For a fixed strike W and initial asset price S_0, let $Y_T := \ln(S_T/S_0)$ and $x := \ln(S_0/W)$. Given a European payoff $g_W(S_0e^{Y_T}) := v(x,T)$, the price at time $t_0 \leq T$ is approximated by

$$v(x,t_0) \approx e^{-r\Delta t}\int_l^u v(y,T)f_T(y|x)dy,$$

where $f_T(y|x)$ is the conditional density of $y := \ln(S_T/W) = x+Y_T$ over the time increment $\Delta t := T - t_0$, and $[l,u]$ is chosen in a manner described shortly. This choice is important, as it can have a significant influence on the speed and even the attainment of convergence to true values.

For a Levy process, the chf of $f_T(y|x)$ satisfies $\widehat{f}_T(\xi|x) = \widehat{f}_T(\xi)e^{i\xi x}$, where $\widehat{f}_T(\xi)$ is the chf of Y_T as before. The value approximation is given by the Fourier cosine series

$$v(x,t_0) \approx e^{-rT}{\sum}'_{n=0}^{N_{COS}-1}\Re\left\{\widehat{f}_T\left(\frac{n\pi}{u-l}\right)e^{in\pi\frac{x-l}{u-l}}\right\}V_n,$$

where

$$V_n := \frac{2}{u-l}\int_l^u v(y,T)\cos\left(n\pi\frac{y-l}{u-l}\right)dy$$

and $\sum'$ indicates that the first term is weighted by one-half. A similar representation holds for Heston's model. For many payoff functions such as vanilla options and digitals, the cosine series coefficients V_n have a known form.

3.7.3 Carr-Madan-Geman-Yor (CGMY)

The CGMY family of exponential Levy models [32] is characterized by four parameters: $C \geq 0$ accounts for the overall activity level, $G \geq 0$ and $M \geq 0$ control the skewness, and $Y < 2$ dictates the fine structure of the process. Specifically, $Y < 0$ determines a finite activity process, $0 \leq Y \leq 1$ a process with finite variation but infinite activity, and $1 \leq Y < 2$ a process of infinite activity and variation. The risk-neutral Levy symbol is given by

$$\psi(\xi) = i\xi(r - \psi_L(-i)) + C\Gamma(-Y)\left((M-i\xi)^Y - M^Y + (G+i\xi)^Y - G^Y\right),$$

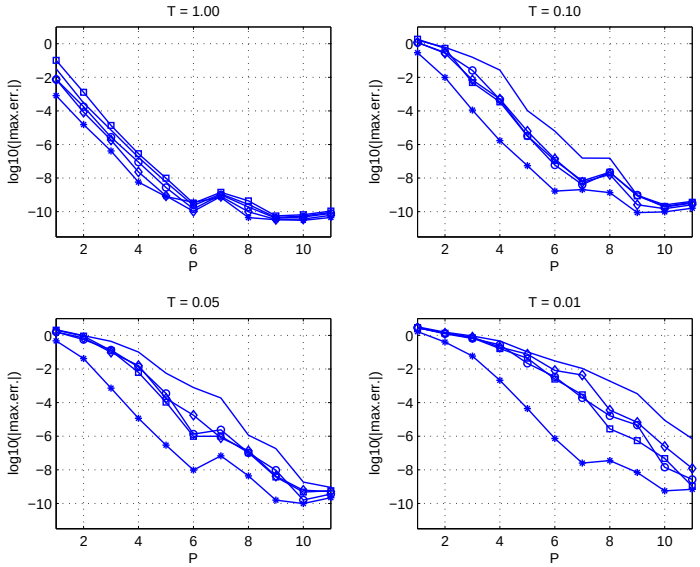

Figure 4: (C, G, M, Y): convergence of PROJ for different parameter settings; 50 strikes priced in each trial.

where

$$\psi_L(-i) = C\Gamma(-Y)\left((M-1)^Y - M^Y + (G+1)^Y - G^Y\right),$$

and $\Gamma = \Gamma(y)$ is the Gamma function.

For COS implementation, the truncation interval $[l, u]$ for CGMY and other Levy models is determined by

$$[l, u] := \left[x + c_1 - L_1\sqrt{|c_2| + \sqrt{|c_4|}}, x + c_1 + L_1\sqrt{|c_2| + \sqrt{|c_4|}}\right], \tag{106}$$

where c_n denotes the n-th cumulant of $\ln(S_T/S_0) = \ln(Y_T)$, and $x := \ln(S_0/W)$.

Reference values for Levy models are generated by the COS method with $N_{COS} = 2^{18}$ and truncation parameter $L_1 = 20$ for $T \geq 0.1$ and $L_1 = 25$ for $T < .01$. For comparison to

Table 2: $(C, G, M, Y) = (1, 5, 5, .7)$; $r = .05$, $S_0 = 100$, $W = 80, 80.5, ..., 140$; ref. values: (20.883609452,...,0.407753168).

$T = 0.1$						
	a	8	16	32	64	128
PROJ	max. err.	6.780e-02	5.245e-03	5.746e-05	1.013e-06	1.202e-07
	avg. err.	2.810e-02	1.226e-03	6.955e-06	1.669e-07	1.039e-07
	(msec)	(0.985)	(0.967)	(1.281)	(1.584)	(2.380)
	N_{COS}	40	80	160	240	280
COS	max. err.	5.966e-02	2.766e-03	3.068e-05	8.378e-07	1.753e-07
	avg. err.	2.812e-02	1.184e-03	1.132e-05	2.845e-07	5.592e-08
	(msec)	(1.073)	(1.456)	(2.319)	(3.131)	(3.499)

Table 3: $(C, G, M, Y) = (1, 5, 5, .7)$; $r = .05$, $S_0 = 100$, $W = 100, 100.5, ..., 160$; ref. values: (3.435256997,...,0.070426192).

$T = 0.05$						
	a	16	32	64	128	256
PROJ	max. err.	1.363e-02	1.010e-03	4.280e-05	7.163e-06	5.375e-07
	avg. err.	2.182e-03	5.681e-05	7.455e-07	2.494e-07	1.698e-08
	(msec)	(1.029)	(1.195)	(1.447)	(2.106)	(3.833)
	N_{COS}	90	180	360	620	800
COS	max. err.	3.733e-02	2.537e-03	5.181e-05	8.841e-07	8.288e-08
	avg. err.	1.035e-02	5.804e-04	1.062e-05	1.480e-07	1.167e-08
	(msec)	(1.589)	(2.372)	(4.760)	(7.458)	(9.369)

Table 4: $(C, G, M, Y) = (1, 5, 5, .7)$; $r = .05$, $S_0 = 100$, $W = 100, 100.25, ..., 130$; ref. values: (1.066783348,...,0.047881851).

$T = 0.01$						
	a	32	64	128	256	512
PROJ	max. err.	3.988e-02	9.910e-03	1.466e-03	1.427e-04	3.160e-05
	avg. err.	6.171e-03	7.222e-04	6.063e-05	2.676e-06	3.004e-07
	(msec)	(1.107)	(1.567)	(2.152)	(4.123)	(6.738)
	N_{COS}	180	360	600	1200	1600
COS	max. err.	3.812e-02	6.826e-03	1.354e-03	7.133e-05	1.255e-05
	avg. err.	5.056e-03	6.752e-04	1.114e-04	5.526e-06	7.753e-07
	(msec)	(2.715)	(4.389)	(7.307)	(14.376)	(20.188)

PROJ, the recommended value $L_1 = 10$ is set for $T \geq 0.1$, and $L_1 = 15$ is set for $T < 0.1$.

Tables 2-4 display results for European call options under the CGMY model with parameters (C,G,M,Y) = (1,5,5,.7), where $K = 121$ evenly spaces strikes are priced for three maturities. For $T = .01$, COS is approximately 1.5-2 times slower than PROJ to achieve each accuracy above e-02. This increases to a factor of 2-3.5 times slower for $T \leq .05$, as shown in Tables 3 and 4. Robustness of PROJ is demonstrated in Figure 4, which presents the results of five parameter settings of the CGMY model, given by

$$C = (4, 4, 6, 3, 3), \qquad G = (5, 5, 15, 5, 5)$$

$$M = (60, 6, 20, 30, 65), \qquad Y = (.3, .4, .5, .6, 1.1).$$

Convergence is demonstrated for four maturity times as a function of P. As expected, shorter maturities lead to slower convergence, though PROJ maintains impressive cpu times even for short maturities.

Table 5: Heston: $(u_0, \bar{u}, \lambda, \eta, \rho) = (.0175, .0398, 1.5768, .5751, -0.5711)$; $r = 0$, $S_0 = 100$, $W = 90, 91, ..., 120$; ref. values: (12.7095317748,...,0.4828281379).

$T = 1$						
	a	8	16	32	64	128
PROJ	max. err.	5.636e-02	1.656e-03	2.163e-05	2.983e-07	2.869e-08
	avg. err.	2.919e-02	5.814e-04	5.328e-06	9.511e-08	1.669e-08
	(msec)	(0.425)	(0.486)	(0.740)	(1.160)	(2.081)
	N_{COS}	32	64	128	256	350
COS	max. err.	3.443e-02	8.039e-04	4.583e-05	4.494e-05	4.494e-05
	avg. err.	1.999e-02	4.068e-04	4.496e-05	4.494e-05	4.494e-05
	(msec)	(0.322)	(0.398)	(0.599)	(0.971)	(1.218)

3.7.4 Heston's Model

In Heston's model, the log return $Y_t := \ln(S_t/S_0)$ and the variance process U_t are modeled jointly by the following equations:

$$dY_t = (r - \frac{1}{2}U_t)dt + \sqrt{U_t}dW_{1,t}$$
$$dU_t = \lambda(\bar{U} - U_t)dt + \eta\sqrt{U_t}dW_{2,t},$$

where $\lambda \geq 0, \bar{U}$ and $\eta \geq 0$ represent the speed of mean reversion of variance, the mean variance level, and the "volatility" of the variance diffusion process. Here $W_{1,t}$ and $W_{2,t}$ are correlated Brownian motions with correlation coefficient ρ. The chf $\widehat{f}_T$ of Y_T in Heston's model becomes

$$\widehat{f}_T(\xi) = \exp\left(A(\xi) + B(\xi)U_0 + i\xi rT\right),$$

where U_0 is the initial variance, and

$$A(\xi) = \frac{\lambda\bar{U}}{\eta^2}\left((\lambda - i\rho\eta\xi - D(\xi))\,T - 2\ln\left(\frac{1 - G(\xi)e^{-D(\xi)T}}{1 - G(\xi)}\right)\right)$$
$$B(\xi) = \frac{1}{\eta^2}(\lambda - i\rho\eta\xi - D(\xi))\frac{1 - e^{-D(\xi)T}}{1 - G(\xi)e^{-D(\xi)T}}$$

where

$$D(\xi) := \sqrt{(\lambda - i\rho\eta\xi)^2 + (\xi^2 + i\xi)\eta^2} \quad \text{and} \quad G(\xi) := \frac{\lambda - i\rho\eta\xi - D(\xi)}{\lambda - i\rho\eta\xi + D(\xi)}.$$

The recommend truncation range for COS is

$$[l, u] := [x + c_1 - L_2\sqrt{|c_2|}, x + c_1 + L_2\sqrt{|c_2|}], \tag{107}$$

with $L_2 = 12$ for maturities $T \geq 0.1$. We set $L_2 = 18$ for maturities $T < 0.1$.

Table 6: Heston: $(u_0, \bar{u}, \lambda, \eta, \rho) = (.02, .01, .01, .2, -.5)$; $r = 0.05$, $S_0 = 100$, $W = 90, 91, ..., 120$; ref. values: (15.693589734,...,0.795285535)

$T = 1$						
	a	4	8	16	32	64
PROJ	max. err.	3.880e-01	8.065e-02	3.670e-03	6.710e-05	5.543e-07
	avg. err.	2.039e-01	3.917e-02	1.377e-03	1.167e-05	1.636e-07
	(msec)	(0.341)	(0.372)	(0.466)	(0.787)	(1.113)
	N_{COS}	90	180	360	600	900
COS	max. err.	4.250e-01	4.826e-02	1.859e-03	4.448e-05	6.952e-07
	avg. err.	2.192e-01	2.387e-02	9.543e-04	2.360e-05	3.473e-07
	(msec)	(0.458)	(0.684)	(1.171)	(1.923)	(2.795)

Table 7: Heston: $(u_0, \bar{u}, \lambda, \eta, \rho) = (.02, .01, .01, .2, -.5)$; $r = 0.05$, $S_0 = 100$, $W = 105, 105.5, ..., 120$; ref. values: (0.330008569,...,4.2044e-06)

$T = 0.1$						
	a	8	16	32	64	128
PROJ	max. err.	3.804e-01	3.215e-02	4.495e-04	5.591e-06	1.053e-07
	avg. err.	2.077e-01	1.476e-02	8.186e-05	9.078e-07	2.252e-08
	(msec)	(0.337)	(0.368)	(0.473)	(0.750)	(1.136)
	N_{COS}	50	120	190	280	340
COS	max. err.	3.407e-01	1.188e-02	3.199e-04	3.625e-06	2.093e-07
	avg. err.	2.037e-01	6.962e-03	1.953e-04	2.103e-06	1.203e-07
	(msec)	(0.359)	(0.553)	(0.739)	(1.025)	(1.226)

Parameters for the first experiment are initialized exactly as described in [61], though we price the strikes $90, 91, ..., 120$ (instead of a single strike):

$$S_0 = 100, r = 0, \lambda = 1.5768, \eta = .5751, \bar{u} = 0.0398, u_0 = 0.0175, \rho = -0.5711.$$

Reference prices for Heston's model are generated by Carr and Madan's (CM) method, which is the industry standard. The number of inversion points to obtain reference values by CM is set to $N = 2^{25}$, as opposed to 2^{17}, as used in [61]. Moreover, reference values are confirmed by direct integration.

With the more accurate reference values obtained, we observe from Table 5 a failure of the COS method to achieve accuracy beyond $e - 05$ when $T = 1$, even when N_{COS} is taken as large as 2^{19}. What we observe here is the sensitivity of COS to the choice of L_2 in equation (107). Taking the recommended value of $L_2 = 12$ impedes convergence in this case, yet for other parameter settings a value of $L_2 = 2$ provides much better convergence results (this is true in the next case). In fact, by taking $L_2 = 28$ we obtain convergence for the COS method to the true values, and all three methods agree. However, setting $L_2 = 28$

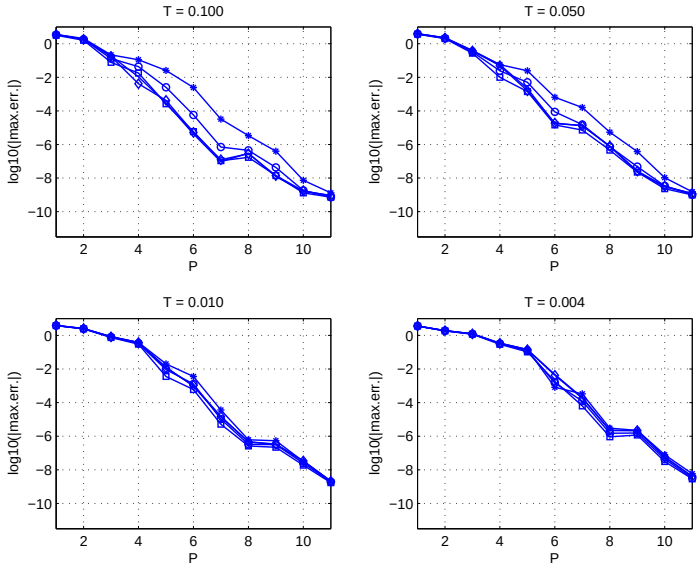

Figure 5: Heston: convergence of PROJ for different parameter settings; 50 strikes priced in each trial.

as the default for COS would produce very slow convergence in general, so $L_2 = 12$ seems to be a reasonable compromise.

In Tables 6 and 7, a new set of Heston experiments is presented, and both methods obtain convergence. With fewer strikes priced, in this case just $K = 31$, the speed advantage of PROJ is less pronounced, though it is still the faster and more robust method. Uncharacteristically, COS converges faster for $T = 0.1$ than it does for $T = 1$. To test the convergence of PROJ, five additional parameter settings are analyzed:

$$u_0 = (.02, .02, .03, .025, .02), \quad \bar{u} = (.02, .03, .04, .025, .02)$$

$$\lambda = (.2, .5, .8, 1.2, 2.4), \quad \eta = (.2, .2, .4, .5, .6), \quad \rho = (-.2, -.5, -.6, -.7, -.9).$$

The results are presented in Figure 5, where an accuracy of about e-06 is obtained for all parameter settings and maturities $T = 0.1, 0.05, 0.01, 0.004$ when $P = 8$. When $P = 11$, an accuracy of e-08 is surpassed for each trial.

3.7.5 Normal Inverse Gaussian (NIG)

The NIG(α, β, δ) return process Y_t of Barndorff-Nielsen [12] is constructed by time changing a standard Brownian motion via the inverse Gaussian subordinator I_t, which has parameters

Table 8: NIG: $r = 0.05$, $S_0 = 100$, $W = 80, 80.25, ..., 120$; $(\alpha, \beta, \delta) = (7, 0.5, 0.1)$; ref. values: (20.409894090,...,0.051059342)

$T = .1$						
	a	32	64	128	256	512
PROJ	max. err.	5.901e-02	1.302e-02	1.301e-04	5.535e-05	7.845e-07
	avg. err.	8.797e-03	1.156e-03	6.974e-06	1.035e-06	3.354e-08
	(msec)	(1.384)	(1.869)	(2.603)	(4.005)	(7.662)
	N_{COS}	70	140	280	560	1220
COS	max. err.	4.628e-02	5.183e-03	1.952e-04	4.837e-06	3.975e-06
	avg. err.	9.721e-03	9.450e-04	3.172e-05	3.976e-06	3.968e-06
	(msec)	(1.871)	(2.821)	(4.921)	(8.956)	(18.643)

Table 9: NIG: $r = 0.05$, $S_0 = 100$, $W = 85, 85.25, ..., 125$; $(\alpha, \beta, \delta) = (7, 0.5, 0.1)$; ref. values: (15.224429485,...,0.016176744)

$T = 0.05$						
	a	32	64	128	256	512
PROJ	max. err.	1.184e-01	4.157e-02	7.240e-03	6.486e-04	6.975e-06
	avg. err.	1.422e-02	3.035e-03	2.454e-04	8.676e-06	1.813e-07
	(msec)	(1.467)	(1.660)	(2.132)	(4.707)	(7.664)
	N_{COS}	70	140	280	560	1000
COS	max. err.	1.482e-01	3.586e-02	5.167e-03	2.660e-04	6.098e-06
	avg. err.	2.753e-02	5.234e-03	6.214e-04	3.052e-05	7.556e-07
	(msec)	(1.479)	(2.485)	(4.096)	(7.636)	(13.419)

$a = 1$ and $b = \delta\sqrt{\alpha^2 - \beta^2}$:

$$Y_t = \beta\delta^2 I_t + \delta W_t,$$

where $\alpha > 0, \beta \in (-\alpha, \alpha), \delta > 0$. The density, while known in closed form, is given in terms of the modified Bessel function of the third kind. The risk-neutral Levy symbol is given simply by

$$\psi(\xi) = i\xi\left(r + \delta\left(\sqrt{\alpha^2 - (\beta+1)^2} - \gamma\right)\right) - \delta\left(\sqrt{\alpha^2 - (\beta + i\xi)^2} - \gamma\right),$$

where $\gamma := \sqrt{\alpha^2 - \beta^2}$.

Tables 8-10 compare the convergence of PROJ and COS for $K = 161$ strikes. In this case, COS is about 1.5-2.5 times slower to achieve each accuracy level, in terms of maximum error. Moreover, the corresponding average errors tend to be smaller than those for COS, an observation that held for most of the experiments conducted, including those not reported. Figure 6 displays the convergence of PROJ for five additional tests, with parameter settings:

$$\alpha = (7, 6, 5, 4, 9), \quad \beta = (.6, -.6, -.2, .5, .5), \quad \delta = (.4, .3, .4, .2, .7).$$

Table 10: NIG: $r = 0.05$, $S_0 = 100$, $W = 85, 85.25, ..., 125$; $(\alpha, \beta, \delta) = (7, 0.5, 0.1)$; ref. values: (15.044912035,...,0.003106500)

$T = 0.01$						
	a	32	64	128	256	512
PROJ	max. err.	2.137e-01	1.261e-01	2.609e-02	1.044e-02	4.750e-04
	avg. err.	1.929e-02	6.385e-03	8.480e-04	2.048e-04	5.200e-06
	(msec)	(1.282)	(1.740)	(2.098)	(4.643)	(7.555)
	N_{COS}	70	140	280	560	1000
COS	max. err.	1.675e-01	6.108e-02	1.824e-02	3.607e-03	4.843e-04
	avg. err.	1.818e-02	4.736e-03	1.015e-03	1.868e-04	2.429e-05
	(msec)	(1.737)	(2.658)	(4.768)	(8.368)	(14.987)

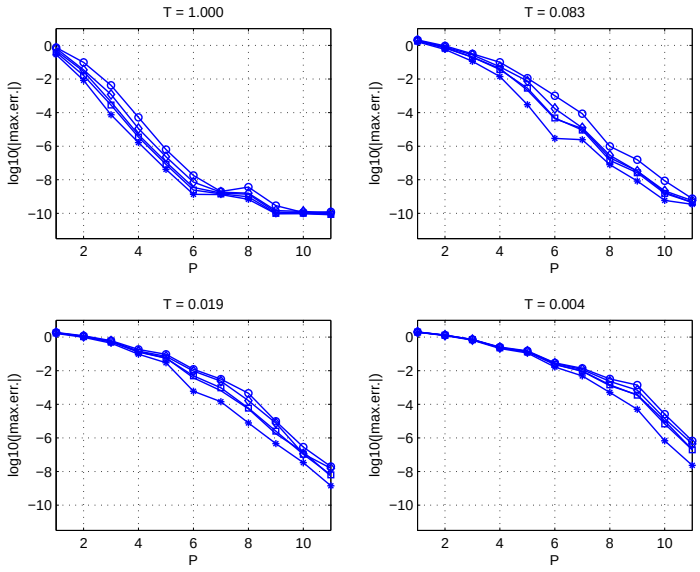

Figure 6: NIG: convergence of PROJ for different parameter settings; 50 strikes priced in each trial.

For maturities of one year, month, week and day we observe convergence to at least within e-06 (which, for $T = 1$ is surpassed for all parameter settings when $P = 5$).

3.8 Conclusions

This paper introduced a novel method for calculating expectations when the characteristic function of log return is known. We utilized the duality theory of Riesz bases to analytically derive orthogonal projections of return densities onto spaces of compactly supported elements, building the foundations for further extensions to the pricing of path-dependent exotic options.

An algorithm called PROJ was presented, which combined two implementations of the method. A numerical analysis was conducted to study the theoretical convergence rate of the algorithm, including the demonstration of exponentially convergent coefficient errors. A numerical example demonstrating the convergence for geometric Asian options was provided. Experiments were conducted to assess its efficiency compared to alternative pricing methods. The closest competitor for pricing multiple strikes simultaneously, COS, was presented for comparison.

In all tests conducted, both PROJ and COS demonstrated impressive performance when pricing multiple options, with PROJ faster in nearly every case to reach the same accuracy, typically by a factor of 1.5-3.5. Similarly, while COS experienced sensitivity to the choice of truncation parameters, PROJ demonstrated robustness throughout. For a fixed desired accuracy, the computation time for PROJ increases much more slowly than for COS as more strikes are priced, which could be valuable for pricing baskets of options in actively traded markets. Due to compact support of B-splines, the FFT implementation developed, and the convergence acceleration afforded by the orthogonally projected density, the utility of PROJ in the context of pricing path dependent options, such as Asian, barrier, and Bermudan options, is even more pronounced, and is the subject of several extensions including [84, 85] which rely on the framework and analysis introduced in this paper.

In addition to the piecewise linear and quadratic basis, other compactly supported generators were studied. For example, the Hanning and Hamming windows from signal

processing were considered, in addition to a cubed cosine basis, but with little success for the cases considered. Two other B-spline bases, the Harr basis (with generator $\varphi^{[0]}$), and the cubic basis ($\varphi^{[3]}$) were analyzed, but with inferior performance relative to linear and quadratic projection. This finding was surprising for the cubic basis, and future research aims at investigating this basis further for long maturity contracts.

CHAPTER IV

THE B-SPLINE ORDER OF DENSITY PROJECTION

This chapter is based on the paper [87], accepted to the Journal of Computational Finance.

4.1 Introduction

To price and hedge complex derivative products, and calibrate model parameters to observed prices, advanced models for asset dynamics require more intensive numerical procedures to guarantee sufficient accuracy than was once the case. As models capture realistic features of asset returns, such as extreme peaks and heavy-tails, traditional pricing methods are compelled beyond their limit.

A new direction in efficient numerical pricing based on fast Fourier transforms was pioneered in [35], and analyzed in greater detail in [91,102] (related approaches can be found in [19,96]). Inspired by the success of these early works, extensive research on pricing in the Fourier domain has emerged. Efficient and robust methods have developed for the pricing of particular products, for example arithmetically averaged Asian options [42] or Bermudan options [100], or under particular asset dynamics, such as the fast Gauss transform method of [26, 27] for mixture of Gaussian distributions.

Few general purpose pricing methods, capable of handling general exponential Levy dynamics, have been able to consistently compete with the cosine series expansion method (COS) of [61], except in special cases such as for extreme strikes. For example, the saddlepoint method [37] has been shown effective at pricing deeply out-of-the-money options, for which other methods may ascribe negative value. Our paper analyzes a general purpose pricing method, like COS, capable of pricing vanilla options robustly and efficiently, and applicable to the pricing of complex exotic products. We also consider the problem of density support truncation, as it applies to density methods in general, and introduce a new approach based on the Hilbert transform (HT) (see [64, 65, 67] for applications of HT to option pricing).

The option pricing method of density projection by frame duality, PROJ, was introduced in [83] as an efficient means of pricing large sets of European options, and later for pricing barrier and Asian options [84, 85]. In our extension to quadratic and cubic bases we are confronted with the numerical stability of valuation formulas that was mostly absent for low order B-splines (in [83], pricing with a quadratic basis became unstable beyond a moderate resolution, so linear interpolation was used instead). We provide a simple stabilization approach that overcomes this difficulty, and even improves the performance and stability of linear projection. Without this stabilization, higher order B-spline approximations would be infeasible.

We provide general formulas for obtaining European prices and Greeks, as well as pricing formulas for digital and forward starting options. PROJ is also found to be robust with respect both maturity extremes. Moreover, for heavy-tailed processes such as CGMY with maturities in the range of one week or less (as arise in discretely monitored contexts), observed convergence tends to dominate that of COS on average, which is in theory exponential (compared to the algebraic convergence of PROJ). In theory, PROJ expansions converge at a rate of one plus the B-spline order (so fourth order convergence for cubic projection), but in practice we often observe up to double this rate of convergence.

As the pricing of exotic options often reduces to a sequence of vanilla-type pricing problems, the simple European setting provides a controlled environment for experimentation and error analysis with a consensus of reference prices available to high precision. Given that similar sources of error arise in European as in exotic pricing, much of the added uncertainty can be quantified and controlled by experiments with the former, facilitating an informed selection of algorithm parameters (user-supplied inputs). We find that the contract maturity (or equivalently the time step for discretely monitored contracts) is a key determinant of the optimal B-spline order.

Section 4.2 introduces the PROJ for the class of B-spline scaling functions, and motivates the use of fixed-width truncation intervals for model robustness. We correct for a substantial numerical instability inherent in compact basis methods, demonstrating how to

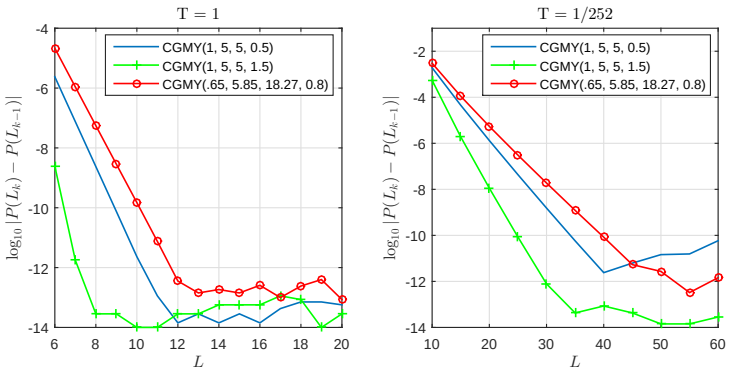

Figure 7: Truncation Parameter with COS: change in price estimates of ATM European call options with changes in truncation parameter $L = L_k \in \{6, ..., 80\}$, with $N = 2^{20}$ fixed. Even within a model class, convergence is highly dependent on the particular model and time to maturity. CGMY models from [61, 62, 64], with $r = .03$, $q = 0$, $S_0 = W = 100$. Prices found by put-call parity.

stabilize the procedure in general. Formulas for option prices with general B-splines are provided, along with the basic algorithm inputs. Section 4.3 conducts an extensive numerical comparison of the first four B-spline orders with respect to features of the pricing problem. Parameter choices are motivated, including a set of experiments to guide the selection of truncated density supports. Several implementations are investigated which apply to expansion methods in general. Finally, option Greeks are obtained and the paper is concluded in Section 4.4.

4.2 Option Pricing With B-Spline Projected Densities

For a general discussion of frames and Riesz bases, we refer the reader to [44,78]. The work of [127] considers approximation properties of B-splines, and applications to static hedging are considered in [88]. By transitioning to the Fourier domain, characteristic functions become sufficient for capturing the transition density of a process. The idea of PROJ, like other expansion methods such as COS [61, 112, 113], is to use this information to represent the density of log return. While the approach applies to a more general class of approximation spaces, the B-spline bases provide excellent approximations with varying degrees of smoothness.

There are three basic considerations that determine a density approximation using PROJ. The first is a choice of *generator* (or *scaling function*), denoted by φ, which is

a basic "shape" function that will be rescaled and shifted to form an approximation space of interlacing shapes on which to project the density. The approximation space is determined initially by its *resolution*. Higher resolutions imply more basis elements for any given interval and the ability to capture finer features of a density, such as extreme peaks. In theory, frame/basis projections are given in terms of an infinite dimensional basis spanning the entire real line on which lies the density support. In practice, finitely many basis elements are used, so the third consideration is the location of a density approximation, which implies a *truncated support*, determined by the right and left-most basis elements to be included.[1]

We consider three basic implementations, which are applied in different contexts. We first propose the use of a fixed truncation width approach to density expansion, which applies to any expansion method. We call this approach implementation I, and it is reviewed shortly. To motivate the advantage in robustness and model independence of a fixed-width approach over say a cumulant based approach, as suggested by [61], we plot in Figures 7 and 8 the convergence of the COS method as a function of the truncation width parameter L, with $N = 2^{21}$ fixed.

For three CGMY models, taken from the literature, the first two from [61,62,64], and the third from [42, 68], we plot for $T = 1$ and $T = 1/252$ the changes in value approximations, $P(L_k)$, that result from an increase of L from L_{k-1} to L_k, where $\{L_k\}$ is plotted on the x-axis. We repeat this experiment for three NIG models, also taken from the literature [42, 68, 121].

For a maturity $T = 1$, the NIG and CGMY models differ substantially in the required choice of L for any fixed accuracy, demonstrating an instability of parameter choice between model classes. Within each model class as well there is great variation with respect to this choice. We later demonstrate a much greater stability across and within model classes when a fixed interval width is chosen according to a model-independent rule of thumb.[2]

[1] We note that this is not the same as a projection of the truncated density, but rather a restriction of the infinite dimensional projection onto a finite support.

[2] In practice, a combination of the fixed and variable width approaches can be applied, using one to soften (or strengthen) the prescription of another. One simple approach is to impose caps and floors on support widths while allowing variability within bounds.

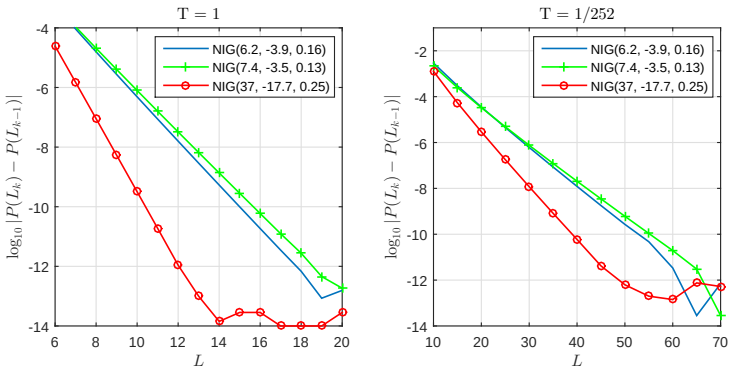

Figure 8: Truncation Parameter with COS: change in price estimates with changes in L for NIG models from $[42, 68, 121]$, with $N = 2^{20}$ fixed. Even larger values of L are required for these NIG examples, indicating a disparity across model classes as well as within. Other parameters: $r = .03$, $q = 0$, $S_0 = W = 100$. Prices found by put-call parity.

Table 11: Symbols, parameter restrictions and strip of analyticity $\mathcal{I}_L$ for tractable Levy processes.

Model	$\psi_L(\xi)$	Param. Restrict.	$\mathcal{I}_L$
BSM	$-\frac{\sigma^2}{2}\xi^2$	$\sigma > 0$	$\mathbb{R}$
MJD	$-\frac{\sigma^2}{2}\xi^2 + \lambda\left(e^{i\xi\mu_J - \frac{\sigma_J^2}{2}\xi^2} - 1\right)$	$\lambda, \sigma_J, \sigma > 0$	$\mathbb{R}$
CGMY	$C\Gamma(-Y)\left((M - i\xi)^Y - M^Y + (G + i\xi)^Y - G^Y\right)$	$C, G > 0, M > 1$ $Y \in (0,1) \cup (1,2)$	$[-M, G]$
NIG	$-\delta\left(\sqrt{\alpha^2 - (\beta + i\xi)^2} - \sqrt{\alpha^2 - \beta^2}\right)$	$\alpha, \delta > 0$ $\beta \in (-\alpha, \alpha - 1)$	$[\beta \pm \alpha]$
KOU	$-\frac{\sigma^2}{2}\xi^2 + \lambda\left(\frac{(1-p)\eta_2}{\eta_2 + i\xi} + \frac{p\eta_1}{\eta_1 - i\xi} - 1\right)$	$\lambda, \sigma > 0$, $p \in [0,1]$ $\eta_1 > 1, \eta_2 > 0$	$(-\eta_1, \eta_2)$
VG	$-\frac{\sigma^2}{2}\xi^2 - \frac{1}{\nu}\ln\left(1 - i\nu\theta\xi + \nu\frac{\sigma_V^2}{2}\xi^2\right)$	$\nu, \sigma_V > 0$, $\sigma \geq 0$ $\zeta := \sqrt{\frac{\theta^2}{\sigma_V^4} + \frac{2}{\nu\sigma_V^2}}$	$\left[\frac{\theta}{\sigma^2} \pm \zeta\right]$

It is important to mention that, for the Black-Scholes-Merton (BSM) model and other light-tailed distributions, convergence of COS is astonishingly fast, independent of essentially all problem data, e.g. strike, volatility, interest rate, maturity, etc. The benefits of using PROJ as opposed to the COS method are most readily observed in pricing contexts in which short-term transition densities (say $T \leq 1/52$, the case of weekly or more frequent observations for discretely monitored exotics) hinder the exponential convergence of cosine series expansion, and the local basis structure of PROJ outperforms the global cosine basis.

4.2.1 Characteristic Functions of Model Processes

Levy processes form a tractable class of models for the logarithmic return process of an asset price [46,117,121] (see [120] for a theoretical introduction). As particularly promising members from this class (representing a vast range of density behavior), for numerical experiments we consider mainly the Normal Inverse Gaussian (NIG) process of Barndorff-Nielsen (1995) and the CGMY process of Carr, Geman, Madan and Yor (2002) (see Boyarchenko and Levendorskii [16, 17] for a related class, the KoBoL processes). The variance gamma process [73,104,105] is another prominent example, which has fallen out of modeling favor in recent years (though is still used to test pricing methods). Characteristic functions for these and other processes are provided in Table 43 for reference. Other classes to which the PROJ method applies are the stochastic volatility models/affine jump diffusions [57, 71, 79, 101].

In this work, we assume that an underlying Levy process, $L(t), t \geq 0$, has been selected. The *characteristic exponent(symbol)* $\psi_L(\xi) := \ln \mathbb{E}[\exp(i\xi L(1))]$ uniquely specifies the processes at all times $t \geq 0$ by the corresponding characteristic function

$$\phi_{L(t)}(\xi) := \mathbb{E}[e^{iL(t)\xi}] = e^{t\psi_L(\xi)}, \quad t \geq 0,$$

where $\psi_L(z)$ is complex analytic in the strip $\mathcal{D}_{(\lambda_-,\lambda_+)} := \{z \in \mathbb{C} : \Im(z) \in (\lambda_-, \lambda_+)\}$. Figure 43 gives several characteristic functions and the associated strips of analyticity, which are of the form $\mathcal{I}_L \supset (-d, d)$ for some $0 < d \leq \infty$. From a defining symbol, we form the exponential Levy processes

$$S(t) = S(0)e^{Y(t)} = S(0)e^{(r-q+\omega)t+L(t)}, \quad \omega = -\psi_L(-i),$$

as a model of the *risk-neutral evolution* of an underlying asset[3], as required to price contingent claims. The characteristic function of log return $Y(T)$, assumed to possess the density $f_T(y)$, is given by

$$\widehat{f}_T(\xi) = e^{i\xi(r-q-\psi_L(-i))T}e^{\psi_L(\xi)T}, \quad T > 0. \tag{108}$$

With the exception of finite activity models (ie pure compound Poisson processes) that are of little practical interest, the assumption of a continuous density is without loss of

[3]Risk-neutrality is enforced by the martingale adjusted drift, $(r - q - \psi_L(-i))t$.

generality.

4.2.2 Orthogonal Projection Onto B-Spline Bases

The B-spline scaling functions represent a class of compactly supported Reisz basis generators. To derive analytical formulas for orthogonal projections onto each approximation space, we appeal to the frame representation[4] theorem [44, 78]. Coefficient functionals of the orthogonally projected density are given by a convolution of the density with a *dual* scaling function, using the unerlying's characteristic function.

With the Haar scaling function defined by $\varphi^{[0]}(y) := \mathbb{1}_{[-\frac{1}{2},\frac{1}{2}]}(y)$, we can define the p-th order B-spline scaling functions successively by the convolution

$$\varphi^{[p]}(x) = \varphi^{[0]} \star \varphi^{[p-1]}(x) = \int_{-\infty}^{\infty} \varphi^{[p-1]}(y-x)\mathbb{1}_{[-\frac{1}{2},\frac{1}{2}]}(y)dy. \tag{109}$$

The parity of order can determine how easy a basis is to work with. For example, the linear scaling function is found by convolving the Haar generator with itself, $\varphi^{[1]}(y) = (1+y)\mathbb{1}_{[-1,0]}(y) + (1-y)\mathbb{1}_{[0,1]}(y)$. Two more generators are considered in detail in this work. An additional convolution unveils the quadratic scaling function

$$\varphi^{[2]}(y) = \begin{cases} y^2/2 + 3y/2 + 9/8, & y \in [-3/2, -1/2] \\ 3/4 - y^2, & y \in [-1/2, 1/2] \\ y^2/2 - 3y/2 + 9/8, & y \in [1/2, 3/2]\,, \end{cases}$$

followed by the cubic scaling function

$$\varphi^{[3]}(y) = \begin{cases} (y+2)^3/6, & y \in [-2, -1] \\ 2/3 - y^3/2 - y^2, & y \in [-1, 0] \\ 2/3 + y^3/2 - y^2, & y \in [0, 1] \\ (2-y)^3/6, & y \in [1, 2]. \end{cases}$$

Approximation smoothness increases with the B-spline order while the generator support, $[-(p+1)/2, (p+1)/2]$, increases by a unit for each increment in order. Regularity

[4]While frame duality underlies much of the theory of dual wavelet construction, it is seldom used directly to obtain the projection. Rather, scaling functions are considered secondary to the corresponding wavelets. In this sense, our approach diverges from traditional applications.

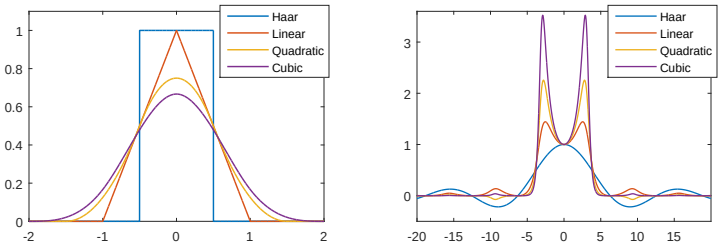

Figure 9: B-Spline generators (left) and their dual Fourier transforms (right).

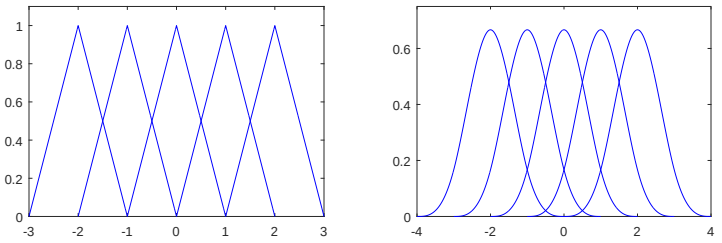

Figure 10: Approximation spaces of linear (left) and cubic (right) bases.

of the B-spline approximations is reflected in each generator's Fourier transform, which exhibits faster tail decay for higher orders. From equation (194), the p-th order B-spline generator has Fourier transform

$$\widehat{\varphi}^{[p]}(\xi) = \left(\frac{\sin(\xi/2)}{(\xi/2)}\right)^{p+1}, \quad \widehat{\varphi}^{[p]}(0) = \int_{-\infty}^{\infty} \varphi^{[p]}(x)dx = 1, \tag{110}$$

which decays at a polynomial rate of one more than the B-spline order. Similarly, greater regularity produces dual generators with Fourier transforms concentrated more tightly around the point of symmetry, with greater decay on the periphery as demonstrated in the right panel of Figure 9.

The method introduced in [83] proceeds as follows. If we denote by $P_{\mathcal{M}_a^{[p]}} f_T(y)$ the orthogonal projection of a density $f_T(y)$ onto the closed span $\mathcal{M}_a^{[p]} := \overline{\text{span}}\{\varphi_{a,k}^{[p]}\}_{k\in\mathbb{Z}}$ of the p-th order B-spline scaling function, a unique dual scaling function (generator) $\widetilde{\varphi}^{[p]}$ is guaranteed to exist for each order, by which the orthogonal projection is given analytically by the frame representation

$$P_{\mathcal{M}_a^{[p]}} f_T(y) = \sum_{k\in\mathbb{Z}} \left(\int_{-\infty}^{\infty} f_T(x)\widetilde{\varphi}_{a,k}^{[p]}(x)dx\right) \varphi_{a,k}^{[p]}(y) = \sum_{k\in\mathbb{Z}} \beta_{a,k}^{[p]} \cdot \varphi_{a,k}^{[p]}(y).$$

For a finite representation restricted to the set of basis elements $\{\varphi_{a,k}^{[p]}\}_{k=1}^{N}$, where each is centered respectively over the grid point $x_k = x_1 + (k-1)/a$, the coefficients are given

analytically by

$$\beta_{a,k}^{[p]} = \frac{a^{-1/2}}{\pi} \Re \left\{ \int_0^\infty \exp(-ix_k\xi) \cdot \widehat{f}_T(\xi) \cdot \widehat{\widetilde{\varphi}}^{[p]}(\xi/a) d\xi \right\}, \quad k = 1, ..., N. \tag{111}$$

These correspond to the infinite dimensional projection coefficients, shifted in alignment with the grid defined by x_1 (see Section 4.2.2.1 for a choice of x_1). While we provide Fourier transforms of dual generators up to the third order, higher order dual transforms are found by

$$\widehat{\widetilde{\varphi}}^{[p]}(\xi) = \left(\frac{\sin(\xi/2)}{(\xi/2)} \right)^{p+1} \left(\int_{-\frac{p+1}{2}}^{\frac{p+1}{2}} \varphi^{[p]}(x)^2 dx + 2 \sum_{k=1}^{p+1} \cos(k\xi) \int_{-\frac{p+1}{2}}^{\frac{p+1}{2}} \varphi^{[p]}(x) \varphi^{[p]}(x-k) dx \right)^{-1}$$

For a fixed point $x_1 \in \mathbb{R}$, the projection coefficients are approximated efficiently by the fast Fourier transform (FFT) implementation of the discrete Fourier transform, defined by :

$$\mathcal{D}_n\{y_j\} = \sum_{j=1}^{N} e^{-i\frac{2\pi}{N}(j-1)(n-1)} y_j, \quad n = 1, ..., N.$$

The projection coefficients are recovered in the Fourier domain according to

$$\left\{ \bar{\beta}_{a,k}^{[p]} \right\}_{k=1}^{N} := \Re \left\{ \mathcal{D} \left\{ H_j^{[p]} \right\}_{j=1}^{N} \right\}, \tag{112}$$

where $H_j^{[p]}$, $j = 1, ..., N$ are defined in Table 12 for each scaling function, $p = 0, ..., 3$. FFT inputs inputs $H_j^{[p]}$ are derived from $\widehat{\widetilde{\varphi}}^{[p]}$, the Fourier transform of the p-th scaling function. For a fixed N, a, step sizes in the Fourier domain are fixed by the Nyquist frequency:

$$\Delta_\xi = 2\pi a/N, \qquad \xi_j = (j-1)\Delta_\xi, \quad j = 1, ..., N. \tag{113}$$

4.2.2.1 Implementation I

In the first implementation, the grid is centered roughly over the mean return and such that $\ln(W/S_0)$ is a member, where $W > 0$ is the strike of a European option (vanilla, digital, etc.). We assume an underlying model $S_t = S_0 e^{Y_t}$ where $\mu_{Y_t} := \mathbb{E}[Y_t]$. With $\bar{P} \in \mathbb{N}$ fixed, a density approximation with support width 2α, centered over $[\mu_{Y_t} - \alpha, \mu_{Y_t} + \alpha]$, is chosen by[5] $\alpha = 2^{\bar{P}}/2$. The resolution is chosen as $\Delta = 2^{-P}$, $P \in \mathbb{N}_+$.

[5]In terms of the original implementation in [83], $\alpha = \bar{a}/2$, where $\bar{a} = 2^{\bar{P}}$. The notation α is used for consistency with non-dyadic implementations.

Table 12: FFT input and other parameters from dual generators derived in [83].

p	$H_1^{[p]}$	$H_j^{[p]}, \quad j = 2, ..., N$	$\Upsilon_{a,N}^{[p]}$	$N^{[p]}$
0	$\frac{1}{4a}$	$\exp(-ix_1\xi_j) \cdot \widehat{f}_T(\xi_j) \cdot (\sin(\xi_j/2a)/\xi_j)$	$e^{-rT} \cdot \frac{4a}{N}$	$\bar{n}$
1	$\frac{1}{24a^2}$	$\exp(-ix_1\xi_j) \cdot \widehat{f}_T(\xi_j) \cdot \frac{(\sin(\xi_j/(2a))/\xi_j)^2}{2+\cos(\xi_j/a)}$	$e^{-rT} \cdot \frac{24a^2}{N}$	$\bar{n}$
2	$\frac{1}{960a^3}$	$\exp(-ix_1\xi_j) \cdot \frac{\widehat{f}_T(\xi_j) \cdot (\sin(\xi_j/(2a))/\xi_j)^3}{33+26\cos(\xi_j/a)+\cos(2\xi_j/a)}$	$e^{-rT} \cdot \frac{960a^3}{N}$	$\bar{n}+1$
3	$\frac{1}{32a^4}$	$\frac{\exp(-ix_1\xi_j) \cdot \widehat{f}_T(\xi_j) \cdot 2520(\sin(\xi_j/(2a))/\xi_j)^4}{1208+1191\cos(\xi_j/a)+120\cos(2\xi_j/a)+\cos(3\xi_j/a)}$	$e^{-rT} \cdot \frac{32a^4}{N}$	$\bar{n}+1$

To ensure that $\ln(W/S_0)$ lies on the grid, we define

$$\bar{n} := \lfloor a\left(\ln(W/S_0) - \lambda\right) + 1 \rfloor, \quad \lambda := \mu_{Y_t} - (N/2 - 1)\,\Delta, \tag{114}$$

where $N := 2^{P+\bar{P}}$ is the total number of grid points along the truncated support. The grid is then determined by

$$x_1 = \ln(W/S_0) - (\bar{n} - 1)\Delta, \quad x_n = x_1 + (n-1)\Delta, \quad n = 1, ..., N, \tag{115}$$

and we have $\ln(W/S_0) = x_{\bar{n}} = x_1 + (\bar{n} - 1)\Delta$. For vanilla options, $x_{\bar{n}}$ is a discontinuity in the payoff's first derivative, and for digital options it marks a discontinuity in the payoff itself.[6]

Remark 8. We also note that, to avoid evaluating characterstic functions beyond the point at which they become negligible, zero padding should be used for $|\widehat{f}_T(\xi_j)| < \tau_\xi$, where for example $\tau_\xi = 10^{-15}$. To determine the zero-padding point, a simple procedure is to set $d = 2^{\bar{P}+2}$, initialize $c \leftarrow 1$ and $\tau \leftarrow |\widehat{f}_T(\Delta_\xi N/d)|$. Then, while $\tau > \tau_\xi$ and $c < d$, update $c \leftarrow c + 1$ and $\tau \leftarrow |\widehat{f}_T(\Delta_\xi N c/d)|$. After returning $\tilde{N} \leftarrow Nc/d$, we set $H_j^{[p]}$ for $j = 1, ..., \tilde{N}$ according to table 12, and $H_j^{[p]} = 0$ for $j = \tilde{N} + 1, ..., N$.

[6]With the truncated support chosen wide enough to control truncation error, implementation I is the most appropriate for studying convergence properties and different bases, as it allows us to isolate the errors arising from discretization and truncation. Alternative implementations are introduced in later sections to provide greater flexibility.

4.2.2.2 Valuation with Projected Densities

Consider a terminal payoff $g(S_T)$ which depends only on $S_T = S_0 e^{Y_T}$, where the log return process Y_T has an unknown density f_T, and define $G_{S_0}(y) := g(S_0 e^y)$. For a fixed choice of B-spline order $p \geq 0$, the value of g as a function of S_0, denoted $\mathcal{V} \circ g(S_0)$, is approximated in the following manner:

$$\mathcal{V} \circ g(S_0) = e^{-rT} \langle G_{S_0}, f_T \rangle \approx e^{-rT} \sum_{k \in \mathbb{Z}} \beta_{a,k}^{[p]} \cdot \langle G_{S_0}, \varphi_{a,k}^{[p]} \rangle \approx e^{-rT} \sum_{k=1}^{N^{[p]}} \beta_{a,k}^{[p]} \cdot \langle G_{S_0}, \varphi_{a,k}^{[p]} \rangle,$$

where the errors associated with each approximation are analyzed in [83]. The index of summation $N^{[p]}$ is given in Table 12, and depends on the overlap of $x_{\bar{n}}$ with neighboring basis elements $\varphi_{a,k}^{[p]}$. Further defining $\Upsilon_{a,N}^{[p]} := e^{-rT}/(N \cdot H_1^{[p]})$ (see Table 12), we have the p-th order value approximation

$$\mathcal{V}_N^{[p]} \circ g(S_0) := \Upsilon_{a,N}^{[p]} \sum_{k=1}^{N^{[p]}} \bar{\beta}_{a,k}^{[p]} \cdot a^{1/2} \langle G_{S_0}, \varphi_{a,k}^{[p]} \rangle, \tag{116}$$

where the term $a^{1/2}$ serves as a simplifying constant in the evaluation of *payoff coefficients*, $a^{1/2}\langle G_{S_0}, \varphi_{a,k}^{[p]} \rangle$. While these coefficients are analytically obtainable for many contracts, including vanilla options, one of the contributions of this work is to show that inexact formulas for the coefficients produce more stable results. We propose a quadrature based approximation approach, described in generality in Section 4.4.1, to restore valuation accuracy which enables the use of higher order (and faster converging) B-spline projections. Vanilla options are considered as a special case in Section 4.2.4, followed by forward starting options.

4.2.3 Quadrature and Stabilization of Coefficient Formulas

In this subsection, we provide an overview of the general procedure for evaluating integrals that arise for B-spline pricing methods. The method is described in detail in the appendix to facilitate extensions to alternative applications. The same methodology applies method applies, for example, to the terminal payoffs (and in the case of discretely monitored exotics, to the intermediate value formulas) of Asian (geometric/arithmetic), digital, power, lookback, swing, and cliquet options, variance swaps and so on, all with possible barriers and even tranches. A special case of the methodology was applied to barrier options in [85] for the linear basis, which we extend to general payoffs and for higher order splines.

4.2.3.1 Integral Partitioning

As indicated in Section 4.2.2.2, analytical formulas for payoff coefficients, when they exist, are prone to numerical instability. Although it seems like moving in the wrong direction, we are actually able to restore valuation accuracy by using inexact formulas for coefficients, obtained by applying quadrature rules with strictly positive weights. Positivity of the weights ensures stability of coefficient approximations. Given that value approximations decay polynomially (although at a faster rate than basic theory would suggest), it suffices to consider Newton-Cotes quadrature formulas[7].

For a general payoff $G_{S_0}(y) := g(S_0 e^y)$, valuation formula (116) requires the evaluation of payoff coefficients $g^{[p]}_{a,n} = a^{1/2}\langle G_{S_0}, \varphi^{[p]}_{a,n}\rangle$, $n = 1, ..., N$. For B-spline order p, define the generator support $I^{[p]} := \left[-\frac{p+1}{2}, \frac{p+1}{2}\right]$. By a change of variable, we can write

$$g^{[p]}_{a,n} = a^{1/2}\int_{x_n-\frac{p+1}{2a}}^{x_n+\frac{p+1}{2a}} G_{S_0}(y)a^{1/2}\varphi^{[p]}(a(y-x_n))dy = \int_{I^{[p]}} G_{S_0}\left(\frac{y}{a}+x_n\right)\varphi^{[p]}(y)dy. \quad (117)$$

In order to apply quadrature rules systematically to obtain *exact formulas* for coefficient approximations, we break the coefficient integrals into sections of at most unit length. The sections are then subdivided according to payoff singularities, and the same rule is applied to each subdivision. As a concrete example, we apply this approach to the European put option with strike price $W > 0$, and terminal payoff $G_{S_0} = (W - S_0 e^y)^+ = (W - S_0 e^y)\mathbb{1}_{[y\le \ln(W/S_0)]}$. To derive coefficient formulas, we define for $n = 1, ..., N$

$$\begin{aligned} g^{[p]}_{a,n} &= a^{1/2}\langle G_{S_0}, \varphi^{[p]}_{a,n}\rangle(y) = a^{1/2}\int_{-\infty}^{\infty}(W - S_0 e^y)\varphi^{[p]}_{a,n}(y)\mathbb{1}_{[y\le \ln(W/S_0)]}dy \\ &= a^{1/2}W\int_{-\infty}^{\ln(W/S_0)}\varphi^{[p]}_{a,n}(y)dy - a^{1/2}S_0\int_{-\infty}^{\ln(W/S_0)} e^y\varphi^{[p]}_{a,n}(y)dy. \end{aligned} \quad (118)$$

This payoff has only the singularity $\ln(W/S_0)$ which is aligned with the grid (Section 4.2.5 considers a misalignment).

[7] Boole's rule is sufficient for the quadratic and cubic splines to value vanilla options (increasing to the seven-point rule provides no gain). Gaussian quadrature with three points also provides the same results, but it makes the derivation of coefficient approximations slightly more involved (Newton-Cotes are a great starting point for extensions to other payoffs). We will, however, apply Gaussian quadrature in the vanilla option case for calibration, in which a grid misalignment requires the basic integrals be augmented slightly, and the fewer Guassian nodes is desirable.

4.2.4 Stable Coefficient Formulas for Vanilla Options

For vanilla options, the formulas for $g_{a,n}^{[p]}$ are separable in x_n, and thus closed form approximations to the coefficient functions are obtained by integrals that are nearly independent of the grid. However, the way in which "kink" points of the payoff are handled is vital to the rate and smoothness of convergence of price approximations. With a, x_1 fixed, anticipating the change of variables we define for each $p \geq 0$ the quantities

$$\bar{\vartheta}_*^{[p]} := \int_{\left[-\frac{p+1}{2}, \frac{p+1}{2}\right]} \varphi^{[p]}(y)dy, \qquad \vartheta_*^{[p]} := \int_{\left[-\frac{p+1}{2}, \frac{p+1}{2}\right]} \varphi^{[p]}(y)e^{\frac{y}{a}}dy, \tag{119}$$

and for each $j \in \{-n_p, ..., n_p\}$, where $n_p := \lceil (p+1)/2 \rceil - 1$, define

$$\bar{\vartheta}_j^{[p]} := \int_{-\frac{p+1}{2}}^{-j} \varphi^{[p]}(y)dy, \qquad \vartheta_j^{[p]} := \int_{-\frac{p+1}{2}}^{-j} \varphi^{[p]}(y)e^{\frac{y}{a}}dy. \tag{120}$$

For the B-splines of order up to three, $n_p \leq 1$, while $n_p = 2$ for the quartic and quintic B-splines. When $\ln(W/S_0)$ is not located on the grid, as is the case for calibration to multiple strikes, there will be an additional integral as well, which will be defined similarly as in the present case and is treated in Section 4.2.5. The next result summarizes the coefficient formulas for pricing put options with p-th order B-splines.[8]

Lemma 4.2.1. *For $p \geq 0$, and $n_p := \lceil (p+1)/2 \rceil - 1$, the vanilla put coefficients satisfy*

$$g_{a,n}^{[p]} = \begin{cases} W \cdot \bar{\vartheta}_*^{[p]} - S_0 e^{x_n} \cdot \vartheta_*^{[p]}, & n \leq \bar{n} - n_p - 1 \\ W \cdot \left(\bar{\vartheta}_{n-\bar{n}}^{[p]} - e^{(n-\bar{n})\Delta} \cdot \vartheta_{n-\bar{n}}^{[p]} \right), & |n - \bar{n}| \leq n_p \end{cases} \tag{121}$$

where $1 \leq n \leq N$, and $x_{\bar{n}} = \ln(W/S_0)$. Note that $g_{a,n}^{[p]} = 0$ for $n \geq \bar{n} + n_p + 1$.

For the B-spline orders considered in this work, we have the following simplification:

Corollary 4.2.2. *For the Haar and linear bases, put options are priced with the coefficients*

$$p = 0, 1: \quad g_{a,n}^{[p]} = \begin{cases} W - S_0 e^{x_n} \cdot \vartheta_*^{[p]}, & n \leq \bar{n} - 1 \\ W \cdot \left(\frac{1}{2} - \vartheta_0^{[p]} \right), & n = \bar{n} \end{cases} \tag{122}$$

[8] The terms $\bar{\vartheta}_*^{[p]}$ and $\bar{\vartheta}_j^{[p]}$ are just constants, and are evaluated precisely.

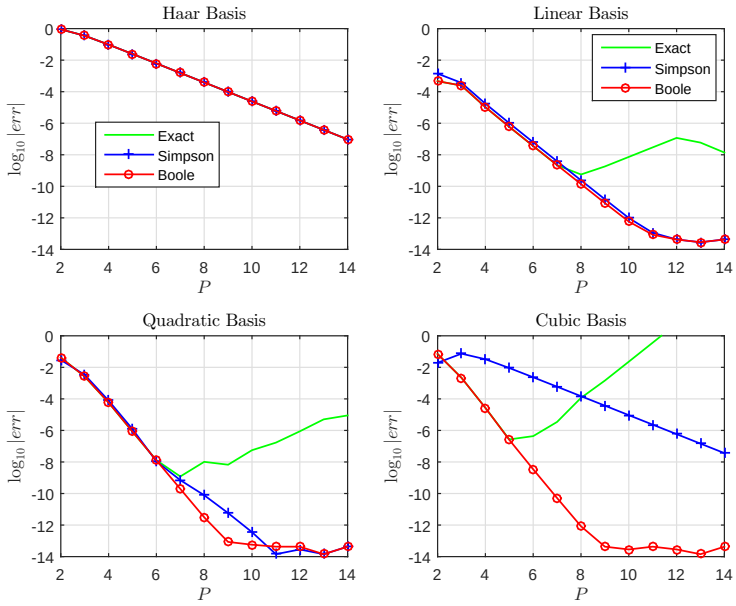

Figure 11: Quadrature and Stabilization: example of convergence restored by replacing exact payoff coefficient formulas with closed-form Newton-Cotes approximations in the CGMY(1,25,30,1.5) model; $r = .05, q = 0, T = 1/52$, $S_0 = W = 100$; support parameter $\bar{P} = 4$. Reference prices computed by COS with $N = 2^{19}$ and $L = 12$ (confirmed by Hilbert Transform method [64]).

For quadratic and cubic bases, put options are priced with the coefficients

$$p = 2, 3: \quad g_{a,n}^{[p]} = \begin{cases} W - S_0 e^{x_n} \cdot \vartheta_*^{[p]}, & n \leq \bar{n} - 2 \\ W \cdot \left(\bar{\vartheta}_{-1}^{[p]} - e^{-\Delta} \cdot \vartheta_{-1}^{[p]} \right), & n = \bar{n} - 1 \\ W \cdot \left(\frac{1}{2} - \vartheta_0^{[p]} \right), & n = \bar{n} \\ W \cdot \left(\bar{\vartheta}_1^{[p]} - e^{\Delta} \cdot \vartheta_1^{[p]} \right), & n = \bar{n} + 1 \end{cases} \tag{123}$$

Applying Boole's rule (see Section 4.2.4.1 below) to evaluate the integrals in (119) and (120) leads to the formulas found in Table 28, which are used in conjunction with Corollary 4.2.2 to evaluate put options, and hence call options by put-call parity:

$$\mathcal{V}_C(S_0, W) = \mathcal{V}_P(S_0, W) + S_0 \cdot \exp(-qT) - W \cdot \exp(-rT), \tag{124}$$

where $\mathcal{V}_C(S_0, W)$ and $\mathcal{V}_P(S_0, W)$ represent the call and put option values for a given model with strike $W > 0$ and initial price $S_0 > 0$. Note that regardless of the quadrature rule employed, the generic formulas in Corollary 4.2.2 have separated all integrals from the option

data, namely S_0 and W, as a result of the variable change. Once the values of $\vartheta^{[p]}_{(\cdot)}, \bar{\vartheta}^{[p]}_{(\cdot)}$ are found, option Greeks will be obtained as byproducts of the pricing formula. Aside from pricing vanilla options, these integrals (and hence stable approximations) reappear for other payoffs and in many exotic contexts.

4.2.4.1 Example: Vanilla Coefficient Formulas by Boole's Rule

We show how the formulas in Table 28 are derived. Recall (or refer to Table 17) the closed five-point Newton-Cotes formula, *Boole's rule*, on $[0, 1]$, which prescribes the nodes and weights

$$\eta_m := (m-1)/4, \quad m = 1, ..., 5, \qquad w_m \in \tfrac{1}{90}\{7, 32, 12, 32, 7\}.$$

Considering the quadratic basis, the first integral is approximated by

$$\vartheta^{[2]}_1 := \int_{-\frac{3}{2}}^{-1} \varphi^{[2]}(y) e^{\frac{y}{a}} dy \approx \frac{1}{2} \sum_{m=1}^{5} w_m \cdot \varphi^{[2]}(\gamma_{1,m}) \cdot e^{\frac{\gamma_{1,m}}{a}},$$

where the nodes $\gamma_{1,m} := -3/2 + (1/2)\eta_m$, and the $1/2$ accounts for the interval width (see equation (151)). Similarly,

$$\vartheta^{[2]}_0 := \int_{-\frac{3}{2}}^{0} \varphi^{[2]}(y) e^{\frac{y}{a}} dy \approx \sum_{m=1}^{5} w_m \left(\varphi^{[2]}(y_{1,m}) \cdot e^{\frac{y_{1,m}}{a}} + \frac{1}{2} \cdot \varphi^{[2]}(\gamma_{2,m}) \cdot e^{\frac{\gamma_{2,m}}{a}} \right),$$

where (by equations(150) and (151)) we have $y_{1,m} := -3/2 + \eta_m$, and $\gamma_{2,m} := -1/2 + (1/2)\eta_m$. The approximation of $\vartheta^{[2]}_{-1}$ is found analogously. Finally we have

$$\vartheta^{[2]}_* := \int_{-\frac{3}{2}}^{\frac{3}{2}} \varphi^{[2]}(y) e^{\frac{y}{a}} dy \approx \sum_{m=1}^{5} w_m \left(\varphi^{[2]}(y_{1,m}) \cdot e^{\frac{y_{1,m}}{a}} + \varphi^{[2]}(y_{2,m}) \cdot e^{\frac{y_{2,m}}{a}} + \varphi^{[2]}(y_{3,m}) \cdot e^{\frac{y_{3,m}}{a}} \right),$$

where $y_{l,m} = a_l + \eta_m$, $m = 1, ...5$, and $(a_1, a_2, a_3) := (-3/2, -1/2, 1/2)$. After simplifying each expression, we have reusable formulas for the approximations of vanilla put coefficients.

Figure 11 demonstrates the dramatic stabilization of coefficients values, and the consequent restoration of call price convergence, by using the approximations given in Table 28 with Corollary 4.2.2 (by put-call parity (PCP)), compared to the exact analytical formulas. Especially for the smoother quadratic and cubic bases, value approximations made with exact coefficients become highly unstable as the resolution is refined. In terms of higher order quadrature, increasing to a seven-point rule (for the bases considered) provides no additional gain (nor do the Gaussian quadratures).

Table 13: Stable coefficient approximations for use with call and put terminal payoffs (vanilla or otherwise). For use with Corollary 4.2.2, and other payoff functions.

Boole's Stable Approximation of Coefficients		
Linear	$\bar{\vartheta}_j^{[1]}$	$\vartheta_j^{[1]}$
$j = *$	1	$\frac{1}{15}\left[\frac{7}{3} + \frac{8}{3}\cosh(3\Delta/4) + 2\cosh(\Delta/2) + 8\cosh(\Delta/4)\right]$
$j = 0$	$\frac{1}{2}$	$\frac{1}{15}\left[\frac{7}{6} + \frac{4}{3}e^{-3\Delta/4} + e^{-\Delta/2} + 4e^{-\Delta/4}\right]$
Quadratic	$\bar{\vartheta}_j^{[2]}$	$\vartheta_j^{[2]}$
$j = *$	1	$\frac{1}{5}\left[\frac{1}{2} + \frac{1}{9}\left(\cosh(5\Delta/4) + 7\cosh(\Delta/2) + 22\cosh(\Delta/4)\right) + \cosh(3\Delta/4) + \frac{1}{6}\cosh(\Delta)\right]$
$j = -1$	$\frac{47}{48}$	$\frac{1}{10}\left[1 + \frac{1}{9}\left(e^{-5\Delta/4} + 7e^{-\Delta/2} + 44\cosh(\Delta/4)\right) + e^{-3\Delta/4} + \frac{1}{6}e^{-\Delta} + \frac{7}{12}e^{\Delta/2} + \frac{49}{72}e^{5\Delta/8} + \frac{25}{72}e^{7\Delta/8} + \frac{3}{16}e^{3\Delta/4} + \frac{7}{144}e^{\Delta}\right]$
$j = 0$	$\frac{1}{2}$	$\frac{1}{10}\left[\frac{7}{24} + \frac{1}{9}e^{-5\Delta/4} + \frac{1}{6}e^{-\Delta} + e^{-3\Delta/4} + \frac{7}{12}e^{-\Delta/2} + \frac{13}{12}e^{-3\Delta/8} + \frac{11}{24}e^{-\Delta/4} + \frac{47}{36}e^{-\Delta/8}\right]$
$j = 1$	$\frac{1}{48}$	$\frac{1}{80}\left[e^{-9\Delta/8} + \frac{1}{6}e^{-5\Delta/4} + \frac{1}{9}e^{-11\Delta/8} + \frac{7}{18}e^{-\Delta}\right]$
Cubic	$\bar{\vartheta}_j^{[3]}$	$\vartheta_j^{[3]}$
$j = *$	1	$\frac{1}{90}\left[\frac{14}{3}\left(2 + \cosh(\Delta)\right) + \frac{1}{2}\left(\cosh(3\Delta/2) + 9\cosh(5\Delta/4) + 23\cosh(\Delta/2)\right) + \frac{1}{6}\left(\cosh(7\Delta/4) + 121\cosh(3\Delta/4) + 235\cosh(\Delta/4)\right)\right]$
$j = -1$	$\frac{23}{24}$	$\frac{1}{90}\left[\frac{1}{3}\left(28 + 7e^{-\Delta}\right) + \frac{1}{12}\left(14e^{\Delta} + e^{-7\Delta/4} + 242\cosh(3\Delta/4) + 470\cosh(\Delta/4)\right) + \frac{1}{4}\left(e^{-3\Delta/2} + 9e^{-5\Delta/4} + 46\cosh(\Delta/2)\right)\right]$
$j = 0$	$\frac{1}{2}$	$\frac{1}{20}\left[\frac{28}{27} + \frac{1}{54}\left(e^{-7\Delta/4} + 121e^{-3\Delta/4} + 235e^{-\Delta/4}\right) + \frac{1}{18}\left(e^{-3\Delta/2} + 23e^{-\Delta/2}\right) + \frac{1}{2}e^{-5\Delta/4} + \frac{14}{27}e^{-\Delta}\right]$
$j = 1$	$\frac{1}{24}$	$\frac{1}{20}\left[\frac{1}{54}e^{-7\Delta/4} + \frac{1}{18}e^{-3\Delta/2} + \frac{1}{2}e^{-5\Delta/4} + \frac{7}{27}e^{-\Delta}\right]$

In all subsequent calculations with the B-spline bases, stable coefficient formulas are employed. The coefficient approximation derived from Boole's rule is applied with orders 1,2, and 3, while exact coefficients are used with the Haar basis. When approximations to option Greeks are made, stable formulas will be used as well.

4.2.4.2 Digital Options

A simple payoff which arises as a building block for more complicated products is the digital (or binary) option. For example, the digital put has payoff $g(S_0 e^y) = \mathbb{1}_{[y \leq \ln(W/S_0)]}$, so that $\mathcal{V} \circ g(S_0) = e^{-rT} \int_{-\infty}^{\ln(W/S_0)} f_T(y)dy = e^{-rT} F_T(\ln(W/S_0))$. The PROJ valuation formula is trivial to derive. For example, in the linear case (the same formula holds for Haar) and cubic cases, the closed form approximation is

$$\mathcal{V} \circ g(S_0) \approx \Upsilon^{[1]}_{a,N} \left(\frac{\bar{\beta}^{[1]}_{a,\bar{n}}}{2} + \sum_{k=1}^{\bar{n}-1} \bar{\beta}^{[1]}_{a,k} \right),$$

$$\mathcal{V} \circ g(S_0) \approx \Upsilon^{[3]}_{a,N} \left(\frac{23}{24} \bar{\beta}^{[3]}_{a,\bar{n}-1} + \frac{1}{2} \bar{\beta}^{[3]}_{a,\bar{n}} + \frac{1}{24} \bar{\beta}^{[3]}_{a,\bar{n}+1} + \sum_{k=1}^{\bar{n}-2} \bar{\beta}^{[3]}_{a,k} \right).$$

For European options, the Hilbert transform has exponential convergence for pricing digital options. However, given that digitals arise in exotic contexts, these formulas apply.[9]

4.2.5 Gaussian Quadrature Adjustment for Grid Misalignment

In the case that $\ln(W/S_0)$ is not a member of the grid, which is true for calibration of multiple options as well as when pricing many exotic options (barrier [85], swing, etc.), an adjustment is made to the coefficient formulas to account for the "misalignment". Suppose that x_1 has been fixed, as well as a step size Δ, and grid budget N. Then the nearest grid point $x_{\bar{n}}$ left of $\ln(W/S_0)$, along with the difference and normalized difference are defined by

$$\bar{n} := \lfloor a \cdot (\ln(W/S_0) - x_1) + 1 \rfloor, \qquad \rho := \ln(W/S_0) - x_{\bar{n}}, \qquad \zeta := a \cdot \rho. \tag{125}$$

Starting with the odd orders, the coefficient adjustments for grid misalignment are defined for $j = -\frac{p+1}{2} + 1, ..., \frac{p+1}{2}$ by

$$\bar{\delta}^{[p]}_j := \int_{-j}^{-j+\zeta} \varphi^{[p]}(y)dy, \qquad \delta^{[p]}_j := \int_{-j}^{-j+\zeta} \varphi^{[p]}(y) e^{\frac{y}{a}} dy. \tag{126}$$

[9] The convergence of digital prices with PROJ is quite rapid, albeit not exponential.

Table 14: Define $\kappa_j := \zeta - j$, $\zeta_\pm := \zeta \cdot q_\pm$, and $\rho_\pm := \rho \cdot q_\pm$. Coefficient adjustments derived from a three point Gaussian quadrature.

Gaussian Quadrature Adjustment for Calibration		
Linear	$\bar{\delta}_j^{[1]}$	$\delta_j^{[1]}$
$j=0$	$\zeta\left(1-\frac{1}{2}\zeta\right)$	$\frac{\zeta}{18}\left[4(2-\zeta)e^{\rho/2}+5\cdot((1-\zeta_-)e^{\rho_-}+(1-\zeta_+)e^{\rho_+})\right]$
$j=1$	$\zeta-\bar{\delta}_0^{[1]}$	$\frac{\zeta}{18}\cdot e^{-\Delta}\cdot\left[4\zeta\cdot e^{\rho/2}+5\left(\zeta_- e^{\rho_-}+\zeta_+ e^{\rho_+}\right)\right]$
Cubic	$\bar{\delta}_j^{[3]}$	$\delta_j^{[3]}$
$j=-1$	$\frac{4}{3}\zeta+\frac{17}{24}+\kappa_{-1}^2\left(\kappa_{-1}\left(\frac{1}{3}-\frac{1}{24}\kappa_{-1}\right)-1\right)$	$\frac{e^{\Delta}}{6}\frac{\zeta}{18}\left[5\left((1-\zeta_-)^3e^{\rho_-}+(1-\zeta_+)^3e^{\rho_+}\right)+(2-\zeta)^3e^{\rho/2}\right]$
$j=0$	$\zeta\left(\frac{2}{3}+\zeta^2\left(\frac{1}{8}\zeta-\frac{1}{3}\right)\right)$	$\frac{\zeta}{18}\left[10\left(\frac{2}{3}+\zeta_-^2\left(\frac{1}{2}\zeta_--1\right)\right)e^{\rho_-}+8\left(\frac{2}{3}+\zeta^2\left(\frac{1}{2}\zeta-1\right)\right)e^{\rho/2}\right]$
$j=1$	$\frac{2}{3}\zeta-\frac{5}{24}-\kappa_1^4\left(\frac{1}{8}\kappa_1+\frac{1}{3}\right)$	$e^{-\Delta}\frac{\zeta}{18}\left[10\left(\frac{2}{3}-\frac{1}{2}\left(\zeta_--1\right)^2\left(\zeta_-+1\right)e^{\rho_-}\right)\right.$ $\left.+8\left(\frac{2}{3}-\frac{1}{2}\left(\frac{\zeta}{2}-1\right)^2\left(\frac{\zeta}{2}+1\right)\right)e^{\rho/2}\right]$
$j=2$	$\kappa_2^2\left(1+\kappa_2\left(\frac{1}{3}+\frac{1}{24}\kappa_2\right)\right)+\frac{4}{3}\zeta-2$	$\frac{e^{-2\Delta}}{6}\frac{\zeta}{18}\left[10\zeta_-^3e^{\rho_-}+\zeta^3e^{\rho/2}\right]$

These adjustments are then added to the original coefficients from equation (120) (and (119) when applicable), to obtain for example

$$\vartheta_j^{[p]}+\delta_j^{[p]} := \int_{-\frac{p+1}{2}}^{-j}\varphi^{[p]}(y)e^{\frac{y}{a}}dy+\int_{-j}^{-j+\zeta}\varphi^{[p]}(y)e^{\frac{y}{a}}dy=\int_{-\frac{p+1}{2}}^{-j+\zeta}\varphi^{[p]}(y)e^{\frac{y}{a}}dy. \tag{127}$$

In general, it is straightforward to verify the following.

Lemma 4.2.3. *Suppose $\zeta \geq 0$. For $p \geq 0$, and $n_p := \lceil (p+1)/2 \rceil - 1$, the vanilla put coefficients under grid misalignment satisfy*

$$g_{a,n}^{[p]} = \begin{cases} W\cdot\bar{\vartheta}_*^{[p]} - S_0e^{x_n}\cdot\vartheta_*^{[p]} & n \leq \bar{n}-n_p-1 \\ W\cdot\left(\bar{\vartheta}_{(n-\bar{n})}^{[p]}+\bar{\delta}_{(n-\bar{n})}^{[p]}-e^{(n-\bar{n})\Delta-\rho}\cdot\left(\vartheta_{(n-\bar{n})}^{[p]}+\delta_{(n-\bar{n})}^{[p]}\right)\right) & |n-\bar{n}|\leq n_p \\ W\cdot\left(\bar{\delta}_{(n-\bar{n})}^{[p]}-e^{(n-\bar{n})\Delta-\rho}\cdot\delta_{(n-\bar{n})}^{[p]}\right) & n=\bar{n}+n_p+1 \end{cases} \tag{128}$$

where $1 \leq n \leq N$.

In the presence of grid misalignments, we take advantage of the fewer nodes required by Gaussian quadrature, as opposed to Newton-Cotes rules of comparable order. For B-spline orders up to cubic, we find that a three point Gaussian rule preserves the overall

convergence rate. We consider odd spline orders for ease of notation. First we define the constants

$$q_- := \left(1 - \sqrt{3/5}\right)/2, \qquad q_+ := \left(1 + \sqrt{3/5}\right)/2. \tag{129}$$

For a fixed $l = 1, ..., p+1$, we define the Gaussian nodes and weights on $[-j, -j+\zeta]$ for $m = 1, 2, 3$ by

$$\eta_m \in \{-j + \zeta \cdot q_-,\ -j + \zeta/2,\ -j + \zeta \cdot q_+\}, \qquad w_m \in \tfrac{\zeta}{18} \cdot \{5, 8, 5\}. \tag{130}$$

These weights are used to define the quadrature adjustments found in Table 37, which together with Lemma 4.2.3 provides the following closed-form expressions, where most coefficients are unaffected by the misalignment.[10]

Corollary 4.2.4. *For the linear basis, put options are priced with the coefficients*

$$g^{[1]}_{a,n} = \begin{cases} W - S_0 \cdot \vartheta^{[1]}_* \cdot \exp(x_n) & n \le \bar{n} - 1 \\ W \cdot \left(\bar{\vartheta}^{[1]}_0 + \bar{\delta}^{[1]}_0 - e^{-\rho} \cdot \left(\vartheta^{[1]}_0 + \delta^{[1]}_0\right)\right) & n = \bar{n} \\ W \cdot \left(\bar{\delta}^{[1]}_1 - e^{-\rho} \cdot e^{\Delta} \cdot \delta^{[1]}_1\right) & n = \bar{n} + 1 \end{cases} \tag{131}$$

For the cubic basis, put options are priced with the coefficients

$$g^{[3]}_{a,n} = \begin{cases} W - S_0 \cdot \vartheta^{[3]}_* \cdot \exp(x_n) & n \le \bar{n} - 2 \\ W \cdot \left(\bar{\vartheta}^{[3]}_{-1} + \bar{\delta}^{[3]}_{-1} - e^{-\rho} \cdot e^{-\Delta} \cdot \left(\vartheta^{[3]}_{-1} + \delta^{[3]}_{-1}\right)\right) & n = \bar{n} - 1 \\ W \cdot \left(\bar{\vartheta}^{[3]}_0 + \bar{\delta}^{[3]}_0 - e^{-\rho} \cdot \left(\vartheta^{[3]}_0 + \delta^{[3]}_0\right)\right) & n = \bar{n} \\ W \cdot \left(\bar{\vartheta}^{[3]}_1 + \bar{\delta}^{[3]}_1 - e^{-\rho} \cdot e^{\Delta} \cdot \left(\vartheta^{[3]}_1 + \delta^{[3]}_1\right)\right) & n = \bar{n} + 1 \\ W \cdot \left(\bar{\delta}^{[3]}_2 - e^{-\rho} \cdot e^{2\Delta} \cdot \delta^{[3]}_2\right) & n = \bar{n} + 2 \end{cases} \tag{132}$$

For brevity, Table 37 provides the necessary adjustments for orders $1, 3$, while ordinary constants are still given by Table 28. Aside from calibration, this adjustment scheme is applied to the derivation of payoff coefficients for barrier options [85], since placing barriers on the grid introduces a strike misalignment.

[10] For calibration, the original coefficients are the same for every strike. Only the coefficient adjustments are strike dependent. Further, the exponentials e^{x_n}, $n = 1, ..., \bar{n} - n_p - 1$, are calculated once at initialization, and are then used by each of the strikes. Moreover, the density is projected only once, so the cost of most computations is spread over the set of strikes.

4.2.6 Forward Starting Options

Forward starting options are contracts whose strike is determined by the underlying process at a future date. Given an a expiry T, and a fixing date t_*, forward starting call and put options are defined by their respective terminal payoffs $(S_T - S_{t_*})^+$ and $(S_{t_*} - S_T)^+$, and S_0 is the known underlying price at some time $t_0 < t_* < T$. It is simple to derive the parity

$$\mathcal{V}_C(S_0) = \mathcal{V}_P(S_0) + S_0(\exp(-qT) - \exp(-r\tau - qt_*)), \qquad \tau := T - t_*,$$

from which the call value $\mathcal{V}_C(S_0)$ is found upon determining the put value $\mathcal{V}_P(S_0)$. The put value is defined with respect to the European price at time t_*, $\mathcal{V}_P^{Eur}(S_{t_*}) = e^{-r\tau}\mathbb{E}[(1 - \exp(X_\tau))^+] \cdot S_{t_*}$, since $(S_{t_*} - S_T)^+ = S_{t_*}(1 - \exp(X_\tau))^+$, where $X_\tau := \ln(S_T/S_{t_*})$.

The problem is solved in two stages with the same P and $\bar{P}$ in each stage for simplicity (similarly, we maintain the same order p in both stages). First, we obtain the value $\Lambda := e^{-r\tau}\mathbb{E}[(1 - \exp(X_\tau))^+]$ by an expansion

$$\Lambda \approx \Lambda^{[p]}(\tau) := \Upsilon_{a,N}^{[p]}(\tau) \sum_{k=1}^{N^{[p]}} \bar{\beta}_{a,k}^{[p]}(\tau) \cdot g_{a,k}^{[p]}(1,1),$$

where the dependence on τ is to emphasize that the coefficients $\beta_{a,k}^{[p]}(\tau)$ and the constant $\Upsilon_{a,N}^{[p]}(\tau)$ are obtained for a time horizon of τ, with chf $\widehat{f}_\tau(\xi)$. The coefficients $g_{a,k}^{[p]}(1,1)$ correspond to a European put option with $S_0 = W = 1$, and are given by Corollary 4.2.2 with stable coefficients derived from Table 28. To find $\bar{\beta}_{a,k}^{[p]}(\tau)$, we set a grid $x_k = (k - N/2)\Delta$, $k = 1, \ldots, N$, so that $x_{N/2} = x_{\bar{n}} = 0$ is aligned with the kink ($\bar{n} \equiv N/2$).

Next, we define the "payoff" $G_{S_0}(x) = \Lambda^{[p]}(\tau) \cdot S_0 \exp(x)$, where $x = \ln(S_{t_*}/S_0)$. A second expansion over $\{x_k\}_{k=1}^N$, now with chf $\widehat{f}_{t_*}(\xi)$, yields the coefficients $\bar{\beta}_{a,k}^{[p]}(t_*)$, from which we derive

$$\begin{aligned}
\mathcal{V}_P(S_0) &\approx \Upsilon_{a,N}^{[p]}(t_*) \sum_{k=1}^{N} \bar{\beta}_{a,k}^{[p]}(t_*) a^{1/2} \int_{-\infty}^{\infty} G_{S_0}(x) \varphi_{a,k}^{[p]}(x) dx \\
&= \Lambda^{[p]}(\tau) \cdot S_0 \cdot \Upsilon_{a,N}^{[p]}(t_*) \sum_{k=1}^{N} \bar{\beta}_{a,k}^{[p]}(t_*) \exp(x_k) \int e^{\frac{y}{a}} \varphi^{[p]}(y) dy \\
&= C^{[p]}(\tau, t_*) \sum_{k=1}^{N} \bar{\beta}_{a,k}^{[p]}(t_*) \exp(x_k)
\end{aligned}$$

Table 15: Abs. errors for forward starting call options in BSM with $r = 0.1$, $q = 0$, $S_0 = 100$, $t_* = 0.25$ and $T = 1$; Cubic PROJ with $\bar{P} = 1$. Ref. values obtained by analytical formula: $[7.2257, 7.2962, 8.1163, 9.4125, 12.4133]$.

P	$\sigma = 0.01$	$\sigma = 0.05$	$\sigma = 0.10$	$\sigma = 0.15$	$\sigma = 0.25$
2	8.293e-01	4.784e-01	1.537e-01	2.947e-02	7.210e-02
3	2.684e-01	7.643e-02	2.335e-03	3.862e-04	7.601e-05
4	6.056e-02	2.204e-03	4.297e-05	3.347e-06	4.751e-07
5	1.268e-02	1.678e-05	2.161e-07	4.329e-08	6.470e-09
6	2.224e-04	1.841e-07	1.977e-09	6.408e-10	9.758e-11
7	3.887e-08	2.627e-09	2.611e-11	9.873e-12	1.515e-12
9	1.688e-14	6.342e-13	0.000e+00	0.000e+00	7.105e-15

where $C^{[p]}(\tau, t_*) := \Lambda^{[p]}(\tau) \cdot S_0 \cdot \vartheta_*^{[p]} \cdot \Upsilon_{a,N}^{[p]}(t_*)$ is a constant, with $\vartheta_*^{[p]}$ obtained via Table 28. Note that in the second expansion, the summation ranges up to N rather than $N^{[p]}$, since the payoff $G_{S_0}(y)$ has an unbounded support.

Convergence for cubic PROJ is demonstrated in Table 15 for BSM with five volatility settings (the first corresponds to the challenging BSM model designated in BENCHOP [124]), where analytical formulas are used to obtain reference values. Arbitrary precision is readily obtained for each model, while smoother densities (corresponding to larger σ) result in faster convergence.

4.3 Numerical Analysis Of B-Spline Orders

In this section we present an extensive numerical study of the various implementations of PROJ. The focus is on identifying robust rules for fixed-width density truncation, exploring model-based truncation methods for density expansions using cumulants and tail probabilities, and analyzing the properties of PROJ specific to each of the B-spline orders from Haar to cubic. Of special interest is the comparative performance as a function of contract maturity. Exotic pricing with discrete monitoring requires the repeated integration of intermediate value functions or characteristic function approximations with monthly, weekly, daily, or nearly continuous monitoring, so quantifying the relative behavior of B-spline projections is essential for exotic applications. This includes determination of appropriate truncation supports and of the subsequent discretization mesh size.

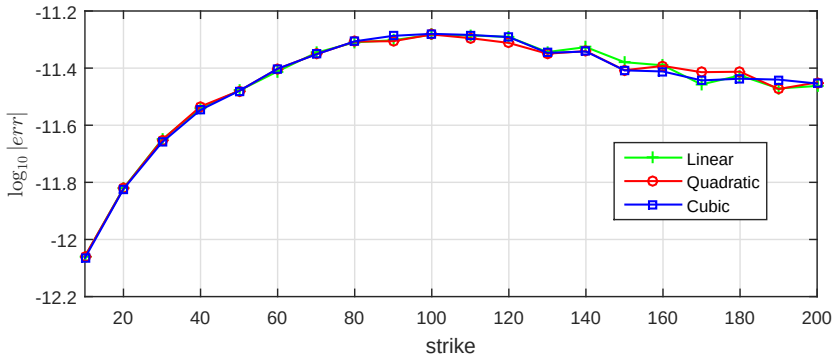

Figure 12: Errors Across Strike: calls priced in CGMY models by PROJ with $\bar{P} = 4$, $P = 13$ and PCP. Average errors over 200 Randomly chosen parameter settings. Other parameters: $r = .05, q = 0$, $S_0 = 100$, $T = 1$. Reference values by COS with $N = 2^{18}$, $L = 14$.

Table 16: Absolute errors (pricing and Greeks) for standard and challenging BSM parameters from [124]. Cubic PROJ is used for standard and Linear PROJ for challenging, both with $\bar{P} = 1$.

	BSM, Standard Parameters					BSM, Challenging Parameters			
P	Price	Delta	Gamma	Vega	P	Price	Delta	Gamma	Vega
2	7.90e-02	5.44e-03	1.68e-04	5.31e+00	5	1.39e-02	2.52e-03	1.25e-01	1.71e+00
3	5.73e-04	1.21e-04	9.48e-05	2.12e-02	6	4.57e-05	3.20e-02	3.89e-02	6.47e-02
4	4.29e-06	8.23e-07	3.82e-06	1.58e-04	7	4.32e-08	4.10e-04	4.24e-03	4.82e-04
5	5.01e-08	1.07e-08	2.05e-07	1.68e-06	8	1.37e-11	5.17e-08	6.61e-07	3.17e-08
6	7.25e-10	1.60e-10	1.23e-08	2.30e-08	9	1.14e-13	1.49e-08	3.15e-07	2.37e-09

Reference values for experiments are obtain by the COS method [61], the Hilbert transform method [64], and by PROJ in cases of extreme maturities where other methods routinely fail. Given the unacceptable sensitivity of cumulant based approaches for weekly or shorter maturities (recall Figures 7 and 8), at least for consistently obtaining reference prices to near arbitrary precision, we use a fixed-width truncation support when COS or PROJ are applied to obtain reference prices when $T < 1$.

For many of the experiments that follow, we specify a model class and sample permissible parameters from that class randomly. Each experiment involves a new set of randomly selected parameters, typically of size 200. For the CGMY model, uniform sampling is from

the set of values[11]

$$C \in [0.5, 4], \qquad G \in [0.5, 30], \qquad M \in [5, 30], \qquad Y \in [0.5, 1.5], \tag{133}$$

where we later consider values of $Y \in (0, 2)$ to identify within-class behavior of the truncation decision. For every random parameter drawing, a separate (pseudo)-random number is used to determine each parameter. Similarly, NIG parameters are drawn uniformly (and separately) from the ranges

$$\alpha \in [2, 20], \qquad \beta \in [-\alpha, 2\alpha - 1], \qquad \delta \in [0.1, 1], \tag{134}$$

where the value of β is drawn uniformly from the set of permissible values $[-\alpha, 2\alpha - 1]$ that are implied by each choice of α. Finally, we consider Merton's Jump Diffusion (MJD), with parameters drawn at random from

$$\sigma \in [0.05, 0.35], \qquad \lambda \in [0.1, 0.4], \qquad \mu_J \in [-0.3, -0.01], \qquad \sigma_J \in [0.05, 0.4]. \tag{135}$$

Figure 12 demonstrates that convergence (of absolute error) is more rapid for deeply away-from-the-money options, so our experiments consider the case of $S_0 = W = 100$. This observation is overwhelmingly model independent. We also find that smoother bases provide more rapid convergence deeply out of the money, due to their ability to capture the smoothness of the tail distribution.

In Table 16, we consider pricing and Greek errors for two BSM models, designated in BENCHOP [124] as standard and challenging, where $S_0 = W = 100$ and $q = 0$. For the standard model, $\sigma = 0.15$, $r = 0.03$ and $T = 1$. For the challenging model, $\sigma = 0.01$, $r = 0.10$ and $T = 0.25$. Appealing to the flexibility of multiple basis orders, we use cubic PROJ for the standard model (which is the preferred basis for smooth problems and moderate to long maturities, as demonstrated in Section 4.3.1) and linear PROJ (the preferred basis for spiked densities and short maturities) for the challenging model. As expected, prices converge faster than Greeks (see Section 4.3.3 for details) to the closed-form reference values for BSM. High precision is readily obtained for both models. Our

[11] Unless otherwise specified, as in Figure 16. In this case, the value of Y is taken outside the normal ranges.

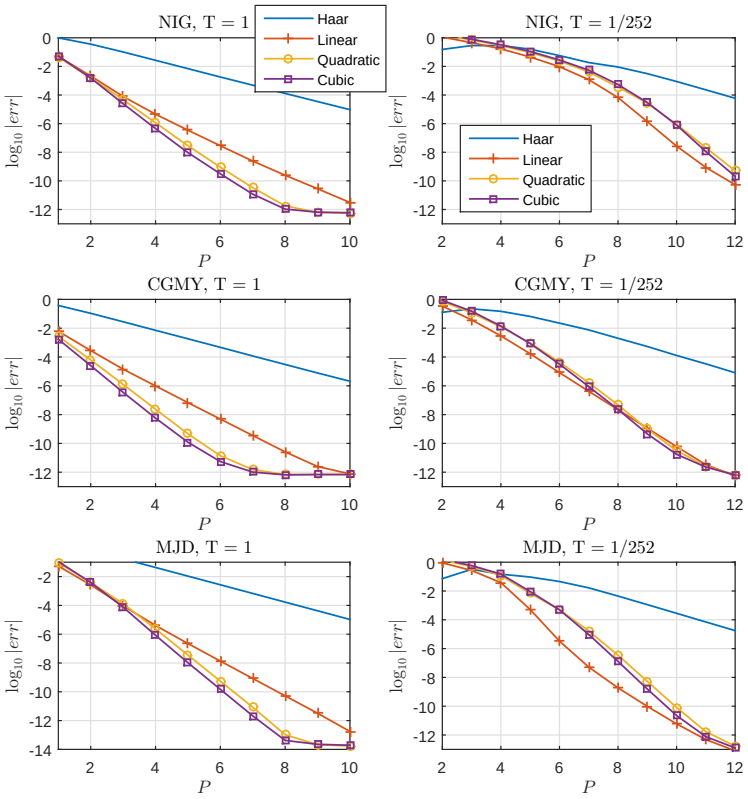

Figure 13: Maturity and Convergence (Standard Maturities): calls priced in NIG, CGMY, and MJD models by PROJ with $\bar{P} = 5$ and PCP. Average errors over 200 randomly chosen parameter settings for each model. Other parameters: $r = .05, q = 0$, $S_0 = W = 100$. Reference values by COS with $N = 2^{18}$, fixed-width $\alpha = 10$.

focus in the remaining experiments is on the CGMY and NIG models, which tend to be more computationally intensive.

4.3.1 Convergence and Option Maturity

One test of robustness is the pricing of options at extreme maturities, a problem for which most methods suffer at one or both of the extremes. For example, the COS method is well known to perform poorly at extremely long maturities [113] (as they arise in problems of insurance, long term bonds, and real options pricing). We also find that while the convergence of COS is theoretically exponential, in practice for $T \leq 1/52$, the algebraic convergence of PROJ is often superior for heavy tailed distributions (see Figure 17). One of the findings of this work is that PROJ is robust to extreme maturities.

For experiments in this subsection, choices of truncation width parameters are guided

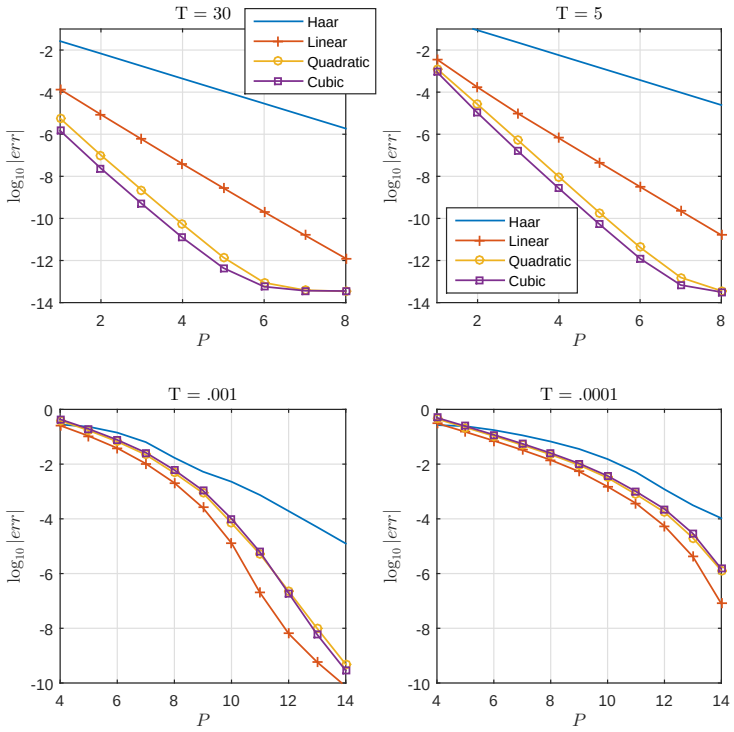

Figure 14: Maturity and Convergence (Extreme Maturities): calls priced in NIG models by PROJ with PCP. For $T \in \{30, 5\}$ $\bar{P} = 6$, while for $T \in \{.001, .0001\}$ $\bar{P} = 2$. Average errors over 200 randomly chosen parameter settings. Other parameters: $r = .03, q = 0$, $S_0 = W = 100$. Reference values by linear PROJ with $P = 2^{16}$.

by the analysis in Section 4.3.2. Two standard maturities $T \in \{1, 1/252\}$ are illustrated in Figure 13 for the CGMY, NIG, and MJD models. Convergence (in terms of $\log_{10}(|err|)$) is rapid for all B-spline bases, with the exception of Haar. Given the similar rate of convergence for weekly, monthly, and daily options, linear PROJ is appropriate in the context of discretely monitored exotics, and is often easier to implement when complications arise.[12] We also note the slightly faster convergence of CGMY and MJD model values over the NIG class.

As one might expect, longer maturities favor the smoother bases with a wider support, namely the quadratic and cubic B-splines, while the linear and Haar B-splines provide natural candidates for extremely short maturities. While the former observation seems to hold, it is perhaps surprising that the quadratic and cubic splines perform quite admirably

[12] An exception is for discretely monitored Asian options, which greatly favor the smoother bases [84], as one might expect for payoffs on averages.

for short maturities, although linear projection is the victor in this case, typically providing about an extra order of precision, and at less of an expense. Naturally, a finer resolution is required to price contracts of short maturity, a cost that is offset by a shorter density support. Higher order B-splines, such as quartics and quintics, are natural candidates for future research with regard to long term contracts.

Rapid convergence for lengthy maturities $T \in \{5, 30\}$ is evident by inspection of Figure 14. While a greater disparity between cubic and quadratic PROJ was expected, the relatively poor performance of Haar B-splines is no surprise. As the option maturity increases, so does the density smoothness and with it the performance of smoother approximation spaces. High accuracy is still attainable for extremely short maturities, illustrated for $T \in \{.001, .0001\}$.

4.3.2 On the Width of Density Truncation

We turn our attention now to the selection of truncated density supports as it applies to density expansion methods, which is a particularly delicate problem for processes beyond the Black-Scholes-Merton model.

4.3.2.1 Implementation I: Fixed-Width

The fixed-width implementation was introduced in Section 4.2.2.1 as a robust approach to obtaining highly accurate prices. This approach provides a more controlled setting to study discretization errors, and is quite effective for obtaining reference prices or during the course of calibration to avoid truncation-induced pricing errors that send search routines in misguided directions. Indeed, within a given model class, such a variety of density shapes and tail-heaviness are routinely encountered that encouraging a routine to select razor-edge truncation intervals is inviting disaster. Model-based approaches have their merits, however, so we consider two such implementations in Sections 4.3.2.2 and 4.3.2.3.

In Figure 15, the convergence in $\bar{P}$, for a fixed width of $2\alpha = 2^{\bar{P}}$ is demonstrated for the NIG class, where we isolate truncation error by fixing $P = 14$. Reference values are obtained by COS with $N = 2^{18}$ and a fixed-width support. In general we find that the required support is independent of B-spline order, so rule-of-thumb prescriptions for $\bar{P}$ can

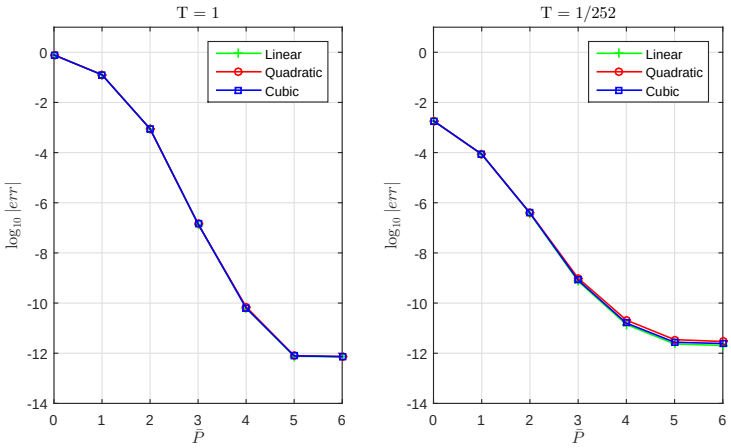

Figure 15: Truncation Support and Convergence (Fixed-Width): calls priced in NIG models by PROJ with $P = 14$ for each basis and PCP. Average errors over 200 randomly chosen parameter settings. Other parameters: $r = .05, q = 0$, $S_0 = W = 100$. Ref. values by COS with $N = 2^{18}$, fixed-width $\alpha = [10, 8]$.

be applied uniformly.

Figure 16 considers the within-model variation of errors for the fixed-width method. We choose the CGMY model class which we partition according to the parameter Y, which controls the "fine" behavior of the process [32]. Within each of five tranches of Y values, the remaining parameters C, G, M are uniformly selected from the ranges specified in equation (133). Compared with the NIG model, a smaller value of $\bar{P}$ tends to suffice for CGMY. By experimentation, we can develop rule-of-thumb settings for $\bar{P}$ to use in future calculations, which depend on tranches of model parameters. In general, any rules should take maturity into account, while larger $\bar{P}$ for greater maturity.

4.3.2.2 Implementation II: Cumulant

In cases where speed is a primary consideration, it may be preferable to fix a desired budget rather than a resolution in order to fix the computational cost in a predictable manner. With the total number of grid points $N \in \mathbb{N}$ fixed as a power of two[13], and a support width of 2α for $\alpha > 0$, we define $\Delta := 2\alpha/(N-1)$, after which the grid is determined by equations (114) and (115) as before, with $x_{\bar{n}} = \ln(W/S_0)$ a member.

[13]This is not essential but it is preferred for subsequent calculations involving fast Fourier transforms. We also note a slight difference in the definition of Δ. With a dyadic partition, $\Delta = 2\alpha/N$, although the support is slightly larger (by Δ) on one side of μ_{Y_t}.

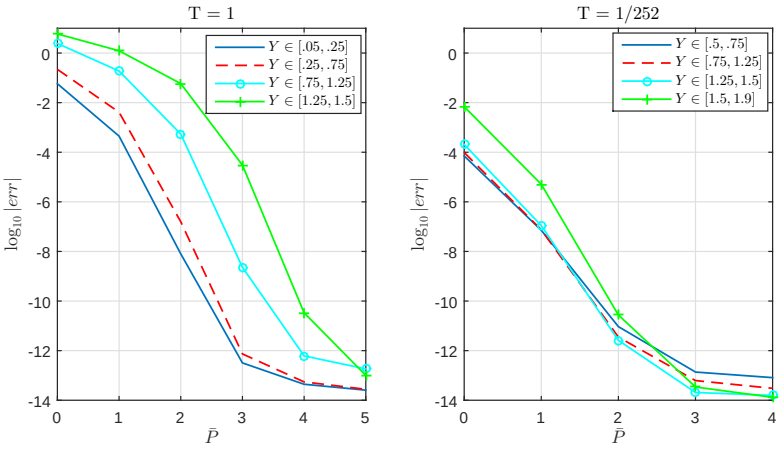

Figure 16: Truncation Support and Convergence by Tail-Heaviness (Fixed-Width): calls priced in CGMY models with five values of Y taken from each subset, and for each, 25 settings of C, G, M are chosen at random. Calls are priced by linear PROJ with PCP for each $\bar{P}$ where $P = 14$ is fixed. Other parameters: $r = .05, q = 0$, $S_0 = W = 100$. Ref. values: for $T = 1$, cubic PROJ with $P = 14$, $\bar{P} = 7$; for $T = 1/252$, linear PROJ with $P = 14$, $\bar{P} = 6$.

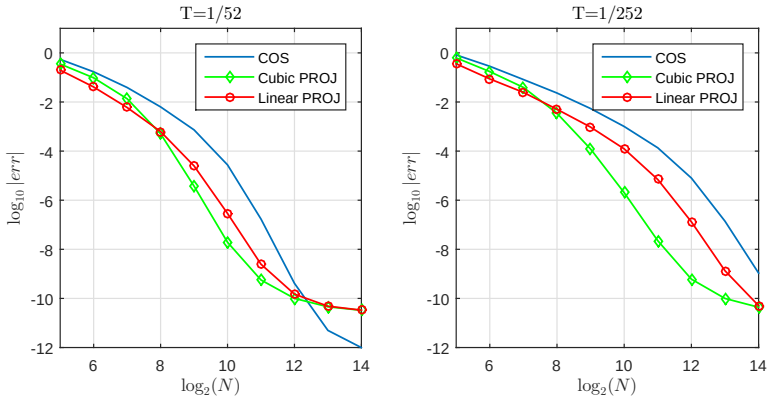

Figure 17: COS vs PROJ Convergence with Implementation II (Cumlant-Based): average call price error over 250 random parameter selections of NIG model using PCP, and strikes drawn randomly from $[80, 120]$. For $T = 1/52$, $L := 35$ (for both methods). For $T = 1/252$, $L := 60$, as suggested by Figure 8. $S_0 = 100$, $r = .05, q = 0$. Reference values: Hilbert transform method: $N = 2^{19}$, step size $h = h(N/2)$ as prescribed in [67].

There are several competing approaches when selecting α. Traditional methods prescribe a multiple of standard deviations, which is inappropriate for heavy-tailed densities and short maturities. To account for this, [62] uses the first, second, and fourth cumulants of the return process to determine a truncated support for Levy models. Modified slightly in our case, the support width is determined by

$$\alpha := L\sqrt{|c_2|t + \sqrt{|c_4|t}}, \tag{136}$$

where c_n denotes the n-th cumulant of $\ln(S_1/S_0) = \ln(Y_1)$, and L is a user-supplied parameter. The first cumulant is incorporated by equation (114) where $\mu_{Y_t} = tc_1$. Again, when speed is a primary motivation, this approach is capable of obtaining decent approximations without "over-prescribing" the support.[14] As demonstrated in Figure 8, cumulant-based approaches should be used with caution, especially for short maturities, as the required value of L (to satisfactorily control truncation error) can vary whimsically between and within model classes.

In Figure 17, we compare the convergence of PROJ to that of COS using implementation II (this choice of truncated support was originally introduced with the COS method [62], though it relates to the approach of [100]). For the NIG model, with reference parameters obtained by Hilbert transform for 250 randomly chosen parameter settings and strikes drawn at random from $[80, 120]$, we can see that the performance of COS begins to deteriorate as the maturity shortens. For $T = 1/52$, linear and cubic PROJ outperform COS for every grid size up to an accuracy of $e - 10$, after which the exponential convergence of COS advances it ahead. For $T = 1/252$, linear PROJ is consistently about 10 times more accurate than COS, while cubic projection is up to 10000 times more accurate for the same N. This finding often extends to discretely monitored contracts where T is replaced by Δ_t, the time between monitoring dates.[15]

[14] Of course one can add a cumulant based specification as a safeguard to identify when the fixed-width is insufficient (allowing a less conservative initial choice), in which case the support should be extended accordingly. With bounded payoffs, the risk is in under-specifying the support, while unbounded payoffs present additional challenges in the absence of parity relations (this is an issue for pricing exotics and American options).

[15] Compared with Figure 17, we see the effect of moneyness on the convergence rate for B-Splines. In particular, the cubic basis outperforms linear for $T = 1/252$ because we are pricing a spectrum of strikes,

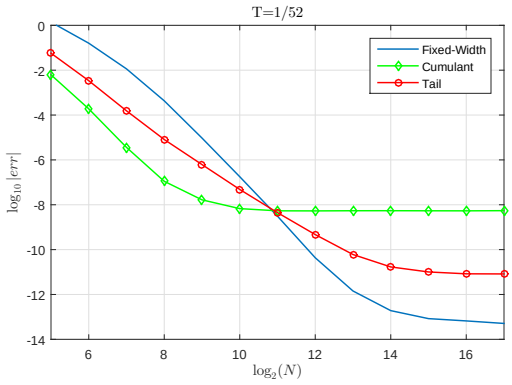

Figure 18: Support Truncation: comparison of implementations with cubic PROJ. Average over 200 randomly chosen parameters of CGMY model; $r = .05$, $q = 0$, $S_0 = W = 100$. Fixed-width uses implementation I with $\bar{P} = 4$; cumulant uses implementation II with $L = 12$; Tail uses implementation III with $P_H = 5$, $\bar{P}_H = 3$, $h = \pi/4$, $\alpha_{\max} = 7$, $TOL = 10^{-10}$.

4.3.2.3 Implementation III: Tail estimation

For robust model-based truncation decisions, an approach which offers greater control over the valuation error can be achieved by approximating the cumulative mass left of the truncation boundary. Especially in situations for which the density will be reused, having control over the error is very desirable.

From [64], the left-tail of the log return Y_t over any truncated support can be computed efficiently using the Hilbert transform which is defined as the Cauchy principal value

$$\mathcal{H}f(x) := \frac{1}{\pi} \cdot \mathrm{PV} \int_{-\infty}^{\infty} \frac{f(y)}{x-y} dy.$$

For a fixed step size $h > 0$ and budget $N_H \in \mathbb{N}_+$, $\mathcal{H}f(x)$ is approximated by

$$H_{h,N_H} f(x) := \sum_{n=-N_H/2}^{N_H/2} f(nh) \frac{1 - \cos(\pi(x-nh)/h)}{\pi(x-nh)/h}, \tag{137}$$

which follows from the Hilbert transform of a sinc expansion of f. Namely, we approximate

$$F_{Y_t}(y) := \mathbb{P}[Y_T \le y] = \mathcal{F}(\mathbb{1}_{(-\infty,y]} \cdot f_T)(0) = \frac{1}{2} - \frac{i}{2}\mathcal{H}(e^{-i\xi y}\widehat{f}_T(\xi))(0).$$

While a model dependent selection of h is easy to implement [64], for clarity we choose h and N_H as follows. For a fixed $\bar{P}_H$, P_H, we simply set[16] $N_H := 2^{P_H + \bar{P}_H}$, $\quad h := 2\pi/2^{\bar{P}_H}$.

some of which are deeply OTM. If we restrict the strike space to be very close to ATM, linear PROJ outperforms cubic.

[16] A decent choice for $\bar{P}_H$ is guided by the same analysis as for $\bar{P}$ with PROJ.

For a fixed value L_H, we start with the initial cumulant-based guess of Section 4.3.2.2, and $x = c_1 - \alpha$ (the left-most grid point). Since the procedure is adaptive, we can take $L_H = 8$ (on the smaller end of standard recommendations). A grid-width multiplier, λ, extends the grid (symmetrically about c_1).[17] The procedure then approximates by Hilbert transform the left tail value, $F_{Y_t}(x)$. As long as $F_{Y_t}(x) > TOL$ (or until $\lambda \cdot \alpha \leq \alpha_{max}$), the grid width is multiplied by λ. Psuedo-code is provided in Algorithm 4. For a modest value of N_H, we can typically obtain within an order or two of the set TOL.[18]

Figure 18 demonstrates with linear PROJ the relationship between support truncation methods. Cumulant-based approaches are useful to achieve rapid convergence for small budgets, but are limited in terms of maximum attainable accuracy.[19] Fixed-width approaches may have slower initial convergence, but given a sufficiently large width selection, they provide a robust implementation by trading the potential of a shortened support for greater insurance against under-prescribing. Depending on how TOL is chosen, the tail estimation approach offers more control over eventual (and hence initial) convergence. For discretely monitored exotics, the added cost of this approach is spread over many subsequent computations.

Algorithm 4 Implementation III: Tail Estimation

$N_H := 2^{\bar{P}_H + P_H}; \quad h := 2\pi/2^{\bar{P}}$
$\alpha \leftarrow L_H \cdot \left(\sqrt{|c_2| + \sqrt{|c_4|}}\right); \quad x \leftarrow c_1 - \alpha$
$\theta_n \leftarrow n - .5, \quad n = -N_H/2, ..., N_H/2$
$\Omega \leftarrow 1/(\pi \cdot \theta); \quad \theta \leftarrow h \cdot \theta$
$\Omega \leftarrow \widehat{f_T}(\theta) \circ \Omega; \quad \nu \leftarrow \exp(-ix\theta)$
$\mathcal{P} \leftarrow \Re\left\{.5(1 + i \cdot \nu^\top \Omega)\right\}$
while $\mathcal{P} > TOL$ & $\lambda \cdot \alpha \leq \alpha_{max}$ **do**
  $\alpha \leftarrow \lambda\alpha; \quad x \leftarrow c_1 - \alpha; \quad \nu \leftarrow \exp(-ix\theta)$
  $\mathcal{P} \leftarrow \Re\left\{.5(1 + i \cdot \nu^\top \Omega)\right\}$
end while
return α

[17] Larger values of λ reduce the number of iterations in the procedure, but limit how close one can get to a specified tolerance.

[18] If $\lambda \approx 1$, the algorithm is quite consistent to within an order. For $\lambda = 1.5$, within two orders of TOL is generally expected. Naturally, the tradeoff is how many iterations until α is selected. The value of α_{max} plays an obvious role in limiting the maximum possible accuracy.

[19] Assuming L is chosen for this purpose, otherwise large values of L slow initial convergence while increasing eventual accuracy set by truncation error.

4.3.3 Option Greeks

As an example, consider the European put option with strike W. To calculate the option Delta, we can differentiate the value formula to obtain

$$\begin{aligned}\Delta_{S_0}^{put} &:= \frac{\partial}{\partial S_0}\mathcal{V} \circ g(S_0) = e^{-rT}\frac{\partial}{\partial S_0}\left(\int_{-\infty}^{\ln(W/S_0)}(W - S_0 e^y) f_T(y)dy\right) \\ &= -e^{-rT}\int_{-\infty}^{\ln(W/S_0)} e^y f_T(y)dy \end{aligned} \tag{138}$$

which follows from Leibniz's rule. Given that the PROJ expansion separates the log return density coefficients, $\bar{\beta}_{a,n}^{[p]}$ (which are independent of S_0), from the payoff coefficients, $g_{a,n}^{[p]}$, which by a change of variable the dependence on S_0 has been separated from the integral, the option Delta coefficients are given in terms of values used to compute option prices. Hence, using quantities already computed in the pricing algorithm, we obtain the option Deltas as follows.

Corollary 4.3.1. *For $p \geq 0$, the put option Deltas are approximated by*

$$\Delta_{S_0}^{put} \approx \Upsilon_{a,N}^{[p]} \sum_{n=1}^{N^{[p]}} \bar{\beta}_{a,n}^{[p]} \cdot \Delta_{a,n}^{[p]}, \tag{139}$$

where for the Haar and linear bases,the Delta coefficients $\Delta_{a,n}^{[p]}$ are given by

$$p = 0, 1: \quad \Delta_{a,n}^{[p]} = \begin{cases} -\exp(x_n) \cdot \vartheta_*^{[p]}, & n \leq \bar{n} - 1 \\ \kappa \cdot \vartheta_0^{[p]}, & n = \bar{n} \end{cases} \tag{140}$$

where $\kappa := -W/S_0$. For quadratic and cubic bases, the Delta coefficients satisfy

$$p = 2, 3: \quad \Delta_{a,n}^{[p]} = \begin{cases} -\exp(x_n) \cdot \vartheta_*^{[p]}, & n \leq \bar{n} - 2 \\ \kappa \cdot e^{-\Delta} \cdot \vartheta_{-1}^{[p]}, & n = \bar{n} - 1 \\ \kappa \cdot \vartheta_0^{[p]}, & n = \bar{n} \\ \kappa \cdot e^{\Delta} \cdot \vartheta_1^{[p]}, & n = \bar{n} + 1 \end{cases} \tag{141}$$

Differentiating the put-call parity formula (124) *with respect to S_0,*

$$\Delta_{S_0}^{call} = \Delta_{S_0}^{put} + \exp(-qT), \tag{142}$$

where $\exp(x_n)$ remains bounded for put options.

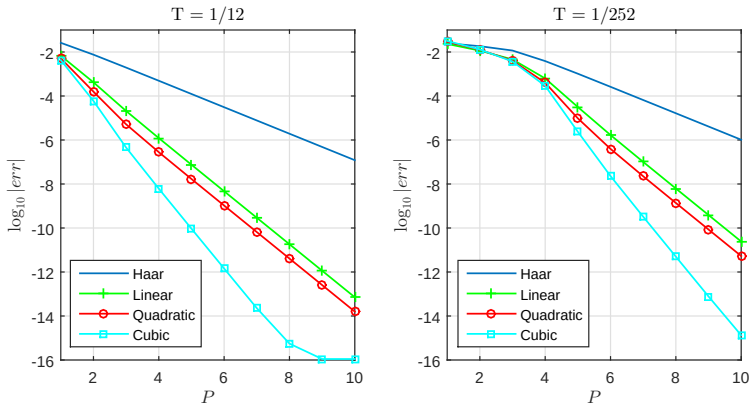

Figure 19: Delta Convergence: CGMY(1, 5, 5,1.5), $r = .05, q = 0$, $S_0 = W = 100$, call option Deltas. $\bar{P} = 4$ for $T = 1/12$, $\bar{P} = 3$ for $T = 1/252$. References in first case obtained by cubic PROJ, $\bar{P} = 4$, $P = 14$, and in second case by linear, $\bar{P} = 3$, $P = 14$.

As demonstrated in Figure 19, Delta values are easily obtained to high precision as by-products of the pricing routine. On-the-other-hand, the method of direct integration (which uses characteristic function values that have also been computed previously in the process of pricing with any B-spline order of PROJ) is ideal for obtaining the option Gamma, which for vanilla calls and puts is given by

$$\Gamma_{S_0} := \frac{\partial^2}{\partial S_0^2}\mathcal{V} \circ g(S_0) = \frac{\partial}{\partial S_0}\Delta_{S_0} = e^{-rT}\frac{W}{S_0^2} \cdot f_T\left(\ln\left(\frac{W}{S_0}\right)\right). \tag{143}$$

Using direct integration of the density, we have

$$\Gamma_{S_0} = \frac{W}{S_0^2}\frac{e^{-rT}}{\pi}\Re\left\{\int_0^\infty \widehat{f}_T(\xi)e^{-i\xi\ln\left(\frac{W}{S_0}\right)}d\xi\right\} \approx \frac{W}{S_0^2}\frac{e^{-rT}}{\pi}\Re\left\{\sum_{j=1}^{N} e^{-i\xi_j\ln\left(\frac{W}{S_0}\right)}\widehat{f}_T(\xi_j)v_j\Delta_\xi\right\},$$

and from [64,123] the discretization error can be seen to decay exponentially in $1/\Delta_\xi$.

In more complex applications, such as the pricing of arithmetic Asian options [84], density values are unknown, while the projected density is given. For this reason, it is insightful to study the error convergence of Γ_{S_0} with respect to the various bases to determine at which resolutions one would obtain decent approximations. The formulas are quite simple, for example the call option Gamma approximations:

$$\Gamma_{S_0} \approx a^{1/2}e^{-rT}\frac{W}{S_0^2} \cdot \begin{cases} \Upsilon^{[p]}_{a,N} \cdot \bar{\beta}^{[p]}_{a,\bar{n}} & p = 0, 1, \\ \Upsilon^{[p]}_{a,N} \cdot \left(\varphi^{[p]}(0)\bar{\beta}^{[p]}_{a,\bar{n}} + \varphi^{[p]}(1)\left(\bar{\beta}^{[p]}_{a,\bar{n}-1} + \bar{\beta}^{[p]}_{a,\bar{n}+1}\right)\right) & p = 2, 3, \end{cases}$$

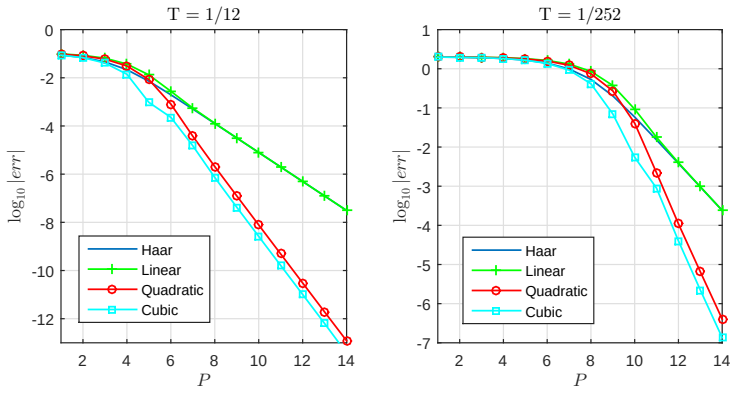

Figure 20: Gamma Convergence: NIG(6, 0.7, 0.4), $r = .05, q = 0$, $S_0 = W = 100$. $\bar{P} = 4$ for $T = 1/12$, $\bar{P} = 2$ for $T = 1/252$. References by direct inversion with $N = 2^{20}$.

where $\varphi^{[2]}(0) = 3/4, \varphi^{[2]}(1) = 1/8, \varphi^{[3]}(0) = 2/3$, and $\varphi^{[3]}(1) = 1/6$. Note too that we are not restricted to Gamma values along grid points, since the projection defines a continuous density approximation along the entire truncated support. Similar formulas apply to Gamma values at arbitrary points, and Greeks can be obtained simultaneously for a portfolio of options as the byproduct of the pricing routine at a negligible cost.[20]

For smoother densities the projections agree more closely with the true density values than in the presence of extreme peaks. As demonstrated in Figure 20 for a highly peaked NIG example, Gamma values for short maturities can only be reliably obtained at a high resolution, so the natural alternative is to use a finite difference scheme, as suggested in [83].

Finally, we consider the option Vega, which is defined as $\mathcal{V}_\sigma = \frac{\partial}{\partial \sigma}\mathcal{V} \circ g$, where σ is the model volatility. This parameter is easily estimated by a central difference

$$\mathcal{V}_N^{[p]}(\sigma) := \Upsilon_{a,N}^{[p]} \cdot \frac{1}{h} \sum_{k=1}^{N^{[p]}} \left(\bar{\beta}_{a,k}^{[p]}(\sigma - h/2) - \bar{\beta}_{a,k}^{[p]}(\sigma + h/2) \right) \cdot g_{a,k}^{[p]}, \tag{144}$$

where $g_{a,k}^{[p]}$ is the same set of coefficients to value the option itself, and $\bar{\beta}_{a,k}^{[p]}(\sigma)$ are the coefficients as a function of volatility parameter σ. A value of $h = .00001$ works well in practice. Given the linearity of the discrete Fourier transform, Vega can be estimated with only one FFT. Other Greeks such as Rho are obtained analogously.

[20] For option Gammas, errors are actually smaller away from grid points by the nature of projection, which seeks to minimize errors along each subinterval as a whole, rather than at particular points.

4.4 Conclusion

This paper extends and refines a recent methodology for pricing European and exotic options under exponential Levy dynamics, based on the frame duality method of Kirkby (2014). The fruitful case of B-spline projection is analyzed in detail. By treating European put pricing as a controlled environment for experimentation, we are able to systematically compare the convergence properties of each order with respect to features of the problem. In particular, contract maturity is a key determinant of the ideal B-spline order.

The approach of coefficient stabilization is developed in generality for use in exotic contexts. Exact coefficient formulas, which are often analytically available and easy to derive, are highly unstable as the basis resolution is refined, and cause extreme accuracy loss for B-spline orders beyond Haar. Without stabilization, application of quadratic and cubic B-splines is severely limited. Formulas and algorithm input for the first four B-spline orders are provided for immediate applications, including stabilized formulas for payoff coefficients that arise in European as well as exotic contexts.

Discretely-monitored exotic options are price by a sequence European-style valuations of very short maturity. We demonstrate the advantage of PROJ, as compared with the COS method, for pricing with short-term transitional densities. Linear PROJ is ideally suited for such highly peaked densities, while the convergence rate of COS slows substantially. Given that similar sources of error arise for exotic option pricing, the analysis conducted in this work serves additionally as a guide for expanding the PROJ methodology to more complex scenarios.

Extensive experiments address the choice of truncated density support, with implications that extend to option pricing methods in general. We compare three implementations, including a novel Hilbert transform-based procedure which offers greater control over value errors. The popular cumulant-based approach is analyzed and compared to a fixed-width alternative, which we propose as a robust choice for pricing with heavy-tailed returns.

4.4.1 Appendix: Quadrature and Stabilization of Coefficient Formulas

This section details the stabilization approach for general payoffs given a B-spline basis of order p, which is based on interval partitioning. For each $p \geq 0$, there is a natural partition of $I^{[p]}$ as

$$I^{[p]} = \left[-\tfrac{p+1}{2}, \tfrac{p+1}{2}\right] = \bigcup_{l=1}^{p+1} I_l^{[p]}, \qquad I_l^{[p]} := [a_l^{[p]}, b_l^{[p]}], \tag{145}$$

which depends on the parity of p:

$$p \geq 2 \text{ even:} \quad I^{[p]} = \left[-\tfrac{p+1}{2}, -\tfrac{p}{2}\right] \cup \left[-\tfrac{p}{2}, -\tfrac{p}{2}+1\right] \cup \cdots \cup \left[\tfrac{p}{2}-1, \tfrac{p}{2}\right] \cup \left[\tfrac{p}{2}, \tfrac{p+1}{2}\right] \tag{146}$$

$$p \geq 1 \text{ odd:} \quad I^{[p]} = \left[-\tfrac{p+1}{2}, -\tfrac{p+1}{2}+1\right] \cup \cdots \cup \left[\tfrac{p+1}{2}-1, \tfrac{p+1}{2}\right]. \tag{147}$$

In the odd case each subinterval $I_l^{[p]}$ is of unit length and has integer endpoints. For $p \geq 2$ even, all interior subintervals are of unit length with integer endpoints, while the two boundary subintervals are half of a unit interval. Equation (117) becomes

$$g_{a,n}^{[p]} = \sum_{l=1}^{p+1} \int_{I_l^{[p]}} G_{S_0}\left(\frac{y}{a} + x_n\right) \varphi^{[p]}(y) dy, \tag{148}$$

which, for a C^∞ payoff, is evaluated by applying a standard quadrature formula each of the integrals over $I^{[p]}$. Since most payoffs posses at least one singularity, a further refinement is needed.

4.4.1.1 Quadrature on Subintervals

Uniform spacing produces very neat closed-form approximations that combine seamlessly in composition. Our basic tools are the Newton-Cotes formulas on $[0, 1]$. For a fixed quadrature order, determined by the number N_q of nodes on $[0, 1]$, let us define these points by

$$\eta_m = (m-1)/(N_q - 1), \qquad m = 1, .., N_q,$$

and w_m the respective quadrature weights. Useful examples are given in Table 17. To evaluate $g_{a,n}^{[p]}$, we separate $1 \leq n \leq N$ into two sets, $N = N^c \cup N^d$, where $n \in N^c$ if , as a function of $y \in I^{[p]}$, $G_{S_0}(y/a + x_n) \in C^\infty(I^{[p]})$, and $n \in N^d$ if $G_{S_0}(y/a + x_n)$ or any of its derivatives[21] are discontinuous on $I_l^{[p]}$, for some $l = 1, ..., p+1$.

[21] Strictly speaking, to maintain smooth convergence, we only need G_{S_0} on $I^{[p]}$ to be continuously differentiable up to the order of projection convergence.

Table 17: Quadrature weights on $[0, 1]$.

Newton-Cotes Quadrature		
N_q	Rule	Weights, w_m
3	Simpson	$\frac{1}{6}\{1, 4, 1\}$
5	Boole	$\frac{1}{90}\{7, 32, 12, 32, 7\}$
7	Seven-Point	$\frac{1}{840}\{41, 216, 27, 272, 27, 216, 41\}$

For the Haar case, supports of basis elements are disjoint, so the points $n \in N^d$ are isolated. For the linear basis, if $n \in N^d$, then unless the discontinuity occurs at a grid point (which we strive for when possible), one of $n-1$ or $n+1$ also belongs to N^d. For all orders $p \geq 1$, $n \in N^d$ implies $n-1, n+1 \in N^d$. Suppose first that $n \in N^c$. For these indices, the approximation is just composite quadrature applied to $I^{[p]}$:

$$\begin{aligned} g_{a,n}^{[p]} &= \sum_{l=1}^{p+1} \left(b_l^{[p]} - a_l^{[p]}\right) \cdot \sum_{m=1}^{N_q} G_{S_0}\Big(\frac{y_{l,m}^{[p]}}{a} + x_n\Big) \cdot \varphi^{[p]}(y_{l,m}^{[p]}) \cdot w_m \\ &= \sum_{l=1}^{p+1} \sum_{m=1}^{N_q} G_{S_0}\Big(\frac{y_{l,m}^{[p]}}{a} + x_n\Big) \cdot \zeta_{l,m}^{[p]}, \end{aligned} \tag{149}$$

where

$$\zeta_{l,m}^{[p]} := w_m \cdot \varphi^{[p]}(y_{l,m}^{[p]}) \cdot \left(b_l^{[p]} - a_l^{[p]}\right), \qquad y_{l,m}^{[p]} = a_l^{[p]} + (m-1) \cdot \frac{b_l^{[p]} - a_l^{[p]}}{N_q - 1} \tag{150}$$

For each interior subinterval (which for odd p is all intervals), $b_l^{[p]} - a_l^{[p]} = 1$, while for boundary intervals (in the even p case), it equals one half. To ensure smooth convergence, the same quadrature order (determined by the number of points N_q) is applied to each subinterval (of possibly varying width).

Now suppose that $n \in N^d$, so $G_{S_0}(y/a + x_n)$ is singular[22] somewhere on $I^{[p]}$. We assume an individual singularity, as the case of multiple singularities is entirely similar. If $G_{S_0}(x)$ is singular at the point x^*, then in transformed coordinates, $G_{S_0}(y/a + x_n)$ is singular at the point $y^* = a(x^* - x_n)$, where $y^* \in I_{l^*}^{[p]}$, for some $1 \leq l^* \leq p+1$. Splitting at the singularity,

[22]In the case of calibrating multiple vanilla options, the singularity is a discontinuous first derivative, generally not coinciding with a grid point. For barrier options, there can also be a discontinuity in the payoff, as with binary options. Staircase type payoffs posses many discontinuities. For Bermudan options, there is a discontinuity in the second derivative at the point of pasting, ie the free (optimal exercise) boundary.

$I_{l^*}^{[p]} = [a_{l^*}^{[p]}, y^*] \cup [y^*, b_{l^*}^{[p]}]$ we define the two sets of nodes

$$\gamma_{l^*,m}^{[p]} := a_{l^*}^{[p]} + (m-1)\frac{y^* - a_{l^*}^{[p]}}{N_q - 1}, \qquad \lambda_{l^*,m}^{[p]} := y^* + (m-1)\frac{b_{l^*}^{[p]} - y^*}{N_q - 1}, \tag{151}$$

corresponding respectively to $[a_{l^*}^{[p]}, y^*]$ and $[y^*, b_{l^*}^{[p]}]$. Equation (149) becomes

$$\begin{aligned} g_{a,n}^{[p]} = &\sum_{l \neq l^*} \sum_{m=1}^{N_q} G_{S_0}\Big(\frac{y_{l,m}^{[p]}}{a} + x_n\Big) \cdot \zeta_{l,m}^{[p]} \\ &+ \sum_{m=1}^{N_q} w_m \Bigg[G_{S_0}\Big(\frac{\gamma_{l^*,m}^{[p]}}{a} + x_n\Big) \cdot \varphi^{[p]}(\gamma_{l^*,m}^{[p]}) \cdot \Big(y^* - a_{l^*}^{[p]}\Big) \\ &\qquad + G_{S_0}\Big(\frac{\lambda_{l^*,m}^{[p]}}{a} + x_n\Big) \cdot \varphi^{[p]}(\lambda_{l^*,m}^{[p]}) \cdot \Big(b_{l^*}^{[p]} - y^*\Big) \Bigg]. \end{aligned} \tag{152}$$

As a special case, we consider the calibration example in Section 4.2.5.

4.4.1.2 One-Sided Payoffs

Consider first a payoff of the form $G_{S_0}(y) = h_{S_0}(y) \cdot \mathbb{1}_{[y \leq \ln(W/S_0)]}$, where h_{S_0} may itself have singularities (e.g. in the case of down-and-out barrier and Bermudan put options). For such payoffs we assume a grid that enforces $\ln(W/S_0)$ as a member[23], say $\ln(W/S_0) = x_{\bar{n}}$. After the change of variables, we have

$$G_{S_0}\left(\frac{y}{a} + x_n\right) = h_{S_0}\left(\frac{y}{a} + x_n\right) \cdot \mathbb{1}_{[y \leq a(\ln(W/S_0) - x_n)]} = h_{S_0}\left(\frac{y}{a} + x_n\right) \cdot \mathbb{1}_{[y+n \leq \bar{n}]}, \tag{153}$$

since $\ln(W/S_0) - x_n = x_{\bar{n}} - x_n = \bar{n} - n$. Hence, for $I^{[p]} = \left[-\frac{p+1}{2}, \frac{p+1}{2}\right]$,

$$g_{a,n}^{[p]} = \sum_{l=1}^{p+1} \int_{I_l^{[p]}} h_{S_0}\left(\frac{y}{a} + x_n\right) \varphi^{[p]}(y) dy, \qquad n \leq \bar{n} - \frac{p+1}{2}. \tag{154}$$

For the coefficients of $\bar{n} - (p+1)/2 < n < \bar{n} + (p+1)/2$, the formula depends on the parity of $p \geq 0$:

$$\begin{aligned} p \text{ odd:} \quad g_{a,n}^{[p]} &= \sum_{l=1}^{\frac{p+1}{2} + (\bar{n} - n)} \int_{I_l^{[p]}} h_{S_0}\left(\frac{y}{a} + x_n\right) \varphi^{[p]}(y) dy \\ p \text{ even:} \quad g_{a,n}^{[p]} &= \sum_{l=1}^{\lceil \frac{p+1}{2} \rceil + (\bar{n} - n)} \int_{a_l^{[p]}}^{b_l^{[p]} \wedge (\bar{n} - n)} h_{S_0}\left(\frac{y}{a} + x_n\right) \varphi^{[p]}(y) dy. \end{aligned}$$

[23]For misaligned grids, as in section 4.2.5, the basic formula will simply be augmented, rather than re-derived. This is just a (frequently occurring) special case of equation 152.

Coefficients of $n \geq \bar{n} + (p+1)/2$ are identically zero. For call-like payoffs, that is $G_{S_0}(y) = h_{S_0}(y) \cdot \mathbb{1}_{[y \geq \ln(W/S_0)]}$, the formulas are very similar.

CHAPTER V

STATIC HEDGING AND PRICING

This chapter is based on the paper [88], which is in Revision with Mathematical Finance.

5.1 Introduction and Literature Review

To accommodate the growing demand for nonstandard derivative payoffs, markets have developed to facilitate their trading. The sources of risk on which these contingent payoffs depend have become increasingly diverse, as have the payoff structures specified in their contracts. Naturally, the introduction of contingent payoffs necessitates robust pricing and hedging strategies to preempt the admission of arbitrage.

One strand of research in the continuously-expanding derivatives pricing literature focuses on the model-free static-hedging approach to pricing through statically or semi-statically replicating the complex derivative payoffs with simple payoffs which are more amenable to valuation (see [11, 30, 33, 36, 40, 107, 108] and the references therein). The critical feature that distinguishes static hedging from ordinary function approximation is that traditional numerical approaches take mesh refinement for granted, whereas static hedging is constrained by the availability of market payoffs, which in turn define the mesh. This distinction motivates the pursuit of approximation with limited mesh refinement, where "basis" functions are chosen according to their availability and liquidity in a given market. We show that by recasting the problem as one of projection onto a suitably chosen frame space, the optimal static hedge is efficiently obtained. Furthermore, such approximations are shown to produce exact representations in the limit as the mesh is refined, much like the integral representations provided by [36].

The contributions of our analysis are threefold. First, we advance a new theoretical framework for pricing contingent claims and studying their perfect static replication strategies, with implications for security design. Specifically, new financial instruments can be introduced according to the richness of payoffs they are able to synthesize, and in a way

that generates standardized markets such as those for plain vanilla options. Frames provide the flexibility to study spaces of claims spanned by simpler securities.

Second, we provide a systematic scheme for hedging exotic derivatives including path-dependent options through a new means of static replication that can be implemented in markets with a reasonable spectrum of strikes on European options spanning practical trading ranges. By improving the accuracy of static replication, fewer instruments are required to achieve a desired hedge, and hedges are obtained with greater efficiency using methods developed in this work. Specifically, our approach consistently reduces the relative hedge error by more than half, while at a cost within fractions of a millisecond of basic interpolation. The risk reduction across a portfolio of exotic payoffs can be substantial. Not only is the hedging of nonlinear European options improved, but the method extends to procedures designed to hedge path dependent options. Specifically, semi-static hedges for barrier and American options as well as mixed static-dynamic strategies employed for products such as realized variance swaps are improved by the new methods.

Finally, this framework presents a new model-free enhancement of exotic derivatives pricing by building on recent advances in transform-based numerical procedures. Numerical studies on the pricing of various exotic options demonstrate that this method is fast and accurate in comparison to existing methods proposed in the literature. Prices computed from projected payoffs converge at a rate that is often several orders faster than when pricing the payoffs directly. Hence, once payoff coefficients are obtained, subsequent valuations are implemented at a fraction of the cost. This method is particularly well suited for pricing baskets of options simultaneously, and is robust to discontinuities of payoffs. In addition, the method enables a systematic comparison of the value of a payoff (or portfolio) across a set of competing model specifications.

Traditional approaches to static hedging typically impose restrictions on the underlying's risk-neutral dynamics, though superior results relative to dynamic hedging have been documented when the assumptions hold and even when these assumptions are relaxed. In [31], a put-call symmetry is established which yields a parity between call and put prices

at different strikes, assuming a particular symmetry holds for the underlying or an auxiliary process. A powerful result (which inspired the present work) is found in [36], where a static integral representation is shown to hold for a large class of functions in terms of liquid assets along a spectrum of strikes. A similar representation is derived in [40] which relates call prices to a spectrum of nearer-expiry calls. Static hedging of exotic options has experienced great success in recent years (see [55] for an early account). Numerical and simulation studies demonstrating the superiority (in terms of replication error) and robustness to model misspecification relative to discrete delta hedging are given in [40], [59] and [108] (see also [125] for simulation studies involving Asian, barrier, lookback, and quanto options).

The approach to static hedging via orthonormal basis representation has been studied in [107] and [49], where special features of the underlying risk-neutral dynamics are used to construct an orthonormal basis for the claim space using the valuation operator. Option representation (spanning) in terms of characteristic functions is introduced and analyzed in [11]. As in [36], our approach is based on synthesizing a target payoff function with a set of simple, liquidly traded payoffs (that is, contingent claims on specific payoff forms), where hedging instruments are prescribed according to features of the physical payoff to be received, independent of the underlying pricing model. Once hedging is accomplished (or eschewed if prices are the only risk source), valuation follows either by observing market prices for the simple payoffs, or by specifying a model and then pricing the simple payoffs simultaneously. Hedging the payoff itself is unaffected by the modeling choice of the underlying, so that the hedging portfolios carry over from one specification to the next.

The remainder of the paper is organized as follows. Section 2 presents several applications of pricing and hedging exotic derivatives and path-dependent options where our proposed framework can be effectively applied. Section 3 describes alternative hedging instruments in the form of frames and the background of frame theory. In Section 4, frame theory is applied to the current state of option markets by utilizing a basis formed from actively traded vanilla options, coined the butterfly basis, whereby we obtain an analytical representation of the "dual basis". Given the immediate application, we develop efficient methods for hedging (extended in Section 6 to pricing) with respect to this basis, which

are verified by a set of numerical experiments including the static hedging of knock-out barrier options. Analytical and quasi-analytical hedges are derived in special cases. Section 5 develops the general theory of frame pricing and discusses the application to higher dimensional payoffs. Concluding remarks are provided in Section 7. An additional set of numerical pricing experiments is conducted with respect to the butterfly basis in the Appendix, demonstrating the method's acceleration of value convergence. Proofs are provided in the appendix as well.

5.2 Motivating Applications

In this section we consider several financial applications to motivate the framework presented. In each of these applications the unifying strategy is to identify a static representation of some or all of the risk inherent in a financial position, expressed as a function $g(S_T)$ of the underlying risk-factor S_T, where T indexes a static time horizon. Given a suitably chosen basis $\{\Psi_k(S_T)\}$, we form an approximation

$$g(S_T) \approx \sum_k \alpha_k \Psi_k(S_T),$$

where several schemes are provided to obtain α_k. If possible, we will decompose $\Psi_k(S_T)$ into tradable market securities, which provides an implementable hedge. Regardless, pricing of $g(S_T)$ is accomplished by pricing the component functions, either using a model or inferring their prices from traded instruments. As discussed in Section 5.4.7, problems with multiple decision periods can be handled as well, by identifying a series of static exposures.

5.2.1 Static Hedging: Nonlinear Risks

Despite the prevalence of nonlinear risk in financial applications, its idiosyncratic nature often leads firms to seek customized over-the-counter payoffs to offset exposure. For example, demand elasticities faced by commodity producers cause revenues to vary nonlinearly with realized commodity prices. If the price risk of future revenues can be quantified it is possible to acquire protection in the form of financial contracts [132]. For instruments with interest rate sensitivities, convexity risk poses a similar problem which can be eliminated by an offsetting *power straddle* position (see [126] and the references therein), which has

a terminal payoff $g(S_T) = (S_T - K)^2$, where S_T is an underlying source of randomness. Additionally, power straddles can be used as tool for capturing implied volatility (*vega*) risk faced by options traders [122]. According to [126] power straddles face constant exposure to future implied volatility, allowing the holder to lock in future levels. In addition to power straddles, one often encounters the *powered call* option [77]

$$g(S_T) = (\max\{S_T - K, 0\})^2 = \left([S_T - K]^+\right)^2,$$

and the *power call* option

$$g(S_T) = \max\{S_T^2 - K^2, 0\} = [S_T^2 - K^2]^+.$$

In particular, the power straddle can be decomposed in terms of a powered call and put option $(S_T - K)^2 = ([S_T - K]^+)^2 + ([K - S_T]^+)^2$, so any one of these contracts can be priced or hedged in terms of the other two. To avoid catastrophically large payoffs, one can consider the capped power payoffs. For example, a p-th order capped power call pays

$$g(S_T) = (S_T - K)^p \mathbb{1}_{[K \leq S_T \leq C]} + (C - K)^p \mathbb{1}_{[S_T > C]},$$

for some $C > K$. From the perspective of the option supplier, we develop methods to hedge the sale of general nonlinear contracts in terms of more liquid instruments. Moreover, rather than offer standardized markets for a plethora of nonstandard products, the framework we develop can be used to design standardized markets capable of approximating a multitude of nonstandard payoffs with high accuracy. Experiments illustrating the effectiveness of this framework for exotic European options are given in Appendix 5.8.

5.2.2 Mixed Static-Dynamic Hedging: Volatility Derivatives

Due to the inextricable presence of volatility in the trading of many derivative products, it should come as no surprise that extensive markets have developed to exchange volatility contingent securities. An especially important product is the realized variance swap. Given a set of trading dates $\{t_0, ..., t_n\}$ at which an investor can trade in (generic) futures contracts with prices denoted by F_i, a standard variance swap specification is the terminal payoff

$$VS_n = \frac{N}{n} \sum_{i=1}^{n} \ln^2 \left(\frac{F_i}{F_{i-1}} \right),$$

where N is a trading day count specified in the contract. From Carr and Lee [33], a semi-static hedging strategy can be used to offset a position in the variance swap. In terms of the simple returns $R_i := (F_i - F_{i-1})/F_{i-1}$, $i = 1, ..., n$, a Taylor series expansion yields

$$\ln^2\left(\frac{F_i}{F_{i-1}}\right) = 2R_i - 2(\ln F_i - \ln F_{i-1}) - \frac{1}{3}R_i^3 + \mathcal{O}(R_i^4),$$

from which

$$VS_n = \frac{N}{n}\left[\sum_{i=1}^{n}\frac{2}{F_{i-1}}(F_i - F_{i-1}) - 2(\ln F_n - \ln F_0) - \frac{1}{3}\sum_{i=1}^{n}R_i^3 + \sum_{i=1}^{n}\mathcal{O}(R_i^4)\right].$$

The first term in the approximation represents a dynamic position in futures contracts, namely a holding of

$$e^{-r(t_n - t_i)}\frac{2N}{n}\left(\frac{1}{F_{i-1}} - \frac{1}{F_0}\right)$$

futures contracts during the period t_{i-1} to t_i. Given the existence of a traded log contract (as advocated in [110]), $g(F_n) = -2(\ln F_n - \ln F_0)$ represents a static position initiated at t_0. In the absence of log contracts, the methods presented in this paper facilitate the accurate approximation of such contracts in terms of liquidly traded assets, namely call and or put options.Hedging of the log contract is considered in Section 5.4.1.5.

5.2.3 Semi-Static Hedging: Barrier and American Options

Semi-static refers to a hedging strategy that requires finitely many trades during the life of a contract. In [29], an approach to semi-static hedging of barrier options using only European options maturing on the same date is developed that requires at most one transaction during the barrier option's life ([31] extends the approach to include rolldown, ratchet and lookback options as well). This approach is used as well by [115] to price and hedge barrier and lookback options.

While a Black-Scholes economy is required for the hedge to provide perfect replication, simulation studies have shown superior performance (in terms of hedge error variance and as well for mean errors when an adjustment for the implied volatility smiled is incorporated) relative to dynamic hedging strategies for specifications including Heston's stochastic volatility model, Merton's jump diffusion model, and the variance gamma model [108].

These results are further extended rigorously to local/stochastic volatility models and time-changed Levy processes when a symmetry condition is satisfied [33].

Take for example the down-and-in claim which pays out $f(S_T)$ at time T as long as a lower barrier $H < S_0$ is breached during $[0, T]$. Based on the result of [29, 30] (later extended to more general dynamics in [33]), we define the adjusted payoff

$$\tilde{f}^{DI}(S_T) = \left[f(S_T) + \left(\frac{S_T}{H}\right)^p f\left(\frac{H^2}{S_T}\right) \right] \mathbb{1}_{[S_T<H]}.$$

If S_t fails to reach the lower barrier for $t \in [0, T]$ this European payoff expires worthless, as does the down-and-in claim. However, if the barrier is hit at some $\tau_H \in [0, T]$, then the value of $\left(\frac{S_T}{H}\right)^p f\left(\frac{H^2}{S_T}\right) \mathbb{1}_{[S_T<H]}$ coincides at time τ_H with the value of $f(S_T)\mathbb{1}_{[S_T>H]}$. Thus, if the proceeds generated by selling $\left(\frac{S_T}{H}\right)^p f\left(\frac{H^2}{S_T}\right) \mathbb{1}_{[S_T<H]}$ at time τ_H are used to purchase the payoff $f(S_T)\mathbb{1}_{[S_T>H]}$, the position held over $[\tau_H, T]$ is the payoff $f(S_T)$, which matches that of the down-and-in claim. Hence the semi-static hedge coincides perfectly with the down-and-in position for any path of the underlying. For a concrete example, the adjusted payoff corresponding to the down-and-out and up-and-out calls satisfy

$$\tilde{f}^{DO}(S_T) = \begin{cases} h(S_T) & \text{if } S_T > H \\ -\left(\frac{S_T}{H}\right)^p h\left(\frac{H^2}{S_T}\right) & \text{if } S_T \leq H \end{cases}$$

and

$$\tilde{f}^{UO}(S_T) = \begin{cases} -\left(\frac{S_T}{H}\right)^p h\left(\frac{H^2}{S_T}\right) & \text{if } S_T > H \\ h(S_T) & \text{if } S_T \leq H \end{cases},$$

where $h(S_T) = (S_T - K)^+$. In Section 5.4.6, we demonstrate the application of butterfly basis hedging to down-and put options.

In a similar pursuit, certain options with early exercise features such as American binary claims [38] offer perfect static replication strategies in a Black Scholes economy. Given the pair of *stationary* securities $S_T^{\gamma \pm \epsilon}$ whose values are invariant over $[0, T]$, an American binary claim is perfectly replicated by the European payoff

$$\left[\left(\frac{S_T}{H}\right)^{\gamma+\epsilon} + \left(\frac{S_T}{H}\right)^{\gamma-\epsilon} \right] \mathbb{1}_E, \tag{155}$$

where $E = [S_T < H]$ for a put, $E = [S_T > H]$ for a call, $\gamma := \frac{1}{2} - \frac{r-d}{\sigma^2}$, and $\epsilon := \sqrt{\gamma^2 + \frac{2r}{\sigma^2}}$. In all of these cases, the success of a static or semi-static replicating strategy depends on the existence of a liquid market in nonlinear European payoffs. Of course no such markets exist, so the task of replication is again to find a suitable approximation for nonlinear payoffs using actively traded instruments. The analysis to follow is in response to these demands for accurate nonlinear payoff approximations.

5.3 Frames of Hedging Instruments and the Basis Theory

In what follows, we consider a generic European option market on the time T realization of an underlying process (e.g an interest rate, equity, index, etc.), denoted S_T, in which a set of payoff forms $\mathcal{M}_T$ are currently traded. For example, $f \in \mathcal{M}_T$ where $f(S_T) = (S_T - k)^+$ would denote the payoff of a European call option on S_T. The present work analyzes how to "optimally" approximate a general payoff $h \notin \mathcal{M}_T$ by assembling traded payoffs from $\mathcal{M}_T$.

The standard approach to static replication, aside from simple linear interpolation, is to discretize an integral representation of the desired payoff provided by [36]. Assuming that $h(S_T)$ is (weakly) twice differentiable, Carr and Madan provide the integral representation

$$\begin{aligned} h(S_T) = h(F_0) + h'(F_0) \cdot (S_T - F_0) \\ + \int_0^{F_0} h''(K)(K - S_T)^+ dK + \int_{F_0}^{\infty} h''(K)(S_T - K)^+ dK, \end{aligned} \tag{156}$$

which decomposes the payoff in terms of bonds, forwards (with current price F_0), and a continuum of calls and puts (see also [34]). To operationalize the integral representation, a discrete approximation is required (see [132] for details). Their method performs reasonably well for smooth payoffs but in practice it is ill-suited for discontinuities, which is one of the drawbacks addressed by our approach.

We develop a method which is similar to Carr and Madan's in that the payoff itself, instead of the valuation operator particular to a given model, is approximated by a discrete set of payoffs in $\mathcal{M}_T$. However, instead of working with market payoffs directly, we selectively

"fuse" them together to form a set $\{\Psi_k\}_{k\in\mathcal{K}}$ of more amenable payoff forms.[1] By mandating $\Psi_k \in \mathcal{H} := L^2(\mathbb{R})$ (or $\mathcal{H}^+ := L^2(\mathbb{R}_+)$), we recast the problem of static replication in terms of optimal approximation (in the L^2 norm) from the set $\mathcal{M} := \overline{\text{span}}\{\Psi_k\}_{k\in\mathcal{K}}$. A careful design of the payoffs $\{\Psi_k\}_{k\in\mathcal{K}}$ will enable us to then re-express the optimal approximation from $\mathcal{M}$ in terms of the original elements of $\mathcal{M}_T$, thereby producing an optimal hedge in traded payoffs.

As with any practical method of static replication, only a finite number of payoffs will be used in the approximation. In particular, no method is capable of capturing the global behavior of arbitrary payoffs with a fixed set of traded instruments. After a certain point, the tail behavior of an approximation is constrained by market availability, perhaps linear when $\mathcal{M}_T$ consists only of vanilla payoffs and the underlying. For this reason, it is without much loss of generality that restrict we our analysis to the hedging of payoffs in $\mathcal{H}$, which can be thought to capture the local behavior of a desired payoff.[2] Once a local approximation is made, the global approximation is given by specifying the tail behavior desired, given the set of traded payoffs.[3]

5.3.1 Basis Theory and Frames for Hedging

We present here only the rudiments of frame and basis theory that are necessary to understand our presentation. Rigorous introductions to the field include [78], [44] and [134].

Our primary objective is to approximate payoffs in $\mathcal{H}$ as linear combinations of the payoffs $\{\Psi_k\}_{k\in\mathcal{K}}$, $f \approx \sum_{k\in\mathcal{K}} \alpha_k \Psi_k$, for some coefficient functionals $\alpha_k = \alpha_k(f)$, which we refer to as *hedge coefficients*. By restricting attention to *Bessel sequences* $\{\Psi_k\}_{k\in\mathcal{K}}$, which for some $B > 0$ satisfy $\sum_{k\in\mathcal{K}} |\langle f, \Psi_k\rangle|^2 \leq B\|f\|^2$, $\forall f \in \mathcal{H}$, the approximation $\sum_{k\in\mathcal{K}} \alpha_k \Psi_k$ converges unconditionally[4] for any $\{\alpha_k\}_{k\in\mathcal{K}} \in l^2(\mathcal{K})$. Unless otherwise specified, $\|\cdot\|$ will denote the L^2 norm. For $\{\Psi_k\}_{k\in\mathcal{K}}$ to admit useful representations, both a lower and upper bound must be satisfied for arbitrary $f \in \overline{\text{span}}\{\Psi_k\}_{k\in\mathcal{K}} := \mathcal{M}$. Specifically, $\{\Psi_k\}_{k\in\mathcal{K}} \subset \mathcal{H}$

[1] Here, $\mathcal{K}$ is just an arbitrary indexing which will later represent a collection of available strikes.

[2] All that is required for our methods to apply is that the payoff remains bounded over the desired hedge interval. Payoffs with singularities can be handled by a locally bounded approximation near the singularity.

[3] Only to study the asymptotic accuracy of approximations as the strike space is refined do we allow for a countably infinite position in an arbitrarily dense market, $\mathcal{M}_T$.

[4] Irrespective of how the Ψ_k are ordered.

is called a *frame sequence* (or a frame for $\mathcal{M}$) if for some dense subset $\widetilde{\mathcal{M}} \subset \mathcal{M}$, it satisfies

$$A\|f\|^2 \leq \sum_{k\in\mathcal{K}} |\langle f, \Psi_k\rangle|^2 \leq B\|f\|^2, \quad \forall f \in \widetilde{\mathcal{M}},$$

for some $0 < A \leq B$.[5] In fact, every frame sequence defines a bounded linear operator $T : l^2(\mathcal{K}) \to \mathcal{H}$ by $T\{c_k\} = \sum_{k\in\mathcal{K}} c_k\Psi_k$. The adjoint, $T^* : \mathcal{H} \to l^2(\mathcal{K})$ is given by $T^*f = \{\langle f, \Psi_k\rangle\}_{k\in\mathcal{K}}$. Upon composing T with T^*, we obtain the *frame operator* $S : \mathcal{M} \to \mathcal{M}$ by $Sf = TT^*f = \sum_{k\in\mathcal{K}}\langle f, \Psi_k\rangle\Psi_k$, which is bounded, invertible and self-adjoint. Furthermore, for any $f \in \mathcal{M}$, $f = \sum_{k\in\mathcal{K}}\langle f, S^{-1}\Psi_k\rangle\Psi_k$, which is called the *frame representation*, and $\{\widetilde{\Psi}_k\}_{k\in\mathcal{K}} := \{S^{-1}\Psi_k\}_{k\in\mathcal{K}}$ the *cannonical dual*. For a general frame sequence, the canonical dual is unique although the representation is not.[6] Moreover, $\{\widetilde{\Psi}_k\}_{k\in\mathcal{K}}$ is also a frame for $\mathcal{M}$.

Frame sequences can be thought of as spanning sets which relax the unique representation requirement of bases. A frame sequence for which $\{c_k\}_{k\in\mathcal{K}} \equiv 0$ is implied whenever $\sum_{k\in\mathcal{K}} c_k\Psi_k = 0$ is called a *Riesz sequence* (or a Riesz basis for $\mathcal{M} = \overline{\text{span}}\{\Psi_k\}_{k\in\mathcal{K}}$).[7] In fact, a Riesz sequence is a (non-orthogonal) basis for its closed span. This implies that $f = \sum_{k\in\mathcal{K}}\langle f, \widetilde{\Psi}_k\rangle\Psi_k$ is the unique representation of any $f \in \mathcal{M}$, where the canonical dual $\{\widetilde{\Psi}_k\}_{k\in\mathcal{K}}$ is now *biorthogonal* to $\{\Psi_k\}_{k\in\mathcal{K}}$: $\langle\Psi_k, \widetilde{\Psi}_m\rangle = \delta_{k,m} = \mathbb{1}_{\{k=m\}}$, for any $k, m \in \mathcal{K}$.

Whenever $\{\Psi_k\}_{k\in\mathcal{K}}$ is a frame or Riesz sequence, the orthogonal projection $P_{\mathcal{M}} : \mathcal{H} \to \mathcal{M}$ of $\mathcal{H}$ onto $\mathcal{M}$ is given by $P_{\mathcal{M}}f = \sum_{k\in\mathcal{K}}\langle f, \widetilde{\Psi}_k\rangle\Psi_k$, $\forall f \in \mathcal{H}$. As for our objective, the L^2 optimal static hedge of $f \in \mathcal{H}$ in terms of the available payoffs in $\mathcal{M}$ is given by $P_{\mathcal{M}}f$. When $\{\Psi_k\}_{k\in\mathcal{K}}$ is a frame (so the representation is not necessarily unique), $P_{\mathcal{M}}f$ selects among all L^2 optimal hedges the one for which the coefficients are $l^2(\mathcal{K})$ minimal. That is, $\|\{\langle f, \widetilde{\Psi}_k\rangle\}\|_{l^2(\mathcal{K})} \leq \|\{\langle f, c_k\rangle\}\|_{l^2(\mathcal{K})}$ whenever $\sum_{k\in\mathcal{K}}\langle f, \widetilde{\Psi}_k\rangle\Psi_k = \sum_{k\in\mathcal{K}} c_k\Psi_k$, so $P_{\mathcal{M}}f$ uses the fewest assets (in the l^2 norm sense).

---

[5] If these bounds hold $\forall f \in \mathcal{H}$ (or a dense subset thereof), $\{\Psi_k\}_{k\in\mathcal{K}}$ is called a *frame*. In particular, a frame is complete for $\mathcal{H}$, $\overline{\text{span}}\{\Psi_k\}_{k\in\mathcal{K}} = \mathcal{H}$.

[6] There may be other coefficients α_k for which $f = \sum_{k\in\mathcal{K}} \alpha_k\Psi_k$, for $f \in \mathcal{M}$.

[7] This criterion, which is a stronger form of linear independence, is known as ω-independence.

5.3.2 Hedging with Frames of Simple Payoffs and Hedging-error Bounds

The simplest procedure for manufacturing a frame sequence, which is often the most relevant prerequisite for static-hedging from a financial perspective, is to take $\mathcal{M} = \overline{\text{span}}\{\phi_k\}_{k\in\mathcal{K}}$ where $\phi_k(S_T) := T_k\phi(S_T) = \phi(S_T - k)$ for some fixed payoff $\phi \in \mathcal{H}$, and T_k the translation operator. The payoff ϕ is called the *generator* of the frame of translates $\{\phi_k\}_{k\in\mathcal{K}} = \{T_k\phi\}_{k\in\mathcal{K}}$, and the corresponding frame operator $S : \mathcal{M} \to \mathcal{M}$ is given by $Sf = \sum_{k\in\mathcal{K}}\langle f, T_k\phi\rangle T_k\phi$. Although our primary interest is hedging payoffs in $\mathcal{H}_+$, it is easier to modify representations for $\mathcal{H}$ than to frame $\mathcal{H}_+$ directly. Similarly, by allowing (at most) countable frame sequences, we take $\mathcal{K} = \mathbb{Z}$ unless otherwise specified, where non-integer translations will be handled shortly.

For frames of translates, the commuter relations $ST_k = T_kS$ and $S^{-1}T_k = T_kS^{-1}$ for all $k \in \mathbb{Z}$ imply an especially simple characterization of the canonical dual frame:

$$\{\widetilde{T_k\phi}\}_{k\in\mathbb{Z}} = \{S^{-1}T_k\phi\}_{k\in\mathbb{Z}} = \{T_kS^{-1}\phi\}_{k\in\mathbb{Z}} = \{T_k\widetilde{\phi}\}_{k\in\mathbb{Z}} := \{\widetilde{\phi}_k\}_{k\in\mathbb{Z}},$$

where $\widetilde{\phi} := S^{-1}\phi$ is the canonical *dual generator* corresponding to ϕ. The verification of a frame of translates and the computation of $\widetilde{\phi}$ are closely related to the Fourier transform (FT) of ϕ.

Consistent with the financial literature, we define the FT of an L^1 or L^2 function[8] as

$$\mathcal{F}f(\xi) = \widehat{f}(\xi) = \int_{\mathbb{R}} e^{i\xi x} f(x)dx.$$

If ϕ generates a Riesz sequence, then $\widetilde{\phi} := S^{-1}\phi$ is given by

$$\widehat{\widetilde{\phi}}(\xi) = \frac{\widehat{\phi}(\xi)}{\mathbf{\Phi}(\xi)}, \quad \text{where} \quad \mathbf{\Phi}(\xi) = \sum_{k\in\mathbb{Z}} \left|\widehat{\phi}(\xi + 2\pi k)\right|^2.$$

In fact, $\{T_k\phi\}_{k\in\mathbb{Z}}$ is a Riesz (resp. frame) sequence iff $A \le \mathbf{\Phi}(\xi) \le B$ for almost every $\xi \in [0, 2\pi]$ (resp. $\xi \in \mathcal{N}$, where $\mathcal{N} := [0, 2\pi]/\{\xi : \mathbf{\Phi}(\xi) = 0\}$) for some $A, B > 0$. For a frame, the dual generator is given by $\widehat{\phi}(\xi)/\mathbf{\Phi}(\xi) \cdot \mathbb{1}_{\mathcal{N}}(\xi)$. As outlined in the appendix, one way to determine $\mathbf{\Phi}$ is by Fourier series expansion.

[8]The case of an L^2 function is handled by Plancherel's extension, in which case the integral is interpreted as a Cauchy principal value.

A further generalization is to generate sequences of translated dilations of a single generator $\phi \in \mathcal{H}$, where the dilation operator D_a ($a \neq 0$) acts on $f \in \mathcal{H}$ according to $D_a f(x) = |a|^{1/2} f(ax)$. If $\{T_k \phi\}_{k\in\mathbb{Z}}$ has already been verified as a frame (Riesz) sequence, the same is true of $\{D_a T_k \phi\}_{k\in\mathbb{Z}}$ for any $a \neq 0$. The canonical dual is given by $\{T_{\frac{k}{a}} \theta\}_{k\in\mathbb{Z}}$, where $\theta := S^{-1} D_a \phi$, and $P_{\mathcal{M}_a} f = \sum_{k\in\mathbb{Z}} \langle f, T_{\frac{k}{a}} \theta \rangle T_{\frac{k}{a}} \phi$ is the projection of $f \in \mathcal{H}$ onto $\mathcal{M}_a := \overline{\text{span}}\{T_{\frac{k}{a}} D_a \phi\}_{k\in\mathbb{Z}}$. An advantage of Riesz bases over general frames is that the dual of $\{D_a T_k \phi\}$ is simply $\{D_a T_k \widetilde{\phi}\}$ for $\widetilde{\phi}$ defined above, which yields the following.

Theorem 5.3.1. *Let $\{T_k \phi\}_{k\in\mathbb{Z}}$ be a Riesz sequence in $\mathcal{H}$ with real-valued generator ϕ and canonical dual $\widetilde{\phi}$. Further, define $\mathcal{M}_a = \overline{span}\{\phi_{a,k}\}_{k\in\mathbb{Z}}$, where $\phi_{a,k} := D_a T_k \phi$. Then the following hold:*

(i) $\widetilde{\phi}_{a,k} := D_a T_k \widetilde{\phi}$ is the unique biorthogonal dual Riesz basis in $\mathcal{M}_a$ corresponding to $\{\phi_{a,k}\}_{k\in\mathbb{Z}}$.

(ii) For any $f \in \mathcal{H}$ the projection of f onto $\mathcal{M}_a$ is given by

$$P_{\mathcal{M}_a} f(S_T) = \sum_{k\in\mathbb{Z}} \beta_{a,k} \cdot \phi_{a,k}(S_T),$$

where for real-valued $f \in \mathcal{H}$,

$$\beta_{a,k} := \frac{a^{1/2}}{2\pi} \int_{\mathbb{R}} e^{-ik\xi} \widehat{f}(a\xi) \widehat{\widetilde{\phi}}(-\xi) d\xi = \frac{a^{1/2}}{\pi} \int_0^\infty \Re \left[e^{-ik\xi} \frac{\widehat{f}(a\xi) \widehat{\phi}(-\xi)}{\mathbf{\Phi}(-\xi)} \right] d\xi.$$

Computationally speaking, in order to switch between scales a Riesz sequence is preferred since a single calculation of $\widetilde{\phi}$ reveals the dual at all scales.

For a Riesz sequence generated by ϕ, the convergence rate of approximations from $\mathcal{M}_a$ to $f \in \mathcal{H}$ of the form

$$f_a(S_T) := a^{1/2} \sum_{k\in\mathbb{Z}} \vartheta_{a,k} \phi(aS_T - k), \quad \{\vartheta_{a,k}\}_{k\in\mathbb{Z}} \in l_2(\mathbb{Z}),$$

can be characterized in terms of $\widehat{\phi}$ and its derivatives. In particular, a Riesz generator ϕ is called an L^{th} *order Riesz generator* if

$$\widehat{\phi}(0) = 1, \quad \text{and for } m = 0, ..., L-1, \quad \widehat{\phi}^{(m)}(2\pi k) = 0, \quad k \in \mathbb{Z}/\{0\}, \tag{157}$$

where $\widehat{\phi}^{(m)}$ denotes the mth derivative of ϕ. The analysis of [**?**] establishes hedging error bounds and the speed of convergence with respect to a. Namely, if $(\phi, \widetilde{\phi})$ form a L^{th} order Riesz generator/dual pair, then the projection error for sufficiently smooth $f \in \mathcal{H}$ satisfies

$$\inf_{f_a \in \mathcal{M}_a} \|f - f_a\| \leq \|f - P_{\mathcal{M}_a} f\| \leq C(\phi) a^{-L} \|f^{(L)}\|,$$

where $C(\phi)$ is independent of f. From the perspective of hedging, in which mesh refinement is limited, [127] observes that coarse scale least-squares approximations behave like an interpolation but with twice the order of accuracy. In particular,

$$\|f - P_{\mathcal{M}_a} f\| \leq K_{2L}(\phi) \|f^{(2L)}\| \cdot a^{-2L} + \sqrt{K_{2L}(\phi)} \|f^{(L)}\| \cdot a^{-L}, \tag{158}$$

for some $K_{2L}(\phi)$ independent of f. While asymptotically the error decays as $\mathcal{O}(a^{-L})$, it exhibits $\mathcal{O}(a^{-2L})$ decay for coarse resolutions. Moreover, the swift initial decay translates into accelerated valuation algorithms when applied to projected payoffs.

5.4 The Butterfly Basis

Given the current state of many financial markets, we study in detail a surprisingly effective method of payoff replication which utilizes the compactly supported, real-valued payoff generator φ:

$$\varphi(S_T) = (1 - |S_T|)^+ = (1 - |S_T|) \mathbb{1}_{[-1,1]}(S_T).$$

For a fixed $a > 0$, we define the scale-a *butterfly basis*[9] as the sequence $\varphi_{a,k} := T_{\frac{k}{a}} D_a \varphi \equiv D_a T_k \varphi$ given by:

$$\begin{aligned} \varphi_{a,k}(S_T) &= a^{1/2} \left(1 - |a\left(S_T - k/a\right)|\right) \mathbb{1}_{[-\frac{1}{a}, \frac{1}{a}]}\left(S_T - k/a\right) \\ &= a^{1/2} (1 - |aS_T - k|) \mathbb{1}_{[\frac{k-1}{a}, \frac{k+1}{a}]}(S_T). \end{aligned}$$

For example, at the initial resolution of $a = 1$, $T_k \varphi(S_T)$ has the representation

$$\varphi(S_T - k) = (S_T - (k-1))^+ - 2(S_T - k)^+ + (S_T - (k+1))^+,$$

[9] Readers may recognize φ as the hat, tent, or linear B-spline scaling function, depending on the context. Our terminology is a reference to the butterfly spread commonly used in option markets. The critical feature distinguishing this analysis from say a finite element approximation is the calculation of basis element coefficients, as will soon become apparent.

which for $k > 1$ is a butterfly spread position centered at k, in terms of call options. The value $1/a$ represents the step size of a uniform spacing of strikes. For short-term S&P 500 index options, a value of $a = 1/5$ provides a five dollar spacing between strikes, at least near the forward price.

In most markets, asset prices (and the support of any contingent payoffs) are assumed to be positive. In this case, $\varphi_{a,0}$ is easily adjusted by truncating its support, while $\varphi_{a,k}$ for $k \geq 1$ is supported over $[\frac{k-1}{a}, \frac{k+1}{a}] \subset \mathbb{R}_+$. Specifically, when working in $\mathcal{H}_+$ we define the left boundary put

$$\varphi_{a,0}(S_T) = a^{1/2}(1 - aS_T)\mathbb{1}_{[0,\frac{1}{a}]}(S_T) = a^{3/2}\Big(\frac{1}{a} - S_T\Big)^+,$$

and we would like to represent arbitrary payoffs in $\mathcal{H}_+$ by taking linear combinations of butterfly basis elements:

$$f(S_T) \approx \beta_0\varphi_{a,0}(S_T) + \sum_{k\geq 1}\beta_k\varphi_{a,k}(S_T), \tag{159}$$

for a set of hedging coefficients $\{\beta_{a,k}\}$ to be determined.[10]

When hedging $f \in \mathcal{H}_+$ with payoffs from $\mathcal{M}_a^+ := \overline{\text{span}}\{\varphi_{a,k}\}_{k\geq 0}$, we define the $\mathcal{H}_+$-projection $P_{\mathcal{M}_a^+}$ as follows. Starting with the true orthogonal projection $P_{\mathcal{M}_a}$ of f onto $\mathcal{M}_a := \overline{\text{span}}\{\varphi_{a,k}\}_{k\in\mathbb{Z}}$, the basis is truncated to $\varphi_{a,0} \cup \{\varphi_{a,k}\}_{k\geq 1}$. When only the function values of f over the desired support are given, a choice of $\beta_0 := f(0)/a^{1/2}$ may be taken to mitigate boundary effects.[11] We will denote by $\sum'$ a series of truncated basis elements, allowing for a possible adjustment to the coefficient of $\varphi_{a,0}$. Note that even for a payoff in $\mathcal{H}_+$, the coefficients prescribed to c_k for $k < 0$ may be nonzero, although they must converge to zero as a increases. Since our available hedging instruments generally have support on $\mathbb{R}_+$, truncation is necessary to obtain implementable hedges.

[10] A simple choice is the set of interpolation coefficients $\beta_{a,k} = a^{-1/2}f(k/a)$, which will be shown to provide inferior hedges an pricing approximations relative to the methods developed in this work.

[11] Similarly, to hedge a payoff over the support $[L, R]$, where $0 < L < R$ are integer multiples of the natural market spacing $1/a$, we can adjust the original projection by truncating the basis to coincide closely with $[L, R]$ with the left and right most coefficients possibly redefined as $f(L)/a^{1/2}$ and $f(R)/a^{1/2}$. These modifications improve the approximation when hedging a payoff with discontinuities at the edges of its support, as is the case when a general nonlinear payoff is localized with upper and lower support barriers. It should be noted, however, that if the original function, not just its values after truncation, is known, it is preferable to obtain hedge coefficients using the original function itself. This will become clear when we discuss implementations.

Corollary 5.4.1. *The butterfly basis, with generator φ and scale parameter $a > 0$ fixed, is a Riesz basis for its closed span on $\mathcal{H}$. Furthermore, the $\mathcal{H}_+$-projection of $f \in \mathcal{H}_+$ onto $\mathcal{M}_a^+$ is given by*

$$P_{\mathcal{M}_a^+} f(S_T) = {\sum_{k\geq 0}}' \langle f, \widetilde{\varphi}_{a,k}\rangle \varphi_{a,k}(S_T) = \beta_{a,0}\varphi_{a,0}(S_T) + \sum_{k\geq 1} \beta_{a,k}\varphi_{a,k}(S_T),$$

where for $k \geq 1$

$$\beta_{a,k} = \frac{12a^{1/2}}{\pi} \Re\left[\int_0^\infty e^{-ik\xi} \widehat{f}(a\xi) \frac{\sin^2(\xi/2)}{\xi^2(2+\cos(\xi))} d\xi\right] \tag{160}$$

In particular, as it is straightforward to show that the Butterfly generator φ is a second order Riesz generator, the following error bound of hedging the payoff f with the butterfly basis is obtained by applying equation (158),

$$\|f - P_{\mathcal{M}_a} f\| \leq K_4(\varphi)\|f^{(4)}\| \cdot a^{-4} + \sqrt{K_4(\varphi)}\|f^{(2)}\| \cdot a^{-2},$$

for a constant $K_4(\varphi)$, independent of f.

Naturally, different prescriptions for the numerical computation of hedge coefficients yield a variety of implementations of the butterfly basis method, which offer trade-offs between speed (and storage) and accuracy. There are at least five different approaches for computing the hedging coefficients of the butterfly basis: the transform-based implementation, dual approximation, Alternative Biorthogonal Sequences (ABS), discrete least squares (DLS), and a continuous least squares (Galerkin) approach used in finite element analysis.

5.4.1 Alternative Methods for Computing the Hedging Coefficients

Using the structure specific to the butterfly basis, a "dual method" is introduced which leads to an exponentially convergent approximation to the true projection and in some cases to analytical formulas for true coefficients. After deriving properties of the true dual, a second method is developed which significantly reduces the computational effort for arbitrary payoffs when analytical coefficient formulas are unknown.[12] Two least-squares based methods are also described. In Appendix 5.10, we present a purely numerical method which works well for smooth payoffs and can be applied to more general Riesz bases for which $\mathcal{F}[\widetilde{\phi}]$ is known.

[12]Moreover, this method is less susceptible to Gibb's oscillations caused by payoff discontinuities.

5.4.1.1 The Dual Method

By expanding the dual generator $\widetilde{\phi}$ itself in the basis generated by ϕ, we arrive at a more robust (yet expensive) procedure for approximating hedging coefficients. One advantage of this approach is that, given an approximation of $\widetilde{\phi}$, hedging coefficients can be calculated using $f(S_T)$ itself, rather than its Fourier transform. It also leads in some cases to analytical formulas for payoff projections, in which case the associated cost is reduced dramatically. Moreover, we will use this method as a control for the development of efficient approximations to the true projection.

Corollary 5.4.2. *Let $\phi \in \mathcal{H}$ be a symmetric real-valued Riesz generator with canonical dual generator $\widetilde{\phi}$. Then*

$$\widetilde{\phi} = \sum_{k\in\mathbb{Z}} \alpha_k T_k \phi, \quad \textit{where} \quad \alpha_k = \frac{1}{\pi}\int_0^\infty \cos(k\xi)\frac{\widehat{\phi}^2(\xi)}{\mathbf{\Phi}^2(\xi)}d\xi.$$

We can apply Corollary 5.4.2 to generate the dual of general Riesz generators when more explicit descriptions are unavailable. It also gives a procedure to check the validity of alternative descriptions as we show next for the butterfly basis. Applying Corollary 5.4.2 to the butterfly basis generator φ, we conclude that $\widetilde{\varphi}$ has coefficients

$$\alpha_k = \frac{36}{\pi}\int_0^\infty \cos(xk)\frac{(1-\cos(x))^2}{x^4(2+\cos(x))^2}dx,$$

the first five of which are given by

$$\alpha_0 = 1.73205,\ \alpha_1 = -0.46410,\ \alpha_2 = 0.12436,\ \alpha_3 = -0.03332,\ \alpha_4 = 0.00893.$$

In fact, for the butterfly basis we can obtain a much cleaner description of the dual using biorthogonality in a different way, which can be verified using the previous Corollary.

Proposition 5.4.1. *The coefficients α_m of $\widetilde{\varphi}$ with respect to the linear basis converge to zero exponentially in m. In particular,*

$$\widetilde{\varphi}(x) = \sum_{m\in\mathbb{Z}} \left(\frac{3}{\sqrt{3}}(\sqrt{3}-2)^{|m|}\right)\varphi(x-m). \tag{161}$$

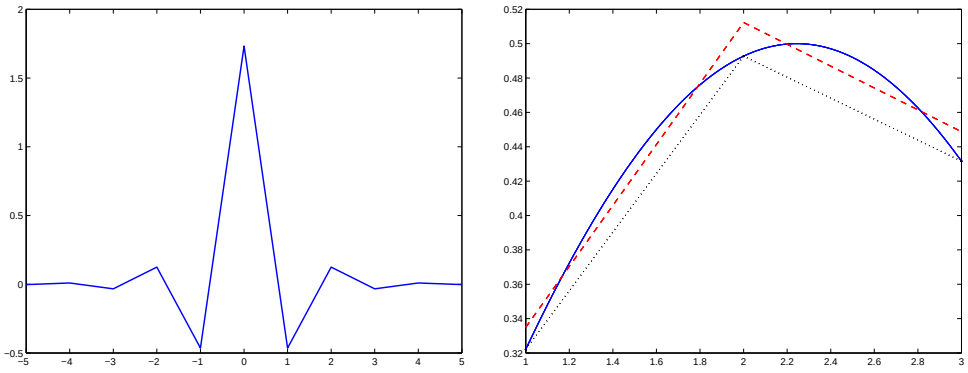

Figure 21: Left: cannonical dual, $\widetilde{\varphi}$. Right: comparison of dual method (dashed line) vs. linear interpolation (dotted line) for a continuous payoff (solid line).

Hence, the dual butterfly generator, illustrated in Figure 22, is a piecewise continuous function which is well approximated over a small, compact interval. In particular, we can approximate the biorthogonal dual on $[-(\gamma+1), \gamma+1]$ by

$$\widetilde{\varphi} \approx \sum_{|m| \leq \gamma} \alpha_m T_m \varphi,$$

for some $\gamma \in \mathbb{N}_+$. Given a payoff $f(S_T)$ supported on $[\bar{L}, \bar{R}] = [k_{\bar{L}}/a, k_{\bar{R}}/a]$, to obtain a hedge over $[L, R] = [k_L/a, k_R/a]$ we use the approximation

$$\begin{aligned} f(S_T) &\approx \sum_{k=k_L}^{k_R} \langle f, \widetilde{\varphi}_{a,k} \rangle \varphi_{a,k}(S_T) \\ &= \sum_{k=k_L}^{k_R} \langle f, D_a T_k \sum_{m \in Z} \alpha_m T_m \varphi \rangle \varphi_{a,k}(S_T) \\ &\approx \sum_{k=k_L}^{k_R} \Big(\sum_{|m| \leq \gamma} \alpha_m \langle f, \varphi_{a,k+m} \rangle \Big) \varphi_{a,k}(S_T) := f_a^{\gamma}(S_T). \end{aligned} \tag{162}$$

Hence, if we calculate $\theta_a = (\theta_{a,k_L-\gamma}, \theta_{a,k_L-\gamma+1}, ..., \theta_{a,k_R+\gamma})$ defined by

$$\theta_{a,k} := \langle f, \varphi_{a,k} \rangle = \int_{[\frac{k-1}{a}, \frac{k+1}{a}]} f(s) \varphi_{a,k}(s) ds, \tag{163}$$

where $k_{\bar{L}} := k_L - \gamma$ and $k_{\bar{R}} := k_R + \gamma$, then β_k is approximated by

$$\beta_k \approx \sum_{|m| \leq \gamma} \alpha_m \theta_{a,k-m} = (\alpha * \theta)_k, \tag{164}$$

the circular convolution of θ with $\alpha = (\alpha_{-\gamma}, ..., \alpha_{\gamma})$. The resulting implementation, which refer to as the *dual method*, converges exponentially in γ to the true projection over any

hedge interval $[L, R]$, and for any resolution $a > 0$. As a result, the size of γ (hence the required computational effort) increases slowly with higher resolutions. Figure 21 demonstrates the local behavior of $f_a^\gamma(S_T)$ compared with interpolation when $\gamma = 12$.

Proposition 5.4.2. *Let f be square integrable on $[L, R]$. With $f_a^\gamma(S_T)$ defined by (162), the deviation from the true orthogonal projection, $P_{\mathcal{M}_a}$, is characterized by:*

$$\|f_a^\gamma - P_{\mathcal{M}_a} f\|_j^{[L,R]} \leq a^{1/2} C_j \cdot \tau(\gamma), \quad j = 1, 2,$$

where

$$C_1 := (R - L + 1)^{3/2} \|f\|_\infty^{[L,R]}, \quad C_2 := \frac{2}{\sqrt{3}}(R - L + 1)\|f\|_\infty^{[L,R]},$$

and

$$\tau(\gamma) := \left(\frac{6}{1 - \nu^2}\right)^{1/2} \nu^{\gamma+1}, \quad \nu := \sqrt{3} - 2 \approx -0.268.$$

Hence, for any resolution $a > 0$, the L^1 and L^2 errors over $[L, R]$ converge exponentially in γ.

A distinct advantage of the dual method, rather than say a least squares approach to be discussed, is that when the particular form of a payoff is known, and the hedging or pricing of such a payoff is frequently required, analytical formulas for the vector θ_a can often be derived. For example, if

$$f(S_T) := (S_T - K)^p, \quad p \in \mathbb{N},$$

$$\theta_{a,k} = C(a, p)\left[(k - Ka - 1)^{(p+2)} - 2(k - Ka)^{(p+2)} + (k - Ka + 1)^{(p+2)}\right], \tag{165}$$

where $C(a, p) := \frac{a^{-(p+\frac{1}{2})}}{(p+1)(p+2)}$, which can be used to derive the coefficients for any polynomial, resulting in a considerable cost reduction. However, in the particular case of polynomial payoffs, the exact beta coefficients are known analytically. Moreover, we can derive the pth moments of $\widetilde{\varphi}$, which will be used to develop efficient approximations to the true projection.

Corollary 5.4.3. *The pth moment of $\widetilde{\varphi}$, M^p, is finite for all $p \in \mathbb{N}$, and is given by*

$$M^p = \int_R \widetilde{\varphi}(x) x^p dx = \begin{cases} \dfrac{6(\nu - 2 + \nu^{-1})}{\sqrt{3}(p+1)(p+2)} \cdot \dfrac{d^{p+2}}{d\zeta^{p+2}} \left[\dfrac{1}{1 - \nu e^\zeta}\right]\Big|_{\zeta=0}, & p \text{ even} \\ 0, & p \text{ odd,} \end{cases} \tag{166}$$

where $\nu = \sqrt{3}-2$. *Hence, the dual coefficients* $\beta_{a,k}^{[p]}$ *are known analytically for any polynomial according to*

$$\beta_{a,k}^{[p]} := \int_R \widetilde{\varphi}_{a,k}(x) x^p dx = a^{-(p+\frac{1}{2})} \sum_{n=0}^{\lfloor \frac{p}{2} \rfloor} \binom{p}{2n} k^{p-2n} M^{2n}. \tag{167}$$

For example, the first four even moments are found to be

$$M^0 = 1, \quad M^2 = -\frac{1}{6}, \quad M^4 = \frac{1}{15}, \quad M^6 = \frac{17}{84},$$

and higher order moments are easily derived. Note as well that for any payoff of the form $f(S_T) := (S_T - K)^p$, if $K = \bar{k}/a$ for some $\bar{k} \in \mathbb{N}$, the corresponding coefficients are found by shifting the index of those for S_T^p by $\bar{k}$. Thus, for any $K = \bar{k}/a$, the projection[13] of the power straddle $f(S_T) := (S_T - K)^2$ over $[L, R] = [k_L/a, k_R/a]$ is given simply by

$$P_{\mathcal{M}_a} f(S_T) = a^{-5/2} \sum_{k=k_L}^{k_R} \left[(k - \bar{k})^2 - \frac{1}{6} \right] \varphi_{a,k}(S_T). \tag{168}$$

Similarly, the projection of $f(S_T) := (S_T - K)^3$ restricted to $[L, R]$ is found using

$$\beta_{a,k} = a^{-7/2}(k - \bar{k}) \left((k - \bar{k})^2 - \frac{1}{2} \right), \qquad k_L \le k \le k_R.$$

Given that polynomial payoffs offer exact formulas for the corresponding projection, an immediate consequence is the ability to transform a Taylor series (or other polynomial approximation method) into a portfolio of liquid contracts. Specifically, if $f \in C^{p+1}$,

$$f(S_T) = f(K) + \sum_{n=1}^{p} \frac{f^{(n)}(K)}{n!} (S_T - K)^n + \frac{f^{(n+1)}(\xi)}{(n+1)!}, \quad \xi \in (L, R).$$

By projection the expansion onto $\{\varphi_{a,k}\}$, the coefficients for $k_L \le k \le k_R$ satisfy

$$\beta_{a,k} = a^{-1/2} \left[f(K) + \sum_{n=1}^{p} \left(\frac{f^{(n)}(K) a^{-n}}{n!} \right) \sum_{m=0}^{\lfloor \frac{n}{2} \rfloor} \binom{n}{2m} (k - \bar{k})^{n-2m} M^{2m} \right].$$

For near expiry contracts, low order projected Taylor expansions about S_t can provide accurate approximations at a low cost.

[13] Strictly speaking, since x^2 is not in L^2, we cannot speak of the orthogonal projection on $\mathcal{M}_a$. However, the exponential decay of $\widetilde{\varphi}$ allows us to obtain the analogous representation, which can be though of as a localized projection, valid upon restricting the representation to compact intervals. This is explored in the next subsection.

In the next subsection, we introduce an alternative to the dual method which approximates the projection at a reduced cost. The appeal of the so-called ABS approximations is that rather than integrating the payoff against $\widetilde{\varphi}_{a,k}$, which has infinite (though safely truncated) support, we can obtain accurate approximations by integrating the payoff against a function with much narrower support. Hence, not only do the coefficients requires less work to obtain, but the extended support $[\bar{L}, \bar{R}]$ can be shortened as well. Consequently, ABS methods are more robust to the presence of discontinuities and are better equipped to handle isolated singularities.

5.4.1.2 Alternative Biorthogonal Sequences (ABS)

As we noted before, the canonical *dual* to a Riesz sequence $\{\phi_{a,k}\} \subset \mathcal{H}$ at any scale is the unique biorthogonal sequence living within the *same* space as the Riesz sequence, $\mathcal{M}_a = \overline{\text{span}}\{\phi_{a,k}\}_k$, and is also a Riesz basis for $\mathcal{M}_a$. However, our search for biorthogonal *sequences* (as opposed to duals) is not limited to $\mathcal{M}_a$. For a given Riesz sequence $\{\phi_k\}$, we will refer to any sequence in $\mathcal{H}$ which is biorthogonal to $\{\phi_k\}$ as an *alternative biorthogonal sequence* (ABS). By using an ABS instead of the canonical dual to approximate the hedging coefficients, an approximation to the true orthogonal projection is obtained, often at a significant reduction in computational effort.

5.4.1.3 ABS Construction

In the butterfly case, starting at the initial resolution, we begin our search for a viable ABS at one higher resolution and supported on $[-1, 1]$, posited to be a symmetric linear function of the form:

$$\breve{\varphi}(x) = \begin{cases} \lambda - 2(\lambda + \nu)x, & [0, 1/2) \\ -2\nu(1 - x), & [1/2, 1], \end{cases}$$

for some constants λ, ν, where $\breve{\varphi}(x) = \breve{\varphi}(-x)$ for $x \in [-1, 0]$. To solve for λ, ν, biorthogonality imposes requires $\int_0^1 \varphi(x)\breve{\varphi}(x)dx = 1/2$ and $\int_0^1 \varphi(x)\breve{\varphi}(x-1)dx = 0$, which yields the following.

Result 5.4.1. *The butterfly basis, with generator φ and scale parameter $a > 0$ fixed, admits*

an ABS with generator

$$\breve{\varphi}^{[1]}(x) = \begin{cases} 3 - 7|x|, & |x| < 1/2 \\ |x| - 1, & 1/2 \leq |x| \leq 1. \end{cases}$$

We designed the ABS generator $\breve{\varphi}^{[1]}$ shown in figure 22 to have narrow support, thereby reducing the computational burden of calculating the hedge coefficients, while mitigating boundary effects[14]. Note as well that by imposing symmetry of $\breve{\varphi}^{[1]}$ about the origin the following odd moments condition is satisfied:

$$\int_{\mathbb{R}} \breve{\varphi}^{[1]}(x) \cdot x^{2p+1} dx = \int_{\mathbb{R}} \widetilde{\varphi}(x) \cdot x^{2p+1} dx = 0, \quad p \in \mathbb{N}.$$

By increasing the support of $\breve{\varphi}$ to $[-2, 2]$, we gain an additional degree of freedom with which we impose a second moment condition, which is solved for to obtain the ABS denoted by $\breve{\varphi}^{[2]}$:

$$\int_{\mathbb{R}} \breve{\varphi}^{[2]}(x) \cdot x^{2} dx = \int_{\mathbb{R}} \widetilde{\varphi}(x) \cdot x^{2} dx = -\frac{1}{6},$$

from Corollary 5.4.3. We show in Proposition 5.4.3 that specifying an ABS by equating its first γ moments to those of the dual is tantamount to obtaining the true projection for all polynomials of degree $p \leq 2\gamma - 1$. This engenders a direct trade-off between the computational effort and the resulting accuracy on an ABS approximation.

In general, we define an ABS_γ generator as the ABS generator supported on $[-\gamma, \gamma]$ for which all moments $p \leq 2\gamma - 1$ coincide with the true dual (in addition to sharing all odd moments by the imposition of symmetry). The ABS_γ generators are of the form

$$\breve{\varphi}^{[\gamma]}(x) = \sum_{|m| \leq 2\gamma - 1} c_m^{[\gamma]} \varphi(2x - m) = \sum_{|m| \leq 2\gamma - 1} \frac{c_m^{[\gamma]}}{\sqrt{2}} \varphi_{2,m}(x), \tag{169}$$

where $c_m^{[\gamma]}$ are determined as follows.

Proposition 5.4.3. *For any $\gamma \geq 2$, the unique set of coefficients $c_m^{[\gamma]}$, $|m| \leq 2\gamma - 1$, for*

[14] We have found the ABS generated by $\breve{\varphi}^{[1]}$ to roughly double the approximation accuracy of interpolation in terms of hedging and pricing errors. However, the ABS_2 defined below provides a substantial improvement, especially for pricing, and the added cost is insignificant.

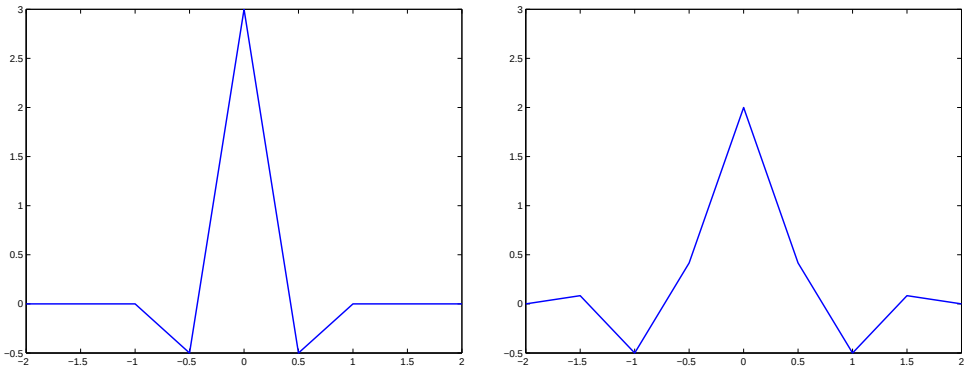

Figure 22: Left: ABS_1 generator supported on $[-1,1]$. Right: ABS_2 generator supported on $[-2,2]$.

which $\breve{\varphi}^{[\gamma]}$ is an ABS_γ generator is given by the solution of the system

$$
\begin{aligned}
1 &= \lambda_0 c_0 + 2\lambda_1 c_1 + 2\lambda_2 c_2 \\
0 &= \lambda_2(c_{2k-2} + c_{2k+2}) + \lambda_0 c_{2k} + \lambda_1(c_{2k-1} + c_{2k+1}), \quad 1 \le k \le \gamma - 2 \\
0 &= \lambda_2 c_{2\gamma-4} + \lambda_0 c_{2\gamma-2} + \lambda_1(c_{2\gamma-3} + c_{2\gamma-1}) \\
0 &= \lambda_2 c_{2\gamma-2} + \lambda_1 c_{2\gamma-1} \\
M^{2k} &= \frac{2^{-2k}}{(2k+1)(2k+2)} \left(c_0 + \sum_{m=1}^{2\gamma-1} c_m \nu_m^{2k} \right), \quad 1 \le k \le \gamma - 1,
\end{aligned}
$$

where

$$\nu_m^{2k} = (m-1)^{2k+2} - 2m^{2k+2} + (m+1)^{2k+2}, \quad m = 1, ..., 2\gamma - 1, \tag{170}$$

$$\lambda_0 = \frac{5}{12}, \quad \lambda_1 = \frac{3}{12}, \quad \lambda_2 = \frac{1}{24}, \tag{171}$$

$c_k = c_{-k}$ $\forall 1 \le k \le 2\gamma - 1$, and M^{2k} are the dual moments which are found by equation (166)*. Moreover, the ABS_γ coefficients agree with those of the true projection for all polynomials of degree $p \le 2\gamma - 1$, and for all odd degrees.*

Application of Proposition 5.4.3 leads to the ABS_2 generator, which very closely approximates the coefficients obtained by the true dual for the functions tested. Moreover, in Table 18 we verify the equivalence of the dual and ABS_2 methods for quadratic payoffs.

Result 5.4.2. *The ABS_2 generator is given by $\breve{\varphi}^{[2]}(x) = \sum_{|m|\le 3} c_{|m|}\varphi(2x - m)$, where*

$$(c_0, c_1, c_2, c_3) = \left(2, \frac{5}{12}, -\frac{1}{2}, \frac{1}{12}\right),$$

and is depicted in figure 22.

We now outline the steps required to implement the ABS_2. To ease notation, we calculate the coefficients of $\bar{f}(x) := f(x+L)$, which requires function values of f on $[\bar{L}, \bar{R}] := [L-2\Delta, R+2\Delta]$. To obtain the hedge coefficients of $\bar{f}$ with respect to $\breve{\varphi}^{[2]}$, the first step is to calculate

$$\begin{aligned}\bar{\theta}_{2a,k} &:= \frac{1}{\sqrt{2}} \int_{[\frac{k-1}{2a}, \frac{k+1}{2a}]} \bar{f}(s)\varphi_{2a,k}(s)ds \\ &= 2a^{3/2}\left[\int_{[\frac{k-1}{2a}, \frac{k}{2a}]} \bar{f}(s)\left(s - \frac{k-1}{2a}\right)ds + \int_{[\frac{k}{2a}, \frac{k+1}{2a}]} \bar{f}(s)\left(\frac{k+1}{2a} - s\right)ds\right],\end{aligned}$$

for $k = -3, -2, ..., 2a(R-L)+3$ (here $\theta_{2a,0}$ is centered over 0). Using a Newton-Cotes rule reduces the number of required function evaluations by uniform sampling. As an example, a simple application of Simpson's rule with function values sampled over $\eta_{4a,k} := L + \frac{k}{4a}$, $k = -7, ..., 4a(R-L)+7$ yields the approximation

$$\bar{\theta}_{2a,k} = \frac{a^{-1/2}}{6}\left[f(\eta_{4a,2k-1}) + f(\eta_{4a,2k}) + f(\eta_{4a,2k+1})\right] + \mathcal{O}(a^{-5}), \tag{172}$$

where the convergence rate is understood in the context of sufficiently smooth functions. With

$$\{d_k\}_{k=-3}^{3} := \{c_3, c_2, c_1, c_0, c_1, c_2, c_3\},$$

the coefficients of $\bar{f}$ on $[0, R-L]$ are approximated by

$$\bar{\beta}_{a,j} \approx \sum_{k=-3}^{3} \bar{\theta}_{2a,k+2(j-1)} \cdot d_k, \quad j = 0, ..., a(R-L),$$

and the desired coefficients of f are found as $\beta_{a,j} = \bar{\beta}_{a,k_L+j}$.

5.4.1.4 ABS Projector

To ensure that convergent representations are still obtained, it is essential that the ABS satisfies a Bessel upper bound. This can be trivial to verify with the following proposition.

Proposition 5.4.4. *([44], p.63) Let $\{f_k\}_{k\in\mathcal{K}} \in \mathcal{H}$ be any sequence satisfying*

$$\sum_{k\in\mathcal{K}} |\langle f_j, f_k\rangle| \leq B, \quad \forall j \in \mathcal{K},$$

where $B > 0$ is some constant. Then $\{f_k\}$ is a Bessel sequence with bound B.

Likewise, we will make use of the fact that a frame sequence, as opposed to a frame for all of $\mathcal{H}$, is actually a Bessel sequence on $\mathcal{H}$.

Lemma 5.4.4. *If $\{\Psi_k\}_{k\in\mathcal{K}}$ is a frame sequence in a Hilbert space $\mathcal{H}$, then $\{\Psi_k\}_{k\in\mathcal{K}}$ is a Bessel sequence (on all of $\mathcal{H}$). That is, $\sum_{k\in\mathcal{K}} |\langle f, \Psi_k\rangle|^2 < \infty$, $\forall f \in \mathcal{H}$.*

With the previous two results in hand, we can characterize an ABS approximation, denoted by $\breve{P}$, which is most appropriate for our purposes. With $\mathcal{M} := \overline{\text{span}}\{\phi_k\}_{k\in\mathbb{Z}}$, we have

$$\breve{P}_{\mathcal{M}} f := \sum_{k\in\mathbb{Z}} \langle f, \breve{\phi}_k\rangle \phi_k, \quad f \in \mathcal{H}. \tag{173}$$

Proposition 5.4.5. *Let ϕ be a Riesz generator in $\mathcal{H}$. If $\breve{\phi} \in \mathcal{H}$ is a compactly supported function such that the sequences of translates $\{\phi_k\}$ and $\{\breve{\phi}_k\}$ are biorthogonal, then the mapping $\breve{P}_{\mathcal{M}} : \mathcal{H} \to \mathcal{M}$ defined in equation* (173) *is a bounded linear projection operator on $\mathcal{M}$ which commutes with the orthogonal projection $P_{\mathcal{M}}$ of $\mathcal{H}$ onto $\mathcal{M}$. However, $\breve{P}_{\mathcal{M}} = P_{\mathcal{M}}$ iff $\breve{P}_{\mathcal{M}}$ is the null operator on $\mathcal{M}^\perp$, that is $\breve{P}_{\mathcal{M}}(\mathcal{M}^\perp) = \{0\}$, which occurs iff $\breve{\phi} \in \mathcal{M}$.*

By commutativity, the true projection preserves that of the ABS and conversely. Moreover, while we can design an ABS to provide identical representations as the dual for polynomials of arbitrarily high order, there will always be $f \in \mathcal{H}$ for which the projections disagree.

5.4.1.5 Numerical Comparison of Alternative Hedging Methods

Before delving further into the theory of frame hedging and pricing, we demonstrate the effectiveness of the dual and ABS_2 methods with two practical examples. The controls are taken to be linear interpolation and the method of Carr and Madan (CM), which results from a discretization of equation (156) (see [132] for details).

Given a payoff function $f(S_T)$ and a fixed hedge interval $[L, R]$ contained in the support of f, we compare for each butterfly method and for several resolutions the *relative absolute hedge error*

$$\text{RAHE} = \frac{\sum_{i=1}^{N_s} |\tilde{f}_{[L,R]}(x_i; a) - f(x_i)|}{\sum_{i=1}^{N_s} |f(x_i)|}, \tag{174}$$

Table 18: RAHE of $f(S_T) = S_T^2$ on $[L, R] = [0, 10]$.

Scale(Δ)	2	1	.5	.25	.1	.01
Interp	2.000e-02	5.000e-03	1.250e-03	3.125e-04	5.000e-05	5.000e-07
Dual_{12}	7.698e-03	1.924e-03	4.811e-04	1.203e-04	1.922e-05	2.254e-07
ABS_2	7.698e-03	1.925e-03	4.811e-04	1.203e-04	1.925e-05	1.925e-07
CM	1.000e-02	7.500e-02	3.750e-02	1.875e-02	7.500e-03	7.500e-04

where $\{x_i\}_{i=1}^{N_s}$ is a uniform sampling of $[L, R]$, and $\tilde{f}_{[L,R]}(x_i; a)$ is a prescribed approximation on $[L, R]$ at resolution a ($\Delta := 1/a$). For the dual method, we take $\gamma = 12$, which corresponds to a dual approximation on the interval $[-13, 13]$. Interpolation approximations can be represented in the butterfly basis by

$$f_{[L,R]}^{Interp}(S_T; a) = \sum_{k=k_L}^{k_R} a^{-1/2} f\Big(\frac{k}{a}\Big)\varphi_{a,k}(S_T).$$

Table 18 presents hedge errors for the payoff $f(S_T) = S_T^2$ on $[0, 10]$. As expected from Proposition 5.4.3, the dual and ABS errors are nearly identical since the payoff is a second order polynomial. Moreover, the dual and ABS methods are more than twice as accurate as interpolation at each resolution, and many times more accurate than CM. Similar results for $f(S_T) = \ln(S_T)$ over $[1, 11]$ are given in Table 19. Note that we have avoided the singularity in our computation, since none of the methods are able to reasonably hedge a payoff near a singularity without carefully adjusting the resolution. Moreover, to keep the singular behavior near $S_T = 0$ from affecting the coefficients, it is advantageous to use an auxiliary linear approximation of the form

$$\ln(S_T)\mathbb{1}[S_T \geq \tau] + [\ln(\tau) + (S_T - \tau)/\tau]\mathbb{1}[S_T < \tau],$$

which replaces the left singular tail by a linear Taylor approximation. While any value of $\tau \in (s, L]$ is reasonable, where s denotes the singularity ($s = 0$ for $\ln(S_T)$),as τ approaches s the approximation deteriorates (especially for the dual method, since the ABS has narrower support). We find that a value of $\tau = 1/2$ works well in this case[15].

[15]For the ABS_2, an approximation can be made arbitrarily close to s by choosing Δ so that $s \leq L - 2\Delta$, and using the auxiliary payoff with $\tau(\Delta) := L - \Delta$. This can be applied to functions other than $\ln(S_T)$, and also at interior and right boundary singularities by similarly defining the auxiliary payoff.

Table 19: RAHE of $f(S_T) = \ln(S_T)$ on $[L, R] = [1, 11]$.

Scale(Δ)	2	1	.5	.25	.1	.01
Interp	1.689e-02	4.487e-03	1.147e-03	2.885e-04	4.624e-05	4.626e-07
Dual_{12}	8.778e-03	2.064e-03	4.853e-04	1.165e-04	1.816e-05	2.707e-07
ABS_2	8.918e-03	2.088e-03	4.908e-04	1.174e-04	1.820e-05	1.784e-07
CM	2.866e-02	2.625e-02	1.174e-02	5.572e-03	2.163e-03	2.124e-04

5.4.1.6 Least-squares Based Methods

Finally, we describe two approaches based on the least-squares idea: discrete least squares (DLS), and a continuous least squares (Galerkin) approach used in finite element analysis. These two approaches have accuracy comparable to the dual method, but at a higher cost especially for wide hedging intervals.

5.4.1.7 Galerkin and DLS Methods

The Galerkin method is derived by the following Hilbert space argument. In order for $\{\beta_{a,k}\}$ to yield the orthogonal projection of f onto $\mathcal{M}_a := \text{span}\{\varphi_{a,k}\}_{k=0}^{\bar{K}}$, it is necessary and sufficient that the approximation error be orthogonal to $\mathcal{M}_a$:

$$f - \sum_{k=0}^{\bar{K}} \beta_{a,k}\varphi_{a,k} \perp \mathcal{M}_a \quad \Leftrightarrow \quad \langle f - \sum_{k=0}^{\bar{K}} \beta_{a,k}\varphi_{a,k}, \varphi_{a,m}\rangle = 0, \quad m = 0, ..., \bar{K}.$$

The resulting (continuous) *normal equations* are expressed as the system

$$\sum_{k=0}^{\bar{K}} \beta_{a,k}\langle\varphi_{a,k}, \varphi_{a,m}\rangle = \langle f, \varphi_{a,m}\rangle, \quad m = 0, ..., \bar{K},$$

which can be solved for $\beta_{a,k}$. While the $\langle\varphi_{a,k}, \varphi_{a,m}\rangle$ are known explicitly, the $\langle f, \varphi_{a,m}\rangle$ are computed numerically.

The Galerkin method also suggests a discrete alternative based on a simple least squares procedure, which can also be used in the context of more general frames. Specifically, we start with a (uniform) grid $\{x_i\}_{i=0}^{N_s}$ of $[L, R]$ and define $A_{i,k} := \varphi_{a,k}(x_i)$ and $f_i := f(x_i)$, $k = 0, ..., \bar{K}$, $i = 0, ..., N_s$. Minimizing the squared residuals over grid points yields the discrete normal equations $A^\top A\beta = A^\top f$, which can be expressed as

$$\sum_{k=0}^{\bar{K}} \beta_{a,k} \sum_{i=0}^{N_s} \varphi_{a,m}(x_i)\varphi_{a,k}(x_i) = \sum_{i=0}^{N_s} \varphi_{a,m}(x_i)f(x_i), \quad m = 0, ..., \bar{K}.$$

Note that by multiplying both sides by $1/(N_s+1)$ and passing to the limit in N_s yields the continuous normal equations (for Riemann integrable f).[16]

In general, the dual method and both least squares approaches are well suited to handle a frame based hedging procedure with a "custom" designed frame, as opposed to one that has been generated by a single "shape" function. To keep the presentation at a reasonable length, numerical results in the remaining part of this paper focus on the ABS and dual implementations with interpolation as the control.

5.4.2 Algorithms

To ease implementation, this section summarizes several of the algorithms considered in this work. We assume a hedge support of $[L, R]$ and a resolution of $a > 0$. Since the market dictates the size of a, the only user-supplied parameters (for hedging) are L and R, which are highly application dependent. With the S&P 500 example given in Section 5.4.5, $\Delta = 1/a$ can be chosen as $5 \cdot c$ where $c \in \{1, 2, ..., 20\}$, depending on the desired resolution. When $\Delta = 5$, we can take $L = 1300$ and $R = 2250$, although by choosing a larger value of Δ, we can extend the boundaries L and R if desired, since the granularity of available vanilla option strikes increases outside of these boundaries. More basis elements require transacting in more traded assets, which introduces additional costs. Unlike with option pricing, where the resolution leads to an unknown (but estimable) error, the payoff is a known measurable function, and the approximation error can be quantified precisely (given a distance measure, such as relative mean-square error). Hence, the resolution can be chosen so that the resulting hedge error is within a prescribed tolerance, subject to the market resolution.

Algorithm 5 Interpolation Coefficients

$\bar{K} := (R - L)/a$
$B_k := f(L + k/a), \quad k = 0, ..., \bar{K}$
return $\{B\}_{k=0}^{\bar{K}}$

Assuming that $L > 1/a$, we take $\bar{K} := (R-L)/a$ to be one less than the number of basis

[16] Robust implementations of discrete least squares utilize QR factorization, and the normal equations are not explicitly solved.

elements. Each butterfly basis algorithm below will take a payoff function f and return a set of coefficients $\{B_k\}_{k=0}^{\bar{K}}$. In this case, B_0 corresponds to the basis element centered at L, B_1 corresponds to $L + 1/a$, and B_k corresponds to $L + k/a$. Algorithm 5 is a direct application of linear interpolation to calculate hedging coefficients.

Algorithm 6 ABS_1 coefficients

$\bar{K} := (R - L)/a$
$g := a^{-1/2}/12$
$z_k \leftarrow f(L + k/4a)$, $k = 0, ..., 4\bar{K}$
$B_k \leftarrow 0$, $k = 0, ..., \bar{K}$
for $k = 0, ..., \bar{K} - 1$ **do**
    $B_k \leftarrow B_k + g \cdot (5 \cdot z_{4k} - z_{4k+1} - z_{4k+2})$
    $B_{k+1} \leftarrow g \cdot (-z_{4k} - z_{4k+1} + 5 \cdot z_{4k+2} + 6 \cdot z_{4k+3})$
end for
$B_0 \leftarrow 2/5 \cdot \sum_{k=0}^{4} z_k - B_1$
$B_{\bar{K}} \leftarrow 2/5 \cdot \sum_{k=\bar{K}-4}^{\bar{K}} z_k - B_{\bar{K}-1}$
return $\{B\}_{k=0}^{\bar{K}}$

In Algorithm 6, we employ a slight variation of the direct ABS_1 approach such that, in the spirit of linear regression, the boundary coefficients are determined so that the line from B_0 to B_1 passes through the average function value midway through the interval $[L, L+1/a]$, and similarly for $B_{\bar{K}}$. This illustrates how one can apply the ABS methods when function values are unknown outside of $[L, R]$. Given the superiority of the ABS_2 method over ABS_1, numerical results for hedging applications are restricted to the ABS_2 method. However, the two methods are compared in the context of pricing in Section 5.8.3.

The application of the ABS_2 method, summarized in Algorithm 7, assumes that function values are known outside of $[L, R]$, as is generally the case. This algorithm is employed when we consider semi-static hedging of barrier options, in Section 5.4.6. The Dual method, which is more involved, is omitted. We find that the ABS_2 method provides the same level of accuracy at a fraction of the cost. Moreover, it behaves better in the presence of payoff discontinuities and is easier to implement.

A basic implementation of the Carr Madan method [36] is provided in Algorithm 8 where we assume the first and second order derivatives of the (smooth) payoff are available, otherwise a finite difference approximation may be substituted. For this method, we supply

Algorithm 7 ABS_2 coefficients

$\bar{K} := (R-L)/a$
$c_0 := 2; \quad c_1 := 5/12; \quad c_2 := -1/2; \quad c_3 := 1/12$
$\{d_k\}_{k=0}^{7} = \{c_3, c_2, c_1, c_0, c_1, c_2, c_3\}$
$\lambda := a^{-1/2}/6$
$\widetilde{K} := 4a(R-L) + 14$
$z_k := f(L - 7/4a + k/4a), \quad k = 0, ..., \widetilde{K}$
for $k = 0, ..., \widetilde{K}/2 - 1$ **do**
    $\theta_k \leftarrow \lambda \cdot [z_{2k} + z_{2k+1} + z_{2k+2}]$
end for
for $j = 0, ..., \widetilde{K}/2 - 1$ **do**
    $B_k = \sum_{k=0}^{7} \theta_{k+2(j-1)} \cdot d_k$
end for
return $\{B\}_{k=0}^{\bar{K}}$

L, R the resolution ($a > 0$) and F_0, which is the T-forward price of the underlying. Algorithm 8 returns the positions in each option with strikes $L, L + 1/a, ..., R - 1/a, R$, where strikes less than F_0 are taken in put options, and strikes greater than F_0 are taken in call options (the corresponding positions are denoted by $\widetilde{B}_k$, to distinguish them from positions in butterfly basis elements). In addition, we hold $f(F_0)$ units in a bond, and $f'(F_0)$ forward contracts. A derivation of the approximation given in Algorithm 8 can be found in [132].

Algorithm 8 Carr-Madan coefficients

$\bar{K} := (R-L)/a$
for $k = 0, ..., \bar{K}$ **do**
    $\widetilde{B}_k = .5 \cdot [f'(L + (k+1)/a) - f'(L + (k-1)/a)]$
end for
return $\{\widetilde{B}_k\}_{k=0}^{\bar{K}}$

5.4.3 Characterization of Applicable Payoff Spaces: Localized Projections

Given a complete description of the dual in Section 5.4.1.1, we are able to characterize the classes of functions for which butterfly projection methods apply, relaxing the ostensible requirement that f belongs to $L^2(\mathbb{R})$. For most practical payoffs, coefficients of a localized projection can be obtained using the global behavior of the function, even for functions which are not L^2 on all of $\mathbb{R}$. We define two such classes of $L^2_{loc} := \{f : f \in L^2([L, R]), \forall L <$

$R \in \mathbb{R}\}$, the first is given by

$$\bar{C} := \{f \in L^2_{loc} : \forall a > 0, \|f\|_2^{I^a_{m^+}} \leq C\|f\|_2^{I^a_m} \text{ eventually, where } |C\nu| < 1\},$$

where *eventually* is defined as the existence of M such that $\forall |m| \geq M$ the bound holds, $I^a_m := [(m-1)/a, (m+1)/a]$, and $I^a_{m^+} := I^a_{m+\text{sign}(m)}$. For example, if $f(x) := \sum_{k=0}^p c_k x^k$, then with respect to $\|\cdot\|_\infty$

$$\frac{\|f\|_\infty^{I^a_{m^+}}}{\|f\|_\infty^{I^a_m}} \sim \left|\frac{m+2}{m+1}\right|^p = \mathcal{O}(1).$$

Hence, for any $\epsilon > 0$, $\exists M$ so that $\|f\|_\infty^{I^a_{m^+}} \leq (1+\epsilon)\|f\|_\infty^{I^a_m}$ $\forall |m| \geq M$, independent of $a > 0$. By taking ϵ small enough that $|(1+\epsilon)\nu| < 1$, we verify $f \in \bar{C}$. Hence $\bar{C}$ contains all polynomials.

The second class, $\bar{C}(a)$, allows the choice of $a > 0$ for which the bound holds:

$$\bar{C}(a) := \{f \in L^2_{loc} : \exists a > 0 \text{ s.th } \|f\|_2^{I^a_{m^+}} \leq C\|f\|_2^{I^a_m} \text{ eventually, where } |C\nu| < 1\}.$$

As an example, let $f(x) := e^{\tau x}$, $\tau > 0$. Then $\|f\|_\infty^{I^a_m} = \exp(\tau(m+1)/a)$, so

$$\|f\|_\infty^{I^a_{m^+}} = \exp(\tau/a)\|f\|_\infty^{I^a_m},$$

and $a > 0$ can be chosen so that $|\exp(\tau/a)\nu| < 1$. Hence functions with exponential growth belong to $\bar{C}(a)$. In particular, $\bar{C}$ characterizes the functions f such that $f \cdot \widetilde{\varphi}_{a,k} \in L^2(\mathbb{R})$, $\forall a > 0, k \in \mathbb{Z}$, and $\bar{C}(a)$ characterizes those for which $\exists \bar{a} \geq 0$ such that $f \cdot \widetilde{\varphi}_{a,k} \in L^2(\mathbb{R})$, $\forall a > \bar{a}, k \in \mathbb{Z}$.

Given a function f in either class, with $[L, R] = [k_L/a, k_R/a]$ a fixed hedge interval, we define for $[k_{\bar{L}}/a, k_{\bar{R}}/a] = [\bar{L}, \bar{R}] \supset [L, R]$ the *localized projections*

$$\bar{P}_{\mathcal{M}_a} f(S_T) = \sum_{k=k_L}^{k_R} \beta_{a,k}\varphi_{a,k}(S_T), \qquad \beta_{a,k} = \langle f, \widetilde{\varphi}_{a,k}\rangle,$$

$$\widehat{P}_{\mathcal{M}_a} f_{[\bar{L},\bar{R}]}(S_T) = \sum_{k=k_L}^{k_R} \widehat{\beta}_{a,k}\varphi_{a,k}(S_T), \qquad \widehat{\beta}_{a,k} = \langle f\mathbb{1}_{[\bar{L},\bar{R}]}, \widetilde{\varphi}_{a,k}\rangle.$$

For localized projection to make sense, $\widehat{P}_{\mathcal{M}_a} f_{[\bar{L},\bar{R}]}$ should be a consistent approximation to $\bar{P}_{\mathcal{M}_a}$, which is indeed the case.

Proposition 5.4.6. *If $f \in \bar{C}$, $a > 0$ and $[L, R]$ is fixed, then $\forall \epsilon > 0$, $\exists [\bar{L}, \bar{R}]$ such that*

$$\|\bar{P}_{\mathcal{M}_a} f - \widehat{P}_{\mathcal{M}_a} f_{[\bar{L},\bar{R}]}\|_2 < \epsilon.$$

Similarly, if $f \in \bar{C}(a)$, $\exists \bar{a} > 0$ such that $\forall a > \bar{a}$ fixed and $\forall \epsilon > 0$, $\exists [\bar{L}, \bar{R}]$ such that the bound holds. Moreover, both projections are finite.

Hence, for $f \in \bar{C}$, and $f \in \bar{C}(a)$ with a sufficiently large, $\bar{P}_{\mathcal{M}_a} f$ is the limit in $L^2([L, R])$ of $\widehat{P}_{\mathcal{M}_a} f_{[\bar{L},\bar{R}]}$ as $[\bar{L}, \bar{R}]$ increases to $(-\infty, \infty)$. For payoffs which do not belong to either class, the coefficients of $f \mathbb{1}_{[\bar{L},\bar{R}]}$ will diverge as $[\bar{L}, \bar{R}]$ grows, while taking $[\bar{L}, \bar{R}]$ too close to $[L, R]$ can lead to large approximation errors, especially near the boundaries. Fortunately, most payoffs of practical interest belong to one of these classes, so localized projections obtained through truncated payoffs will converge, and any of the butterfly methods can be successfully applied. For payoffs with isolated singularities, well behaved approximations to the payoff near singularities can be used to obtain the coefficients of accurate hedges. This will be demonstrated for the log contract, which is well behaved away from the origin.

5.4.4 Quasi-analytical Hedges

Many practical nonlinear payoffs can be expressed in the form $\Psi(S_T) = h \circ f(S_T)$, or $f \circ h(S_T)$ where $f(S_T)$ is a given payoff. For example, a simple generalization of the powered call is the payoff $(\max\{\lambda S_T - K, 0\})^2$. If analytical hedges of f are known, then in some cases an analytical or quasi-analytical hedge of Ψ is given by specifying the original payoff f along with the type of transformation h any transformation parameters, adding to the efficiency of pricing/hedging routines. The idea is to find formulas for transformed payoffs in terms of known or analytically given coefficients.

5.4.4.1 Basic Transforms

We start with the coefficients $\beta_{a,k}(\Psi)$ of some more obvious transforms when the coefficients $\beta_{a,k}$ are known for f:

$$\begin{aligned}
&\text{Shift}: \quad \beta_{a,k}(T_{\frac{\bar{k}}{a}} f) = T_{\bar{k}}\beta_{a,k} = \beta_{a,k-\bar{k}} \\
&\text{Scale}: \quad \beta_{a,k}(\lambda f + c) = \lambda\beta_{a,k} + ca^{-1/2} \\
&\text{Dilation}: \quad \beta_{a,k}(f(\gamma\cdot)) = \gamma^{-1/2}\beta_{\frac{a}{\gamma},k}
\end{aligned}$$

To avoid a resolution change, we fixed the shift $\bar{k}/a$ to remain at the market spacing, although this is not required in general. Similarly, in the case of dilation, we are finding the coefficients at the market spacing $a > 0$ in terms of those at a potentially unavailable resolution.

5.4.4.2 Caps, Floors and Composition

To avoid catastrophically large payouts or simply to reduce the option premium, caps are often introduced so that $\Psi(S_T) = f(S_T)\mathbb{1}_{f(S_T)\leq C} + C\mathbb{1}_{f(S_T)>C} = \min\{f(S_T), C\}$. Floors serve a similar purpose of allowing for upside potential while restricting the maximum attainable loss for the option holder. These payoffs satisfy $\Psi^C(S_T) = \max\{C, f(S_T)\} = C\mathbb{1}_{f(S_T)\leq C} + f(S_T)\mathbb{1}_{f(S_T)>C}$, the classic example being the standard vanilla option $\Psi(S_T) = (\alpha(S_T - K))^+ = \max\{0, \alpha(S_T - K)\}$, where $\alpha = \pm 1$ and $C = 0$.

For a capped payoff when $f(S_T)$ is monotone and x^c satisfies $f(x^c) = C$, given the coefficients of $\beta_{a,k}$ of f, we set $k^c := \lfloor ax^c \rfloor$, $\lambda^c := ax^c - k^c = (x^c - k^c/a)/(1/a)$, and define

$$\beta^C_{a,k} = \begin{cases} \beta_{a,k} & k < k^c \\ \lambda^c\beta_{a,k^c} + (1-\lambda^c)Ca^{-1/2} & k = k^c \\ Ca^{-1/2} & k > k^c \end{cases}. \tag{175}$$

Hence, the coefficient at the "pasting" point k^c is weighted according to its proximity to the two separate payoffs, $f(S_T)\mathbb{1}_{f(S_T)\leq C}$ and $C\mathbb{1}_{f(S_T)>C}$, and on either side of k_c the coefficients are set according to which payoff is active.

Of course caps and floors can be combined to form collar type payoffs,

$$\Psi^D(S_T) = \max\{F, \min\{f(S_T), C\}\} = F\mathbb{1}_{f(S_T)\leq F} + f(S_T)\mathbb{1}_{f(S_T)\in(F,C)} + C\mathbb{1}_{f(S_T)\geq C},$$

where f is typically monotone on (F, C). With $f(x_F) = F$, $k_F := \lceil ax_F \rceil$, and $\lambda_F = ax_F - k_F$, an analogous formula for floored and capped payoffs is found:

$$\beta^D_{a,k} = \begin{cases} Fa^{-1/2} & k < k_F \\ (1-\lambda_F)\beta_{a,k_F} + \lambda_F F a^{-1/2} & k = k_F \\ \beta_{a,k} & k_F < k < k^c \\ \lambda^c \beta_{a,k^c} + (1-\lambda^c)Ca^{-1/2} & k = k^c \\ Ca^{-1/2} & k > k^c \end{cases}. \tag{176}$$

Formulas for compositions of transforms can be specified as well. For example, the capped powered call is the composition of $(\min\{C, \cdot\})^2$ with $\min\{0, S_T - K\}$, where the payoff satisfies $([S_T - K]^+)^2\mathbb{1}_{[S_T\leq K+C^{1/2}]} + C\mathbb{1}_{[S_T>K+C^{1/2}]}$ with $K = \bar{k}/a$ ($\bar{k} = k_F$) and $k^c := \lfloor a(K + C^{1/2})\rfloor$. Hence, the coefficients for $\bar{k} < k < k^c$ are given by equation (168), $\beta^D_{a,k} = 0$ for $k < \bar{k}$ and $\beta^C_{a,k^c} = \lambda a^{-5/2}[(k^c - \bar{k})^2 - \frac{1}{6}] + (1-\lambda)a^{-1/2}C$.

Similarly, at a high enough resolution[17], the payoff $\Psi(S_T) = \max\{f_1(S_T), f_2(S_T)\}$ is accurately represented by the pairwise maximum of the coefficients $\beta^{\max}_{a,k} = \max\{\beta^1_{a,k}, \beta^2_{a,k}\}$. A call on a scaled maximum of the payoffs, $(\gamma\Psi(S_T))^+$ can be found by applying equation (176) with the dilation coefficients $\frac{1}{\gamma}\beta^{\max}_{\frac{a}{\gamma},k}$ in place of $\beta_{a,k}$. When $K = \gamma\bar{k}/a$, the coefficients of $(\gamma\Psi(S_T) - K)^+$ are found by the flooring formula with $F = 0$ and the set of beta coefficients $\frac{1}{\gamma}T_{\frac{\gamma\bar{k}}{a}}\beta^{\max}_{\frac{a}{\gamma},k} = \frac{1}{\gamma}\beta^{\max}_{\frac{a}{\gamma},k-\bar{k}}$. Of course an arbitrary K can be specified, but the coefficients will need to be calculated at a different resolution.

5.4.4.3 Piecewise Continuous Payoffs

As an example, consider the case of a profit hedging commodity supplier whose future expenses vary nonlinearly with an unknown supply quantity, according to a set of tranche-dependent fixed and marginal costs (e.g. according to infrastructure utilization, outsourcing,

[17] This qualitative statement is left to be specified by the user, with the condition that at low resolutions, ie large spacing between strikes, a method such as ABS_2 is used. For pricing resolutions, this approximation will generally be sufficient.

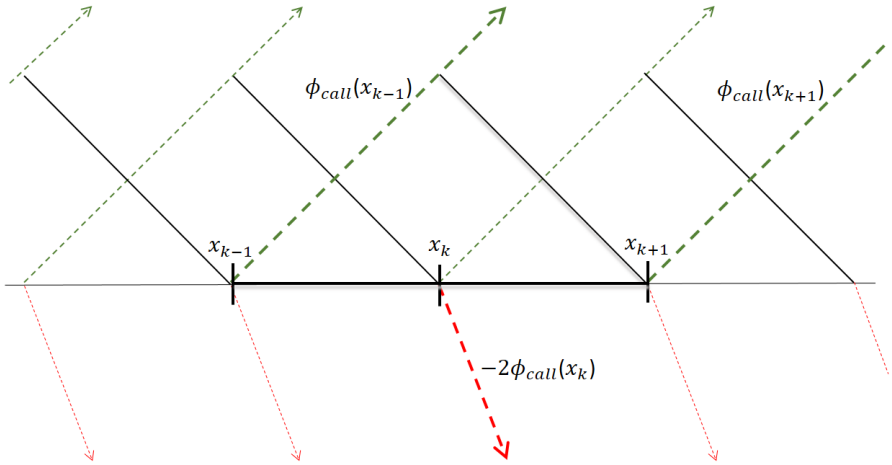

Figure 23: Butterfly basis in terms of call options along some grid $\{x_k\}$, where $\phi_{call}(x_k)$ is a call option with strike x_k.

stock-out, etc.). By capturing the correlation between price and quantity, the joint exposure can be mitigated by a payoff on realized price over $[L, R] = [k_L/a, k_R/a]$. Fixing tranches $I_m = [\frac{\tau_m}{a}, \frac{\tau_{m+1}}{a}]$, $m = 1, ..., M-1$, where $\mathcal{T} = \{\tau_1, ..., \tau_M\}$ are the left tranche boundaries, set to the nearest market strike, $\tau_1 := k_L, \tau_R := k_R$, and $\delta_m := f(\tau_m^+) - f(\tau_m^-)$, $m = 1, ..., M$ are the corresponding payoff jumps, we assume that to each I_m there corresponds a payoff function $f^m := (f - \bar{\delta}_m)\mathbb{1}\{I_m\}$ with known coefficients $\beta_{a,k}^m$, where $\bar{\delta}_m := \sum_{j=1}^m \delta_j = f(\tau_m^+)$. The coefficients of $f = \sum_{m=1}^M (\bar{\delta}_m \mathbb{1}\{I_m\} + f^m)$ are given by

$$\beta_{a,k}^{pc} = \begin{cases} a^{-1/2}\bar{\delta}_m + \beta_{a,k}^m & k \in \mathcal{T}^c \cup \{k_L, k_R\} \\ a^{-1/2}[\bar{\delta}_{m-1} + \delta_m/2] + \dfrac{\beta_{a,k}^{m-1} + \beta_{a,k}^m}{2} & k = \tau_m \end{cases}.$$

Of course, the projection methods can still be applied directly to f, without specifying any known discontinuities. The ABS methods in particular are robust to payoff jumps, since their narrow support mitigates the effect of Gibbs phenomenon. When the jumps are known, and the payoffs corresponding to each tranch are analytically hedged, this approach is preferred.

5.4.5 From Butterflies to Plain "Vanilla" Payoffs

By construction, we can utilize the butterfly basis to approximate a given payoff f, which can then be expressed simply in terms of a payoff position in the underlying S_T, one strike

of a put payoff $\psi_K^{put}(S_T) = (K - S_T)^+$, and call payoffs $\psi_K^{call}(S_T) = (S_T - K)^+$ with strikes along the support of f:

Result 5.4.3. *Let $f \in \mathcal{H}_+$, and suppose we have an order $\bar{K}+1$ approximation of f in terms of the scale-a butterfly basis given by*

$$f(S_T) \approx \beta_0 \varphi_{a,0}(S_T) + \sum_{k=1}^{\bar{K}} \beta_k \varphi_{a,k}(S_T),$$

where the β_k for $k \geq 0$ are computed by any means. Noting that $\varphi_{a,0}(S_T) = \psi_{\frac{1}{a}}^{put}(S_T)$, we have the following static hedge in terms of positions in liquid assets:

$$f(S_T) \approx a^{3/2} \left[\beta_0 \psi_{\frac{1}{a}}^{put}(S_T) + \beta_1 S_T + \sum_{k=1}^{\bar{K}+1} c_k \cdot \psi_{\frac{k}{a}}^{call}(S_T) \right],$$

where the call positions are given by

$$c_k = \begin{cases} \beta_2 - 2\beta_1 & k = 1 \\ \beta_{k-1} - 2\beta_k + \beta_{k+1} & k \in \{2, ..., \bar{K} - 1\} \\ \beta_{\bar{K}-1} - 2\beta_{\bar{K}} & k = \bar{K} \\ \beta_{\bar{K}} & k = \bar{K} + 1. \end{cases}$$

Note too that we can avoid holding the asset itself if we use the put representation of $\varphi_{a,1}(S_T) = a^{3/2} \left[\psi_{\frac{2}{a}}^{put}(S_T) - 2\psi_{\frac{1}{a}}^{put}(S_T) \right]$. Figure 23 illustrates the butterfly basis decomposition into call option positions.

In effect, the butterfly basis takes a set of vanilla payoffs which are not members of $\mathcal{H}$ and fashions a Riesz basis to which the theory and algorithms apply. In active options markets such as those traded on S&P 500 assets or indices, call prices are directly observable and the pricing problem is immediate. In this case, smile effects are imputed in the prices obtained, free of charge. A mixed representation, in terms of both calls and puts, and a pure put representation can be obtained as well.

Recall the position prescribed by the integral representation of Carr and Madan, in which $h''(K)dK$ calls are held for $K \in [0, F_0]$, and $h''(K)dK$ puts are held for $K \in [F_0, \infty)$, where F_0 is the T-forward asset price (alternatively F_0 could be the current market price

of the underlying). An analogous butterfly representation is simple to derive from the relationship

$$\begin{aligned} a^{-3/2}\varphi_{a,k}(S_T) &= \Big(\frac{k+1}{a} - S_T\Big)^+ - 2\Big(\frac{k}{a} - S_T\Big)^+ + \Big(\frac{k-1}{a} - S_T\Big)^+ \\ &= \psi^{put}_{\frac{k+1}{a}}(S_T) - 2\psi^{put}_{\frac{k}{a}}(S_T) + \psi^{put}_{\frac{k+1}{a}}(S_T). \end{aligned}$$

Hence, by utilizing puts for butterfly elements with $k < F_0$ and calls for $k > F_0$, one can derive an out-of-the-money (OTM) representation. Specifically, we assume that vanilla options are available over the interval $[L - 1/a, R + a]$ with listed strikes $\{L - 1/a, L, L + 1/a, ..., R, R + 1/a\}$, where $[L, R]$ is the desired support for our hedge and $F_0 \in [L, R]$ (otherwise a representation in terms of calls or in terms puts is available). We assume that $R = L + \bar{K}/a$ for some $\bar{K} \in \mathbb{N}$, so that $\bar{K} = (R - L)/a$. Now define $\beta^L_k := \beta_{k_L+k}$, where $k_L := L/a$, so β^L_0 corresponds to the basis element centered over L, β^L_1 corresponds to $L + 1/a$, and so on. We can then obtain an OTM representation as

$$\begin{aligned}
\psi^{put}_{L-\frac{1}{a}} &: \quad a^{3/2}\beta^L_0 \\
\psi^{put}_{L+\frac{k}{a}} &: \quad a^{3/2}[\beta^L_{k-1} - 2\beta^L_k + \beta^L_{k+1}], \quad k = 0, ..., k^* - 1 \\
\psi^{put}_{L+\frac{k^*}{a}} &: \quad a^{3/2}[\beta_{k^*-1} - 2\beta_{k^*}] \\
\psi^{put}_{L+\frac{k^*+1}{a}} &: \quad a^{3/2}\beta_{k^*} \\
\psi^{call}_{L+\frac{k^*}{a}} &: \quad a^{3/2}\beta_{k^*+1} \\
\psi^{call}_{L+\frac{k^*+1}{a}} &: \quad a^{3/2}[\beta_{k^*+2} - 2\beta_{k^*+1}] \\
\psi^{call}_{L+\frac{k}{a}} &: \quad a^{3/2}[\beta_{k-1} - 2\beta_k + \beta_{k+1}], \quad k = k^* + 2, ..., \bar{K} \\
\psi^{call}_{L+\frac{\bar{K}+1}{a}} &: \quad a^{3/2}\beta_{\bar{K}},
\end{aligned}$$

where $k^* = \lfloor (F_0 - L)/a \rfloor$. In practice, the set of available strikes will dictate our choice of which instruments to include in a hedge, namely our selection of $[L, R]$. For liquid products such as options on Brent Crude Oil futures (traded on Intercontinental Exchange, ICE), agricultural commodities (for example white sugar options), and index products (such as

Table 20: RAHE of three payoffs on $[L, R] = [1300, 2200]$, corresponding to the S&P 500 example, with payoff strike set to $K = (L + R)/2$. Ratio gives the ratio of the RAHE for interpolation (Interp) over that of ABS_2. The errors are taken relative to a uniformly sampled "value" over the interval $[L, R]$. The values for the three payoffs are respectively 694.125, 27.677, 297.574.

$f(S_T) = \lvert S_T - K\rvert^{6/5}$					
Scale(Δ)	100	50	25	10	5
Interp	1.335e-02	1.757e-03	4.703e-04	8.084e-05	2.111e-05
ABS_2	1.056e-02	6.663e-04	1.788e-04	3.082e-05	8.061e-06
Ratio	1.264	2.637	2.630	2.623	2.619
$f(S_T) = (R-L)^{1/2} \cdot \exp\big(-\big((S_T-K)/(R-L)\big)^2\big)$					
Scale(Δ)	100	50	25	10	5
Interp	1.739e-03	4.344e-04	1.086e-04	1.737e-05	4.342e-06
ABS_2	6.739e-04	1.675e-04	4.181e-05	6.686e-06	1.671e-06
Ratio	2.580	2.594	2.597	2.598	2.598
$f(S_T) = \log(S_T) \cdot (S_T - K)^2/S_T$					
Scale(Δ)	100	50	25	10	5
Interp	2.665e-02	6.667e-03	1.667e-03	2.667e-04	6.668e-05
ABS_2	1.025e-02	2.565e-03	6.415e-04	1.027e-04	2.566e-05
Ratio	2.601	2.599	2.598	2.598	2.598

S&P 500 index options) active trading occurs for uniformly spaced strikes surrounding the ATM strike, although trading is not limited to contracts which have open interest (there is a higher transaction cost associated with less liquid strikes).

For example, on December 17, 2015, strikes for the February 16th maturity of ICE Brent options on futures (with a futures closing price of 36.95 USD) are offered for calls and puts. Call strikes are listed at 50 cent increments from 37 to 60 USD and put strikes from 29 to 53 USD (naturally the strike ranges for calls and puts overlap), which defines the finest granularity that can be chosen for the resolution parameter $\Delta = 1/a$. Beyond these boundaries, strikes are listed in dollar increments.

Similarly, on December 17, 2015, with a market close of 2,041.89 USD on the S&P 500 index, strikes for December 2015 options are quoted in increments of 5 USD from about 1,300 USD to 2,250 USD (see for example CBOE), straddling the current index level. Beyond these boundaries, the granularity increases, and likewise as the time to maturity grows, although a similarly fine strike space is observed for several months following the

prompt month. At a maturity of two years (December 2017), a granularity of 25 or 50 USD is to be expected. As a static hedge draws closer to maturity, the portfolio can be adjusted to add finer granularity if desired.

In Table 20, we provide three exotic European payoff examples for the S&P 500 market with $[L, R] = [1300, 2200]$. The first is a power straddle with rational exponent, the second is a Gaussian-style payoff, and the third is the product of a power straddle with a damping term $\log(S_T)/S_T$. For each of these payoffs, we consider strikes which are spaced uniformly Δ USD apart, with $\Delta \in \{100, 50, 25, 10, 5\}$, and record the relative absolute hedge error (RAHE) defined in Section 5.4.1.5 for a fine mesh. Comparing the ABS_2 method to linear interpolation, we see that interpolation incurs about 2.6 times the error of the ABS_2 method, and the difference in computational effort is negligible. Experimenting with many smooth payoff forms, an interesting finding is that a constant of about 2.6 holds in general, while this constant holds for non-smooth payoffs once a threshold resolution is reached. For the first example payoff, which is non-smooth, the threshold is reached for Δ between 100 and 50.

Remark 9. While it is useful to unwind a butterfly hedge in terms of underlying options, trading the butterfly positions themselves has an advantage with respect to the margining practices used by clearing houses, since the finite risk associated with such products is well understood, and margins are set accordingly. The required margin for an equivalent position in vanilla instruments, when transacted separately, will be higher in general under margining methods such as SPAN (Standard Portfolio Analysis of Risk).

5.4.6 Semi-Static Hedging of Barrier Options

As demonstrated in [30, 31], barrier options are natural candidates for semi-static hedging. While the ability to *perfectly* hedge such contracts depends on very specific market conditions, such as a Black-Scholes-Merton (BSM) economy, and the assumption that portfolios can be liquidated immediately upon barrier breach and at the BSM price, imperfect hedging is still possible under relaxed assumptions. Moreover, in cases where delta hedging is known to fail dramatically such as for down-and-out put (DOP) and up-and-out-call (UOC)

contracts [108], the performance of semi-static hedging is much more satisfactory, although it is still far from a perfect hedge.

In the following set of experiments we consider the problem of semi-static hedging a DOP option, as discussed in section 5.2.3, where the adjusted payoff is defined as

$$\tilde{f}(S_T) = \begin{cases} (K - S_T)^+ & \text{if } S_T > B \\ -\left(\frac{S_T}{B}\right)^p \left(K - \frac{B^2}{S_T}\right)^+ & \text{if } S_T \leq B \end{cases} \tag{177}$$

with strike K, barrier $B < K$, interest rate $r \geq 0$, dividend yield $d \geq 0$, volatility $\sigma > 0$, and $p := 1 - 2(r-d)/\sigma^2$. The adjusted payoff is constructed using a prescribed volatility (for now it is taken to be σ, the true market volatility), and a butterfly hedge is established in vanilla options using the ABS_2 methodology. In particular, we set $[L, R] = [B^2/K, K]$, fix a number N, and obtain the butterfly coefficients at strikes $L + k/a$ for $k = 0, ..., \bar{K} := N - 1$, where $a := (R - L)/\bar{K}$. By setting the coefficients at L ($k = 0$) and R ($k = \bar{K}$) equal to zero, we obtain a hedge that requires N strikes in vanilla options. We have chosen our strike space for simplicity and to illustrate the method.

For each experiment, we simulate the underlying dynamics up to the first barrier breach, or contract expiry $T = 1$, whichever occurs first. If breach occurs, the vanilla portfolio is liquidated at the BSM prices, and is then discounted to obtain the profit and loss (P&L) for that simulation run (at breach, the true adjusted payoff has zero value). Otherwise, the portfolio results in a European-style payoff at time T, and the difference between this payoff and $(K - S_T)^+$ is discounted to the present to obtain the P&L. Monitoring is allowed every other day ($M = 252/2$ monitoring dates), so if a breach occurs the underlying can drift significantly away from the barrier prior to liquidating the vanilla portfolio, resulting in a nonzero P&L. Hence, there are two sources of error: the error arising from approximating the adjusted payoff, as well as the error from a drift in the underlying away from the barrier at liquidation. With a finite monitoring frequency, even the true adjusted payoff results in an imperfect hedge. The simulation is then repeated 10,000 times, and relative P&Ls are recorded, where each P&L is relative to the discretely monitored DOP option value. In all experiments $r = 0.06$ and $d = 0.02$.

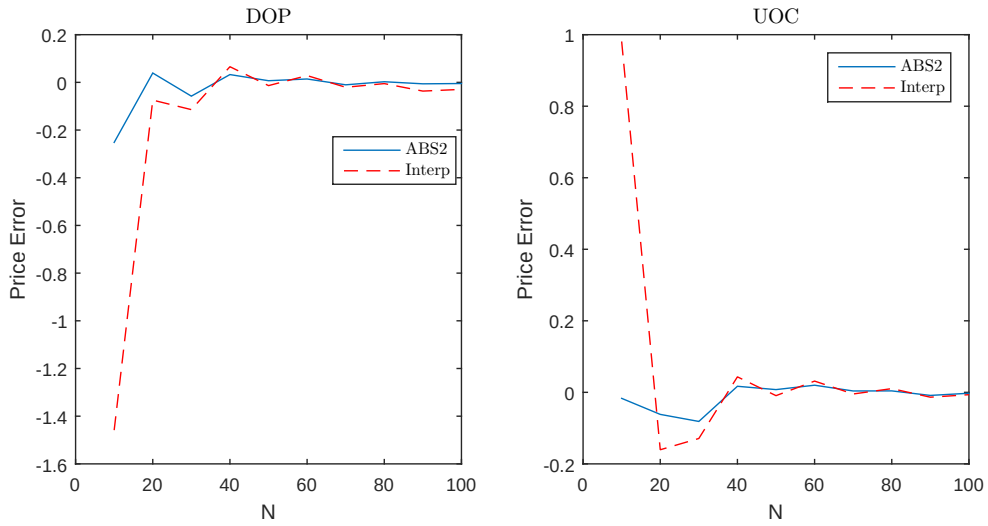

Figure 24: Pricing error as a function of the number of strikes N for a DOP with $K = 100$ and $B = 80$ (left) and a UOC with $K = 100$ and $B = 120$ (right). Comparison of linear interpolation and ABS_2 when the approximated adjusted payoff is sold.

Figure 24 illustrates the difference in pricing error (profit and loss) that occurs when selling the vanilla portfolio for each of the two methods linear interpolation and ABS_2 as a function of N. The left panel considers a DOP option with $K = 100$ and $B = 80$, and the right panel a UOC option with $K = 100$ and $B = 120$. In both cases, the time to maturity is $T = 1$ and the portfolio is sold exactly when the underlying touches the barrier, so the only source of error is in approximating the adjusted payoff. In both cases the ABS_2 methodology outperforms linear interpolation, for small (practical) values of N as well as when N is taken very large. The difference in errors is most pronounced for small values of N.

Figure 25 illustrates the butterfly approximation to the adjusted payoff (left) using $N = 9$ options, as well as the P&Ls for the first 500 simulations (right). Note that the previous example illustrates the error that occurs when the underlying is equal to the barrier upon liquidation, and the true adjusted payoff should have zero value. However, this value becomes nonzero as the underlying deviates from the barrier prior to liquidation. Moreover, in the absence of a breach, the adjusted payoff does not always coincide with the vanilla option at delivery. These errors can be relatively large, as seen in the right panel of Figure 25. Unlike the second source of error, the first of these can be mitigated by

Table 21: Performance of semi-static DOP hedge for BSM model, relative to discretely monitored value, 3.6249, with breach percentage = 10.77. Parameters: $S_0 = 65$, $K = 70$, $B = 50$, $\sigma = 0.18$, $r = 0.06$, $d = 0.02$, $M = 252/2$.

N	6	8	10	12	25	50	100
mean	-0.05	-0.054	-0.135	-0.044	-0.061	-0.045	-0.053
MAD	0.34	0.121	0.174	0.062	0.077	0.049	0.054
std	0.79	0.397	0.493	0.232	0.339	0.265	0.284
min	-6.27	-4.094	-5.457	-4.363	-6.611	-5.879	-5.970
max	1.31	0.987	0.427	0.751	1.291	1.441	0.905

increasing the monitoring frequency.

Remark 10. Given that the alternative to semi-static hedging is a dynamic hedging strategy, we replicate an experiment in [108] to obtain a context for the errors observed with our framework.[18] A UOC contract with $K = 110$, $B = 140$ and $S_0 = 100$ is considered in a BSM model where $\sigma = 0.2$, and other parameters are as before. Relative to the price 2.277 (calculated in [108]), the delta hedging strategy has a mean error of -0.007 and standard deviation of 0.949. This compares to a mean error of -0.077 and a standard deviation of 0.5036 with the ABS_2 method using $N = 11$ options. While the mean error is somewhat larger, dynamic hedging is nearly twice as risky when measured by standard deviation. While not reported for dynamic hedging, the relative min and max deviation for ABS_2 were -9.34 and 1.89 respectively, so even with half the standard deviation of dynamic hedging, large errors can still be expected. This is observed in Figure 25 for DOP options as well.

Table 21 illustrates the performance of the semi-static hedging strategy for a DOP contract with $K = 70$ and $B = 50$, in terms of the mean error (mean), mean absolute deviation (MAD), minimum error (min), maximum error (max) and standard deviation of errors (std), all relative to the discretely monitored option value with the same monitoring frequency. As the number of vanilla options, N, increases, we expect that the approximation error and standard deviation should decline. While this is typically true, the convergence is far from monotone, and due to the discrete monitoring frequency there will be errors

[18]Implementing the dynamic delta hedge is a delicate matter for DOP and UOC call options, especially as the underlying approaches the barrier (see [22] for examples). A careful implementation and description of such a strategy is outside the scope of the present work. Our focus is on introducing a new static hedging method, and illustrating its potential for application.

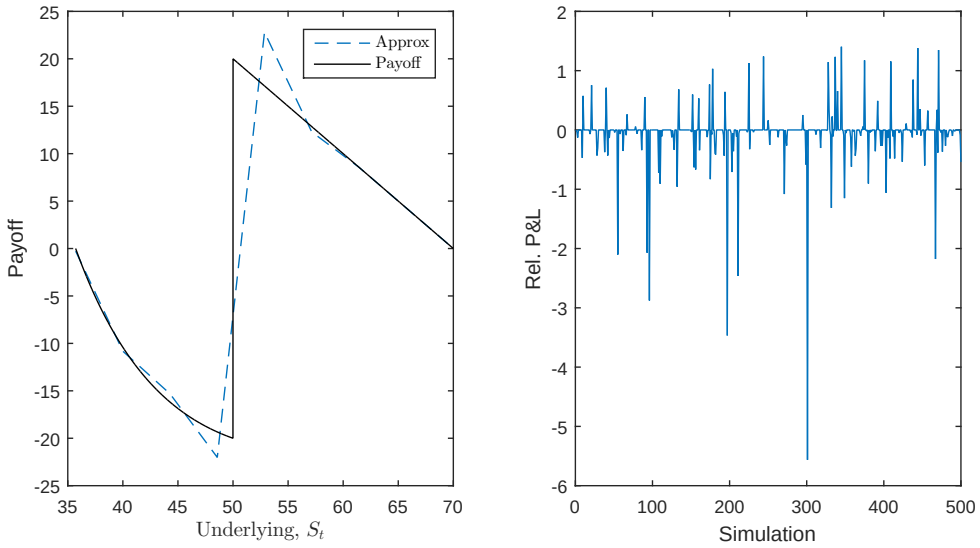

Figure 25: The left panel illustrates the DOP adjusted payoff for a contract with strike $K = 70$ and knock-out barrier $B = 50$, along with the ABS_2 approximation with $N = 9$ options, uniformly spaced within $(B^2/K, K)$. Additional parameters: $r = .06$, $d = .02$, $T = 1$, $M = 252/2$, $\sigma = .18$, $S_0 = 65$. The right panel illustrates the profit and loss for the semi-static hedging strategy in a BSM market, where each bar represents the outcome of a single simulation.

associated with the hedging policy even in the limit. Table 22 repeats the experiment with a barrier $B = 60$ placed nearer the underlying (and strike). In this case, the performance actually improves in terms of MAD and standard deviation, though we must keep in mind that the strike set used to establish the hedge differs in the two experiments. In particular, the second experiment spreads the same number of strikes across a narrower support $[L, R] = [B^2/K, K]$, which is $[35.7, 70]$ in the first case and $[51.4, 70]$ in the second. The number of breaches also increases from 10.77 percent of the simulations to 58.45 percent. Table 23 illustrates the effect of increasing volatility from 0.18 to 0.25, again with $B = 60$ and $K = 70$. While the number of breaches rises from 58.45 to 69.98 percent, the effect is a decrease in MAD and standard deviation, as well as a narrowing of the range of errors.

In the final set of experiments, we relax the BSM model assumption, and consider a stochastic volatility driven market. In particular, consider Heston's model, which posits

$$dS_t = (r - d)S_t dt + \sqrt{\nu_t} S_t dW_{1,t} \tag{178}$$

$$d\nu_t = \kappa(\theta - \nu_t)dt + \sigma_\nu \sqrt{\nu_t} dW_{2,t} \tag{179}$$

Table 22: Performance of semi-static DOP hedge for BSM model, relative to discretely monitored value, 3.086, with breach percentage = 58.45. Parameters: $S_0 = 65$, $K = 70$, $B = 60$, $\sigma = 0.18$, $r = 0.06$, $d = 0.02$, $M = 252/2$.

N	6	8	10	12	25	50	100
mean	-0.11	0.043	-0.003	-0.033	-0.031	-0.027	-0.026
MAD	0.14	0.070	0.037	0.043	0.034	0.028	0.027
std	0.30	0.162	0.165	0.178	0.151	0.134	0.140
min	-4.26	-2.936	-3.285	-3.636	-3.546	-3.630	-3.775
max	0.85	0.768	0.764	0.760	0.743	0.413	0.364

Table 23: Performance of semi-static DOP hedge for BSM model, relative to discretely monitored value, 3.9125, with breach percentage = 69.98. Parameters: $S_0 = 65$, $K = 70$, $B = 60$, $\sigma = 0.25$, $r = 0.06$, $d = 0.02$, $M = 252/2$.

N	6	8	10	12	25	50	100
mean	-0.07	0.031	0.001	-0.017	-0.017	-0.014	-0.014
MAD	0.08	0.045	0.021	0.022	0.018	0.015	0.014
std	0.18	0.099	0.103	0.112	0.102	0.092	0.098
min	-3.32	-2.288	-2.567	-2.845	-2.758	-2.743	-3.033
max	0.67	0.602	0.586	0.581	0.595	0.269	0.249

where $W_{1,t}$ and $W_{2,t}$ are correlated Brownian motions with correlation $\rho = -0.58$. The initial *variance* is $\nu_0 = 0.18$. While the market volatility is allowed to change, we assume that traders still price the underlying portfolio using Black-Scholes but with prevailing market volatility. Since a single volatility must be used to establish the original hedge, we take this to be the long term average volatility, $\sqrt{\theta} = 0.4243$. We consider the original contract parameters $K = 70$ and $B = 50$, with the remaining model parameters (obtained from a calibration to AUDJPY call options on September 16, 2008, [45, 94]) summarized in Table 24. Since the prevailing volatility at the time of liquidation differs from the volatility used establish the hedge, a new source of error is introduced in this case. Even so, the results are similar to what we have observed in a pure BSM market. In this case, even if the monitoring frequency becomes arbitrarily large, hedging errors will persist at large values of N.

5.4.7 Hedging with Multiple Decision Periods

The examples considered so far require portfolio rebalancings at up to two distinct times, once at initialization to establish the static hedge, and possibly an additional rebalancing at

Table 24: Performance of semi-static DOP hedge for Heston's model, relative to discretely monitored value, 8.9836, with breach percentage = 52.56. Parameters: $S_0 = 65$, $K = 70$, $B = 50$, $\nu_0 = 0.1800$, $\sigma_v = 2.4400$, $\kappa = 0.3800$, $\rho =$ -0.5800, $\theta = 0.1800$, $r = 0.06$, $d = 0.02$, $M = 252/2$

N	6	8	10	12	25	50	100
mean	-0.01	-0.015	-0.037	-0.014	-0.018	-0.014	-0.016
MAD	0.03	0.020	0.040	0.016	0.020	0.015	0.016
std	0.15	0.095	0.122	0.093	0.103	0.092	0.096
min	-2.48	-1.927	-2.163	-2.420	-2.649	-2.321	-2.295
max	0.52	0.525	0.249	0.547	0.506	0.551	0.529

a single stopping time prior to expiry. As demonstrated in [30], the semi-static approach can be extended to multiple rebalancing (decision) periods. For example, consider a rolldown call option which is described by a set of barriers, $B_1 > B_2 > \ldots > B_n$, each less than S_0. If $S_t > B_1$ for $0 \leq t \leq T$, the option pays $(S_T - K_0)^+$ at maturity. However, if B_1 is breached priory to expiry, the prevailing strike rolls down from K_0 to $K_1 < K_0$, and likewise with each successive B_i which is hit, the strike rolls down from K_{i-1} to K_i. This contract, denoted RDC, can be represented as the following portfolio of down-and-out call options

$$RDC = DOC(K_0, B_1) + \sum_{i=1}^{n-1} \{DOC(K_i, B_{i+1}) - DOC(K_i, B_i)\}$$

where $DOC(K_j, B_m)$ represents a strike K_j option with knock out barrier B_m. Hence, at initialization we establish a hedge portfolio of European payoffs

$$\tilde{f}(S_T; K_0, B_1) + \sum_{i=1}^{n-1} \left\{ \tilde{f}(S_T; K_i, B_{i+1}) - \tilde{f}(S_T; K_i, B_i) \right\}, \tag{180}$$

where the individual adjusted payoffs are defined by

$$\tilde{f}(S_T; K_j, B_m) = \begin{cases} (S_T - K_j)^+ & \text{if } S_T > B_m \\ -\left(\frac{S_T}{B_m}\right)^p \left(\frac{B_m^2}{S_T} - K_j\right)^+ & \text{if } S_T \leq B_m \end{cases}, \tag{181}$$

and the butterfly methodology can be applied to each individually to obtain an aggregated position in butterfly (or vanilla) payoffs. For each B_i that is breached, the positions in $\tilde{f}(S_T; K_j, B_{j+1})$ and $\tilde{f}(S_T; K_j, B_j)$ are liquidated at the market price, while the remaining positions are left untouched. Hence, this strategy faces at most n rebalancings, including initialization. A similar strategy holds for ratchet options [30].

5.5 General Theory of Frame Pricing

The butterfly basis is especially well suited for the current state of option markets. As more products become standard, the applicability of frame pricing and hedging will expand accordingly. Moreover, the ability of frames to systematically generate spaces of general payoff forms suggests the use of a frame based analysis to guide the design of new instruments so that arbitrary risk exposures can be readily hedged. We show that frame methods in general are consistent in the sense that hedges built from frame elements converge to exact representations of the payoffs they approximate, and prices converge to their true values as the strike space is arbitrarily refined. This consistency holds for a large class of models for the underlying.

5.5.1 Convergence of Frame Representations

When implementing a hedge in practice, it is natural to establish an appropriate frame sequence with a scale fixed according to available market payoffs. However, to facilitate the theoretical development of frame based pricing and hedging, it becomes advantageous to partition the domain space dyadically in the following manner, consistent with the approach taken in the frame (and wavelet) literature.

Starting with a frame generator $\phi \in \mathcal{H}$, consider first the space $V_0 := \overline{\text{span}}\{T_k\phi\}_{k\in\mathbb{Z}} = \overline{\text{span}}\{\phi_{0,k}\}_{k\in\mathbb{Z}}$, where $\phi_{0,k}(S_T) := \phi(S_T - k)$. To transition between approximations at different scales[19] we define the operator D by $Df(x) = 2^{1/2}f(2x)$. By composing D with itself j times, it follows that $D^j f(x) = 2^{j/2}f(2^j x)$. By slicing the translation granularity in half, the next finer space is $V_1 := D\overline{\text{span}}\{T_k\phi\}_{k\in\mathbb{Z}} = \overline{\text{span}}\{\phi_{1,k}\}_{k\in\mathbb{Z}}$, where $\phi_{1,k}(S_T) := 2^{1/2}\phi(2S_T - k)$. Proceeding similarly we obtain

$$V_j := D^j\overline{\text{span}}\{T_k\phi\}_{k\in\mathbb{Z}} = \overline{\text{span}}\{\phi_{j,k}\}_{k\in\mathbb{Z}}, \tag{182}$$

where $\phi_{j,k}(S_T) := 2^{j/2}\phi(2^j S_T - k) = D^j T_k\phi(S_T)$.

As long as ϕ has been appropriately selected, with selection criteria provided shortly,

[19] To maintain consistency $j \in \mathbb{Z}$ will always correspond to the dyadic spacing of 2^{-j}, while $a > 0$ indicates a spacing of $1/a$. In general, we could study the dyadic spacing of $1/2^j a$, though $a = 1$ is taken to simplify notation.

any function in $\mathcal{H}$ can be approximated arbitrarily well for some fixed resolution level j by forming linear combinations of $\phi_{j,k}$ as k varies over $\mathbb{Z}$. Appropriately chosen generators ϕ induce a special structure on the space $\mathcal{H}$.

Definition 5.5.1. (Frame Multiresolution Analysis) A function $\phi \in \mathcal{H}$ which generates a frame sequence $\{T_k\phi\}_{k\in\mathbb{Z}}$ is said to generate a *frame multiresolution analysis* (FMRA)[20] if the spaces $\{V_j\}_{j\in\mathbb{Z}}$ defined in (182) satisfy

(i) $\cdots V_{-1} \subset V_0 \subset V_1 \cdots,$ (ii) $\overline{\cup_j V_j} = \mathcal{H}.$

From [44](p.289), it is verified that the butterfly basis on $\mathcal{H}$ with generator $\varphi(S_T) = (1 - |S_T|)\mathbb{I}_{[-1,1]}(S_T)$ generates an FMRA.

In addition to standardizing the approximation process, FMRAs provide assurance that our approximation strategy is asymptotically valid. Specifically, we can guarantee improved approximations by increasing the resolution of our chosen frame sequence. Likewise, we can easily balance the trade-off between a coarser approximation and a smaller basket of basis payoffs in any particular application. In the context of hedging, when the market dictates the available resolution, there is a point after which strikes are no longer traded. For pure pricing, this is not an issue.

Now let ϕ be a frame generator and define $\theta_j = S^{-1}D_j\phi$. For $f \in \mathcal{H}$, an approximation in terms of the scale j frame sequence is given by the orthogonal projection operator

$$P_J f(S_T) = \sum_{k\in\mathbb{Z}} \langle f, T_{2^{-j}k}\theta_j\rangle \phi_{j,k}(S_T),$$

where $J := V_j$, and convergence is obtained in the limit (the statement $J \to \infty$ is interpreted as $j \to \infty$):

Proposition 5.5.1. *If ϕ generates an FMRA, then for each $j \in \mathbb{Z}$ the following hold:*

(i) $\{\phi_{j,k}\}_{k\in\mathbb{Z}}$ is a frame for $V_j = \overline{span}\{\phi_{j,k}\}_{k\in\mathbb{Z}}$.

(ii) $\forall f \in \mathcal{H}$, $\|P_J f\| \le \|f\|$ and $\lim_{J\to\infty}\|P_J f - f\| = 0$.

[20]The reader should be aware that this definition is significantly shorter than equivalent ones given in most (especially older) treatments of FMRAs. See [44] chapter 13 for details.

In summary, if we start with a payoff $\phi(S_T)$ which generates an FMRA, then scaled and shifted versions of ϕ enable an approximate hedge of any $f \in \mathcal{H}$ which approaches (in L^2) the true payoff as the support of f is partitioned into a finer strike space. The next step is to price f by pricing elements of the frame. Once frame elements have been priced, then at any fixed resolution, the pricing of arbitrary $f \in \mathcal{H}$ is reduced to the computation of its hedge coefficients.

5.5.2 The Pricing Functional

We can now consider a sequential approximation of the pricing problem in the case of positive asset prices. We assume for concreteness an exponential Levy model of the risk-neutral dynamics $S_T = S_0 e^{X_T}$, where S_T is a non-dividend paying asset, and X_T is a process with known characteristic function $\widehat{\mu}_T(\xi)$. For example, X_T could follow a Levy process, an affine jump diffusion or a stochastic volatility model (such as Heston's model). For simplicity, we assume that X_T has a density, μ_T, though little changes conceptually if a probability measure on $\mathbb{R}$ is used instead. We denote the density of $\ln(S_T)$ by q_T, and note that $\ln(S_T) = \ln(S_0) + X_T$, where S_0 is assumed to be known at the time of pricing. The characteristic functions are related by

$$\widehat{q}_T(\xi) \equiv \mathbb{E}[e^{i(\ln(S_0)+X_T)\xi}] = e^{i\xi \ln(S_0)}\mathbb{E}[e^{iX_T\xi}] = e^{i\xi \ln(S_0)}\widehat{\mu}_T(\xi).$$

For a given risk neutral density q_T (with S_0 fixed), define the *pricing functional* $\mathcal{V} : \mathcal{H} \to \mathbb{C}$ by

$$\mathcal{V}(f) = e^{-rT}\int_{\mathbb{R}} f(e^y)q_T(y)dy = e^{-rT}\int_{\mathbb{R}} f(S_0e^x)\mu_T(x)dx.$$

For simplicity, the interest rate is assumed constant. However, prices obtained from a spectrum of observed calls and puts will incorporate market views of the stochastic behavior of interest rates, volatility and even dividends. A mild restriction on q_T enables the pricing of any $f \in \mathcal{H}$.

Theorem 5.5.1. *Suppose q_T is essentially bounded ($q_T \in L^\infty(\mathbb{R})$), and $|\widehat{q}_T(i)| < \infty$. Then the pricing functional satisfies $\mathcal{V} \in \mathcal{H}^*$, i.e $\mathcal{V}$ is a bounded linear functional over $\mathcal{H}$.*

For example, if $\widehat{q}_T \in L^1(\mathbb{R})$, it follows that for every continuity point of $\widehat{q}_T(x)$, $|q_T(\xi)| = \int_{\mathbb{R}} |e^{ix\xi}\widehat{q}_T(x)|dx \leq \|\widehat{q}_T\|_1$, so $q_T \in L^\infty(\mathbb{R})$.

In terms of a frame sequence $\{\phi_{j,k}\}_{k\in\mathbb{Z}}$ with dual frame sequence $\{T_{2^{-j}k}\theta_j\}_{k\in\mathbb{Z}}$, the approximate pricing functional at resolution j can be defined similarly as

$$\mathcal{V}_J := \mathcal{V} \circ P_J, \quad \mathcal{V}_J f = e^{-rT} \int_{\mathbb{R}} \left(\sum_k \langle f, T_{2^{-j}k}\theta_j \rangle \phi_{j,k}(e^y) \right) q_T(y) dy.$$

Theorem 5.5.2. *Suppose the conditions of Theorem 5.5.1 hold, and let ϕ be a frame generator with $\theta_j := S^{-1}D_j\phi$. Then for each $j \in \mathbb{N}$, $\mathcal{V}_J : \mathcal{H} \to \mathbb{C}$ is a well defined bounded linear functional which satisfies*

$$\mathcal{V}_J f = \sum_k \langle f, T_{2^{-j}k}\theta_j \rangle \mathcal{V} \circ \phi_{j,k}, \qquad f \in \mathcal{H}.$$

Moreover, if ϕ generates a FMRA, $\mathcal{V}_J \to \mathcal{V}$ uniformly in $\mathcal{H}$. That is,

$$\lim_{J\to\infty} \sup_{f\in\mathcal{H}, \|f\|=1} |\mathcal{V}_J f - \mathcal{V} f| = 0.$$

In particular, frame pricing is a (uniformly) consistent approximation to the pricing problem. Moreover, payoff representations are valid independently of the underlying dynamics, since any such pricing operator $\mathcal{V}$ yields a consistent approximation in terms of the frame elements. Likewise, admissible payoffs are specified independently of $\mathcal{V}$, and so can be used from one model to the next.

5.5.3 Pricing with Riesz Bases

While frames are certainly sufficient to guarantee the representation properties we desire, and they provide enough structure to conduct fruitful analysis, the elegant dual structure of Riesz bases greatly simplifies their implementation. In particular, the butterfly basis is a special class of FMRA in which the the generator ϕ is compactly supported and generates a Riesz sequence of translates. Recall that for $\phi \in \mathcal{H}$, $\{T_k\phi\}_{k\in\mathbb{Z}}$ is a Riesz basis for $\mathcal{M} := \overline{\text{span}}\{T_k\phi\}_{k\in\mathbb{Z}}$ if

1. $\exists \widetilde{\phi} \in \mathcal{M}$ such that $\{T_k\widetilde{\phi}\}_{k\in\mathbb{Z}}$ is biorthogonal to $\{T_k\phi\}_{k\in\mathbb{Z}}$, and

2. $\exists B \geq A > 0$ such that $A\|f\|^2 \leq \sum_{k\in\mathbb{Z}} |\langle f, T_k\phi\rangle|^2 \leq B\|f\|^2$, $\forall f \in \mathcal{M}$.

By replacing the frame condition with the requirement that ϕ generates a Riesz sequence which satisfies (i) and (ii) of definition 5.5.1 for the spaces $\{V_j\}_{j\in\mathbb{Z}}$ defined in (182), we have what is called a *Riesz multiresolution analysis* (RMRA). For $f \in \mathcal{H}$, an approximation in terms of the scale j Riesz sequence is given by the orthogonal projection operator

$$P_J f(S_T) = \sum_{k\in\mathbb{Z}} \langle f, \widetilde{\phi}_{j,k}\rangle \phi_{j,k}(S_T),$$

where $J := V_j$. Similarly, to restrict attention to payoffs $f \in \mathcal{H}_+$, we define the $\mathcal{H}_+$-projection $P_{J^+} : \mathcal{H}_+ \to V_{J^+} := \overline{\text{span}}\{\phi_{j,k}\}_{k\geq 0}$ as $P_{J^+} f(S_T) = {\sum_{k\geq 0}}' \langle f, \widetilde{\phi}_{j,k}\rangle \phi_{j,k}(S_T)$, where $\sum'$ indicates that each $\phi_{j,k}$ has been restricted to $\mathbb{R}_+$ ($\phi_{j,k}(x)\mathbb{1}_{x\geq 0}$), and the coefficient of $\phi_{j,0}$ may be adjusted. By theorem 5.5.2, the approximate pricing functional at resolution j can be defined in the RMRA case as $\mathcal{V}_J := \mathcal{V} \circ P_J, \quad \mathcal{V}_J f = \sum_{k\in\mathbb{Z}} \langle f, \widetilde{\phi}_{j,k}\rangle \mathcal{V} \circ \phi_{j,k}$, for $f \in \mathcal{H}$.

The value convergence can also be characterized formally by following:

Corollary 5.5.3. *If $\phi \in \mathcal{H}$ generates a Riesz sequence, then for each $j \in \mathbb{Z}$ the following hold:*

(i) $\{\phi_{j,k}\}_{k\in\mathbb{Z}}$ *is a Riesz basis for* $V_j = \overline{span}\{\phi_{j,k}\}_{k\in\mathbb{Z}}$.

(ii) If ϕ generates an RMRA, then $\forall f \in \mathcal{H}$, $\|P_J f\| \leq \|f\|$ *and* $\lim_{J\to\infty} \|P_J f - f\| = 0$. *Moreover,* $\mathcal{V}_J \to \mathcal{V}$, *uniformly in* $f \in \mathcal{H}$.

(iii) For $f \in \mathcal{H}_+$, $\lim_{J^+\to\infty} \|P_{J^+} f - f\| = 0$, *and* $\lim_{J^+\to\infty} |\mathcal{V} \circ P_{J^+} f - \mathcal{V} f| = 0$.

When the basis elements (or their components) are priced in a market (e.g. a butterfly basis), valuation is reduced to an observation of market prices. If irregular strikes, or perhaps strikes at values different from the payoff representation are available, a continuous approximation to the market prices (e.g. by interpolation of some form) can be constructed and sampled at the required strike points.

Using a well designed ABS, the computational expense can be reduced, without compromising consistency as the strike space is refined. As long as $\{T_k\phi\}_k$ and $\{T_k\breve{\phi}\}_k$ are biorthogonal, by a change of variables $\langle \phi_{j,k}, \breve{\phi}_{j,m}\rangle = \langle T_k\phi, T_m\breve{\phi}\rangle = \delta_{k,m}$, so biorthogonality

is preserved from one resolution to the next. If $\breve{P}_J f = \sum_{k\in\mathbb{Z}} \langle f, \breve{\phi}_{j,k}\rangle \phi_{j,k}$ denotes the ABS projection operator defined on the refinement $V_j := \overline{\text{span}}\{\phi_{j,k}\}_{k\in\mathbb{Z}}$,

$$\begin{aligned}\breve{P}_J\breve{P}_J f &= \sum_m \Big\langle \sum_k \langle f, \breve{\phi}_{j,k}\rangle \phi_{j,k}, \breve{\phi}_{j,m}\Big\rangle \phi_{j,m} \\ &= \sum_m \Big(\sum_k \langle f, \breve{\phi}_{j,k}\rangle \delta_{k,m}\Big)\phi_{j,m} = \sum_k \langle f, \breve{\phi}_{j,k}\rangle \phi_{j,k}, \end{aligned} \tag{183}$$

so $\breve{P}_J\breve{P}_J f = \breve{P}_J f$. We then have the following:

Proposition 5.5.2. *Let $\phi \in \mathcal{H}$ be an RMRA generator, and $\breve{\phi}$ a compactly supported ABS generator. Then*

$$\lim_{J\to\infty} \|\breve{P}_J f - f\| = 0, \quad \textit{and} \quad \lim_{J\to\infty} |\mathcal{V}\circ\breve{P}_J f - \mathcal{V} f| = 0,$$

where $\breve{P}_J$ is a bounded linear (non-orthogonal) projection of $\mathcal{H}$ onto V_j, for all $j \in \mathbb{N}$. In fact, for each $f \in \mathcal{H}$, $\|\breve{P}_J f\|$ is uniformly bounded over $j \in \mathbb{Z}$.

5.5.3.1 Pricing on the Level of Randomness

While exponential (Levy) models are very popular in equity and other markets with strictly positive asset prices or indices, in some cases pricing on the level of randomness is more appropriate, and we can utilize duality for a Riesz basis to price a payoff when the risk-neutral characteristic function for the underlying is known, as opposed to that of the log underlying. The pricing functional is then given by $\mathcal{V}(f) = e^{-rT}\int_{\mathbb{R}} f(s)p_T(s)ds$, $\forall f \in \mathcal{H}$. By duality, $\sum_k \langle f, \widetilde{\phi}_{j,k}\rangle \phi_{j,k} = \sum_k \langle f, \phi_{j,k}\rangle \widetilde{\phi}_{j,k}$. Hence

$$\begin{aligned}\mathcal{V}_J(f) = \mathcal{V}\left(\sum_k \langle f, \phi_{j,k}\rangle \widetilde{\phi}_{j,k}\right) &= e^{-rT}\sum_k \langle f, \phi_{j,k}\rangle \langle p_T, \widetilde{\phi}_{j,k}\rangle \\ &= \frac{e^{-rT}}{2\pi}\sum_k \langle f, \phi_{j,k}\rangle \langle \widehat{p}_T, \widehat{\widetilde{\phi}}_{j,k}\rangle,\end{aligned}$$

whereby the coefficients $\langle \widehat{p}_T, \widehat{\widetilde{\phi}}_{j,k}\rangle$ represent the projection coefficients of p_T, and the payoff is now integrated directly against $\phi_{j,k}$.

Before concluding with numerical results, we briefly outline the application of frames to higher dimensions, which is the focus of ongoing research.

5.5.4 Higher Dimensional Extensions

In order to price multi-dimensional payoffs, for instance the basket call option with terminal payout $f(S_{1,T},...,S_{d,T}) = \left(\sum_{n=1}^{d} \gamma_n S_{n,T} - K\right)^+$, basis theory suggests the use of the tensor product basis $\prod_{n=1}^{d} \varphi_{a_n,k_n}(s_n)$, where each dimension is alloted a separate resolution. Fixing $a_1 = a_2 = a$ in the two dimensional case, and $\varphi^a_{k_1,k_2}(S_{1,T}, S_{2,T}) := \varphi_{a,k_1}(S_{1,T})\varphi_{a,k_2}(S_{2,T})$, the projection is formed by

$$\begin{aligned} P_{\mathcal{M}^2_a} f(S_{1,T}, S_{2,T}) &= \sum_{k_1} \varphi_{a,k_1}(S_{1,T}) \sum_{k_2} \varphi_{a,k_2}(S_{2,T}) \langle f(s_1,s_2), \widetilde{\varphi}^a_{k_1,k_2}(s_1,s_2)\rangle \\ &= \sum_{k_1,k_2} \beta^a_{k_1,k_2} \cdot \varphi^a_{k_1,k_2}(S_{1,T}, S_{2,T}), \end{aligned}$$

where $\widetilde{\varphi}^a_{k_1,k_2}(s_1,s_2) = \widetilde{\varphi}_{a,k_1}(s_1)\widetilde{\varphi}_{a,k_2}(s_2)$. In higher dimensions, the ABS schemes become even more essential to reduce the computational cost of $\beta^a_{k_1,k_2}$, where we simply replace the product dual by the product of one dimensional ABS elements. Given a joint pricing kernel (or joint characteristic function), prices for the basis elements are used to price f:

$$\mathcal{V} \circ f(S_{1,0}, S_{2,0}) \approx \sum_{k_1,k_2} \beta^a_{k_1,k_2} \cdot \mathcal{V} \circ \varphi^a_{k_1,k_2}(S_{1,0}, S_{2,0}).$$

Moreover, once payoff coefficients have been obtained for the payoff form, products on various asset pairs are priced by computing the corresponding basis prices, using the same set of $\beta^a_{k_1,k_2}$. Alternatively, higher dimensions offer the possibility of designing frames to efficiently price specific payoff forms.[21] For example, a difference frame space could be tailored to the pricing of rainbow options such as $(\max\{S_{1,T}, S_{2,T}\} - K)^+$.

5.6 Pricing Exotic Payoffs by Density Projection

The preceding analysis utilizes frames to decompose physical payoffs in terms of simpler components. Utilizing the same theory, the methodology developed in [83] obtains orthogonal projections of risk-neutral return densities for processes with known characteristic functions, enabling the efficient pricing of any finitely valued claim (see also [84, 85]). In particular, vanilla options along a spectrum of strikes are priced simultaneously at low cost.

[21] While frame hedging in higher dimensions using tensor product bases is perhaps unrealistic, decomposition in terms of simpler components is still beneficial from a risk management perspective.

Given that butterfly approximations are themselves composed of vanilla options, prices of butterfly elements follow immediately and arbitrary payoffs are priced by obtaining their hedge coefficients. Moreover, storing hedge coefficients (as opposed to function values) results in a significant information reduction for subsequent pricing, as finer resolutions are required for direct pricing to obtain a similar accuracy.

5.6.1 Exponential Levy Models

While butterfly basis methods are independent of an underlying model, we continue to assume an exponential model of the form $S_T = S_0 e^{X_T}$, where S_T is a non-dividend paying asset, and X_T is a Levy process with known characteristic function $\widehat{\mu}_T(\xi) = \exp(T\psi_{RN}(\xi))$, where ψ_{RN} is the risk-neutral *(Levy) symbol* (see [21] for a development of Exponential Levy-based modeling in finance). Examples are reviewed in Sections 5.8.1 and 5.8.2 of the appendix. We assume that the symbol is chosen (e.g. martingale adjustment) so that arbitrage-free prices are obtained after discounting, where we fix a constant interest rate $r = 0.05$ (and zero dividend yield). In this case, efficient pricing methods such as the COS method [62] and PROJ [83] can be used to price the butterfly basis instruments simultaneously. Also see [22] for efficient extensions of FFT techniques, and their relation to the COS method.

5.6.2 Projection of Risk-Neutral Densities

In [83], the risk-neutral log return density μ_T is projected onto the space $\Omega_\alpha := \overline{\text{span}}\{\mu_{\alpha,l}\}_{l\in\mathbb{Z}}$, where $\mu_{\alpha,l}$ are elements of a compactly supported Riesz sequence of translates at the resolution $\alpha = 2^P$, for some $P \in \mathbb{N}$. In particular, truncated projections onto quadratic and linear spline spaces are used to obtain $\mu_T(y) \approx \bar{P}_{\Omega_\alpha}\mu_T(y) = \sum_{l\in\mathcal{L}} \beta^\mu_{\alpha,l}\mu_{\alpha,l}(y)$, where $\beta^\mu_{\alpha,l} := \langle \mu_T, \widetilde{\mu}_{\alpha,l}\rangle$. Efficient calculation of $\beta^\mu_{\alpha,l}$ is detailed in [83], along with an error analysis. For example we can utilize the linear spline basis $\mu_{\alpha,l} := \varphi_{\alpha,\frac{x_0}{\alpha}+l}$, $l \geq 0$, which is shifted so that $\mu_{\alpha,0}$ is centered over some $x_0 \in \mathbb{R}$, and $\mu_{\alpha,l}$ is centered over $x_0 + l/\alpha$. The coefficients are calculated by

$$\beta^\mu_\alpha = \Re[\mathcal{D}\{H_j\}_{j=0}^{N-1}], \quad H_j = \exp(-ix_0\xi_j + T\psi_{RN}(\xi_j))\frac{\sin^2(\xi_j/2a)}{\xi_j^2(2+\cos(\xi_j/a))} \quad j \geq 1, \qquad (184)$$

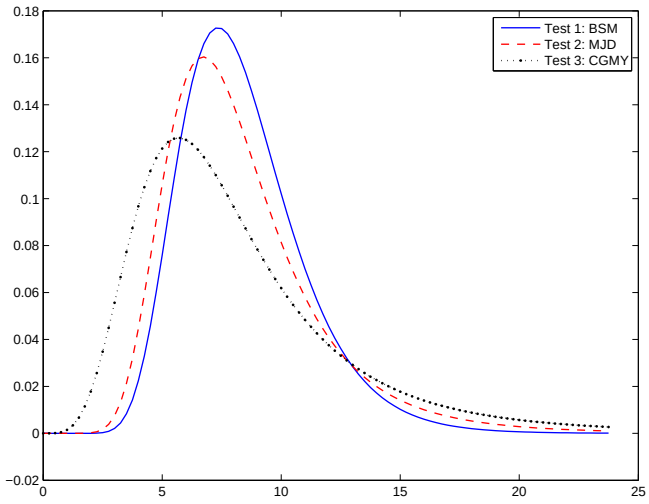

Figure 26: A plot of scaled butterfly prices, $a^{-1/2}\{\mathcal{V} \circ \varphi_{a,k}\}_{k\geq 0}$, for each test case with $a = 2^{10}$.

where $H_0 := 1/24a^2$. Here $\mathcal{D}$ denotes the discrete transform (implemented efficiently using the FFT), and $N = 2\bar{N}$ where $\bar{N} = \alpha 2^{\bar{P}} = 2^{P+\bar{P}}$ for some $\bar{P} \in \mathbb{N}$ which depends on the time to maturity T. For example, when $T \leq 1$, $\bar{P} = 2$ or 3 is a sufficient choice for most reasonable pricing models with heavy tails. More details on the choice of density support (here parameterized by $\bar{P}$) can be found in [87]. In general, once the density support is fixed, the parameter P is incremented until the change in value approximation (given by equation (185) below) is less than a specified tolerance, say e-04. A starting value of $P = 5$ will result in one or two pricing iterations beyond the first for most processes, where at least two approximations are required in order to test that the tolerance has been met (one can then apply Richardson extrapolation if desired). The benefit of transform methods such as [22, 51, 95] is that a reliable starting value for the parameters which govern convergence can be found based on the characteristic function of the underlying process.

To price a set of payoffs $g = \{g_k(S_0 e^{X_T})\}_{k=1}^K$, we determine the coefficient matrix G with elements

$$G_{k,l} := \alpha^{1/2} \int_{x_0+\frac{l-1}{\alpha}}^{x_0+\frac{l+1}{\alpha}} \mu_{\alpha,l}(y) g_k(S_0 e^x) dx, \quad l = 0, ...\bar{N} - 1,$$

from which the vector of prices is approximated by

$$\mathcal{V}_{\bar{N}} \circ g = \frac{24\alpha^2 e^{-rT}}{N} G\{\beta^{\mu}_{\alpha,l}\}_{l=0}^{\bar{N}-1}. \tag{185}$$

For example, to price a set of European puts (or calls by put-call parity), with strike set $\{W_1, ..., W_K\}$ and payoffs $g_k(S_0 e^{X_T}) = (W_k - S_0 e^{X_T}) \mathbb{1}_{X_T \leq \ln(W_k/S_0)}$, we proceed with $x_0 := \ln(W_K/S_0) - (\bar{N} - 1)/\alpha$, so that the final basis element $\mu_{\alpha,\bar{N}-1}$ straddles the largest strike in log space, $\ln(W_K/S_0)$. Here the coefficient matrix G is known analytically, although a modification can be made to improve performance at high resolutions [83]. Once put options have been priced, the corresponding butterfly basis is priced (for $k \geq 2$) using

$$\mathcal{V} \circ \varphi_{a,k}(S_0) = a^{3/2} \left[P_T \left(\frac{k-1}{a}; S_0 \right) - 2P_T \left(\frac{k}{a}; S_0 \right) + P_T \left(\frac{k+1}{a}; S_0 \right) \right], \tag{186}$$

where $P_T(K; S_0)$ is the price of a strike-K put with maturity T and current asset price level S_0. Similarly, $\mathcal{V} \circ \varphi_{a,0}(S_0) = a^{3/2} P_T \left(\frac{1}{a}; S_0 \right)$, and $\mathcal{V} \circ \varphi_{a,1}(S_0) = a^{3/2} \left[P_T \left(\frac{2}{a}; S_0 \right) - 2P_T \left(\frac{1}{a}; S_0 \right) \right]$.

With prices for butterfly elements calculated by equation (186), the subsequent valuation of arbitrary claims reduces to the computation of hedge coefficients. The set of butterfly basis values is illustrated in figure 26 for the three test cases considered, where, at fine resolutions a smooth risk-neutral density emerges. This reflects the Breeden and Litzenberger result [23], $\frac{\partial}{\partial K} \mathbb{P}[S_T \leq K] = e^{rT} \frac{\partial^2 P_T}{\partial K^2}(K; S_0)$.

As illustrated in Appendix 5.8, value approximations of projected payoffs converge very quickly with respect to the resolution of the payoff projection. Hence, once the basis is priced, the marginal computations for subsequent payoffs are very modest compared with pricing each payoff directly.

5.7 Conclusions

We propose a new theoretical framework for pricing contingent claims and studying their static replication strategies utilizing basic financial instruments whose payoffs form frames. This generates standardized markets such as those for plain vanilla options, and frames provide the flexibility to study spaces of claims spanned by simpler securities. We provide a systematic scheme for pricing exotic derivatives including path-dependent options through a new means of static replication that can be implemented in markets with a reasonable spectrum of strikes on European options spanning practical trading ranges. Numerical studies on the pricing of various exotic options demonstrate that this method is fast and accurate in comparison to existing methods proposed in the literature. Namely, our approach

outperforms alternative methods based on interpolation as well as the integral representations of Carr and Madan [36], providing more accurate hedges and faster converging value approximations which reduce the required number of basis elements to achieve a desired accuracy. Future research includes extensions to higher dimensional payoffs, as well as the design of frames to capture particular model features with sparse representations.

5.8 Appendix: Pricing Experiments

In this section we consider a set of pricing experiments for exotic European options given exponential Levy models for the underlying. Three such models are reviewed and in Sections 5.8.1 and 5.8.2, along with parameter sets that will be used in the subsequent experiments. Comparisons of the various hedging methods, applied to several exotic payoffs are provided in Section 5.8.3.

5.8.1 BSM and MJD

The Black-Scholes-Merton (BSM) model is described by its volatility, σ, and is represented by the Levy symbol

$$\psi_L(\xi) = -\frac{\sigma^2}{2}\xi^2,$$

prior to martingale adjustment. For this model we consider the test case

$$\text{Test 1}: \quad \sigma = .3 \tag{187}$$

By adding a Poisson jump process with normally distributed jump sizes, we arrive at

$$\psi_L(\xi) = -\frac{\sigma^2}{2}\xi^2 + \lambda_J\left(\exp\left(i\mu_J\xi - \frac{\sigma_J^2}{2}\xi^2\right) - 1\right),$$

where σ is the diffusion volatility, μ_J, σ_J are the jump size mean and volatility, and λ_J the rate of jump arrivals. For this model, we consider the test case

$$\text{Test 2}: \quad \sigma = .3, \quad \mu_J = .15, \quad \sigma_J = .2, \quad \lambda_J = .7 \tag{188}$$

5.8.2 CGMY

The CGMY processes form a four parameter family of exponential Levy models [32]: $C \geq 0$ accounts for the activity level of jumps, $G, M \geq 0$ determine the skewness, and $Y < 2$

Table 25: Capped powered call: $f(S_T) = (S_T - 8)^2 \mathbb{1}_{[8,23]}(S_T) + (15)^2 \mathbb{1}_{(23,\infty)}(S_T)$, strikes in $[0, 30]$ at spacing Δ, $S_0 = 8$, $T = 1$, ref.: $[4.759375, 7.684145, 12.143187]$.

	Test 1: BSM				
Δ	2.00	1.00	0.50	0.25	0.10
Interp	6.688e-02	1.685e-02	4.216e-03	1.054e-03	1.686e-04
ABS1	3.260e-02	8.370e-03	2.104e-03	5.268e-04	8.432e-05
ABS2	1.274e-03	7.259e-05	4.242e-06	2.676e-07	7.701e-09
Quasi	5.804e-04	1.124e-04	7.167e-06	4.437e-07	1.103e-08
	Test 2: MJD				
Δ	2.00	1.00	0.50	0.25	0.10
Interp	3.405e-02	9.104e-03	2.278e-03	5.699e-04	9.151e-05
ABS1	1.590e-02	4.485e-03	1.132e-03	2.838e-04	4.576e-05
ABS2	1.114e-03	9.408e-05	1.218e-05	2.104e-06	1.805e-08
Quasi	2.105e-03	1.204e-04	1.335e-05	2.085e-06	2.588e-08
	Test 3: CGMY				
Δ	2.00	1.00	0.50	0.25	0.10
Interp	1.549e-02	4.741e-03	1.187e-03	2.980e-04	4.897e-05
ABS1	6.691e-03	2.300e-03	5.802e-04	1.465e-04	2.474e-05
ABS2	7.282e-04	1.241e-04	2.560e-05	4.987e-06	5.065e-07
Quasi	3.839e-03	1.223e-04	2.436e-05	4.762e-06	5.236e-07

dictates the fine structure, where $Y < 0$ specifies a finite activity process, $0 \leq Y \leq 1$ a process with finite variation but infinite activity, and $1 \leq Y < 2$ a process of infinite activity and variation. The risk-neutral Levy symbol is given by

$$\psi_{RN}(\xi) = i\xi(r - \psi_L(-i)) + C\Gamma(-Y)\left((M - i\xi)^Y - M^Y + (G + i\xi)^Y - G^Y\right),$$

where

$$\psi_L(-i) = C\Gamma(-Y)\left((M - 1)^Y - M^Y + (G + 1)^Y - G^Y\right),$$

and $\Gamma = \Gamma(y)$ is the Gamma function. Our third test corresponds to the CGMY model with parameters

$$\text{Test 3}: \quad C = 2, \quad M = 5, \quad G = 6, \quad Y = .5, \tag{189}$$

which generates a density with much heavier tails than the BSM or MJD models, as depicted in figure 26.

5.8.3 Experiments

The first valuation test is of the capped powered call,

$$f(S_T) = (S_T - 8)^2 \mathbb{1}_{[8,23]}(S_T) + (15)^2 \mathbb{1}_{(23,\infty)}(S_T),$$

where strikes are available on $[0, 30]$. To keep the truncation error from dominating the overall error, we price the payoff with support restricted to $[0, 30]$, using the method outlined in Appendix 5.9. We include as well the quasi-analytical hedge suggested in Section 5.4.4, which is labeled Quasi in table 25. This example illustrates a general observation that ABS_1 reduces the error of interpolation by around fifty percent, in terms of valuation and relative hedge error. ABS_2 performs substantially better in this case, as well as for many other functions tested. For all resolutions and for each method tested, the marginal cost after basis prices were obtained was between .1 and .2 milliseconds[22], where Quasi (which avoided calculating coefficients below the strike) incurred the least expense, followed by interpolation. Moreover, for all resolutions the ABS methods were within .06 milliseconds of interpolation. Hence, as the cost of pricing the basis is by far the dominant expense (see [62,83] for pricing of multiple strikes in Levy and Heston models), ABS is able to reduce the total computational cost by reducing the number of basis elements that are needed. For example, in the BSM test, to reach an accuracy of $e-04$, interpolation requires 10 times the number of basis elements as ABS_2.

We next consider the amortizing option of [71]:

$$f(S_T) = \frac{(S_T - K)^+}{S_T}, \quad S_0 = 14, K = 15, T = .5,$$

the results of which are shown in table 26. In the BSM case, ABS_2 significantly outperforms interpolation, where at the resolution $\Delta = 0.1$, an interpolation accuracy of $e-05$ compares to an ABS_2 accuracy of $e-10$, demonstrating that while ABS_2 generally outperforms interpolation, the discrepancy can be extreme. For the CGMY model, with $\Delta = 2$, the accuracy of ABS_2 has already reached $e-06$, and accuracy which is not reached by interpolation even for $\Delta = 0.1$.

[22] For all experiments conducted, the code is written in MATLAB 8.1, and the computer has an Intel(R) Core(TM) i5-3470T CPU, 2.90GHz with 3MB cache size.

Table 26: Amortizing option: $f(S_T) = \frac{(S_T-15)^+}{S_T}\mathbb{1}_{[0,50]}(S_T)$, strikes in $[10, 50]$ at spacing Δ, $S_0 = 14$, $T = .5$, ref.: $[0.048274, 0.056238, 0.073304, 0.423509]$.

	Test 1: BSM			Test 2: MJD		
Δ	Interp	ABS1	ABS2	Interp	ABS1	ABS2
2.00	6.433e-02	4.659e-02	2.730e-03	4.525e-02	3.239e-02	8.193e-04
1.00	3.810e-03	1.888e-03	1.136e-05	2.816e-03	1.396e-03	3.742e-06
0.50	9.558e-04	4.768e-04	6.488e-07	7.068e-04	3.537e-04	1.903e-06
0.25	2.391e-04	1.195e-04	3.774e-08	1.772e-04	8.904e-05	9.711e-07
0.10	3.827e-05	1.914e-05	8.865e-10	2.875e-05	1.465e-05	5.523e-07
	Test 3: CGMY			RAHE		
Δ	Interp	ABS1	ABS2	Interp	ABS1	ABS2
2.00	2.378e-02	1.711e-02	7.499e-06	2.838e-03	2.483e-03	2.481e-03
1.00	1.928e-03	9.754e-04	3.198e-05	2.983e-04	1.843e-04	1.286e-04
0.50	4.864e-04	2.490e-04	1.218e-05	7.460e-05	4.504e-05	3.048e-05
0.25	1.249e-04	6.556e-05	6.285e-06	1.865e-05	1.112e-05	7.403e-06
0.10	2.354e-05	1.406e-05	4.571e-06	2.984e-06	1.766e-06	1.163e-06

Table 27: $f(S_T) = [\sin(S_T)/2 + 3\ln(5 + S_T)]\mathbb{1}_{[0,40]}(S_T)$, strikes in $[0, 40]$ at spacing Δ, $S_0 = 8$, $T = 1$, reference values: $[7.399143, 7.336068, 7.194016, 9.2647738]$.

	Test 1: BSM			Test 2: MJD		
Δ	Interp	ABS1	ABS2	Interp	ABS1	ABS2
2.00	2.385e-03	1.473e-03	6.359e-04	1.150e-03	6.036e-04	7.736e-05
1.00	6.414e-04	3.436e-04	4.518e-05	3.079e-04	1.592e-04	1.054e-05
0.50	1.631e-04	8.306e-05	2.839e-06	7.757e-05	3.928e-05	9.686e-07
0.25	4.095e-05	2.057e-05	1.775e-07	1.947e-05	9.822e-06	1.745e-07
0.10	6.560e-06	3.282e-06	4.595e-09	3.161e-06	1.614e-06	6.761e-08
	Test 3: CGMY			RAHE		
Δ	Interp	ABS1	ABS2	Interp	ABS1	ABS2
2.00	2.595e-04	3.866e-04	5.066e-04	1.092e-02	8.416e-03	7.854e-03
1.00	1.046e-04	6.853e-05	3.072e-05	2.850e-03	1.838e-03	1.375e-03
0.50	2.823e-05	1.434e-05	2.075e-07	7.264e-04	4.383e-04	2.991e-04
0.25	6.915e-06	3.122e-06	6.920e-07	1.827e-04	1.082e-04	7.161e-05
0.10	9.192e-07	2.976e-07	3.249e-07	2.924e-05	1.722e-05	1.129e-05

As a final example, we constructed the payoff

$$f(S_T) = [\sin(S_T)/2 + 3\ln(5 + S_T)]\mathbb{1}_{[0,40]}(S_T), \quad S_0 = 8, T = 1,$$

to demonstrate the potential for pricing highly nonlinear contracts. Table 27 demonstrates again the superiority of ABS methods in terms of both pricing convergence and relative hedge errors. At a resolution $\Delta = .5$, the ABS_2 method is about two orders more accurate than interpolation, for each model tested, and its relative hedge error is less than half. It should also be noted that average errors for ABS methods are generally much smaller than average *absolute* errors due to their tendency to "hug" payoffs, as seen in figure 21. In contrast, interpolation has a tendency to systematically under or over hedge a payoff depending on its local convexity.

Many other exotic payoffs such as the log contract were tested as well, with similar findings. For the American binary hedge in equation (155), we found similar results for each method, where in the BSM model a value of 1 was taken as the reference for $S_T = H$.

5.9 Appendix: Direct Pricing of General Payoffs

As a control, we determine prices for general payoffs g directly by using a version of the procedure given in section 5.6.2. For payoffs with finite support $[L, R]$, we set $x_0 = \ln(L/S_0)$ (when $L = 0$, $x_0 := -4$) and $\bar{P} = \lceil \log_2(\ln(R/S_0) - x_0 + 1/\alpha \rceil$ to ensure that $x_{\bar{N}-1} \geq \ln(R/S_0)$, where $\bar{N} = \alpha 2^{\bar{P}}$, $N = 2\bar{N}$. That is, $\bar{P}$ is taken as the smallest integer such that the basis elements $\mu_{\alpha,l}$, $0 \leq l \leq \bar{N} - 1$, cover $[L, R]$. Note that if $R = \infty$, truncation is required. To avoid pricing outside of the desired support, we set $N^* := \lfloor (\ln(R/S_0) - x_0)\alpha + 1 \rfloor$, and only compute the payoff coefficients for $l = 0, ..., N^* - 1$. Here μ_{α,N^*-1} is roughly centered over R, and $\mu_{\alpha,0}$ is centered over L. Then $\mathcal{V}_{N^*} \circ g = (24a^2 e^{-rT}/N) \cdot G\{\beta^{\mu}_{\alpha,l}\}_{l=0}^{N^*-1}$, where G is a row vector of payoff coefficients.

For payoffs in the numerical section, this method is used to obtain reference prices, where we take $\alpha = 2^P$ for $P = 13$. Since the butterfly basis on $[L, R]$ for $L > 0$ has support on $[L - \Delta, R + \Delta]$, to compare direct with butterfly pricing over finite intervals we divide the prices of the boundary butterfly elements corresponding to L and R by two to account for the spillover (when $L = 0$, only the price corresponding to R is halved). Alternatively,

we could price the boundary elements separately after truncation, but the convergence rate is unaffected in our examples.

5.10 Appendix: Transform-Based Method

Direct application of Corollary 5.4.1 leads to a procedure which applies when the payoff form of $f(S_T)$ is known on an interval $[\bar{L}, \bar{R}]$ containing $[L, R]$, the desired hedge support. We assume that for some k_L, $k_R \in \mathbb{N}$, the endpoints satisfy $L = k_L/a$, $R = k_R/a$. Two applications of the fast Fourier transform (FFT) are required, where the desired coefficients c_k, $k = k_L, ..., k_R$, are recovered from those corresponding to $[\bar{L}, \bar{R}]$. Hence, with $P \in \mathbb{N}_+$, we define $k_{\bar{R}} := k_{\bar{L}} + 2^P - 1$ so that $[k_{\bar{L}}/a, k_{\bar{R}}/a] = [\bar{L}, \bar{L} + (2^P - 1)/a)] = [\bar{L}, \bar{R}]$ straddles $[L, R]$.

By utilizing the function defined over $[\bar{L}, \bar{R}]$, coefficients corresponding to the projection over $[L, R]$ are obtained with superior accuracy. To begin, we define

$$\bar{f}(y) = f(\bar{L} + y) - f(\bar{L}) - y\Delta_f, \quad \text{where} \quad \Delta_f := \frac{f(\bar{R}) - f(\bar{L})}{\bar{R} - \bar{L}},$$

and determine the coefficients $\bar{c}_k$ of the projection

$$\bar{f}(S_T) \approx \sum_{k=0}^{N_F - 1} \bar{c}_k \varphi_{a,k}(S_T),$$

where $N_F := 2^P$. We then define

$$h(\xi) := \frac{a^2(1 - \cos(\xi/a))}{\xi^2(2 + \cos(\xi/a))},$$

which we sample over the grid $\xi_j := (j-1)\Delta_\xi$, $j = 1, ..., N_F$, where $\Delta_\xi = \frac{2\pi a}{N_F}$.We determine the coefficients of $\bar{f}$ over $[0, \bar{R} - \bar{L}]$, corresponding to the points $y_k = (k-1)/a$, $k = 1, ..., N_F$

$$\begin{aligned}
\bar{c}_{k-1} &\approx 12 \cdot \Re \int_0^{2\pi a} e^{-iy_k\xi} h(\xi) \hat{\bar{f}}(\xi) d\xi \\
&\approx 12 \cdot \Re \sum_{j=1}^{N_F} e^{-i\frac{(k-1)}{a}\xi_j} h(\xi_j) \hat{\bar{f}}(\xi_j) \Delta_\xi \\
&= \frac{24\pi}{N_F} \cdot \Re \sum_{j=1}^{N_F} e^{-i(k-1)(j-1)\frac{2\pi}{N_F}} h(\xi_j) \hat{\bar{f}}(\xi_j) = \frac{24\pi}{N_F} \cdot \Re \left[\mathcal{D}_{k-1} \{ h(\xi_j) \hat{\bar{f}}(\xi_j) \}_{j=1}^{N_F} \right], \qquad (190)
\end{aligned}$$

where $\mathcal{D}$ denotes the discrete Fourier transform, and $\mathcal{D}^{-1}$ will denote its inverse. To determine $\{\hat{\bar{f}}(\xi_j)\}_{j=1}^{N_F}$, using the fact that $y_{N_F} = (2^P - 1)/a = \bar{R} - \bar{L}$ we compute

$$\begin{aligned}\hat{\bar{f}}(\xi_j) \approx \int_0^{\bar{R}-\bar{L}} e^{i\xi_j y}\bar{f}(y)dy &\approx \frac{1}{a}\sum_{n=1}^{N_F} e^{a(j-1)\frac{2\pi}{N_F}y_n}\bar{f}(y_n) \\ &= \frac{1}{a}\sum_{n=1}^{N_F} e^{(j-1)(n-1)\frac{2\pi}{N_F}}\bar{f}(y_n) = \frac{N_F}{a}\mathcal{D}_j^{-1}\{\bar{f}(y_n)\}_{n=1}^{N_F}. \qquad (191)\end{aligned}$$

Combining equations (190) and (191), we arrive at

$$\bar{c}_{k-1} \approx \frac{24\pi}{a}\cdot\Re\left[\mathcal{D}_{k-1}\left\{h(\xi_j)\cdot D_j^{-1}\{\bar{f}(y_n)\}\right\}\right]. \qquad (192)$$

From the set $\{\bar{c}_k\}_{k=0}^{2^P-1}$, we extract the desired coefficients

$$c_{k_L+j} = \bar{c}_{k_0+j}, \quad j = 0, ..., k_R - k_L,$$

where $k_0 := k_L - k_{\bar{L}}$. This procedure, which is applicable to general Reisz sequences of translates, is easy to implement and produces highly accurate approximations for smooth functions, but is not as robust to payoff discontinuities as the ABS and Dual methods.

5.11 Appendix: Auxiliary Results

One way to obtain an expression for $\mathbf{\Phi}$ is via Fourier series (FS) expansion:

Theorem 5.11.1. *[44] Let $\phi \in L^2(\mathbb{R})$. Then $\mathbf{\Phi} \in L^1(0, 2\pi)$, and the Fourier coefficients of $\mathbf{\Phi}$ with respect to the orthonormal basis $\{\frac{1}{\sqrt{2\pi}}e^{-ikx}\}_{k\in\mathbb{Z}}$ are given by*

$$c_k = \sqrt{2\pi}\int_{-\infty}^{\infty}\phi(x)\overline{\phi(x-k)}dx, \qquad k \in \mathbb{Z}.$$

Moreover, when ϕ is a compactly supported real-valued function, the FS expansion has only finitely many terms:

$$\mathbf{\Phi}(\gamma) = \frac{c_0}{\sqrt{2\pi}} + \frac{2}{\sqrt{2\pi}}\sum_{k=1}^{N} c_k\cos(k\gamma),$$

for some $N \leq \lceil |supp(\phi)| \rceil$.

The following proposition concerns the alteration of projection coefficients and its effect on convergence. The proof is omitted.

Proposition 5.11.1. *Let $(\phi, \widetilde{\phi})$ be a Riesz generator-dual pair in $\mathcal{H}$. Fix an initial spacing $1/a$ and define $\{\alpha_j\}_{j\geq 0}$ by $\alpha_j = 2^j a$. Choose any finite set of points $\{x^m\}$ of the form $x^m = k_m/\alpha_{j_m}$, where $k_m \in \mathbb{Z}$ and $j_m \leq J^* \in \mathbb{Z}_+$. For each m, choose a bounded sequence $\{v_j^m\}_{j\geq j_m}$ of modifications. Then $\forall \epsilon > 0$, $\exists J \geq J^* \in \mathbb{Z}_+$, such that $\forall j' \geq J \in \mathbb{Z}_+$*

$$\|\widetilde{P}_{J'} f - P_{J'} f\| < \epsilon, \quad \forall f \in \mathbb{Z},$$

where $P_{J'}$ is the orthogonal projection of $\mathcal{H}$ onto $J' := \overline{span}\{D_{\alpha_{j'}} T_k \phi\}_{k\in\mathbb{Z}}$, and $\widetilde{P}_{J'}$ is obtained by replacing for each m and $\forall j' \geq j_m$ the coefficients of $D_{2^{j'}a} T_{2^{j'-j_m}k_m} \phi$ (those of the basis elements centered over x_m at each resolution above j_m) by $v_{j'}^m/(\alpha_{j'})^{1/2}$.

5.12 Appendix: Proofs

Proof of Theorem 5.3.1. To prove (i), note that $D_a T_k \widetilde{\phi}$ is a frame sequence with the same bounds $0 < A \leq B$ as for $\{T_k\phi\}$. Indeed, $\langle D_a T_m \phi, D_a T_k \widetilde{\phi}\rangle = \langle \phi, T_{k-m}\widetilde{\phi}\rangle$, and $\text{span}\{D_a T_m \phi\}_m$ is of course dense in $\mathcal{M}_a$, so the bounds remain valid. From the biorthogonality of $\{T_k\phi\}$ and $\{T_k\widetilde{\phi}\}$, $\delta_{m,k} = \langle T_m\phi, T_k\widetilde{\phi}\rangle = \langle D_a T_m\phi, D_a T_k\widetilde{\phi}\rangle$, and the result follows since there is at most one sequence in $\mathcal{M}_a$ biorthogonal to $\{D_a T_k\phi\}$. For (ii), we have by frame representation and Parseval's identity

$$P_{\mathcal{M}_a} f = \sum_k \langle f, \widetilde{\phi}_{a,k}\rangle \phi_{a,k} = \frac{1}{2\pi} \sum_k \langle \widehat{f}, \mathcal{F}[D_a T_k \widetilde{\phi}]\rangle \phi_{a,k}.$$

With the modulation operator $E_b : \mathcal{H} \to \mathcal{H}$ defined by $(E_b f)(x) = e^{ibx} f(x)$,

$$\begin{aligned}\langle \widehat{f}, \mathcal{F}[D_a T_k \widetilde{\phi}]\rangle = \langle \widehat{f}, D_{\frac{1}{a}} E_k \widehat{\widetilde{\phi}}\rangle = \langle D_a \widehat{f}, E_k \widehat{\widetilde{\phi}}\rangle &= a^{1/2} \int_{-\infty}^{\infty} \widehat{f}(a\xi) \overline{e^{ik\xi} \widehat{\widetilde{\phi}}(\xi)} d\xi \\ &= a^{1/2} \int_{-\infty}^{\infty} e^{-ik\xi} \widehat{f}(a\xi) \widehat{\widetilde{\phi}}(-\xi) d\xi.\end{aligned}$$

The reality of f and $\widetilde{\phi}$ then implies

$$\langle f, \widetilde{\phi}_{a,k}\rangle = \Re\langle f, \widetilde{\phi}_{a,k}\rangle = a^{1/2} \Re \int_{-\infty}^{\infty} e^{-ik\xi} \widehat{f}(a\xi) \widehat{\widetilde{\phi}}(-\xi) d\xi.$$

But for $z \in \mathbb{C}$, $\Re z = \Re \bar{z}$, so upon splitting the integral

$$\begin{aligned}\langle f, \widetilde{\phi}_{a,k}\rangle &= a^{1/2} \Re \int_{-\infty}^{0} \overline{e^{-ik\xi} \widehat{f}(a\xi) \widehat{\widetilde{\phi}}(-\xi)} d\xi + a^{1/2} \Re \int_0^{\infty} e^{-ik\xi} \widehat{f}(a\xi) \widehat{\widetilde{\phi}}(-\xi) d\xi \\ &= 2a^{1/2} \int_0^{\infty} \Re \left[e^{-ik\xi} \widehat{f}(a\xi) \widehat{\widetilde{\phi}}(-\xi) d\xi \right].\end{aligned}$$

□

Proof of Corollary 5.4.1. A simple calculation yields $\widehat{\varphi}(\xi) = 4\sin^2(\xi/2)/\xi^2$. By Theorem 5.11.1 in the appendix, using the fact that φ is compactly supported we derive $\mathbf{\Phi}(\xi) = \frac{1}{3}(1 + 2\cos^2(\xi/2))$, from which

$$\widehat{\widetilde{\varphi}}(\xi) = \widehat{\varphi}(\xi)\mathbf{\Phi}(\xi)^{-1} = \frac{12\sin^2(\xi/2)}{\xi^2(1 + 2\cos^2(\xi/2))} = \frac{12\sin^2(\xi/2)}{\xi^2(2 + \cos(\xi))}.$$

Finally, noting that $\widehat{\widetilde{\varphi}}(\xi) = \widehat{\widetilde{\varphi}}(-\xi)$, the result follows from Theorem 5.3.1. □

Proof of Corollary 5.4.2. Since ϕ is real-valued and symmetric, the same is true of $\widehat{\phi}$. Further

$$\mathbf{\Phi}(\xi) = \sum_k |\widehat{\phi}(\xi + 2\pi k)|^2 = \sum_k |\widehat{\phi}(-\xi - 2\pi k)|^2 = \sum_k |\widehat{\phi}(-\xi + 2\pi k)|^2 = \mathbf{\Phi}(-\xi),$$

so $\widehat{\widetilde{\phi}}$ and hence $\widetilde{\phi}$ is real-valued and symmetric. The fact that $\widetilde{\phi}$ is the unique biorthogonal dual implies that $\widetilde{\phi} \in \overline{\text{span}}\{T_k\phi\}$, from which the representation $\widetilde{\phi} = \sum_k \langle \widetilde{\phi}, T_k\widetilde{\phi}\rangle T_k\phi$ is valid. Hence,

$$\langle \widetilde{\phi}, T_k\widetilde{\phi}\rangle = \frac{1}{2\pi}\int_{-\infty}^{\infty} \widehat{\widetilde{\phi}}(\xi)\overline{\widehat{\widetilde{\phi}}(\xi)e^{i\xi k}}d\xi = \frac{1}{2\pi}\int_{-\infty}^{\infty} \widehat{\widetilde{\phi}}(\xi)\widehat{\widetilde{\phi}}(-\xi)e^{-i\xi k}d\xi.$$

Moreover, $\widetilde{\phi}$ real-valued implies $\langle \widetilde{\phi}, T_k\widetilde{\phi}\rangle = \Re\langle \widetilde{\phi}, T_k\widetilde{\phi}\rangle\ \forall k$. By the symmetry and reality of $\widehat{\widetilde{\phi}}$, $\Re[\widehat{\widetilde{\phi}}(\xi)\widehat{\widetilde{\phi}}(-\xi)e^{-i\xi k}] = (\widehat{\widetilde{\phi}}(\xi))^2\Re(e^{-i\xi k})$. Thus

$$\langle \widetilde{\phi}, T_k\widetilde{\phi}\rangle = \frac{1}{2\pi}\int_{-\infty}^{\infty} \frac{\widehat{\phi}^2(\xi)}{\mathbf{\Phi}^2(\xi)}\Re(e^{-i\xi k})d\xi = \frac{1}{\pi}\int_0^{\infty} \frac{\widehat{\phi}^2(\xi)}{\mathbf{\Phi}^2(\xi)}\cos(\xi k)d\xi,$$

since the integrand is even. □

Proof of Proposition 5.4.1. From biorthogonality, $\widetilde{\varphi}$ necessarily satisfies $\int_{\mathbb{R}} = \widetilde{\varphi}(x)\varphi(x - k)dx = 0$ for $|k| \geq 1$, or equivalently

$$\begin{aligned}
0 &= \int_{\mathbb{R}} \left(\sum_{m\in\mathbb{Z}} \alpha_m\varphi(x - m)\right)\varphi(x - k)dx \\
&= \alpha_{k-1}\int_{k-1}^{k} T_{k-1}\varphi \cdot T_k\varphi + \alpha_k\int_{k-1}^{k+1} T_k\varphi \cdot T_k\varphi + \alpha_{k+1}\int_{k}^{k+1} T_{k+1}\varphi \cdot T_k\varphi \\
&= \frac{1}{6}(\alpha_{k-1} + 4\alpha_k + \alpha_{k+1}),
\end{aligned}$$

so $\alpha_{k+1} = -4\alpha_k - \alpha_{k-1}$. If we posit the ansatz $\alpha_k = \alpha_0\nu^{|k|}$ for $|k| \geq 1$, the difference equation becomes $\alpha_0\nu^2 + 4\alpha_0\nu + \alpha_0 = 0$, which has a stationary (non-divergent) solution

$\nu = \sqrt{3}-2$. When $k = 0$, we can use the fact that $\alpha_{-1} = \alpha_1$ and the biorthogonality relation $\int_{\mathbb{R}} = \widetilde{\varphi}(x)\varphi(x)dx = 1$ to obtain the equation $\alpha_1 = 3 - 2\alpha_0$. Combined with the ansatz $\alpha_1 = \alpha_0\nu$, we find that $\alpha_0 = 3/\sqrt{3}$. Uniqueness of the biorthogonal dual gives the result, after verifying that $\widetilde{\varphi} \in L^2$ by a geometric series, with $\widetilde{\varphi}$ defined by equation (161). □

Proof of Proposition 5.4.2. We derive the L^2 error, with the L^1 error following similarly. Note first that

$$|\langle f, \varphi_{a,k}\rangle| \leq \|f\|_\infty^{[L,R]} \int_{[\frac{k-1}{a}, \frac{k+1}{a}]} \varphi_{a,k}(s)ds = a^{-1/2}\|f\|_\infty^{[L,R]}.$$

Moreover, from equation (161) we have by a geometric series

$$\sum_{|m|>\gamma} |\alpha_m|^2 = 2\sum_{m>\gamma} \left(\frac{3}{\sqrt{3}}\right)^2 \nu^{2m} = \frac{6}{1-\nu^2}\nu^{2(\gamma+1)} = \tau(\gamma)^2.$$

Hence,

$$\begin{aligned}
\|f_a^\gamma - P_{\mathcal{M}_a} f\|_2^2 &= \int \Big| \sum_{k_L}^{k_R} \Big(\sum_{|m|\leq\gamma} \alpha_m \langle f, \varphi_{a,k+m}\rangle \Big) \varphi_{a,k}(s) - \beta_{a,k}\varphi_{a,k}(s) \Big|^2 ds \\
&\leq \int \left(\sum_{k_L}^{k_R} \Big| \sum_{|m|\leq\gamma} \alpha_m \langle f, \varphi_{a,k+m}\rangle - \beta_{a,k} \Big| |\varphi_{a,k}(s)| \right)^2 ds \\
&\leq \int \left(\sum_{k_L}^{k_R} |\varphi_{a,k}(s)| \sum_{|m|>\gamma} |\alpha_m| |\langle f, \varphi_{a,k+m}\rangle| \right)^2 ds \\
&\leq \int \left(\sum_{k_L}^{k_R} |\varphi_{a,k}(s)| \left(\sum_{|m|>\gamma} |\alpha_m|^2 \right)^{1/2} \left(\sum_{|m|>\gamma} |\langle f, \varphi_{a,k+m}\rangle|^2 \right)^{1/2} \right)^2 ds \\
&\leq \Big(\tau(\gamma)\|f\|_\infty^{[L,R]} \Big)^2 (R-L+1) \int \left(\sum_{k_L}^{k_R} |\varphi_{a,k}(s)| \right)^2 ds.
\end{aligned}$$

Expanding the square,

$$\begin{aligned}
\int \left(\sum_{k_L}^{k_R} |\varphi_{a,k}(s)| \right)^2 &\leq \sum_{k_L}^{k_R} \int \varphi_{a,k}^2(s)ds + \sum_{\substack{k\neq j \\ k_L\leq k,j\leq k_R}} \int \varphi_{a,k}(s)\varphi_{a,j}(s)ds \\
&\leq \frac{4}{3}a(R-L+1).
\end{aligned}$$

□

Proof of Corollary 165. From Proposition 5.4.1 with $\alpha_0 := 3/\sqrt{3}$,

$$\int_R \widetilde{\varphi}(x)x^p dx = \alpha_0 \sum_{m\in\mathbb{Z}} \nu^{|m|} \int_R \varphi(x-m)x^p dx = \alpha_0 \sum_{m\in\mathbb{Z}} \nu^{|m|}\theta_{1,m},$$

where $\theta_{1,m}$ is derived from equation (165). Thus, with $c_p := \alpha_0/(p+1)(p+2)$,

$$\begin{aligned} M^p &= c_p \sum_{m\in\mathbb{Z}} \nu^{|m|} \left[(m-1)^{p+2} - 2m^{p+2} + (m+1)^{p+2}\right] \\ &= c_p \left(1+(-1)^{p+2}\right)\left(1 + \sum_{m=1}^{\infty} \nu^m \left[(m-1)^{p+2} - 2m^{p+2} + (m+1)^{p+2}\right]\right) \\ &= c_p \left(1+(-1)^{p+2}\right)\cdot\left(1 + \nu G^{p+2} - 2G^{p+2} + \nu^{-1}(G^{p+2}-\nu)\right), \end{aligned}$$

where $G^q := \sum_{m=0}^{\infty} \nu^m m^q$. The result follows upon noting that $(1-\nu)G^q$ is the qth moment of a geometric random variable with success probability $1-\nu$, which is found by differentiating its moment generating function. To determine the coefficients,

$$\begin{aligned} \int_R \widetilde{\varphi}_{a,k}(x)x^p dx &= a^{1/2}\int \widetilde{\varphi}(a(x-k/a))x^p \\ &= a^{-(p+\frac{1}{2})}\int \widetilde{\varphi}(x)(x+k)^p dx = a^{-(p+\frac{1}{2})}\sum_{n=0}^{p}\binom{p}{n}k^{p-n}\int \widetilde{\varphi}(x)x^n dx, \end{aligned}$$

by a change of variables and binomial expansion. The result follows after eliminating odd moments. □

Proof of Proposition 5.4.6. We prove the case of $f \in \bar{C}$, the other being entirely similar. With $\epsilon_{a,k} := |\beta_{a,k} - \widehat{\beta}_{a,k}| = |\int_{[\bar{L},\bar{R}]^c} f\cdot\widetilde{\varphi}_{a,k}|$,

$$\begin{aligned} \|\bar{P}_{\mathcal{M}_a} f - \widehat{P}_{\mathcal{M}_a} f_{[\bar{L},\bar{R}]}\|_2^2 &\le \int \left(\sum_{k_L}^{k_R} \epsilon_{a,k}\varphi_{a,k}(x)\right)^2 dx \\ &\le \int \left[\left(\sum_{k_L}^{k_R}\epsilon_{a,k}^2\right)^{1/2}\left(\sum_{k_L}^{k_R}\varphi_{a,k}(x)^2\right)^{1/2}\right]^2 dx \\ &= \sum_{k_L}^{k_R}\epsilon_{a,k}^2 \cdot \sum_{k_L}^{k_R}\int \varphi_{a,k}(x)^2 dx \le \epsilon_a^* \cdot \frac{2}{3}a^2(R-L+1)^2, \end{aligned}$$

where $\epsilon_a^* := \max_{k_L\le k\le k_R}\{\epsilon_{a,k}^2\}$. By Corollary 5.4.1, $\widetilde{\varphi}_{a,k} = \alpha_0\sum_{m\in\mathbb{Z}}\nu^{|m|}\varphi_{a,k+m}$, from which

we determine a bound on ϵ_a^*. With $\bar{A}_k := \{m \in \mathbb{Z} : m + k \leq k_{\bar{L}} \text{ or } m + k \geq k_{\bar{R}}\}$

$$\begin{aligned}
\epsilon_{a,k} &\leq \alpha_0 \sum_{m \in \bar{A}_k} |\nu|^{|m|} \int |f(x)\varphi_{a,k+m}(x)|dx \\
&\leq \sqrt{2} \sum_{m \in \bar{A}_k} |\nu|^{|m|} \|f\|_2^{I_{k+m}^a} \\
&\leq \sqrt{2}\|f\|_2^{I_k^a} \sum_{m \in \bar{A}_k} |C\nu|^{|m|} \leq \kappa \cdot \tau([\bar{L}, \bar{R}]), \quad \forall k_L \leq k \leq k_R,
\end{aligned}$$

where $\kappa := \sqrt{2}\|f\|_2^{[L-1/a, R+1/a]}$ is independent of $[\bar{L}, \bar{R}]$, and decreases in a, and $\tau([\bar{L}, \bar{R}]) := \sum_{m \in \bar{A}_k} |C\nu|^{|m|}$ is finite since $|C\nu| < 1$. Hence, we can choose $[\bar{L}, \bar{R}] = [k_{\bar{L}}/a, k_{\bar{R}}/a]$ such that this tail series is arbitrarily small. Finiteness of the coefficients, hence of the representation, follows similarly by splitting the expression for $\beta_{a,k}$ into a finite component and a convergent tail series. □

Proof of Proposition 5.4.3. By symmetry, the biorthogonality condition $\langle \breve{\varphi}^{[\gamma]}(x), \varphi(x-k)\rangle = 0$ for $|k| \geq 1$ is equivalent to

$$0 = \int \breve{\varphi}^{[\gamma]}(x)\varphi(x-k)dx = \sum_{m=0}^{2\gamma-1} c_m^{[\gamma]} \lambda_{|m-k|}, \quad 1 \leq k \leq \gamma,$$

where $\lambda_{|m-k|} := \langle \varphi(x-m), \varphi(2x-k)\rangle$ can be shown to satisfy equation (171), and $\lambda_j = 0$ for $j \geq 3$. This gives the second through fourth equations above, which represent γ equations in all. The first equation is derived similarly from $\langle \breve{\varphi}^{[\gamma]}(x), \varphi(x)\rangle = 1$, bringing the total to $\gamma + 1$ equations. Since $2\gamma - 1$ coefficients are needed, there are $\gamma - 1$ remaining degrees of freedom, which are consumed by the moment matching conditions:

$$\begin{aligned}
M^{2k} &= \int \breve{\varphi}^{[\gamma]}(x)x^{2k}dx \\
&= \frac{1}{\sqrt{2}} \left(c_0^{[\gamma]} \int \varphi(2x)x^{2k}dx + 2 \sum_{m=1}^{2\gamma-1} c_m^{[\gamma]} \int \varphi(2x-m)x^{2k}dx \right),
\end{aligned}$$

where the integrals are evaluated using equation (165). Linear independence is then easily verified from the corresponding matrix.

To verify the final claim, Let $f(x) := \sum_{k_L}^{k_R} \varphi_{1,k}(x) \in \mathcal{M}_1$, where $k_L := -\gamma, k_R := \gamma$. From Proposition 5.4.5, any ABS approximation is a projector onto $\mathcal{M}_1$, so in particular

with $a = 1$ the coefficient corresponding to $k = 0$ in the ABS_γ approximation satisfies

$$1 = \int f\breve{\varphi}^{[\gamma]} = \int_{-\gamma}^{\gamma} \sum_{k_L}^{k_R} \varphi_{1,k}\varphi^{[\gamma]} = \int_{-\gamma}^{\gamma} \sum_{k\in\mathbb{Z}} \varphi_{1,k}\breve{\varphi}^{[\gamma]} = \int_{-\gamma}^{\gamma} \breve{\varphi}^{[\gamma]} = \int_{\mathbb{R}} \breve{\varphi}^{[\gamma]},$$

where we have used $1 = \sum_{k\in\mathbb{Z}} \varphi_{1,k}$. Thus $\int_{\mathbb{R}} \breve{\varphi}^{[\gamma]} = M^0$ is satisfied for any γ. For $\gamma \geq 1$ fixed, by Corollary 5.4.3 with $p \leq 2\gamma - 1$,

$$\begin{aligned}
\int x^p \widetilde{\varphi}_{a,k}(x)dx &= a^{-(p+\frac{1}{2})} \int (x+k)^p \widetilde{\varphi}(x)dx \\
&= a^{-(p+\frac{1}{2})} \sum_{n=0}^{\lfloor \frac{p}{2} \rfloor} \binom{p}{2n} k^{p-2n} M^{2n} \\
&= a^{-(p+\frac{1}{2})} \sum_{n=0}^{\lfloor \frac{p}{2} \rfloor} \binom{p}{2n} k^{p-2n} \int x^{2n} \breve{\varphi}^{[\gamma]}(x)dx = \int x^p \breve{\varphi}^{[\gamma]}_{a,k}(x)dx,
\end{aligned}$$

which follows upon equating the moments, and then reversing the change of variables and binomial expansion. □

Proof of Lemma 5.4.4. Since $\mathcal{M} := \overline{\text{span}}\{\Psi_k\}_{k\in\mathcal{K}}$ is a closed subspace of $\mathcal{H}$, there exists a unique decomposition $\mathcal{H} = \mathcal{M} \bigoplus \mathcal{M}^\perp$, which we denote by $f = P_{\mathcal{M}} f + P_{\mathcal{M}^\perp} f$. Then for any $f \in \mathcal{H}$ and k given, $\langle f, \Psi_k \rangle = \langle P_{\mathcal{M}} f, \Psi_k \rangle$. Thus if B denotes the upper frame bound on $\mathcal{M}$,

$$\sum_{k\in\mathcal{K}} |\langle f, \Psi_k \rangle|^2 = \sum_{k\in\mathcal{K}} |\langle P_{\mathcal{M}} f, \Psi_k \rangle|^2 \leq B\|P_{\mathcal{M}} f\|^2 \leq B\|f\|^2,$$

since $P_{\mathcal{M}} f \in \mathcal{M}$. □

Proof of Proposition 5.4.5. To simplify notation, let $\breve{P} := \breve{P}_{\mathcal{M}}$. Idempotence of $\breve{P}$ at all scales is demonstrated in equation (183). As for continuity, the compact support of $\breve{\phi}$ implies that $\sum_k |\langle \breve{\phi}_j, \breve{\phi}_k \rangle| \leq B$ from some $B > 0$ and for all $j \in \mathbb{Z}$. Hence by Proposition 5.4.4

$$\|\{\langle f, \breve{\phi}_k \rangle\}\|^2_{l^2(\mathbb{Z})} = \sum_k |\langle f, \breve{\phi}_k \rangle|^2 \leq B\|f\|^2 < \infty \quad \forall f \in \mathcal{H},$$

so $\{\langle f, \breve{\phi}_k \rangle\} \in l^2(\mathbb{Z})$, and the mapping $T_1 : f \to \{\langle f, \breve{\phi}_k \rangle\}$ is a well-defined, bounded linear map of $\mathcal{H}$ into $l^2(\mathbb{Z})$. The fact that $\{\phi_k\}$ is a Riesz sequence, and hence a Bessel sequence on all of $\mathcal{H}$ by Lemma 5.4.4, implies that $\sum_k c_k \phi_k$ converges unconditionally $\forall \{c_k\} \in l^2(\mathbb{Z})$. Moreover, $T_2 : \{c_k\} \to \sum_k c_k \phi_k$ is a well-defined bounded linear mapping of $l^2(\mathbb{Z})$ into $\mathcal{H}$.

Hence the composition $\breve{P} = T_2 \circ T_1$ is a bounded linear map from $\mathcal{H}$ into M. In fact, idempotence implies that $\breve{P}$ is onto $\mathcal{M}$.

Denoting the unique canonical dual generator by $\widetilde{\phi}$, the *orthogonal* projection of $\mathcal{H}$ onto $\mathcal{M}$ is given by $P_{\mathcal{M}} f = \sum_k \langle f, \widetilde{\phi}_k \rangle \phi_k$. If $f \in \mathcal{M}$, $f = P_{\mathcal{M}} f$ so by biorthogonality

$$\langle f, \breve{\phi}_m \rangle = \langle P_{\mathcal{M}} f, \breve{\phi}_m \rangle = \Big\langle \sum_k \langle f, \widetilde{\phi}_k \rangle \phi_k, \breve{\phi}_m \Big\rangle = \langle f, \widetilde{\phi}_m \rangle,$$

so that $\breve{P} f = P_{\mathcal{M}} f = f \ \forall f \in \mathcal{M}$. Thus we have for any $f, g \in \mathcal{H}$

$$\langle f, \breve{P} g \rangle = \langle P_{\mathcal{M}} f, \breve{P} g \rangle + \langle P_{\mathcal{M}^\perp} f, \breve{P} g \rangle = \langle P_{\mathcal{M}} f, \breve{P} g \rangle = \langle P_{\mathcal{M}} f, \breve{P}(P_{\mathcal{M}} g + P_{\mathcal{M}^\perp} g) \rangle.$$

Therefore $\langle f, \breve{P} g \rangle = \langle P_{\mathcal{M}} f, P_{\mathcal{M}} g + \breve{P} P_{\mathcal{M}^\perp} g \rangle$.

Although $P_{\mathcal{M}^\perp} g \in \mathcal{M}^\perp \subset \text{Range}(\breve{P})^\perp \Rightarrow \langle \breve{P} P_{\mathcal{M}^\perp} g, P_{\mathcal{M}^\perp} g \rangle = 0$, it is not true in general that $\breve{P} P_{\mathcal{M}^\perp} g = 0$. But $\langle P_{\mathcal{M}} f, \breve{P} P_{\mathcal{M}^\perp} g \rangle = \langle f, \breve{P} P_{\mathcal{M}^\perp} g \rangle$, so in order for $\langle f, \breve{P} g \rangle = \langle P_{\mathcal{M}} f, \breve{P} P_{\mathcal{M}} g \rangle$, it is necessary and sufficient that $\breve{P} P_{\mathcal{M}^\perp}(\mathcal{H}) = \{0\}$. In this case, $\langle f, \breve{g} \rangle = \langle P_{\mathcal{M}} f, P_{\mathcal{M}} g \rangle$, and likewise for the equality $\langle P_{\mathcal{M}} f, P_{\mathcal{M}} g \rangle = \langle \breve{P} f, g \rangle$, which is equivalent to self-adjointness of $\breve{P}$. Since idempotence holds, this is equivalent to $\breve{P} = P_{\mathcal{M}}$.

Finally, $\breve{P}(\mathcal{M}^\perp) = \{0\}$ is in turn equivalent to $\breve{\phi} \in \mathcal{M}$. Indeed, if $\breve{\phi} \in \mathcal{M}$, biorthogonality implies that $\{\breve{\phi}_k\}$ is the unique dual which satisfies $f = \breve{P} f + (I - \breve{P}) f = P_{\mathcal{M}} f + P_{\mathcal{M}^\perp} f$. Hence $\breve{P}(\mathcal{M}^\perp) = P_{\mathcal{M}}(\mathcal{M}^\perp) = \{0\}$. Conversely, if $\breve{P}(\mathcal{M}^\perp) = \{0\}$, then $\sum_k \langle f, \breve{\phi}_k \rangle \phi_k = 0 \ \forall f \in \mathcal{M}^\perp$. But $\{\phi_k\}$ is a Riesz sequence, so ω-independence implies $\langle f, \breve{\phi}_k \rangle = 0 \ \forall k \in \mathbb{Z}$. Hence, $\{\breve{\phi}_k\} \in (\mathcal{M}^\perp)^\perp = \mathcal{M}$ since $\mathcal{M}$ is closed, so $\breve{\phi} \in \mathcal{M}$. □

Proof of Proposition 5.5.1. While this result is standard in the literature, the proof of (ii) highlights the essence of a multiresolution analysis. Accordingly, fix any $\epsilon > 0$, and any $f \in \mathcal{H}$. By condition (ii) of the definition of FMRA, there exists $j \in \mathbb{Z}$ such that for some $h \in V_j$, $\|f - h\| < \epsilon/2$. By condition (i) of this proposition and the fact that $h \in V_j$, $P_{J'} h(x) = h(x)$ for all $j' \geq j$. Hence

$$\begin{aligned} \|f - P_{J'} f\|_2 &= \|f - h + P_{J'} h - P_{J'} f\|_2 \\ &\leq \|f - h\|_2 + \|P_{J'}(f - h)\|_2 \leq 2\|f - h\|_2 < \epsilon. \end{aligned}$$

The multiresolution structure ensures that approximations can only improve with mesh refinement. □

Proof of Theorem 5.5.1. We have for $f \in \mathcal{H}$

$$e^{rT}|\mathcal{V}f| \leq \int_{-\infty}^{\infty} |f(e^y)|q_T(y)dy = \int_0^{\infty} |f(x)|\frac{q_T(\ln(x))}{x}dx$$
$$\leq \|f\|_2 \left[\int_0^{\infty} \frac{q_T^2(\ln(x))}{x^2}dx\right]^{1/2},$$

so by a change of variables

$$e^{rT}|\mathcal{V}f| \leq \|f\|_2 \left[\int_{-\infty}^{\infty} \frac{q_T^2(z)}{e^z}dz\right]^{1/2} \leq \|f\|_2\|q_T\|_{\infty}^{1/2}\left[\int_{-\infty}^{\infty} q_T(z)e^{-z}dz\right]^{1/2}.$$

Thus, $|\mathcal{V}f| \leq C\|f\|_2$, where $C := e^{-rT}\left(\|q_T\|_{\infty}\hat{q}_T(i)\right)^{1/2}$, and $\hat{q}_T(i) = e^{-\ln(S_0)}\widehat{\mu}_T(i)$. Linearity is clear. □

Proof of Theorem 5.5.2. To verify the first claim, note that by Proposition 5.5.1, $\|P_J f\| \leq \|f\|$, so $f \in \mathcal{H}$ implies $|\mathcal{V} \circ P_J f| \leq \|\mathcal{V}\|\|P_J f\| \leq \|\mathcal{V}\|\|f\|$, so $\mathcal{V}_J : \mathcal{H} \to \mathbb{C}$. In fact, by the Uniform Boundedness Principle, $\sup_J\|\mathcal{V}_J\| < \infty$, so $\mathcal{V}_J$ is a uniformly bounded class in $\mathcal{H}^*$. Since continuous linear functionals preserve convergent series,

$$\mathcal{V}_J f = \mathcal{V}\Big(\lim_{K\to\infty}\sum_{|k|\leq K}\langle f, T_{2^{-j}k}\theta_j\rangle\phi_{j,k}\Big) = \lim_{K\to\infty}\sum_{|k|\leq K}\langle f, T_{2^{-j}k}\theta_j\rangle\mathcal{V}\circ\phi_{j,k},$$

by Theorem 5.5.1. To prove the second claim, $\mathcal{V}$ bounded implies that by the Riesz Representation theorem, $\exists h \in \mathcal{H}$ for which $\mathcal{V}f = \langle f, h\rangle, \forall f \in \mathcal{H}$. Hence,

$$|\mathcal{V}_J f - \mathcal{V}f| = |\mathcal{V} \circ (P_J - I)f| = |\langle (P_J - I)f, h\rangle$$
$$= \langle f, (P_J - I)h\rangle$$
$$\leq \|f\|\|(P_J - I)h\|,$$

since P_J is self-adjoint. Taking the supremum over $f \in \mathcal{H}$, $\|f\| = 1$, uniform convergence is obtained as $\|(P_J - I)h\| \to 0$. □

Proof of Corollary 5.5.3. The first two claims are immediate from previous results. To prove (iii), fix any $f \in \mathcal{H}_+$. Then

$$\|P_J f - P_{J^+}f\| \leq \|(P_J f - P_{J^+}f)\mathbb{1}_{x\geq 0}\| + \|(P_J f - P_{J^+}f)\mathbb{1}_{x<0}\|$$
$$= \|(P_J f - P_{J^+}f)\mathbb{1}_{x\geq 0}\| + \|P_J f\mathbb{1}_{x<0}\|$$
$$= \|(\langle f, \widetilde{\phi}_{j,0}\rangle - f(0)2^{-j/2})\cdot\phi_{j,0}(x)\cdot\mathbb{1}_{x\geq 0}\| + \|(P_J f - f)\mathbb{1}_{x<0}\|$$
$$\leq \|(\langle f, \widetilde{\phi}_{j,0}\rangle - f(0)2^{-j/2})\cdot\phi_{j,0}(x)\| + \|P_J f - f\|,$$

which converges to zero by proposition 5.11.1 and (ii) of this proposition. Hence

$$\|P_{J^+}f - f\| \leq \|P_{J^+}f - P_J f\| + \|P_J f - f\| \to 0, \text{ as } J \to \infty.$$

Similarly,

$$|\mathcal{V} \circ P_{J^+}f - \mathcal{V}f| = |\mathcal{V}(P_{J^+} - I)f| \leq \|\mathcal{V}\|\|(P_{J^+} - I)f\|.$$

But $\|(P_{J^+} - I)f\| \to 0$, and the claim follows. □

Proof of Proposition 5.5.2. By compactness of $\breve{\phi}$, we've seen that $\sum_k |\langle T_k\breve{\phi}, T_m\breve{\phi}\rangle| \leq B$ for some $B > 0$ and $\forall m \in \mathbb{Z}$. But

$$\sum_k |\langle T_k\breve{\phi}, T_m\breve{\phi}\rangle| = \sum_k |\langle D_j T_k\breve{\phi}, D_j T_m\breve{\phi}\rangle| \leq B,$$

from which

$$\|\{\langle f, \breve{\phi}_{j,k}\rangle\}\|^2_{l^2(\mathbb{Z})} = \sum_k |\langle f, \breve{\phi}_{j,k}\rangle|^2 \leq B\|f\|^2, \quad \forall f \in \mathcal{H},$$

where B is constant $\forall j \in \mathbb{Z}$. Hence the continuous linear map $A_{1,j} : f \to \{\langle f, \breve{\phi}_{j,k}\rangle\}$ is point-wise bounded over $f \in \mathcal{H}$, uniformly in $j \in \mathbb{Z}$. By the uniform boundedness principle (UBP), $\sup_{j\in\mathbb{Z}}\|A_{1,j}\| \leq A_1$, for some $A_1 > 0$. Likewise, the fact that ϕ generates an RMRA implies the map $A_{2,j} : \{c_k\} \to \sum_k c_k\phi_{j,k}$ for $\{c_k\} \in l^2(\mathbb{Z})$ is point-wise bounded for each $f \in \mathcal{H}$, uniformly over $j \in \mathbb{Z}$. Again, the UBP implies $\sup_{j\in\mathbb{Z}}\|A_{2,j}\| \leq A_2$, for some $A_2 > 0$. By composition, $\breve{P}_J = A_{2,j} \circ A_{1,j}$, and $\|\breve{P}_J\| \leq \|A_{2,j}\|\|A_{1,j}\| \leq A_2A_1$, so $\sup_{j\in\mathbb{Z}}\|\breve{P}_J\| \leq A_2A_1$. Thus, $\breve{P}_J$ is a bounded, linear projection operator on $\mathcal{H}$.

Now let P_J denote the orthogonal projection $P_J f = \sum_k \langle f, \widetilde{\phi}_{j,k}\rangle\phi_{j,k}$, and fix any $\epsilon > 0$. The fact that ϕ is an RMRA generator implies the existence of $j \in \mathbb{Z}$ such that, for some $h \in V_j$, $\|f - h\| < \epsilon(1 + A_1A_2)/2$ for any $f \in \mathcal{H}$. Moreover, the RMRA structure ensures that $h \in V_{j'}$ for all $j' \geq j$, hence $\|f - P_{J'}f\| \leq \epsilon/(1 + A_1A_2)$, $\forall j' \geq j$ by the proof of proposition 5.5.1. Thus

$$\begin{aligned}
\|\breve{P}_{J'}f - f\| &\leq \|\breve{P}_{J'}f - \breve{P}_{J'}P_{J'}f\| + \|\breve{P}_{J'}P_{J'}f - f\| \\
&= \|\breve{P}_{J'}(I - P_{J'})f\| + \|(P_{J'} - I)f\| \\
&\leq (\|\breve{P}_{J'}\| + 1)\|(I - P_{J'})f\| \leq (A_2A_1 + 1)\|(I - P_{J'})f\| < \epsilon,
\end{aligned}$$

for all $j' \geq j$. Thus $\lim_{J\to\infty} \|\breve{P}_J f - f\| = 0$, and $\lim_{J\to\infty} |\mathcal{V} \circ \breve{P}_J f - \mathcal{V} f| = 0$ follows from previous arguments. $\square$

CHAPTER VI

ASIAN OPTIONS

This chapter is based on the paper [84], cccepted to SIAM Journal on Financial Mathematics.

6.1 Introduction

Since their introduction in 1987, Asian options (known also as average rate or average price options) have provided a popular means of risk management in a variety of markets. For example, Eydeland and Wolyniec (2003) document their importance in mitigating the delivery risks present in gas markets. Since Asian options have payoffs that are contingent on the average price of an underlying asset (index, interest rate, exchange rate, commodity, etc.) over a given time horizon, their prices are less sensitive to price manipulations, and they become easier to hedge towards the option's expiry. By taking an average of the underlying, these options are typically much cheaper than standard European contracts. Moreover, their relative stability has led to the hybridization of exotic options that contain an Asian type specification towards the end of the contract, known as an "Asian tail".

As is generally the case with path-dependent contracts, robust pricing of Asian options is very challenging and computationally demanding. Even in the Black-Scholes-Merton (BSM) framework, no analytical formulas exist for the pricing of arithmetic Asian options. The computational approaches can be categorized as analytical approximations and bounds [3,4,93,111], partial differential equation (PDE) methods [5,6,56,129], lattices [48], Monte Carlo [82,119], and transform methods [13,41,42,54,138], to which our approach belongs. Alternative methods include Taylor expansion [81], perturbation [140], direct iterated integration [69], and maturity randomization [68]. In terms of both speed and accuracy, the transform based approaches are generally superior for models with Levy (log) returns, including BSM.

By working in the Fourier domain, we develop a fast and highly accurate method for

pricing generalized Asian options in exponential Levy models, which we call APROJ[1]. This includes discretely monitored contracts as well as the continuously monitored options that pervade foreign exchange markets. In-progress option prices and Greeks are also determined efficiently. Compared to state-of-the-art-methods, the APROJ method provides a 10- to 100-fold improvement in terms of cpu time to reach the same (or better) accuracy. This is confirmed for the methods of [13, 41, 42, 95, 138], most notably the improved convolution method of Cerny and Kyriakou [42], the ASCOS method of Zhang and Oosterlee [138], and the inverse Fourier transform method of Levendorskii and Xie [95], which are (to our knowledge) the fastest available pricing methods for discretely monitored arithmetic Asian options under Levy dynamics.

The paper is organized as follows. Section 2 reviews exponential Levy models and the method of density projection by frame duality. The problem of arithmetic Asian option pricing is formulated in Section 3, along with a derivation of the APROJ method. Section 4 develops extensions to in-progress option pricing and Greeks, generalized averaging, and continuous averaging. An in-depth analysis of error propagation and terminal valuation error is given in Section 5, after which Section 6 demonstrates the accuracy and efficiency of the method with a series of numerical experiments. Comparisons are made to existing methods with parameter sets from the literature. Finally, Section 7 concludes the paper.

6.2 Density Projection Method

The projection method described in this section applies whenever the characteristic function of the underlying random variable is known, which is the case for the family of Levy processes. Since the variance gamma (VG) model was introduced in 1990 to price derivatives [104], the versatility and tractability of Levy processes as generalizations of the BSM framework have generated a surge of research and modeling success. While application of the VG model itself has waned, subsequent developments such as the KoBoL [18, 20] model (with CGMY [32] as a special case) as well as the NIG [12] model have proven to be excellent alternatives which calibrate well to market data [32, 73], and the exponential (semi-heavy)

[1]APROJ is short for Asian PROJection, due to its use of a biorthogonal projection method.

decay of their tails engenders a significant computational advantage over the VG model.

6.2.1 Exponential Levy Models

Suppose $L(t), t \geq 0$, is a Levy process, which is a stochastically continuous process with stationary and independent increments. We denote its *Levy symbol* by $\psi_L(\xi)$, where by the Levy-Khintchine theorem the characteristic function (ChF) satisfies

$$\phi_{L(t)}(\xi) := \mathbb{E}[e^{iL(t)\xi}] = e^{t\psi_L(\xi)}, \quad t \geq 0.$$

Figure 43 in the appendix provides some of the more popular Levy symbols used in financial modeling, along with any parameter restrictions[2].

To model the underlying randomness on which Asian options are contracted, we consider exponential Levy processes of the form

$$S(t) = S(0)e^{Y(t)} = S(0)e^{(r-q+\omega)t+L(t)}, \quad \omega = -\psi_L(-i),$$

where $r, q \geq 0$ are the interest rate and dividend yield. Here ω is a "convexity correction" that is used to ensure that discounted asset processes (with reinvested dividends) behave as martingales. That is, $\mathbb{E}[S(t+\Delta_t)|S(t)] \equiv S(t)\mathbb{E}[e^{R_{\Delta_t}}] = S(t)e^{(r-q)\Delta_t}$, $\Delta_t, t \geq 0$, where

$$R_{\Delta_t} := \log(S(t+\Delta_t)/S(t)) \stackrel{d}{=} (r - q + \omega + L(1))\Delta_t, \quad t, \Delta_t > 0.$$

The ChF of R_{Δ_t} is given by

$$\phi_{R_{\Delta_t}}(\xi) = e^{i\xi(r-q+w)\Delta_t}e^{\psi_L(\xi)\Delta_t}, \quad \Delta_t > 0.$$

Note that the underlying Levy processes satisfies an exponential moment condition $\mathbb{E}[e^{-\alpha L(t)}] < \infty$, $\forall t \geq 0$, where $\mathcal{I}_L = (\lambda_-, \lambda_+)$ denotes the set of all such α. Here $-\infty \leq \lambda_- \leq 0 \leq \lambda_+ \leq \infty$ with possible inclusion of the endpoints. As a function of $z = \xi + iw$, $\psi_L(z)$ is analytic in the strip $\mathcal{D}_{(\lambda_-,\lambda_+)} := \{z \in \mathbb{C} : \Im(z) \in (\lambda_-, \lambda_+)\}$. With the exception of the pure jump VG (ie when $\sigma = 0$), the Levy processes of interest in finance satisfy the following bound for some $c, \kappa > 0$ and $\nu \in (0, 2]$

$$|\phi_{R_{\Delta_t}}(\xi)| = |e^{\psi_L(\xi)\Delta_t}| \leq \kappa e^{-\Delta_t c|\xi|^\nu}. \tag{193}$$

[2]If no restriction is given, the permissible parameter values are taken to be the real line.

6.2.2 Density Recovery and Option Pricing by Frame Projection

In [83], a method of European option pricing, called PROJ, is derived from the theory of frames and Riesz bases. The insight is to project the risk-neutral log return density, given in terms of its ChF, onto a tractable basis of compactly supported functions. The basis is formed by scaling and shifting a fixed *generator* or *scaling function*. The resulting method produces highly accurate localized approximations at low resolutions, where the number of basis elements grows with the resolution. The reader is referred to [83] for more details on the PROJ method, in particular the derivation of dual bases. We refer the reader to [44, 78] for an introduction to frame theory (also see [88] for applications to static hedging).

The B-spline bases of order p are of particular interest, and can be derived as follows. Starting with the Haar scaling function defined by $\varphi^{[0]}(y) := \mathbb{1}_{[-\frac{1}{2},\frac{1}{2}]}(y)$, the p-th order B-spline scaling functions are derived successively by the convolution

$$\varphi^{[p]}(x) = \varphi^{[0]} \star \varphi^{[p-1]}(x) = \int_{-\infty}^{\infty} \varphi^{[p-1]}(y-x)\mathbb{1}_{[-\frac{1}{2},\frac{1}{2}]}(y)dy. \tag{194}$$

With $p = 1$, the linear B-spline basis is generated by

$$\varphi^{[1]}(x) := (1-|x|)^+ = (1-|x|)\mathbb{1}_{[-1,1]}(x),$$

while for $p = 2$ we obtain the quadratic scaling function

$$\varphi^{[2]}(y) = \begin{cases} y^2/2 + 3y/2 + 9/8, & y \in [-3/2, -1/2] \\ 3/4 - y^2, & y \in [-1/2, 1/2] \\ y^2/2 - 3y/2 + 9/8, & y \in [1/2, 3/2]\,. \end{cases}$$

To ease notation, we will write $\varphi = \varphi^{[p]}$ when the context is clear.

Given a *resolution* a, and a grid $x_n = x_1 + (n-1)/a$, the approximation space for a fixed generator φ is given by the span of $\varphi_{a,n}(x) = a^{1/2}\varphi(a(x - x_n))$, which is centered over x_n. To derive finite dimensional approximations in terms of $\{\varphi_{a,n}\}_{n=1}^N$ for N fixed, we will truncate the corresponding projections onto the infinite dimensional space $\mathcal{M}_a := \overline{\text{span}}\{\varphi_{a,n}\}_{n\in\mathbb{Z}}$, using the fact that φ satisfies the *frame bounds*

$$A\|f\|^2 \le \sum_{n\in\mathbb{Z}} |\langle f, \varphi_{a,n}\rangle|^2 \le B\|f\|^2, \quad \forall f \in L^2(\mathbb{R}), \tag{195}$$

for some $0 < A \le B$ (independent of a).

6.2.2.1 Density Projection by Duality

Given a random variable X, with unknown density[3] f_X, we utilize the frame representation theorem [44,78] which states that the orthogonal projection $P_{\mathcal{M}_a} f_X$ of f_X onto $\mathcal{M}_a$ is given by

$$P_{\mathcal{M}_a} f_X = \sum_{n\in\mathbb{Z}} \langle f_X, \widetilde{\varphi}_{a,n}\rangle \varphi_{a,n},$$

where $\{\widetilde{\varphi}_{a,n}\}_{n\in\mathbb{Z}}$ is the *dual basis*, which is guaranteed to exist in some form. As shown in [83], if the ChF $\phi_X(\xi) := \mathbb{E}[e^{iX\xi}]$ is known, the projection coefficients satisfy for $1 \le n \le N$

$$\langle f_X, \widetilde{\varphi}_{a,n}\rangle = \mathbb{E}[\widetilde{\varphi}_{a,n}(X)] = \frac{a^{-1/2}}{\pi} \Re\left[\int_0^\infty \exp(-ix_n\xi)\cdot\phi_X(\xi)\widehat{\widetilde{\varphi}}\Big(\frac{\xi}{a}\Big)d\xi\right], \tag{196}$$

where

$$\widehat{\widetilde{\varphi}}(\xi) = \mathcal{F}\widetilde{\varphi}(\xi) = \int_{\mathbb{R}} e^{i\xi x}\widetilde{\varphi}(x)dx.$$

When $\widehat{\widetilde{\varphi}}(\xi)$ is known, as for the linear and quadratic generators [83]

$$\widehat{\widetilde{\varphi}}^{[1]}(\xi) = \frac{12\sin^2(\xi/2)}{\xi^2(2+\cos(\xi))}, \qquad \widehat{\widetilde{\varphi}}^{[2]}(\xi) = \frac{480\sin^3(\xi/2)}{\xi^3(26\cos(\xi)+\cos(2\xi)+33)}, \tag{197}$$

the coefficients can thus be calculated efficiently using the fast Fourier transform (FFT), as described next.

When $\phi_X(\xi)$ satisfies a growth estimate of the form of equation (193), the truncation error from numerically integrating (196) will decay exponentially, and polynomially otherwise. Even so, multiplication of the chf by $\widehat{\widetilde{\varphi}}(\xi)$ in equation (196) has a damping effect which reduces aliasing caused by an otherwise insufficient choice of a (the discrete Fourier transform implies a truncation interval of $2\pi a$ in Fourier space). This is one factor which contributes to accurate approximations at low resolutions.

6.2.2.2 Coefficient Approximation

To recover the orthogonal projection of the density of a random variable X, the first step is to set a resolution, for example $a = 2^P$ for $P \in \mathbb{N}$. By further specifying $\bar{P} \in \mathbb{N}$, which

[3] Levy models, with the exception of the compound Poisson process (ie no diffusion component and finite jump activity), possess a continuous density [120].

determines the support width of the projected density, and x_1, which determines its location in log return space, a conceptual grid $x_n = x_1 + (n-1)/a$, $n = 1, \ldots, N$, is designated where

$$N = 2^{P+\bar{P}} = a2^{\bar{P}} := a\bar{a},$$

where the choice of parameters is discussed in Section 6.3.6. For example, if $\mathbb{E}[X] := \mu_X$, then to center the grid over μ_X, set $x_1 = \mu_X - \left(\frac{N}{2} - 1\right)\Delta$ (where $\Delta := 1/a$), so that $\mu_X = x_{\frac{N}{2}}$. The density is then recovered on

$$[x_1, x_1 + \bar{a} - \Delta] \approx [\mu_X - \bar{a}/2, \mu_X + \bar{a}/2].$$

To discretize the integral in equation (196), by the Nyquist frequency requirement $\Delta\Delta_\xi = 2\pi/N$ the grid in frequency space is set to $\xi_j = (j-1)\Delta_\xi$, $j = 1, \ldots, N$, where $\Delta_\xi = 2\pi a/N = 2\pi/\bar{a}$. It is shown in [83] that the *truncated* true projection $\widetilde{f}_X(x)$ is well represented by the numerical approximation $\breve{f}_X(x)$, defined respectively by[4]

$$\widetilde{f}_X(x) := \sum_{n=1}^{N} \langle f_X, \widetilde{\varphi}_{a,n} \rangle \varphi_{a,n}(x), \qquad \breve{f}_X(x) := \sum_{n=1}^{N} \left(a^{1/2} C_{a,N} \breve{\beta}^X_{a,n} \right) \varphi_{a,n}(x),$$

where the coefficients $\langle f_X, \widetilde{\varphi}_{a,n} \rangle \approx a^{1/2} C_{a,N} \breve{\beta}^X_{a,n}$ are calculated by the discrete Fourier transform, in the absence of ChF error[5]:

$$a^{1/2} C_{a,N} \cdot \breve{\beta}^X_{a,n} = \frac{a^{-1/2}}{\pi} \Re \left\{ \sum_{j=1}^{N} \exp(-i x_n \xi_j) \cdot \phi_X(\xi_j) \widehat{\widetilde{\varphi}}\left(\frac{\xi_j}{a}\right) v_j \Delta_\xi \right\}, \tag{198}$$

where $\nu_j := 1 - (\delta_{j,1} + \delta_{j,N})/2$ and $C_{a,N}$ is a constant which depends on the selected generator φ. The full set of $\{\breve{\beta}^X_{a,n}\}_{n=1}^N$ are computed with complexity $\mathcal{O}(N \log_2(N))$ by the FFT.

As long as the numerical error is controlled, the overall convergence of the APROJ algorithm will be at least of the order of projection convergence. Define $\mathcal{H}(\mathcal{D}_d)$ to be the set of analytic functions in the strip $\mathcal{D}_d = \{z \in \mathbb{C} : \Im(z) \in (-d, d)\}$ which satisfy

$$\int_{-d}^{d} |h(x + iy)| dy \to 0, \quad \text{as } |x| \to \infty.$$

For $h \in \mathcal{H}(\mathcal{D}_d)$, we define the norm

$$\|h\|^{\mathcal{H}_d} := \lim_{\epsilon \to 0^+} \left[\int_{\mathbb{R}} |h(x + i(d - \epsilon))| dx + \int_{\mathbb{R}} |h(x - i(d - \epsilon))| dx \right].$$

We have the following result for p^{th} order B-spline generators.

[4]The term $a^{1/2}$ will be absorbed by an intermediate calculation.
[5]Error in the characteristic functions will be introduced.

Proposition 6.2.1. *Suppose that $\phi_X(\xi) \in \mathcal{H}(\mathcal{D}_d)$ for some $d > 0$, and let $\bar{\mu} = \bar{\mu}_X$ be an approximation to $\mathbb{E}[X]$. Fix $a = 2^P$ and $N = a \cdot \bar{a}$, where $\bar{a} = 2^{\bar{P}}$ for $\bar{P} > 1 + \log_2 |\bar{\mu}|$. Fix $x_1 = \bar{\mu} + \left(1 - \frac{N}{2}\right)\frac{1}{a}$. Then for some $0 < \gamma \leq d$*

$$\sup_{1 \leq n \leq N} \left| a^{1/2} C_{a,N} \cdot \breve{\beta}^X_{a,n} - \langle f_X, \widetilde{\varphi}_{a,n} \rangle \right| \leq \frac{a^{-1/2}}{\pi} \left(C^{[p]}_\gamma(\phi_X) \frac{e^{-(\bar{a}-2|\bar{\mu}|)\gamma/2}}{1 - e^{-\bar{a}\gamma}} + \tau_a(X) \right),$$

where $C^{[p]}_\gamma(\phi_X)$ is a constant. If for some $c, \kappa > 0$ and $\nu \in (0, 2]$, the tail of ϕ_X satisfies

$$|\phi_X(\xi)| \leq \kappa \exp(-tc|\xi|^\nu), \quad \xi \in \mathbb{R}, \tag{199}$$

where $t > 0$ is some fixed time, then

$$\tau_a(X) = \mathcal{O}(a \exp(-tc \cdot (2\pi a)^\nu). \tag{200}$$

In this case, the largest trapezoidal error converges exponentially in $\bar{a}$, while the truncation error is exponential in a. Moreover, when $a > 2d$, $\gamma = d$.

Proof. See appendix. □

Note that for the linear basis we have the bound $C^{[1]}_\gamma(\phi_X) \leq 24\|\phi_X\|^{\mathcal{H}}$ and $\tau_a(X) \leq \frac{6\kappa}{\pi} \cdot a \exp(-tc \cdot (2\pi a)^\nu)$, although the specific constants will not be required for our implementation.

6.2.2.3 Quadratic Basis Implementation

To implement the APROJ algorithm, we fix the quadratic basis, although the method applies more generally to p^{th} order B-splines and other generators as well. In particular,

$$f_X(x) \approx a^{1/2} C_{a,N} \sum_{n=1}^{N} \breve{\beta}^X_{a,n} \varphi^{[2]}_{a,n}(x), \quad C_{a,N} := \frac{960a^3}{N}. \tag{201}$$

The coefficients $a^{1/2} C_{a,N} \breve{\beta}^X_{a,n}$ are found using the discretization in equation (198). From the dual generator transform $\widehat{\widetilde{\varphi}}^{[2]}(\xi)$ in equation (197), we define

$$H_1 = 1/(960a^3), \qquad H_j = \phi_X(\xi_j)\zeta_j \exp(-ix_1\xi_j), \quad 2 \leq j \leq N, \tag{202}$$

where

$$\zeta_j := \frac{(\sin(\xi_j/2a)/\xi_j)^3}{26\cos(\xi_j/a) + \cos(2\xi_j/a) + 33}, \quad 2 \leq j \leq N. \tag{203}$$

The coefficients $\breve{\beta}^X = \{\breve{\beta}^X_n\}_{n=1}^N$ are recovered by the discrete Fourier transform (DFT)

$$\breve{\beta}^X := \Re[\mathcal{D}\{H_j\}_{j=1}^N], \qquad \mathcal{D}_n\{H_j\} := \sum_{j=1}^N e^{-i\frac{2\pi}{N}(j-1)(n-1)} H_j, \quad n = 1, \ldots, N, \tag{204}$$

For ϕ_X analytic in a strip containing $\mathcal{D}_{(-d,d)}$ with $d > 0$, trapezoidal approximations to the DFT converge exponentially with respect to $a, \bar{a}$, by Proposition 6.2.1.

6.2.3 Arithmetic Asian Options

Our main goal is to price discretely monitored arithmetic Asian options, which are contracts on the average over an observed set of prices of an underlying, with observations taken at a discrete set of $M+1$ monitoring dates, $\{0 = t_0, t_1, \ldots, t_M = T\}$, with $S_0 = S(t_0)$ observed upon entering the contract. We assume a uniform spacing between observations[6], $t_m = m\Delta t = m\frac{T}{M}$, $m = 0, \ldots, M$. If the density of $A_M := \frac{1}{M+1}\sum_{m=0}^M S_m$ is known, say f_{A_M}, then the initial value of an option paying $g(A_M)$ at time T must initially satisfy $\mathcal{V} \circ g(S_0) = e^{-rT}\int_{\mathbb{R}} g(u) f_{A_M}(u; S_0) du$.

Fixed strike vanilla Asian options (calls and puts) are priced according to the terminal payoffs with strike $W > 0$

$$g(A_M) := \begin{cases} \left(\frac{1}{M+1}\sum_{m=0}^M S_m - W\right)^+, & \text{for a call,} \\ \left(W - \frac{1}{M+1}\sum_{m=0}^M S_m\right)^+, & \text{for a put.} \end{cases} \tag{205}$$

By considering a change of numeraire, floating strike arithmetic options can be priced using an analogous formula, but only at inception [58]. On the other hand, frame projection can be used to efficiently obtain bounds on the prices of floating strike arithmetic options in terms of their geometrically averaged counterparts.

6.3 Mean Adjusted APROJ Method

This section details the APROJ method, which combines elements of several different methods to produce a highly efficient pricing algorithm. The first step is to reduce the problem dimension by employing a technique known as the Carverhill-Clewlow-Hodges factorization [41], which has been utilized as well by [42, 68, 69, 138]. The factorization results in

[6]This assumption is easily relaxed at a modest increase in cpu time.

a recursive scheme to recover a single state variable, Y_M, defined by a sequence of intermediate variables $\{Y_m\}_{m=1}^M$. As in [138], we focus on the ChF of this process, which we extend to generalized averaging and in-progress contracts. Analyticity of the chf of Y_m at each stage is proved. To reduce the computational cost and improve accuracy, we explicitly account for the shifting mean of Y_m, by employing an alternative to the lower bound grid shift algorithm proposed in [13]. In particular, we derive upper and lower bounds on the mean of Y_m, and devise an efficient grid shift scheme.

To derive the ChF, we extend the PROJ method of [83]. By utilizing the orthogonally projected density, PROJ obtains highly accurate approximations even at low resolutions. This phenomenon is explained in [127], where for modest resolutions the least squares projection behaves like an interpolation with twice the order of accuracy. Consequently, the use of projected densities results in a substantial reduction in overall cost. Transitioning between time states m requires the calculation of a series of complex valued integrals, for which we derive accurate closed form approximations, taking advantage of the compactly supported basis elements of the PROJ method. In contrast, the globally supported basis elements of a cosine series expansion, for example, require a much more expensive procedure to evaluate the analogous integrals. The resulting algorithm achieves high accuracy at a low computational cost compared with existing methods. Parameters are determined by an iterative procedure which uses the transform method of [64, 67] to estimate truncation error, as well as a proxy for the integration error incurred at each step. Greeks are obtained at a negligible added cost.

6.3.1 Change of Variables

The idea behind the Carverhill-Clewlow-Hodges factorization is to express the average in terms of a random variable Y_M, defined below, so that

$$A_M = \frac{1}{M+1}\sum_{m=0}^{M} S_m = \frac{S_0}{M+1}\left(1+\exp(Y_M)\right). \tag{206}$$

Given an approximation of the density f_{Y_M}, the value of a payoff $g(Y_M; S_0)$ satisfies

$$\mathcal{V}\circ g(S_0) = e^{-rT}\int_{\mathbb{R}} g(y;S_0) f_{Y_M}(y)dy,$$

where for vanilla options

$$g(y) := \begin{cases} \left(\dfrac{S_0(1+\exp(y))}{M+1} - W \right)^+, & \text{for a call,} \\ \left(W - \dfrac{S_0(1+\exp(y))}{M+1} \right)^+, & \text{for a put.} \end{cases} \tag{207}$$

In this way, pricing of a path-dependent Asian option is reduced to the valuation of a European option on the variable Y_M. As will be demonstrated, such a variable can also be found for generalized Asian options with fixed strikes, and for geometric Asian options with fixed and floating strikes (see [83] for the PROJ implementation for geometric Asian options).

The insight of [41] is that the arithmetic average can be expressed as

$$\begin{aligned} A_M &= \frac{S_0}{M+1}\left(1+\frac{S_1}{S_0}\left(1+\frac{S_2}{S_1}\left(\cdots\frac{S_{M-1}}{S_{M-2}}\left(1+\frac{S_M}{S_{M-1}}\right)\right)\right)\right) \\ &= \frac{S_0}{M+1}\left(1+e^{R_1}\left(1+e^{R_2}\left(\cdots e^{R_{M-1}}\left(1+e^{R_M}\right)\right)\right)\right) \\ &= \frac{S_0}{M+1}\left(1+\exp(R_1+\log\left(1+\exp(R_2+\log\left(\cdots R_{M-1}+\log\left(1+\exp(R_M)\right)\right)\right)\right)\right) \end{aligned}$$

where the log return increments are defined by[7]

$$R_m := \log(S_m/S_{m-1}), \quad m = 1, \ldots, M,$$

where we have suppressed the dependence of R_m on the time step $\Delta t = T/M$. By introducing the sequence $\{Y_m\}_{m=1}^M$, defined recursively by

$$Y_1 := R_M, \qquad Y_m := R_{M+1-m} + \log(1+\exp(Y_{m-1})), \quad m = 2, \ldots, M, \tag{208}$$

we have

$$Y_m = \log\left(\frac{1}{S_{(M-m)}}\sum_{j=1}^{m} S_{(M-m)+j}\right), \tag{209}$$

from which it follows that $\exp(Y_M) = \frac{1}{S_0}\sum_{m=1}^M S_m$, and so equation (206) holds. As in [138], we recover the ChF of ϕ_{Y_M} by computing the ChFs of the sequence $\{Y_m\}_{m=1}^M$.

[7] We reserve the notation R to denote the return distribution over a time increment of size Δ_t, while R_m denotes the return random variable itself. To make the dependence on Δ_t explicit, we will at times use R_{Δ_t} to denote a generic return increment.

6.3.2 The Basic Recursion

With $Z_m := \log(1 + \exp(Y_m))$, the characteristic function of Y_M is found recursively from $Y_1 = R_M$ by the equation

$$Y_m = R_{M+1-m} + Z_{m-1}, \quad m = 2, \ldots, M. \tag{210}$$

Assuming exponential Levy dynamics, the log return increments R_m are independent, from which independence of R_{M+1-m} and $\log(1+\exp(Y_{m-1}))$ follow. Moreover, stationarity (and uniform monitoring) implies that $R_{M+1-m} = R$ in law for all m, where R has known ChF for many Levy processes. Hence, starting with $\phi_{Y_1}(\xi) = \phi_R(\xi)$, the ChF of Y_m is derived from that of Y_{m-1} using equation (210):

$$\phi_{Y_1}(\xi) = \phi_R(\xi), \qquad \phi_{Y_m}(\xi) = \phi_R(\xi)\phi_{Z_{m-1}}(\xi), \quad m = 2, \ldots, M.$$

Specifically,

$$\phi_{Z_{m-1}}(\xi) := \mathbb{E}\left[e^{i\xi \log(1+\exp(Y_{m-1}))}\right] = \int_{\mathbb{R}} (e^y + 1)^{i\xi} f_{Y_{m-1}}(y)dy, \tag{211}$$

where $f_{Y_{m-1}}$ is approximated using $\phi_{Y_{m-1}}$.

The next result will ensure that the DFT errors, which are incurred at each density projection step, converge exponentially with respect to $a, \bar{a}$.

Proposition 6.3.1. *Suppose that $\phi_R(z)$ is analytic in the strip $\mathcal{D}_d := \{z \in \mathbb{C} : \Im(z) \in (-d, d)\}$, for some $d > 0$, and satisfies equation (193) for some $\kappa, c > 0$ and $\nu \in (0, 2]$. If $\{Y_m\}_{m=1}^M$ are defined by equation (208), then the ChFs satisfy*

(i) ϕ_{Y_m} is analytic in $\mathcal{D}_d$, $1 \le m \le M$, and

(ii) $|\phi_{Y_m}(\xi)| \le \kappa e^{-\Delta_t c|\xi|^\nu}$, $\xi \in \mathbb{R}$, $1 \le m \le M$.

Hence, the domain of analyticity and the decay of ϕ_{Y_m} are independent of m.

Proof. See appendix. □

It should also be noted that $f_{Y_m}(y) \sim e^{-d|y|}$ as $|y| \to \infty$, ie the densities have exponentially decaying tails[8], determined by the tail behavior of f_R. This follows since analyticity

[8]The rate of decay could be faster than d, but this gives a conservative estimate.

of ϕ_{Y_m} in $\mathcal{D}_d$ implies that $\mathbb{E}[e^{\eta Y_m}] < \infty$ for $\eta \in (-d, d)$. In particular, we are dealing with densities of rapid decrease.

6.3.3 APOJ Algorithm Overview

Before developing the APROJ algorithm in detail, we present the main blocks with references to their derivation in the text:

1. To account for the shifting mean of Y_m, a grid shift algorithm is derived in Section 6.3.4

2. The initial ChF ϕ_{Z_1} is obtained in terms of the closed form ChF ϕ_R in Section 6.3.5.1, where we introduce the integral matrix Ψ

3. The ChFs $\phi_{Z_{m-1}}$ are obtained recursively in Section 6.3.5.2

4. Given $\phi_{Z_{m-1}}$, we obtain ϕ_{Y_m} in Section 6.3.5.3

5. An automated method of parameter selection is detailed in Section 6.3.6, which is summarized by initialization Subroutine 9

6. An approximation of the integral matrix Ψ is given in Section 6.3.7, which is summarized by Subroutine 10

7. The final valuation step (which applies to general payoffs) is presented in Section 6.3.8, after recovering ϕ_{Y_M}

8. Formulas for vanilla option Greeks are provided in Section 6.3.10

After developing the main algorithm blocks, in Section 6.3.9 we summarize the routine in Algorithm 11, which calls initialization Subroutine 9 to determine parameters, and Subroutine 10 to populate the integral matrix Ψ.

6.3.4 Mean-adjusted Grid

We employ a grid shift to ensure that we capture to within a set tolerance the mass of $f_{Y_{m-1}}$, while the grid specific to each Y_m will belong to a single enlarged grid, for $m = 1, \ldots, M-1$.

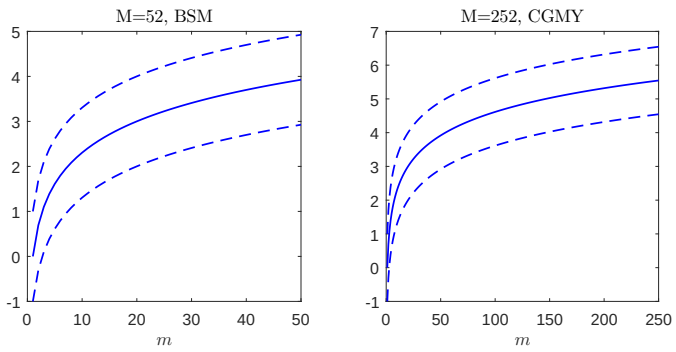

Figure 27: Plot of $\tilde{\mu}_m$, the approximated mean of Y_m, as a function of m with $r = .05$, $q = 0$ in the BSM $\sigma = 0.3$ model (Left) and the CGMY $= (0.27, 17.5, 54.8, 0.8)$ model (Right). The bounds $\bar{\mu}_m \pm \bar{a}/2$ are given by dashed lines, where $\bar{a} = 2$.

The final grid corresponding to Y_M will vary slightly according to the payoff to be priced. Since the distribution of $Y_1 = R_{\Delta_t}$ is roughly centered about its mean, a natural starting grid in log return space is fixed by centering about

$$\mathbb{E}[R_{\Delta_t}] = (r - q + \omega + \mathbb{E}[L(1)])\Delta_t = c_1 \Delta_t,$$

where $c_1 = \mathbb{E}[\log(S_{t+1}/S_t)]$ is the first cumulant of log return over a unit interval, and is provided in Table 43 for common processes. For example, the Black-Scholes-Merton (BSM) model satisfies $\mathbb{E}[R_{\Delta_t}] = (r - q - \sigma^2/2)\Delta_t$, where σ is the rate of volatility.

The approach of Benhamou [13] is to approximate the mean $\mathbb{E}[Y_m] = \mathbb{E}[R_{\Delta_t}] + \mathbb{E}[\log(1 + e^{Y_{m-1}})]$ by

$$\mu_1^B := \mathbb{E}[R_{\Delta_t}], \quad \mu_m^B = \mu_1^B + \log\left(1 + e^{\mu_{m-1}^B}\right), \quad m = 2, \ldots, M. \tag{212}$$

By convexity of $\log(1 + e^y)$, Jensen's inequality implies $\log(1 + \exp(\mathbb{E}[Y_{m-1}])) \leq \mathbb{E}[\log(1 + \exp(Y_{m-1}))]$, so the mean shift underestimates the true mean. We employ an alternative grid-shift scheme, described next.

6.3.4.1 Grid Shift and Bounds

As an alternative to the grid adjustment of [13], and to bound the growth of the grid shift, we derive an upper bound on $\mathbb{E}[Y_m]$ by applying Jensen's inequality(for *concave* functions) to equation (209):

$$\mathbb{E}[Y_m] \leq \log\left(\sum_{j=1}^{m} \mathbb{E}\left[\frac{S_{(M-m)+j}}{S_{(M-m)}}\right]\right) = (r - q)\Delta_t + \log\left(\frac{\exp\left((r - q)\Delta_t m\right) - 1}{\exp\left((r - q)\Delta_t\right) - 1}\right), \tag{213}$$

since $e^{(r-q)j\Delta t} = \mathbb{E}\left[\frac{S_{(M-m)+j}}{S_{(M-m)}}\middle|\mathcal{F}_{M-m}\right] = \mathbb{E}\left[\frac{S_{(M-m)+j}}{S_{(M-m)}}\right]$, where the first equality follows from the martingale property and the second from the fact that Levy increments are independent of the current filtration, $\mathcal{F}_{M-m}$. Similarly,

$$Y_m \geq \log(m) + \frac{1}{m}\sum_{j=1}^{m} \log\left(\frac{S_{(M-m)+j}}{S_{(M-m)}}\right),$$

from which we derive $\mathbb{E}[Y_m] \geq \log(m) + \mathbb{E}[R_{\Delta_t}]\frac{m+1}{2}$. In particular, we obtain a set of upper and lower bounds on the growth of $\mathbb{E}[Y_m]$.

Proposition 6.3.2. *With μ_m^B defined by equation (212), and $\theta := (r-q)\Delta_t$ we have*

$$\mathbb{E}[R_{\Delta_t}]\frac{m+1}{2} + \log(m) \leq \mathbb{E}[R_{\Delta_t}] + \log\left(1 + e^{\mu_{m-1}^B}\right) \tag{214}$$

$$\leq \mathbb{E}[Y_m]$$

$$\leq \theta + \log\left(\frac{\exp(\theta m) - 1}{\exp(\theta) - 1}\right) \leq \log(m) + \theta(m\mathbb{1}_{r\geq q} + \mathbb{1}_{r<q}). \tag{215}$$

With $\mu_0^B := 0$, these bounds hold for all $1 \leq m \leq M$.

Proof. Both inequalities in equation (215) follow from equation (213). To prove equation (214), define $\theta_m = \log(m) + \rho\frac{m+1}{2}$, where $\rho := \mathbb{E}[R_{\Delta_t}]$. We show that $\mu_m^B \geq \theta_m$ by proving $\exp(\mu_m^B - \theta_m) \geq 1$ inductively, where the case of $m = 1$ holds trivially. For $m \geq 2$,

$$\begin{aligned}
\exp(\mu_m^B - \theta_m) &= e^{\rho}\left(1 + e^{\mu_{m-1}^B}\right)e^{-\rho(m+1)/2}\frac{1}{m} \\
&\geq e^{\rho}\left(1 + e^{\rho m/2 + \log(m-1)}\right)e^{-\rho(m+1)/2}\frac{1}{m} \\
&= e^{\rho/2}\left(e^{-\rho m/2}\frac{1}{m} + \frac{m-1}{m}\right)
\end{aligned} \tag{216}$$

where the inequality follows by the inductive hypothesis. For $m = 2$, equation (216) becomes

$$\exp(\mu_2^B - \theta_2) \geq e^{\rho/2}\left(e^{-\rho}\tfrac{1}{2} + \tfrac{1}{2}\right) = \cosh(\rho) \geq 1.$$

It is thus sufficient to show that the lower bound in (216) is nondecreasing in m. In particular,

$$\frac{d}{dm}e^{\rho/2}\left(e^{-\rho m/2}\frac{1}{m} + \frac{m-1}{m}\right) = \frac{e^{\rho(1-m)/2}}{2m^2}\left(2\left(e^{\rho m/2} - 1\right) - \rho m\right).$$

Since $e^{\rho(1-m)/2}/2m^2 > 0$, the result follows from the fact that the second term $2\left(e^{\rho m/2} - 1\right) - \rho m := 2(e^{\lambda/2} - 1) - \lambda$ has a global minimum at $\lambda = 0$. That is, for any $\rho \neq 0$ fixed (the

case of $\rho = 0$ follows immediately), the derivative is a nondecreasing function of m, and equation (214) is proved. □

An immediate consequence of Proposition 6.3.2 is that we obtain a priori a corridor in which $\mathbb{E}[Y_m]$ lies for all $1 \leq m \leq M$, in terms of the mean return and $(r-q)$:

$$\mathbb{E}[R_{\Delta_t}]\frac{m+1}{2} \leq \mathbb{E}[Y_m] - \log(m) \leq |r-q|T\frac{m}{M}, \quad \forall m \leq M. \tag{217}$$

Hence, $\mathbb{E}[Y_m] = \log(m) + \mathcal{O}(m|r-q|\Delta_t)$ and the growth in $\mathbb{E}[Y_m]$ is no faster than $\log(m)$, independently of M (the second term is always bounded by $|r-q|T$). We also note that the upper bounds in equation (215) can be applied when $\mathbb{E}[R_{\Delta_t}]$ is unknown.

6.3.4.2 Grid Shift Algorithm

The APROJ grid shift is implemented by combining the innermost upper and lower bounds of Proposition 6.3.2. In particular, with $\mu_1^B = \mathbb{E}[R_{\Delta_t}] = c_1\Delta_t$ (see Table 43), and for $m = 2, \ldots, M$

$$\mu_m^B := \mu_1^B + \log\left(1 + e^{\mu_{m-1}^B}\right), \qquad \mu_m^U := (r-q)\Delta_t + \log\left(\frac{\exp\left((r-q)\Delta_t m\right) - 1}{\exp\left((r-q)\Delta_t\right) - 1}\right),$$

we define our grid as the lower-upper bound average

$$\tilde{\mu}_1 := c_1\Delta_t, \qquad \tilde{\mu}_m := (\mu_m^B + \mu_m^U)/2, \quad m = 2, \ldots, M, \tag{218}$$

with maximum grid shift error $|\mathbb{E}[Y_m] - \tilde{\mu}_m| \leq (\mu_m^U - \mu_m^B)/2$.

In order to reduce the computations required below (namely in computing a matrix Ψ), we perturb each $\tilde{\mu}_m$ slightly to obtain $\bar{\mu}_m$, which belongs to an extension of the initial grid defined by $\tilde{\mu}_1$:

$$\bar{\mu}_m := \tilde{\mu}_1 + N_m\Delta, \quad N_m := \lfloor a(\tilde{\mu}_m - \tilde{\mu}_1)\rfloor, \quad m = 2, \ldots, M, \tag{219}$$

and $\bar{\mu}_1 \equiv \tilde{\mu}_1$, $N_1 := 0$. Hence, we define the mean-adjusted grids

$$x_n^m = x_1^m + (n-1)\Delta, \quad x_1^m := \bar{\mu}_m + (1 - N/2)\,\Delta, \quad m = 1, \ldots, M-1, \tag{220}$$

each corresponding to a subset of the linear basis $\{\varphi_{a,n}\}_{n=1}^{N+N_{M-1}}$, with $\varphi_{a,1}$ centered over x_1^1. In particular, the density of Y_m is recovered over $[\bar{\mu}_m - \bar{a}/2, \bar{\mu}_m + \bar{a}/2]$, $m = 1, \ldots, M$,

which is illustrated in Figure 27. The choice of x_1^M will be detailed in Section 6.3.8. To implement the algorithm, only $\{x_1^m\}_{m=1}^M$ and $\{N_m\}_{m=1}^M$ are needed (there is no need to actually generate the grids at each stage).

6.3.5 Characteristic Function Recovery

We now derive the ChF recovery by successive PROJ expansions on the mean-adjusted grid. The algorithm is summarized in Section 6.3.9, along with a discussion of its complexity. In the algorithm description, we will denote by $\bar{\beta}_X$ the DFT approximation in the presence of ChF error, to distinguish it in the error analysis from $\breve{\beta}_X$ (which is absent ChF error).

6.3.5.1 Initialization

To initialize the characteristic function recursion we need

$$\phi_{Z_1}(\xi) := \mathbb{E}\left[e^{i\xi \log(1+\exp(R))}\right] = \int_{\mathbb{R}} (e^y+1)^{i\xi} f_R(y)dy.$$

Since $\phi_R(\xi)$ is known, $\phi_{Z_1}(\xi)$ is approximated by a (quadratic) PROJ expansion of $f_R(y)$, with coefficients $\breve{\beta}_n = \breve{\beta}_{a,n}$ to yield[9]

$$\begin{aligned}
\phi_{Z_1}(\xi) &\approx \int_{\mathbb{R}} (e^y+1)^{i\xi} \left(a^{1/2} C_{a,N} \sum_{n=1}^{N} \breve{\beta}_n \varphi_{a,n}(y) \right) dy \\
&= C_{a,N} \sum_{n=1}^{N} \breve{\beta}_n \cdot a^{1/2} \int_{I_n} (e^y+1)^{i\xi} \varphi_{a,n}(y)dy \\
&\approx C_{a,N} \sum_{n=1}^{N} \bar{\beta}_n^1 \cdot \bar{\Psi}(\xi,n) := \bar{\phi}_{Z_1}(\xi), \qquad (221)
\end{aligned}$$

where for the quadratic basis $I_n := [x_n^1 - 3\Delta/2, x_n^1 + 3\Delta/2]$ and $C_{a,N} = 960a^3/N$.

With the initial grid implied by the choice of $x_1^1 = \mathbb{E}[R] + (1 - N/2)\Delta$, so that ϕ_{Z_1} is approximated by a projected expansion of f_R about $\mathbb{E}[R]$, the column vector $\bar{\beta}^1$ is determined by

$$\bar{\beta}^1 := \Re[\mathcal{D}\{H_j^1\}_{j=1}^N], \qquad H_j^1 := \phi_R(\xi_j) \cdot \zeta_j \exp(-ix_1^1\xi_j), \quad j = 2, \ldots, N, \qquad (222)$$

where $H_1^1 = 1/(960a^3)$ and ζ_j is defined in equation (203). Further,

$$\Psi(\xi,n) := a^{1/2} \int_{I_n} (e^y+1)^{i\xi} \varphi_{a,n}(y)dy, \quad n = 1, \ldots, N + N_{M-1}, \qquad (223)$$

[9] We use the notation $\bar{\beta}^1$ here to be consistent with $\bar{\beta}^m$, $m \geq 2$, although it should be noted that $\bar{\beta}^1 = \breve{\beta}^1$ in this case since ϕ_R is known.

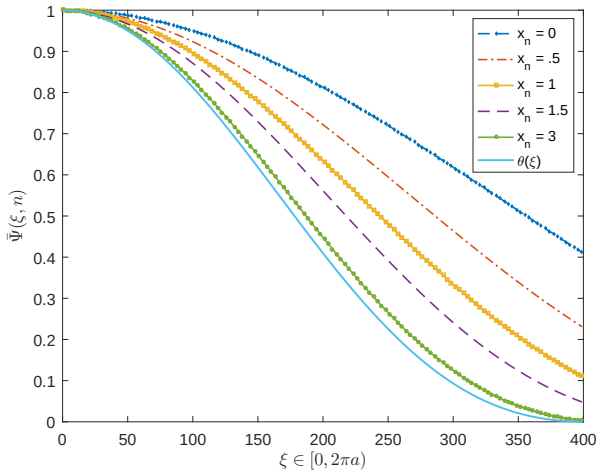

Figure 28: Convergence in x_n of $\Psi(\xi, n)$ to $a^{1/2}\mathcal{F}[\varphi_{a,n}](\xi)$, a plot of the modulus.

and $\bar{\Psi}(\xi, n)$ denotes a Newton-Cotes approximation to $\Psi(\xi, n)$ (discussed in Section 6.3.7). From here we obtain $\bar{\phi}_{Y_2}(\xi) = \phi_R(\xi)\bar{\phi}_{Z_1}(\xi)$, which concludes the initialization.

Remark 11. As demonstrated in Figure 28, for increasing x_n the columns in $\Psi(\xi, n)$ become progressively closer to the values of $a^{1/2}\mathcal{F}[\varphi_{a,n}]$ on $[0, 2\pi a)$. This is illustrated with the linear basis in terms of the scaled modulus

$$\theta(\xi) := \left(\frac{\sin(\xi/2a)}{\xi/(2a)}\right)^2 = a^{1/2}\left|a^{-1/2}e^{ix_n\xi}\left(\frac{\sin(\xi/2a)}{\xi/(2a)}\right)^2\right| = a^{1/2}|\mathcal{F}[\varphi_{a,n}]|,$$

and reflects the fact that

$$\left|\int_{I_n}(e^y+1)^{i\xi}\varphi_{a,n}(y)dy - \int_{I_n}e^{i\xi y}\varphi_{a,n}(y)dy\right| \to 0, \quad \text{as } x_n \to +\infty.$$

For a p^{th} order B-spline basis, we have the following characterization for large x_n.

Lemma 6.3.1. *With $a > 0$ fixed, the elements of $\bar{\Psi}$ behave as*

$$\Psi(\xi, n) \sim e^{ix_n\xi}\left(\frac{\sin(\xi/2a)}{\xi/(2a)}\right)^{(p+1)} + \mathcal{O}(a \cdot \exp(-x_{n-1})),$$

when x_n is large, with respect to the B-spline basis of order p.

Proof. See appendix. □

Especially when M is large (in which case a significant portion of $\bar{\Psi}$ will be well approximated by Lemma 6.3.1), the algorithm can be improved to use this result.

6.3.5.2 Recovery of $\phi_{Z_{m-1}}$

From the definition of Z_{m-1}, the characteristic function is approximated in terms of the PROJ expansion of $f_{Y_{m-1}}$, recovered over $[\bar{\mu}_{m-1} - \frac{\bar{a}}{2}, \bar{\mu}_{m-1} + \frac{\bar{a}}{2}]$, and corresponding to the subset of basis elements $\varphi_{a,n}$, $n = N_{m-1}+1, \ldots, N_{m-1}+N$:

$$\begin{aligned}\phi_{Z_{m-1}}(\xi) &= \int_{\mathbb{R}} (e^y + 1)^{i\xi} f_{Y_{m-1}}(y) dy \\ &\approx \int_{\mathbb{R}} (e^y + 1)^{i\xi} \left(a^{1/2} C_{a,N} \sum_{n=1}^{N} \bar{\beta}_n^{m-1} \varphi_{a,N_{m-1}+n}(y) \right) dy \\ &\approx C_{a,N} \sum_{n=1}^{N} \bar{\beta}_n^{m-1} \cdot \bar{\Psi}(\xi, N_{m-1}+n) := \bar{\phi}_{Z_{m-1}}(\xi). \end{aligned} \tag{224}$$

As before, the grid is fixed by x_1^{m-1}, and the column vector $\bar{\beta}^{m-1} := \Re[\mathcal{D}\{H_j^{m-1}\}_{j=1}^N]$ is determined via

$$H_1^{m-1} = 1/(960a^3), \quad H_j^{m-1} := \bar{\phi}_{Y_{m-1}}(\xi_j) \cdot \zeta_j \exp(-ix_1^{m-1}\xi_j), \quad j = 2, \ldots, N. \tag{225}$$

In fact, we only need the values of $\bar{\phi}_{Y_m}(\xi)$ for the discrete set of points $\xi_j = (j-1)\Delta_\xi$, $j = 1, \ldots, N$. Accordingly, if we define the $N \times (N_{M-1}+N)$ matrix $\bar{\Psi}$ by

$$\bar{\Psi}(j,n) := \bar{\Psi}(\xi_j, n), \quad j, n = 1, \ldots, N_{M-1}+N,$$

the computation at each stage can be represented as

$$\bar{\Phi}_{Z_{m-1}} = C_{a,N} \bar{\Psi}_{m-1} \bar{\beta}^{m-1} \tag{226}$$

where $\bar{\Phi}_{Z_{m-1}} = (\bar{\phi}_{Z_{m-1}}(\xi_1), \ldots, \bar{\phi}_{Z_{m-1}}(\xi_N))^\top$, and for $m = 2, \ldots, M$,

$$\bar{\Psi}_{m-1}(j,n) = \bar{\Psi}(j, N_{m-1}+n), \quad j, n = 1, \ldots, N.$$

Here, $\bar{\Psi}_{m-1}$ is defined for notational compactness and to indicate that only a subset of $\bar{\Psi}$ takes part in the matrix-vector product.

6.3.5.3 Recovery of ϕ_{Y_m}

To determine $\bar{\Phi}_{Y_m}$, equation (224) yields

$$\bar{\phi}_{Y_m}(\xi) = \bar{\phi}_{Z_{m-1}}(\xi)\phi_R(\xi) = C_{a,N} \sum_{n=1}^{N} \bar{\Psi}(\xi, N_{m-1}+n) \cdot \bar{\beta}_n^{m-1} \cdot \phi_R(\xi). \tag{227}$$

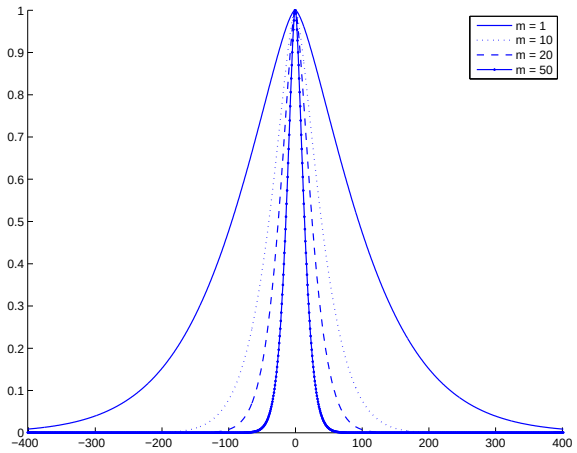

Figure 29: Modulus of ϕ_{Y_m}: $\Delta_t = 1/50$ for $(C, G, M, Y) = (.0244, .0765, 7.5515, 1.2945)$, and $r = .0367$. x-axis: $\xi \in [-2\pi a, 2\pi a]$, $\Delta_\xi = 2\pi/\bar{a}$, where $a = 2^6$, $\bar{a} = 2^3$.

In matrix form the algorithm reads

$$\Phi_R^C := C_{a,N}\Phi_R, \qquad \bar{\Phi}_{Y_m} = \left(\bar{\Psi}_{m-1}\bar{\beta}^{m-1}\right) \circ \Phi_R^C, \quad m = 2, \ldots, M, \tag{228}$$

where $\circ$ denotes the Hadamard product and $\Phi_R = (\phi_R(\xi_1), \ldots, \phi_R(\xi_N))^\top$.

An example of the modulus of recovered ChFs for the CGMY model with $M = 50$ is given in Figure 29, where the line corresponding to $m = 1$ is just $|\phi_R(\xi)|$. Notice how the ChFs collapse about the origin as m approaches M. The reflects the fact that, as m increases, the density of f_{Y_m} becomes less peaked (ie smoother), which translates into a more rapid decay of ϕ_{Y_m}.

6.3.6 Parameter Selection

The two parameters required to apply the APROJ method are $\bar{a}$ and N (or equivalently Δ). For several experiments in the numerical section, we fix a value of $\bar{a} = 2^{\bar{P}}$ (often excessively large to isolate the resolution error) and increase the parameter $a = 2^P$, which allows us to illustrate the convergence behavior as a function of resolution.[10] For example, Figure 33 in appendix illustrates the convergence in a for several levels of $\bar{a}$ fixed.

[10] One could use the value of $\bar{a} = 2^{\bar{P}}$ prescribed in Corollary 6.5.1 which ensures $\bar{a} - 2|\bar{\mu}_M| > 0$, and hence the exponential convergence in $\bar{a}$; it is usually around $\bar{P} = 3$ for $M \leq 50$, or $\bar{P} = 4$ when $M = 250$. Since this controls the *largest* coefficient error, it tends to be conservative although robust for heavy tailed returns (for BSM, $\bar{P} = 2$ is more than sufficient for $M \leq 250$ and $\sigma \leq .5$, and practical accuracy of greater than e-04 is achieved with $\bar{P} = 0 \sim 1$). In practice, a conservative rule of thumb is to choose $\bar{P} = 4$ for heavy tailed distributions, and $\bar{P} = 1$ for diffusion models.

This section provides an automated approach to parameter selection, requiring no user input, which should facilitate implementation in practical pricing scenarios. We first fix an initial value for N and truncation multiplier L_1. For $\Delta_t \geq 1/80$ we find that $N = 2^6$ and $L_1 = 12$ provide good starting values. Similarly we initialize $N = 2^7$ and $L_1 = 16$ for $\Delta_t < 1/80$. We then initialize $\bar{a}$ given according to the cumulants of R_{Δ_t}, as proposed in [61] (without the lower bound):

$$\bar{a} \leftarrow 2 \cdot \max\left\{1,\ L_1\sqrt{c_2\Delta_t + \sqrt{c_4\Delta_t}}\right\},$$

and set $\Delta \leftarrow \bar{a}/N$ (see Table 43 for c_n). Finally, we estimate the truncation error, with a tolerance ϵ_1, and a proxy for the valuation error, with a tolerance ϵ_2, increasing the values for N and $\bar{a}$ according to a set of rules.

First we estimate the truncation error. As shown in [64] (see also [67]), the probability mass of a random variable over and interval $[l, u]$ is given by

$$\mathbb{P}[l < R < u] = \int_{-\infty}^{\infty} e^{-i\xi(u+l)/2}\frac{\sin(\xi(u-l)/2)}{\pi\xi}\phi_R(\xi)d\xi.$$

Fixing $N > 0$ and $\Delta_\xi > 0$, we have the approximation

$$\mathbb{P}[l < R < u] \approx F_{\Delta_\xi,N}(l,u) := \frac{\Delta_\xi}{\pi}\left[\gamma_1 + \sum_{1\leq|n|\leq N-1} e^{-i\gamma_2(n\Delta_\xi)}\frac{\sin(\gamma_1(n\Delta_\xi))}{n\Delta_\xi}\phi_R(n\Delta_\xi)\right]$$

where $\gamma_1 = (u-l)/2$ and $\gamma_2 = (u+l)/2$. From Section 6.3.4.2, we know the grid shift error is bounded by $|\mathbb{E}[Y_m] - \tilde{\mu}_m| \leq (\mu_m^U - \mu_m^B)/2 := \tau_m$, and in practice we find that τ_M is the largest such error. Hence, given a grid estimate (l, u), we estimate the mass of f_R on $(\tilde{l}, \tilde{u}) = (l + \tau_M, u - \tau_M)$. If $|1 - F_{\Delta_\xi,N}(\tilde{l}, \tilde{u})| > \epsilon_1$, we double the grid size N, set $\bar{a} \leftarrow \sqrt{2}\bar{a}$, and reestimate.

As a second verification, by the martingale property of $e^{-(r-q)t}S_t$, we can utilize the following estimate to obtain a proxy for integration error incurred at each step:

$$E_N := C_{a,N} \cdot \vartheta_*^{[2]} \cdot \sum_{n=1}^{N} \bar{\beta}_n^1 \exp(x_1^1 + (n-1)\Delta) = \int \breve{f}_R(x)e^x dx \tag{229}$$

where $\vartheta_*^{[2]}$ is defined in Table 28. E_N approximates $\mathbb{E}[\exp(R_{\Delta_t})] = \exp((r-q)\Delta_t)$ using the projected density. Hence, once the truncation criterion is satisfied, we will further double

the grid size as long as $|E_N - \exp((r-q)\Delta_t)| \cdot M > \epsilon_2$. The multiplier M is to account for the number of such approximations made during the algorithm. The resulting initialization routine is summarized in Subroutine 9. After the main algorithm, a final check will be made (see Remark 13).

Note that the parameter ϵ_1 = 5e-04, along with ϵ_2 = 5e-04 are set in Subroutine 9 to satisfy an overall valuation error tolerance of TOL:= 5e-04 or better, uniformly across models, and tends to be conservative. This is illustrated in Table 36 of the numerical section.

Algorithm 9 Initialization by automated parameter selection

For $\Delta_t \geq 1/80$, Set: $L_1 = 12, N = 2^6$; For $\Delta_t < 1/80$, Set: $L_1 = 16, N = 2^7$
Set error tolerances $\epsilon_1 = 5e\text{-}04$; $\epsilon_2 = 5e\text{-}04$
Calculate cumulants c_1, c_2, c_4 of R_1 (see Table 43)
$\tilde{\mu}_1 \leftarrow c_1\Delta_t$; $\theta \leftarrow (r-q)\Delta_t$; $\mu_1^B \leftarrow c_1\Delta_t$
Initialize $\bar{a} \leftarrow 2 \cdot \max\left\{1,\ L_1\sqrt{c_2\Delta_t + \sqrt{c_4\Delta_t}}\right\}$
Set(Δ, a, Δ_ξ): $\Delta \leftarrow \bar{a}/N$; $a \leftarrow 1/\Delta$; $\Delta_\xi \leftarrow 2\pi/2\bar{a}$
for $m = 2 \ldots M$ **do**
$\mu_m^B \leftarrow \mu_1^B + \log\left(1 + e^{\mu_{m-1}^B}\right)$; $\tilde{\mu}_m \leftarrow \frac{1}{2}\left(\mu_m^B + \theta + \log\left(\frac{\exp(\theta m)-1}{\exp(\theta)-1}\right)\right)$
end for
Max grid shift error: $\tau_M := \frac{1}{2}\left(\theta + \log\left(\frac{\exp(\theta M)-1}{\exp(\theta)-1}\right) - \mu_M^B\right)$
$x_1^1 \leftarrow \tilde{\mu}_1 + (1 - N/2)\Delta$
$l \leftarrow x_1^1 + \tau_M$; $u \leftarrow (x_1^1 + \bar{a}) - \tau_M$; $\gamma_1 \leftarrow \frac{u-l}{2}$; $\gamma_2 \leftarrow \frac{u+l}{2}$
while $|1 - F_{\Delta_\xi, N}(l, u)| > \epsilon_1$ **do**
$N \leftarrow 2N$; $\bar{a} \leftarrow \sqrt{2}\bar{a}$; Set$(\Delta, a, \Delta_\xi)$
$x_1^1 \leftarrow \tilde{\mu}_1 + (1 - N/2)\Delta$; Update: l, u, γ_1, γ_2
end while
$\{\xi_j\}_{j=1}^N = (j-1)\Delta_\xi$, $\Phi \leftarrow \{\phi_R(\xi_j)\}_{j=1}^N$; Calculate $\{\zeta_j\}_{j=2}^N$ from (203)
Calculate $\{H_j\}_{j=1}^N$ from (222); $\{\bar{\beta}_n\}_{n=1}^N \leftarrow \Re\{\text{FFT}\{H_j\}_{j=1}^N\}$
Calculate E_N from (229)
while $|E_N - \exp(\theta)| \cdot M > \epsilon_2$ **do**
$N \leftarrow 2N$; $\bar{a} \leftarrow \sqrt{2}\bar{a}$; Set$(\Delta, a, \Delta_\xi)$
Recalculate: $\{\xi_j\}_{j=1}^N$, Φ, $\{\zeta_j\}_{j=2}^N$, $\{H_j\}_{j=1}^N$, $\{\bar{\beta}_n\}_{n=1}^N$ and E_N
end while
$N_m \leftarrow \lfloor a(\tilde{\mu}_m - \tilde{\mu}_1)\rfloor$; $x_1^m \leftarrow (\tilde{\mu}_1 + N_m\Delta) + (1 - N/2)\Delta$, $m = 1, \ldots, M$

6.3.7 Approximation of Ψ

We now discuss the numerical integration of the matrix Ψ. From equation (223), for $j = 1, \ldots, N$, From equation (223), for $j = 1, \ldots, N$,

$$\Psi(j,n) := a^{1/2} \int_{I_n} (e^y + 1)^{i\xi_j} \varphi_{a,n}(y) dy, \quad n = 1, \ldots, N + N_{M-1},$$

which we approximate by $\bar{\Psi}$ using Newton-Cotes quadrature. By fixing the grids with $\{x_1^m\}_{m=1}^{M-1}$ defined by equation (220), each can be considered as a subset of $x_1^1 + (n-1)\Delta$, $n = 1, \ldots, N + N_{M-1}$, so quadrature points (and function evaluations) can be reused in subsequent approximations. Moreover, the induced grid overlap reduces the computation[11] of $\bar{\Psi}$ from $N \times ((M-1)N)$ elements to $N \times (N + N_{M-1}) \leq N \times (\log(M-1)N)$ (see Section 6.3.9).

To obtain the matrix $\bar{\Psi}$ we evaluate the integrals by applying a seven point Newton-Cotes rule to each subinterval I_n^l, $l = 1, 2, 3$, where

$$I_n := [x_n - 3\Delta/2, x_n - \Delta/2] \cup [x_n - \Delta/2, x_n + \Delta/2] \cup [x_n + \Delta/2, x_n + 3\Delta/2] := I_n^1 \cup I_n^2 \cup I_n^3.$$

Combined with the known values of $\varphi^{[2]}(y)$ at each quadrature point, this results in the (composite) seven-point rule on I_n

$$\begin{aligned} Q(\nu) = &\frac{1}{840}\Big\{3\big[\nu_1 + \nu_{17} + 25(\nu_5 + \nu_{13}) + 46(\nu_7 + \nu_{11})\big] \\ &+ \frac{27}{18}\big[\nu_2 + \nu_{16} + 4(\nu_4 + \nu_{14}) + 13(\nu_8 + \nu_{10})\big] \\ &+ 34\left[\nu_3 + \nu_{15} + 6\nu_9\right] + 41\left[\nu_6 + \nu_{12}\right]\Big\}, \end{aligned}$$

where ν is defined in Subroutine 10, and represents generic values of the integrand for some (j,n) fixed.[12].

To calculate all integrals in $\Psi(j,\cdot)$ for j fixed thus requires a full grid $\{\eta_k\}_{k=1}^{N_\eta}$ of size $N_\eta = 17 + 6(N + N_{M-1} - 1)$, where[13]

$$\{\eta_k\}_{k=1}^{N_\eta} = x_1^1 - 8\Delta/6, \ldots, x_1^1 + (N + N_{M-1} - 1)\Delta + 8\Delta/6, \qquad \eta_k - \eta_{k-1} = \Delta/6.$$

[11] For example, when $N = 2^{11}$ and $M = 250$, the size of $\bar{\Psi}$ is reduced from 1.04×10^8 to 7.08×10^5 elements.

[12] Note that $Q(\nu)$ requires only 17 points to evaluate to populate $\Psi(j,n)$, since $x_n - \Delta/2$ and $x_n + \Delta/2$ are each shared by two subintervals, and on the boundaries $\varphi^{[2]}(y) = 0$

[13] This grid is used to initialize the algorithm, after which the value of η is updated.

Algorithm 10 Calculation of $\bar{\Psi}$

$N_\eta = 17 + 6(N + N_{M-1} - 1)$
$\eta_k \leftarrow x_1^1 + (k-9)\Delta/6, \quad k = 1, \ldots, N_\eta$
$\theta_k \leftarrow \exp\left(i\Delta_\xi \log\left(1 + \exp(\eta_k)\right)\right), \quad k = 1, \ldots, N_\eta$
$\eta \leftarrow \theta$
$\bar{\Psi}(1, n) \leftarrow 1, \quad n = 1, \ldots, N + N_{M-1}$
for $j = 2 \ldots N$ **do**
  for $n = 1, \ldots, N + N_{M-1}$ **do**
    $\nu_k \leftarrow \eta_{k+6(n-1)}, \quad k = 1, \ldots, 17$
    $\bar{\Psi}(j, n) \leftarrow Q(\nu)$
  end for
  $\eta \leftarrow \eta \circ \theta$
end for

Using the fact that

$$(e^y + 1)^{i\xi_j} = \exp\left(i\xi_j \log\left(1 + e^y\right)\right) = \exp\left(i(\xi_{j-1} + \Delta_\xi) \log\left(1 + e^y\right)\right)$$
$$= \exp\left(i\Delta_\xi \log\left(1 + e^y\right)\right) \cdot \exp\left(i\xi_{j-1} \log\left(1 + e^y\right)\right),$$

we obtain Subroutine 10 for $\bar{\Psi}$, where $\eta \circ \theta$ denotes the Hadamard product[14]. Since the quadrature rule is fixed (e.g. seven-point in our case, although alternative quadratures can be used as well), no user-supplied inputs are required. This simplifies the implementation as compared to a procedure such as ASCOS [138], which requires a specification of n_q (quadrature points for the Clenshaw-Curtis integration rule), which can vary substantially from one application to the next.

6.3.8 The Valuation Step

Given the approximation $\bar{\Phi}_{Y_M}$, the final step is analogous to the valuation problem for a European option. Rather than specify x_1^M as before, the valuation accuracy can be further improved by perturbing the terminal grid so that the vanilla option "kink", defined by

$$y^* := \log\big((M+1)W/S_0 - 1\big), \tag{230}$$

[14] To evaluate the complexity, η requires on the order of $\mathcal{O}(N_\eta)$ operations to initialize (as θ), followed by $N-1$ Hadamard products for a total cost of $\mathcal{O}((N-1)N_\eta)$ operations. Each quadrature application across a row $\bar{\Psi}(j, \cdot)$ of $\bar{\Psi}$, of which there are $N-1$, requires $\mathcal{O}(N + N_{M-1})$ operations. Hence, $\bar{\Psi}$ is populated at a cost of $\mathcal{O}((N-1)(N + N_{M-1}))$ operations.

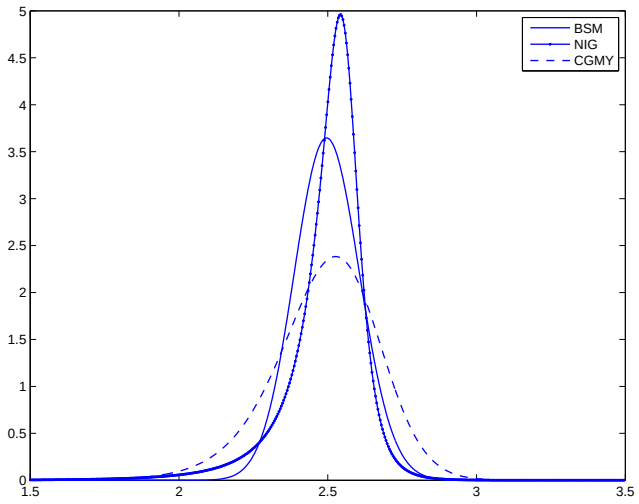

Figure 30: Plotted densities f_{Y_M}, $M = 12$, recovered by PROJ for models: BSM(.17801), NIG(6.1882, -3.8941, .1622), CGMY(.6509, 5.853, 18.27, .8) in section 6.6.

is a member. In this case, equation (207) can be expressed as

$$g(y) := \begin{cases} \left(\dfrac{S_0(1+\exp(y))}{M+1} - W \right) \mathbb{1}[y \geq y^*], & \text{for a call,} \\ \left(W - \dfrac{S_0(1+\exp(y))}{M+1} \right) \mathbb{1}[y \leq y^*], & \text{for a put.} \end{cases} \tag{231}$$

Initially defining $\tilde{x}_1^M = \tilde{\mu}_1 + N_M\Delta + (1 - N/2)\Delta$ and $n^* = \lfloor (y^* - \tilde{x}_1^M)a + 1 \rfloor$, we set

$$x_1^M := y^* - (n^* - 1)\Delta, \qquad x_n^M = x_1^M + (n-1)\Delta, \quad n = 1, .., N. \tag{232}$$

from which $y^* = x_{n^*}^M$. If we then define the terminal basis $\{\varphi_{a,n}^M(y)\}_{n=1}^N$ where $\varphi_{a,n}^M(y)$ is centered over x_n^M, the density is approximated by

$$f_{Y_M}(y) \approx \frac{1}{2\pi} \sum_{n=1}^{N} \langle \bar{\phi}_{Y_M}, \widehat{\bar{\varphi}}_{a,n}^M \rangle \cdot \varphi_{a,n}^M(y) \approx a^{1/2} C_{a,N} \sum_{n=1}^{N} \bar{\beta}_n^M \varphi_{a,n}^M(y)$$

where $\varphi_{a,N/2}^M(y)$ is roughly centered over the mean of Y_M, and $\bar{\beta}^M := \Re[\mathcal{D}\{H_j^M\}_{j=1}^N]$ is determined using

$$H_1^M = 1/(960a^3), \qquad H_j^M := \bar{\phi}_{Y_M}(\xi_j)\zeta_j \exp(-ix_1^M\xi_j), \quad j = 2, \ldots, N. \tag{233}$$

The final step is to approximate the initial value by integrating the terminal payoff against the PROJ expansion of f_{Y_M} (see Figure 30):

$$\mathcal{V} \circ g(S_0) = e^{-rT} \int_{\mathbb{R}} g(y; S_0) f_{Y_M}(y) dy \approx e^{-rt_M} C_{a,N} \sum_{n=1}^{n^*+1} \bar{\beta}_n^M g_n, \tag{234}$$

where the terminal payoff coefficients are defined for $n = 1, \ldots, N$ by

$$g_n := a^{1/2} \int_{x_n^M - 3\Delta/2}^{x_n^M + 3\Delta/2} \varphi_{a,n}^M(y) g(y) dy = \int_{-3/2}^{3/2} \varphi(y) g\left(x_n^M + \frac{y}{a}\right) dy. \tag{235}$$

Remark 12. For a general payoff $g(y)$, equation (235) can be numerically integrated, by taking into account the piecewise definition of φ and any payoff discontinuities. In general, even when analytical formulas for g_n are known, closed form quadrature rules (such as those in Table 28 for put options) provide more numerically stable coefficients as the resolution is refined (see [87] for more discussion).

As for European options, put-call parity can be used to price Asian call options (see equation (237)). This approach is preferred numerically since the put has a bounded payoff. For vanilla options defined in equation(231), define $C := \frac{S_0}{M+1}$ and $D := W - C$, and

$$E_n := \exp(x_n^M) = \exp(x_1^M + (n-1)\Delta), \qquad n = 1, \ldots, n^* + 1.$$

The payoff coefficients of a put option are given by $g_n^{put} = 0$ for $n = n^* + 2, \ldots, N$, and

$$g_n^{put} := \begin{cases} D \cdot \bar{\vartheta}_*^{[2]} - C \cdot \vartheta_*^{[2]} \cdot E_n & n = 1, \ldots, n^* - 2 \\ D \cdot \bar{\vartheta}_{-1}^{[2]} - C \cdot \vartheta_{-1}^{[2]} \cdot E_n & n = n^* - 1 \\ D \cdot \bar{\vartheta}_0^{[2]} - C \cdot \vartheta_0^{[2]} \cdot E_n & n = n^* \\ D \cdot \bar{\vartheta}_1^{[2]} - C \cdot \vartheta_1^{[2]} \cdot E_n & n = n^* + 1 \end{cases} \tag{236}$$

where $\vartheta_j^{[2]}$ and $\bar{\vartheta}_j^{[2]}$, derived in [87], are provided in Table 28 for reference. The value is then approximated by substituting g_n^{put} for g_n in equation (234). Once the put value $\mathcal{V}^{put}$ is determined, the call value $\mathcal{V}^{call}$ satisfies (see Section 6.4.3)

$$\mathcal{V}^{call} = \mathcal{V}^{put} + \frac{S_0 e^{-rT}}{M+1} \left(\frac{e^{(r-q)\Delta_t (M+1)} - 1}{e^{(r-q)\Delta_t} - 1} \right) - e^{-rT} W. \tag{237}$$

Remark 13. While the two checks in Section 6.3.6 are designed to prevent an insufficient choice of Δ and $\bar{a}$ at initialization, we can use the following quantity

$$\mathbb{E}[e^{Y_M}] = \frac{M+1}{S_0} \mathbb{E}[A_M] - 1 = \frac{e^{(r-q)\Delta_t (M+1)} - 1}{e^{(r-q)\Delta_t} - 1} - 1$$

to estimate the final valuation error. In particular, the error in estimating $\mathbb{E}[e^{Y_M}]$,

$$\mathcal{E}_M := \mathbb{E}[e^{Y_M}] - C_{a,N} \cdot \vartheta_*^{[2]} \cdot \sum_{n=1}^{N} \bar{\beta}_n^M \exp(x_n^M) \tag{238}$$

Table 28: Stable closed form coefficient approximations using Boole's rule for use with terminal payoffs.

Quadratic	$\bar{\vartheta}_j^{[2]}$	$\vartheta_j^{[2]}$
$j = *$	1	$\frac{1}{5}\left[\frac{1}{2} + \frac{1}{9}\left(\cosh(5\Delta/4) + 7\cosh(\Delta/2) + 22\cosh(\Delta/4)\right) + \cosh(3\Delta/4) + \frac{1}{6}\cosh(\Delta)\right]$
$j = -1$	$\frac{47}{48}$	$\frac{1}{10}\left[1 + \frac{1}{9}\left(e^{-5\Delta/4} + 7e^{-\Delta/2} + 44\cosh(\Delta/4)\right) + e^{-3\Delta/4} + \frac{1}{6}e^{-\Delta}\right.$ $\left. + \frac{7}{12}e^{\Delta/2} + \frac{49}{72}e^{5\Delta/8} + \frac{25}{72}e^{7\Delta/8} + \frac{3}{16}e^{3\Delta/4} + \frac{7}{144}e^{\Delta}\right]$
$j = 0$	$\frac{1}{2}$	$\frac{1}{10}\left[\frac{7}{24} + \frac{1}{9}e^{-5\Delta/4} + \frac{1}{6}e^{-\Delta} + e^{-3\Delta/4} + \frac{7}{12}e^{-\Delta/2} + \frac{13}{12}e^{-3\Delta/8} + \frac{11}{24}e^{-\Delta/4} + \frac{47}{36}e^{-\Delta/8}\right]$
$j = 1$	$\frac{1}{48}$	$\frac{1}{80}\left[e^{-9\Delta/8} + \frac{1}{6}e^{-5\Delta/4} + \frac{1}{9}e^{-11\Delta/8} + \frac{7}{18}e^{-\Delta}\right]$

serves as a proxy for the error in $\mathcal{V} \circ g(S_0)$. Given an value error tolerance TOL = 5e-04, we set a mean error tolerance for $\mathcal{E}_M$ of $\epsilon_3 := \text{TOL}/10 = 5\text{e-}03$. If $\mathcal{E}_M < \epsilon_3$, the algorithm terminates. Otherwise, if this threshold is exceeded, we reenter the main loop in Algorithm 11. We will then have the new value estimate, $\mathcal{V}_N$, and the previous estimate $\mathcal{V}_{N/2}$. Hence, the new stopping criteria becomes $|\mathcal{V}_N - \mathcal{V}_{N/2}| <$TOL.

6.3.9 The Algorithm and its Complexity

We now summarize the proceeding steps which define the quadratic APROJ algorithm, while alternative bases can be accommodated similarly. The algorithm calls initialization Subroutine 9, although one can instead select N and Δ directly. After Subroutine 10 is called to compute $\bar{\Psi}$, the main loop begins. Note that we have designed the routine for memory efficiency by reusing the arrays H and $\bar{\beta}$.

6.3.9.1 Complexity

We begin with cost of initializing the matrix $\bar{\Psi}$. From Section 6.3.7, for a given quadrature rule the complexity associated with calculating $\bar{\Psi}$ is $\mathcal{O}((N-1)(N+N_{M-1}))$. From equation (217), we can bound the growth of N_{M-1}, and hence the dimensions of $\bar{\Psi}$. With $\tilde{\mu}_m$ defined in equation (218), it follows that

$$\begin{aligned}\tilde{\mu}_{M-1} - \tilde{\mu}_1 &\leq \log(M-1) + \frac{T}{M}\left((M-2)(r-q) - (w + \mathbb{E}[L(1)])\right) \\ &\leq 2\log(M-1),\end{aligned}$$

Algorithm 11 Main Algorithm

Value error tolerance TOL:=5e-04
Call Subroutine 9 to obtain:
    Input 1: Final parameters $N, \Delta, \bar{a}, \Delta_\xi$
    Input 2: Grids $\{\xi_j\}_{j=1}^N,\ \{N_m\}_{m=1}^M,\ \{x_1^m\}_{m=1}^M$
    Input 3: Coefficient input $\Phi,\ \{\zeta_j\}_{j=2}^N,\ \{\bar{\beta}_n\}_{n=1}^N$
Call Subroutine 10 to compute $\bar{\Psi}$
$\Phi \leftarrow C_{a,N}\Phi; \quad C_1 \leftarrow 1/(960a^3)$
$H_j \leftarrow \Phi_j \cdot \sum_{n=1}^N \bar{\Psi}_{j,n}\bar{\beta}_n, \quad j = 1, \ldots, N$
$\bar{\beta} \leftarrow H$
for $m = 3, \ldots, M$: **do**
    $H_1 \leftarrow C_1; \quad H_j \leftarrow \zeta_j \cdot \bar{\beta}_j \cdot \exp(-i\xi_j \cdot x_1^{m-1}), \quad j = 2, \ldots, N$
    $\bar{\beta} \leftarrow \Re[\mathrm{FFT}(H)]$
    $H_j \leftarrow \Phi_j \cdot \sum_{n=1}^N \bar{\Psi}_{j,N_{m-1}+n}\bar{\beta}_n, \quad j = 1, \ldots, N$
    $\bar{\beta} \leftarrow H$
end for
Redefine x_1^M by equation (232)
$H_1 \leftarrow C_1; \quad H_j \leftarrow \zeta_j \cdot \bar{\beta}_j \cdot \exp(-i\xi_j \cdot x_1^M), \quad j = 2, \ldots, N$
$\bar{\beta} \leftarrow \Re[\mathrm{FFT}(H)]$
Find put value $\mathcal{V}^{put}$ using equation (234) with g_n^{put} defined in (236)
For a call, use put-call parity equation (237)
Compute final error proxy $\mathcal{E}_M$ in eq. (238), and proceed as directed in Remark 13

for sufficiently large M, by Proposition 6.3.2. For $\bar{a} \geq 2$,

$$N_{M-1} = \lfloor a(\tilde{\mu}_{M-1} - \tilde{\mu}_1) \rfloor \leq \lfloor 2N \log(M-1)/\bar{a} \rfloor \leq N \log(M-1). \tag{239}$$

Thus, $N + N_{M-1} \leq (N+1)\log(M-1) = \mathcal{O}(N\log(M))$, so the complexity of $\bar{\Psi}$ is $\mathcal{O}(N^2 \log(M))$. Given that the computational cost of determining x_1^m and H^m, $m = 1, \ldots, M$, is on the order $\mathcal{O}(MN)$, and the final value cost is $\mathcal{O}(N)$, the remaining contribution to the algorithm's complexity resides in the cost of $\bar{\beta}^m$, $m = 1, \ldots, M$, which is on the order $\mathcal{O}(MN\log_2(N)$ when the fast Fourier transform is utilized, the matrix vector multiplications $\bar{\Psi}_{m-1}\bar{\beta}^{m-1}$, $m = 2, \ldots, M$, at a cost of $\mathcal{O}((M-1)N^2)$, and the Hadamard products $\left(\bar{\Psi}_{m-1}\bar{\beta}^{m-1}\right) \circ \Phi_R^C$, $m = 2, \ldots, M$, at a cost of $\mathcal{O}((M-1)N)$. Hence, the total cost is $\mathcal{O}(MN\log_2(N) + N^2\log(M) + MN^2) = \mathcal{O}(MN^2)$.

6.3.10 Greeks

We now demonstrate how price sensitivities are calculated at almost no additional cost from the valuation algorithm. Consider first the put option payoff $g(y; S_0)$ defined in equation

(231), where $y^* = y^*(S_0) = \log\Big((M+1)\frac{W}{S_0} - 1\Big)$. First we observe that Y_M is independent of S_0. Indeed,

$$\exp(Y_M) = \frac{1}{S_0}\sum_{m=1}^{M} S_m = \frac{1}{S_0}\sum_{m=1}^{M} S_0 \exp\left(\sum_{k=1}^{m} R_k\right) = \sum_{m=1}^{M} \exp\left(\sum_{k=1}^{m} R_k\right).$$

From equation (234), Leibniz rule is used to determine the put option Delta, noting that $g(y^*(S_0), S_0) = 0$:

$$\mathbf{\Delta} := \frac{\partial \mathcal{V} \circ g}{\partial S_0} = e^{-rT}\int_{-\infty}^{y^*(S_0)} \frac{\partial g(y; S_0)}{\partial S_0} f_{Y_M}(y)dy = \frac{-e^{-rT}}{M+1}\int_{-\infty}^{y^*(S_0)} (1+e^y) f_{Y_M}(y)dy.$$

Using quantities that were already computed during the valuation stage, we find that

$$\mathbf{\Delta}^{put} \approx C_{a,N}\frac{-e^{-rT}}{M+1}\sum_{n=1}^{n^*+1} \bar{\beta}_n^M g_n(\mathbf{\Delta}^{put}). \tag{240}$$

The coefficients $g_n(\mathbf{\Delta}^{put})$ are defined similarly to equation (236), but instead of $D \cdot \bar{\vartheta}_j^{[2]} - C \cdot \vartheta_j^{[2]} \cdot E_n$ for $j \in \{*, -1, 0, 1\}$, we use $g_n(\mathbf{\Delta}^{put}) = \bar{\vartheta}_j^{[2]} + \vartheta_j^{[2]} \cdot E_n$. To determine the call Delta, equation (237) leads to the put-call parity formula

$$\mathbf{\Delta}^{call} = \mathbf{\Delta}^{put} + \frac{e^{-rT}}{M+1}\left(\frac{e^{(r-q)\Delta_t(M+1)} - 1}{e^{(r-q)\Delta_t} - 1}\right)$$

Likewise, the put (and call) option Gamma is given by

$$\begin{aligned}\mathbf{\Gamma} := \frac{\partial^2 \mathcal{V} \circ g}{\partial S_0^2} &= \frac{-e^{-rT}}{M+1}\frac{\partial}{\partial S_0}\int_{-\infty}^{y^*(S_0)} (1+e^y) f_{Y_M}(y)dy \\ &= \frac{-e^{-rT}}{M+1}\left(1+e^{y^*}\right) f_{Y_M}(y^*)\frac{\partial y^*(S_0)}{\partial S_0} = \left(\frac{W}{S_0}\right)^2 \frac{(M+1)\cdot e^{-rT} f_{Y_M}(y^*)}{W(M+1) - S_0}.\end{aligned} \tag{241}$$

For the quadratic basis we use the approximation[15]

$$f_{Y_M}(y^*) \approx a \cdot C_{a,N} \cdot \Big(\varphi^{[2]}(0)\bar{\beta}_{n^*}^M + \varphi^{[2]}(1)\big(\bar{\beta}_{n^*-1}^M + \bar{\beta}_{n^*+1}^M\big)\Big),$$

where $\varphi^{[2]}(0) = 3/4, \varphi^{[2]}(1) = 1/8$ and n^* is given in the previous subsection. Thus $\mathbf{\Delta}$ and $\mathbf{\Gamma}$ are computed as byproducts of the pricing algorithm.

6.4 Extensions

In this section we illustrate in-progress option pricing, generalized arithmetic averaging and continuously monitored option pricing.

[15]For the linear basis, $f_{Y_M}(y^*) \approx a \cdot C_{a,N} \cdot \bar{\beta}_{n^*}^M$

6.4.1 In-Progress Options: Pricing and Greeks

Only a slight modification is required to price Asian options at arbitrary times after averaging has begun. With the arithmetic average A_M defined in equation (206), then for $\tau \in [M_s\Delta t, (M_s+1)\Delta t)$, for some $M_s < M-1$, we find a variable Y_{M-M_s} such that

$$A_M = \frac{1}{M+1}\left[\sum_{m=0}^{M_s} S_m + S(\tau)\cdot\exp(Y_{M-M_s})\right].$$

That is, M_s indexes the most recent monitoring date, and $U_{M_s} := \sum_{m=0}^{M_s} S_m$ as well as $S(\tau)$ are known at the time of pricing. Noting that for $h := (M_s+1)\Delta_t - \tau$, $S_{M_s+1} = S(\tau)e^{R(h)}$ where $R(h) \overset{d}{=} \log(S_{t+h}/S_t)$, it follows from stationarity and independence of increments that Y_{M-M_s} can be found recursively by

$$\begin{aligned}
&\phi_{Y_1} = \phi_R, \qquad \bar{\phi}_{Y_m} = \phi_R \cdot \bar{\phi}_{Z_{m-1}}, \quad m = 2,\ldots,M-M_s-1,\\
&\bar{\phi}_{Y_{M-M_s}} = \phi_{R(h)} \cdot \bar{\phi}_{Z_{M-M_s-1}}.
\end{aligned}$$

When $\tau = M_s\Delta t$, $\phi_R \equiv \phi_{R(h)}$. As before, the final grid defined by $x_1^{M-M_s}$ is shifted so that the kink point

$$y^* := \log\left((M+1)W - U_{M_s}\right) - \log(S(\tau)) \tag{242}$$

is a member. For in-progress vanilla options, the payoff is expressed as

$$g(y) := \begin{cases} \left(\frac{1}{M+1}\left(U_{M_s} + S(\tau)e^y\right) - W\right)\mathbb{1}[y \geq y^*], & \text{for a call,}\\ \left(W - \frac{1}{M+1}\left(U_{M_s} + S(\tau)e^y\right)\right)\mathbb{1}[y \leq y^*], & \text{for a put,}\end{cases} \tag{243}$$

and payoff coefficients are derived analogously. Perhaps of even more interest than the price for an in-progress option are the Greeks. For the fixed strike Asian put,

$$\boldsymbol{\Delta} := \frac{\partial \mathcal{V}^\tau \circ g}{\partial S(\tau)} = \frac{-e^{-r(T-\tau)}}{M+1}\int_{-\infty}^{y^*} e^y f_{Y_{M-M_s}}(y)dy,$$

where $\mathcal{V}^\tau \circ g(U_{M_s}, S(\tau)) = e^{-r(T-\tau)}\mathbb{E}[g(A_M)|U_{M_s}, S(\tau)]$. Similarly, the put (and call) option Gamma is given by

$$\boldsymbol{\Gamma} := \frac{\partial^2 \mathcal{V}^\tau \circ g}{\partial S^2(\tau)} = \frac{e^{-r(T-\tau)}}{(S(\tau))^2} f_{Y_{M-M_s}}(y^*)\left(W - \frac{U_{M_s}}{M+1}\right),$$

where $f_{Y_{M-M_s}}(y^*)$ is calculated as before.

6.4.2 Generalized Arithmetic Asian Pricing

By a slight modification of the original algorithm, the ARPOJ method is capable of pricing payoffs on generalized averages of the underlying[16]

$$A_M^\lambda := \frac{1}{M+1}\sum_{m=0}^{M}\lambda_m S_m, \tag{244}$$

where $\lambda_m > 0$, $m = 0, \ldots, M$. We have the following extension, which is proved in a similar fashion to the Carverhill-Clewlow result, noting that

$$A_M^\lambda = \frac{S_0}{M+1}\left(\lambda_0 + e^{R_1}\left(\lambda_1 + e^{R_2}\left(\cdots e^{R_{M-1}}\left(\lambda_{M-1} + \lambda_M e^{R_M}\right)\right)\right)\right).$$

In alternative representation is provided in Corollary 6.4.1, which prevents the matrix $\bar{\Psi}$ from becoming stage dependent, and results in an efficient algorithm.

Corollary 6.4.1. *Fix a set of positive weights $\lambda = \{\lambda_m\}_{m=0}^M$, and define $X_m := \frac{\lambda_m}{\lambda_{m-1}}\exp(R_m)$, $m = 1, \ldots, M$, where $R_m = \log(S_m/S_{m-1})$. Set $Y_1 = \log(X_M) = \log(\lambda_M/\lambda_{M-1}) + R_M$, and define recursively*

$$Y_m = \log\left(\frac{\lambda_{M+1-m}}{\lambda_{M+1-(m-1)}}\right) + R_{M+1-m} + Z_{m-1}, \quad m = 2, \ldots, M,$$

where $Z_m := \log(1 + \exp(Y_m))$. Then

$$A_M^\lambda \equiv \frac{\lambda_0 S_0}{M+1}\left(1 + \exp(Y_M)\right). \tag{245}$$

Proof. The proof relies on an equivalent factorization of A_M^λ,

$$A_M^\lambda = \frac{\lambda_0 S_0}{M+1}\left(1 + \frac{\lambda_1 S_1}{\lambda_0 S_0}\left(1 + \frac{\lambda_2 S_2}{\lambda_1 S_1}\left(\cdots\frac{\lambda_{M-1}S_{M-1}}{\lambda_{M-2}S_{M-2}}\left(1 + \frac{\lambda_M S_M}{\lambda_{M-1}S_{M-1}}\right)\right)\right)\right),$$

which can be verified by multiplying each of the terms. The remainder of the proof is similar to standard construction, and follows algebraically. □

This form of the recursion requires that $\lambda_m > 0$ for each m, in which case the structure of the APROJ algorithm is unaffected. Namely, the matrix $\bar{\Psi}$ is the same for each m, and the only real change is the grid shift, where we add $\tilde{\lambda}_m := \log(\lambda_{M+1-m}/\lambda_{M+1-(m-1)})$ to each $\tilde{\mu}_m$. The perturbed grid shifts $\bar{\mu}_m$ are defined still by equation (219).

[16] We include the term $1/(M+1)$ so that the standard average is obtained when all $\lambda_m = 1$.

6.4.3 Put-Call Parity

Just as for vanilla European options, put-call parity can be used to price Asian call options in terms of puts and conversely (this will be used for all numerical experiments). In the generalized setting, we have

$$e^{-rT}\mathbb{E}\left[(A_M^{\lambda})^+ - (-A_M^{\lambda})^+\right] = \frac{e^{-rT}}{M+1}\mathbb{E}\left[\sum_{m=0}^{M}\lambda_m S_m\right] = \frac{S_0 e^{-rT}}{M+1}\sum_{m=0}^{M}\lambda_m e^{(r-q)\Delta_t m},$$

where q is the continuous dividend yield, and $\Delta_t = T/M$ in the uniform case. Considering the fixed and floating strikes[17] together, with $\alpha = \pm 1$,

$$(\alpha(A_M - K_1 S_T - K_2))^+ = (\alpha A_M^{\lambda})^+,$$

where

$$\lambda_0 = 1 - \frac{K_2}{S_0}(M+1), \quad \lambda_M = 1 - (M+1)K_1, \quad \lambda_m = 1, \quad m = 1, \ldots, M-1.$$

In this setting, with $C_M(S_0, T)$ and $P_M(S_0, T)$ denoting the call and put prices,

$$C_M(S_0,T) - P_M(S_0,T) = \frac{S_0 e^{-rT}}{M+1}\left(\frac{e^{(r-q)\frac{T(M+1)}{M}} - 1}{e^{(r-q)\frac{T}{M}} - 1}\right) - S_0 K_1 e^{-qT} - e^{-rT}K_2,$$

from which the fixed and floating strike parities are derived. Moreover, the forward contract, $g(\{S_m\}) = A_M - K_2$, is priced immediately by setting $K_1 = 0$.

It should be noted that put-call parity is a useful tool for maintaining robustness when pricing call options. Since the density of Y_M is recovered approximately over $[\bar{\mu}_M - \frac{\bar{a}}{2}, \bar{\mu}_M + \frac{\bar{a}}{2}]$, this implies a lower bound on the truncation error for pricing call options:

$$\epsilon_{trunc} \geq e^{-rT}\left(\frac{S_0(1+\exp(\bar{\mu}_M + \bar{a}/2))}{M+1} - W\right)\int_{\bar{\mu}_M + \bar{a}/2}^{\infty} f_{Y_M}(y)dy.$$

For a heavy-tailed density, the implied truncation error can be unacceptable, in which case put-call parity can be used to price call options in terms of the *bounded* put prices.

[17] For example, a floating strike call has payoff $(A_M - K_1 S_T)^+$.

Table 29: Continuously monitored Asian option values by Richardson Extrapolation. NIG model with parameters from [69]. Values obtained by quadratic APROJ with $P = 7, \bar{P} = 4$, and seven point rule. ASCOS values given in [138].

	$W = 90$		$W = 100$	
d	ASCOS	APROJ	ASCOS	APROJ
1	–	12.67415	–	5.11827
2	–	12.67441	–	5.11855
3	–	12.67443	–	5.11859
4	12.6748	12.67443	5.1191	5.11859
5	12.6744	12.67443	5.1186	5.11859
6	12.6743	12.67443	5.1185	5.11859

6.4.4 Continuous Monitoring

As a final extension, we consider the case of continuously monitored contracts, with terminal payoffs

$$g(S) = \begin{cases} \left(\frac{1}{T}\int_0^T S(t)dt - W\right)^+ & \text{for a call,} \\ \left(W - \frac{1}{T}\int_0^T S(t)dt\right)^+ & \text{for a put.} \end{cases}$$

Let $\mathcal{V}_N(M)$ denote the discretely monitored value approximation with M monitoring dates, and with N fixed. By fixing a positive integer d, the continuously monitored option value can be approximated by a four-point Richardson extrapolation:

$$\mathcal{V}_N^\infty(d) := \frac{1}{21}\left(64\mathcal{V}_N(2^{d+3}) - 56\mathcal{V}_N(2^{d+2}) + 14\mathcal{V}_N(2^{d+1}) - \mathcal{V}_N(2^d)\right),$$

as demonstrated in [138]. We compare the extrapolation procedure[18], when applied with APROJ, to the values obtained by [138] in Table 29. For both strikes, agreement in prices is to at least three decimals.

6.5 Error Analysis

In this section, we provide a stability analysis of the error propagation of ChFs for $1 \leq m \leq M$, after which we conclude with the terminal valuation error for pricing options on the arithmetic average.

Recall that the characteristic functions for Levy processes of interest satisfy

$$|\phi_{R_{\Delta_t}}(\xi)| \leq \kappa \exp(-\Delta_t c|\xi|^\nu), \quad \xi \in \mathbb{R}. \tag{246}$$

[18]For greatest efficiency, a common $\bar{\Psi}$ can be used for all four settings of M in the extrapolation procedure, by perturbing the means slightly so they align.

For the BSM, KOU (double exponential), and MJD (Merton's Jump Diffusion) models from Table 43, the ChF of log return satisfies $|\phi_{R_{\Delta_t}}(\xi)| \leq \exp\left(-\Delta_t \frac{\sigma^2}{2}|\xi|^2\right)$, so equation (193) holds with $\nu = 2$ and $c = \frac{\sigma^2}{2}$. For the CGMY model, $\nu = Y$ and c can be taken as $c = 2C|\Gamma(-Y)\cos(\pi Y/2)| \cdot \epsilon$, for any $\epsilon \in (0,1)$. With the Normal Inverse Gaussian (NIG) model, $\nu = 1$ and $c = \delta$. For the pure jump VG, $|\phi_{R_{\Delta_t}}(\xi)| \leq \kappa|\xi|^{-2\Delta_t/\nu}$, so that $\phi_{R_{\Delta_t}}$ fails to be integrable for $\Delta_t \leq \nu/2$. However, by adding a Brownian motion component, $-\frac{\sigma^2}{2}\xi^2$, equation (193) is satisfied with $\nu = 2$. We have the following Corollary of Proposition 6.2.1.

Corollary 6.5.1. *Suppose that $\phi_{R_{\Delta_t}}(\xi) \in \mathcal{H}(\mathcal{D}_d)$ for some $d > 0$. Fix $a = 2^P$ and $N = a \cdot \bar{a}$, where $\bar{a} = 2^{\bar{P}}$ for $\bar{P} > 1 + \log_2|\bar{\mu}_M|$. Assume for some $c, \kappa > 0$ and $\nu \in (0,2]$, $\phi_{R_{\Delta_t}}(\xi)$ satisfies equation(246). Then for some $0 < \gamma \leq d$, and a constant $C_M = \mathcal{O}(\max_{m=1,\ldots,M}\|\phi_{Y_m}\|^{\mathcal{H}_d})$,*

$$\sup_{1\leq n\leq N}\left|a^{1/2}C_{a,N}\cdot\breve{\beta}^m_{a,n} - \langle f_{Y_m}, \widetilde{\varphi}_{a,n}\rangle\right| \leq \frac{a^{-1/2}}{\pi}\left(C_M\frac{e^{-(\bar{a}-2|\bar{\mu}_M|)\gamma/2}}{1-e^{-\bar{a}\gamma}} + \tau_a(R_{\Delta_t})\right) \tag{247}$$

independently of $1 \leq m \leq M$ where $\tau_a(R_{\Delta_t}) = \mathcal{O}(a\exp(-\Delta tc\cdot(2\pi a)^\nu))$ is as in equation (200). For large enough $a > 0$, and $d < \infty$, γ will approach d.

6.5.1 Error Propagation

We can now state the core result concerning the propagation of ChF error for a given number of monitoring dates M.

Proposition 6.5.1. *Suppose that $\phi_{R_{\Delta_t}}(\xi) \in \mathcal{H}(\mathcal{D}_d)$ for some $d > 0$, and consider a p^{th} order B-spline basis generated by φ. Fix $a = 2^P$ and $N = a \cdot \bar{a}$, where $\bar{a} = 2^{\bar{P}}$ for $\bar{P} > 1 + \log_2|\bar{\mu}_M|$. Assume for some $c, \kappa > 0$ and $\nu \in (0,2]$, the tail of $\phi_{R_{\Delta_t}}(\xi)$ satisfies equation (246). The terminal ChF error satisfies $\epsilon(\bar{\phi}_{Y_M}(\xi_1)) = 0$ and*

$$|\epsilon(\bar{\phi}_{Y_M}(\xi_j))| = \mathcal{O}\left(\Delta^{(p+1)}\cdot e^{-\tilde{c}\Delta_t\left(\frac{(j-1)}{\bar{a}}\right)^\nu}\bar{a}^{1/2}\|\xi^{(p+1)}\phi_{R_{\Delta_t}}(\xi)\|_2\right), \quad 2 \leq j \leq N, \tag{248}$$

where $\tilde{c} := (2\pi)^\nu c$. The dependence on M is governed by the behavior of $\phi_{R_{\Delta t}}$.

Proof. Fix any $\xi \geq 0$, and let $G := \cup_{m=1,..,M}G_m$ the full truncated integration range implied by $\bar{P}$, where $G_m = [\bar{\mu}_m - \frac{\bar{a}}{2}, \bar{\mu}_m + \frac{\bar{a}}{2}]$. To manage notation, we will suppress the

dependence of certain objects on m. For example, we assume by the indexing on $\bar{\beta}_n^m$ that the corresponding elements $\varphi_{a,n}$ have been shifted appropriately.

We start by fixing $m \geq 3$, for which

$$\begin{aligned}
\epsilon(\bar{\phi}_{Z_{m-1}}(\xi)) &:= \phi_{Z_{m-1}}(\xi) - \bar{\phi}_{Z_{m-1}}(\xi) \\
&= \int_{\mathbb{R}} (e^y+1)^{i\xi} f_{Y_{m-1}}(y)dy - C_{a,N} \sum_{n=1}^{N} \bar{\beta}_n^{m-1} \bar{\Psi}(\xi, n) \\
&= \int_{\mathbb{R}/G_{m-1}} (e^y+1)^{i\xi} f_{Y_{m-1}}(y)dy \\
&+ \left(\int_{G_{m-1}} (e^y+1)^{i\xi} f_{Y_{m-1}}(y)dy - C_{a,N} \sum_{n=1}^{N} \beta_n^{m-1} \Psi(\xi, n) \right) \\
&+ C_{a,N} \sum_{n=1}^{N} \beta_n^{m-1} (\Psi(\xi, n) - \bar{\Psi}(\xi, n)) + C_{a,N} \sum_{n=1}^{N} \bar{\Psi}(\xi, n)(\beta_n^{m-1} - \bar{\beta}_n^{m-1}) \\
&:= \big(\tau(G_{m-1}) + J_1^{m-1}(\xi) + J_2^{m-1}(\xi)\big) + J^{m-1}(\xi),
\end{aligned}$$

where the error term $J^{m-1}(\xi)$ will be further split into two components. Here we have defined β_n^{m-1} so that $a^{1/2} C_{a,N} \beta_n^{m-1} = \langle f_{Y_{m-1}}, \widetilde{\varphi}_{a,n} \rangle$, from which

$$\widetilde{f}_{Y_{m-1}}(y) := a^{1/2} C_{a,N} \sum_{n=1}^{N} \beta_n^{m-1} \varphi_{a,n}(y)$$

is the true projection truncated to the set $\{\varphi_{a,n}\}_{n=1}^N$.

Since $|(e^y+1)^{i\xi}| = |\exp(i\xi \log(1+e^y))| = 1$, the truncation error satisfies

$$\tau(G_{m-1}) = \int_{\mathbb{R}/G_{m-1}} (e^y+1)^{i\xi} f_{Y_{m-1}}(y)dy \leq \int_{\mathbb{R}/G_{m-1}} f_{Y_{m-1}}(y)dy \leq \tau_M(G),$$

for $m = 1, \ldots, M$, where $\tau_M(G)$ bounds the largest such truncation error (typically, $\tau_M(G) \approx \tau(G_1)$, since f_R has the heaviest tails). The next result characterizes the convergence of J_1^{m-1}, which is governed by the projection error.

Lemma 6.5.2. *For $\xi \in \mathbb{R}$, $1 \leq m \leq M$, and $C_1(R_{\Delta_t}) := C_1(\varphi) \cdot \|\xi^2 \phi_{R_{\Delta_t}}(\xi)\|_2/(2\pi)$, J_1^{m-1} satisfies*

$$|J_1^{m-1}(\xi)| \leq \sqrt{a} \cdot C_1(R_{\Delta_t}) \Delta^{(p+1)},$$

with the constant $C_1(\varphi)$ from (250), independent of $\phi_{R_{\Delta_t}}$.

Proof. In particular, by Cauchy-Schwartz

$$\begin{aligned} J_1^{m-1}(\xi) &= \int_{G_{m-1}} (e^y+1)^{i\xi} f_{Y_{m-1}}(y)dy - C_{a,N}\sum_{n=1}^{N}\beta_n^{m-1}\Psi(\xi,n) \\ &= \int_{G_{m-1}} (e^y+1)^{i\xi}\left(f_{Y_{m-1}}(y) - a^{1/2}C_{a,N}\sum_{n=1}^{N}\beta_n^{m-1}\varphi_{a,n}(y)\right)dy \\ &\leq \|(e^y+1)^{i\xi}\|_2^{G_{m-1}} \cdot \|f_{Y_{m-1}} - \widetilde{f}_{Y_{m-1}}\|_2^{G_{m-1}} \\ &\leq \|(e^y+1)^{i\xi}\|_2^{G_{m-1}} \cdot \|f_{Y_{m-1}} - P_{\mathcal{M}_a} f_{Y_{m-1}}\|_2^{\mathbb{R}}. \end{aligned}$$

To characterize the convergence rate of density projections onto B-spline bases, we note that φ is Riesz generator which satisfies

$$\widehat{\varphi}(0) = 1, \quad \text{and for } m \in \{0,1\}, \quad \widehat{\varphi}^{(m)}(2\pi k) = 0, \quad k \in \mathbb{Z}/\{0\}, \tag{249}$$

where $\widehat{\varphi}^{(m)}$ denotes the mth derivative of φ. In particular, the p^{th} order B-spline generator φ is a $(p+1)^{th}$ *order Riesz generator*. It then follows that for any $f_X \in L^2(\mathbb{R})$, the projection error satisfies

$$\inf_{f_a \in \mathcal{M}_a} \|f_X - f_a\|_2 \leq \|f_X - P_{\mathcal{M}_a} f_X\|_2 \leq C_1(\varphi) a^{-(p+1)} \|f_X^{(p+1)}\|_2, \tag{250}$$

where $C_1(\varphi)$ is a constant independent of f_X (see [**?**]). It follows that

$$\|f_{Y_m}^{(p+1)}\|_2 = \frac{1}{2\pi}\|\mathcal{F}[f_{Y_m}^{(p+1)}]\|_2 = \frac{1}{2\pi}\|(-i\xi)^{(p+1)}\phi_{Y_m}(\xi)\|_2 \leq \frac{1}{2\pi}\|\xi^{(p+1)}\phi_{R_{\Delta_t}}(\xi)\|_2 < \infty, \tag{251}$$

since for $\xi \in \mathbb{R}$, $|\phi_{Y_m}(\xi)| \leq |\phi_{R_{\Delta_t}}(\xi)|$, and the $(p+1)^{th}$ moment is finite by exponential decay of $\phi_{R_{\Delta_t}}(\xi)$. Thus if we define $C_1(R_{\Delta_t})$ as in the statement of the Lemma,

$$\|f_{Y_{m-1}} - P_{\mathcal{M}_a} f_{Y_{m-1}}\|_2^{\mathbb{R}} \leq C_1(R_{\Delta_t})\Delta^{(p+1)}, \quad \forall m \geq 2.$$

Hence, for $m \geq 2$ and $\xi \in \mathbb{R}$

$$|J_1^{m-1}(\xi)| \leq \|(e^y+1)^{i\xi}\|_2^{G_{m-1}} C_1(R_{\Delta_t})\Delta^{(p+1)} \leq \sqrt{\bar{a}} \cdot C_1(R_{\Delta_t})\Delta^{(p+1)},$$

since $|(e^y+1)^{i2\xi}| = 1$ and $|G_{m-1}| \leq \bar{a}$. □

Remark 14. We should note that, while the bound in (251) is chosen to be independent of m, the behavior of this term is truly a decreasing function of m, although is difficult to quantify. This can be seen by examining the behavior of ϕ_{Y_m} from the approximations given in Figure 29 for a CGMY model.

The next source of error materializes from the approximation of Ψ by $\bar{\Psi}$.

Lemma 6.5.3. *For $\xi \in \mathbb{R}$ $1 \leq m \leq M$, and $C_2(R_{\Delta_t}) := C_2(\varphi)\|\phi_{R_{\Delta_t}}\|_2/2\pi$,*

$$|J_2^{m-1}(\xi)| \leq \sqrt{\bar{a}} \cdot \epsilon(\bar{\Psi}) C_2(R_{\Delta_t}), \tag{252}$$

where the constant $C_2(\varphi)$ is the lower frame bound defined in equation (195) *for the piecewise linear basis, and*

$$\epsilon(\bar{\Psi}) := \sup\{|\Psi(\xi_j, n) - \bar{\Psi}(\xi_j, n)| : 1 \leq j \leq N, 1 \leq n \leq N + N_{M-1}\}.$$

Proof. By the discrete version of Cauchy-Schwartz,

$$\begin{aligned} J_2^{m-1}(\xi) &= C_{a,N} \sum_{n=1}^{N} \beta_n^{m-1} (\Psi(\xi, n) - \bar{\Psi}(\xi, n)) \\ &\leq a^{-1/2} \left(\sum_{n=1}^{N} \left(\Psi(\xi, n) - \bar{\Psi}(\xi, n) \right)^2 \right)^{1/2} \left(\sum_{n=1}^{N} \left(a^{1/2} C_{a,N} \beta_n^{m-1} \right)^2 \right)^{1/2} \\ &\leq \sqrt{\bar{a}} \cdot \epsilon(\bar{\Psi}) \cdot \Big(\sum_{n \in \mathbb{Z}} |\langle f_{Y_{m-1}}, \widetilde{\varphi}_{a,n} \rangle|^2 \Big)^{1/2} \leq \sqrt{\bar{a}} \cdot \epsilon(\bar{\Psi}) \cdot C_2(\varphi) \| f_{Y_{m-1}} \|_2. \end{aligned}$$

The term $C_2(\varphi)\|f_{Y_{m-1}}\|_2$ follows from Bessel's inequality, which is the upper *frame bound* corresponding to the piecewise linear basis. Noting that

$$\|f_{Y_{m-1}}\|_2 = \|\phi_{Y_{m-1}}\|_2/2\pi \leq \|\phi_{R_{\Delta_t}}\|_2/2\pi,$$

we have

$$|J_2^{m-1}(\xi)| \leq \sqrt{\bar{a}} \cdot \epsilon(\bar{\Psi}) \cdot C_2(\varphi) \|\phi_{R_{\Delta_t}}\|_2/2\pi.$$

□

Remark 15. While the definition of $\epsilon(\bar{\Psi})$ is made so that we obtain an overall convergence rate in Δ when $\bar{a}$ has been fixed and a sufficiently accurate quadrature rule has been selected, the the error in $\bar{\Psi}$ tends to be much smaller for $\xi_j \in [0, 2\pi a]$ near zero than for ξ_j near $2\pi a$. If we define

$$\epsilon_j(\bar{\Psi}_{m-1}) := \sup_{1 \leq n \leq N} |\Psi(\xi_j, N_{m-1} + n) - \bar{\Psi}(\xi_j, N_{m-1} + n)|$$

then $J_2^{m-1}(\xi_j) \leq \epsilon_j(\bar{\Psi}_{m-1})\sqrt{\bar{a}} \cdot C_2(R_{\Delta_t})$. This is more than offset, however, when multiplied by $\phi_{R_{\Delta_t}}(\xi_j)$ to obtain the error in $\bar{\phi}_{Y_m}$, since $\phi_{R_{\Delta_t}}(\xi_j)$ is close to one for ξ_j near zero, and

decays exponentially for larger ξ_j. In practice, the contribution of $\epsilon(\bar{\Psi})$ is dominated by the projection error when using a seven-point Newton-Cote's rule. Although Boole's rule is often sufficient (and cheaper) for $M \leq 52$, we opt for the more conservative seven-point rule in general.

For the final term, which reflects the discrete Fourier transform error inherent in $\bar{\beta}^m$, we have

$$J^{m-1}(\xi) := C_{a,N} \sum_{n=1}^{N} \bar{\Psi}(\xi, n)(\beta_n^{m-1} - \bar{\beta}_n^{m-1}) = a^{-1/2} \sum_{n=1}^{N} \bar{\Psi}(\xi, n) \cdot \epsilon(\bar{\beta}_n^{m-1}),$$

where $\epsilon(\bar{\beta}_n^{m-1}) := a^{1/2} C_{a,N}(\beta_n^{m-1} - \bar{\beta}_n^{m-1})$.

Lemma 6.5.4. *The error source $J^{m-1}(\xi)$ can be bounded by*

$$|J^{m-1}(\xi)| \leq \frac{\bar{a}}{\pi} \epsilon^M(a, \bar{a}) + C(J_4) \cdot \epsilon(\bar{\phi}_{Z_{m-2}}) a^{-1/2} |\bar{\phi}_{Z_1}(\xi)| \tag{253}$$

where $C(J_4)$ is a constant, and

$$\epsilon^M(a, \bar{a}) := C_M \frac{e^{-(\bar{a} - 2|\bar{\mu}_M|)\gamma/2}}{1 - e^{-\bar{a}\gamma}} + \tau_a(R_{\Delta_t}). \tag{254}$$

Proof. Splitting $\epsilon(\bar{\beta}_n^{m-1})$ in terms of the discrete Fourier transform and ChF errors, where $a^{1/2} C_{a,N} \breve{\beta}_n^{m-1}$ is the discrete Fourier transform approximation using the true $\phi_{Y_{m-1}}$ (see equation (198)), it follows that

$$\begin{aligned} \epsilon(\bar{\beta}_n^{m-1}) &= \left(\langle f_{Y_{m-1}}, \widetilde{\varphi}_{a,n} \rangle - a^{1/2} C_{a,N} \breve{\beta}_n^{m-1} \right) + a^{1/2} C_{a,N} \left(\breve{\beta}_n^{m-1} - \bar{\beta}_n^{m-1} \right) \\ &:= \epsilon_1(\bar{\beta}_n^{m-1}) + \epsilon_2(\bar{\beta}_n^{m-1}). \end{aligned}$$

Hence,

$$\epsilon(\bar{\phi}_{Z_{m-1}}(\xi)) = \left(\tau(G_{m-1}) + J_1^{m-1}(\xi) + J_2^{m-1}(\xi) + J_3^{m-1}(\xi) \right) + J_4^{m-1}(\xi),$$

where we have defined

$$J_3^{m-1}(\xi) := a^{-1/2} \sum_{n=1}^{N} \bar{\Psi}(\xi, n) \cdot \epsilon_1(\bar{\beta}_n^{m-1}), \quad J_4^{m-1}(\xi) := a^{-1/2} \sum_{n=1}^{N} \bar{\Psi}(\xi, n) \cdot \epsilon_2(\bar{\beta}_n^{m-1}).$$

Moreover, for the Newton-Cotes quadrature rules, $|\bar{\Psi}(\xi_j, n)| \leq 1$ for any $1 \leq j, n \leq N$, and by Corollary 6.5.1

$$|\epsilon_1(\bar{\beta}_n^{m-1})| \leq \frac{a^{-1/2}}{\pi} \epsilon^M(a, \bar{a}),$$

where $\epsilon^M(a,\bar{a})$ is defined in equation (254).

Hence,

$$|J_3^{m-1}(\xi_j)| \leq \frac{a^{-1/2}}{\pi}\epsilon^M(a,\bar{a}) \cdot a^{-1/2}\sum_{n=1}^{N}|\bar{\Psi}(\xi_j,n)| \leq \frac{\bar{a}}{\pi}\epsilon^M(a,\bar{a})$$

Note that $J_4^{m-1}(\xi)$ alone depends on $\epsilon(\bar{\phi}_{Z_{m-2}}(\xi_j))$, since

$$\begin{aligned}\epsilon_2(\bar{\beta}_n^{m-1}) &= \frac{a^{-1/2}}{\pi}\Re\left(\Delta_\xi {\sum_{j=1}^{N}}' h_{a,n}(\xi_j)\left(\phi_{Y_{m-1}}(\xi_j) - \bar{\phi}_{Y_{m-1}}(\xi_j)\right)\right)\\ &= \frac{a^{-1/2}}{\pi}\Re\left(\Delta_\xi {\sum_{j=1}^{N}}' h_{a,n}(\xi_j)\phi_{R_{\Delta_t}}(\xi_j)\epsilon(\bar{\phi}_{Z_{m-2}}(\xi_j))\right), \end{aligned} \tag{255}$$

where $h_{a,n}(\xi)$ and $h_a(\xi)$ are defined in equation (260) for the linear basis (and in general is determined by $\widehat{\bar{\varphi}}(\xi)$), and $\sum'$ indicates that the first and last terms in the sum are halved. If we define $\epsilon(\bar{\phi}_{Z_{m-2}}) := \max_{1\leq j\leq N}|\epsilon(\bar{\phi}_{Z_{m-2}}(\xi_j))|$, it follows that

$$\left|\Re\left(\Delta_\xi {\sum_{j=1}^{N}}' h_{a,n}(\xi_j)\phi_{R_{\Delta_t}}(\xi_j)\epsilon(\bar{\phi}_{Z_{m-2}}(\xi_j))\right)\right| \leq \epsilon(\bar{\phi}_{Z_{m-2}})\Delta_\xi {\sum_{j=1}^{N}}' h_a(\xi_j)\Re(\phi_{R_{\Delta_t}}(\xi_j)),$$

which is bounded above for all N and a, since $\Re(\phi_{R_{\Delta_t}})$ admits an upper frame bound. To derive an upper bound on $J_4^{m-1}(\xi)$, we recall the dependence of $\bar{\Psi}$ and $h_{a,n}$ on $m-1$ (through the shift x_1^{m-1}, denoted by $h_{a,n}^{m-1}$), from which equation (255) yields

$$\begin{aligned} J_4^{m-1}(\xi) &= a^{-1/2}\sum_{n=1}^{N}\bar{\Psi}_{m-1}(\xi,n)\cdot\epsilon_2(\bar{\beta}_n^{m-1})\\ &= a^{-1/2}\sum_{n=1}^{N}\bar{\Psi}_{m-1}(\xi,n)\frac{a^{-1/2}}{\pi}\Re\left(\Delta_\xi {\sum_{j=1}^{N}}' h_{a,n}^{m-1}(\xi_j)\phi_{R_{\Delta_t}}(\xi_j)\epsilon(\bar{\phi}_{Z_{m-2}}(\xi_j))\right)\\ &= \mathcal{O}\left(\frac{\epsilon(\bar{\phi}_{Z_{m-2}})}{a^{1/2}}\left|\sum_{n=1}^{N}\bar{\Psi}_{m-1}(\xi,n)\frac{a^{-1/2}}{\pi}\Re\left(\Delta_\xi {\sum_{j=1}^{N}}' h_{a,n}^{m-1}(\xi_j)\phi_{R_{\Delta_t}}(\xi_j)\right)\right|\right)\\ &= \mathcal{O}\left(\frac{\epsilon(\bar{\phi}_{Z_{m-2}})}{a^{1/2}}\left|\sum_{n=1}^{N}\bar{\Psi}_{m-1}(\xi,n)\cdot a^{1/2}C_{a,N}\bar{\beta}^1_{N_{m-1+n}}\right|\right). \end{aligned}$$

As a final simplification, we note that

$$J_4^{m-1}(\xi) = \mathcal{O}\left(\epsilon(\bar{\phi}_{Z_{m-2}})a^{-1/2}\left|\sum_{n=1}^{N}\bar{\Psi}(\xi,n)a^{1/2}C_{a,N}\bar{\beta}^1_n\right|\right) \leq \frac{C(J_4)}{a^{1/2}}\cdot\epsilon(\bar{\phi}_{Z_{m-2}})|\bar{\phi}_{Z_1}(\xi)|,$$

for some $C(J_4)$. To see that $C(J_4)$ can be chosen independently of N_{m-1}, from the decay of $\phi_{R_{\Delta_t}}(\xi)$, it follows that $f_{R_{\Delta_t}} \in C^\infty(\mathbb{R})$ has exponential decay at infinity, along with all of its derivatives [18] (see also [120]). □

Summarizing the obtained bounds, it follows that

$$\begin{aligned}|\epsilon(\bar{\phi}_{Z_{m-1}}(\xi))| &= \left|\big(\tau(G_{m-1}) + J_1^{m-1}(\xi) + J_2^{m-1}(\xi) + J_3^{m-1}(\xi)\big) + J_4^{m-1}(\xi)\right| \\ &\leq C^M(a,\bar{a}) + B(a,\xi)\epsilon(\bar{\phi}_{Z_{m-2}}).\end{aligned}$$

where

$$C^M(a,\bar{a}) := \tau_M(G) + \sqrt{\bar{a}}\cdot C_1(R_{\Delta_t})\Delta^{(p+1)} + \sqrt{\bar{a}}\cdot C_2(R_{\Delta_t})\epsilon(\bar{\Psi}) + \frac{\bar{a}}{\pi}\epsilon^M(a,\bar{a}), \tag{256}$$

and $B(a,\xi) := C(J_4)|\bar{\phi}_{Z_1}(\xi)|a^{-1/2}$. Iterating from $M-1$ we obtain

$$\begin{aligned}|\epsilon(\bar{\phi}_{Z_{M-1}}(\xi))| &\leq C^M(a,\bar{a})\sum_{j=0}^{M-3} B(a,\xi)^j + B(a,\xi)^{M-2}\epsilon(\bar{\phi}_{Z_1}) \\ &= C^M(a,\bar{a})\frac{1-B(a,\xi)^{M-2}}{1-B(a,\xi)} + B(a,\xi)^{M-2}\epsilon(\bar{\phi}_{Z_1}).\end{aligned}$$

Moreover, the error in $\bar{\phi}_{Z_1}$ satisfies

$$\begin{aligned}\epsilon(\bar{\phi}_{Z_1}(\xi)) &:= \phi_{Z_1}(\xi) - \bar{\phi}_{Z_1}(\xi) \\ &= \int_{\mathbb{R}}(e^y+1)^{i\xi} f_{R_{\Delta_t}}(y)dy - C_{a,N}\sum_{n=1}^{N}\bar{\beta}_n^1\bar{\Psi}(\xi,n) \\ &= \int_{\mathbb{R}/G_1}(e^y+1)^{i\xi} f_{R_{\Delta_t}}(y)dy \\ &+ \left(\int_{G_1}(e^y+1)^{i\xi} f_{R_{\Delta_t}}(y)dy - C_{a,N}\sum_{n=1}^{N}\beta_n^1\Psi(\xi,n)\right) \\ &+ C_{a,N}\sum_{n=1}^{N}\beta_n^1(\Psi(\xi,n)-\bar{\Psi}(\xi,n)) + C_{a,N}\sum_{n=1}^{N}\bar{\Psi}(\xi,n)(\beta_n^1-\bar{\beta}_n^1) \\ &:= \big(\tau(G_1) + J_1^1(\xi) + J_2^1(\xi)\big) + J_3^1(\xi),\end{aligned}$$

where we note that $\bar{\beta}_n^1 = \breve{\beta}_n^1$, since $\phi_{R_{\Delta t}}(\xi)$ is known exactly. Hence $\epsilon(\bar{\phi}_{Z_1}) \leq C^M(a,\bar{a})$, from which we derive

$$\begin{aligned}|\epsilon(\bar{\phi}_{Z_{M-1}}(\xi))| &\leq \frac{C^M(a,\bar{a})}{1-B(a,\xi)}\left(1-B(a,\xi)^{M-2} + (1-B(a,\xi))B(a,\xi)^{M-2}\right) \\ &\leq C^M(a,\bar{a})\frac{1-B(a,\xi)^{M-1}}{1-B(a,\xi)} \leq 2C^M(a,\bar{a}),\end{aligned} \tag{257}$$

for a sufficiently large.

The behavior of $C^M(a,\bar{a})$ can be characterized by noting that with $\bar{a}$ chosen sufficiently large, the truncation error $\tau_M(G)$ is dominated by the other sources. Further, as $\epsilon(\bar{\Psi})$ can be made negligible by a sufficient choice of quadrature, and $\epsilon^M(a,\bar{a})$ converges exponentially in $\bar{a}, a$, the error behaves like $\mathcal{O}(\Delta^{(p+1)})$, which is the projection convergence with respect to the B-spline basis of order p. In particular, from equation (256) we have

$$C^M(a,\bar{a}) = \mathcal{O}(\sqrt{\bar{a}} \cdot C_2(R_{\Delta_t})\Delta^{(p+1)}).$$

Recalling that $\bar{\phi}_{Y_M} = \bar{\phi}_{Z_{M-1}}\phi_{R_{\Delta t}}$,

$$|\epsilon(\bar{\phi}_{Y_M}(\xi_j))| \leq 2C^M(a,\bar{a}) \cdot |\phi_{R_{\Delta_t}}(\xi_j)| = \mathcal{O}(\sqrt{\bar{a}} \cdot \Delta^{(p+1)}|\phi_{R_{\Delta_t}}(\xi_j)|), \quad 2 \leq j \leq N,$$

where we note that $\epsilon(\bar{\phi}_{Y_M}(\xi_1)) = 0$, since $\bar{\phi}_{Y_M}(\xi_1) = 1$ is enforced by the algorithm. Equation (248) then follows from the assumed decay of $\phi_{R_{\Delta_t}}$. □

6.5.2 Valuation Error

The terminal valuation error for a contract on the arithmetic average is now characterized. We show that for bounded payoffs[19] (as for a put, with put-call parity to price a call), the error converges on the order of projection error, $\mathcal{O}(\Delta^{(p+1)})$. If we define $\mathcal{E}(\mathcal{V}_N) := e^{rT}\left(\mathcal{V} \circ g(S_0) - \mathcal{V}_N \circ g(S_0)\right)$, we obtain

$$\begin{aligned}
\mathcal{E}(\mathcal{V}_N) &= \int_{\mathbb{R}} g(y) f_{Y_M}(y)dy - C_{a,N}\sum_{n=1}^{N} \bar{\beta}_n^M g_n \\
&= \int_{\mathbb{R}/G_M} g(y) f_{Y_M}(y)dy + \left(\int_{G_M} g(y) f_{Y_M}(y)dy - C_{a,N}\sum_{n=1}^{N} \beta_n^M g_n\right) \\
&\quad + C_{a,N}\sum_{n=1}^{N}\left(\beta_n^M - \breve{\beta}_n^M + \breve{\beta}_n^M - \bar{\beta}_n^M\right) g_n := \tilde{\tau}_M(G) + \mathcal{E}_1 + \mathcal{E}_2.
\end{aligned}$$

Assuming g is bounded, we have

$$\tilde{\tau}_M(G) = \int_{\mathbb{R}/G_M} g(y) f_{Y_M}(y)dy \leq \|g\|_\infty \cdot \mathbb{P}[Y_M \in G_M^c] = \|g\|_\infty \cdot \tau_M(G),$$

which is controlled by the choice of $\bar{a}$ sufficiently large.[20]

[19] This assumption is not essential, although it simplifies the analysis.

[20] For unbounded g, as long as the price is finite, the integral $\int_{\mathbb{R}} g(y) f_{Y_M}(y)dy < \infty$, hence $\int_{\mathbb{R}/G_M} g(y) f_{Y_M}(y)dy \to 0$ as $G_M \uparrow \mathbb{R}$. That is, $\tau_M(G) \to 0$ as the truncation error decreases.

Since the coefficients g_n are exact[21], the second source of error satisfies

$$\begin{aligned}\mathcal{E}_1 &= \int_{G_M} g(y) f_{Y_M}(y) dy - C_{a,N} \sum_{n=1}^{N} \beta_n^M g_n \\ &= \int_{G_M} g(y) f_{Y_M}(y) dy - \sum_{n=1}^{N} \langle f_{Y_M}, \widetilde{\varphi}_{a,n} \rangle \int_{G_M} g(y) \varphi_{a,n}(y) dy \\ &= \int_{G_M} g(y) \left(f_{Y_M}(y) - \sum_{n=1}^{N} \langle f_{Y_M}, \widetilde{\varphi}_{a,n} \rangle \varphi_{a,n}(y) \right) dy \\ &\leq \|g\|_2^{G_M} \cdot \|f_{Y_M} - P_{\mathcal{M}_a} f_{Y_M}\|_2^{\mathbb{R}} = \mathcal{O}(\Delta^{(p+1)}). \end{aligned} \tag{258}$$

The third source of error, which accounts for the trapezoidal approximation to the projection coefficients as well as the terminal ChF error, satisfies

$$\begin{aligned}\mathcal{E}_2 &= C_{a,N} \sum_{n=1}^{N} \left(\beta_n^M - \breve{\beta}_n^M + \breve{\beta}_n^M - \bar{\beta}_n^M \right) g_n \\ &= \sum_{n=1}^{N} a^{1/2} C_{a,N} \left(\beta_n^M - \breve{\beta}_n^M + \breve{\beta}_n^M - \bar{\beta}_n^M \right) \cdot \int_{G_M} g(y) \varphi_{a,n}(y) dy.\end{aligned}$$

We will need the following result.

Lemma 6.5.5. *For any $N_M \in \mathbb{Z}$, it holds that*

$$\sum_{n=1}^{N} C_{a,N} \breve{\beta}_{N_M+n}^1 = \mathcal{O}(1),$$

where $\breve{\beta}_{N_M+n}^1$ are the DFT coefficients of $f_{R_{\Delta_t}}$ corresponding to x_n^M, which are absent of ChF error since $\phi_{R_{\Delta_t}}$ is known (these are not calculated explicitly). For $\bar{a}$ sufficiently large, $\tilde{a} > 0$ can be chosen so that the sum is strictly less than one $\forall a \geq \tilde{a}$.

Proof. We have the following bound

$$\begin{aligned}\sum_{n=1}^{N} C_{a,N} \breve{\beta}_{N_M+n}^1 &\leq \int_{G_M} \left(\sum_{n \in \mathbb{Z}} a^{1/2} C_{a,N} |\breve{\beta}_n^1| \cdot \varphi_{a,n}(y) \right) dy \\ &= \int_{G_M} |\breve{f}_R(y)| dy \leq \int_{G_M} |f_R(y)| dy + \int_{G_M} |\breve{f}_R(y) - f_R(y)| dy,\end{aligned}$$

and the result follows from Corollary 6.5.1 after applying Cauchy-Swartz inequality to the second integral, and a similar argument as the proof of Lemma 6.5.2. □

[21]For numerical reasons we have elected instead to use a more stable approximation than the exact coefficients.

We can now provide the convergence rate for the third error source.

Lemma 6.5.6. *The term $\mathcal{E}_2$ is characterized by*

$$\mathcal{E}_2 = O\left(C^M(a,\bar{a})\right), \tag{259}$$

where $C^M(a,\bar{a})$ is defined in equation (256)*.*

Proof. We consider each error $\epsilon_1(\bar{\beta}_n^M) := a^{1/2}C_{a,N}(\beta_n^M - \breve{\beta}_n^M)$ and $\epsilon_2(\bar{\beta}_n^M) := a^{1/2}C_{a,N}(\breve{\beta}_n^M - \bar{\beta}_n^M)$ in turn. Noting that, by Corollary 6.5.1

$$\sup_{1\leq n\leq N}|\epsilon_1(\bar{\beta}_n^M)| = a^{1/2}C_{a,N}\sup_{1\leq n\leq N}\left|\beta_n^M - \breve{\beta}_n^M\right| \leq \frac{a^{-1/2}}{\pi}\epsilon^M(a,\bar{a}),$$

where $\epsilon^M(a,\bar{a})$ is defined in equation (254), we have

$$\begin{aligned}
&\sum_{n=1}^{N} a^{1/2}C_{a,N}\left(\beta_n^M - \breve{\beta}_n^M\right)\int_{G_M} g(y)\varphi_{a,n}(y)dy \\
&\leq \left(\sum_{n=1}^{N}\left(\frac{a^{-1/2}}{\pi}\epsilon^M(a,\bar{a})\right)^2\right)^{1/2}\left(\sum_{n=1}^{N}\left(\int_{G_M} g(y)\varphi_{a,n}(y)dy\right)^2\right)^{1/2} \\
&= \frac{\bar{a}^{1/2}}{\pi}\epsilon^M(a,\bar{a})\cdot\left(\sum_{n=1}^{N}|\langle g\mathbb{1}_{G_M},\varphi_{a,n}\rangle|^2\right)^{1/2} \leq \frac{\bar{a}^{1/2}}{\pi}\epsilon^M(a,\bar{a})\cdot C_3(\varphi)\cdot\|g\|_2^{G_M},
\end{aligned}$$

where $C_3(\varphi)$ is the upper frame bound of the *dual basis*, $\{\widetilde{\varphi}_{a,n}\}_{n\in\mathbb{Z}}$, and is the inverse of the lower from bound of the "primal" basis[22]. Since $\|g\|_2^{G_M} \leq \|g\|_\infty \bar{a}^{1/2}$ (for bounded payoffs), the final inequality is on the order $\mathcal{O}(\bar{a}\epsilon^M(a,\bar{a}))$.

Considering $\epsilon_2(\bar{\beta}_n^M)$, we have (noting the dependence of $h_{a,n}^M(\xi_j)$ on the grid $\{x_n^M\}$)

$$\begin{aligned}
\epsilon_2(\bar{\beta}_n^M) &= \frac{a^{-1/2}}{\pi}\Re\left\{\Delta_\xi\sum_{j=1}^{N}{}'h_{a,n}^M(\xi_j)\phi_{R_{\Delta_t}}(\xi_j)\epsilon(\bar{\phi}_{Z_{M-1}}(\xi_j))\right\} \\
&= \mathcal{O}\Big(\frac{\epsilon(\bar{\phi}_{Z_{M-1}})}{a^{1/2}\pi}\Re\Big\{\Delta_\xi\sum_{j=1}^{N}{}'h_{a,n}^M(\xi_j)\phi_{R_{\Delta_t}}(\xi_j)\Big\}\Big) = \mathcal{O}\big(\epsilon(\bar{\phi}_{Z_{M-1}})\sqrt{a}C_{a,N}\breve{\beta}_{N_M+n}\big),
\end{aligned}$$

where $\epsilon(\bar{\phi}_{Z_{M-1}}) := \sup_{1\leq j\leq N}|\epsilon(\bar{\phi}_{Z_{M-1}}(\xi_j))|$. Hence,

$$\begin{aligned}
\sum_{n=1}^{N} g_n\frac{\epsilon_2(\bar{\beta}_n^M)}{a^{1/2}} &= \mathcal{O}\left(\epsilon(\bar{\phi}_{Z_{M-1}})\sum_{n=1}^{N}\left|\int_{G_M} g(y)\varphi_{a,n}(y)dy\right|a^{1/2}C_{a,N}\breve{\beta}_{N_M+n}\right) \\
&= \|g\|_\infty^{G_M}\epsilon(\bar{\phi}_{Z_{M-1}})\mathcal{O}\left(\sum_{n=1}^{N}a^{1/2}C_{a,N}\breve{\beta}_{N_M+n}\right) = \mathcal{O}\left(\|g\|_\infty^{G_M}\epsilon(\bar{\phi}_{Z_{M-1}})\right)
\end{aligned}$$

[22]Duality is used here to obtain a tighter bound, by a factor of $\bar{a}^{1/2}$, than if the standard techniques were applied, which in turn allows us to dominate this source of error by the one derived from $\epsilon_2(\bar{\beta}_n^M)$ next.

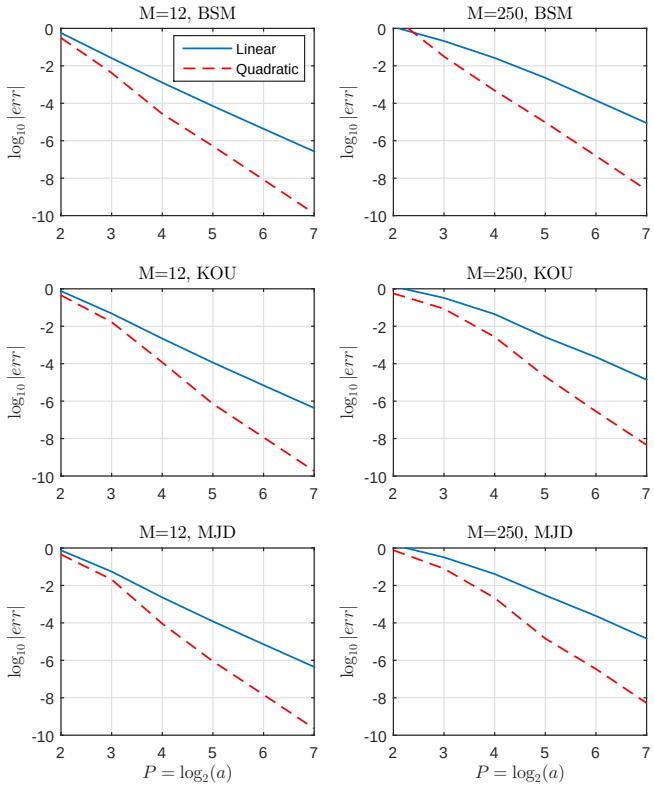

Figure 31: Convergence of linear vs. quadratic APROJ. Parameters as in [68]. Errors are max over strikes $\{90, 100, 110\}$. For MJD and BSM, $\bar{P} := \log_2(\bar{a}) = 3$; for KOU $\bar{P} = 4$. Reference values by linear APROJ with $P = 10$ given in Table 35.

by Lemma 6.5.5, and $\left|\int_{G_M} g(y)\varphi_{a,n}(y)dy\right| \leq \|g\|_\infty^{G_M} \int_{G_M} \varphi_{a,n}(y)dy = a^{-1/2}\|g\|_\infty^{G_M}$.

For bounded payoffs, $\|g\|_\infty^{G_M} \leq \|g\|_\infty < \infty$, and $\epsilon(\bar{\phi}_{Z_{M-1}}) = \mathcal{O}(C^M(a, \bar{a}))$ by equation (257). Hence, by the definition of $C^M(a, \bar{a})$,

$$\mathcal{E}_2 = \mathcal{O}\left(C^M(a, \bar{a}) + \bar{a}\epsilon^M(a, \bar{a})\right) = O\left(C^M(a, \bar{a})\right).$$

□

Remark 16. Combining equations (258) and (259), and assuming that $\bar{a}$ is chosen to make $\tau_M(G)$ (and hence $\tilde{\tau}_M(G)$) negligible, we conclude

$$\mathcal{V} \circ g(S_0) - \mathcal{V}_N \circ g(S_0) = \mathcal{O}\left(e^{-rT} \cdot C^M(a, \bar{a})\right) = \mathcal{O}(\Delta^{(p+1)}).$$

This of course requires that the error contributed by $\bar{\Psi}$ has been controlled by the choice

Table 30: Calibrated parameters from [42]; values reported here to an additional decimal, obtained by quadratic APROJ with $P = 9, \bar{P} = 3$. Other parameters: $M = 50$, $r = .04$, $q = 0$, $T = 1$.

Model (Param.)	vol	Calibrated Parameters	Strike 90	100	110
	0.1	(0.1)	11.581134	3.338617	0.273759
BSM	0.3	(0.3)	13.669816	7.698599	3.896399
(σ)	0.5	(0.5)	17.192393	12.091536	8.314413
	0.1	(0.1222, 0.0879, -0.1364)	11.640247	3.323853	0.158354
NIG	0.3	(0.1222, 0.2637, -0.4091)	13.700850	7.342655	3.278604
(ν, σ, θ)	0.5	(0.1222, 0.4395, -0.6819)	16.763062	11.235866	7.168361
	0.1	(0.2703, 17.56, 54.82, 0.8)	11.639881	3.324584	0.157877
CGMY	0.3	(0.6509, 5.853, 18.27, 0.8)	13.701604	7.347424	3.283082
(C, G, M, Y)	0.5	(0.9795, 3.512, 10.96, 0.8)	16.768352	11.244236	7.176236

of quadrature, a choice which may vary by basis. Figure 31 illustrates the difference in convergence rates for the APROJ method with linear and quadratic B-splines.

6.6 Numerical Experiments

A major improvement over the breakthrough pricing methods of Clewlow (1990), Benhamou (2002), and later Fusai and Meucci (2008), referred to as FM, was the improved convolution method of Cerny and Kyriakou (2009), referred to as CK. The method of CK represented a major improvement in speed[23], but also demonstrated that references prices reported by the other three are less precise than the four to five decimal places claimed, often correct to only two or three decimals. The ASCOS method of [138] is capable of obtaining precise estimates of prices, but it does not seem to compete with CK in terms of cpu time[24]. The primary drawbacks of ASCOS are its global basis functions, which require several hundred quadrature points per element of a matrix analogous to $\bar{\Psi}$, and the fixed truncation support (no mean-adjustment)[25]. We also compare to the recent method of Levendorskii and Xie [95], denoted LX, which takes two forms: LX(f) for the flat iFT method, and LX(p) for the parabolic iFT method[26]

[23]The results for CK were obtained in MATLAB 7.2 on Dell Latitude 620 Intel(R) Dual Core T7200, 2GHz, 2Gb RAM.

[24]The results for ASCOS were obtained in MATLAB 7.7 with Intel(R) Core(TM)2 Duo CPU E6550, 2.33GHz and 4MB cache size.

[25]The author's indicate that a grid adjustment is possible, but to do so would require re-computation of the matrix analogous to $\bar{\Psi}$ at each step (or every several steps), and would incur a substantial cost.

[26]The results of LX were obtained in MATLAB 7.11.0, with an Intel(R) Celeron(R) Processor T1600, 1.66GHz, 667MHz FSB and 1MB cache.

Through numerical experiments[27] we demonstrate that APROJ is not only highly accurate (on the level of CK and LX), but is also faster than the state-of-the-art methods to obtain the same or superior accuracy, typically on the order of a 10- to 100-fold improvement. This is true for both linear and quadratic implementations. Given that the initial peak of f_R is quickly softened to obtain f_{Y_m}, we find that quadratic APROJ is remarkably accurate for Asian option pricing, and is presented next. Numerical results for linear APROJ (not presented), are also impressive.

In the first few sets of experiments, to isolate the rate of convergence of APROJ, we conservatively fix $\bar{P} = 3$ for pure diffusion models, and $\bar{P} = 3 \sim 4$ for heavy-tailed models, such as CGMY and NIG. For most cases, a smaller value of $\bar{P}$ would have sufficed (especially with BSM experiments), and reduced the computation time.[28] Sensitivity of APROJ with respect to the choice of $\bar{P}$ is illustrated in Figure 33. The final set of experiments investigates the automated approach to parameter selection which is often much more efficient, improving cpu times even further.

Our first set of experiments compares the convergence and cpu time of APROJ against the method of CK for $M = 50$ and strikes $\{90, 100, 110\}$. The specifications considered are the log-normal, ie Black-Scholes-Merton (BSM), the Normal Inverse Gaussian (NIG), and the Carr-Geman-Madan-Yor (CGMY) model. Three test cases are considered for each model, with parameters calibrated by [42] to a fixed volatility (vol) in the set $\{0.1, 0.3, 0.5\}$. Recovered values, as well as calibrated parameters are provided for each strike in Table 30. For the NIG model, we use the alternative ChF form with parameters (ν, σ, θ) to maintain consistency with [42], which has Levy symbol

$$\psi_L(\xi) = \frac{1}{\nu}\left(1 - \sqrt{1 - 2\theta\nu i\xi + \nu\sigma^2\xi^2}\right).$$

In Table 31, we see rapid convergence of the quadratic APROJ method, which is implemented with the seven point rule and $\bar{P} = 3$. By $P = 5$, accuracy on the order e-07$\sim$e-09 is

[27] The results for APROJ were obtained in MATLAB 8.0 with Intel(R) Core(TM) i5-3470T CPU, 2.90GHz with 3MB cache size.

[28] Moreover, Boole's rule, which is faster than the seven point rule, obtains nearly identical results in many of the cases. However, it is safer in practice to use the more accurate method, so this is how we present the results.

Table 31: Parameters from CN [42]. For ARPOJ with $\bar{P} = 3$ and the seven point rule, each cpu pair $\cdot/\cdot$ reports the time to achieve an error of $\mathrm{TOL}_1/\mathrm{TOL}_2$, where TOL_1 is on the order of e-03∼e-04 and TOL_2 is on the order of e-06∼e-07. The error is taken as the maximum abs. error over the strike set $\{90, 100, 110\}$. CK prices are on the order of e-05∼e-06. Ref prices are provided in Table 30.

		Quadratic APROJ, $P = \log_2(a)$							APROJ	CK
	vol	1	2	3	4	5	6	7	cpu(sec)	cpu(sec)
BSM	.1	4.8e+00	1.1e+00	1.6e-01	7.3e-03	3.1e-05	2.4e-07	3.1e-09	.008/.202	1.0
	.3	3.8e+00	9.2e-02	8.8e-04	5.6e-06	6.2e-08	8.8e-10	1.3e-11	.003/.009	.3
	.5	1.7e+00	4.8e-03	3.0e-05	2.9e-07	3.9e-09	5.8e-11	9.5e-13	.001/.008	.3
NIG	.1	4.3e+00	1.1e+00	1.5e-01	1.7e-02	2.2e-04	1.3e-06	1.1e-08	.026/.203	3.7
	.3	2.9e+00	1.8e-01	6.4e-03	4.4e-05	1.4e-07	2.6e-09	3.9e-11	.003/.028	1.8
	.5	2.6e+00	2.1e-02	2.2e-04	1.6e-06	5.9e-09	6.8e-09	4.8e-09	.003/.009	1.8
CGMY	.1	3.3e+00	1.1e+00	1.5e-01	1.6e-02	2.2e-04	1.3e-06	9.9e-09	.027/.201	8.5
	.3	2.9e+00	1.7e-01	6.2e-03	4.2e-05	1.1e-07	2.4e-09	3.6e-11	.004/.027	4.1
	.5	3.0e+00	2.1e-02	2.1e-04	1.5e-06	3.9e-08	1.4e-08	7.7e-09	.004/.009	2.1

achieved for vol $\in \{0.3, 0.5\}$ and for all models. With $P = 7$, accuracy on the order e-08 is achieved for all models and levels of vol. In the far right column of Table 31 we provide the cpu times reported by [42] to achieve within four to five correct decimals, which are at least a factor of 10 more than the time required for APROJ to reach e-06∼e-07 accuracy (with only one exception), and are often *more than 100 times* that of APROJ. This is consistent across all models and specifications as well as strikes tested. Similar results hold for the linear implementation of APROJ.

For the set of experiments in Table 31 involving the CMGY (KoBoL) model, we can also compare our results to those of LX [95], using the parabolic method LX(p). When vol = 0.1, they report a max error of 6.7e-05 over strikes in $\{90, 100, 110\}$ at a cost of 1.581 seconds (compared to an APROJ accuracy of 1.3e-06 in 0.201 seconds). When vol =0.3, they achieve 3.9e-06 in 1.037 seconds (compared to 1.2e-07 in 0.027 seconds), and when vol =0.5 they achieve 4.6e-06 in 0.684 seconds (compared to 1.5e-06 in 0.009 seconds). In each of these cases, APROJ obtains greater accuracy and at the same time provides a 7.8, 38, and 76-fold time reduction respectively.

The second set of experiments compares the convergence and cpu time of APROJ against the ASCOS method for $M \in \{12, 50, 250\}$ and strikes $\{90, 100, 110\}$. For this case, we specify the NIG model with parameter set in [69],

$$(\alpha, \beta, \delta) = (6.1882, -3.8941, 0.1622), \quad r = 0.0367, \quad q = 0, \quad T = 1, \quad S_0 = 100,$$

Table 32: NIG parameters from FM [69], $(\alpha, \beta, \delta) = (6.1882, -3.8941, 0.1622)$, and $r = 0.0367, q = 0, T = 1, S_0 = 100$. Convergence for quadratic APROJ with $\bar{P} = 4$ and seven-point rule. Reference values obtained by quadratic APROJ with $P = 9, \bar{P} = 4$, and seven point rule.

		Quadratic APROJ, $P = \log_2(a)$							NIG
M	strike	1	2	3	4	5	6	7	reference
	90	5.3e-01	2.0e-01	6.4e-03	1.7e-04	3.4e-08	2.2e-09	3.8e-11	12.62243
12	100	1.9e+00	4.0e-01	1.9e-03	8.4e-04	8.4e-06	7.2e-08	1.1e-09	5.06060
	110	1.5e+00	3.0e-01	9.2e-03	9.1e-04	1.6e-05	6.3e-08	1.3e-09	1.01355
	90	6.6e-01	4.2e-01	4.3e-02	2.5e-03	1.9e-07	1.1e-09	6.6e-11	12.66126
50	100	2.3e+00	5.0e-01	1.4e-02	8.3e-03	2.7e-05	1.0e-07	1.9e-09	5.10370
	110	2.1e+00	6.1e-01	9.8e-02	2.3e-03	2.0e-04	7.6e-07	4.4e-09	1.03770
	90	3.3e-01	4.4e-01	5.6e-02	6.4e-03	6.6e-05	6.0e-07	2.3e-08	12.67176
250	100	1.9e+00	3.9e-01	3.6e-02	1.8e-02	3.6e-05	2.9e-06	1.7e-07	5.11556
	110	1.8e+00	6.2e-01	1.3e-01	1.1e-02	2.5e-04	3.7e-06	3.0e-07	1.04448

Table 33: NIG parameters from FM [69], $(\alpha, \beta, \delta) = (6.1882, -3.8941, 0.1622)$, and $r = 0.0367, q = 0, T = 1, S_0 = 100$. APROJ with $\bar{P} = 4$, seven point rule. Corresponding values of P for each accuracy are given in Table 32. Absolute errors for strike $W = 110$.

		ASCOS			Quadratic APROJ		
		$N = 128$	$N = 256$	$N = 384$	$\bar{P} = 4$		
M		$n_q = 200$	$n_q = 400$	$n_q = 600$	Seven-Point		
12	|err.|	2.0e-03	1.74e-04	5.16e-06	9.1e-04	1.6e-05	6.3e-08
	(sec)	(2.41)	(15.13)	(46.09)	(.017)	(.085)	(.314)
50	|err.|	2.26e-04	6.94e-05	2.17e-06	2.0e-04	7.6e-07	4.4e-09
	(sec)	(2.43)	(15.16)	(46.22)	(.190)	(.731)	(2.94)
250	|err.|	7.8e-03	9.33e-05	8.49e-06	2.5e-04	3.7e-06	2.8e-07
	(sec)	(2.42)	(15.23)	(46.68)	(.717)	(2.94)	(11.42)

Table 34: CGMY (KoBoL) Parameters from Levendorskii and Xie [95]: $S_0 = 100$, $M = 12$, $T = 1$, $r = 0.04$, $q = 0$, $CGMY = (1.1136, 3, 10, 0.2)$; in terms of KoBoL parameterization, $(c, \lambda_-, \lambda_+, \nu) = (1.1136, -10, 3, 0.2)$. Convergence for quadratic APROJ with $\bar{P} = 4$ and seven-point rule. Reference values obtained by quadratic APROJ with $P = 11, \bar{P} = 5$, and seven point rule, and verified to seven decimals with prices of [95]. The LX(f) and LX(p) methods are respectively the flat and parabolic Fourier transform methods of [95].

		Quadratic APROJ, $P = \log_2(a)$				LX(f)	LX(p)
strike	Ref.	2	3	4	5		
90	14.795530855	6.349e-02	1.161e-04	1.136e-05	9.312e-09	2.1e-07	2.1e-07
100	8.281218252	2.973e-02	2.641e-04	3.467e-05	7.533e-08	7.8e-07	7.8e-07
110	3.718094231	1.523e-01	1.040e-03	1.951e-04	5.002e-06	1.7e-06	1.8e-06
	cpu (sec)	0.003	0.007	0.016	0.082	27.77	0.792

and ChF given in Table 43 of the appendix. Table 32 reports the convergence of quadratic APROJ, along with the reference prices. Reference prices as well as reported cpu times are provided for $\bar{P} = 4$ and the seven point rule[29]. In Table 33 the performance of APROJ is compared to ASCOS, with similar findings as in the first set of experiments. For example, when $M = 12$, ASCOS requires 15.13 seconds to achieve 1.74e-04 accuracy, while APROJ reaches 1.6e-05 accuracy in 0.085 seconds, an almost 200-fold improvement. To reach 6.3e-08 accuracy takes APROJ 0.314 seconds compared to 46.09 seconds for ASCOS to reach 5.15e-06. For other cases of *comparable accuracy*, the improvement is by at least a factor of 10 or more.

We next consider a KoboL (CGMY) model from Levendorskii and Xie [95], with parameters $CGMY = (1.1136, 3, 10, 0.2)$, or in terms of the KoBoL [18, 20] parameterization $(c, \lambda_-, \lambda_+, \nu) = (1.1136, -10, 3, 0.2)$. As demonstrated in Table 34, the APROJ method converges rapidly to high accuracy. Two methods from [95] are provided for comparison, the LX(f) method and LX(p), neither of which seems to dominate the other in terms of speed or accuracy from the experiments provided in [95]. In this case, LX(f) is slower to converge (in terms of cpu), but for strikes $\{90, 100, 100\}$, both methods of [95] reach an accuracy of about (2.1e-07, 7.8e-07, 1.7e-06) respectively. The APROJ method with $P = 5$ achieves accuracy of (9.3e-09, 7.5e-08, 5.0e-06), with a cpu time reduction factor of 9.65 for the LX(p) method and a 338-fold reduction for LX(f).

[29]The necessarily larger value of $\bar{P}$ is detected by recovering the value of $\bar{\beta}_1^1$ prior to the algorithm's initialization.

Table 35: Model parameters from [68,69], and $r = 0.0367, q = 0, T = 1, S_0 = 100$. Reference values by Linear APROJ, $P = 10$. For MJD and BSM, $\bar{P} = 3$; for KOU $\bar{P} = 4$.

Model	Parameters	Strike	Reference Values $M = 12$	Reference Values $M = 250$
BSM	$\sigma = 0.17801$	90	11.9049157	11.9405632
		100	4.8819616	4.9521569
		110	1.3630380	1.4133670
KOU	$\sigma = 0.120381$	90	12.713070	12.753177
	$\lambda = 0.330966, \quad p = 0.2071$	100	5.017859	5.070220
	$\eta_1 = 9.65997, \quad \eta_2 = 3.13868$	110	1.041531	1.076568
MJD	$\sigma = 0.126349$	90	12.710669	12.749182
	$\lambda = 0.174814$	100	5.011290	5.063823
	$\mu_J = -0.390078, \quad \sigma_J = 0.338796$	110	1.051633	1.087406

Now we consider the BSM model, Merton's Jump Diffusion (MJD), and Kou's double exponential (KOU) model, which characteristic functions given in Figure 43. Parameters are as in [69] (later used in [68]), which are provided in Table 35 along with reference values. The parameter setting for BSM is also considered in [42]. Convergence is compared for the linear and quadratic implementation of APROJ in Figure 31.

The first observation is that the prices obtained for BSM agree with those of CK [42] to 7 decimals (the other two models are not reported in [42]), while the method of FM [69] is accurate to only about 2-3 decimals in most cases with cpu times in excess of 5 seconds (this is pointed out as well in [42]). Greater accuracy is obtained by APROJ in just milliseconds. When $M = 250$, $K = 100$, the price to seven decimals is given by 4.9521569, as computed by CK and APROJ. FM obtains 4.95233, while the maturity randomization methods of Fusai, Marazzina and Marena (FMM) [68] report prices of 4.95212 and 4.95242, using density recursion and price recursion respectively, with cpu times of 38.32 seconds and 95.80 seconds[30]. We find similar results for the models of KOU and MJD, where the prices of FMM agree with those computed by ARPOJ (given in Table 35) to 3 or 4 decimals with FMM cpu times in the dozens of seconds, compared to milliseconds for APROJ.

The previous experiments illustrate the convergence of APROJ as a function of the resolution when the grid width is fixed a priori. The final set of experiments analyzes the ability of the APROJ algorithm to accurately select parameters without user input, as

[30]The results for FMM were obtained in MATLAB 7.4 on a personal computer with Intel(R) Core 2 Quad Q6600, 2.4GHz, 4Gb RAM.

Table 36: Call price errors for quadratic APROJ with automated parameter selection. Cpu times represent full cost including parameter determination. Columns NL_1 and NL_2 are the number of loops required in initialization (Subroutine 9) and the main algorithm (Algorithm 11) before tolerance is met, where $\epsilon_1 = 5e\text{-}04, \epsilon_2 = 5e\text{-}04$, and $\epsilon_3 = 5\text{e-}03$ in Algorithm 11. N is the final grid size. In all cases, $S_0 = 100$, $r = 0.05$, $q = 0$, $T = 1$. MJD params: $(\sigma, \lambda, \mu_J, \sigma_J)$. Kou params: $(\sigma, \lambda, p, \eta_1, \eta_2)$. NIG params: (α, β, δ)

Model	W	M	Ref	|Err|	cpu(sec)	NL_1	NL_2	$\log_2(N)$
CGMY	90	12	11.999099	2.33e-06	0.006	1	1	6
(0.2703, 17.56, 54.82, 0.8)	100	250	3.643684	7.01e-07	0.083	2	1	8
CGMY	90	12	15.061188	5.63e-04	0.005	1	1	6
(1.1136, 3, 10, 0.2)	100	250	8.644264	7.80e-06	0.471	2	2	9
MJD	90	12	13.134793	6.10e-04	0.005	1	1	6
(0.13, 0.17, -0.39, 0.34)	100	250	5.480458	1.02e-04	0.103	1	2	8
MJD	90	12	12.704098	1.02e-06	0.005	1	1	6
(0.1, 3, -0.05, 0.086)	100	250	5.620436	6.79e-06	0.030	1	1	7
BSM	90	12	11.949574	4.22e-07	0.006	1	1	6
$\sigma = 0.1$	100	250	3.639486	2.02e-06	0.029	1	1	7
BSM	90	12	13.854399	1.96e-06	0.006	1	1	6
$\sigma = 0.3$	100	250	7.939288	4.92e-06	0.028	1	1	7
NIG	90	12	12.290729	5.89e-05	0.005	1	1	6
(8, -1, 0.2)	100	250	4.610758	1.70e-07	0.423	3	1	9
Kou	90	12	13.564345	9.71e-04	0.005	1	1	6
(0.15, 0.4, 0.2, 9, 3)	100	250	6.297930	2.33e-05	0.473	2	2	9

described in Section 6.3.6 (and implemented in Subroutine 9) to achieve a practical accuracy of about TOL = 5e-04 or better.[31] Table 36 considers several models and settings for M and W, with reference prices obtained by APROJ with $N = 2^{13}$. Based on the prescription given in Section 6.3.6, for $M = 12$ the algorithm is initialized with $N = 2^6$ and and grid width multiplier $L_1 = 12$, while for $M = 250$ we set $N = 2^7$ and $L_1 = 16$. The column labeled $\log_2(N)$ reports the final value after satisfying all error tolerances. The column labeled NL_1 is the number of iterations required in initialization Subroutine 9 before the error tolerances ϵ_1 and ϵ_2 were satisfied (so $\mathrm{NL}_1 = 1$ implies that the initial estimate of N and $\bar{a}$ were sufficient). Column NL_2 is the number of loops in the main Algorithm 11 before the terminal valuation criteria was satisfied.

Ideally, since the cost of Subroutine 9 is negligible, we would prefer it to identify insufficient settings of N and $\bar{a}$ prior to entering Algorithm 11. Either way we see that these three consistency checks are more than sufficient to achieve high accuracy. Column cpu(sec)

[31] We have selected to the parameters $\epsilon_1, \epsilon_2, \epsilon_3$ to attain an accuracy of TOL = 5e-04 or better. However, these parameters, as well as the initial value of N and L_1 can be increased if the desired accuracy is beyond what is required in practice.

reports the time in seconds for the full procedure, which is generally fractions of a second, including the cost of demeriting initial values for N and $\bar{a}$. We conclude that APROJ is capable of obtaining accurate prices at a very small computational cost when the algorithm, rather than the user, determines the required values of N and $\bar{a}$ needed to achieve the designated tolerance.

6.7 Conclusions

In this article, we introduced a novel method, APROJ, for pricing arithmetic Asian options driven by exponential Levy processes. This method is based on a recursive characteristic function recovery by density projection, using frame duality on a shifted grid. Continuously monitored Asian options are also priced in this framework. After an extensive investigation of its theoretical behavior, numerical experiments demonstrate the rapid convergence of APROJ, for both the linear and quadratic implementations. A variety of models and parameter settings from the literature are considered.

Compared to recently developed breakthrough methods, APROJ achieves higher accuracy at a fraction of the cost, consistently reducing cpu times by a factor of 10-100, and often much greater. Moreover, the algorithm is able to accurately select the required parameter settings needed to achieve a supplied tolerance. The computational cost of pricing and calculating sensitivities of an important path-dependent derivate is now within milliseconds of the cost associated with vanilla European options. The extension to discretely monitored barrier options facilitates a similar cost reduction, and will appear in a subsequent work.

6.8 Appendix: Proofs

Proof of Proposition 6.3.1. We proceed by induction where $m = 1$ follows from $Y_1 = R_M$. Fix $m \geq 2$ and assume (i) and (ii) hold for $m-1$. First we show finiteness of $\phi_{Z_{m-1}}(z)$ for any fixed $z = x + i\eta \in \mathcal{D}_d$. Consider the case of $\eta \in (-d, 0)$ (finiteness for $\eta \in [0, d)$ follows immediately). Since $\phi_{Y_{m-1}}(x+i\eta) = \int_{\mathbb{R}} e^{i(x+i\eta)y} f_{Y_{m-1}}(y)dy < \infty$, ie the integral exists and is finite, $e^{i(x+i\eta)y} f_{Y_{m-1}}(y)$ must be absolutely integrable in y, from which $\int_{\mathbb{R}} e^{-\eta y} f_{Y_{m-1}}(y)dy <$

Model	$\psi_L(\xi), \quad \omega = -\psi_L(-i), \quad$ Param. Restrictions	Cumulants
BSM	$\psi_L(\xi) = -\frac{\sigma^2}{2}\xi^2$	$c_1 = \gamma$
	$\omega = -\frac{\sigma^2}{2}$	$c_2 = \sigma^2$
	$\sigma > 0, \quad \mathcal{I}_L = \mathbb{R}$	$c_4 = 0$
MJD	$\psi_L(\xi) = -\frac{\sigma^2}{2}\xi^2 + \lambda\Big(\exp(i\xi\mu_J - \frac{\sigma_J^2}{2}\xi^2) - 1\Big)$	$c_1 = \gamma + \lambda\mu_J$
	$\omega = -\frac{\sigma^2}{2} - \lambda\Big(\exp(\mu_J + \frac{\sigma_J^2}{2}) - 1\Big)$	$c_2 = \sigma^2 + \lambda(\mu_J^2 + \sigma_J^2)$
	$\lambda, \sigma_J, \sigma > 0, \quad \mathcal{I}_L = \mathbb{R}$	$c_4 = \lambda(\mu_J^4 + 6\sigma_J^2\mu_J^2 + 3\sigma_J^4\lambda)$
CGMY	$\psi_L(\xi) = C\Gamma(-Y)\left((M - i\xi)^Y - M^Y + (G + i\xi)^Y - G^Y\right)$	$c_1 = \gamma + C\Gamma(1-Y)(M^{Y-1} - G^{Y-1})$
	$\omega = -C\Gamma(-Y)((M-1)^Y - M^Y + (G+1)^Y - G^Y)$	$c_2 = C\Gamma(2-Y)(M^{Y-2} + G^{Y-2})$
	$C, G > 0, M > 1, Y \in (0,1) \cup (1,2), \quad \mathcal{I}_L = [-M, G]$	$c_4 = C\Gamma(4-Y)(M^{Y-4} + G^{Y-4})$
NIG	$\psi_L(\xi) = -\delta\left(\sqrt{\alpha^2 - (\beta + i\xi)^2} - \sqrt{\alpha^2 - \beta^2}\right)$	$c_1 = \gamma + \delta\beta/\sqrt{\alpha^2 - \beta^2}$
	$\omega = \delta\left(\sqrt{\alpha^2 - (\beta+1)^2} - \sqrt{\alpha^2 - \beta^2}\right)$	$c_2 = \delta\alpha^2(\alpha^2 - \beta^2)^{-3/2}$
	$\alpha, \delta > 0,\ \beta \in (-\alpha, \alpha - 1), \quad \mathcal{I}_L = [\beta \pm \alpha]$	$c_4 = 3\delta\alpha^2(\alpha^2 + 4\beta^2)(\alpha^2 - \beta^2)^{-7/2}$
KOU	$\psi_L(\xi) = -\frac{\sigma^2}{2}\xi^2 + \lambda\Big(\frac{p\eta_1}{\eta_1 - i\xi} + \frac{(1-p)\eta_2}{\eta_2 + i\xi} - 1\Big)$	$c_1 = \gamma + \frac{\lambda p}{\eta_1} - \frac{\lambda(1-p)}{\eta_2}$
	$\omega = -\frac{\sigma^2}{2} - \lambda\Big(\frac{p\eta_1}{\eta_1 - 1} + \frac{(1-p)\eta_2}{\eta_2 + 1} - 1\Big)$	$c_2 = \sigma^2 + 2\frac{\lambda p}{\eta_1^2} + 2\frac{\lambda(1-p)}{\eta_2^2}$
	$\lambda, \sigma > 0,\ p \in [0,1],\ \eta_1 > 1, \eta_2 > 0, \quad \mathcal{I}_L = (-\eta_1, \eta_2)$	$c_4 = 24\lambda(\frac{p}{\eta_1^4} + \frac{1-p}{\eta_2^4})$
VG	$\psi_L(\xi) = -\frac{\sigma^2}{2}\xi^2 - \frac{1}{\nu}\log\left(1 - i\nu\theta\xi + \nu\frac{\sigma_V^2}{2}\xi^2\right)$	$c_1 = \gamma + \theta$
	$\omega = -\frac{\sigma^2}{2} + \frac{1}{\nu}\log\left(1 - \nu\theta - \nu\frac{\sigma_V^2}{2}\right)$	$c_2 = \sigma^2 + \sigma_V^2 + \nu\theta^2$
	$\nu, \sigma_V > 0,\ \sigma \geq 0, \quad \mathcal{I}_L = \left[\frac{\theta}{\sigma_V^2} \pm \sqrt{\frac{\theta^2}{\sigma_V^4} + \frac{2}{\nu\sigma_V^2}}\right]$	$c_4 = 3(\sigma_V^4\nu + 2\theta^4\nu^3 + 4\sigma_V^2\theta^2\nu^2)$

Figure 32: Symbols $\psi_L(\xi)$, cumulants c_n of $\log(S_{t+1}/S_t)$, parameter restrictions and strip of analyticity $\mathcal{I}_L$ for tractable Levy processes. $\gamma := r - q - \psi_L(-i) = r - q + \omega$. Note that $\mathbb{E}[\log(S_{t+1}/S_t)] = c_1 = r - q + w + \mathbb{E}[L(1)]$, and $\mathbb{E}[R_{\Delta_t}] = c_1\Delta_t$.

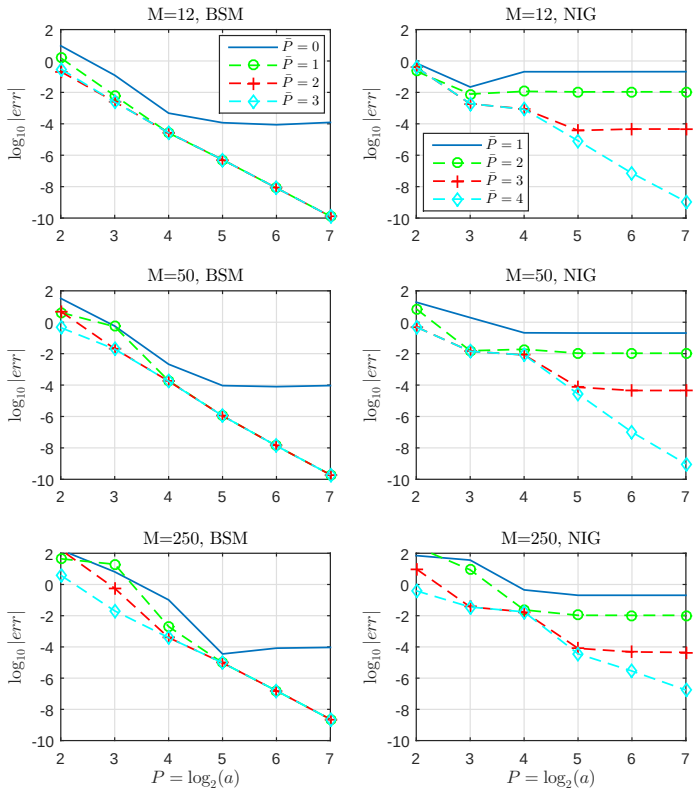

Figure 33: Convergence in $\bar{P}$ of quadratic APROJ prices for BSM and NIG models (one legend for each model). Parameters and reference values as in Table 35, strike $W = 100$.

∞. Note that

$$\int_{\mathbb{R}} |e^{i(x+i\eta)\log(1+e^y)} f_{Y_{m-1}}(y)|dy \leq e^{-\eta\log(2)} \int_{-\infty}^{0} f_{Y_{m-1}}(y)dy + \int_{0}^{\infty} e^{-\eta\log(1+e^y)} f_{Y_{m-1}}(y)dy.$$

To bound the second integral, note that $\exists\tilde{\eta} \in (-d, \eta)$, and $\tau > 0$ s.th $\forall y > \tau$, $-\tilde{\eta}y > -\eta\log(1+e^y)$. Hence,

$$\int_{\tau}^{\infty} e^{-\eta\log(1+e^y)} f_{Y_{m-1}}(y)dy \leq \int_{\tau}^{\infty} e^{-\tilde{\eta}y} f_{Y_{m-1}}(y)dy \leq \int_{\mathbb{R}} e^{-\eta y} f_{Y_{m-1}}(y)dy < \infty,$$

so $\phi_{Z_{m-1}}(z)$ exists and is finite $\forall z \in \mathcal{D}_d$. To prove continuity, fix any $\{z_n\} \in \mathcal{D}_d$ with $z_n \to z \in \mathcal{D}_d$. Let $G \subset \mathcal{D}_d$ be a bounded open set containing the tail of $\{z_n\}$, so $\bar{G} \subset \mathcal{D}_d$. With $\bar{\eta} := \max\{|\eta| : z = x + i\eta \in \bar{G}\}$, note that for any $z \in \bar{G}$ it holds

$$|e^{iz\log(1+e^y)} f_{Y_{m-1}}(y)| \leq e^{\bar{\eta}\log(1+e^y)} f_{Y_{m-1}}(y) = |e^{i\bar{z}\log(1+e^y)} f_{Y_{m-1}}(y)|,$$

where $\bar{z} = x - i\bar{\eta}$ for arbitrary $x \in \mathbb{R}$, since $\log(1+e^y) \geq 0$ for all $y \in \mathbb{R}$. Hence

$$\sup_{z\in\bar{G}} |\phi_{Z_{m-1}}(z)| \leq |\phi_{Z_{m-1}}(\bar{z})| < \infty,$$

where finiteness of $\bar{z} \in \bar{G} \subset \mathcal{D}_d$ was proved above, so by dominated convergence

$$\lim_{z_n\to z} \phi_{Z_{m-1}}(z_n) = \int_{\mathbb{R}} \lim_{z_n\to z} \exp\left(iz_n\log(1+e^y)\right) f_{Y_{m-1}}(y)dy = \phi_{Z_{m-1}}(z).$$

Analyticity is now proved as follows. Fix any positively oriented triangle $\Gamma \in \mathcal{D}_d$. By Fubini's theorem

$$\int_{\Gamma} \phi_{Z_{m-1}}(z)dz = \int_{\mathbb{R}} f_{Y_{m-1}}(y) \int_{\Gamma} \exp\left(iz\log(1+e^y)\right) dzdy = 0,$$

where the final equality holds by Cauchy's theorem. Hence, by Morera's theorem, we conclude that $\phi_{Z_{m-1}}(z)$ is analytic on $\mathcal{D}_d$, and so too is $\phi_{Y_m}(z) = \phi_R(z)\phi_{Z_{m-1}}(z)$. The growth estimate (ii) follows immediately from $|\phi_{Z_{m-1}}(\xi)| \leq 1$ for $\xi \in \mathbb{R}$. $\square$

Proof of Lemma 6.3.1. Let $[-\lambda, \lambda]$ be the support of φ. For $a > 0$, $\xi \in [0, 2\pi a)$,

$$\begin{aligned}
\left| a^{1/2}\mathcal{F}[\varphi_{a,n}](\xi) - \bar{\Psi}(\xi, n) \right| &\leq a^{1/2} \int \varphi_{a,n}(y) \left| e^{i\xi y} - e^{i\xi \log(1+\exp(y))} \right| dy \\
&= \int_{-\lambda}^{\lambda} \varphi(y) \left| e^{i\xi(x_n + \frac{y}{a})} \right| \left| 1 - e^{i\xi\left(\log(1+\exp(x_n+\frac{y}{a})) - (x_n+\frac{y}{a})\right)} \right| \\
&\leq |\xi| \int_{-\lambda}^{\lambda} \varphi(y) \left| \log\left(1 + \exp\left(x_n + \frac{y}{a}\right)\right) - \left(x_n + \frac{y}{a}\right) \right| dy \\
&\leq 2\pi a \left(\log(1 + \exp(x_{n-1})) - x_{n-1}\right) \int_{-\lambda}^{\lambda} \varphi(y) dy \\
&= 2\pi a \left(\log(1 + \exp(x_{n-1})) - x_{n-1}\right),
\end{aligned}$$

where the next to last line follows since $\log(1 + \exp(x)) - x$ is strictly decreasing. An asymptotic expansion yields

$$\log(1 + \exp(x_{n-1})) - x_{n-1} \sim e^{-x_{n-1}} - e^{-2x_{n-1}}/2 + \mathcal{O}(e^{-3x_{n-1}}),$$

and the result follows from $\mathcal{F}[\varphi_{a,n}](\xi)$. □

Proof of Proposition 6.2.1. We provide a proof here for linear case, with a bound on the term $C_\gamma^{[1]}(\phi_X)$. The more general case of a p^{th} order basis is discussed in [83]. First define

$$h_{a,n}(\xi) := 12 \frac{\sin^2(\xi/2a)}{(\xi/a)^2(2 + \cos(\xi/a))} \exp(-ix_n\xi) := h_a(\xi) \exp(-ix_n\xi), \tag{260}$$

and $\xi_j = (j-1)\Delta_\xi$ where $\Delta_\xi = 2\pi a/N$. We have that $\epsilon(\breve{\beta}_{a,n}^X) := a^{1/2} C_{a,N} \cdot \bar{\beta}_{a,n}^X - \langle f_X, \widetilde{\varphi}_{a,k} \rangle$ satisfies

$$\begin{aligned}
\epsilon(\breve{\beta}_{a,n}^X) &= \frac{a^{-1/2}}{\pi} \Re \left(\Delta_\xi \sum_{j=1}^{N} \nu_j \phi_X(\xi_j) h_{a,n}(\xi_j) - \int_0^\infty \phi_X(\xi) h_{a,n}(\xi) d\xi \right) \\
&= \frac{a^{-1/2}}{\pi} \Re \left(\Delta_\xi \sum_{j=1}^{\infty} \tilde{\nu}_j \phi_X(\xi_j) h_{a,n}(\xi_j) - \int_0^\infty \phi_X(\xi) h_{a,n}(\xi) d\xi \right. \\
&\qquad \left. + \Delta_\xi \sum_{j=N}^{\infty} \bar{\nu}_j \phi_X(\xi_j) h_{a,n}(\xi_j) \right) := \frac{a^{-1/2}}{\pi} \left(\epsilon_{trap}(a, \bar{a}) + \tau_a(X) \right),
\end{aligned}$$

where $\nu_j := 1 - (\delta_{j,1} + \delta_{j,N})/2$, $\tilde{\nu}_j = 1 - \delta_{j,1}/2$, and $\bar{\nu}_j = 1 - \delta_{j,N}/2$. To apply Theorem 3.2.1 in [123], we must show that the presence of $h_a(\xi)$ does not affect the integrand's analyticity or the finiteness of the Hardy norm, both of which will follow if we can bound $h_a(\xi)$ in a

strip contained within $\mathcal{D}_d$ (note that Proposition 3.1 of [83] demonstrates the existence of a bound). Consider $\widehat{\widetilde{\varphi}}(\xi) = \frac{12\sin^2(\xi/2)}{\xi^2(2+\cos(\xi))} = h_a(a\xi)$, and let $z = x + iy$. Note first that

$$\begin{aligned}|2 + \cos(x+iy)| &= \tfrac{1}{2}\left|4 + e^{-y}(\cos(x) + i\sin(x)) + e^{y}(\cos(x) - i\sin(x))\right| \\ &= \left(\sinh^2(y)\sin^2(x) + (\cosh(y)\cos(x)+2)^2\right)^{1/2}.\end{aligned}$$

For $|y| \leq 1/2$, $\cosh(y) \leq 3/2$, from which $(\cosh(y)\cos(x)+2)^2 \geq 1/4$, and $|2+\cos(x+iy)| \geq 1/2$, uniformly in x. Similarly, for $|y| \leq 1$,

$$\left|\frac{\sin\left(\frac{x+iy}{2}\right)}{x+iy}\right|^2 = \frac{\sinh^2\left(\frac{y}{2}\right)\cos^2\left(\frac{x}{2}\right) + \cosh^2\left(\frac{y}{2}\right)\sin^2\left(\frac{x}{2}\right)}{y^2+x^2} \leq 1,$$

uniformly in x. Hence, $\forall |y| \leq 1/2$, $|\widehat{\widetilde{\varphi}}(x+iy)| \leq 24$, so for $|y| \leq a/2$, $|\widehat{\widetilde{\varphi}}((x+iy)/a)| \leq 24$, $\forall x \in \mathbb{R}$. Thus, $\phi_X \cdot h_{a,n} \in \mathcal{H}(\mathcal{D}_\gamma)$ where $\gamma = \gamma(a) = d \wedge a/2$, and $C_\gamma(\phi_X) := \|\phi_X \cdot h_{a,n}\|^{\mathcal{H}_\gamma} \leq 24\|\phi_X\|^{\mathcal{H}_\gamma}$. For a sufficiently large, the integrand is bounded within $\mathcal{D}_d$ (for any finite $d > 0$). Moreover, since $\bar{P} > 1 + \log_2|\bar{\mu}|$, it holds that $\bar{a}/2 > |\bar{\mu}|$ and so $|x_n| \leq |\bar{\mu}| + \bar{a}/2 < \bar{a}$, $\forall 1 \leq n \leq N$. Thus by Theorem 3.2.1 in [123], $\epsilon_{trap}(a, \bar{a})$ converges exponentially in $\bar{a}$, according to the bound given.

The truncation error depends on the tail behavior of ϕ_X. Since $|h_{a,n}(\xi)| \leq \frac{12a^2}{\xi^2}$, and $|\phi_X(\xi)|$ satisfies equation (199), the truncation error is bounded by

$$\Delta_\xi \sum_{j=N}^{\infty} \bar{\nu}_j \phi_X(\xi_j) h_{a,n}(\xi_j) \leq 12\kappa a^2 \int_{2\pi a}^{\infty} \frac{e^{-tc|\xi|^\nu}}{\xi^2} d\xi \leq 12\kappa a^2 e^{-tc|2\pi a|^\nu} \int_{2\pi a}^{\infty} \frac{1}{\xi^2} d\xi,$$

and the result follows after simplifying. □

CHAPTER VII

BARRIER AND PARISIAN OPTIONS

This chapter is based on the paper [85], currently in Revision with Applied Mathematical Finance.

7.1 Introduction

Discretely monitored barrier and Parisian options are an important class of path-dependent exotic contracts for which no analytical valuation formulas exist. Pricing such contracts robustly and efficiently is a challenging problem outside of the Black-Scholes-Merton (BSM) framework, especially for Parisian options for which few studies exist beyond BSM. Even within the BSM framework, considerable effort has been applied to relate the prices of continuously and discretely monitored contracts [24, 25] in order to approximate the latter. In general, the payoff of a barrier option at maturity depends on whether the price of an underlying asset (or index) remains within a pre-specified range for each of a fixed set of monitoring dates. Consequently, the contract value can be obtained by backward induction on a sequence of intermediate value functions, starting from the payoff at maturity.

Various numerical methods exist for pricing standard barrier options. In the Gaussian framework, Eyedeland (1994) employed backward induction by convolving the transition density at each stage with the value function at one time step into the future, an approach which has since been extended to more general Lévy dynamics. Significant progress was made by Feng and Linetsky (2008) who compute the Fourier transform of the valuation operator recursively by expressing it as a Hilbert transform, followed by an inversion in the final stage. The COS method of Fang and Oosterlee (2009) represents the value at each stage by a cosine series expansion, based on the framework developed in Fang and Oosterlee (2008). Similar to the Hilbert transform (HT) approach, De Innocentis and Levendorskii (2014) represent the valuation operator in terms of its Fourier transform in the previous stage, which is then approximated by the Fourier transform of a polynomial interpolation

of the value. In the special case of Gaussian (or mixture of Gaussian) return distributions, the fast Gauss transform is applied by Broadie and Yamamoto [26, 27].

Compared to the pricing of other path-dependent options, efficient barrier option pricing has enjoyed a great deal of success. However, existing analytical/numerical methods for Parisian options, introduced in [43], are still very limited in terms of the model dynamics they can accommodate. The vast majority of works are restricted to the BSM model, for example [14, 43, 76, 130], although recently [2] has extended the existing Laplace transform methods to include the double-sided jump diffusion of [90].

Novelty aside, the burden of any new barrier pricing method is that not only must it be fast enough to warrant consideration, but it should be robust as well. Moreover, this robustness should extend to general Lévy processes. With an eye towards calibrating model dynamics directly to barrier option markets, rather than borrowing parameters calibrated to vanilla prices, an efficient *and* robust pricing method capable of pricing general barrier options including Parisian barrier options (both cumulative and resetting) would be a valuable contribution to the field of option pricing.

In this paper, we devise a backward induction method based on the frame projection approach (PROJ) of Kirkby (2015), which is derived from the duality theory of frames and Riesz bases. In contrast to the cosine series expansion approach [61], we consider *non-orthogonal* basis expansions for which we utilize a *biorthogonal* (*dual*) basis to determine the orthogonally projected density. In fact, the cosine basis is a special case for which the frame is orthogonal. However, because of the global nature of the cosine basis, the implementation using locally supported B-splines considered in this work differs substantially.

Supplied only the characteristic function of the log return process, analytical expressions for the orthogonally projected density (onto a space of compactly supported basis elements) are convolved with the valuation operator at each stage. Not only does frame projection represent a transition density in terms of its characteristic function, but the process of projection facilitates rapidly converging value approximations at each stage, resulting in a substantial reduction of computational cost. Discrete convolution of the projected density with a set of value coefficients, interpreted as coefficients of a dual expansion of the previous

stage value, is represented as a Toeplitz matrix-vector multiplication, which is computed by the fast Fourier transform (FFT). An augmentation is devised to reduce the required grid size and correct for the value contribution neglected by traditional discrete convolution, which engenders a robust implementation that safeguards against underestimating the density truncation interval.

To facilitate direct calibration, we devise a method of automated parameter selection, which adjusts the grid size and resolution to meet a provided tolerance. The enables pricing without user interference. The method, called BPROJ, applies to knock-out barrier options (or knock-in by parity) with single or double barriers, with or without (time-dependent) rebates. By a simple extension, Parisian and Parasian (delayed barrier/ cumulative Parisian) options are priced in the same framework. This is the first method that can price such contracts with general Lévy dynamics. We demonstrate that even when the exact density is known, frame projection results in a substantial convergence acceleration over a direct convolution-based approach.

The paper is organized as follows. Section 7.2 briefly reviews the Lévy model class and the concept of option pricing by frame duality. Section 7.3 presents the projection algorithm for discretely monitored barrier options, with single and double barriers, and with rebates or binary payoffs. An augmentation procedure is designed to enhance the robustness of convolution schemes with respect to the choice of density truncation intervals. Moreover, an anti-aliasing approach for density recovery is provided for double barrier options. Stable formulas for payoff coefficients are derived along with a recursive algorithm for the intermediate value coefficients. A novel method of automated parameter selection is introduced, which facilitates hands-off pricing and contributes to the algorithm's robustness. Parisian options are considered in Section 7.4. An error analysis is provided in Section 7.5. In Section 7.6, we perform a series of numerical experiments to justify claims of efficiency and robustness. Finally, the paper is concluded in Section 7.7.

7.2 Pricing by Frame Projection

We consider models driven by an underlying Lévy process [46, 117, 120, 121], which is characterized by independent, stationary increments. Given a Lévy process $L(t)$, $t \geq 0$, defined in terms of its *characteristic exponent* or *symbol* $\psi_L(\xi)$ (see Table 43 for symbols used in this work), the characteristic function satisfies

$$\phi_{L(t)}(\xi) := \mathbb{E}[e^{iL(t)\xi}] = e^{t\psi(\xi)}, \quad t \geq 0.$$

We assume a constant risk-free interest rate, $r \geq 0$, and dividend yield, $q \geq 0$. To model the underlying, we posit an exponential Lévy model of the form

$$S(t) = S(0)e^{Y(t)} = S(0)e^{(r-q-\psi_L(-i))t+L(t)},$$

where $-\psi_L(-i)$ is the additive martingale (convexity) adjustment which ensures that $e^{-(r-q)t}S(t)$ is a martingale, that is $\mathbb{E}[S(T)|S(t)] = e^{(r-q)(T-t)}S(t)$. The characteristic exponent of $Y(t)$ is given by

$$\psi_Y(\xi) = r - q - \psi_L(-i) + \psi_L(\xi),$$

which is the *risk-neutral (pricing) symbol*. We denote by p_{Δ_t} the density[1] of log return over the increment Δ_t, $\ln(S_{t+\Delta_t}/S_t)$, which is independent of the value of S_t and satisfies

$$\phi_{\Delta_t}(\xi) = \int e^{i\nu\xi} p_{\Delta_t}(\nu)d\nu = e^{i\xi(r-q-\psi_L(-i))\Delta_t} e^{\psi_L(\xi)\Delta_t} = e^{\psi_Y(\xi)\Delta_t}. \tag{261}$$

7.2.1 European Option Valuation

It turns out that discretely monitored barrier options can be priced by a sequence of problems, each equivalent to pricing a European option. Given a T-maturity European payoff $g(S_T)$, the value at any time $t \in [0, T]$ satisfies

$$\mathcal{V} \circ g(S_t) = e^{-r\Delta_t}\mathbb{E}[g(S_T)|S_t] = e^{-r\Delta_t} \int_{\mathbb{R}} g(S_t e^{\nu}) p_{\Delta_t}(d\nu),$$

where $\Delta_t = T - t$. The valuation procedure proposed in this paper is based on the PROJ methodology introduced in [83] (extended to Asian options in [84]), whereby the log return

[1] Lévy models, with the exception of the compound Poisson process, possess a continuous density [120].

density is approximated by its *orthogonal projection* onto a Riesz sequence. For a fixed *resolution* $a > 0$, and a symmetric *generator* φ, we obtain analytical (and efficiently computable) representations of the orthogonally projected density onto a space of compactly supported basis elements $\{\varphi_{a,k}\}_{k\in\mathbb{Z}}$. The basis elements are defined by $\varphi_{a,k}(\nu) := a^{1/2}\varphi(a(\nu - \nu_k))$, where $\{\nu_k\}_{k\in\mathbb{Z}}$ are the points on a uniformly spaced grid of width $\Delta = 1/a$.

The contribution of PROJ is not in the choice of basis per se, but rather the determination of coefficients to accelerate convergence of subsequent integral approximations. Namely, by making direct use of the dual theory of frames[2], we obtain analytical formulas for the orthogonally projected density. The representations are provided by a *dual basis*, generated by $\widetilde{\varphi}(\nu)$, with which we convolve the density to obtain projection coefficients. Fixing a subset of basis elements of size $N \in \mathbb{N}_+$, the log return density is approximated by

$$p_{\Delta_t}(\nu) \approx \sum_{k=1}^{N} \left(\int_{-\infty}^{\infty} p_{\Delta_t}(\nu) \cdot a^{1/2} \widetilde{\varphi}(a(\nu - \nu_k)) d\nu \right) \varphi_{a,k}(\nu), \tag{262}$$

which provides the L^2 projection restricted to $\{\varphi_{a,k}\}_{k=1}^{N}$.

Guided by the analysis of [87], we project p_{Δ_t} onto the linear B-spline basis[3], which we define in terms of translated dilations of the generator

$$\varphi(\nu) := (1 - |\nu|)^+ = (1 - |\nu|)\mathbb{1}_{[-1,1]}(\nu).$$

With a left-most grid point ν_1 fixed (discussed in Section 7.3.3), the piecewise linear approximation space is spanned by the functions $\{\varphi_{a,k}\}_{k=1}^{N}$ given by

$$\varphi_{a,k}(\nu) = \begin{cases} a^{3/2}\left[\nu - \left(\nu_1 + \frac{k-2}{a}\right)\right] & \text{if } \nu \in \left[\nu_1 + \frac{k-2}{a}, \nu_1 + \frac{k-1}{a}\right] \\ a^{3/2}\left[\left(\nu_1 + \frac{k}{a}\right) - \nu\right] & \text{if } \nu \in \left[\nu_1 + \frac{k-1}{a}, \nu_1 + \frac{k}{a}\right], \end{cases} \tag{263}$$

where $\varphi_{a,k}(\nu)$ is centered over $\nu_k = \nu_1 + (k-1)/a$. After introducing the barrier pricing problem (which determines the appropriate grid), Section 7.3.3 reviews an efficient implementation for acquiring the orthogonally projected transition density.

[2] A theory which is used primarily to motivate the search for biorthogonal wavelets.

[3] In addition to its simplicity, we find that the linear basis often outperforms smoother spline bases for weekly or more frequent monitoring, especially for extremely peaked transitional densities.

7.3 Discretely-Monitored Barrier Options

Barrier options are separated into two basic categories. Knock-out barrier options become worthless if the underlying (stock, interest rate, index, etc.) breaches a specified barrier by expiration, while knock-in barrier options have a zero payoff unless the barrier is breached. Continuous monitoring, which is impossible in practice but provides a reasonable approximation for frequently monitored barrier options such as those on Forex, leads to analytical formulas for barrier options in certain models, namely pure diffusion specifications. When monitoring occurs at a discrete set of times (daily, monthly, etc.), analytic pricing formulas are no longer available, necessitating the use of numerical methods. By parity, knock-in options are priced in terms of a knock-out option with the same barrier, and a vanilla option, all with the same strike (see [114]).

7.3.1 Knock-Out Options: Backward Induction

The BPROJ pricing method relies on a recursive description of the barrier option value, which is computed at a time $t_0 \leq T$, where T is the contract expiration date. Monitoring occurs at a discrete set of times $\mathcal{T} := \{t_1, ..., t_M\}$, where $t_0 < t_1 < t_M = T$. Assuming for now that no rebates are awarded upon barrier breach, the contract's value at time t_0 is given by

$$\mathcal{V}^*(x, t_0) = e^{-rt_M} \mathbb{E}_{x,0} \left[\mathbb{1}_{[S_{t_1} \in C]} \cdot \mathbb{1}_{[S_{t_2} \in C]} \cdots \mathbb{1}_{[S_{t_M} \in C]} \cdot g(S_{t_M}) \right], \tag{264}$$

where $\mathbb{E}_{x,0}[\ \cdot\ ] = \mathbb{E}[\ \cdot\ | S_{t_0} = S_0 e^x]$, for some fixed $S_0 > 0$. Typically, $S_{t_0} \equiv S_0$ (so $x = 0$), but option values will be computed across a set of initial prices, S_{t_0}, in this form. The set C is the continuation region implied by any knock-out barriers (if for any $t \in \mathcal{T}$, $S_t \in C^c$, then the option expires worthless), and $g(S_T) = g(S_{t_M})$ is the terminal payoff. For example, $g(S_T) = (S_T - W)^+$ for a knock-out call option.

The induction procedure determines $\mathcal{V}^*(x, t_0)$ as follows. First, we define

$$\mathcal{V}^*(y, t_M) := g(S_0 e^y) \mathbb{1}_{[y \in \widetilde{C}]},$$

where $y \in \widetilde{C}$ iff $S_0 e^y \in C$. Note that the true contractual payoff is given by $g(S_0 e^y) \mathbb{1}_{[S_t \in C, t \in \mathcal{T}]}$. By the induction's end, this path requirement will have been enforced. Given $\mathcal{V}^*(y, t_m)$, we

define for $m = M-1, M-2, .., 1$

$$\mathcal{V}^*(x, t_{m-1}) := e^{-r(t_m - t_{m-1})} \mathbb{E}_{x,m-1} \left[\mathcal{V}^* \left(x + \ln \left(\frac{S_{t_m}}{S_{t_{m-1}}} \right), t_m \right) \mathbb{1}_{\left[x + \ln \frac{S_{t_m}}{S_{t_{m-1}}} \in \widetilde{C} \right]} \right],$$

where $\mathbb{E}_{x,m-1}[\ \cdot\ ] = \mathbb{E}[\ \cdot\ | S_{t_{m-1}} = S_0 e^x]$. It follows that $\mathcal{V}^*(x, t_0)$, calculated inductively, is equivalent to the definition in equation (264).

7.3.1.1 Single Barrier Options

To introduce the BPROJ method, we consider a single barrier knock-out option, initiated at time t_0, which is monitored discretely at the set of observation dates $t_m = t_0 + m\Delta_t$, $m = 1, ..., M$, where we assume for simplicity that $t_m - t_{m-1} = T/M := \Delta_t$ is constant.[4] Suppose that $[L, U]$ represents the continuation region for $\{S_{t_m}\}_{m=1}^M$, with L denoting the lower boundary ($L = 0$ for an up-and-out option) and U the upper boundary ($U = \infty$ for a down-and-out[5]). At maturity t_M, the option payoff is $g(S_{t_M})$, unless a knock-out event (barrier breach) is observed for some $t_m \in \mathcal{T}$, in which case the payoff is zero[6], so the option expires worthless.

7.3.2 Log Asset Grid

Suppose we fix a grid budget $K \in \mathbb{N}_+$, taken to be a power of two, and a grid-width $\alpha > 0$. At each iteration of the pricing algorithm, option values are calculated along a grid of size K with spacing Δ, determined below. At time t_{m-1}, grid points in this space are denoted by $x = \ln(S_{t_{m-1}}/S_0)$, and those at time t_m are denoted by $y = \ln(S_{t_m}/S_0)$, for $m = M, M-1, ..., 1$. Specifically, we fix the *log asset grid*

$$x_n = x_1 + (n-1)\Delta, \quad n = 1, ..., K,$$

where x_1 is chosen according to the type of barrier option to be priced, and $\{y_n\}_{n=1}^K \equiv \{x_n\}_{n=1}^K$. Barriers in log asset space are denoted by $l := \ln(L/S_0)$ and $u := \ln(U/S_0)$. In Section 7.3.12.1, we provide a method to determine the two input parameters to BPROJ,

[4] The case of $t_1 - t_0 \neq \Delta_t$, that is for an arbitrary time between monitoring points, is easily handled as well.

[5] Practically speaking U is an upper limit obtained by truncating the support.

[6] Rebates will be introduced later.

$N = 2K$ and α, along with a grid adjustment to include discontinuities in the payoff as well as $\ln(S_0/S_0)$. For now, it suffices to note that $x_1 = l$ for a down-and-out contract, while $x_K = u$ for an up-and-out.

7.3.3 Density Projection and Log Return Grid

We will denote points in the log return space by $\nu = \ln(S_{t_m}/S_{t_{m-1}})$, where the resolution $a = 1/\Delta > 0$ is the same as in Section 7.3.2, and the number of basis elements is $N = 2K \in \mathbb{N}_+$. We fix the *log return grid*

$$\nu_1 := (1 - N/2)\Delta, \quad \nu_k = \nu_1 + (k-1)\Delta, \quad k = 1, ..., N,$$

where ν_1 has been chosen so that $\nu_{N/2} = 0$. Hence $[\nu_1, \nu_N] \approx [-\alpha, \alpha]$, which centers the log return density about the origin (where we note that the log asset grid width is α). Moreover, the log asset and log return grids have identical resolution, but the log return grid is twice as large. Specifying the piecewise-linear spline basis $\{\varphi_{a,k}\}_{k=1}^N$, with $\varphi_{a,k}(\nu)$ centered over ν_k, the frame projected return density is given by

$$\begin{aligned} p_{\Delta_t}(\nu) &\approx \sum_{k=1}^{N} \frac{a^{-1/2}}{\pi} \Re\left\{ \int_0^\infty \exp(-ix_k\xi) \cdot \phi_{\Delta_t}(\xi) \frac{12\sin^2(\xi/2a)}{(\xi/a)^2(2+\cos(\xi/a))} \right\} \cdot \varphi_{a,k}(\nu) \\ &\approx \frac{24a^{5/2}}{N} \sum_{k=1}^{N} \bar{\beta}_{a,k} \cdot \varphi_{a,k}(\nu), \end{aligned}$$

which is derived from the Fourier transform of the dual generator $\widetilde{\varphi}$

$$\widehat{\widetilde{\varphi}}(\xi) = \frac{12\sin^2(\xi/2)}{\xi^2(2+\cos(\xi))}.$$

The (rescaled) coefficients are computed efficiently using the fast Fourier transform (FFT)

$$\left\{\bar{\beta}_{a,k}\right\}_{k=1}^N := \Re\left\{\mathcal{D}\left[\{H_j\}_{j=1}^N\right]\right\}, \tag{265}$$

with input values

$$H_1 = 1/24a^2, \quad H_j = \exp(-ix_1\xi_j) \cdot \phi_{\Delta_t}(\xi_j) \cdot \frac{\sin^2(\xi_j/2a)}{\xi_j^2(2+\cos(\xi_j/a))} \quad j \geq 2, \tag{266}$$

where the discrete Fourier transform, $\mathcal{D}$, is defined by

$$\mathcal{D}_n\left[\{y_j\}_{j=1}^N\right] = \sum_{j=1}^{N} e^{-i\frac{2\pi}{N}(j-1)(n-1)} y_j, \quad n = 1, ..., N.$$

Algorithm 12 summarizes the coefficient recovery, where we define the function

$$h_a(\xi) := \frac{\sin^2(\xi/2a)}{\xi^2(2+\cos(\xi/a))}. \tag{267}$$

Algorithm 12 Projection Coefficients of Transition Density

1: Input: Δ, N
2: $\nu_1 \leftarrow (1-N/2)\Delta; \quad a \leftarrow 1/\Delta; \quad \Delta_\xi \leftarrow 2\pi a/N$
3: $\Omega_k \leftarrow k\Delta_\xi, \quad k = 1, ..., N-1$
4: $\Omega_k \leftarrow \exp(-i\nu_1\Omega_k) \cdot \phi_{\Delta_t}(\Omega_k) \cdot h_a(\Omega_k), \quad k = 1, ..., N-1$
5: $\bar{\beta} \leftarrow \Re\left\{\text{FFT}\left([1/(24a^2), \Omega_1, ..., \Omega_{N-1}]\right)\right\}$
6: **return** : $\bar{\beta}$

7.3.4 Value Iteration with Projected Densities

With a log asset grid chosen according to Section 7.3.2, value iteration proceeds as follows. At time t_{M-1}, and for each of $\{x_n\}_{n=1}^K$, the option value $\mathcal{V}^*(x_n, t_{M-1})$ is approximated using the terminal payoff $\mathcal{V}^*(y, t_{M-1}) = g(S_0 e^y)$ at the points $\{y_n\}_{n=1}^K$ and the projected density. To ease notation, we write $\bar{\beta}_k \equiv \bar{\beta}_{a,k}$. With $\{\bar{\beta}_k\}_{k=1}^{2K}$ obtained from equation (265), we have for $n = 1, ..., K$

$$\begin{aligned}
\mathcal{V}^*(x_n, t_{M-1}) &= e^{-r\Delta_t} \int_l^u g(S_0 e^y) p_{\Delta_t}(y - x_n) dy \\
&\approx \frac{24a^2 e^{-r\Delta_t}}{N} \sum_{k=1}^{N} \bar{\beta}_k \cdot a^{1/2} \int_l^u g(S_0 e^y) \varphi_{a,k}(y - x_n) dy \\
&= \Upsilon_{a,N}^{\Delta_t} \sum_{k=K-n+1}^{N-n} \bar{\beta}_k \cdot a^{1/2} \int_l^u g(S_0 e^y) \cdot a^{1/2} \varphi(a(y - (x_n + v_k))) dy \\
&= \Upsilon_{a,N}^{\Delta_t} \sum_{k=1}^{K} \bar{\beta}_{K+(k-n)} \cdot a^{1/2} \int_l^u g(S_0 e^y) \cdot a^{1/2} \varphi(a(y - y_k)) dy \\
&= \Upsilon_{a,N}^{\Delta_t} \sum_{k=1}^{K} \bar{\beta}_{K+(k-n)} \theta_{M,k} := \mathcal{V}_{M-1}(x_n),
\end{aligned} \tag{268}$$

where

$$\Upsilon_{a,N}^{\Delta_t} := \frac{24a^2 e^{-r\Delta t}}{N}, \qquad \theta_{M,k} = a^{1/2} \int_l^u g(S_0 e^y) \cdot a^{1/2} \varphi(a(y - y_k)) dy, \tag{269}$$

for $k = 1, ..., K$. In particular, the dependence on x_n has been passed from the integrals to the projection coefficients, so $\theta_{M,k}$ are independent of n.

Note the use of $\mathcal{V}^*$ to denote the true value, and $\mathcal{V}$ the approximation. Values at time t_{m-1} are calculated recursively using values at time t_m, $m = M-1, ..., 1$, as follows. For $t_{m-1} \in \mathcal{T}$,

$$\begin{aligned}\mathcal{V}^*(x_n, t_{m-1}) &= e^{-r\Delta_t} \int_l^u \mathcal{V}^*(y, t_m) p_{\Delta_t}(y - x_n) dy \\ &\approx \Upsilon_{a,N}^{\Delta_t} \sum_{k=1}^{K} \bar{\beta}_{K+(k-n)} \cdot a^{1/2} \int_l^u \mathcal{V}^*(y, t_m) \cdot a^{1/2} \varphi(a(y - y_k)) dy, \end{aligned} \tag{270}$$

for $n = 1, ..., K$. Since only an approximation to $\mathcal{V}^*(y, t_m)$ is known, we will devise an approximation to the integrals arising in the final equation. From the perspective of frame theory, these integrals represent coefficients of the value with respect to the dual basis, $\{\widetilde{\varphi}_{a,k}\}_{k=1}^K$, and we refer to them as *value coefficients*.

7.3.5 Convergence Acceleration

Before moving on, we demonstrate within the traditional BSM framework the remarkable disparity between pricing with the actual density versus using a PROJ expansion with the same set of grid points. In particular, the use of frame projected densities should not be thought of as simply an approximation tool when the underlying density is unknown. Rather, the use of projection facilitates much more rapidly converging value approximations due to the way it represents the density (see [88] for a discussion in the context of payoff function approximation). Hence, while methods such as [51] require only an approximation to the value function at each recursive step (since the characteristic function is known), our use of the projected density (even when the density is known in closed form) is by design.

In this experiment, log return density points for the "direct" method are recovered exactly from the normal distribution, $p_{\Delta_t} \sim \mathcal{N}((r - q - \sigma^2/2)\Delta_t, \sigma^2\Delta_t)$, rather than by projection. Integrals in each stage are computed by Toeplitz matrix-vector multiplication using a trapezoidal rule adjustment, as discussed in Lord et. al. (2008) (see also Eyedeland (1994)). From Figure 34, the advantage of utilizing a frame projected density, in terms of its acceleration of value approximations, is clearly demonstrated. This is perhaps the reason why the direct approach has been mostly ignored, despite its amenability to Toeplitz-FFT methods. It should also be noted that, while the direct approach approximates values

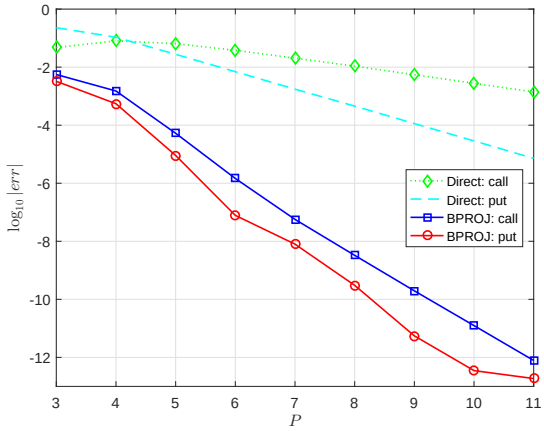

Figure 34: BPROJ vs. Direct: a convergence comparison of barrier option pricing with frame projected density (recoved from chf) versus using the actual density (Direct) for monthly monitored up-and-out contracts in the BSM model: $\sigma = .3$, $T = 1$, $M = 12$, $r = .05$, and $q = .02$, $S_0 = W = 100$, $U = 120$. Reference values obtained by COS [62] with $N = 2^{16}$ over $[-2^3, 2^3]$. Both methods use the same set of grid points on $[-\alpha, \alpha]$ for $\alpha = 4$, with resolution determined by P, where $K = \alpha \cdot 2^P$.

by discretely convolving density points with the previous stage value, BRPOJ discretely convolves projected density points with a set of value coefficients that arise as the orthogonal projection coefficients of an expansion of the previous stage value with respect to the dual basis.

7.3.6 Recursion on Value Coefficients

Given the value approximations in equations (268) and (270), we propose a recursive scheme for approximating the value coefficients. At time t_M, value coefficients are known explicitly, while a local polynomial interpolation of the value function is used to approximate the integrals for t_m, $m \leq M - 1$. The procedure presented in this subsection applies to all varieties of knock-out options.

7.3.6.1 Coefficients at t_M

With an expression for $\mathcal{V}(x_n, t_{M-1})$ in terms of the terminal payoff g, we determine the payoff coefficients (these are the value coefficients at time t_M) with respect to the linear basis:

$$\theta_{M,k} = a^{1/2} \int_{y_{k-1}}^{y_{k+1}} g(S_0 e^y) \cdot a^{1/2} \varphi(a(y - y_k)) dy, \quad k = 1, ..., K, \tag{271}$$

where multiplication by $a^{1/2}$ serves to simplify constants in the final expressions for $\theta_{M,k}$ and $\mathcal{V}(x_n, t_{M-1})$. Equation (268) can be written as

$$\mathcal{V}(x_n, t_{M-1}) = \Upsilon_{a,N}^{\Delta_t} \sum_{k=1}^{K} \bar{\beta}_{K+(k-n)} \cdot \theta_{M,k}, \quad n = 1, ..., K, \tag{272}$$

where the $\theta_{M,k}$ are derived shortly for vanilla and digital options. While analytical coefficient formulas are available, the analysis in [87] demonstrates an instability of exact formulas as the basis is refined, which leads to an alternative approach.

In addition to their simplicity, notice that the same set of payoff coefficients, $\theta_{M,k}$, are used for each x_n. Thus, to efficiently compute (272), we introduce the Toeplitz matrix

$$\boldsymbol{T}_0^{\Delta_t} = \Upsilon_{a,N}^{\Delta_t} \cdot \begin{bmatrix} \bar{\beta}_K & \bar{\beta}_{K+1} & \bar{\beta}_{K+2} & \cdots & \bar{\beta}_{2K-1} \\ \bar{\beta}_{K-1} & \bar{\beta}_K & \bar{\beta}_{K+1} & \cdots & \bar{\beta}_{2K-2} \\ \bar{\beta}_{K-2} & \bar{\beta}_{K-1} & \bar{\beta}_K & & \bar{\beta}_{2K-3} \\ \vdots & \vdots & \vdots & \ddots & \vdots \\ \bar{\beta}_1 & \bar{\beta}_2 & \bar{\beta}_3 & \cdots & \bar{\beta}_K \end{bmatrix}.$$

While $\boldsymbol{T}_0^{\Delta_t}$ is not formed explicitly, it leads to an efficient computation. In particular, to calculate $\boldsymbol{T}_0^{\Delta_t} v$, for $v = (v_1, ..., v_K)^\top$, we define

$$\mu_0 := \mathcal{D}\left\{\Upsilon_{a,N}^{\Delta_t} \cdot (\bar{\beta}_K, ..., \bar{\beta}_1, 0, \bar{\beta}_{2K-1}, ..., \bar{\beta}_{K+1})^\top\right\}, \tag{273}$$

and $\boldsymbol{T}_0^{\Delta_t} v$ is given by the first K elements of

$$p = \mathcal{D}^{-1}\left\{\mu_0 \circ \mathcal{D}\left\{(v_1, ..., v_K, 0, ..., 0)^\top\right\}\right\}, \tag{274}$$

where $v \circ u$ is the element-wise (Hadamard) product of v with u, and the vector of zeros is of length K. Since $\boldsymbol{T}_0^{\Delta_t} v$ is required at each step of the algorithm, we will store μ_0 at initialization for future use.

Now let $\boldsymbol{\mathcal{V}}_{M-1} := (\mathcal{V}(x_1, t_{M-1}), ..., \mathcal{V}(x_K, t_{M-1}))^\top$. With the vector $\theta_M := (\theta_{M,1}, ..., \theta_{M,K})^\top$, equation (272) becomes

$$\boldsymbol{\mathcal{V}}_{M-1} = \boldsymbol{T}_0^{\Delta_t} \theta_M, \tag{275}$$

where the matrix-vector product $\boldsymbol{T}_0^{\Delta_t} \theta_M$ is computed efficiently using the fast Fourier transform (FFT).

7.3.6.2 *Coefficients at t_m*

At time t_{m-1}, the algorithm has just generated the approximated value vector $\boldsymbol{\mathcal{V}}_m := (\mathcal{V}(y_1, t_m), ..., \mathcal{V}(y_K, t_m))^\top$ in the previous time step. From equation (270), it remains only to calculate

$$\theta_{m,k} := a^{1/2} \int_l^u \mathcal{V}(y, t_m) \cdot a^{1/2} \varphi(a(y - y_k)) dy, \quad k = 1, ..., K.$$

Note that the subscript m on $\theta_{m,k}$ is for the purpose of exposition only. In practice, there is no need to store θ coefficients from previous time steps.

In contrast to the first iteration in which θ_M can be computed explicitly from the terminal payoff $g(S_0 e^y)$, an exact formula for $\mathcal{V}^*(y, t_m)$ is unavailable, so θ_m must be approximated. What is known, however, is the set of values $\{\mathcal{V}_{m,n}\}_{n=1}^K$, where $\mathcal{V}_{m,n} := \mathcal{V}(y_n, t_m)$. Hence, for each interior interval $I_k := [y_{k-1}, y_{k+1}]$, $k = 2, ..., K-1$, we define the local quadratic interpolation[7] of $\mathcal{V}(y, t_m)$ on I_k by

$$\begin{aligned} \widetilde{\mathcal{V}}_{m,k}(y) = \mathcal{V}_{m,k-1} \frac{(y - y_k)(y - y_{k+1})}{2\Delta^2} - \mathcal{V}_{m,k} \frac{(y - y_{k-1})(y - y_{k+1})}{\Delta^2} \\ + \mathcal{V}_{m,k+1} \frac{(y - y_{k-1})(y - y_k)}{2\Delta^2}. \end{aligned} \tag{276}$$

Since $\varphi(a(y - y_k))\widetilde{\mathcal{V}}_{m,k}(y)$ is piecewise cubic on I_k, by splitting the interval in half, integration by Simpson's rule on each subinterval is exact:

$$a^{1/2} \int_{I_k} \widetilde{\mathcal{V}}_{m,k}(y) \cdot a^{1/2} \varphi(a(y - y_k)) dy = [\widetilde{\mathcal{V}}_{m,k-1/2} + \widetilde{\mathcal{V}}_{m,k} + \widetilde{\mathcal{V}}_{m,k+1/2}]/3, \tag{277}$$

where $\widetilde{\mathcal{V}}_{m,k-1/2} := \widetilde{\mathcal{V}}_{m,k}(y_k - \Delta/2)$, $\widetilde{\mathcal{V}}_{m,k+1/2} := \widetilde{\mathcal{V}}_{m,k}(y_k + \Delta/2)$, and $\widetilde{\mathcal{V}}_{m,k} = \mathcal{V}_{m,k}$. From equation (276),

$$\begin{aligned} \widetilde{\mathcal{V}}_{m,k-1/2} &= \frac{3}{8}\mathcal{V}_{m,k-1} + \frac{3}{4}\mathcal{V}_{m,k} - \frac{1}{8}\mathcal{V}_{m,k+1} \\ \widetilde{\mathcal{V}}_{m,k+1/2} &= -\frac{1}{8}\mathcal{V}_{m,k-1} + \frac{3}{4}\mathcal{V}_{m,k} + \frac{3}{8}\mathcal{V}_{m,k+1}. \end{aligned}$$

[7] This step is similar to an intermediate computation in [51]. They use a B-spline interpolation over the full grid to approximate the Fourier transformed value. In contrast, our approach uses a local Lagrange interpolation applied separately to overlapping subintervals. This allows us to obtain the explicit form of $\theta_{m,k}$.

To handle the boundary intervals $I_1 := [y_1, y_2]$ and $I_K := [y_{K-1}, y_K]$, we fit a cubic interpolating polynomial. The coefficients are thus approximated by[8]

$$\theta_{m,k} := \begin{cases} \left[13\mathcal{V}_{m,1} + 15\mathcal{V}_{m,2} - 5\mathcal{V}_{m,3} + \mathcal{V}_{m,4}\right]/48 & k = 1 \\ \left[\mathcal{V}_{m,k-1} + 10\mathcal{V}_{m,k} + \mathcal{V}_{m,k+1}\right]/12 & k = 2, ..., K-1 \\ \left[13\mathcal{V}_{m,K} + 15\mathcal{V}_{m,K-1} - 5\mathcal{V}_{m,K-2} + \mathcal{V}_{m,K-3}\right]/48 & k = K \end{cases} \tag{278}$$

Finally, we compute

$$\mathcal{V}(x_n, t_{m-1}) = \Upsilon_{a,N}^{\Delta_t} \sum_{k=1}^{K} \bar{\beta}_{K+(k-n)} \cdot \theta_{m,k}, \quad n = 1, ..., K, \tag{279}$$

which is represented in matrix vector notation as

$$\boldsymbol{\mathcal{V}}_{m-1} = \boldsymbol{T}_0^{\Delta_t} \theta_m, \qquad m = M-1, ..., 1. \tag{280}$$

The errors generated by this procedure are studied in the error analysis section. In general, the pricing of single barrier knock-out options follows this basic procedure, with coefficients θ_M specialized to the payoff at expiration. For certain payoffs such as DOC options and options with rebates, modifications are made to the basic algorithm to improve accuracy, as discussed below.

7.3.7 Payoff Coefficients

While the derivation of payoff coefficients is seemingly obvious, there is an important subtlety which must be addressed. For single barrier knock-out options, there are two basic integrals that are evaluated to determine payoff coefficients for all four contract types. These are denoted by

$$\vartheta_{[-1,0]} := \int_{[-1,0]} \varphi(y) \cdot e^{\frac{y}{a}} dy, \qquad \vartheta_{[0,1]} := \int_{[0,1]} \varphi(y) \cdot e^{\frac{y}{a}} dy. \tag{281}$$

While these integrals have analytical solutions, the analysis of [87] demonstrates an inherent numerical instability of the exact formulas, advocating instead the use of low order quadrature approximations which are also given in closed-form. Further defining

$$\vartheta_* := \int_{[-1,1]} \varphi(y) \cdot e^{\frac{y}{a}} dy = \vartheta_{[-1,0]} + \vartheta_{[0,1]}, \tag{282}$$

[8] The aggregate cost of this step is about $(M-1) \cdot 5N/2$ basic operations.

we evaluate each integral using a three point Gaussian quadrature. With

$$b_3 := \sqrt{15}, \quad b_4 := \sqrt{15}/10, \tag{283}$$

the *stable* Gaussian approximations satisfy

$$\vartheta_{[-1,0]} \approx \frac{e^{-\Delta/2}}{18}\left(5\cosh(b_4\Delta) + b_3\sinh(b_4\Delta) + 4\right) \tag{284}$$

$$\vartheta_{[0,1]} \approx \frac{e^{\Delta/2}}{18}\left(5\cosh(b_4\Delta) - b_3\sinh(b_4\Delta) + 4\right). \tag{285}$$

We will introduce several more integrals as they arise for different payoff types.

7.3.8 Down-and-Out Put Coefficients

The valuation of DOP options is a straightforward application of the generic algorithm, where the terminal payoff satisfies

$$(W - S_0e^y)\mathbb{1}_{[\ln(L/S_0),\ln(W/S_0)]}(y).$$

As for all knock-out options, the grid (for both x and y) is fixed by setting the leftmost point as the out barrier $l = \ln(L/S_0)$, which is the point of discontinuity of the terminal payoff. The nearest grid point left of $\ln(W/S_0)$ is given by

$$\bar{n} := \lfloor (a \cdot (\ln(W/S_0) - x_1) + 1 \rfloor, \tag{286}$$

and the difference and normalized difference are defined by

$$\rho := \ln(W/S_0) - x_{\bar{n}}, \qquad \zeta := a \cdot \rho. \tag{287}$$

For indices $2 \le k \le \bar{n} - 2$, the terminal payoff coefficients from equation (271) are defined after a simple variable change by

$$\theta^{DOP}_{M,k} = \int_{[-1,1]} \left(W - S_0e^{y_k} \cdot e^{\frac{y}{a}}\right)\varphi(y)dy = W - S_0e^{y_k} \cdot \vartheta_*.$$

Noting that $y_1 = \ln(L/S_0)$, we have $S_0e^{y_1} = L$, and the left boundary coefficient follows similarly (see equation (297)). For the coefficients of $\varphi_{a,\bar{n}}$ and $\varphi_{a,\bar{n}+1}$, the grid misalignment requires a slight modification, to account for the payoff nonlinearity. Because of the basis structure, accuracy is retained for $\rho > 0$. Hence, we define the set of adjustments

$$\bar{\delta}^{put}_0 := \int_0^\zeta \varphi(y)dy, \qquad \delta^{put}_0 := \int_0^\zeta \varphi(y)e^{\frac{y}{a}}dy \tag{288}$$

$$\bar{\delta}_1^{put} := \int_{-1}^{-1+\zeta} \varphi(y)dy, \qquad \delta_1^{put} := \int_{-1}^{-1+\zeta} \varphi(y)e^{\frac{y}{a}}dy. \tag{289}$$

Stable coefficient approximations are derived by applying a three point Gaussian rule, so we define the constants

$$q_- := \frac{1}{2}\left(1 - \sqrt{3/5}\right), \qquad q_+ := \frac{1}{2}\left(1 + \sqrt{3/5}\right). \tag{290}$$

Taking δ_1^{put} as an example, we define the Gaussian nodes and weights on $[-1, -1+\zeta]$ for $m = 1, 2, 3$ by

$$\eta_m \in \Big\{ -1 + \zeta \cdot q_-,\ \ -1 + \zeta/2,\ \ -1 + \zeta \cdot q_+ \Big\}, \qquad w_m \in \frac{\zeta}{18} \cdot \{5, 8, 5\}. \tag{291}$$

Hence,

$$\begin{aligned}\delta_1^{put} &\approx \frac{\zeta}{18}\left[5 \cdot \varphi(\eta_1)\exp\left(\frac{\eta_1}{a}\right) + 8 \cdot \varphi(\eta_2)\exp\left(\frac{\eta_2}{a}\right) + 5 \cdot \varphi(\eta_3)\exp\left(\frac{\eta_3}{a}\right)\right] \\ &= \frac{\zeta}{18}e^{-\Delta}\left[5 \cdot (\zeta_- \cdot e^{\rho_-} + \zeta_+ \cdot e^{\rho_+}) + 4\zeta \cdot e^{\rho/2}\right],\end{aligned}$$

where

$$\rho_\pm := \rho \cdot q_\pm, \qquad \zeta_\pm := \zeta \cdot q_\pm. \tag{292}$$

With the formulas defined in Table 37, we can derive the DOP payoff coefficients:

$$\theta_{M,k}^{DOP} = \begin{cases} \dfrac{W}{2} - L \cdot \vartheta_{[0,1]}, & k = 1 \\ W - e^{y_k} \cdot S_0 \cdot \vartheta_*, & k = 2, ..., \bar{n} - 1 \\ W\left(\dfrac{1}{2} + \bar{\delta}_0^{put} - e^{-\rho}\left(\vartheta_{[-1,0]} + \delta_0^{put}\right)\right), & k = \bar{n} \\ W\left(\bar{\delta}_1^{put} - e^{\Delta-\rho} \cdot \delta_1^{put}\right), & k = \bar{n} + 1 \\ 0, & k = \bar{n} + 2, ..., K. \end{cases} \tag{293}$$

We note that the main cost to acquire θ, which has complexity $\mathcal{O}(K)$, arises from the computation of about $\bar{n}$ exponentials and a like number of multiplications.

7.3.9 Down-and-Out Call Coefficients

Of all the knock-out barrier options, only the DOC has an unbounded payoff. The pricing algorithm for DOC options follows the basic structure given above, but with an augmentation

Table 37: Coefficients derived from a three point Gaussian quadrature.

Gaussian Quadrature Adjustment for Payoff Coefficients		
Puts	$\bar{\delta}_j^{put}$	δ_j^{put}
$j=0$	$\zeta\left(1-\frac{1}{2}\zeta\right)$	$\frac{\zeta}{18}\left[4(2-\zeta)e^{\rho/2}+5\cdot((1-\zeta_-)e^{\rho_-}+(1-\zeta_+)e^{\rho_+})\right]$
$j=1$	$\frac{\zeta^2}{2}$	$\frac{\zeta}{18}\cdot e^{-\Delta}\cdot\left[4\zeta\cdot e^{\rho/2}+5\left(\zeta_- e^{\rho_-}+\zeta_+ e^{\rho_+}\right)\right]$
Calls	$\bar{\delta}_j^{call}$	δ_j^{call}
$j=0$	$\frac{1}{2}+\zeta\left(\frac{\zeta}{2}-1\right)$	$e^{(\rho+\Delta)/2}\frac{\sigma^2}{18}\left[5\cdot\left((1-q_-)e^{\Delta\sigma_-}+(1-q_+)e^{\Delta\sigma_+}\right)+4\right]$
$j=1$	$\sigma-\frac{1}{2}\sigma^2$	$e^{(\rho-\Delta)/2}\frac{\sigma}{18}\cdot\left[4(\zeta+1)+5\left(\left(\frac{\zeta+1}{2}+\sigma_-\right)e^{\Delta\sigma_-}+\left(\frac{\zeta+1}{2}+\sigma_+\right)e^{\Delta\sigma_+}\right)\right]$

to the value at each iteration for improved accuracy. We define the perturbed down-and-out grid from equations (316)-(317). To derive DOC payoff coefficients, we again define $\bar{n}, \rho, \zeta$ as in equations (287) and (286), and further

$$\sigma := 1-\zeta, \qquad \sigma_\pm := \sigma(q_\pm - 1/2) = \pm\frac{\sigma}{2}\sqrt{3/5}, \tag{294}$$

where $q_\pm$ is given in equation (290). Coefficients corresponding to the points $x_{\bar{n}}$ and $x_{\bar{n}+1}$ are affected by the grid misalignment, so we introduce the following integrals:

$$\bar{\delta}_0^{call} := \int_{1-\sigma}^{1}\varphi(y)dy, \qquad \delta_0^{call} := \int_{1-\sigma}^{1}\varphi(y)e^{\frac{y}{a}}dy \tag{295}$$

$$\bar{\delta}_1^{call} := \int_{-\sigma}^{0}\varphi(y)dy, \qquad \delta_1^{call} := \int_{-\sigma}^{0}\varphi(y)e^{\frac{y}{a}}dy. \tag{296}$$

Taking δ_0^{call} as an example, we have the Gaussian approximation

$$\begin{aligned}\delta_0^{call} &\approx \frac{\sigma}{18}\left[5\cdot\left((\sigma/2-\sigma_-)e^{\Delta\sigma_-}+(\sigma/2-\sigma_+)e^{\Delta\sigma_+}\right)+4\sigma\right]\\ &= e^{\frac{\rho+\Delta}{2}}\frac{\sigma^2}{18}\left[5\cdot\left((1-q_-)e^{\Delta\sigma_-}+(1-q_+)e^{\Delta\sigma_+}\right)+4\right],\end{aligned}$$

and similarly for δ_1^{call}. The coefficients for $\bar{\delta}_0^{call}, \bar{\delta}_1^{call}$ are given exactly. Table 37 summarizes the resulting approximations. Hence, we can derive the DOC coefficients

$$\theta_{M,k}^{DOC} = \begin{cases} 0 & k=1,\ldots,\bar{n}-1\\ W\left(\delta_0^{call}e^{-\rho}-\bar{\delta}_0^{call}\right) & k=\bar{n}\\ W\left(e^{\Delta-\rho}\left(\vartheta_{[0,1]}+\delta_1^{call}\right)-\left(1/2+\bar{\delta}_1^{call}\right)\right) & k=\bar{n}+1\\ S_0\exp(y_k)\cdot\vartheta_* - W & k=\bar{n}+2,...,K\end{cases} \tag{297}$$

For simplicity we have assumed that $L \leq W$, though a only slight modification to the coefficients in (297) is needed if $L > W$.

Algorithm 13 BRPOJ Pricing Algorithm

Parameters: L or U; $W,\ \Gamma,\ S_0,\ r,\ q,\ T,\ M$
Calculate $\bar{\beta},\ N,\ \Delta,\ \alpha,\ n_0$ from Algorithm 12
$a \leftarrow 1/\Delta; \quad K \leftarrow N/2; \quad \Delta_t \leftarrow T/M; \quad \Upsilon_{a,N} \leftarrow 24a^2/N$
$\bar{n} \leftarrow \lfloor (a(\ln(W/S_0) - x_1) + 1 \rfloor; \quad \rho \leftarrow \ln(W/S_0) - x_{\bar{n}}; \quad \zeta := a \cdot \rho$
$q_\pm \leftarrow (1 \pm \sqrt{3/5})/2,\ \rho_\pm \leftarrow \rho \cdot q_\pm,\ \zeta_\pm \leftarrow \zeta \cdot q_\pm,\ \sigma \leftarrow 1 - \zeta,\ \sigma_\pm \leftarrow \sigma(q_\pm - 1/2)$
For call options, set $\bar{\delta}_j^{call}, \delta_j^{call},\ j = 0, 1$ from Table 37
For put options, set $\bar{\delta}_j^{put}, \delta_j^{put},\ j = 0, 1$ from Table 37
DOC: Initialize θ by equation (297)
UOC: Initialize θ by equation (298)
DOP: Initialize θ by equation (293)
UOP: Initialize θ by equation (299)
$\mu_0 \leftarrow \Upsilon_{a,N} \cdot e^{-r\Delta_t}[\bar{\beta}_K, ..., \bar{\beta}_1, 0, \bar{\beta}_{2K-1}, ..., \bar{\beta}_{K+1}]; \quad \mu_0 \leftarrow \text{FFT}(\mu_0)$
$p \leftarrow \text{iFFT}(\mu_0 \circ \text{FFT}([\theta, \vec{0}_K])); \quad \mathcal{V} \leftarrow \{p_k\}_{k=1}^K$
for $m \leftarrow M - 2, \ldots, 0$ **do**
    $\theta_1 \leftarrow [13\mathcal{V}_1 + 15\mathcal{V}_2 - 5\mathcal{V}_3 + \mathcal{V}_4]/48$
    $\theta_k \leftarrow [\mathcal{V}_{k-1} + 10\mathcal{V}_k + \mathcal{V}_{k+1}]/12, \quad k = 2, \ldots, K-1$
    $\theta_K \leftarrow [13\mathcal{V}_K + 15\mathcal{V}_{K-1} - 5\mathcal{V}_{K-2} + \mathcal{V}_{K-3}]/48$
    $p \leftarrow \text{iFFT}(\mu_0 \circ \text{FFT}([\theta, \vec{0}_K])); \quad \mathcal{V} \leftarrow \{p_k\}_{k=1}^K$
end for
return : $\mathcal{V}_{n_0}$

7.3.10 Up-and-Out Vanilla Options

For up-and-out vanilla options, the x, y grids are set according to equations (318)-(319) to ensure that $y_K = u = \ln(U/S_0)$ and $y = 0$ belongs to the grid. For UOC options, with the exception of $\theta_{M,K}^{UOC}$, the coefficients are identical to equation (297):

$$\theta_{M,K}^{UOC} := \begin{cases} \theta_{M,k}^{DOC} & k \leq K-1 \\ U \cdot \vartheta_{[-1,0]} - W/2 & k = K. \end{cases} \tag{298}$$

Similarly, for UOP options

$$\theta_{M,k}^{UOP} = \begin{cases} W - \exp(y_k) S_0 \cdot \vartheta_* & k = 1 \\ \theta_{M,k}^{DOP} & k = 2, ..., K \end{cases} \tag{299}$$

where $\theta_{M,k}^{DOP}$ are defined in equation (293). Other than the terminal coefficients, the algorithm is otherwise identical.

Algorithm 13 presents the BPROJ method for pricing single barrier options, which includes a call to Algorithm 12 to initialize the grids. The overall complexity is $\mathcal{O}(M \cdot N \log_2(N))$, which is driven by the two FFTs for each iteration. Overhead from the payoff coefficients and intermediate value coefficients contributes a total of $\mathcal{O}(M \cdot N)$ operations (roughly $(7N/2)\log_2(N)$ at each step). The next section describes a procedure for augmenting value coefficients for added robustness, which requires a few straightforward modifications to Algorithm 13 for DOC and UOP options.

7.3.11 Boundary Augmentation

For down-and-out options, the upper bound u is not imposed by the barrier, but is rather a truncation of the upper integration limit. Down-and-out calls are affected by this limit more so than down-and-out puts, whose values decay rapidly out of the money. As described next, we can efficiently add protection against underestimating an appropriate truncated density support for DOC and UOP options.

7.3.11.1 DOC Coefficient Augmentation

Rather than extend the convolution grid, we devise an augmentation that is considerably cheaper, yet results in a highly robust implementation. In particular, pricing is more robust to insufficient choices of the transition density's truncated support, which is a common occurrence when pricing and calibrating with heavy tailed return families.

Recall the martingale property $E[S_{t_M}|S_{t_m}] = S_{t_m}\exp((r-q)(t_M - t_m))$. To mitigate the truncation error for $\mathcal{V}_{m-1}$ for $t_{m-1} < t_{M-1}$, we use the fact that the true value at time t_m satisfies

$$\mathcal{V}^*(y, t_m) \sim S_0 e^{-q(t_M - t_m)} e^y - e^{-r(t_M - t_m)} W, \tag{300}$$

for large values of $y = \ln(S_{t_m}/S_0)$. This reflects the asymptotic behavior of European call options, since for large values of y, the probability of knock-out becomes negligible. We will use this insight to mitigate the error caused by artificially imposing an upper

barrier u. Assuming that y_K is large enough so that equation (300) is a reasonable approximation[9] for $\mathcal{V}_{m,K+k} := \mathcal{V}(y_K + k\Delta, t_m), k = 1, ..., K$, the corresponding coefficients $\bar{\theta}_m := (\bar{\theta}_{m,1}, ..., \bar{\theta}_{m,K})^\top$ are found explicitly (where $I_{K+k} := [y_K - (k-1)\Delta, y_K + (k+1)\Delta]$, and $\varphi_{a,K+k}$ is centered over I_{K+k}) as

$$\begin{aligned}\bar{\theta}_{m,k} &= a^{1/2} \int_{I_{K+k}} \mathcal{V}(y, t_m)\varphi_{a,K+k}(y)dy \\ &\approx a^{1/2} \left[S_0 e^{-q\tau(m)} \int_{I_{K+k}} e^y \varphi_{a,K+k}(y)dy - e^{-r\tau(m)} W \int_{I_{K+k}} \varphi_{a,K+k}(y)dy \right] \\ &= \exp(y_{K+k}) \cdot S_0 \vartheta_* - e^{-r\tau(m)} W, \end{aligned} \tag{301}$$

where $\tau(m) := t_M - t_m = (M-m)\Delta t$ is the only dependence of either term on t_m. Using values of $\bar{\beta}_k$ that have already been calculated, we can define the Toeplitz matrix

$$\boldsymbol{T}_1 = \Upsilon_{a,N} \cdot \begin{bmatrix} \bar{\beta}_{2K} & 0 & 0 & \cdots & 0 \\ \bar{\beta}_{2K-1} & \bar{\beta}_{2K} & 0 & \cdots & 0 \\ \bar{\beta}_{2K-2} & \bar{\beta}_{2K-1} & \bar{\beta}_{2K} & \ddots & \vdots \\ \vdots & \vdots & \vdots & \ddots & 0 \\ \bar{\beta}_{K+1} & \bar{\beta}_{K+2} & \bar{\beta}_{K+3} & \cdots & \bar{\beta}_{2K} \end{bmatrix}, \qquad \Upsilon_{a,N} := \frac{24a^2}{N},$$

and we note that $\Upsilon_{a,N} = e^{r\Delta_t} \Upsilon_{a,N}^{\Delta_t}$. The matrix $\boldsymbol{T}_1$ is a natural extension of $\boldsymbol{T}_0^{\Delta_t}$, which accounts for values that are neglected by the original convolution.[10] Moreover, given the asymptotic approximation, we are not required to calculate value function for points beyond the original grid, $\{y_k\}_{k=1}^K$, so we can correct for the neglected value contribution at a marginal cost. To evaluate $\boldsymbol{T}_1 v$ for $v = (v_1, ..., v_K)^\top$, we define

$$\mu_1 := \mathcal{D}\left\{ \Upsilon_{a,N} \cdot (\bar{\beta}_{2K}, ..., \bar{\beta}_{K+1}, 0, 0, ..., 0)^\top \right\}, \tag{302}$$

where there are K zeros in all. Equation (274) is then applied with μ_1 in place of μ_0.

We thus have the augmented value approximation

$$\boldsymbol{\mathcal{V}}_{m-1} = \boldsymbol{T}_0^{\Delta_t} \theta_m + e^{-q\tau(m)} \cdot \widetilde{\theta}^{(2)} - e^{-r\tau(m)} \cdot \widetilde{\theta}^{(1)}(W), \quad m = M-1, ..., 1, \tag{303}$$

[9] Even for small y_K, the approximation is far better than setting the peripheral values (those beyond the grid) to zero, as is done with traditional discrete convolution.

[10] This matrix is used as well for the case of up-and-out options with rebates.

where $\widetilde{\theta}^{(1)}(W)$ and $\widetilde{\theta}^{(2)}$ are the constant vectors defined by

$$\widetilde{\theta}^{(1)}(W) = W \cdot \boldsymbol{T}_1 \begin{bmatrix} 1 \\ 1 \\ \vdots \\ 1 \end{bmatrix}, \qquad \widetilde{\theta}^{(2)} = S_0 \vartheta_* \cdot \boldsymbol{T}_1 \begin{bmatrix} \exp(y_K + \Delta) \\ \exp(y_K + 2\Delta) \\ \vdots \\ \exp(y_K + K\Delta) \end{bmatrix}, \tag{304}$$

and we replace $\theta_{m,K}$ with $2\theta_{m,K}$, to account for the boundary, for $m = M-1, \ldots, 1$. Again, $\boldsymbol{T}_1$ is not actually generated and $\widetilde{\theta}^{(2)}$ is computed efficiently using the FFT and only once at initialization. Likewise, $\widetilde{\theta}^{(1)}$ is computed only once, and its elements represent a cumulative sum:

$$\widetilde{\theta}^{(1)}_k(W) = W \cdot \Upsilon_{a,N} \cdot \sum_{j=0}^{k-1} \bar{\beta}_{2K-j}, \quad k = 1, ..., K. \tag{305}$$

The coefficients at t_M are given by a simple extension of the terminal payoff. We simply augment the value approximation in (275) to obtain

$$\boldsymbol{\mathcal{V}}_{M-1} := \boldsymbol{T}_0^{\Delta_t} \theta_M^{DOC} + e^{-r\Delta_t} \left(\widetilde{\theta}^{(2)} - \widetilde{\theta}^{(1)}(W) \right). \tag{306}$$

7.3.11.2 DOP Coefficient Augmentation

Similar to the DOC case, the pricing of DOP options is made significantly more robust (to the choice of truncation interval) by a simple augmentation that relies on the value's asymptotic convergence to that of a plain vanilla put. The asymptotic approximation for UOP options, with y sufficiently small, is given by

$$\mathcal{V}^*_m(y) \sim e^{-r\tau(m)} W - S_0 e^{-q\tau(m)} e^y, \tag{307}$$

where $\tau(m) := t_M - t_m$.

To correct for the values neglected by a traditional discrete convolution, we introduce

an additional Toeplitz matrix, T_{-1}, used to price UOP options and those with rebates:

$$\boldsymbol{T}_{-1} = \Upsilon_{a,N} \cdot \begin{bmatrix} 0 & \bar{\beta}_1 & \bar{\beta}_2 & \bar{\beta}_3 & \cdots & \bar{\beta}_{K-1} \\ & 0 & \bar{\beta}_1 & \bar{\beta}_2 & \cdots & \bar{\beta}_{K-2} \\ & & \ddots & \ddots & \ddots & \vdots \\ & & & \ddots & \bar{\beta}_1 & \bar{\beta}_2 \\ & & & & \ddots & \bar{\beta}_1 \\ & & & & & 0 \end{bmatrix},$$

where we again note the use of $\Upsilon_{a,N}$ in place of $\Upsilon_{a,N}^{\Delta_t}$. Efficient computation of $\boldsymbol{T}_{-1}v$ is accomplished by defining the vector

$$\mu_{-1} := \mathcal{D}\left\{\Upsilon_{a,N} \cdot (0, ..., 0, 0, \bar{\beta}_{K-1}, ..., \bar{\beta}_1)^\top\right\}, \tag{308}$$

where there are $K+1$ zeros in all, after which equation (274) is applied with μ_{-1} in place of μ_0. We then have the augmented value approximation

$$\boldsymbol{\mathcal{V}}_{M-1} = \boldsymbol{T}_0^{\Delta_t}\theta_M^{UOP} + e^{-r\Delta_t}\left(\widetilde{\theta}^{(3)}(W) - \widetilde{\theta}^{(4)}\right) \tag{309}$$

$$\boldsymbol{\mathcal{V}}_{m-1} = \boldsymbol{T}_0^{\Delta_t}\theta_m + e^{-r\tau(m)} \cdot \widetilde{\theta}^{(3)}(W) - e^{-q\tau(m)} \cdot \widetilde{\theta}^{(4)}, \quad m = M-1, ..., 1, \tag{310}$$

where $\widetilde{\theta}^{(3)}$ and $\widetilde{\theta}^{(4)}$ are the constant vectors defined by

$$\widetilde{\theta}^{(3)}(W) = W \cdot \boldsymbol{T}_{-1}\begin{bmatrix} 1 \\ 1 \\ \vdots \\ 1 \end{bmatrix}, \qquad \widetilde{\theta}^{(4)} = S_0\vartheta_* \cdot \boldsymbol{T}_{-1}\begin{bmatrix} \exp(y_1 - K\Delta) \\ \exp(y_1 - (K-1)\Delta) \\ \vdots \\ \exp(y_1 - \Delta) \end{bmatrix}, \tag{311}$$

and we replace $\theta_{m,1}$ with $2\theta_{m,1}$, to account for the boundary, for $m = M-1, \ldots, 1$. The elements of $\widetilde{\theta}^{(3)}$ represent a cumulative sum:

$$\widetilde{\theta}_K^{(3)}(W) = 0, \quad \widetilde{\theta}_k^{(3)}(W) = W \cdot \Upsilon_{a,N} \cdot \sum_{j=1}^{K-k} \bar{\beta}_j, \quad k = 1, ..., K-1.$$

Remark 17. When speed is a primary concern, choosing too large of a truncation interval can waste resources. At the same time, a parsimonious choice is risky when dealing with heavy-tailed return distributions. The augmentations offer protection against under-specifying

the truncation support, allowing faster implementations to be applied more robustly. For calibration to barrier option markets, this is especially useful to safeguard against poor price approximations that lead the parameter search astray.

7.3.11.3 Greeks

Since the BPROJ algorithm returns value approximation across a grid of S_{t_0}, Delta and Gamma values are trivial to compute using high order finite difference approximations, and at a negligible cost. Other pricing methods require a separate recursion to recover these coefficients, so all cpu times reported for BPROJ should be thought of as including the cost to obtain these Greeks. It should be noted that, given a log asset grid spacing of Δ, for numerical stability it may be better to use points at a spacing $\lambda\Delta$ for some integer $\lambda \geq 1$, depending on the finite difference scheme employed.

7.3.12 Grid Choice and Automated Parameter Selection

There are two parameters required to apply BPROJ, $N = 2K \in \mathbb{N}_+$ which defines the number of basis elements, and $\alpha > 0$ which determines the log asset grid width. With $L_1 = 10$, and fixing an initial $\widetilde{N}$ (see Remark 19), we initialize α and Δ as $\widetilde{\alpha}$ and $\widetilde{\Delta}$:

$$\widetilde{\alpha} = L_1\sqrt{T \cdot c_2 + \sqrt{T \cdot c_4}}, \qquad \widetilde{\Delta} = 2\widetilde{\alpha}/(\widetilde{N} - 1) \tag{312}$$

where c_2, c_4 are the second and fourth cumulants of $\ln(S_{t+1}/S_t)$ (see [61, 62]). Cumulants for common Lévy processes are given in Table 43.

Remark 18. In [51], concerns are raised about the robustness of the cumulant based approach, namely equation (312). They show that if, instead of using $T \cdot c_i$ in equation (312), the grid was determined by $\Delta_t \cdot c_i$, the COS method became unstable and prices diverged. However, our goal is to price a contract which can at expiry deliver a payoff in terms of S_T, rather than S_{Δ_t}. Hence, the terminal grid should be chosen in terms of the cumulants of $\ln(S_T/S_0)$, as we have initialized in equation (312), rather than $\ln(S_{\Delta_t}/S_0)$.

Even with the cumulants chosen based on $\ln(S_T/S_0)$, we provide additional layers of protection against under-specifying α. The first is the augmentation procedure introduced in Section 7.3.11. By intentionally under-specifying L_1 (and hence α), Figure 35 illustrates

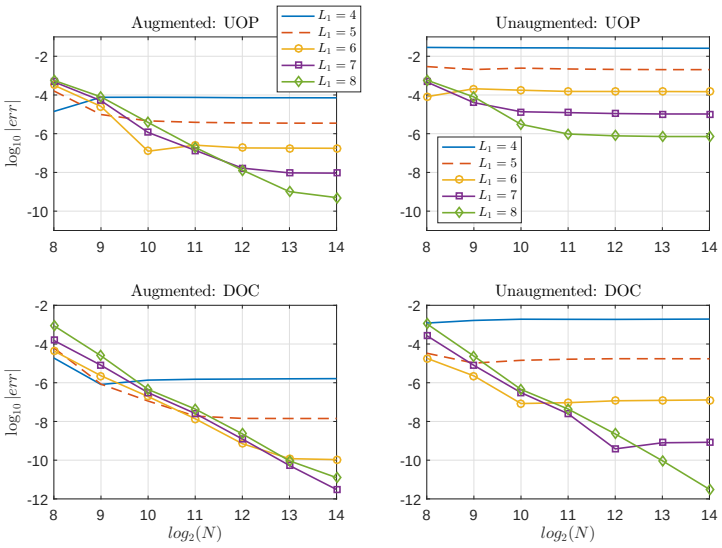

Figure 35: Comparison of BPROJ with and without augmentation for weekly-monitored knock-out options, with values of L_1 lower than the recommended range (with α, Δ fixed by (312)). We consider the exceptionally heavy-tailed model: NIG(15,-5, 0.5), with $r = .05, q = .02, T = 1$, and $S_0 = W = 100$. For up-and-out, $U = 120$, while $L = 80$ for down-and-out. Reference prices obtained by COS [62] with $N = 2^{16}$ and $L_1 = 10$. For this example, the method of automated parameter selection is not applied.

that some accuracy can be recovered by the boundary augmentation, since the value function has known asymptotic behavior. The left panels compare the augmented prices with the un-augmented prices in the right panels, for several insufficient values of L_1. While the attainable accuracy is still limited, there is an appreciable gain for exceptionally heavy-tailed models. Two additional layers of protection are provided in Section 7.3.12.1, which automates the selection of grid parameters to avoid under-specifying α and N.

7.3.12.1 Automated Parameter Selection

In practical pricing applications, such as calibration, an automated procedure is required to determine the algorithm parameters α and N (or equivalently Δ), without user intervention. We develop a procedure which utilizes an estimate for the probability error on the terminal grid, as well as the a proxy for error in intermediate integrations during recursions. From

[64, 67] we can represent the cumulative distribution of log return $Y_T = \ln(S_T/S_0)$ by

$$\begin{aligned} F(x) &= \int_{-\infty}^{x} p_T(y)dy = \int_{\mathbb{R}} p_T(y)\mathbb{1}_{(-\infty,x)}dy \\ &= \mathcal{F}(\mathbb{1}_{(-\infty,x)} \cdot p_T)(0) = \frac{1}{2} - \frac{i}{2}\mathcal{H}(e^{-i\xi x}\phi_T(\xi))(0), \end{aligned} \tag{313}$$

where $\mathcal{H}$ denotes the Hilbert transform

$$\mathcal{H}f(z) = \frac{1}{\pi}\mathrm{PV}\int_{\mathbb{R}} \frac{f(y)}{z-y}dy.$$

Applied to equation (313), we have the discrete approximation

$$F(x) \approx F_{\Delta_\xi,N}(x) := \frac{1}{2} + \frac{i}{2}\sum_{n=-(N-1)}^{N-1} \phi_T((n-\tfrac{1}{2})\Delta_\xi)\frac{\exp(-ix(n-\frac{1}{2})\Delta_\xi)}{(n-\frac{1}{2})\pi}. \tag{314}$$

We start by fixing a value of $L_1 = 10$ which initializes the grid-width α according to equation (312), with a slight modification to impose a lower bound on α in terms of $\ln(W/S_0)$ and the barrier (see Algorithm 14 which summarizes the full procedure). We then estimate the probability mass of $\ln(S_T/S_0)$ which is neglected by our grid choice, and increase the grid-width by a fixed multiplier $\tau > 1$, until a probability tolerance $\epsilon_1 > 0$ is met. Moreover, since a grid for $\ln(S_T/S_0)$ is much larger than required for any individual log return over an increment Δ_t, the truncation error for intermediate valuations is negligible.

For a down-and-out option, if the right tail estimate $|1-F_{\Delta_\xi,N}(x_{N/2})|\cdot\max\{S_0, W\} > \epsilon_1$, we double the grid size N, set $\alpha \leftarrow \tau\alpha$, and reestimate. For an up-and-out option, we similarly expand the grid as long as $|F_{\Delta_\xi,N}(x_1)| \cdot \max\{S_0, W\} > \epsilon_1$, which estimates the error in the left tail. Note that in either case, we are only concerned with the probability within the continuation region.

In addition to controlling truncation error we utilize the martingale property of $e^{-(r-q)t}S_t$, namely $E[S_{t+\Delta_t}|S_{t_m}] = S_{t_m}\exp((r-q)\Delta_t)$, to obtain a proxy for integration error incurred at each step:

$$E_N := \Upsilon_{a,N} \cdot \vartheta_* \cdot \sum_{n=1}^{N} \bar{\beta}_n \exp(x_1 + (n-1)\Delta) \tag{315}$$

which approximates the expectation of log-return $\mathbb{E}[\exp(Y_{\Delta_t})] = \exp((r-q)\Delta_t)$ using the projected density (calculated from ϕ_{Δ_t}). In particular, the error in estimating $\bar{\beta}_n$, and our

ability to accurately calculate intermediate value integrals, is reflected in equation (315). Hence, once the probability tolerance ϵ_1 is satisfied, we further double the grid size as long as $|E_N - \exp((r-q)\Delta_t)| \cdot M > \epsilon_2$, where the multiplier M accounts for the number of integral approximations made during the algorithm.

Remark 19. In order to apply the automated parameter selection approach, an initial starting value of L_1 and N are required. We find that $L_1 \leftarrow 10$ is a good choice (for Parisian options, $L_1 \leftarrow 12$ to account for excursions beyond the barrier), while the initial value of N depends on $\Delta_t = T/M$. For $\Delta_t \leq 1/100$ (which includes daily monitoring), we initialize $N \leftarrow 2^{10}$. Else if $\Delta_t \leq 1/40$, we initialize $N \leftarrow 2^9$. Else, we initialize $N \leftarrow 2^8$. In Algorithm 14, we set $\tau \leftarrow 1.1$, so at each stage the probability threshold is not satisfied, we increase the grid-width by ten percent. We set the tolerance thresholds $\epsilon_1 \leftarrow$5e-08 and $\epsilon_2 \leftarrow$1e-05 to conservatively achieve overall valuation error tolerance goal of TOL = 5e-04, which is sufficient for practical purposes. In general, a maximum value of N, for example $N = 2^{17}$, should be enforced as a stopping criteria for automated parameter selection.

Once sufficiently large values of α and N are determined, the grid will be perturbed slightly to improve the convergence rate and smoothness. In particular, we face a choice of which *two* select points to align with the grid. Our first choice ensures that the knock-out barrier belongs to the grid, which is essential for smooth (and rapid) convergence. For the second choice, rather than place the payoff kink, $\ln(W/S_0)$, on the grid (to account for a discontinuous first derivative), a better alignment is found by ensuring that $\ln(S_0/S_0) = 0$ is a member, to avoid an interpolation at the recursion's end (for double barrier options, interpolation is required). Because of the basis representation, and the way in which value coefficients are later computed, no accuracy is lost by failing to align $\ln(W/S_0)$ with the grid. Hence, by starting with an initial resolution, an adjustment is made to place $y = 0$ on the grid as follows.

7.3.12.2 Down-and-out Grid

For down-and-out options (vanilla or otherwise), $x_1 := l$ coincides with the knock-out barrier. Given values for N and α (for example, generated by the procedure in Section

Algorithm 14 Initialization by Automated Parameter Selection

Set $L_1 \leftarrow 10$; Initialize N as in Remark 19
$\epsilon_1 \leftarrow$5e-08; $\epsilon_2 \leftarrow$1e-05; $\tau \leftarrow 1.1$
if Down-and-out: **then**
  $\alpha \leftarrow \max\left\{\tau \cdot (\max\{0, \ln(W/S_0)\} - l),\ L_1\sqrt{c_2 T + \sqrt{c_4 T}}\right\}$
  $x^* \leftarrow l + \alpha$; $\Delta_\xi \leftarrow \pi(N-1)/(\alpha N)$
  while $|1 - F_{\Delta_\xi, N}(x^*)| \cdot \max\{S_0, W\} > \epsilon_1$ **do**
    $\alpha \leftarrow \tau\alpha$; $N \leftarrow 2N$; $x^* \leftarrow l + \alpha$; $\Delta_\xi \leftarrow \pi(N-1)/(\alpha N)$
  end while
  $\mathcal{E} \leftarrow 2\epsilon_2$; $N \leftarrow N/2$
  while $\mathcal{E} > \epsilon_2$ **do**
    $N \leftarrow 2N$; $\Delta \leftarrow 2\alpha/(N-1)$; $n_0 \leftarrow \lfloor 1 - l/\Delta \rfloor$
    if $\Delta <= l$, **then** $\Delta \leftarrow l/(1 - n_0)$ **end if**
    Call Algorithm 12 to obtain $\bar{\beta}$
    $\epsilon_2 \leftarrow |E_N - \exp((r-q)\Delta_t)| \cdot M$ (E_N defined in equation (315))
  end while
else Up-and-out:
  $\alpha \leftarrow \max\left\{\tau \cdot (u - \min\{0, \ln(W/S_0)\}),\ L_1\sqrt{c_2 T + \sqrt{c_4 T}}\right\}$
  $x^* \leftarrow u - \alpha$; $\Delta_\xi \leftarrow \pi(N-1)/(\alpha N)$
  while $|F_{\Delta_\xi, N}(x^*)| \cdot \max\{S_0, W\} > \epsilon_1$ **do**
    $\alpha \leftarrow \tau\alpha$; $N \leftarrow 2N$; $x^* \leftarrow u - \alpha$; $\Delta_\xi \leftarrow \pi(N-1)/(\alpha N)$
  end while
  $\mathcal{E} \leftarrow 2\epsilon_2$; $N \leftarrow N/2$
  while $\mathcal{E} > \epsilon_2$ **do**
    $N \leftarrow 2N$; $\Delta \leftarrow 2\alpha/(N-1)$; $n_0 \leftarrow \lfloor N/2 - u/\Delta \rfloor$
    if $\Delta \leq u$, **then** $\Delta \leftarrow u/(N/2 - n_0)$ **end if**
    Call Algorithm 12 to obtain $\bar{\beta}$
    $\epsilon_2 \leftarrow |E_N - \exp((r-q)\Delta_t)| \cdot M$ (E_N defined in equation (315))
  end while
end if
return : $\bar{\beta},\ N,\ \Delta,\ \alpha,\ n_0$

7.3.12.1), we define $\bar{\Delta} = 2\alpha/(N-1)$ and $K = N/2$. As long as $\bar{\Delta} \leq |l|$, we define[11]

$$n_0 := \lfloor 1 - l/\bar{\Delta} \rfloor, \quad \Delta := l/(1-n_0), \quad a := 1/\Delta, \tag{316}$$

which establishes the perturbed grid

$$x_1 = l, \quad x_n = x_1 + (n-1)\Delta, \quad n = 1, ..., K. \tag{317}$$

After the perturbation, $x_{n_0} = 0$.

7.3.12.3 Up-and-out Grid

For up-and-out options, $x_K := u$, and as long as $\bar{\Delta} \leq u$ we define[12]

$$n_0 := \lfloor K - u/\bar{\Delta} \rfloor, \quad \Delta := u/(K-n_0), \quad a := 1/\Delta, \tag{318}$$

which establishes the perturbed grid

$$x_1 = u - (K-1)\Delta, \quad x_n = x_1 + (n-1)\Delta, \quad n = 1, ..., K. \tag{319}$$

The selection of log-asset grids for barrier options is summarized in Algorithm 14, which additionally provides a method of automated parameter selection for the two input parameters to BPROJ, namely N and α. The approach, which facilitates hands-off calibration, is detailed in Section 7.3.12.1 .

7.3.12.4 Robustness

We previously addressed the robustness to under-specifying the truncated density support with respect to the support width parameter L_1 (recall Figure 35). We now illustrate the robustness of our method using automated parameter selection. In particular, we address a concern raised in [51] (see Remark 18) by reproducing the experiment in which the COS method diverged using a cumulant-based grid-width selection. By comparison, we are able to achieve the desired TOL = 5e-04 (for absolute pricing errors) as discussed in Remark 19. The model is KoBoL with $\lambda_- = -60, \lambda_+ = 50, \nu = 0.7, c = 4$ (or in terms of $(C, G, M, Y) =$

[11] In the case of $|l| < \widetilde{\Delta}$, we set $\Delta = \widetilde{\Delta}$, $n_0 = 1$, and at the algorithm's end we use linear interpolation between the points n_0 and $n_0 + 1$ to determine the value.

[12] In the case of $0 < u < \bar{\Delta}$, we set $\Delta = \bar{\Delta}$, $n_0 = K - 1$, and at the algorithm's end we use linear interpolation between the points n_0 and $n_0 + 1$ to determine the value.

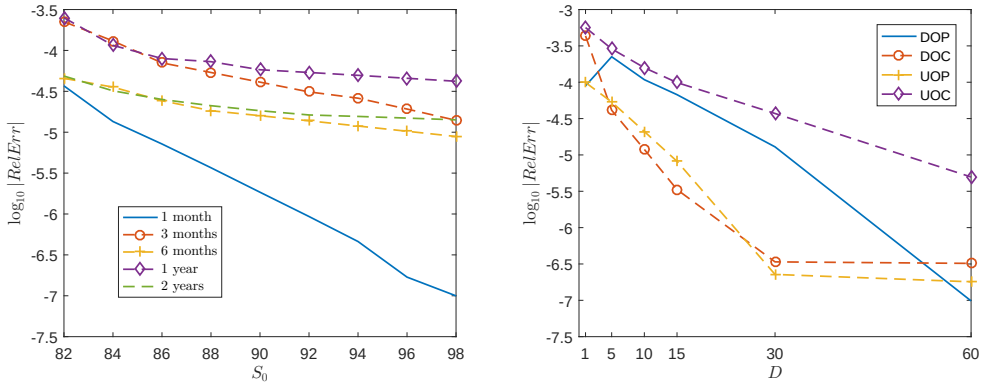

Figure 36: Robustness of automated parameter selection for the divergent COS example in [51].

$(4, 50, 60, 0.7))$ with $r = 0.04, q = 0.02$. A DOP contract with $L = 80$ and $W = 100$ is priced along a spectrum of S_0.

The left panel of Figure 36 illustrates the *relative* pricing errors for contracts of various time to maturity, with $\Delta_t = 1/252$ fixed (where we note that the value approaches zero as S_0 nears $L = 80$). While the experiment of [51] resulted in an explosion of prices for COS, our method of parameter selection performs robustly, achieving the desired tolerance (for absolute error) uniformly. Moreover, to demonstrate that this robustness extends to each of the alternative contacts types (including the DOC with unbounded payoff), the right panel of Figure 36 provides relative pricing errors for each type as a function of $D = |S_0 - H|$. Here H denotes the barrier, with $H = L$ for down-and-out and $H = U$ for up-and-out. Even as H approaches S_0, the method maintains its accuracy. To illustrate robustness across models, additional experiments are provided in Table 41 with the same desired TOL = 5e-04.

7.3.13 Rebates and Digital Options

Barrier option contracts often specify a rebate which is paid to the holder of a knock-out option in the event of barrier breach. We consider time dependent rebates, $RB(t)$, which award the holder at the time of breach (rebate payments deferred to contract maturity are analogous). In particular, if $\mathcal{V}_{m-1}^{aug}$ denotes the value augmentation (for UOP and DOC

options), then the rebate augmented formula for $m = M, ..., 1$ is simply

$$\mathcal{V}_{m-1} = \boldsymbol{T}_0^{\Delta_t}\theta_m + \mathcal{V}_{m-1}^{aug} + \mathcal{V}_{m-1}^{RB},$$

where for $\widetilde{\theta}^{(3)}(W)$ and $\widetilde{\theta}^{(1)}(W)$ defined in equations (311) and (304) respectively

$$\mathcal{V}_{m-1}^{RB} := \begin{cases} RB(t_m) \cdot \widetilde{\theta}^{(3)}(1) & \text{Down-and-Out} \\ RB(t_m) \cdot \widetilde{\theta}^{(1)}(1) & \text{Up-and-Out.} \end{cases}$$

The terminal payoff coefficients θ_M are unaltered. Digital options are also simple to price using $\widetilde{\theta}^{(3)}(1)$ and $\widetilde{\theta}^{(1)}(1)$, and with augmentations to reflect the fact that, for y sufficiently in-the-money, the value is asymptotically that of a discount bond, $\mathcal{V}(y, t_m) \sim e^{-r(t_M - t_m)}$.

7.3.14 Pricing Double Barrier Options

Double barrier options impose a corridor in which an underlying must remain to receive the payout at maturity. For these contracts, the corridor is generally too narrow for the density to be recovered accurately due to aliasing, especially for infrequently monitored contracts, as illustrated in Figure 37. Here, $L_2 = 1$ corresponds to the density projection over the support width implied by the barriers $[L, U] = [80, 120]$, and the presence of aliasing is clear[13]. By doubling the width, $L_2 = 2$, the effect is mitigated. Hence, rather than equate the support width imposed by the barrier with the one used for projection, we obtain the projected density over a potentially wider support, and then use only those coefficients which correspond to points on the value grid. Equation (321) below prescribes an extended support which is used when the log return process has known cumulants.

Suppose that a double barrier option knocks out when the underlying exits[14] $[L, U]$, denoted in log asset space by $[l, u] = [\ln(L/S_0), \ln(U/S_0)]$. Define the barrier support width by $\alpha := u - l$, and fix a budget of K points on the value grid, for a resolution

$$\Delta := \frac{u - l}{K - 1} = \frac{\alpha}{K - 1}, \qquad a := 1/\Delta. \tag{320}$$

We further define $N_\alpha := 2K$, the number of projection coefficients used in the convolution, which will be a subset of recovered coefficients on a grid of size N specified below. To

[13] The COS method is also susceptible to aliasing error.

[14] The option typically knocks out at either of the points L or U, so the support is truly (L, U), but the distinction is irrelevant from the perspective of pricing.

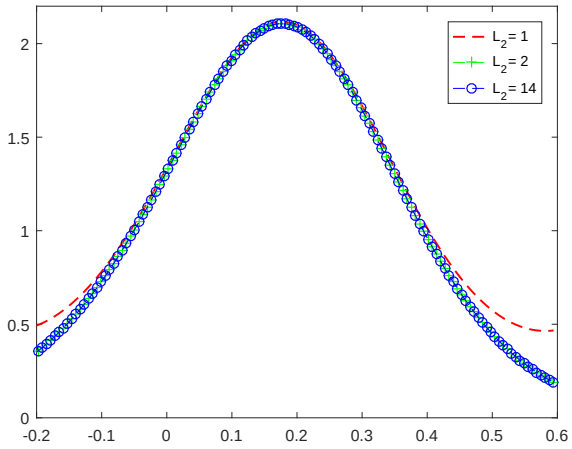

Figure 37: Removal of Aliasing: comparison of projected densities for $\Delta_t = 1/12$ corresponding to double barriers $[80, 120]$ and $S_0 = 100$. Aliasing observed when density support width equated with barrier width, $L_2 = 1$. Setting $L_2 \geq 2$ removes aliasing in this example, and equation (321) prescribes $L_2 = 3$. Model: NIG (10, -1, 5), $r = .05, q = .02$, $T = 1$.

avoid aliasing, we determine a sufficient support by the method of [61, 62], with a slight modification. With $L_1 := 10$, and c_j the jth cumulant of $\ln(S_{t+1}/S_t)$, we fix

$$N := L_2 \cdot N_\alpha, \qquad L_2 := \left\lceil \frac{2L_1}{\alpha} \sqrt{c_2 \Delta_t + \sqrt{c_4 \Delta_t}} \right\rceil . \tag{321}$$

To avoid an excessively large choice of N, we will fix a cap of $N \leq 4 \cdot N_\alpha$ when $M \leq 12$, and $N \leq 3 \cdot N_\alpha$ otherwise (it should also be noted that $N \geq N_\alpha$). For weekly and daily monitored contracts, it is often the case that $N = N_\alpha$, but the definition in equation (321) safeguards against possible aliasing.

The projected density is recovered by Algorithm 15, centered over the origin ($\nu_1 := (1-L_2K)\Delta$), but now the coefficients that participate in the convolution are restricted to $\bar{\beta}_k$, $k = (L_2-1)\cdot K+1, ..., (L_2+1)\cdot K-1$. For a double barrier call (DBC), coefficients are given by the UOC coefficients in Section 7.3.10, while double barrier put (DBP) coefficients are given by the DOP coefficients in Section 7.3.8. Since l, u belong to the grid, but $\ln(S_0/S_0)$ does not, we use a five-point cubic spline interpolation about n_0 to find the value. The algorithm for double-barrier options is otherwise analogous to Algorithm 13 for single-barrier options, and is omitted.

Algorithm 15 Projection Coefficients of Transition Density (Anti-aliasing)

1: Input: Δ, N; Set $\lambda \leftarrow 2$ for double-barrier
2: $\nu_1 \leftarrow (1 - N/2)\Delta$; $a \leftarrow 1/\Delta$
3: $\widetilde{N} \leftarrow \lambda N$
4: $\Delta_\xi \leftarrow 2\pi a/\widetilde{N}$; $\Upsilon_{a,\widetilde{N}} \leftarrow 24a^2/\widetilde{N}$
5: $\Omega_k \leftarrow k\Delta_\xi, \quad k = 1, ..., \widetilde{N} - 1$
6: $\Omega_k \leftarrow \exp(-i\nu_1\Omega_k) \cdot \phi_{\Delta_t}(\Omega_k) \cdot h_a(\Omega_k), \quad k = 1, ..., \widetilde{N} - 1$
7: $\bar{\beta} \leftarrow \Re\left\{\text{FFT}\left([1/(24a^2), \Omega_1, ..., \Omega_{\widetilde{N}-1}]\right)\right\}$
8: Return: $\bar{\beta}, \Upsilon_{a,\widetilde{N}}$

7.4 Parisian and Step Barrier Options

A more exotic type of barrier option, the *Parisian* option, is one for which the underlying must spend a prescribed duration of time inside the knock-out region before the contract becomes worthless (or issues a rebate). A discretely monitored *cumulative* Parisian option allocates a fixed budget Γ, and stipulates that the contract knocks-out the $(\Gamma + 1)$st time it is observed within the knock-out region. That is, the holder will receive a European payoff $G(S_T)$ at delivery if the underlying is observed *at most* Γ times within the knock-out region during the contract's life. A *resetting* Parisian option with budget Γ will deliver a European payoff unless the underlying is observed within the knock-out region on $\Gamma + 1$ *consecutive* monitoring dates. The BPROJ method applies to both specifications, with or without rebates, and with single or double barriers. We denote the single knock-out barrier of a Parisian option by H, and $h := \ln(H/S_0)$. For an up-and-out contract, $H = U > 0$, while for a down-and-out $H = L > 0$. Since the underlying can travel within the knock-out region for up to Γ monitoring dates, our grid in log-asset space must extend beyond h.

7.4.1 Automated Parameter Selection

As before we initialize α using the cumulants of the underlying $\ln(S_T/S_0)$, and a grid on $(-\alpha/2, \alpha/2)$ which is now centered about $\ln(S_0/S_0)$. This defines the grid boundaries x_1 and $x_{N/2}$, from which we estimate the truncation error of log-return. Applying a result of [64] (see also [67]), the probability mass of $\ln(S_T/S_0)$ over the interval $[x, y]$ is given by

$$\mathbb{P}[x < \ln(S_T/S_0) < y] = \int_{-\infty}^{\infty} e^{-i\xi(y+x)/2} \frac{\sin(\xi(y-x)/2)}{\pi\xi} \phi_T(\xi) d\xi.$$

Fixing $N > 0$ and $\Delta_\xi > 0$, we have the approximation $\mathbb{P}[x < Y_T < y] \approx F_{\Delta_\xi,N}(x,y)$ for $Y_T = \ln(S_T/S_0)$, where

$$F_{\Delta_\xi,N}(x,y) := \frac{\Delta_\xi}{\pi}\left[\lambda_1 + \sum_{1\le|n|\le N-1} e^{-i\lambda_2(n\Delta_\xi)}\frac{\sin(\lambda_1(n\Delta_\xi))}{n\Delta_\xi}\phi_T(n\Delta_\xi)\right] \tag{322}$$

where $\lambda_1 = (y-x)/2$ and $\lambda_2 = (y+x)/2$. Fixing a probability tolerance $\epsilon_1 > 0$, and gridwidth multiplier $\tau > 1$, if $|1 - F_{\Delta_\xi,N}(x_1, x_{N/2})| > \epsilon_1$, we double the grid size N, set $\alpha \leftarrow \tau\alpha$, and reestimate. We again employ the proxy for integration error using equation (315), for which the grid size is further increased until a tolerance ϵ_2 is met. Algorithm 16 summarizes this parameter selection method for single-barrier Parisian options. Note that the initial grid-width $\alpha >= 2\tau|h|$, which ensures that the grid extends beyond barrier.

While the choice of n_0, n_h differs depending on the grid, we know in general that $\ln(S_0/S_0)$ satisfies $x_{n_0} \le 0 < x_{n_0+1}$, the payoff kink satisfies $x_{\bar{n}} \le \ln(W/S_0) < x_{\bar{n}+1}$, and the barrier $x_{n_h} = h$ lies on the grid. Whenever feasible, we align the grid so that $x_{n_0} = 0$ as well. In particular, as long as $|h| \ge \Delta$, where Δ is the final grid-width chosen by Algorithm 16, $x_{n_0} = 0$. However, if $0 < |h| < \Delta$, aligning both h and 0 with grid-points risks shrinking the grid-width exceedingly. Hence, in this case we leave the grid unadjusted, and use interpolation upon termination to determine the value at 0.

7.4.2 Up-and-Out Parisian Call

Consider first the cumulative up-and-out Parisian call (UOPC) with budget[15] Γ, which pays $G(S_T) = (S_T - W)^+$ at expiry assuming S_{t_m} is observed above the knock-out barrier $U > 0$ at most Γ times for $m = 0, \dots, M$. The value function $\mathcal{V}_m(x, \gamma_m)$, conditional on $\ln(S_{t_m}/S_0) = x$ now also depends on the variable

$$\gamma_m = \sum_{0\le j\le m} \mathbb{1}_{[S_j > U]}. \tag{323}$$

The value recursion is similar to a standard UOC, with a few modifications. In the first stage we have $\boldsymbol{\mathcal{V}}_{M-1}(\gamma_{M-1}) = \boldsymbol{T}_0^{\Delta_t}\theta_M(\gamma_{M-1})$, where

$$\theta_{M,k}(\gamma_{M-1}) = a^{1/2}\int \mathcal{V}_M(y,\gamma_M)\varphi_{a,k}(y)dx = a^{1/2}\int G(S_0e^y)\mathbb{1}_{[\gamma_M\le\Gamma]}(y)\varphi_{a,k}(y)dy.$$

[15] An in-progress Parisian option with γ_0 credits spent at time t_0 is priced identically, but with a remaining budget of $\widetilde{\Gamma} = \Gamma - \gamma_0$. Note, from definition (323), γ_0 includes any breach which occurs at t_0.

Algorithm 16 Parisian Option: Automated Parameter Selection

Set $L_1 \leftarrow 12$; Initialize N as in Remark 19
$h \leftarrow \ln(H/S_0)$, where $H = U$ for up-and-out, $H = L$ for down-and-out
$\epsilon_1 \leftarrow$5e-08; $\epsilon_2 \leftarrow$1e-05; $\tau \leftarrow 1.1$
$\alpha \leftarrow \max\left\{2\tau|h|,\ L_1\sqrt{c_2T + \sqrt{c_4T}}\right\}$
$\mathcal{E}_1 \leftarrow 2\epsilon_1$; $N \leftarrow N/2$; $\alpha \leftarrow \alpha/\tau$
while $|\mathcal{E}_1| > \epsilon_1$ **do**
    $N \leftarrow 2N$; $\alpha \leftarrow \tau\alpha$; $\Delta \leftarrow 2\alpha/(N-1)$; $\Delta_\xi \leftarrow 2\pi/(\Delta N)$
    $x_1 \leftarrow -\alpha/2$; $x_{N/2} \leftarrow x_1 + (N/2-1)\Delta$
    $\mathcal{E}_1 \leftarrow |1 - F_{\Delta_\xi,N}(x_1, x_{N/2})|$ (see equation (322) for $F_{\Delta_\xi,N}$)
end while
$\mathcal{E}_2 \leftarrow 2\epsilon_2$; $N \leftarrow N/2$
while $|\mathcal{E}_2| > \epsilon_2$ **do**
    $N \leftarrow 2N$; $\Delta \leftarrow 2\alpha/(N-1)$
    $n_h \leftarrow \lfloor (h + \alpha/2)/\Delta + 1 \rfloor$; $x_1 \leftarrow h - (n_h - 1)\Delta$; $n_0 \leftarrow n_h$
    if $h \neq 0$ **then**
        $n_0 \leftarrow \lfloor 1 - x_1/\Delta \rfloor$
        if $|h| \geq \Delta$ **then**
            $\Delta \leftarrow (h-0)/(n_h - n_0)$; $x_1 \leftarrow \Delta(1-n_0)$; $n_h \leftarrow \lfloor n_0 + h/\Delta \rfloor$
        end if
    end if
    Call Algorithm 12 to obtain $\bar{\beta}$
    $\mathcal{E}_2 \leftarrow |E_N - \exp((r-q)\Delta_t)| \cdot M$ (see equation (315) for E_N)
end while
return : $N,\ \Delta,\ x_1,\ n_h,\ n_0,\ \bar{\beta}$

We denote $\theta_M(\gamma_{M-1})$ as a function of γ_{M-1}, since the value of $y = \ln(S_{t_M}/S_0)$ and γ_{M-1} are sufficient to determine $\gamma_M = \gamma_M(y, \gamma_{M-1})$. Any value of $\gamma_{M-1} \leq \Gamma - 1$ will result in the same payoff $G(S_{t_M}) = (S_{t_M} - W)^+$ at maturity. However, if $\gamma_{M-1} = \Gamma$, there is still a possibility of knock-out in the final stage, if $x > u$.

Hence, for $k = 1, \ldots, K$ and $\gamma_{M-1} = \gamma$ the terminal coefficients are defined by

$$\theta_{M,k}(\gamma) = \begin{cases} \theta^{EC}_{M,k} & \gamma = 0, \ldots, \Gamma - 1 \\ \theta^{UOC}_{M,k} & \gamma = \Gamma, \end{cases} \tag{324}$$

where $\theta^{EC}_{M,k}$ are the European call coefficients defined by

$$\theta^{EC}_{M,k} = \begin{cases} 0 & k = 1, \ldots, \bar{n} - 1 \\ W\left(\delta_0^{call} e^{-\rho} - \bar{\delta}_0^{call}\right) & k = \bar{n} \\ W\left(e^{\Delta - \rho}\left(\vartheta_{[0,1]} + \delta_1^{call}\right) - \left(1/2 + \bar{\delta}_1^{call}\right)\right) & k = \bar{n} + 1 \\ S_0 \exp(y_k) \cdot \vartheta_* - W & k = \bar{n} + 2, \ldots, K \end{cases} \tag{325}$$

and

$$\bar{n} \leftarrow \lfloor ((\ln(W/S_0) - x_1)/\Delta + 1 \rfloor, \quad \rho \leftarrow \ln(W/S_0) - x_{\bar{n}}, \quad \zeta := \rho/\Delta. \tag{326}$$

Similarly, $\theta^{UOC}_{M,k} = \theta^{EC}_{M,k}$ for $k = 1, \ldots, n_h - 1$, while $\theta^{UOC}_{M,n_h} = U \cdot \vartheta_{[-1,0]} - W/2$, and $\theta^{UOC}_{M,k} = 0$ for $k = n_h + 1, \ldots, K$, where we recall that $x_{n_h} = h$ is the barrier.

Once $\theta_{M,k}(\gamma_{M-1})$ is obtained for $0 \leq \gamma_{M-1} \leq \Gamma$, we compute each of $\boldsymbol{\mathcal{V}}_{M-1}(\gamma_{M-1}) = \boldsymbol{T}_0^{\Delta_t} \theta_M(\gamma_{M-1})$ to initialize the recursion. For $m = M - 1, \ldots, 1$, we define $\theta_m(\gamma_{m-1})$ by splitting into two cases. For $\gamma_{m-1} = \gamma$, with $0 \leq \gamma \leq \Gamma - 1$ we have

$$\theta_{m,k}(\gamma) = \begin{cases} g_m^{(\gamma^*)}(x_{k-1}, x_{k+1}) & k = 1, \ldots, n_h - 1 \\ g_m^{(\gamma^*)}(x_{k-1}, u) + g_m^{(\gamma+1)}(u, x_{k+1}) & k = n_h \\ g_m^{(\gamma+1)}(x_{k-1}, x_{k+1}) & k = n_h + 1, \ldots, K, \end{cases} \tag{327}$$

where $g_m^{(\gamma)}(b, c)$ is defined by

$$g_m^{(\gamma)}(b, c) := a^{1/2} \int_b^c \mathcal{V}_m(y, \gamma) \varphi_{a,k}(y) dy. \tag{328}$$

At this point, there is a slight difference in implementation for reseting versus cumulative Parisian options, which we capture by the variable γ^*. For $0 \leq \gamma^* \leq \Gamma^*$, we set

$$\begin{aligned} \gamma^* &:= \gamma, \quad \text{Cumulative Parisian Option} \\ \gamma^* &:= 0, \quad \text{Resetting Parisian Option.} \end{aligned}$$

Equation (327) follows from the fact that $\gamma_m = \gamma^*_{m-1}$ when $\ln(S_{t_m}/S_{t_{m-1}}) \leq u$, while $\gamma_m = \gamma_{m-1} + 1$ when $\ln(S_{t_m}/S_{t_{m-1}}) > u$. For the resetting Parisian option, whenever the underlying exits the knock-out region (for any excursion of up to Γ monitoring dates), the counter γ resets to zero.

The integrals defining $\theta_{m,k}(\gamma)$ are split based on the relation between x_k and u. At the barrier, u, the integral defining $\theta_{m,n_h}(\gamma)$ is split evenly between the two value functions, $\mathcal{V}_m(y, \gamma^*)$ and $\mathcal{V}_m(y, \gamma + 1)$, since $x_{n_h} = u$. For $|k - n_h| > 1$, one or the other value function is active. Similarly, for $\gamma_{m-1} = \Gamma$

$$\theta_{m,k}(\Gamma) = \begin{cases} g_m^{(\Gamma^*)}(x_{k-1}, x_{k+1}) & k = 1, \ldots, n_h - 1 \\ g_m^{(\Gamma^*)}(x_{k-1}, u) & k = n_h \\ 0 & k = n_h + 1, \ldots, K, \end{cases} \tag{329}$$

where the second two equations follow from $\mathcal{V}(x, \Gamma + 1) = 0$.

We approximate the coefficients in the same way as for ordinary barrier options in Section 7.3.6.2, using local polynomial interpolation. Based on equation (278), we have three types approximations, defined for $0 \leq \gamma \leq \Gamma$ by

$$\begin{aligned} a_{m,k}(\gamma) &:= \left[13\mathcal{V}_{m,k}(\gamma) + 15\mathcal{V}_{m,k+1}(\gamma) - 5\mathcal{V}_{m,k+2}(\gamma) + \mathcal{V}_{m,k+3}(\gamma)\right]/48 \\ b_{m,k}(\gamma) &:= \left[\mathcal{V}_{m,k-1}(\gamma) + 10\mathcal{V}_{m,k}(\gamma) + \mathcal{V}_{m,k+1}(\gamma)\right]/12 \\ c_{m,k}(\gamma) &:= \left[13\mathcal{V}_{m,k}(\gamma) + 15\mathcal{V}_{m,k-1}(\gamma) - 5\mathcal{V}_{m,k-2}(\gamma) + \mathcal{V}_{m,k-3}(\gamma)\right]/48 \end{aligned} \tag{330}$$

and $a_{m,k}(\Gamma + 1) = b_{m,k}(\Gamma + 1) = c_{m,k}(\Gamma + 1) \equiv 0$. Note that $a_{m,k}(\gamma)$ and $c_{m,k}(\gamma)$ define boundary integral approximations with cubic interpolation, and $b_{m,k}(\gamma)$ defines interior integral approximations with quadratic interpolation. Applying these rules to the integrals in equations (327) and (329), we obtain the set of theta coefficients that are used in the

algorithm for $0 \leq \gamma \leq \Gamma$

$$\theta_{m,k}(\gamma) := \begin{cases} a_{m,k}(\gamma^*) & k = 1 \\ b_{m,k}(\gamma^*) & k = 2, \ldots, n_h - 1 \\ c_{m,k}(\gamma^*) + a_{m,k}(\gamma + 1) & k = n_h \\ b_{m,k}(\gamma + 1) & k = n_h + 1, \ldots, K - 1 \\ c_{m,k}(\gamma + 1) & k = K. \end{cases} \tag{331}$$

Not that these coefficients apply to any type of up-and-out contract, where particular terminal payoffs are handled by the terminal coefficients $\theta_{M,k}(\gamma)$. The recursion then proceeds as before, with $\boldsymbol{\mathcal{V}}_{m-1}(\gamma) = \boldsymbol{T}_0^{\Delta_t}\theta_m(\gamma)$ for $0 \leq \gamma \leq \Gamma$. At termination, a value surface $\boldsymbol{\mathcal{V}}_0(\gamma)$ is obtained (note that we only require $\boldsymbol{\mathcal{V}}_0(0)$).

Algorithm 17 Parisian Option: Initialization

Parameters: $H = L$ or U; $W,\ \Gamma,\ S_0,\ r,\ q,\ T,\ M$; $\quad \Delta_t \leftarrow T/M$
Call Algorithm 16 to obtain: $N,\ \Delta,\ x_1,\ n_h,\ n_0,\ \bar{n},\ \bar{\beta}$
$a \leftarrow 1/\Delta$; $\quad K \leftarrow N/2$; $\quad \Upsilon_{a,N} \leftarrow 24a^2/N$
$\bar{n} \leftarrow \lfloor (a(\ln(W/S_0) - x_1) + 1 \rfloor$; $\quad \rho \leftarrow \ln(W/S_0) - x_{\bar{n}}$; $\quad \zeta := a \cdot \rho$
$q_\pm \leftarrow (1 \pm \sqrt{3/5})/2,\ \rho_\pm \leftarrow \rho \cdot q_\pm,\ \zeta_\pm \leftarrow \zeta \cdot q_\pm,\ \sigma \leftarrow 1 - \zeta,\ \sigma_\pm \leftarrow \sigma(q_\pm - 1/2)$
Define $\vartheta_{[0,1]}, \vartheta_{[-1,0]}$ from equation (284) - (285), $\quad \vartheta_* \leftarrow \vartheta_{[0,1]} + \vartheta_{[-1,0]}$
Initialize $V_{k,\gamma} \leftarrow 0$, $\quad k = 1, \ldots, K$, $\quad \gamma = 0, \ldots, \Gamma$
$\mu_0 \leftarrow e^{-r\Delta_t} \cdot \Upsilon_{a,N}[\bar{\beta}_K, ..., \bar{\beta}_1, 0, \bar{\beta}_{2K-1}, ..., \bar{\beta}_{K+1}]$; $\quad \mu_0 \leftarrow \mathrm{FFT}(\mu_0)$
Up-and-Out Parisian Call:
Set $\bar{\delta}_j^{call}, \delta_j^{call},\ j = 0, 1$ from Table 37
Define $\theta = \{\theta_k\}_{k=1}^K$ by equation (325)
$p \leftarrow \mathrm{iFFT}(\mu_0 \circ \mathrm{FFT}([\theta, \vec{0}_K]))$; $\quad V_{\bullet,\gamma} \leftarrow \{p_k\}_{k=1}^K$, $\quad \gamma = 0, \ldots, \Gamma - 1$
Redefine $\theta_{n_h} \leftarrow U \cdot \vartheta_{[-1,0]} - W/2$; $\quad \theta_k \leftarrow 0$ for $k = n_h + 1, \ldots, K$
$p \leftarrow \mathrm{iFFT}(\mu_0 \circ \mathrm{FFT}([\theta, \vec{0}_K]))$; $\quad V_{\bullet,\Gamma} \leftarrow \{p_k\}_{k=1}^K$
Down-and-Out Parisian put:
Set $\bar{\delta}_j^{put}, \delta_j^{put},\ j = 0, 1$ from Table 37
Define $\theta = \{\theta_k\}_{k=1}^K$ by equation (333)
$p \leftarrow \mathrm{iFFT}(\mu_0 \circ \mathrm{FFT}([\theta, \vec{0}_K]))$; $\quad V_{\bullet,\gamma} \leftarrow \{p_k\}_{k=1}^K$, $\quad \gamma = 0, \ldots, \Gamma - 1$
Redefine $\theta_{n_h} \leftarrow W/2 - L \cdot \vartheta_{[0,1]}$; $\quad \theta_k \leftarrow 0$ for $k = 1, \ldots, n_h - 1$
$p \leftarrow \mathrm{iFFT}(\mu_0 \circ \mathrm{FFT}([\theta, \vec{0}_K]))$; $\quad V_{\bullet,\Gamma} \leftarrow \{p_k\}_{k=1}^K$
return : V, μ_0, n_h, n_0

7.4.3 Down-and-Out Parisian Put

To price the down-and-out Parisian put (DOPP), with European payoff $G(S_T) = (W - S_T)^+$, and knock-out barrier $L > 0$, we define the breach counter γ as in equation (323), but with

Algorithm 18 Up-and-Out Parisian Call: Main Algorithm

Parameters: $H = L$ or U; $W,\ \Gamma,\ S_0,\ r,\ q,\ T,\ M$; $\quad \Delta_t \leftarrow T/M$
Call Algorithm 17 to obtain V, μ_0, n_h, n_0
Cumulative Up-and-Out Parisian Call:
for $m = M-2, \ldots, 0$ **do**
  for $\gamma = 0, \ldots, \Gamma - 1$ **do**
    $\theta_1 \leftarrow a_{m+1,1}(\gamma)$
    $\theta_k \leftarrow b_{m+1,k}(\gamma), \quad k = 2, \ldots, n_h - 1$
    $\theta_{n_h} \leftarrow c_{m+1,n_h}(\gamma) + a_{m+1,n_h}(\gamma+1)$
    $\theta_k \leftarrow b_{m+1,k}(\gamma+1), \quad k = n_h+1, \ldots, K-1$
    $\theta_K \leftarrow c_{m+1,K}(\gamma+1)$
    $p \leftarrow \mathrm{iFFT}(\mu_0 \circ \mathrm{FFT}([\theta, \vec{0}_K])); \quad V_{\bullet,\gamma} \leftarrow \{p_k\}_{k=1}^K$
  end for
  $\theta_{n_h} \leftarrow c_{m+1,n_h}(\Gamma); \quad \theta_k \leftarrow 0, \quad k = n_h+1, \ldots, K$
  $p \leftarrow \mathrm{iFFT}(\mu_0 \circ \mathrm{FFT}([\theta, \vec{0}_K])); \quad V_{\bullet,\Gamma} \leftarrow \{p_k\}_{k=1}^K$
end for
Resetting Up-and-Out Parisian Call:
for $m = M-2, \ldots, 0$ **do**
  $\theta_1 \leftarrow a_{m+1,1}(0)$
  $\theta_k \leftarrow b_{m+1,k}(0), \quad k = 2, \ldots, n_h - 1$
  $\delta \leftarrow c_{m+1,n_h}(0)$
  for $\gamma = 0, \ldots, \Gamma - 1$ **do**
    $\theta_{n_h} \leftarrow \delta + a_{m+1,n_h}(\gamma+1)$
    $\theta_k \leftarrow b_{m+1,k}(\gamma+1), \quad k = n_h+1, \ldots, K-1$
    $\theta_K \leftarrow c_{m+1,K}(\gamma+1)$
    $p \leftarrow \mathrm{iFFT}(\mu_0 \circ \mathrm{FFT}([\theta, \vec{0}_K])); \quad V_{\bullet,\gamma} \leftarrow \{p_k\}_{k=1}^K$
  end for
  $\theta_{n_h} \leftarrow \delta; \quad \theta_k \leftarrow 0, \quad k = n_h+1, \ldots, K$
  $p \leftarrow \mathrm{iFFT}(\mu_0 \circ \mathrm{FFT}([\theta, \vec{0}_K])); \quad V_{\bullet,\Gamma} \leftarrow \{p_k\}_{k=1}^K$
end for
if $0 < |h| < \Delta$ **then**
  price $= V_{n_0,1} + (V_{n_0+1,1} - V_{n_0,1}) \cdot (0 - x_{n_0})/\Delta$
else
  price $= V_{n_0,1}$
end if
return : price

the indicator replaced by $\mathbb{1}[S_{t_j} < L]$. The terminal coefficients are defined by

$$\theta_{M,k}(\gamma_{M-1}) = \begin{cases} \theta^{EP}_{M,k} & \gamma_{M-1} = 0, \dots, \Gamma - 1 \\ \theta^{DOP}_{M,k} & \gamma_{M-1} = \Gamma, \end{cases} \tag{332}$$

where $\theta^{EP}_{M,k}$ are the European put coefficients defined by

$$\theta^{EP}_{M,k} = \begin{cases} W - e^{y_k} \cdot S_0 \cdot \vartheta_*, & k = 1, ..., \bar{n} - 1 \\ W\left(\frac{1}{2} + \bar{\delta}^{put}_0 - e^{-\rho}\left(\vartheta_{[-1,0]} + \delta^{put}_0\right)\right), & k = \bar{n} \\ W\left(\bar{\delta}^{put}_1 - e^{\Delta-\rho} \cdot \delta^{put}_1\right), & k = \bar{n} + 1 \\ 0, & k = \bar{n} + 2, ..., K. \end{cases} \tag{333}$$

with $\bar{n}, \rho, \zeta$ are defined by equation (326). The coefficients $\theta^{DOP}_{M,k}$ are the same as $\theta^{EP}_{M,k}$, except that $\theta^{DOP}_{M,k} = 0$ for $k = 1, \dots, n_h - 1$, and $\theta^{DOP}_{M,n_h} = W/2 - L \cdot \vartheta_{[0,1]}$. For $k = n_1 + 1, \dots, K$, they satisfy $\theta^{DOP}_{M,k} = \theta^{EP}_{M,k}$.

For $m = M - 1, \dots, 1$, we define the theta coefficients by

$$\theta_{m,k}(\gamma) := \begin{cases} a_{m,k}(\gamma + 1) & k = 1 \\ b_{m,k}(\gamma + 1) & k = 2, \dots, n_h - 1 \\ c_{m,k}(\gamma + 1) + a_{m,k}(\gamma^*) & k = n_h \\ b_{m,k}(\gamma^*) & k = n_h + 1, \dots, K \end{cases} \tag{334}$$

where $0 \le \gamma \le \Gamma$. As for the UOC, we have the value recursion $\boldsymbol{\mathcal{V}}_{m-1}(\gamma) = \boldsymbol{T}_0^{\Delta_t}\theta_m(\gamma)$, which terminates with $\boldsymbol{\mathcal{V}}_0(0)$.

Remark 20. Similarly, to price a double-barrier Parisian option (call or put), with $L < W < U$ the terminal coefficients are the same as for the UOPC and UOPP respectively, while

the coefficients for $m = M-1, \ldots, 1$ become

$$\theta_{m,k}(\gamma) := \begin{cases} a_{m,k}(\gamma+1) & k = 1 \\ b_{m,k}(\gamma+1) & k = 2, \ldots, n_l - 1 \\ c_{m,k}(\gamma+1) + a_{m,k}(\gamma^*) & k = n_l \\ b_{m,k}(\gamma^*) & k = n_l+1, \ldots, n_u - 1 \\ c_{m,k}(\gamma^*) + a_{m,k}(\gamma+1) & k = n_u \\ b_{m,k}(\gamma+1) & k = n_u+1, \ldots, K-1 \\ c_{m,k}(\gamma+1) & k = K. \end{cases} \tag{335}$$

For these contracts, we adjust the grid so that $l = x_{n_l}$ and $u = x_{n_u}$ are grid points, and a five point cubic interpolation about n_0 is used to recover the value for $\ln(S_0/S_0) = 0$, which lies between x_{n_0} and x_{n_0+1}.

7.4.3.1 Parisian Algorithm

We summarize the Parisian pricing algorithm for an UOPC in Algorithm 18, which handles both resetting and cumulative specifications. The algorithm for a DOPC is nearly identical, except for the coefficients θ, which are instead updated according to equation (334). During the routine, initialization Algorithm 17 is called (which applies to both UOPC and DOPP options), which determines the grids according to Algorithm 16, and initializes the $K \times (\Gamma + 1)$ value matrix V in terms of the terminal coefficients. After initialization, the main loop is entered, and a price is returned (or if desired, the value surface at time zero for the same cost). Hence, a surface of Greeks is a natural byproduct of the routine, at a negligible cost. Double barrier Parisian options are a straightforward extension as discussed in Remark 20.

7.4.4 Parisian Options in the Black-Scholes-Merton Model

Even for the BSM model, reference prices for discretely monitored Parisian options are difficult to find in the literature for both reseting and cumulation specifications. Hence, we first compare our prices to a basic Monte Carlo scheme in Table 38 (where column R/C specifies Resetting (R) or Cumulative (C)). Reference prices are obtained to high accuracy

using BPROJ, which are confirmed by MC along with a 95% confidence interval. The error column $|Err|$ refers to the error of the BPROJ scheme with automated parameter selection, along with the final value of $\log_2(N)$ determined by Algorithm 16. NL is the number of iterations required before the tolerance is met, given the initial values for N as in Remark 19. The column cpu(sec) is the full cost of Algorithm 18, including initialization and automated parameter selection.[16] Not only is the algorithm fast, but it obtains accurate prices given a desired tolerance of TOL = 5e-04, for both reseting and cumulative options. Note that NL = 1 for each case, which indicates that the initial values for N and α were sufficient to achieve the error tolerance. For heavy-tailed models, more iterations may be required, and our initial values are chosen to be conservative across models. Table 42 in Section 7.6.2 provides reference prices and BPROJ errors for several additional Lévy processes.

7.4.5 Step Options

Motivated by a desire to soften the knock-out feature of a barrier option, the *step option* [99] penalizes cumulative excursions into the knock-out region, $\mathcal{C}^c$. Consider the discretely monitorned cumulative excursion time γ_M

$$\gamma_M = \sum_{0 \le j \le M} \mathbb{1}_{[S_j \in \mathcal{C}^c]}, \quad \tau_M := T \cdot \frac{\gamma_M}{M+1}, \tag{336}$$

where $0 \le \tau_M \le T$ has been normalized so that $\tau_M = T$ for a process which is observed in the knock-out region at each monitoring date. Given a non-increasing function $h : \mathbb{R}_+ \to \mathbb{R}_+$, with $h(0) = 1$, the terminal payoff $G(S_T)$ is softened by $G(S_T) \cdot h(\tau_M)$. One such contract examined by [99] specifies an exponentially discounted call option

$$\exp(-\rho\tau_M)(S_T - W)^+ \tag{337}$$

where $\rho > 0$, called the *proportional step option*. Our algorithm for cumulative Parisian options is modified only slightly to price these contracts. In particular, we set $\Gamma = M + 1$, and redefine just the terminal coefficients $\theta_M^{Par}(\gamma)$ for an otherwise equivalent cumulative

[16] All experiments are conducted in MATLAB 8.0 with Intel(R) Core(TM) i5-2410M CPU, 2.30GHz with 3MB cache size.

Table 38: Parisian value errors and Cpu times for BSM model with $\sigma = 0.18$ and automated parameter selection. In all cases, $S_0 = 100$, $W = 100$, $r = 0.05$, $q = 0$, $T = 1$. For DOPP, $L = 80$, while for UOPC, $U = 120$. Column R/C specifies Resetting (R) or Cumulative (C). The column MC is a Monte Carlo estimate with standard error with 95% CI in column 95CI.

Type	R/C	M	Γ	Ref	$\|Err\|$	cpu(sec)	$\log_2(N)$	NL	MC	95CI
DOPP	R	52	5	3.0713309	1.31e-06	0.016	9	1	3.070	[3.066, 3.073]
DOPP	R	252	15	2.8389278	1.41e-06	0.322	10	1	2.845	[2.837, 2.852]
DOPP	C	52	5	2.8633356	3.46e-06	0.021	9	1	2.863	[2.859, 2.866]
DOPP	C	252	15	2.6063036	1.31e-06	0.365	10	1	2.606	[2.599, 2.613]
UOPC	R	52	5	3.5734667	5.39e-06	0.017	9	1	3.576	[3.572, 3.580]
UOPC	R	252	15	3.1004047	6.19e-07	0.334	10	1	3.108	[3.097, 3.120]
UOPC	C	52	5	3.1272890	1.82e-06	0.019	9	1	3.129	[3.125, 3.133]
UOPC	C	252	15	2.6569707	5.65e-07	0.360	10	1	2.656	[2.649, 2.664]

Parisian contract:

$$\theta_M^{Step}(\gamma) = h\left(T \cdot \frac{\gamma}{M+1}\right) \cdot \theta_M^{Par}(\gamma), \quad \gamma = 0, \ldots, M+1. \tag{338}$$

Note that all varieties of single and double barriers are covered by the choice of knock-out region $\mathcal{C}^c$.

7.5 Error Analysis

For simplicity, we analyze the convergence behavior for the double barrier option with $[l, u] = [\ln(L/S_0), \ln(U/S_0)]$, with payoff denoted by $G(y) := g(S_0 e^y)$. Alternative knock-out regions are analyzed similarly.

7.5.1 Projection Error

To quantify the projection error, which drives the convergence of BPROJ, we define the approximated density projection by

$$\bar{p}_{\Delta_t}(\nu) := \Lambda_{a,N} \sum_{k=1}^{N} \bar{\beta}_{a,k} \varphi_{a,k}(\nu), \qquad \Lambda_{a,N} := \frac{24a^{5/2}}{N} = a^{1/2} \Upsilon_{a,N}, \tag{339}$$

as well as the projected density (restricted to $\{\varphi_{a,k}\}_{k=1}^N$) with exact projection coefficients in the absence of DFT error by

$$\widetilde{p}_{\Delta_t}(\nu) := \Lambda_{a,N} \sum_{k=1}^{N} \beta_{a,k} \varphi_{a,k}(\nu) = \sum_{k=1}^{N} \langle p_{\Delta_t}, \widetilde{\varphi}_{a,k} \rangle \varphi_{a,k}(\nu). \tag{340}$$

For clarity and ease of notation, we proceed as though $[\nu_1, \nu_N] = [-\alpha, \alpha]$.[17] The next result characterizes the discrepancy between exact and approximate orthogonal projections for Lévy models of sufficient regularity.

Corollary 7.5.1. *Let $\alpha > 0$ determine a density expansion over $[-\alpha, \alpha]$. Assume for some $d, c, \kappa > 0$ and $\nu \in (0, 2]$, $\phi_{\Delta_t}(\xi) \in \mathcal{H}_d$ and satisfies*

$$|\phi_{\Delta_t}(\xi)| \leq \kappa \exp(-c|\xi|^\nu \Delta_t), \quad \xi \in \mathbb{R}. \tag{341}$$

Then

(i) For some $0 < \gamma \leq d$, and $C(\phi_{\Delta_t}) \leq 24\|\phi_{\Delta_t}\|^{\mathcal{H}}$, the aggregate coefficient error is bounded by

$$\sum_{n=1}^{N} \left|\Lambda_{a,N} \cdot \bar{\beta}_{a,n} - \langle p_{\Delta_t}, \widetilde{\varphi}_{a,n}\rangle\right| \leq a^{1/2}\mathcal{E}_\alpha(\Delta), \tag{342}$$

where

$$\mathcal{E}_\alpha(\Delta) := \frac{2C(\phi_{\Delta_t})}{\gamma} \exp\left(-\alpha\pi\gamma\right) + \frac{12\kappa}{\pi} \cdot \frac{\alpha}{\Delta} \exp\left(-c \cdot \left(\frac{2\pi}{\Delta}\right)^\nu \Delta_t\right).$$

(ii) The following L^1 -bound holds:

$$\int_{-\alpha}^{\alpha} |\bar{p}_{\Delta_t}(\nu) - \widetilde{p}_{\Delta_t}(\nu)| d\nu \leq \mathcal{E}_\alpha(\Delta).$$

Proof. The coefficient errors are shown in [83] to satisfy

$$\left|\Lambda_{a,N} \cdot \bar{\beta}_{a,n} - \langle p_{\Delta_t}, \widetilde{\varphi}_{a,n}\rangle\right| \leq \frac{a^{-1/2}}{\pi} \left(C(\phi_{\Delta_t}) \frac{e^{-(2\alpha - |\nu_n|)\gamma}}{1 - e^{-2\alpha\gamma}} + \tau_a(\phi_{\Delta_t})\right),$$

where the first term in parentheses is the trapezoidal rule error, which decays exponentially for functions analytic within a strip in the complex plane, and the second term

$$\tau_a(\phi_{\Delta_t}) \leq \frac{6\kappa}{\pi} \cdot a \exp(-c \cdot (2\pi a)^\nu \Delta_t)$$

arises from truncating the Fourier integrals, and its convergence is governed by the tail decay of ϕ_{Δ_t}. By summing over $1 \leq n \leq N$, with $\nu_n = (n - N/2)/a$, we have that

$$\begin{aligned}\sum_{n=1}^{N} e^{-(2\alpha - |\nu_n|)\gamma} = e^{-2\gamma\alpha} \sum_{n=1}^{N} e^{\left|n - \frac{N}{2}\right|\frac{\gamma}{a}} &= e^{-2\gamma\alpha} \left(2e^{\gamma\alpha} \sum_{n=1}^{N/2} e^{-\frac{n\gamma}{a}} - 1\right) \\ &\leq e^{-2\gamma\alpha} \frac{2\left(e^{\gamma\alpha} - 1\right)}{e^{\frac{\gamma}{a}} - 1} \leq \frac{2a}{\gamma}\left(e^{-\gamma\alpha} - e^{-2\gamma\alpha}\right),\end{aligned}$$

[17] This would be the case if we added a single basis element to the boundary.

since by convexity $e^{\gamma/a} - 1 \geq \gamma/a$. Thus,

$$\frac{1}{1-e^{-2\gamma\alpha}} \sum_{n=1}^{N} e^{-(2\alpha-|\nu_n|)\gamma} \leq \frac{2a}{\gamma} e^{-\gamma\alpha} \frac{1-e^{-\gamma\alpha}}{1-e^{-2\gamma\alpha}} \leq \frac{2ae^{-\gamma\alpha}}{\gamma},$$

and the claim follows. For the second part, just note that

$$\int_{-\alpha}^{\alpha} |\bar{p}_{\Delta_t}(\nu) - \widetilde{p}_{\Delta_t}(\nu)| d\nu = \sum_{n=1}^{N} \left| \Lambda_{a,N} \cdot \bar{\beta}_{a,n} - \langle p_{\Delta_t}, \widetilde{\varphi}_{a,n} \rangle \right| \int_{-\alpha}^{\alpha} \varphi_{a,n}(\nu) d\nu,$$

and apply claim (i). □

The notation $\mathcal{E}_\alpha(\Delta)$ emphasizes that, once α has been fixed, the discretization error will decay as a function of Δ. Moreover, for double barrier options, (l, u) is fixed in the contract, and $\alpha = u - l$. Section 7.5.2.3 discusses how to control $\mathcal{E}_\alpha(\Delta)$ for fixed (l, u).

7.5.2 BPROJ Error

To quantify the stability and convergence rate of BRPOJ, we start with the case of double barrier options, which extends to the single barrier case after a few modifications.

7.5.2.1 Stage $M-1$

After the first iteration, we have for $1 \leq n \leq K$

$$\begin{aligned} e^{r\Delta_t} \mathcal{V}^*_{M-1}(x_n) = &\int_l^u G(y) \bar{p}_{\Delta_t}(y - x_n) dy + \int_l^u G(y) \left(p_{\Delta_t}(y - x_n) - \widetilde{p}_{\Delta_t}(y - x_n) \right) dy \\ &+ \int_l^u G(y) \left(\widetilde{p}_{\Delta_t}(y - x_n) - \bar{p}_{\Delta_t}(y - x_n) \right) dy. \end{aligned}$$

Since the integrals $\int_l^u G(y) \varphi_{a,k}(y) dy$ are known exactly[18] , it follows that

$$\begin{aligned} e^{r\Delta_t} |\mathcal{V}^*_{M-1}(x_n) - \mathcal{V}_{M-1}(x_n)| &\leq \|G\|_2^{(l,u)} \|p_{\Delta_t} - \widetilde{p}_{\Delta_t}\|_2 + \|G\|_\infty^{(l,u)} \int_{l-u}^{u-l} |\widetilde{p}_{\Delta_t}(y) - \bar{p}_{\Delta_t}(y)| dy \\ &\leq \gamma_M \cdot \left(\|p_{\Delta_t} - \widetilde{p}_{\Delta_t}\|_2 + \mathcal{E}_\alpha(\Delta) \right), \end{aligned}$$

by part (ii) of Corollary 7.5.1 where

$$\gamma_M \leq \max \left\{ \|G\|_\infty^{(l,u)}, \|G\|_2^{(l,u)} \right\}. \tag{343}$$

[18] Or are approximated for stability purposes, by a sufficiently high order quadrature. For ease of exposition, we treat the initial payoff coefficients as known quantities, although the conclusion is unaffected, since the quadrature error is dominated by that of projection and the local interpolation.

Thus, the maximum error after one iteration satisfies

$$\mathcal{E}^*_{M-1} := \sup_{1\le n\le K} |\mathcal{V}^*_{M-1}(x_n) - \mathcal{V}_{M-1}(x_n)| \le e^{-r\Delta_t}\gamma_M \cdot (\|p_{\Delta_t} - \widetilde{p}_{\Delta_t}\|_2 + \mathcal{E}_\alpha(\Delta)) . \qquad (344)$$

7.5.2.2 Stage $m-1$

After the first step, the error will account for the use of local quadratic interpolation[19] to calculate the coefficients $\theta_{m,k}$, where we define $I_k := [y_{k-1}, y_{k+1}]$ for $2 \le k \le K$, $I_1 := [y_1, y_2]$ and $I_K := [y_{K-1}, y_K]$. While a cubic interpolation is performed on each of the boundary intervals, we assume for simplicity that quadratic interpolation is performed throughout, as the convergence rate is unaffected. We then have

$$\begin{aligned}
e^{r\Delta_t}\mathcal{V}^*_{m-1}(x_n) &= \int_l^u \mathcal{V}^*_m(y)\bar{p}_{\Delta_t}(y-x_n)dy + \int_l^u \mathcal{V}^*_m(y)\left(p_{\Delta_t}(y-x_n) - \bar{p}_{\Delta_t}(y-x_n)\right)dy \\
&\le \int_l^u \mathcal{V}^*_m(y)\bar{p}_{\Delta_t}(y-x_n)dy \\
&\quad + \|\mathcal{V}^*_m\|^{(l,u)}_\infty \int_{-\alpha}^{\alpha} |p_{\Delta_t}(y) - \widetilde{p}_{\Delta_t}(y)|\, dy + \|\mathcal{V}^*_m\|^{(l,u)}_2 \|p_{\Delta_t} - \widetilde{p}_{\Delta_t}\|_2 \\
&\le \int_l^u \mathcal{V}^*_m(y)\bar{p}_{\Delta_t}(y-x_n)dy \\
&\quad + \max\{\|\mathcal{V}^*_m\|^{(l,u)}_\infty, \|\mathcal{V}^*_m\|^{(l,u)}_2\}\left(\mathcal{E}_\alpha(\Delta) + \|p_{\Delta_t} - \widetilde{p}_{\Delta_t}\|_2\right), \qquad (345)
\end{aligned}$$

by Corollary 7.5.1. With $\mathcal{K} := \{k : K \le k \le 2K-1\}$, the first term in equation (345) is decomposed as[20]

$$\begin{aligned}
\int_l^u \mathcal{V}^*_m(y)\bar{p}_{\Delta_t}(y-x_n)dy &= \Lambda_{a,N}\sum_{k\in\mathcal{K}} \bar{\beta}_{k-n+1}\int_{I_k} \mathcal{V}^*_m(y)\varphi_{a,k}(y)dy \\
&= \Lambda_{a,N}\sum_{k\in\mathcal{K}} \bar{\beta}_{k-n+1}\left(\int_{I_k} \widetilde{\mathcal{V}}_{m,k}(y)\varphi_{a,k}(y)dy + \mathcal{E}(\theta_{m,k})\right) \\
&= e^{r\Delta_t}\mathcal{V}_{m-1}(x_n) + \Lambda_{a,N}\sum_{k\in\mathcal{K}} \bar{\beta}_{k-n+1}\mathcal{E}(\theta_{m,k}), \qquad (346)
\end{aligned}$$

where

$$\mathcal{E}(\theta_{m,k}) := \int_{I_k} \left(\mathcal{V}^*_m(y) - \widetilde{\mathcal{V}}_{m,k}(y)\right)\varphi_{a,k}(y)dy,$$

[19] This is not the same as say quadratic B-spline interpolation, since the intervals I_k overlap.

[20] To avoid introducing excessive notation, we assume that the basis elements $\varphi_{a,k}$ are aligned correctly according to the context. For example, $\int_{I_k} \widetilde{\mathcal{V}}_{m,k}(y)\varphi_{a,k}(y)dy$ assumes that $\varphi_{a,k}(y)$ is centered over y_k in log asset space, while $\varphi_{a,k}(\nu)$ is centered over ν_k in log return space.

and $\widetilde{\mathcal{V}}_{m,k}(y)$ is the local quadratic interpolation on I_k defined in equation (276). It follows that

$$\begin{aligned}|\mathcal{E}(\theta_{m,k})| &\leq \int_{I_k} \left|\mathcal{V}_m^*(y) - \widetilde{\mathcal{V}}_{m,k}(y)\right| \varphi_{a,k}(y)dy \\ &\leq \|\mathcal{V}_m^* - \widetilde{\mathcal{V}}_{m,k}\|_\infty^{I_k} \int_{I_k} \varphi_{a,k}(y)dy \\ &\leq a^{-1/2}\left(\|\mathcal{V}_m^* - \widetilde{\mathcal{V}}_{m,k}^*\|_\infty^{I_k} + \|\widetilde{\mathcal{V}}_{m,k}^* - \widetilde{\mathcal{V}}_{m,k}\|_\infty^{I_k}\right), \end{aligned} \tag{347}$$

where $\widetilde{\mathcal{V}}_{m,k}^*$ is the local quadratic interpolation over I_k using the true values. Hence,

$$\|\mathcal{V}_m^* - \widetilde{\mathcal{V}}_{m,k}^*\|_\infty^{I_k} \leq \|\mathcal{V}_m^{*(3)}\|_\infty^{I_k} \cdot \frac{\Delta^3}{12},$$

where the superscript indicates a third derivative, which can be bounded as follows:

$$\begin{aligned} e^{r\Delta_t}\left|\frac{d^n}{dx^n}\mathcal{V}_m^*(x)\right| &= \left|\frac{d^n}{dx^n}\int_l^u \mathcal{V}_{m+1}^*(y)p_{\Delta_t}(y-x)dy\right| \\ &= \left|\int_l^u \mathcal{V}_{m+1}^*(y)\cdot(-1)^n p_{\Delta_t}^{(n)}(y-x)dy\right| \leq \|\mathcal{V}_m^*\|_\infty^{(l,u)} \cdot \|p_{\Delta_t}^{(n)}\|_1^{I(\alpha)}, \end{aligned}$$

where $I(\alpha) := (-\alpha, \alpha)$. Specifically,

$$\|\mathcal{V}_m^* - \widetilde{\mathcal{V}}_{m,k}^*\|_\infty^{I_k} \leq \frac{e^{-r\Delta t}}{12}\|\mathcal{V}_m^*\|_\infty^{(l,u)} \cdot \|p_{\Delta_t}^{(3)}\|_1^{I(\alpha)}\Delta^3.$$

When equation (341) in Corollary 7.5.1 holds, $p_{\Delta_t} \in C^\infty(\mathbb{R})$ and $|p_{\Delta_t}^{(n)}(\nu)| \to 0$ as $|\nu| \to \infty$, $\forall n \in \mathbb{N}$. For a precise bound, one can estimate $p_{\Delta_t}^{(3)}(\nu) = \frac{i}{2\pi}\int_{\mathbb{R}} \xi^3 \exp(-i\nu\xi + \psi_Y(\xi)\Delta_t)d\xi$.

For the second term in equation (347),

$$\|\widetilde{\mathcal{V}}_{m,k}^* - \widetilde{\mathcal{V}}_{m,k}\|_\infty^{I_k} \leq \sup_{1\leq k\leq N} |\mathcal{V}_m^*(x_k) - \mathcal{V}_m(x_k)| := \mathcal{E}_m^*,$$

and let $\gamma_m := \max\left\{\|\mathcal{V}_m^*\|_2^{(l,u)}, \|\mathcal{V}_m^*\|_\infty^{(l,u)}, \|\mathcal{V}_m^*\|_\infty^{(l,u)} \cdot \|p_{\Delta_t}^{(3)}\|_1^{I(\alpha)}/12\right\}$. We then obtain the estimate

$$\begin{aligned}\sup_{k\in\mathcal{K}}|\mathcal{E}(\theta_{m,k})| &\leq a^{-1/2}\left(\frac{e^{-r\Delta t}}{12}\|\mathcal{V}_m^*\|_\infty^{(l,u)} \cdot \|p_{\Delta_t}^{(3)}\|_1^{I(\alpha)}\Delta^3 + \mathcal{E}_m^*\right) \\ &\leq a^{-1/2}\cdot\gamma_m\Delta^3 + \mathcal{E}_m^*. \end{aligned} \tag{348}$$

Hence, combining equations (345)-(348) we have

$$
\begin{aligned}
&e^{r\Delta_t}\left|\mathcal{V}^*_{m-1}(x_n) - \mathcal{V}_{m-1}(x_n)\right| \\
&\leq \left|\Lambda_{a,N}\sum_{k\in\mathcal{K}}\bar{\beta}_{k-n+1}\mathcal{E}(\theta_{m,k})\right| + \int_l^u |\mathcal{V}^*_m(y)|\,|p_{\Delta_t}(y-x_n) - \bar{p}_{\Delta_t}(y-x_n)|\,dy \\
&\leq \Lambda_{a,N}\sum_{k\in\mathcal{K}}\left(|\beta_{k-n+1}| + |\bar{\beta}_{k-n+1} - \beta_{k-n+1}|\right)|\mathcal{E}(\theta_{m,k})| + \gamma_m\cdot(\mathcal{E}_\alpha(\Delta) + \|p_{\Delta_t} - \widetilde{p}_{\Delta_t}\|_2) \\
&\leq \sup_{k\in\mathcal{K}}|\mathcal{E}(\theta_{m,k})|a^{1/2}(1+\mathcal{E}_\alpha(\Delta)) + \gamma_m\cdot(\mathcal{E}_\alpha(\Delta) + \|p_{\Delta_t} - \widetilde{p}_{\Delta_t}\|_2) \\
&\leq (\gamma_m\Delta^3 + \mathcal{E}^*_m)(1+\mathcal{E}_\alpha(\Delta)) + \gamma_m\cdot(\mathcal{E}_\alpha(\Delta) + \|p_{\Delta_t} - \widetilde{p}_{\Delta_t}\|_2) \\
&\leq \mathcal{E}^*_m(1+\mathcal{E}_\alpha(\Delta)) + \gamma_m\left(\|p_{\Delta_t} - \widetilde{p}_{\Delta_t}\|_2 + \Delta^3 + \mathcal{E}_\alpha(\Delta))(1+\Delta^3)\right),
\end{aligned}
$$

with terms multiplying γ_m ordered by their rate of convergence. Thus, with $\bar{\gamma}_M := \max\{\gamma_m : 1 \leq m \leq M\}$, we have

$$
\mathcal{E}^*_{m-1} \leq e^{-r\Delta_t}\left(\vartheta_1(\Delta)\mathcal{E}^*_m + \bar{\gamma}_M\vartheta_2(\Delta)\right), \tag{349}
$$

where we have defined

$$
\begin{aligned}
\vartheta_1(\Delta) &:= 1 + \mathcal{E}_\alpha(\Delta) \\
\vartheta_2(\Delta) &:= \|p_{\Delta_t} - \widetilde{p}_{\Delta_t}\|_2 + \Delta^3 + \mathcal{E}_\alpha(\Delta)(1+\Delta^3).
\end{aligned}
$$

7.5.2.3 Propagation

From equations (349) and (344), we iterate starting with $\mathcal{E}^*_0$:

$$
\begin{aligned}
\mathcal{E}^*_0 &\leq e^{-r\Delta_t}\left(\vartheta_1(\Delta)\mathcal{E}^*_1 + \bar{\gamma}_M\vartheta_2(\Delta)\right) \leq \cdots \\
&\leq \vartheta_2(\Delta)\bar{\gamma}_M e^{-r\Delta_t}\left(\sum_{j=0}^{M-2}\left(e^{-r\Delta_t}\vartheta_1(\Delta)\right)^j\right) + \left(e^{-r\Delta_t}\vartheta_1(\Delta)\right)^{M-2}\mathcal{E}^*_{M-1}
\end{aligned}
$$

where $\mathcal{E}^*_{M-1} \leq e^{-r\Delta_t}\bar{\gamma}_M\cdot(\|p_{\Delta_t} - \widetilde{p}_{\Delta_t}\|_2 + \mathcal{E}_\alpha(\Delta))$. Thus, if we define

$$
\Omega^M_\alpha(\Delta) := \bar{\gamma}_M\cdot e^{-r\Delta_t}\left(\sum_{j=0}^{M-1}\left(e^{-r\Delta_t}\left(1+\mathcal{E}_\alpha(\Delta)\right)\right)^j\right),
$$

it follows that

$$
\mathcal{E}^*_0 = \mathcal{O}\left(\left(\|p_{\Delta_t} - \widetilde{p}_{\Delta_t}\|_2 + \Delta^3 + \mathcal{E}_\alpha(\Delta)\right)\cdot\Omega^M_\alpha(\Delta)\right) \tag{350}
$$

Recall Corollary 7.5.1, which gives

$$\mathcal{E}_\alpha(\Delta) := \frac{2C(\phi_{\Delta_t})}{\gamma}\exp\left(-\alpha\pi\gamma\right) + \frac{12\kappa}{\pi}\cdot\frac{\alpha}{\Delta}\exp\left(-c\cdot\left(\frac{2\pi}{\Delta}\right)^{\nu}\Delta_t\right). \tag{351}$$

In the double barrier case, $\alpha := u-l$ is fixed by the barriers. However, we can control errors in frequency space by choosing $\widetilde{\alpha} \geq \alpha$ so that the first term of $\mathcal{E}_{\widetilde{\alpha}}(\Delta)$ from equation (351), which decays exponentially in $\widetilde{\alpha}$, is negligible. The remaining (truncation) error, with $\widetilde{\alpha}$ fixed, will decay exponentially in Δ. For $\widetilde{\alpha}$ sufficiently large, we have

$$\mathcal{E}_0^* = \mathcal{O}\left(\left(\|p_{\Delta_t} - \widetilde{p}_{\Delta_t}\|_2 + \Delta^3\right)\cdot\Omega_{\widetilde{\alpha}}^M(\Delta)\right). \tag{352}$$

To bound the term $\Omega_{\widetilde{\alpha}}^M(\Delta)$, we note first that $\|G\|_2^{(l,u)} \leq \sqrt{(u-l)}\|G\|_\infty^{(l,u)}$, from which $\gamma_M \leq \max\{1, \sqrt{(u-l)}\}\|G\|_\infty^{(l,u)}$. Moreover, $\|\mathcal{V}_m^*\|_\infty^{(l,u)} \leq \|G\|_\infty^{(l,u)}$, and $\|p_{\Delta_t}^{(3)}\|_1^{I(\alpha)} \leq (u-l)\|p_{\Delta_t}\|_\infty^{\mathbb{R}} < \infty$. Hence, for some $C_{\gamma,M} < \infty$,

$$\bar{\gamma}_M \leq (u-l)\cdot C_{\gamma,M}\|G\|_\infty^{(l,u)}, \tag{353}$$

where the subscript of M indicates the dependence of $\|p_{\Delta_t}^{(3)}\|_\infty^{\mathbb{R}}$ on $\Delta_t = T/M$. Note that for vanilla call and put options, $\|G\|_\infty^{(l,u)} \leq \{U-W, W-L\}$ respectively.

Remark 21. While theoretically, $\|p_{\Delta_t} - \widetilde{p}_{\Delta_t}\|_2 = \mathcal{O}(\Delta^2)$, in practice we observe convergence at a rate of $\mathcal{O}(\Delta^3) \sim \mathcal{O}(\Delta^4)$. Hence, the convergence rate will be dominated by the local interpolation error, which is $\mathcal{O}(\Delta^3)$. We note that by improving the interpolation scheme to a local quartic polynomial, no additional gain is observed. However, for extensions to higher order bases, a commensurate increase in interpolation order is necessary to observe faster convergence.

7.6 Numerical Experiments

We consider BSM [15], MJD (Merton's Jump Diffusion) [106], CGMY (Carr-Madan-Geman-Yor) [32], NIG (Normal Inverse Gaussian) [12] and Kou's double exponential models which are prominent members of the exponential Lévy class. Corresponding characteristic functions are provided for reference in the appendix. To compare with known reference prices, some parameter settings have been borrowed from recent literature on barrier option pricing, while additional reference prices are provided. Moreover, reference prices for Parisian

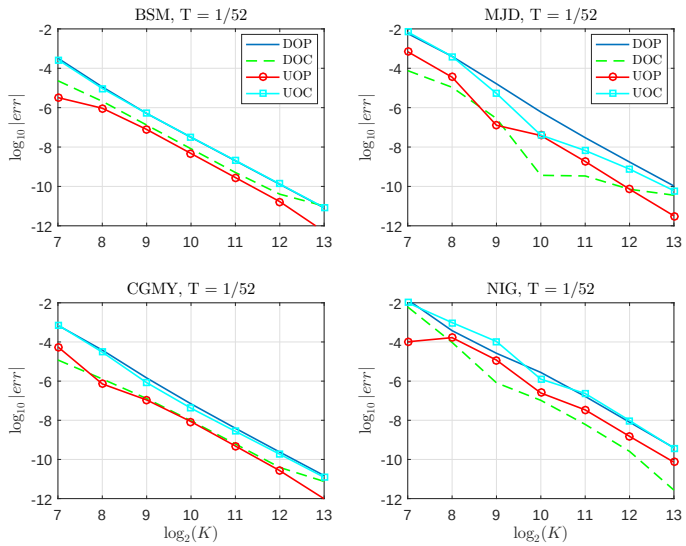

Figure 38: Weekly-Monitored Convergence (Single Barrier): $r = .05, q = .02, T = 1$, $M = 52$, and $S_0 = W = 100$. Models from Table 39. For up-and-out, $U = 120$, while $L = 80$ for down-and-out. Equation (312) determines the grid. Reference prices obtained by COS [62] with $N_C = 2^{16}$ and $L_1 = 12$.

options are presented for the first time for several models, including MJD, CGMY, and NIG. All experiments are conducted in MATLAB 8.0 with Intel(R) Core(TM) i5-2410M CPU, 2.30GHz with 3MB cache size.

7.6.1 Resolution

To assess the convergence of BPROJ with respect to the resolution (governed by K or equivalently $N = 2K$), we perform a series of numerical experiments for which reference prices are known [67]. In this section, equation (312) is used to determine the parameters, rather than by Algorithm 14, so that we can isolate the convergence behavior with respect to resolution. This also allows to compare our results with the COS method with the same grid-width. Convergence of BPROJ is observed to the eight reported decimals in [67], after which the COS method is used to compute reference prices to further digits, with N_C defined as the number of cosine basis elements. The first set of experiments, which are borrowed from [67] in order to verify reference prices, are listed in Table 39. For weekly monitored contracts, the cpu times range from about two to forty milliseconds as K ranges over $2^7 \sim 2^{13}$. Moreover, this is the cost to obtain the *entire* value function along the grid,

Table 39: Test parameters for Lévy models as in [67]; $S_0 = W = 100$, $T = 1$, $r = 0.05$, $q = 0.02$.

Test No.	Model	Parameters	Test No.	Model	Parameters
1	BSM	$\sigma = 0.2$	3	CGMY	$(C, G, M, Y) = (4, 50, 60, 0.7)$
2	MJD	$(\sigma, \lambda, \mu_J, \sigma_J) = (0.1, 3, -0.05, 0.086)$	4	NIG	$(\alpha, \beta, \delta) = (-15, -5, 0.5)$

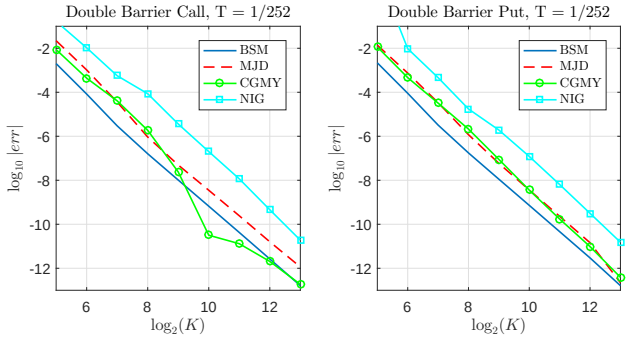

Figure 39: Daily-Monitored Convergence (Double Barrier): $r = .05, q = .02, T = 1$, $M = 252$, and $S_0 = W = 100$. Models from Table 39, $(L, U) = (80, 120)$. Ref. prices by BPROJ with $K = 2^{16}$ and $L_1 = 12$.

so Greeks are obtained at negligible cost. The corresponding convergence is illustrated in Figure 38 for the four models, and for each of the four types of knock-out contracts. The truncation parameter L_1 is set to 12, although as demonstrated in Figure 35, augmentation allows for similar accuracy to be obtained with a smaller value of L_1 (and with more rapid convergence). Even with a larger value of L_1, rapid convergence is observed for all test cases, with similar behavior for each. Moreover, the DOC and UOP, which are the two augmented cases, achieve greater accuracy at each resolution.

The next set of experiments tests the convergence of BPROJ for a daily monitored double barrier option with $(L, U) = (80, 120)$. Reference values are confirmed to eight decimals published in [67], after which BPROJ is used to additional digits. With the models given in Table 39, rapid convergence is observed. As expected, a smaller grid size is required, since a smaller value of $\alpha = u - l$ implies that the step size is smaller for each value of K. Moreover, truncation error is absent in the double barrier case.

While the analyses of [67] and [62] consider ATM options exclusively, the relationship between S_0, W and the barriers is important. Figure 40 demonstrates this relationship for the CMGY model and for each knock-out type, where $S_0 = 100$ is fixed as W varies. In

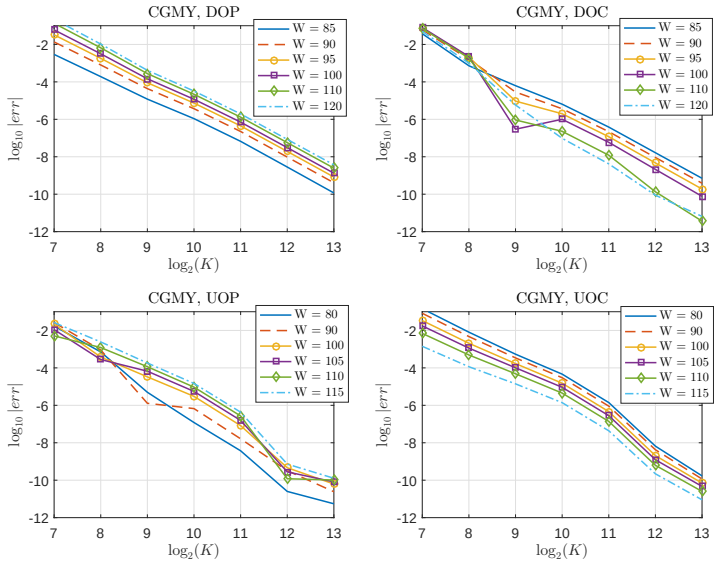

Figure 40: Daily-Monitored Convergence (Single Barrier): $r = .05, q = .02, T = 1$, $M = 252$, and $S_0 = 100$. Models from Table 39, $(L, U) = (80, 120)$. Ref. prices by COS with $N = 2^{16}$ and $L_1 = 12$.

particular, for the unaugmented cases, DOP and UOC, convergence is smoother, even in the presence of a payoff discontinuity. Perhaps most importantly, we observe that accuracy is unaffected when $\ln(W/S_0) \neq 0$, as it would be for other methods that obtain the value function along a grid. Namely, the basis structure of BPROJ permitted a grid choice for which the payoff discontinuity was not a member, without affecting convergence. The observed change in accuracy is due to option moneyness, and it increases as W moves the option away from the money, and decreases conversely.

In the next set of experiments, efficiency of BPROJ is assessed by comparing its performance to the barrier implementation of COS [62], which is a state-of-the-art pricing method for barrier options under exponential Lévy dynamics (see [51] for a comparison with the HT method of [67], as well as an extension and refinement of the Carr Madan approach [35] for barrier options). For the NIG model in [62], we compare the convergence for daily-monitored options, and with reference prices obtained by the COS method. While both methods converge, we see that cpu times for the COS method increase much faster than for BPROJ when more basis elements are needed. For monthly and weekly-monitored options (which are far less common that the daily-monitored cases), both methods converge

Table 40: Daily-monitored performance comparison with COS method [62], with $L_1 = 12$. Test parameters as in [62], given in Table 39. Barriers: $(L, U) = (80, 120)$. For a comparable computational cost, we set $K = N_C$ for BPROJ (where K is the value grid size, and $N = 2K$.). Equation (312) determines the grid. Reference prices are obtained by COS with $L_1 = 12$ and $N_C = 2^{17}$.

NIG(6,0.7,0.4)			COS		BPROJ	
Option Type	Ref. Val.	$\log_2(N_C)$	error	msec	error	msec
DOP	2.08350353	9	3.12e-02	18.2	4.97e-02	18.0
		10	7.38e-03	31.4	3.94e-03	27.5
		11	1.30e-03	65.5	2.44e-04	47.7
		12	1.19e-04	130.1	2.89e-05	99.2
		13	2.97e-06	289.2	2.21e-06	180.1
DOC	10.94944513	9	1.17e-02	17.3	3.53e-02	14.3
		10	1.75e-03	31.5	2.88e-03	24.5
		11	2.40e-04	65.7	4.77e-05	45.3
		12	4.32e-06	131.8	6.03e-06	86.5
		13	7.29e-07	288.8	4.73e-07	174.6
UOP	8.01423621	9	1.25e-02	17.3	1.04e-02	14.1
		10	4.22e-03	32.0	8.79e-04	23.9
		11	3.74e-04	65.6	1.50e-06	44.4
		12	8.44e-06	132.3	4.12e-06	85.3
		13	1.38e-06	293.8	4.81e-07	171.4
UOC	1.20342421	9	2.50e-02	17.5	3.07e-02	17.9
		10	6.60e-03	31.8	3.08e-03	28.2
		11	1.08e-03	66.1	1.74e-04	47.3
		12	9.20e-05	132.8	1.37e-05	97.8
		13	2.20e-06	290.1	1.55e-06	178.3

rapidly to practical accuracies (say $10^{-3} \sim 10^{-6}$) with comparable cpu times, after which the exponential convergence of COS is apparent. For options of greater maturity than $T = 1$ year, or when monitoring in more frequent (as for foreign exchange contracts), the speed advantage of BPROJ is more pronounced.

7.6.2 Automated Parameter Selection

This section illustrates the robustness of the automated parameter selection scheme detailed in Section 7.3.12. We consider two specifications of each of the models CGMY, MJD, NIG, Kou, and BSM, and price a set of DOP and DOC options, with varying H, W, and M. Reference prices are calculated by BPROJ, with absolute ($|Err|$) and relative ($|Rel.Err|$) errors given for the automated scheme. The column NL denotes the number of iterations in Algorithm 14 before the error tolerances are met, with an overall value error goal of TOL = 5e-04 (or better). The column $\log_2(N)$ is the final value determined.

For extremely peaked models such as the CGMY(4, 50, 30, 0.3) or NIG(15, -5, 0.5), the

algorithm correctly detects that a larger resolution is required, resulting in several iterations before satisfying the mean error tolerance. For other models, such as CGMY(0.2703, 17.56, 54.82, 0.8) with $M = 252$, neither the probability nor mean error tolerance are satisfied in the first iteration, requiring and increased grid-width and resolution. For some models, such as BSM, the initialized values of N and α are often more than sufficient. Rather than decreasing the initial grid-width and basis size to avoid excessive accuracy in some cases, we accept that conservative estimates are often obtained, since the algorithm cost is negligible in these cases. Even across a wide variety of models, the method performs robustly, achieving the desired tolerance at a very low cost.

We perform a similar set of experiments for Parisian options in Table 42 with reference prices for Levy processes that have yet to be reported in the literature. Both cumulative (C) and resetting (R) types are considered. As for barrier options, the automated scheme is robust in selecting the necessary parameters to achieve TOL= 5e-04 accuracy in prices, and the cost is very modest. Because of the enlarged grid-width required for Parisian options (due to excursion beyond the barrier), as expected the scheme selects a higher N than before.

7.7 Conclusion

We introduce a novel framework for pricing general discretely monitored barrier and Parisian options under exponential Lévy dynamics. For Parisian options, the existing literature has yet to consider underlying models with this level of generality, and the method applies to both cumulative and reseting Parisian options with single or double barriers. By utilizing the method of density projection by frame duality, rapid convergence of intermediate value approximations is obtained. The convergence is demonstrated by an error analysis and verified by a series of numerical experiments, for which BPROJ easily achieves the eight decimals reported in the literature. By utilizing a Toeplitz representation of the intermediate value coefficients, accurate prices are obtained with great efficiency as well. For practical pricing scenarios, such as calibration, we introduce an automated procedure for parameter selection requiring no user input. The algorithm is demonstrated to be fast and robust.

Table 41: Barrier option errors and cpu times for automated parameter selection. Column NL is number of loops required in initialization Algorithm 14 before tolerance is met. N is the final grid size. In all cases, $S_0 = 100$, $r = 0.05$, $q = 0$, $T = 1$.

Model	Type	H	W	M	Ref	$\|Err\|$	$\|Rel.Err\|$	cpu(sec)	NL	$\log_2(N)$
CGMY	DOP	80	100	12	1.6166109	3.37e-06	2.09e-06	0.003	1	8
(G, G, M, Y)	DOP	80	95	52	0.6114938	5.94e-07	9.72e-07	0.008	2	10
(0.2703, 17.56, 54.82, 0.8)	DOP	90	95	252	0.0652584	3.39e-08	5.19e-07	0.064	3	12
CGMY	UOC	120	100	12	3.3518176	6.49e-05	1.94e-05	0.003	1	8
(G, G, M, Y)	UOC	110	95	52	1.7819262	1.05e-04	5.89e-05	0.008	2	10
(4, 50, 30, 0.3)	UOC	135	105	252	3.8082642	1.88e-05	4.93e-06	0.127	4	13
MJD	DOP	80	100	12	2.0675201	5.17e-05	2.50e-05	0.002	1	8
$(\sigma, \lambda, \mu_J, \sigma_J)$	DOP	80	95	52	0.8629417	3.01e-05	3.49e-05	0.005	1	9
(0.12, 1, -0.06, 0.08)	DOP	90	95	252	0.0462857	6.88e-06	1.49e-04	0.019	1	10
MJD	UOC	120	100	12	0.7673427	1.46e-04	1.90e-04	0.002	1	8
$(\sigma, \lambda, \mu_J, \sigma_J)$	UOC	110	95	52	0.1964608	5.03e-05	2.56e-04	0.005	1	9
(0.25, 2, -0.12, 0.18)	UOC	135	105	252	1.5296553	2.01e-04	1.31e-04	0.019	1	10
NIG	DOP	80	100	12	2.0381739	3.72e-04	1.83e-04	0.003	1	8
(α, β, δ)	DOP	80	95	52	0.8692051	9.30e-05	1.07e-04	0.008	2	10
(8, -1, 0.2)	DOP	90	95	252	0.0747386	1.99e-05	2.66e-04	0.065	3	12
NIG	UOC	120	100	12	2.3592043	6.69e-04	2.83e-04	0.002	1	8
(α, β, δ)	UOC	110	95	52	0.8423634	6.56e-05	7.79e-05	0.007	2	10
(15, -5, 0.5)	UOC	135	105	252	3.9701770	4.38e-05	1.10e-05	0.064	3	12
Kou	DOP	80	100	12	1.0802349	2.57e-04	2.38e-04	0.003	2	9
$(\sigma, \lambda, p, \eta_1, \eta_2)$	DOP	80	95	52	0.4280794	1.70e-04	3.98e-04	0.008	2	10
(0.15, 0.6, 0.2, 9, 3)	DOP	90	95	252	0.0206620	3.23e-05	1.56e-03	0.037	2	11
Kou	UOC	120	100	12	1.7232076	6.54e-05	3.80e-05	0.002	1	8
$(\sigma, \lambda, p, \eta_1, \eta_2)$	UOC	110	95	52	0.5439582	2.64e-05	4.85e-05	0.005	1	9
(0.2, 0.33, 0.5, 10, 10)	UOC	135	105	252	2.9033305	3.25e-05	1.12e-05	0.019	1	10
BSM	DOP	80	100	12	2.4362319	3.72e-06	1.53e-06	0.002	1	8
σ	DOP	80	95	52	1.0397317	2.35e-06	2.26e-06	0.004	1	9
0.15	DOP	90	95	252	0.0507307	7.47e-07	1.47e-05	0.019	1	10
BSM	UOC	120	100	12	0.4228516	1.08e-06	2.57e-06	0.002	1	8
σ	UOC	110	95	52	0.0939105	9.36e-07	9.97e-06	0.004	1	9
0.45	UOC	135	105	252	0.6671245	5.76e-06	8.63e-06	0.019	1	10

Table 42: Parisian option errors and cpu times for automated parameter selection. Column R/C denotes resetting (R) vs cumulative (C). N is the final grid size. In all cases, $S_0 = W = 100$, $r = 0.05$, $q = 0$, $T = 1$. Barrier $H = 80$ for DOPP; $H = 120$ for UOPC.

Model	Type	R/C	M	Γ	Ref	$\lvert Err\rvert$	$\lvert Rel.Err\rvert$	cpu(sec)	NL	$\log_2(N)$
CGMY	DOPP	R	52	5	1.7205409	3.94e-05	2.29e-05	0.028	2	10
(G, G, M, Y)	DOPP	C	52	5	1.7033119	5.58e-05	3.28e-05	0.032	2	10
(0.2703, 17.56, 54.82, 0.8)	UOPC	R	252	12	5.3690123	1.82e-04	3.40e-05	0.673	3	12
	UOPC	C	252	12	5.2919876	2.62e-04	4.95e-05	0.746	3	12
CGMY	DOPP	R	52	5	2.5440428	8.83e-06	3.47e-06	0.042	3	11
(G, G, M, Y)	DOPP	C	52	5	2.5214495	2.35e-05	9.33e-06	0.046	3	11
(4, 50, 30, 0.3)	UOPC	R	252	12	3.7599685	3.61e-05	9.60e-06	2.272	5	14
	UOPC	C	252	12	3.6448328	2.57e-05	7.06e-06	2.489	5	14
MJD	DOPP	R	52	5	2.5226161	5.87e-05	2.33e-05	0.017	1	9
$(\sigma, \lambda, \mu_J, \sigma_J)$	DOPP	C	52	5	2.4175802	2.42e-05	1.00e-05	0.020	1	9
(0.12, 1, -0.06, 0.08)	UOPC	R	252	12	3.8332312	1.34e-04	3.50e-05	0.271	1	10
	UOPC	C	252	12	3.5363449	1.15e-05	3.25e-06	0.299	1	10
MJD	DOPP	R	52	5	2.0566139	9.58e-06	4.66e-06	0.026	2	10
$(\sigma, \lambda, \mu_J, \sigma_J)$	DOPP	C	52	5	1.7219672	1.00e-05	5.81e-06	0.029	2	10
(0.25, 2, -0.12, 0.18)	UOPC	R	252	12	1.2949247	9.48e-06	7.32e-06	0.401	2	11
	UOPC	C	252	12	1.0148030	4.18e-06	4.12e-06	0.439	2	11
NIG	DOPP	R	52	5	2.3560626	1.57e-05	6.65e-06	0.071	4	12
(α, β, δ)	DOPP	C	52	5	2.3139194	1.51e-05	6.54e-06	0.077	4	12
(8, -1, 0.2)	UOPC	R	252	12	3.8540054	3.21e-05	8.32e-06	1.224	4	13
	UOPC	C	252	12	3.7739463	1.72e-04	4.56e-05	1.339	4	13
NIG	DOPP	R	52	5	2.6077264	3.05e-04	1.17e-04	0.026	2	10
(α, β, δ)	DOPP	C	52	5	2.4631476	3.33e-04	1.35e-04	0.029	2	10
(15, -5, 0.5)	UOPC	R	252	12	2.9008918	6.20e-05	2.14e-05	0.667	3	12
	UOPC	C	252	12	2.7112828	2.25e-04	8.31e-05	0.724	3	12

Table 43: Symbols $\psi_L(\xi)$, cumulants c_n of $\log(S_{t+1}/S_t)$, param. restrictions and strip of analyticity $\mathcal{I}_L$. $\gamma := r - q - \psi_L(-i) = r - q + \omega$. $\mathbb{E}[\log(S_{t+1}/S_t)] = c_1 = r - q + w + \mathbb{E}[L(1)]$, and $\mathbb{E}[R_{\Delta_t}] = c_1\Delta_t$.

Model	$\psi_L(\xi)$, $\omega = -\psi_L(-i)$, Param. Restrictions	Cumulants
BSM	$\psi_L(\xi) = -\frac{\sigma^2}{2}\xi^2$	$c_1 = \gamma$
	$\omega = -\frac{\sigma^2}{2}$	$c_2 = \sigma^2$
	$\sigma > 0, \quad \mathcal{I}_L = \mathbb{R}$	$c_4 = 0$
MJD	$\psi_L(\xi) = -\frac{\sigma^2}{2}\xi^2 + \lambda\Big(\exp(i\xi\mu_J - \frac{\sigma_J^2}{2}\xi^2) - 1\Big)$	$c_1 = \gamma + \lambda\mu_J$
	$\omega = -\frac{\sigma^2}{2} - \lambda\Big(\exp(\mu_J + \frac{\sigma_J^2}{2}) - 1\Big)$	$c_2 = \sigma^2 + \lambda(\mu_J^2 + \sigma_J^2)$
	$\lambda, \sigma_J, \sigma > 0, \quad \mathcal{I}_L = \mathbb{R}$	$c_4 = \lambda(\mu_J^4 + 6\sigma_J^2\mu_J^2 + 3\sigma_J^4\lambda)$
CGMY	$\psi_L(\xi) = C\Gamma(-Y)\left((M - i\xi)^Y - M^Y + (G + i\xi)^Y - G^Y\right)$	$c_1 = \gamma + C\Gamma(1 - Y)(M^{Y-1} - G^{Y-1})$
	$\omega = -C\Gamma(-Y)((M - 1)^Y - M^Y + (G + 1)^Y - G^Y)$	$c_2 = C\Gamma(2 - Y)(M^{Y-2} + G^{Y-2})$
	$C, G > 0, M > 1, Y \in (0, 1) \cup (1, 2), \quad \mathcal{I}_L = [-M, G]$	$c_4 = C\Gamma(4 - Y)(M^{Y-4} + G^{Y-4})$
NIG	$\psi_L(\xi) = -\delta\left(\sqrt{\alpha^2 - (\beta + i\xi)^2} - \sqrt{\alpha^2 - \beta^2}\right)$	$c_1 = \gamma + \delta\beta/\sqrt{\alpha^2 - \beta^2}$
	$\omega = \delta\left(\sqrt{\alpha^2 - (\beta + 1)^2} - \sqrt{\alpha^2 - \beta^2}\right)$	$c_2 = \delta\alpha^2(\alpha^2 - \beta^2)^{-3/2}$
	$\alpha, \delta > 0, \beta \in (-\alpha, \alpha - 1), \quad \mathcal{I}_L = [\beta \pm \alpha]$	$c_4 = 3\delta\alpha^2(\alpha^2 + 4\beta^2)(\alpha^2 - \beta^2)^{-7/2}$
Kou	$\psi_L(\xi) = -\frac{\sigma^2}{2}\xi^2 + \lambda\Big(\frac{p\eta_1}{\eta_1 - i\xi} + \frac{(1-p)\eta_2}{\eta_2 + i\xi} - 1\Big)$	$c_1 = \gamma + \frac{\lambda p}{\eta_1} - \frac{\lambda(1-p)}{\eta_2}$
	$\omega = -\frac{\sigma^2}{2} - \lambda\Big(\frac{p\eta_1}{\eta_1 - 1} + \frac{(1-p)\eta_2}{\eta_2 + 1} - 1\Big)$	$c_2 = \sigma^2 + 2\frac{\lambda p}{\eta_1^2} + 2\frac{\lambda(1-p)}{\eta_2^2}$
	$\lambda, \sigma > 0$, $p \in [0, 1]$, $\eta_1 > 1, \eta_2 > 0, \quad \mathcal{I}_L = (-\eta_1, \eta_2)$	$c_4 = 24\lambda(\frac{p}{\eta_1^4} + \frac{1-p}{\eta_2^4})$
VG	$\psi_L(\xi) = -\frac{\sigma^2}{2}\xi^2 - \frac{1}{\nu}\log\left(1 - i\nu\theta\xi + \nu\frac{\sigma_V^2}{2}\xi^2\right)$	$c_1 = \gamma + \theta$
	$\omega = -\frac{\sigma^2}{2} + \frac{1}{\nu}\log\left(1 - \nu\theta - \nu\frac{\sigma_V^2}{2}\right)$	$c_2 = \sigma^2 + \sigma_V^2 + \nu\theta^2$
	$\nu, \sigma_V > 0$, $\sigma \geq 0, \quad \mathcal{I}_L = \left[\frac{\theta}{\sigma_V^2} \pm \sqrt{\frac{\theta^2}{\sigma_V^4} + \frac{2}{\nu\sigma_V^2}}\right]$	$c_4 = 3(\sigma_V^4\nu + 2\theta^4\nu^3 + 4\sigma_V^2\theta^2\nu^2)$

CHAPTER VIII

CONCLUSION

This work develops a new framework for pricing and hedging vanilla and exotic financial options using Fourier techniques. In particular, Frame theory is introduced to the field as a means of tackling many problems in option pricing and hedging. From this theory we derive a new approach for solving pricing problems in the Fourier domain, using the characteristic function of the underlying process. The resulting method is robust, accurate and efficient. Moreover, many types of contracts can be priced in this framework, assuming exponential Levy dynamics and stochastic volatility in the case of vanilla options. This includes many models which extend Black-Scholes-Merton, such as KoBoL (CGMY), Kou's double exponential jump diffusion, Merton's jump diffusion, Meixner and generalized hyperbolic processes, and the Normal Inverse Gaussian model. The only difference for pricing this wide class of models is a specification for the characteristic function, which is often known in closed form. The contracts considered are general European, geometric/arithmetic Asian, forward starting, American/Bermudan, Barrier, Bermudan barrier, Parisian, Par-asian, step, lookback, swing (multi early-exercise) and credit default swaps. Extensions to alternative exotic contracts and stochastic processes are being investigated.

8.1 Future Research Objectives

Up to this point, I have devoted my research efforts towards extending the idea of frame projection to various contexts in exotic option pricing. My intention is to pursue other applications of frame theory that are separate from extensions of the PROJ method.

The first application of frame projection beyond PROJ is in terms of simulating the dynamics of a process by using the characteristic function of process increments. For example, Glasserman and Lin (2010) use Laplace transforms to numerically invert a density, and estimate an appropriate score function by constructing a linear interpolation of the inverted cdf [75]. The question is whether the use of a projected density to perform the

inversion is able to provide a variance reduction (at the cost of introducing additional bias). If so, the implied trade-off between the induced bias and variance reduction is of interest. Alternatively, can the score function itself be projected to hasten convergence? In pricing exotic European options (e.g. straddles) using Monte Carlo, I have found that projected payoffs have value estimates that converge much faster with respect to the number of trials than if the payoff itself is used. The idea of convergence acceleration is very interesting, and I would like to explore the implications further.

Another avenue is to study the relationship between inverse problems and frame projection. This arises, for example, when attempting to identify a process given a set of data. Alternatively, given a set of option prices, can projection be used to more effectively identify an appropriate risk-neutral model. Other basis and related methods are also of interest in this context (e.g. Kriging), as well as in other areas.

Given that [83] identifies calibration as a main application of the PROJ method (in the European context), a natural line of research is that of calibration methodology. This field is more in line with traditional operations research interests, involving high dimensional optimization with noisy data (noisy because option prices are not obtained precisely). For example, how accurately must we calculate prices in order to reach reasonable parameter settings with relatively flat objective functions (e.g. in Heston's model)? Can cumulants or other characteristic function information be used to guide or limit the search? To what extent do the calibrated model parameters matter when determining an appropriate risk-neutral model, and is it consistent across different contract types? To what extent are certain contracts, such as Asian or barrier, more sensitive to the calibrated parameters than others?

Extension to higher dimensional problems is another area of interest, using tensor product bases. This includes hedging as well as pricing applications. Similarly, while Levy processes have been the main focus of this work, stochastic volatility modeling has been widely adopted in practice. Extensions of the PROJ method to stochastic volatility with exotic options are in progress. Also, more exotic structures such as swing options [89] and general stochastic control problems are being studied for Levy models as well.

REFERENCES

[1] Akhiezer, N. and Glazman, I., *Theory of Linear Operators in Hilbert Space: Two Volumes Bound as One*. New York: Dover, 1993.

[2] Albrecher, H., Dominik, K., and Zhou, X., "Pricing of Parisian options for a jump-diffusion model with two-sided jumps," *Applied Mathematical Finance*, vol. 19(2), pp. 97–129, 2012.

[3] Albrecher, H., Mayer, P., and Schoutens, W., "General lower bounds for arithmetic asian option prices.," *App. Math. Fin.*, vol. 15(2), pp. 123–149, 2008.

[4] Albrecher, H. and Predota, M., "Bounds and approximations for discrete Asian options in a variance-gamma model," *Grazer Math. Ber.*, vol. 345, pp. 35–57, 2002.

[5] Alziary, B., Dechamps, J., and Koehl, P., "Pde approach to asian options: analytical numerical evidence," *J. Banking and Fin.*, vol. 21, pp. 613–640, 1997.

[6] Andreasen, J., "The pricing of discretely sampled Asian and lookback options: a change of numeraire approach," *J. Comput. Fin.*, vol. 1(3), pp. 15–36, 1998.

[7] Andricopoulos, A., Widdicks, D., Newton, D., and Duck, P., "Universal option valuation using quadrature methods," *J. Finan. Econ.*, vol. 67, pp. 447–471, 2003.

[8] Andricopoulos, A., Widdicks, D., Newton, D., and Duck, P., "Extending quadrature methods to value multi-asset and complex path dependent options," *J. Finan. Econ.*, vol. 83, pp. 471–499, 2007.

[9] Applebaum, D., *Levy Processes and Stochastic Calculus*. Cambridge, UK: Cambridge University Press, second ed., 2009.

[10] Bakshi, G. and Madan, D., "Spanning and derivative-security valuation," *J. Finan. Econ.*, vol. 55, pp. 205–238, 2000.

[11] Bakshi, G. and Madan, D., "Spanning and derivative-security valuation," *Journal of Financial Economics*, vol. 55, pp. 205–238, 2000.

[12] Barndorff-Nielsen, O., "Processes of normal inverse Gaussian type," *Finance and Stochastics*, vol. 2(1), pp. 41–68, 1997.

[13] Benhamou, E., "Fast Fourier transform for discrete Asian options," *J. Comput. Fin.*, vol. 6(1), pp. 49–61, 2002.

[14] Bernard, C. and Boyle, P., "Monte Carlo methods for pricing discrete Parisian options," *The European J. of Fin.*, vol. 17(3), pp. 169–196, 2011.

[15] Black, F. and Scholes, M., "The pricing of options and corporate liabilities," *J. Political Economy*, vol. 81, pp. 637–659, 1973.

[16] Boyarchenko, S. and Levendorskii, S., "Option pricing for truncated Levy processes," *International J. of Theoretical and Applied Finance*, vol. 3, pp. 549–552, 2000.

[17] Boyarchenko, S. and Levendorskii, S., *Non-Gaussian Merton-Black-Scholes Theory*. River Edge, NJ,: Adv. Ser. Stat. Sci. Appl. Probab. World Scientific Publishing Co., volume 9 ed., 2002.

[18] Boyarchenko, S. and Levendorskii, S., *Non-Gaussian Merton-Black-Scholes Theory*. River Edge, NJ,: Adv. Ser. Stat. Sci. Appl. Probab. World Scientific Publishing Co., volume 9 ed., 2002.

[19] Boyarchenko, S. and Levendorskii, S., "Efficient versions of the Fourier transform in applications to option pricing," *J. Comp. Fin.*, vol. 18(2), 2014.

[20] Boyarchenko, S. and Levendorskii, S., "Option pricing for truncated Levy processes," *International J. of Theoretical and Applied Finance*, vol. 3(3), pp. 549–552, July 2000.

[21] Boyarchenko, S. and Levendorskii, S., *Non-Gaussian Merton-Black-Scholes Theory*. River Edge, NJ: World Scientific Publishing Co., volume 9 of adv. ser. stat. sci. appl. probab. ed., 2002.

[22] Boyarchenko, S. and Levendorskii, S., "Efficient variations of Fourier transform in applications to option pricing," *Journal of Computational Finance*, vol. 18(2), pp. 57–90, 2015.

[23] Breeden, D. and Litzenberger, R., "Prices of state contingent claims implicit in option prices," *Journal of Business*, vol. 51, pp. 621–651, 1978.

[24] Broadie, M. and Glasserman, P., "A continuity correction for discrete barrier options," *Management Science*, vol. 42, pp. 328–344, 1996.

[25] Broadie, M., Glasserman, P., and Kou, S., "Connecting discrete and continuous path-dependent options," *Fin. Stoch.*, vol. 3, pp. 55–82, 1999.

[26] Broadie, M. and Yamamoto, Y., "Application of the fast Gauss transform to option pricing.," *Management Science*, vol. 49(8), p. 2003, 1071-1088.

[27] Broadie, M. and Yamamoto, Y., "A double-exponential fast Gauss transform algorithm for pricing discrete path-dependent options," *Operations Research*, vol. 53(5), pp. 764–779, 2005.

[28] Carmona, R. and Durrleman, V., "Pricing and hedging spread options," *SIAM Review*, vol. 45, pp. 627–685, 2003.

[29] Carr, P. and Chou, A., "Breaking barriers," *Risk*, vol. 10, pp. 139–145, 1996.

[30] Carr, P. and Chou, A., "Hedging complex barrier options." Working paper, 2002.

[31] Carr, P., Ellis, K., and Gupta, V., "Static hedging of exotic options," *Journal of Finance*, vol. 53, pp. 1165–1190, 1998.

[32] Carr, P., Geman, H., Madan, D. B., and Yor, M., "The fine structure of asset returns: an empirical investigation," *J. Business*, vol. 75, pp. 305–332, 2002.

[33] Carr, P. and Lee, R., "Put-call symmetry: Extensions and applications," *Mathematical Finance*, vol. 19(4), pp. 523–560, October 2009.

[34] Carr, P., Lewis, K., and Madan, D., "On the nature of options." Working Paper, 2000.

[35] Carr, P. and Madan, D., "Option valuation using the fast Fourier transform," *J. Comput. Finance*, vol. 2, pp. 61–73, 1998.

[36] Carr, P. and Madan, D., "Optimal positioning in derivative securities," *Quantitative Finance*, vol. 1, pp. 19–37, 2001.

[37] Carr, P. and Madan, D., "Saddlepoint methods for option pricing," *J. Comput. Fin.*, forthcoming.

[38] Carr, P. and Picron, J., "Static hedging of timing risk," *Journal of Derivatives*, vol. 6, No.3, pp. 57–70, Spring 1999.

[39] Carr, P. and Wu, L., "Time-changed Levy processes and option pricing," *J. Finan. Econ.*, vol. 71(1), pp. 113–141, 2004.

[40] Carr, P. and Wu, L., "Static hedging of standard options," *Journal of Financial Econometrics*, vol. 12(1), pp. 3–46, 2014.

[41] Carverhill, A. and Clewlow, L., "Flexible convolution: Valuing average rate (Asian) options," *Risk*, vol. 3(4), pp. 25–29, 1990.

[42] Cerny, A. and Kyriakou, I., "An improved convolution algorithm for discretely sampled Asian options," *Quant. Fin.*, vol. 11, pp. 381–389, 2011.

[43] Chesney, M., Jeanblanc-Picque, M., and Yor, M., "Brownian excursions and Parisian barrier options," *Adv. in App. Prob.*, pp. 165–184, 1997.

[44] Christensen, O., *An Introduction to Frames and Riesz Bases*. Birkhauser Boston, 2003.

[45] Clark, I., *Foreign Exchange Option Pricing: A Practitioners Guide*. Chichester, UK: The Wiley Finance Series, John Wiley & Sons, Ltd, 2011.

[46] Cont, R. and Tankov, P., *Financial Modelling with Jump Processes*. Chapman & Hall / CRC Press, 2004.

[47] Conway, J., *Functions of One Complex Variable I*. New York: Springer, second ed., 1978.

[48] Dai, T. and Lyuu, Y., "Accurate and efficient lattice algorithms for American-style Asian options with range bounds," *Appl. Math. Comput.*, vol. 209, p. 238253, 2009.

[49] Darolles, S. and Laurent, J., "Approximating payoffs and pricing formulas," *Journal of Economic Dynamics and Control*, vol. 24, pp. 1721–1746, 2000.

[50] Daubechies, I., "Orthonormal bases of compactly supported wavelets," in *Commun Pure Appl Math 41:906966*, 1988.

[51] De Innocentis, M. and Levendorskii, S., "Pricing discrete barrier options and credit default swaps under Levy processes," *Quant. Fin.*, vol. 14(8), pp. 1337–1365, 2014.

[52] Debnath, L. and Mikusinski, P., *Introduction to Hilbert Spaces With Applications*. Academic Press, third ed., 2005.

[53] Dempster, M. and Hong, S., "Spread option valuation and the fast Fourier transform," *Mat. Fin.-Bachelier Congress 2000, Springer, Berlin*, pp. 203–220, 2002.

[54] Den Iseger, P. and Oldenkamp, E., "Pricing guaranteed return rate products and discretely sampled Asian options," *J. Comput. Fin.*, vol. 9(3), pp. 1–39, 2006.

[55] Derman, E., Ergener, D., and Kani, I., "Static options replication," *Journal of Derivates*, vol. 2, pp. 78–95, 1995.

[56] Dewynne, J. and Wilmott, P., "Asian options as linear complementary problems," *Advances in Futures and Options Research*, vol. 8, pp. 145–173, 1995.

[57] Duffie, D., Pan, J., and Singleton, K., "Transform analysis and asset pricing for affine jump diffusions," *Econometrica*, vol. 68, pp. 1343–1376, 2000.

[58] Eberlein, E. and Papapantoleon, A., "Equivalence of floating and fixed strike Asian and lookback options," *Stochastic Processes and their Applications*, vol. 115(1), pp. 31–40, 2005.

[59] Engelmann, B., Fengler, M., Nalholm, M., and Schwendner, P., "Static versus dynamic hedges: an empirical comparison for barrier options," *Review of Derivative Research*, vol. 9(3), pp. 239–264, 2006.

[60] Fang, F., Jonsson, H., Oosterlee, C., and Schoutens, W., "Fast valuation and calibration of credit default swaps under Levy dynamics," *J. Comput. Fin.*, vol. 14, pp. 57–86, 2010.

[61] Fang, F. and Oosterlee, C., "A novel pricing method for European options based on Fourier cosine series expansions," *SIAM J. Sci. Comput.*, vol. 31, pp. 826–848, 2008.

[62] Fang, F. and Oosterlee, C., "Pricing early-exercise and discrete barrier options by Fourier-cosine series expansions," *Numerische Mathematik*, vol. 114, pp. 27–62, 2009.

[63] Fang, F. and Oosterlee, C., "A Fourier-based valuation method for Bermudan and barrier options under Heston's model," *SIAM J. Finan. Math.*, vol. 2, pp. 439–463, 2011.

[64] Feng, L. and Lin, X., "Inverting analytic characteristic functions with financial applications," *SIAM J. Finan. Math.*, vol. 4(1), pp. 372–398, 2013.

[65] Feng, L. and Lin, X., "Pricing Bermudan options in Levy process models," *SIAM J. Finan. Math.*, vol. 4(1), pp. 474–493, 2013.

[66] Feng, L. and Linetsky, V., "Computing exponential moments of the discrete maximum of a Levy process and lookback options," *Finan. Stoch.*, vol. 13(4), pp. 501–529, 2009.

[67] Feng, L. and Linetsky, V., "Pricing discretely monitored barrier options and defaultable bonds in Levy process models: a fast Hilbert transform approach," *Math. Finan.*, vol. 18(3), p. 337384, July 2008.

[68] Fusai, G., Marazzina, D., and Marena, M., "Pricing discretely monitored Asian options by maturity randomization," *SIAM J. Finan. Math.*, vol. 2, pp. 383–403, 2011.

[69] Fusai, G. and Meucci, A., "Pricing discretely monitored Asian options under Levy processes," *J. Banking Fin.*, vol. 32(1), pp. 2076–2088, 2008.

[70] Gasquet, C. and Witomski, P., *Fourier Analysis and applications: filtering, numerical computation, wavelets*. New York: Springer, 1998.

[71] Gatheral, J., *The Volatility Suface: a Practicioner's Guide*. New Jersey: John Wiley and Sons, Inc., 2006.

[72] Geman, H., Karoui, N., and Rochet, J., "Changes of numeraire, changes of probability measure and option pricing," *J. App. Prob.*, vol. 32(2), pp. 443–458, 1995.

[73] Geman, H. and Madan, D., *Risks in returns: a pure jump perspective*. In Exotic Option Pricing and Advanced Levy Models, Wiley, 2005.

[74] Gil-Pelaez, J., "Note on the inversion theorem," *Biometrika*, vol. 38(3/4), pp. 481–482, 1951.

[75] Glasserman, P. and Liu, Z., "Sensitivity estimates from characteristic functions," *Operations Research*, vol. 58(6), pp. 1611–1623, 2010.

[76] Haber, R., Schonbucher, P., and Wilmott, P., "Pricing Parisian options," *J. Derivatives*, vol. 6, pp. 71–79, 1999.

[77] Haug, E., *The Complete Guide to Option Pricing Formulas*. McGraw-Hill, second ed., 2006.

[78] Heil, C., *A Basis Theory Primer*. Birkhauser, expanded edition ed., 2011.

[79] Heston, S., "A closed-form solution for options with stochastic volatility with applications to bond and currency options," *Review of Financial Studies*, vol. 6, pp. 327–343, 1993.

[80] Hurd, T. and Zhou, Z., "A Fourier transform method for spread option pricing," *SIAM J. Finan. Math.*, vol. 1(1), pp. 142–157, 2010.

[81] Ju, N., "Pricing asian and basket options via taylor expansion," *J. Comput. Fin.*, vol. 5(3), pp. 79–103, 2002.

[82] Kemna, A. and Vorst, A., "A pricing method for options based on average asset values," *J. of Banking and Fin.*, vol. 14, pp. 113–129, 1990.

[83] Kirkby, J., "Efficient option pricing by frame duality with the fast Fourier transform," *SIAM J. Finan. Math.*, vol. 6(1), pp. 713–747, 2015.

[84] Kirkby, J., "An efficient transform method for Asian option pricing." SIAM J. Finan. Math., Accepted, 2015.

[85] Kirkby, J., "Robust barrier option pricing by frame projection under exponential Levy dynamics." Working Paper, 2015.

[86] Kirkby, J., "American and exotic option pricing with jump diffusions and other Levy processes." Working Paper, 2016.

[87] Kirkby, J., "Robust option pricing with characteristic functions and the B-spline order of density projection." J. Comput. Fin., Forthcoming, 2016.

[88] Kirkby, J. and Deng, S., "Static hedging and pricing of exotic options with payoff frames." Working Paper, 2015.

[89] Kirkby, J. and Deng, S., "Efficient swing option pricing by dynamic programming with B-spline density projection." Working Paper, 2016.

[90] Kou, S. and Wang, H., "Option pricing under a double exponential jump diffusion model," *Management Science*, vol. 50(9), pp. 1178–1192, 2004.

[91] Lee, R., "Option pricing by transform methods: extensions, unification, and error control," *J. Comput. Finance*, vol. 7(3), pp. 50–86, 2004.

[92] Leentvaar, C. and Oosterlee, C., "Multi-asset option pricing using a parallel Fourier-based technique," *J. Comput. Fin.*, vol. 12(1), pp. 1–26, 2008.

[93] Lemmens, D., Liang, L., Tempere, J., and De Schepper, A., "Pricing bounds for discrete arithmetic Asian options under Levy models," *Physica A: Statistical Mechanics and its Applications*, vol. 389(22), pp. 5193–5207, 2010.

[94] Levendorskii, "Efficient pricing and reliable calibration in the heston model," *International Journal of Theoretical and Applied Finance*, vol. 15(7), p. 12050 (44 pages), 2012.

[95] Levendorskii, S. and Xie, J., "Pricing discretely sampled Asian options under Levy processes." Available at SSRN: http://papers.ssrn.com/abstract=2088214, 2012.

[96] Lewis, A., "A simple option formula for general jump-diffusion and other exponential Levy processes." Working Paper, 2001.

[97] Lewis, A., "A simple option formula for general jump-diffusion and other exponential Levy processes." Working Paper, 2001.

[98] Li, M., Deng, S., and Zhou, J., "Closed-form approximations for spread option prices and Greeks," *J. Deriv.*, vol. 15, pp. 58–80, 2008.

[99] Linetsky, V., "Step options," *Math. Finance*, vol. 9, pp. 55–96, 1999.

[100] Lord, R., Fang, F., Bervoets, F., and Oosterlee, C., "A fast and accurate FFT-based method for pricing early-exercise options under Levy processes," *SIAM J. Sci. Comput.*, vol. 10, pp. 1678–1705, 2008.

[101] Lord, R. and Kahl, C., "Jump and stochastic volatility: Exchange rate processes implict in Deutche mark in options," *Review of Financial Studies*, vol. 9, pp. 69–107, 1996.

[102] Lord, R. and Kahl, C., "Optimal Fourier inversion in semi-analytical option pricing," *J. Comput. Fin.*, vol. 10(4), pp. 1–30, 2007.

[103] Lukacs, E. and Szasz, O., "On analytic characteristic functions," *Pacific J. of Math.*, vol. 2(4), pp. 615–625, 1952.

[104] Madan, D. and Seneta, E., "The variance gamma (v.g.) model for share market returns," *J. Business*, vol. 63, pp. 511–524, 1990.

[105] Madan, D. B., Carr, P., and Chang, E., "The variance gamma process and option pricing," *European Finance Review*, vol. 2, pp. 79–105, 1998.

[106] Merton, R., "Option pricing when underlying stock returns are discontinuous," *J. Finan. Econ.*, vol. 3, pp. 125–144, 1976.

[107] Milne, F. and Madan, D., "Contingent claims valued and hedged by pricing and investing in a basis," *Mathematical Finance*, vol. 4(3), pp. 223–245, 1994.

[108] Nalholm, M. and Poulsen, R., "Static hedging and model risk for barrier options," *The Journal of Futures Markets*, vol. 26(5), pp. 449–463, 2006.

[109] Naylor, A. and Sell, G., *Linear Operator Theory in Engineering and Science*. New York: Springer-Verlag, 1982.

[110] Neuberger, A., "The log contract," *J. of Portfolio Management*, vol. 20(2), pp. 74–80, 1994.

[111] Nielsen, J. and Sandmann, K., "Pricing bounds on Asian options.," *J. Fin. and Quant. Anal.*, vol. 38(2), 2003.

[112] Ortiz-Gracia, L. and Masdemont, J., "Peaks and jumps reconstruction with B-splines scaling functions." Working Paper, 2012.

[113] Ortiz-Gracia, L. and Oosterlee, C., "Robust pricing of European options with wavelets and the characteristic function," *SIAM J. Sci. Comput.*, vol. 35(5), pp. B1055–B1084, 2013.

[114] Petrella, G. and Kou, S., "Numerical pricing of discrete barrier and lookback options via Laplace transforms," *J. Comput. Fin.*, vol. 8(1), pp. 1–37, 2004.

[115] Poulsen, R., "Barrier options and their static hedges: simple derivations and extensions," *Quantitative Finance*, vol. 6(4), pp. 327–335, August 2006.

[116] Priestley, H., *Introduction to Complex Analysis*. Oxford University Press, second ed., 2003.

[117] Raible, S., *Levy processes in finance: theory, numerics, and empirical facts*. PhD thesis, Univ. Freiburg, 2000.

[118] Ruijter, M. and Oosterlee, C., "Two-dimensional Fourier cosine series expansion method for pricing financial options," *SIAM J. Sci. Comput.*, vol. 34(5), pp. B642–B671, 2012.

[119] Sabino, P., "Monte Carlo methods and path-generation techniques for pricing multi-asset path- dependent options." SSRN Working Paper, 2007.

[120] Sato, K.-I., *Levy Processes and Infinitely Divisible Distributions*. Cambridge, UK: Cambridge University Press, 1999.

[121] Schoutens, W., *Levy Processes in Finance: Pricing Financial Derivatives*. John Wiley and Sons Ltd., 2003.

[122] Shimko, D., "Non linear risk management," *Financial Derivaties and Risk Management*, vol. 1(4), pp. 36–38, 1995.

[123] Stenger, F., *Numerical Methods based on Sinc and Analytic functions*. New York: Springer-Verlag, 1993.

[124] Sydow, L., Hook, L., Larsson, E., Lindstrom, E., Milovanovic, S., Persson, J., Shcherbakov, V., Shpolyanskiy, Y., Siren, S., Toivanen, J., Walden, J., Wiktorsson, M., Levesley, J., Li, J., Oosterlee, C., Ruijter, M., Toropov, A., and Zhao, Y., "BENCHOP-The BENCHmarking project in option pricing," *International J. of Computer Mathematics*, vol. 92(12), pp. 2361–2379, 2015.

[125] Tompkins, R., "Static versus dynamic hedging of exotic options: an evaluation of hedge performance via simulation," *Journal of Risk Finance*, vol. 3(4), pp. 6–34, 2002.

[126] Tompkins, R., "Power options: Hedging nonlinear risks," *The Journal of Risk*, vol. 2, No.2, pp. 29–45, Winter 1999/2000.

[127] Unser, M. and Daubechies, I., "On the approximation power of convolution-based least squares versus interpolation," *IEEE Transactions on Signal Processing*, vol. 45(7), pp. 1697–1711, July 1997.

[128] Unser, M., "Vanishing moments and the approximation power of wavelet expansions," in *Proceedings of the 1996 IEEE international conference on image processing*, 1996.

[129] Vecer, J., "A new pde approach for pricing arithmetic average Asian options," *J. Comput. Fin.*, vol. 4(4), pp. 105–115, 2001.

[130] Vetzal, K. and Forsyth, P., "Discrete Parisian and delayed barrier options: A general numerical approach," *Adv. in Futures and Options Res.*, vol. 10, pp. 1–16, 1999.

[131] Xiu, D., "Hermite polynomial based expansion of European option prices," *J. Econometrics*, vol. 179(2), pp. 158–177, 2014.

[132] Y. Oum, S. O. and Deng, S., "Hedging quantity risks with standard power options in a competitive wholesale electricity market," *Naval Research Logistics*, vol. 53, pp. 697–712, 2006.

[133] Yamamoto, Y., "Double-exponential fast Gauss transform algorithms for pricing discrete lookback options," *Publ. RIMS, Kyoto University*, vol. 41, pp. 989–1006, 2005.

[134] Young, R., *An Introduction to Nonharmonic Fourier Series*. New York: Academic Press, (revised) ed., 1980.

[135] Zeng, P. and Kwok, Y., "Pricing barrier and Bermudan style options under time-changed Levy processes: fast Hilbert transform approach." Working Paper, Jan. 2014.

[136] Zhang, B., Grzelak, L., and Oosterlee, C., "Efficient pricing of commodity options with early-exercise under the Ornstein-Uhlenbeck process," *App. Numer. Math.*, vol. 62, pp. 91–111, 2012.

[137] Zhang, B. and Oosterlee, C., "An efficient pricing algorithm for swing options based on Fourier cosine expansions," *J. Comput. Fin.*, vol. 16(4), pp. 1–32, 2013.

[138] Zhang, B. and Oosterlee, C., "Efficient pricing of European-style Asian options under exponential Levy processes based on Fourier cosine expansions," *SIAM J. Finan. Math.*, vol. 4, pp. 399–426, 2013.

[139] Zhang, B. and Oosterlee, C., "Pricing of early-exercise Asian options under Levy processes based on Fourier cosine expansions," *App. Numer. Math.*, vol. 78, pp. 14–30, 2014.

[140] Zhang, J., "Pricing continuously sampled Asian options with perturbation method," *J. Futures Markets*, vol. 23(6), pp. 535–560, 2003.

VITA

Justin Lars Kirkby was born in Norfolk, Virginia. He received both a B.S. in Economics in 2010 and a M.A. in Economics in 2011 from Virginia Commonwealth University. He received a M.S. in Mathematics from Georgia Institute of Technology in 2014. In fall 2011, he joined the Ph.D. program in Operations Research within the school of Industrial and Systems Engineering at Georgia Tech and earned his Ph.D. in 2016. Since June 2015, he has been employed by the Clearing Technology group at Intercontinental Exchange in Atlanta, Georgia. He is married to Elise Kirkby. When not working nor writing research papers, he enjoys travelling and casually reading mathematics.